UNIVERSITY
of
GLASGOW

ESTIMATING CHANGES IN MORPHOLOGY AND SEDIMENT SUPPLY USING REMOTE SENSING AND FIELD TECHNIQUES IN THE LAR DAM BASIN, IRAN

Thesis submitted for the degree of Doctor of Philosophy (Ph.D.)

by

Karim Solaimani
(B.A., M.Sc.)

University of Glasgow
Faculty of Science

Department of Geography & Topographic Science
Glasgow G12 8QQ, UK.

October 1996

بِسْمِ اللّٰهِ الرَّحْمٰنِ الرَّحِيْم

(In the name of Allah, the beneficent, the merciful)

Do they not look at camels, how they are created?

And at the Sky, how it is raised high?

And at the Mountains, how they are fixed firm?

And at the Earth, how it is spread out?

(Holy Quran, Sura Qashiyah, Verses 17-20)

CONTENTS

ACKNOWLEDGEMENTS v
ABSTRACT vi

CHAPTER 1: INTRODUCTION
1.1 THE LAR BASIN 1
1.2 AIMS OF RESEARCH 3
1.3 THESIS STRUCTURE 5

CHAPTER 2: LITERATURE REVIEW
Introduction 7
2.1 GLOBAL SEDIMENT BUDGET 7
2.2 EROSION ESTIMATION MODEL AND SEDIMENT YIELD 8
2.2.1 Predicting Soil Erosion Rates 8
2.2.2 The Sediment Delivery Ratio 12
2.3 SUMMARY AND DEFINITION 14
2.4 USING REMOTE SENSING DATA FOR LAND SURFACE CHANGES 15
2.4.1 A Review of Landsat (TM) and SPOT (MSS) For Environmental Sciences 16
2.4.2 Kosmos Satellite Photography (KFA-1000) 18
2.5 APPLICATION OF AERIAL PHOTOGRAPHS AND SATELLITE DATA FOR LAND SURFACE CHANGES AND SEDIMENT DELIVERY 18
2.5.1 Soil Characteristics 19
2.5.2 Soil Erosion 20
2.5.3 Land Use and Land Cover Changes 24
2.5.4 Fluvial Features 26
2.6 SUMMARY 33
2.7 PREVIOUS WORK IN THE STUDY AREA 34
2.7.1 Geology and Petrology 34
2.7.2 Stratigraphy 36
2.7.3 Sedimentology 36
2.8 GENERAL SUMMARY 37

CHAPTER 3: INVESTIGATION TECHNIQUES
Introduction 38
3.1 REMOTE SENSING DATA INVESTIGATION (RSDI) 38
3.1.1 Objectives 38
3.1.2 Aerial Photographs 39
3.1.3 Satellite Remote Sensing Techniques 40
3.1.4 Digital Image Processing 42
3.2 HYDROLOGICAL AND SURVEY METHODS 50
3.3 FIELD AND LABORATORY TECHNIQUES 51
3.3.1 Particle Size 52
3.3.2 Sieving Analysis 52
3.3.3 Particle Shape 55
3.3.4 Echo-Sounding 55
3.3.5 Control Points for Aerial Photos Stereo Model 56
3.3.6 Vegetation Survey 57
3.3.7 Volumetric Calculation of the Lar Basin Sediments 57
3.4 PROBLEMS 58

3.4.1 Topographic and Atmospheric Effects....58
3.4.2 Geometric Correction....59
3.5 MAP PRODUCTION....60
3.6 SUMMARY....62

CHAPTER 4: PHYSICAL CHARACTERISTICS
Introduction....63
4.1 CLIMATE....63
4.1.1 Temperature....64
4.1.2 Precipitation....64
4.1.3 Annual Precipitation....66
4.2 GEOLOGY....68
4.2.1 The Geological History of Study area....68
4.2.2 Damavand Lavas....69
4.2.3 Tectonic Structure of the Lar Basin Using KFA-1000 Imagery....70
4.2.4 Stratigraphy....71
4.2.5 Soils....76
4.3 VEGETATION CHARACTERISTICS....78
4.3.1 Herb Type....78
4.3.2 Shrub-perennial and Grasses-perennial Forbs....78
4.3.3 Shrub and Perennial Grasses....79
4.3.4 Shrub-forbs Types....79
4.3.5 Rocky Land and Cliff....79
4.4 PHYSIOGRAPHIC ANALYSIS....80
4.4.1 Ordering the Network....80
4.4.2 Basin Area and Elevation....82
4.4.3 Hypsometric Analysis of Basin....83
4.5 SUMMARY....91

CHAPTER 5: MORPHOLOGICAL CHANGES AND DEPOSITION
Introduction....94
5.1 SEDIMENTATION CYCLES IN THE BASIN....94
5.2 GENERAL OBSERVATIONS ON SEDIMENT DISTRIBUTION....96
5.2.1 Great Lake Lar....98
5.2.2 Small Lake of Dalichai....98
5.3 SEDIMENT IN THE IMAM-PAHNAK AREA....98
5.4 MORPHOLOGICAL CHANGES IN THE LAR BASIN....98
5.5 CLASSIFICATION OF DEPOSITS IN THE LAR DAM BASIN....100
5.5.1 Lower Lake Deposits....101
5.5.2 The Upper Lake Deposits....106
5.5.3 The Lar Dam Basin Terrace Gravels....109
5.5.4 Lacustrine Terraces....110
5.6 DETECTION OF LANDSLIDES AND SINKHOLES....112
5.6.1 Lassem Landslide Area....115
5.7 SEDIMENT CHARACTERISTICS IN THE LAR BASIN....115
5.7.1 Particle characteristics....116
5.7.2 Size....116
5.7.3 Shape....118
5.8 ESTIMATION OF SEDIMENT YIELD FROM THE BASIN....120
5.8.1 Sediment Volumes....121
5.8.2 Estimation From Comparative Basins....129

5.8.3 Installation of Sediment-Load Measuring Stations and Estimating the Sediment Delivery Ratio....130
5.8.4 Measurement of Sediment Discharge....131
5.9 SUMMARY....134

CHAPTER 6: DIGITAL IMAGE PROCESSING TECHNIQUES AND RESULTS
Introduction....136
6.1 SPECIFIC OBJECTIVES OF THIS STUDY....137
6.1.1 Geometric Correction....138
6.1.2 Ancillary Data....139
6.1.3 Training Area....140
6.2 ESTIMATION OF POPULATION OF STATISTICS (EPS)....140
6.2.1 Supervised Classification....141
6.2.2 Unsupervised Classification....145
6.3 REMOTE SENSING DATA CLASSIFICATION ACCURACY....147
6.3.1 Selection of Sample Area....147
6.3.2 Image Processing and Error....149
6.3.3 Result of Classification....149
6.4 REMOTE SENSING AND THE GEOMORPHOLOGY OF THE LAR BASIN....151
6.4.1 Tectonic Landforms....152
6.4.2 Structure....153
6.4.3 Lineaments....153
6.4.4 Damavand Volcano Landforms....155
6.4.5 Fluvial Features....156
6.4.6 Terrace Investigation....157
6.4.7 Landslides....160
6.5 VEGETATION COVER AND SOIL EROSION....162
6.6 LAND COVER PATTERN ASSESSMENT....168
6.7 SUMMARY....171

CHAPTER 7: DISCUSSION
Introduction....173
7.1 MORPHOLOGICAL CHANGES AND SEDIMENTARY HISTORY IN THE LAR BASIN....173
7.1.1 Late Quaternary Sedimentary History of the Study Area....173
7.2 LANDCOVER ASSESSMENT AND EROSION SOURCES....178
7.2.1 Lithologic Characteristics and Erodibility....181
7.3 THE LAR BASIN EROSION SOURCES AND PATTERNS....185
7.3.1 Surface Erosion....186
7.3.2 Subsurface Erosion....189
7.3.3 Bank Erosion....189
7.3.4 Mass Movement....190
7.3.5 Sinkhole Development and Lake Drainage....191
7.4 PARTICLE SIZE PATTERNS....193
7.5 SEDIMENT YIELD....195
7.5.1 Lar Basin Deposition....195
7.5.2 Infill of the Lar Lake and Rate of Deposition....195
7.5.3 Sediment Delivery Estimation from Gauging Data....196
7.5.4 Patterns of Sediment Delivery From Different parts of the Basin....200
7.5.5 General Relationships....201
7.6 METHOD ASSESSMENT AND CRITIQUE....203

7.6.1 Remote Sensing Technique Assessment....203
7.6.2 Sediment Estimation from Topography Maps....209
7.6.3 Aerial Photos and Sediment Estimation....209
7.6.4 Echosounding Survey....210
7.6.5 Sediment Concentration Analysis....210
7.6.6 Future Work....211
7.7 SUMMARY....212

CHAPTER 8: CONCLUSION
8.1 GENERAL REVIEW OF THE RESEARCH....215
8.1.1 History of Deposits in the Lar Basin....215
8.2 SUMMARY OF FINDINGS....216
8.2.1 Land Surface Mapping from Aerial Photographs and Field Checking....216
8.2.2 SPOT (XS), Landsat (TM) and Land Surface Detection....217
8.3 GENERAL CONCLUSION....219
8.4 SCOPE FOR FUTURE RESEARCH....221

GLOSSARY....224

REFERENCES....228

FOLDED MAPS (in folder at back)
no.1 = The Lar Dam Basin Slope Angle
no.2 = The Lar Dam Basin Vegetation
no.3 = The Lar Dam Basin Soils
no.4 = The Lar Dam Basin Geomorphology

APPENDICES:

Appendix Chapter 5 (Particle Shape Analysis)
[Dalichai Downstream and Upstream, Sefid-Ab, Khoshkehlar and Galehsardab Junction, Gozaldarreh, Imamzadeh Youghidar and Asbkalak]

Appendix Chapter 6
6.1 SPOT-RHV
6.1.1 Orbital and Recording Options
6.1.2 Multispectral Scanner Imagery
6.2 LANDSAT
6.2.1 MSS Sensor
6.2.2 RBV Sensor
6.2.3 TM Sensor
6.3 USED REMOTE SENSING DATA SPECIFICATIONS

Enclosed Floppy Disk;
Appendix Chapter 4 (Climatic Data)
4.1 The Lar Basin Climatic Data
4.1.1 Amol Station
4.1.2 Polour Station
4.1.3 Karehsang Station

Appendix Chapter 5 (Sediment Concentration and Water Discharge Data)
5.1 Karehsanh Station
5.2 Polour Station
5.3 The Lar Basin Pebbleometric Data
5.3.1 Dalichai
5.3.2 Sefid-Ab
5.3.3 Khoshkehlar and Galehsardab Junction
5.3.4 Gozaldarreh
5.3.5 Imamzadeh Yorghidar

ABSTRACT

ESTIMATING CHANGES IN MORPHOLOGY AND SEDIMENT SUPPLY USING REMOTE SENSING AND FIELD TECHNIQUES IN THE LAR DAM BASIN, IRAN

This research aims to establish land surface changes and sediment delivery using both remote sensing and field techniques in the Lar Dam Basin, Northern Iran. The early eruption of Damavand volcano approximately 60 000 years BP blocked the Lar River with volcanic debris and created Lake Lar upstream of the natural dam. Lake Lar became completely infilled with sediments before the natural dam was breached which is taken to have occurred at about 40 000 years BP. At an elevation of about 2150m. a spillway level formed at the southern side of the volcanic cone and then Damavand produced basic lava flows which raised the dam in the Lar valley to about 2700m.

The potential of different remote sensing techniques for assessing land cover changes in mountainous semi-arid areas has been examined in the Lar Basin. The study considers morphological changes by sequential air photographs, KFA-1000, SPOT (XS), Landsat (TM), topographic maps, echosounding survey, sampling and sediment discharges measured at selected stations. Digital image processing of the Landsat TM and SPOT subscenes for the study area was performed using the Dragon image processing system. The land surface classification information derived from the air photographs, KFA-1000, the SPOT and the Landsat TM has been linked to morphological changes and used as an input into vegetation, soils, morphotectonic and geomorphology maps of the Lar Basin.

The amount of sediment infill estimated from different methods as follows;

- from topographic maps amounts to about $1.58\times10^{11}m^3$ for the old Lake deposits;
- from aerial photographs at three selected deltas estimated $8.5\times10^5m^3$;
- from echosounding this value estimated $13.9\times10^5m^3$ for same deltas,
- and by gauging stations at Gozaldarreh suggests is about $169t/km^2a$-1 which at Polour shows a significant value about $223t/km^2a^{-1}$ before the dam reduced to $155t/km^2a^{-1}$.

ACKNOWLEDGMENT

First of all I would like to thank Ministry of Culture and Higher Education of the Islamic Republic of Iran for their financial support throughout the period over which this research work was carried out, student director Dr. Salar-Amoli, Iranian Embassy in London for their supports and Mazandaran University Iran for field support during my field work (summer 1993 and 1994) in Iran.

The completion of thesis would not have been possible without the continuous advice, supervision and support of my supervisor, Dr. James D. Hansom. Thanks are also due to Dr. Trevor B. Hoey my second supervisor for his guidance in statistical analysis and Dr. Marwan Hassan for his guidance and friendship who generously allowed me to use his computer programs and references. Dr. Amin-Sobhani and Mr. Musavi for their field support and assistant in Iran. The author wishes to thank Professor John Briggs the Head of Department for his financial support to presentation my papers in some conferences during my research.

Sincere thanks are also due to the following individuals and organization:
Dr. Alastair Morison for a conversation about this research in the early stage. Professor G. Petrie for 1:25000 topography map of the Lar Basin (1945). Professor I. Thompson for his encouragement. Dr. J. Drummond for her guidance in photogrammetrical analysis. Mr. D. Tait for Dragon image processor. Mr. P. Chung and S. McGinley for their technical support. Mrs. A. Dunlop for helping me to plot from aerial photographs. Department secretarial staff, Mrs. Seena Glassford, Mrs. Helen Boyd, Mis. Eilidh Douglas and Mr. Gorge Fraser for their supports. Mr. I. Gerrard for photography of the images and maps. Mr. M. Shand for his Photoshop and other computer programs. Mr. Mirtabar and staff of the Lar Dam office who provided some useful information and facility for my field work in Iran. Mr. M.J. Valadan and my room mates Mrs. L. Pierce, Mrs. A. Ventura, Mr. D. McDougall, Miss V. Harvey and Mr. D. Shepherd for their encoragement and advice. Mr. Shefaat, director of Iranian National Cartographic Centre, who generously provided some useful documents for my research. Iranian; Geographical Organization, Energy Ministry, Agricultural Ministry, Forestry and Range Organization, Geological Survey for their useful information. Finally, I would like to thank my wife S. Lotfi for her endless support and encouragement.

DEDICATION

I feel pride and pleasure in dedicating this thesis

to leaders of freedom and independence,

Martyrs of 8 years holy defence.

CHAPTER 1: INTRODUCTION

1.1 THE LAR BASIN

The Lar Basin in northern Iran lies in the Central Alborz range and is dominated by Damavand volcano. The Caspian Sea is some 100 kilometres to the north and Tehran is some 50 kilometres to south-west of the study area (Figure 1.1). This basin is the highest watershed in Iran and reaches 2400 metres in the valley and 5671 metres at Damavand summit. The area of the basin is 780 km^2 and the average discharge of the Lar is about 14 m^3/s. The total average annual discharge of the river is about 432 million m^3.

Because of the mountainous terrain and harsh climatic conditions, Iran possesses only limited regions suitable for agriculture. Of the total area of Iran (1648195 km^2) about 20.7% is desert, 54.9% natural sparse grassland, 7.6% forest land, and only the remaining 14.4% is potentially arable land, of which 11.6 million hectares go annually under cultivation and the rest lie fallow. This short description indicates the importance of the Lar Basin for future planning since it has good quality water and also a unique situation between Tehran (needing for its increased population drinking water and electricity) and the Caspian plain (for irrigation).

The Lar dam was built in 1974 to produce hydroelectricity and drinking water for Tehran ($179\times10^6 m^3$) and supply water for Mazandaran province ($249\times10^6 m^3$), but it has not lived up to expectations owing to morphological changes in the dam area. The loss of predicted water from the reservoir affects the life of millions of people due to the reduction of water allocated for farmers in the north (about 3 million people) and the urban dwellers of Tehran (over 10 million people). Future plans in this area need to be reassessed and is one of the reasons for the establishment of this research project. On the other hand conservation of the Lar Basin's natural resources e.g. pastures, water, soil, mines and wild life, needs to be accounted for in the face of future development plans.

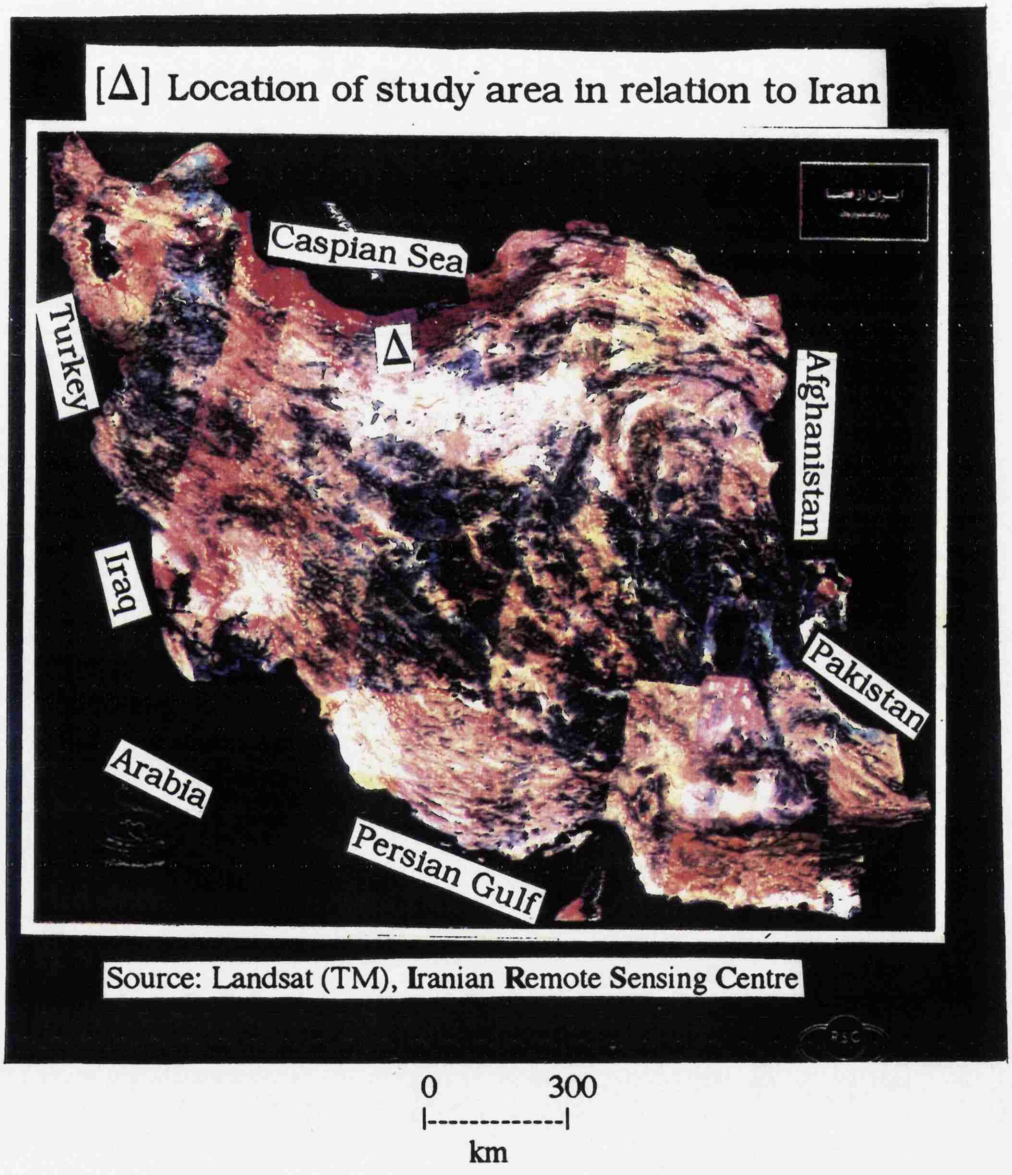

Figure 1.1: Location of the study area.

The limestones in the Lar basin form a series of prominent eastern-western trending ridges that rise to heights of over 3000 metres above sea level and which have imparted a strong east-west trend to the river basin. This is disrupted by a blockage to the valley in east where it joins the Haraz valley. This blockage, caused by the Damavand lavas, created Lake Lar which extended over 25 kilometres upstream of the lava dam. Some hundreds metres of sediment were then deposited in the lake whilst continued eruptions from Damavand gradually raised the elevation of the lava dam (Figure 1.2). The process culminated in the outpouring of large quantities of predominantly intermediate lavas which make up much of Damavand volcano today. Actually this process is the starting point of morphological changes, in the Lar basin which are assessed in this study. Major recent surface and subsurface changes like sinkholes and landslides in the Lake area, influence the former Lake deposits. Similarly, sedimentation estimates show that about 170×10^3 tonnes of soil are annually delivered from upstream, a serious problem for infilling of the reservoir (about 960×10^6 m^3 capacity).

The Lar area has a rather barren appearance for the most part. The limestone formation and Damavand volcano both have only a thin soil cover which supports only a sparse vegetation and about 90% of the basin is covered by these natural pastures. Nevertheless, this proves to be adequate to support the grazing of nomads each summer time. The presence of animals in the valley has led to an almost complete absence of trees. The animals prevent the young trees from becoming established by eating the saplings but where animals are prevented from grazing, as at southern Lake Lar, several trees flourish. The gravel terraces are again dry and barren in appearance for much of the year, although many small plants thrive during the spring when the ground is moist from the snow melt. On the flood plain of the River Lar and near spring discharges, especially in southern side of the Lake the green appearance persists throughout the year. The grass which grows here provides feed for herds of animals brought into the valley each summer time. This grazing has resulted in vegetation cover density decreasing year by year and this seems to have caused enhanced sediment erosion downstream.

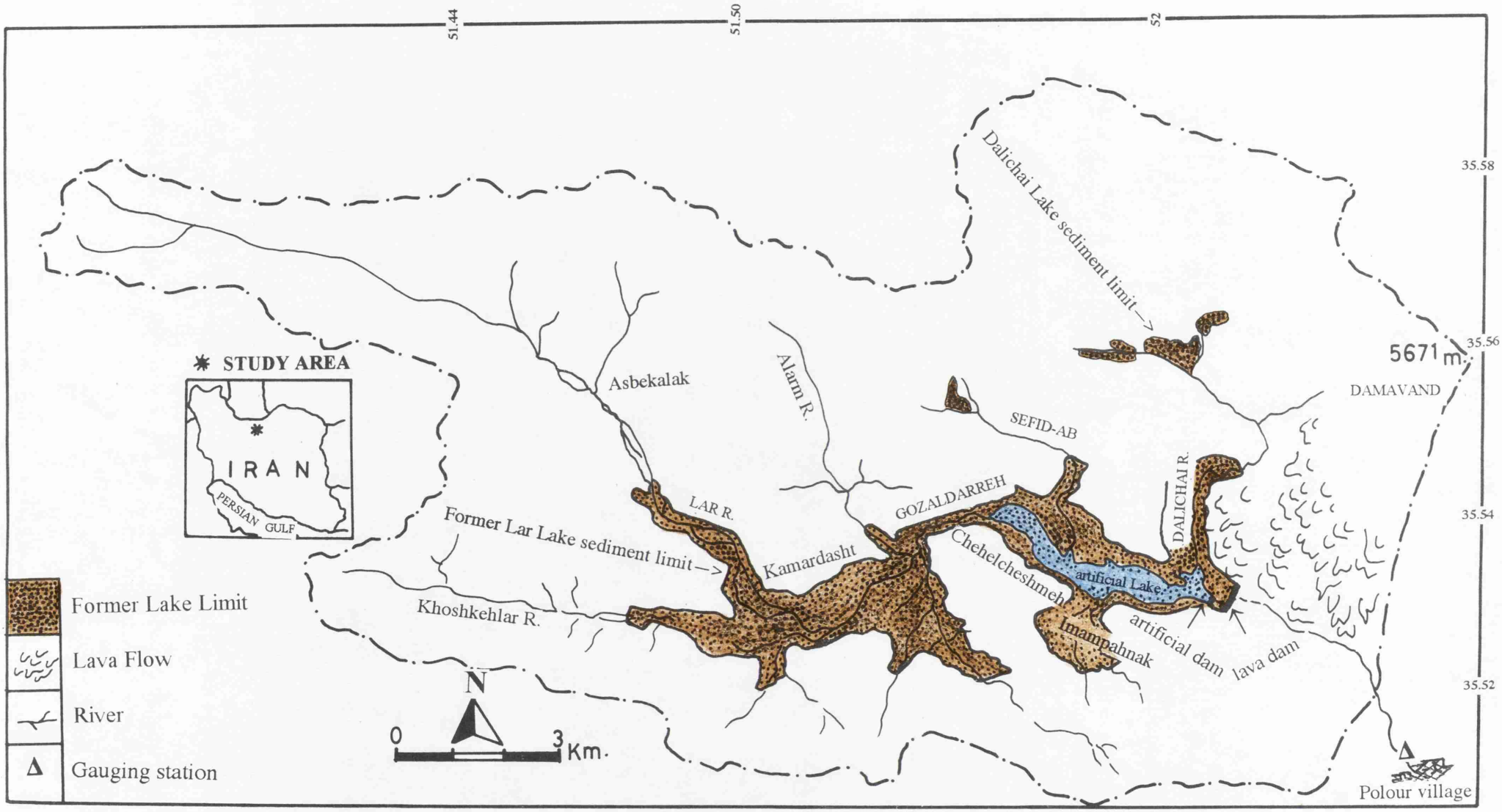

Figure 1.2: Location of the Lar basin, limit of former lake, lava and artificial dam.

1.2 AIMS OF RESEARCH

The aim of this research is to investigate the geomorphological changes in morphology and sediment supply in the Lar Basin. The sediment supply to the river is controlled by the changing nature of the catchment surface sediment and vegetation. In addition to field mapping of geomorphology, remote sensing techniques are used to identify and assess the observed changes at selected sites in the Lar Basin.

In order to achieve these aims the work was divided into two stages, each of which stands alone on specific aspects of the physical environment, but which link together at a later stage in order to achieve the overall aim of the research. The first of these is to assess the extent of morphological changes in the basin and to produce an estimate of sediment delivery into the Lake. The second is to identify the amount of sediment delivery to gauging stations within the basin to allow comparisons through time. Figure 1.2 shows the linkage between geomorphological changes, physical characteristics and the techniques in this research which are eventually integrated within the discussion.

One of the objectives of this research is to examine the potential of remote sensing data to identify land surface and morphological changes in the Lar Basin. As the Lar basin surface types are very complex, a variety of soil/ground variables in combination are required to explain the spectral response of surface cover types. The relative importance of any one or more of these factors may vary within or among the land cover types. Thus, a considerable effort is made to evaluate the spatial and spectral characteristics of different sensors considered in the study.

The most common conventional way of assessing erosion potential is based on field work which is time consuming and costly. Although using remotely sensed images to evaluate a large area is more objective and efficient than comparing data from many individual efforts, remotely sensed data and computer analysis cannot fully replace conventional detailed ground surveys. However, these can help scientists and policy makers to determine the scope of a problem and focus activities to where they will be

most effective (Pelletier, 1985). Among remotely sensed data it has been shown that aerial photography is a very good tool for recognition of all kinds of erosion features and sediment estimation. As mentioned above some parts of the Lar basin are inaccessible to field checking, so it seems that the best tool is remote sensing data. Thus the KFA-1000, sequential aerial photographs, SPOT and Landsat TM imagery will be analysed in order to identify areas of fluvial sediment, vegetation cover, morphological changes and to classify and map the major surface types of the Lar basin. The mapping information thus obtained is then used as an input into a geomorphological and other maps at the study area.

Thus, the major objectives of the research are:

(I) to investigate depositional history and its effects on recent morphological changes in the Lar basin;

(II) to produce morphological, vegetation, lithology and morphotectonic maps of the study area in order to identify changes;

(III) to estimate sedimentation in a former Lake and present sediment delivery in the Lar basin;

(IV) to evaluate the usefulness of remote sensing data in identifying areas that contribute to sediment delivery to the Lar basin.

1.3 THESIS STRUCTURE

The study first reviews similar work and investigation methods elsewhere in relation to land surface cover interpretation, and explains the rationale of selection of the study area followed by background information. Therefore, the aim of **Chapter 2** is to review similar works in traditional and remote sensing techniques with emphasis on river basins in semiarid or mountainous areas elsewhere. This chapter also assesses the

methods used and their advantages and disadvantages. Remote sensing data including aerial photographs are reviewed for different kinds of applications for land use, soil characteristics and erosion, vegetation, landcover changes, fluvial, and lacustrine applications linked to chapters 4 to 7. In **Chapter 3**, the investigation techniques are described in two main stages: remote sensing interpretation, and field work. In this chapter different techniques and data gathering procedures are explained aimed at identifying land surface changes and sediment estimation in the Lar basin.

In **Chapter 4** attention is directed at the physical environment of the basin (climate, physiography, geology and vegetation) in order to provide a preliminary insight into the characteristics of the major surface types considered. The characteristics of different surfaces help to show how morphological changes might affect the Lar basin.

Following morphological changes in the study area in the past, more recent changes are discussed in **Chapter 5**. This chapter also reports sediment characteristics and classification of deposits in the study area derived from field, remote sensing data and laboratory analysis.

Chapter 6 reports the results of classification of the land cover using a digital image processing system to aid the development of prototype maps.

The results of this research are discussed and interpreted in **Chapter 7.** The degree of success of the landcover analysis is assessed and related to those methods most useful in identification of erodable areas. The sources and patterns of erosion are discussed in relation to landcover and then linked to the deposition areas in the Lar basin. Finally sediment concentration and volumetric data are compared as different methods for estimation of sedimentation in the Lar basin. **Chapter 8** comprises the conclusion and summary remarks drawn from the whole thesis (Figure 1.3).

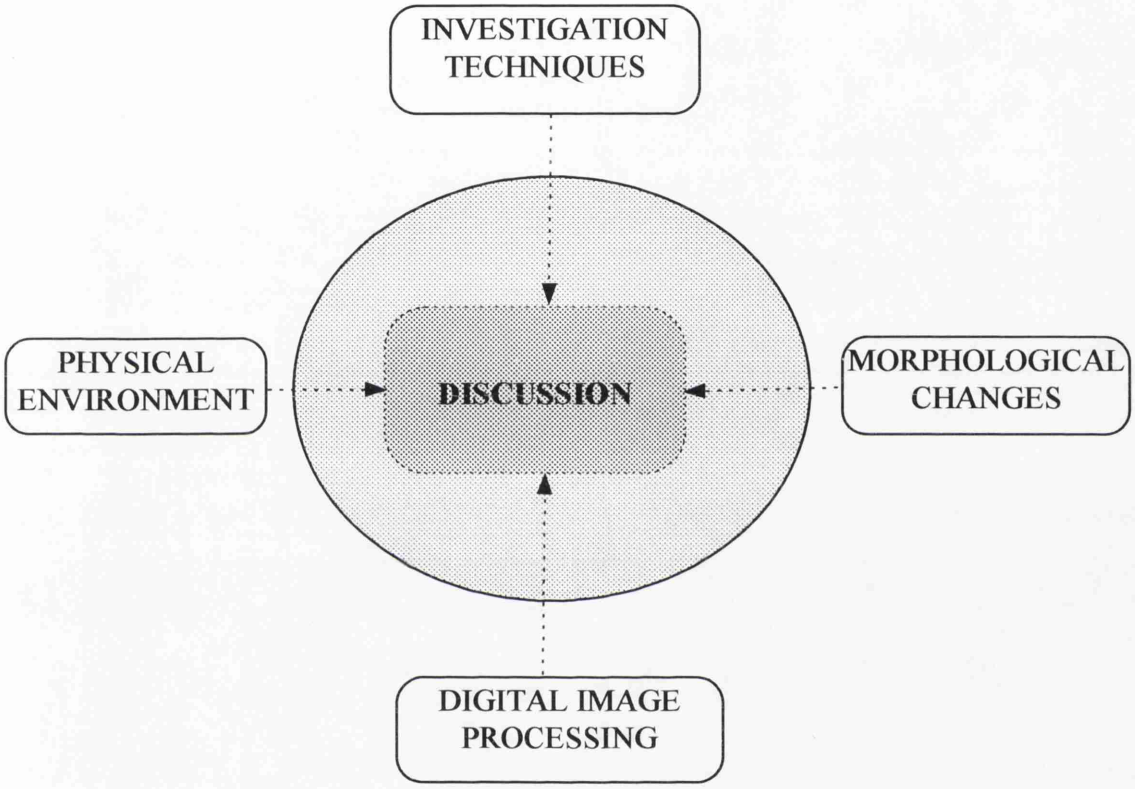

Figure 1.3: Diagram showing the general stages of this thesis.

CHAPTER 2: LITERATURE REVIEW

INTRODUCTION

The aims of this chapter are: to review the rates and mechanisms of soil erosion and sediment delivery in mountainous semi-arid areas, using both remote sensing and field data; and, to identify the possible linkages between these two aspects of research. The few studies which have been carried out on the geology and geomorphology of the Central Alborz Range are also to be reviewed. Sediment yields are acknowledged to reach peak values in mountainous semiarid environments (Clotet and Gallart, 1986; Bogen, 1995), largely because of poor ground protection offered by sparse vegetation and the activity of soil fauna, which serve to reduce infiltration rates and encourage overland flow (Langbein and Schumm, 1958; Scoging et al. 1992).

The chapter examines the literature and background of research involving: (1) erosion rate estimation; (2) assessment of land surface morphological changes and sediment delivery by remote sensing; and, (3) previous work related to this field area.

2.1 GLOBAL SEDIMENT BUDGET

Walling (1984) has estimated that 14×10^9 tonnes of suspended sediment and 1×10^9 tonnes of sediment transported as bed load are discharged into the oceans annually by rivers. These two components of sediment transport are responsible for an average rate of denudation of the land surface of approximately 57.5 mm per one thousand years. This rate of denudation is distributed unequally over the land surfaces of the Earth, and considerable variation is observed (Figures 2.1and 2.2). Woodward (1995) studied pattern of erosion in Mediterranian river basins and demonstrated that soil erosion and sediment yield in this area are encouraged by the high erosivity of precipitation, an active tectonic setting, steep topography, fissile sedimentary geology and easily erodible soil mantles. Its natural vulnerability to erosion has been morphogenic zone than in any other (Dedkov and Mozaherin, 1992). In consequence, some rivers in this region have suspended sediment yields of >4000t km^{-2} yr^{-1}. Sediment yield of almost an order of magnitude greater (39700t km^{-2} yr^{-1}) are

Figure 2.1: A map of global sediment yields based on values-of specific suspended sediment yields for drainage basins with areas of 1000–10 000 km^2 (after Walling and Webb, 1983)

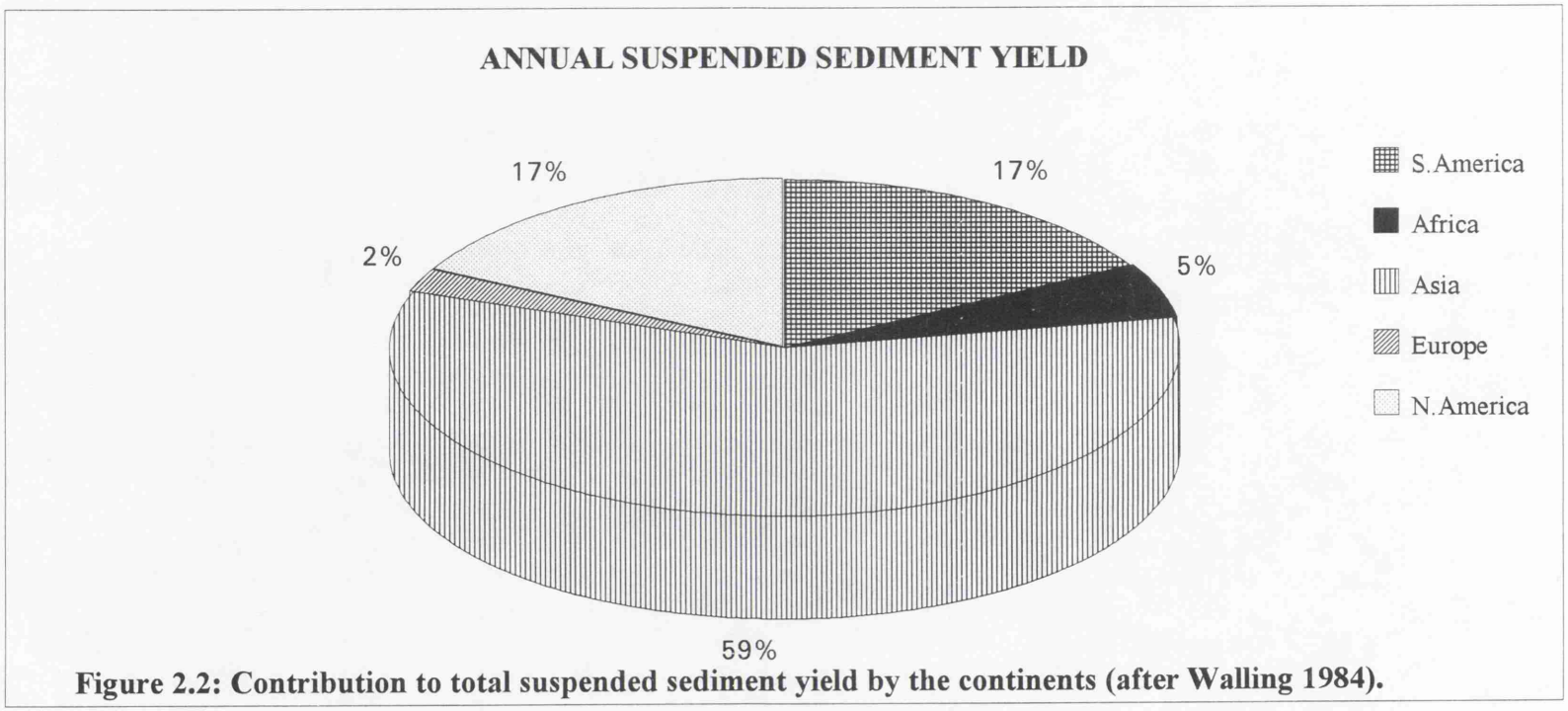

Figure 2.2: Contribution to total suspended sediment yield by the continents (after Walling 1984).

reported by White (1995) for a small basin in the Magat catchment of the Philipines. In this case, the very high transport rates can be attributed to the effects of rainfall on soils exposed through the disturbance of natural vegetation. The annual suspended sediment in four Alpine glacier basins located in the Val d, Herens, Switzerland, may reach 3000t km^{-2} yr^{-1} (Gurnell, 1995), although loads as low as 280t km^{-2} yr^{-1} were also recorded in this area. Walling (1995) collected and interpreted global databases of sediment and solute concentration and yield, which currently reveal, for example, that suspended yields range globally from a minimum of 0.9 to maximum of >53500t km^{-2} yr^{-1} (Figure 2.1). Seen in a world context, sediment concentration and yields of the Lar basin, which are about 200t km^{-2} $yr,^{-1}$ are very low.

2.2 EROSION ESTIMATION MODELS AND SEDIMENT YIELD

2.2.1 Predicting Soil Erosion Rates

Soil erosion studies can be traced back to the late nineteenth Century (Hudson, 1978). A basic understanding of the factors affecting erosion was developed early in the 20th Century starting from the experimental work initiated by the US Forest Service in 1915 (Ayres 1936). The importance of raindrop impact was first appreciated by Low (1967) and later by Ellison (1944). Scientists began to develop empirical equations as data were accumulated. For example, Zingg (1940) proposed an emprical equation for soil loss, and the relationship of rainfall characteristics to the amount of soil eroded was proposed by Musgrave (1947) to estimate gross erosion from watersheds. This is;

$$E = (0.00527)\, I R S^{1.35} L^{0.35} P_{30}^{1.75} \qquad [2/1]$$

E = the soil loss (mm/y), I = the inherent erodibility of a soil at 10% slope and 22 m slope length (mm/y), R = a vegetal cover factor, S = slope angle, (%), L = length of slope, (m), P_{30} = the maximum 30 minute rainfall (mm).

LIoyd and Eley (1952) provided a graphical solution of the Musgrave equation for use in the North Eastern United States. Smith (1941) and Browing et al (1947)

developed factor relationships which later provided a basis for the development of the Universal Soil Loss Equation (USLE).

$$A=RKLSCP \qquad [2/2]$$

A= average annual soil loss per unit area (tons/acre), R= a rainfall erosivity factor, K= the erodibility of the soil, L= slope length factor, S= slope gradient factor, C= cropping management factor, and P= erosion control practice factor (see Wischmeier and Smith 1965, for extended information on the equation).

Van Poren and Batelli (1965) evaluated the applicability of these factors as they affected soil loss in Illinois. In 1954, a re-evaluation of the various factors affecting soil loss was undertaken (Smith and Wischmeier 1957, Wischmeier and Smith 1958, Wischmeier et al 1958) which resulted in the development of the USLE by Wischmeier and Smith (1965). This equation was later refined as more data was received from runoff plots, rainfall simulation, and field experience (Wischmeier and Smith 1978).

The USLE model has also been applied outside the USA. For example, Hudson (1961) proposed an erosion equation for subtropical Africa as follows;

$$E = TSLPMR \qquad [2/3]$$

E= erosion rate (tonnes/acre/year) and the remaining factors are functions of soil type, slope gradient and length, agronomic or agricultural practice, mechanical protection, and rainfall, respectively. Another soil loss equation for South Africa was developed by Elwell (1977);

$$Z = K X C \qquad [2/4]$$

where Z = predicted mean annual soil loss (tonnes/acre/year), K = mean annual soil loss, from a standard field plot 30m×10m at a 4.5% slope for a bare soil of known erodibility, C = the ratio of soil lost from a cropped plot to that lost from the standard plot, and X = the ratio of soil lost from a plot of length L and slope S to that lost from the standard plot.

Field observation at various times of the year suggested that surface water is the principal agent of erosion on the Lar basin. After an extensive literature search for previous work on the use of erosion models in mountainous areas in Iran or indeed from a similar environment elsewhere, only one report, that of Banket et al. (1979) from Moel Faman in Clywd, was found but this is for a humid environment. In this, an essentially field based report, they compared the effectiveness of three predictive models; USLE, Fournier and Kirkby and found that the USLE model gave the best estimate for soil loss. But there is some difficulty to be encountered in assessing its various parameters.

All of the mentioned models have been derived for the prediction of soil loss from agricultural land. Therefore, without valid modification their application to the non-agricultural land such as the Lar Dam Basin would be questionable.

In the many parts of the world, areas with annual precipitation close to the 400-500 mm of the study area, have semiarid vegetation communities. Langbein and Schumm (1958,1965) argued that low sediment yield occurred in the lowest precipitation ranges because there was not enough water and energy to deliver sediments. In the higher precipitation ranges, they suggested that grasslands and forest provided enough cover to retard the erosion process. Their oft-repeated diagram showing the peak sediment yield in the 400-500 mm effective precipitation zone was plotted from sample stations in subdivisions (Figure 2.3). Walling and Webb (1983) have a major criticisms of the Langbein-Schumm curve which shows a decline in sediment yield with an increase in precipitation. Walling and Webb indicate that the group-averaging method causes the plot to be an abstraction of the data that is subject to alteration given small amounts of new data. Although the relationship between sediment yield and mean annual runoff developed by Judson and Ritter (1964) and Dandy and Bolton (1976) reveals curves somewhat similar to the Langbein-Schumm model in the lower precipitation ranges (Figure 2.3), additional data from a variety of climates and conditions do not substantiate the original formulation.

Studies of the sediment yield and precipitation relationship provide three lessons for researchers dealing with semiarid catchments; (i) data from one region, even one large region, are not likely to provide valid generalizations for global use; (ii) the construction of theory from grouped data appears to be risky. The conclusions drawn

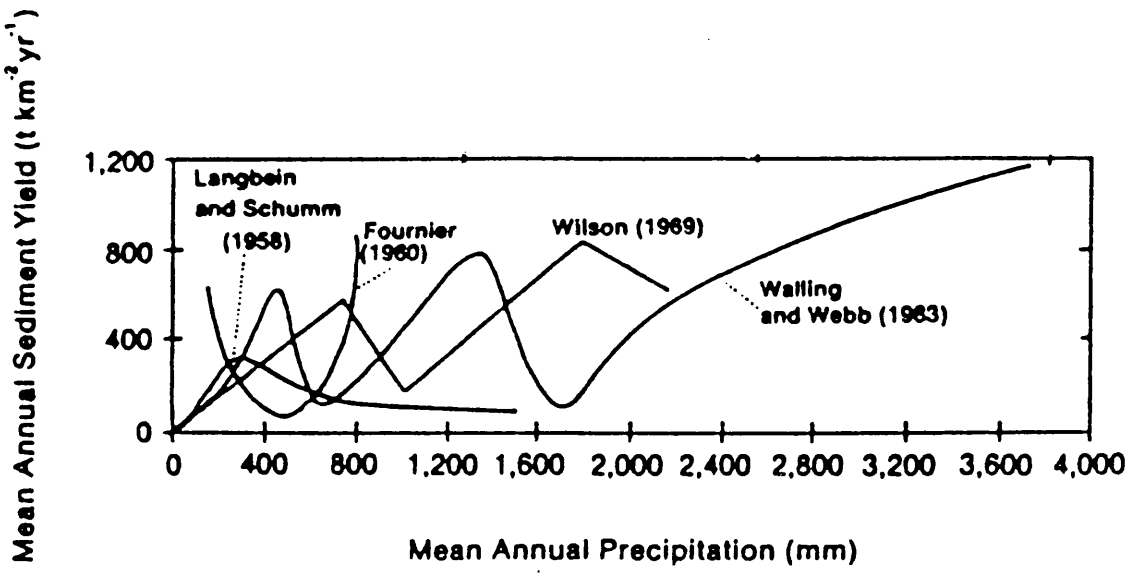

Figure 2.3: The relationships between precipitation and sediment yield plotted with points from grouped data means. Raw data show no relationship (*after Walling and Webb 1983*).

from grouped data strongly reflect the grouping process which obscures the natural variability in the data; (iii) successful theory must grow from the complexity of the data and account for this complexity.

Estimation of catchment sediment yield requires integration of erosion export processes. To predict sediment yield for areas where no sediment data are available, various general models have been suggested. Most take the form of linear regression equations relating sediment yield with one or more climatic and topographic variables. Linear regression models were employed by Fournier (1960), Corbel (1964) and Painter (1974) for the major climatic zones of the world and a similar model was suggested by Flaxman (1972) for the western United States. Williams and Berndt (1972) extended the USLE, to give an estimate of the delivery ratio, for small catchments in part of Texas.

Negev (1967) attempted to simulate erosion-deposition processes by distinguishing between the two main sources of sediment, the land surface and the channel system. On the land surface the most important parameters are the rainfall intensity and the overland flow rate and amount. The approach suggested by Painter et al. (1974) was related to determining the influence of afforestation on erosion and sediment transport from a grassland area.

Langbein and Schumm (1958) proposed a tenuous relation between effective precipitation and sediment yield. Schumm (1956) expanded the relationship and developed supporting theory, and finally a host of subsequent researchers provided wider ranging data, criticisms, and further refinements of explanation. In addition to vegetation and precipitation, soil characteristics directly influence erosion and the contribution of sediment to channels. Generally, soils with low clay contents tend to be most erodible. In a review of erodible soils from England, Canada (Ripley et al. 1961), India (Mehta et al. 1963), and the United States (Magahan 1975), Evans (1980) found that soils with more than 30-35% clay are unlikely to be classified as highly erodible (Figure 2.4). The stability of soil in semiarid areas is dramatically affected by monovalent anions such as sodium, a relatively weak binding agent that is associated with rapid erosion and piping.

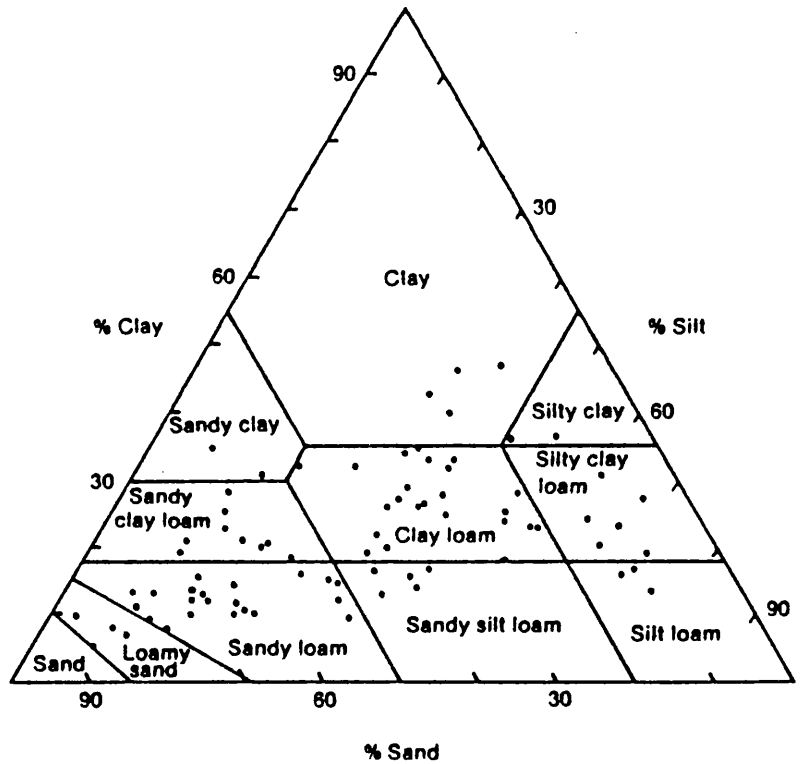

Figure 2.4: Particle size characteristics for soils deemed highly erodible showing the importance of clay content (after Evans 1980).

Finally, slope characteristics also control erosion. Slope angle controls the process of splash erosion (Ellison 1944). Erosion increases with increasing slope angles, especially at angles of less than 10 degrees. Erosion also increases as slope length increases, especially in field-size areas because more runoff is available from upslope areas (Wischmeier et al. 1958).

2.2.2 The Sediment Delivery Ratio

The sediment delivery ratio is the ratio between the amount of material exported from a drainage basin to that eroded from slopes with the basin. If the ratio is equal to 1.0, the amount of material lost from slopes equals the amount leaving the basin as fluvial sediment yield. Sediment delivery ratios, like specific sediment yield values, generally decline with increasing basin area. Because the ratio is dimensionless and does not account for absolute magnitudes, there is increased likelihood that similar ratio/area relationships will exist for different sized areas (Figure 2.5). There are many curves, the most widely based is that by Roehl (1961). The curve by Renfro (1975) is from data from Texas, while the ones by Piest et al. (1975) and Beer et al. (1966) are from a humid-semiarid transition area. The shape of the curves probably reflect the geomorphologic characteristics of the slopes and channels of the basins which determine the nature and distribution of storage sites. There are probably limiting curves determined by the combined possible basin and network geometries. As yet these curves are undefined, and research from dryland areas is noticeably lacking. As a general statement, the available data suggest that;

$$R_S = C\, A_d^{-0.2} \qquad [2/5]$$

where R_S = sediment delivery ratio, A_d=drainage area (km^2), and C=an empirical constant.

The range of calculated sediment delivery ratios indicates varying amounts of internal storage within drainage basins. The maintenance of this arrangement on a geologic time scale would not be possible because sediment in storage would indefinitely increase. Those materials stored along channels as valley alluvium eventually leave

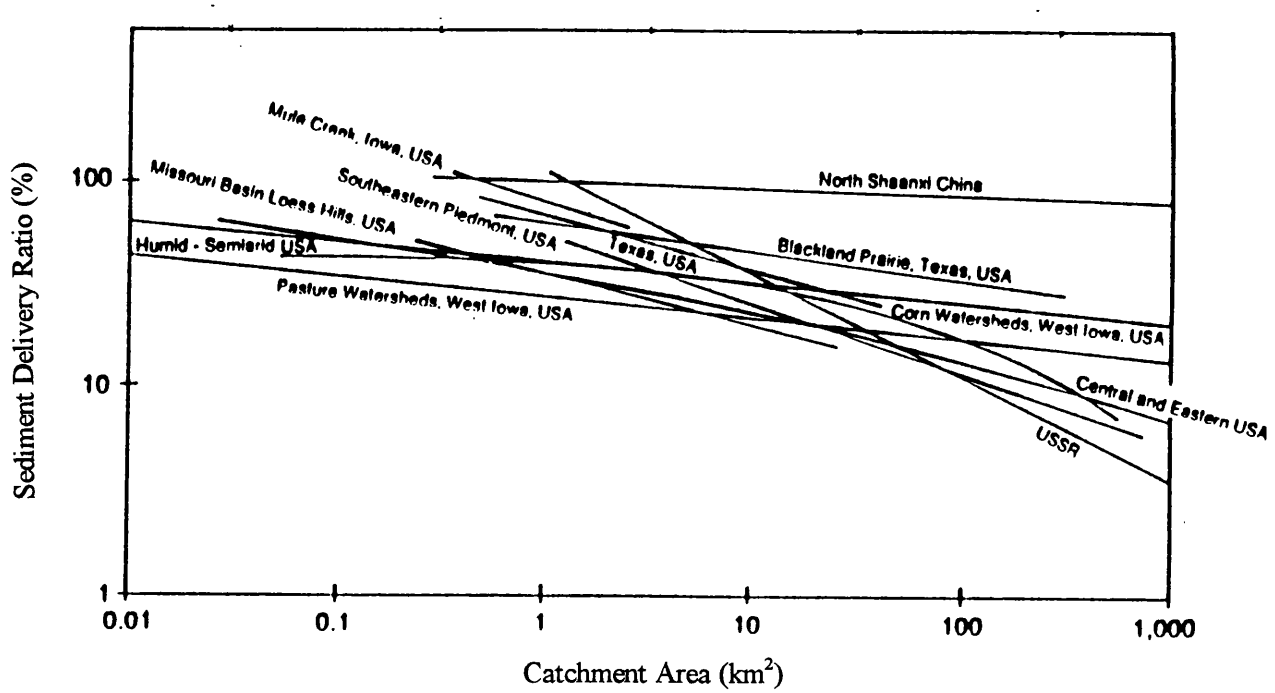

Figure 2.5: Relation between sediment delivery ratios expressed as % and total drainage basin area *(after Branson et al. 1981).*

the basin during intensive erosion episodes as well known in semiarid area settings. Schumm and Hadley (1957) established the process for small channels, and Graf (1983) demonstrated that the cumulative effects of accelerated erosion episodes in the upper Colorado river basin over 40 years produced sediment delivery ratios as high as 1.5 for some semiarid area streams.

The most common methods of estimating sediment yield include analysis of sediment discharge data, evaluation of volumes of sediment deposited in reservoirs in or close to the basin under study, and the use of generalized sediment yield equations (Rooseboom 1975).Attempts to estimate sediment discharge in rivers by using sediment transport equations are usually less successful as availability of sediment often limits the actual transport amounts (Rooseboom, 1975).

The discrepancy between surface erosion and yield can be interpreted in two ways. Firstly it may based purely on the definitions. If all points in a catchment are sampled, and deposition is treated as negative erosion, average erosion and yield must of course balance. Thus delivery ratios less than 1.0 reflect the normal definition of gross erosion as the total mobilization of material from the eroding sites within a basin. Secondly if p is the proportion of a catchment eroding at rate e (measured as a depth of erosion, ma^{-1}), and the proportion experiencing deposition at rate d is q (=1-p), then for any time period;

$$s = pe-qd \qquad [2/6]$$

where s=annual sediment delivery and the percentage delivery ratio is ;

$$Rs = S/E = s/pe = [1-(qd/pe)] \qquad [2/7]$$

The second equation shows that delivery ratios can easily be much less than 100% if q is large (>0.9) and/ or the ratio of deposition to erosion rates is high (>5). A local deposition rate in only 10% of a catchment which is 8.5 times the average erosion rate occurring elsewhere will result in a delivery ratio of 5.5% (Richards, 1993).

Accurate sediment discharge data is one of the main inputs required for sediment yield estimation. Apart from statistical requirements such as adequate sample size, homogeneity and stationarity of data, the actual method used to sample also demands consideration. The latter is very important in sediment transport as it is not always economical and feasible to do detailed sampling in order to obtain measurements which are representative of the total sediment discharge of a river at a particular section. Sediment transport phenomena and sampling methods will therefore be reviewed briefly in chapter 3 before proceeding to discuss statistical requirements and methods of analysis.

Total sediment transport in a stream can be divided into bed load and suspended load. Bed load is the sediment that moves by saltation, rolling and sliding in the bed layer of a channel, whereas suspended load is the sediment that is supported by upward components of turbulent currents and which stays in suspension for an appreciable length of time. Measurement of the bed load component of sediment transport, which is generally considered to be small (in the order of approximately 5 percent) (Walling, 1984, Rooseboom, 1975), is a difficult operation and depends on the nature of the sediment. No single apparatus or procedure, has been universally accepted as completely adequate for determination of bed load discharge (Gregory and Walling 1976). Suspended sediment on the other hand is easier to measure and a wide range of instruments including instantaneous, point-integrating, single stage and pumping samplers, as well as continuous monitoring apparatus (Gregory and Walling, 1973), have been developed for this purpose.

2.3 SUMMARY AND DEFINITION

Not all of the models described above are appropriate for estimation of the sediment yield of the Lar basin, because this area includes some factors which are absent from many models, e.g. stream bank erosion and gully erosion. The nature of the material transport in the rivers and soil particle size data are gaps in existing knowledge for this site.

The construction of volumetric estimates of depositional areas from topographic maps for the Lar basin has not been previously attempted and forms a significant extension to the results of this work (Chapter 5). It is clear from the literature that

very little work has been attempted in the field of estimation of delivered sediment in semi-arid river basins. Therefore the only model which was selected for sediment estimation in the Lar basin is that used for Lake Mead reservoir in USA (Smith et al. 1966). The application of this model is justified because of its inclusion of factors relevant for the Lar basin.

Thus in the light of the models described above, the aims of this part of the thesis are to: i) establish a depth of accumulated valley fill which was measured by seismic exploration and suggests that the channels were occupied by a large lake prior to valleys filling, and also to estimate sediment yield from sediment concentration data, and terrace and river deposition area volumes; ii) examine former lake limits and to calculate an estimate of sediment eroded from the Lar basin; iii) attempt to link aims i and ii through a paleosediment budget in order to assess morphological changes in the Lar basin.

2.4 USING REMOTE SENSING DATA FOR LAND SURFACE CHANGES

Remote sensing is the science of obtaining information about an object, area, or phenomenon through the analysis of data acquired by device that is not in contact with the objects under investigation (Lillesand and Kiefer, 1987). In the interpretation of information for the environmental sciences, it usually refers to the use of electromagnetic radiation sensors to record images of the environment (Curran, 1985). The eye can only capture visible radiation which occupies a very small part of the electromagnetic spectrum. To overcome these deficiencies various instruments or systems have been developed (Figure 2.6). Table 2.1 shows the electromagnetic radiation regions used in remote sensing including; near ultra-violet 'UV' (0.3-0.4μm), visible light (0.4-0.7μm), near shortwave and thermal infrared (0.7-14μm) and mirowave (1mm-1m) . Short wave infrared has more recently been used for geomorphological classification and thermal infrared is primarily used for temperature measurement, while microwave is utilized for radar and microwave radiometry (Figure 2.7).

During the 1940s and 1950s large scale, complete coverage of many countries (including Iran) was undertaken using black and white panchromatic aerial

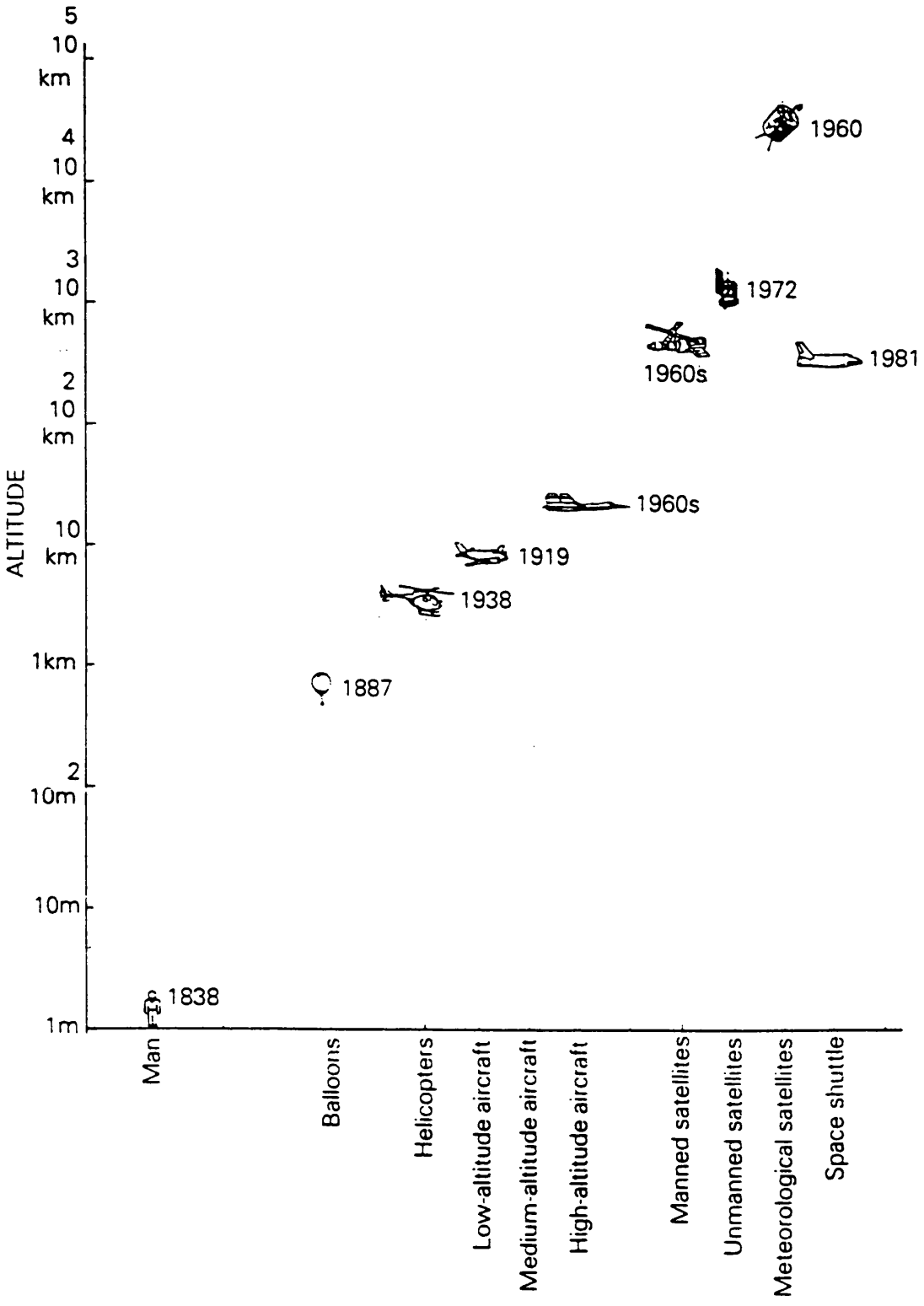

Figure 2.6: Platforms for natural resource investigations (*after Howard, 1988*).

class				wavelength	frequency
ultraviolet				100A ~0.4 μ m	750 ~3,000THz
visible				0.4 ~0.7 μ m	430 ~750THz
infrared	near infrared			0.7 ~1.3 μ m	230 ~430THz
	short wave infrared			1.3 ~3 μ m	100 ~230THz
	intermediate infrared			3 ~8 μ m	38 ~100THz
	thermal infrared			8 ~14 μ m	22 ~38THz
	far infrared			14 μ m ~1mm	0.3 ~22THz
radio wave	submillimeter			0.1 ~1mm	0.3 ~3THz
	micro wave	millimeter	(EHF)	1 ~10mm	30 ~300GHz
		centimeter	(SHF)	1 ~10cm	3 ~30GHz
		decimeter	(UHF)	0.1 ~1m	0.3 ~3GHz
	very short wave		(VHF)	1 ~10m	30 ~300MHz
	short wave		(HF)	10 ~100m	3 ~30MHz
	medium wave		(MF)	0.1 ~1km	0.3 ~3MHz
	long wave		(LF)	1 ~10km	30 ~300kHz
	very long wave		(VLF)	10 ~100km	3 ~30kHz

Table 2.1: Classification of electromagnetic radiations *(source: Japan Association on Remote Sensing 1993).*

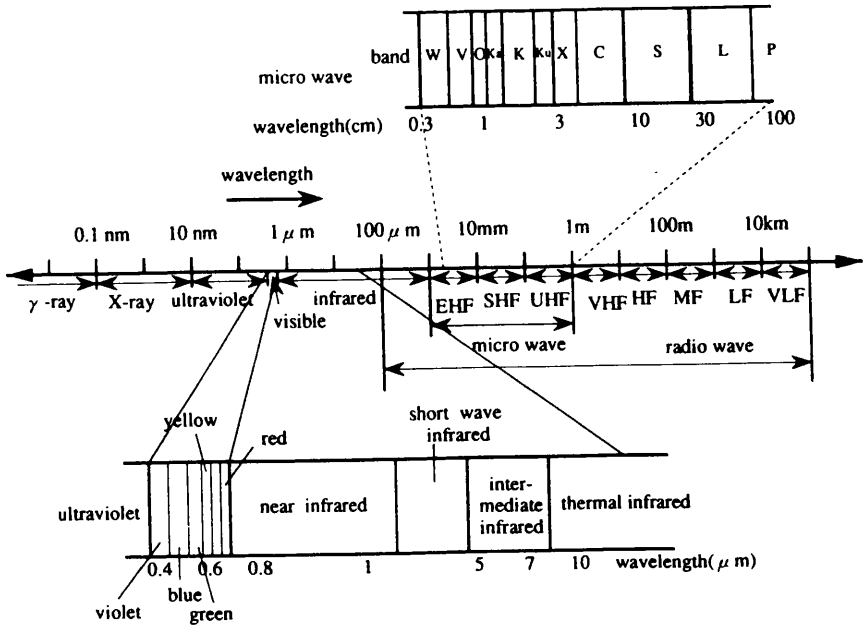

Figure 2.7: The bands used in remote sensing (source: Japan Association on Remote Sensing 1993).

photography. By the 1960s aerial photography had been operative long enough to allow for the study of temporal variations in the environment. The period from the late 1950s has been extremely active for Remote Sensing, with developments in the whole applications field occurring at an increasing rate. With satellite launches occurring regularly, following SPUTNIK-1 in 1957, the interest in Remote Sensing concentrated on the use of this new and unique platform. In 1959 the first earth images were transmitted from EXPLORES-6 and the first meteorological satellite, TIROS-1, was launched in 1960.

Computer technology advances have been vital for all aspects remote sensing and have allowed the huge data streams to be handled efficiently. Remote sensing has also been aided by the influx of new ideas from a variety of related disciplines, by the availability of funding for space related activities and by access to an increasing range of software and hardware. Remote Sensing has a number of positive advantages over other sensing systems. Jackson and Mason (1986) argue that modern remote sensing has now successfully overcome the problems which it had in the 1960s and 1970s of being "technology pushed". As useful applications of Remote Sensing imagery have been developed, especially in the field of environmental awareness, remote sensing is now also being "user pulled". This recent trend has been helped by the growing ability to successfully integrate remotely sensed data into Geographical Information Systems (GIS). If it was not for the functionality offered by GIS, then the future for Remote Sensing might be rather uncertain.

In this research, satellite data at different resolutions is employed. This includes SPOT multispectral, Landsat TM and KFA-1000 satellite photograph (see Appendix Chapter 6 for system technical information). These were usefully applied for mapping of vegetation cover, soil characteristics, erodibility and depositional areas, especially on inaccessible areas of the Lar basin.

2.4.1 A Review of Landsat (TM) and SPOT (MSS) For Environmental Sciences

An unmanned, earth orbiting series of satellites, was initiated by NASA that transmit images to earth receiving stations. They were desined primarily for collection of earth resources data. The current Landsat satellites contain two sensor systems; a 4 channel

multi spectral scanner (MSS) and 7 channel thematic mapper (TM) system. The first Landsat (Earth Resources Technology Satellite 'ERTS') was launched in 1972, Landsat 2 and Landsat 3 were launched in 1975, and 1978.

With the launch of Landsat 4,5 and SPOT satellites in 1982, 1984 and 1986, respectively, a new generation of satellite data have been introduced. Although the geographic area covered by both the Landsat TM and SPOT sensors is virtually identical, SPOT has greatly improved spatial, spectral and radiometric resolutions. These sensor refinements enhance the usefulness of SPOT data relative to MSS and TM (Landsat).

SPOT data, with it's favorable high spatial resolution (20m TM; 10m PA), offered possibilities for the assessment and mapping of vegetation and erosion in the Lar basin. Landsat TM data have also been utilized in the basin, for erosion mapping as well as for classification of land cover. Broad classification, delineation and mapping of some features, such as wet land has been more successful with MSS (Carter 1978, Ernst and Hopper 1979, Caster and Richardson 1981, Bartlett and Klemas 1982), although there was some difficulty with the classification of other aspects. For example, Landsat MSS was less successful in the classification of rangeland region (Beaubien 1979, Harris et al 1978, Bryant et al 1980, Latty and Hoffer 1981, Markham and Townshend 1981) and problems have also been encountered in delineating urban and suburban land cover (Carter and Jackson 1976, Jensen and Toll 1982). These limitations are generally attributed to the poor spatial resolution (79m) of the Landsat MSS (Haak et al 1987).

The critical aspect of the TM data based land surface classification lies in the classification accuracy which in general is a function of the number of boundary pixels and the spatial resolution (30 metres) of the image data (Ioka and Koda, 1986). Extensive effort was made by Williams et al. (1984), Toll (1984, 1985) and Irons et al. (1985) to explain the effects of the Landsat TM improvements on classification accuracy. These studies concluded that TM digital classification can be useful in vegetation and soil identification especially in large areas.

Thus, it appears that the relationship between spatial resolution and classification accuracy are closely integrated. Townshend and Justice (1981) and Markham and Townshend (1981) explained the high spatial resolution effect on classification accuracy. They suggested that increased spatial resolution generally results in an increase in the variance of pixel values. Conversely, increased spatial resolution reduces the number of mixed or boundary pixels, and hence higher accuracy may be achieved (Thomson et al 1975, Pitts and Badlaras 1980, Jackson et al 1983).

2.4.2 Kosmos Satellite Photography (KFA-1000)

Until the end of the 1980s data from the Landsat-TM and SPOT systems were the international leaders in non-military remote sensing applications. The efficiency of both systems (operation and reliability) has not yet been achieved by any other system. The political changes in the former Soviet Union, however, have enabled access to the photographic satellite systems of the Kosmos satellite. Originally designed for military purposes, this system has become a serious competitor for Landsat and SPOT, at least as far as geometric resolution is concerned (Sollner, 1993).

In this project KFA-1000 (Kosmos) images were used for mapping the geomorphology and vegetation of the Lar dam basin. Its camera system acquires colour spectrozonal photography from an average height at 270 kilometers, with an average scale of 1:270 000 (Longoria et al. 1993). The frame size is 30×30 cm which covers an area of 6400 km^2 with 60% longitudinal overlap of photographs. The ground resolution is stated to be 5 meters (Figure 2.8). It's spectral ranges are 570-680nm and 680-810nm. The camera number, focal length and exposure number appear in each frame.

2.5 APPLICATION OF AERIAL PHOTOGRAPHS AND SATELLITE DATA FOR LAND SURFACE CHANGES AND SEDIMENT DELIVERY

Aerial photographs have been used to map sediment delivery processes and to locate changes in the land surface in relation to soil properties. In ideal circumstances, photographs record differences in reflectance from vegetation or the soil surface

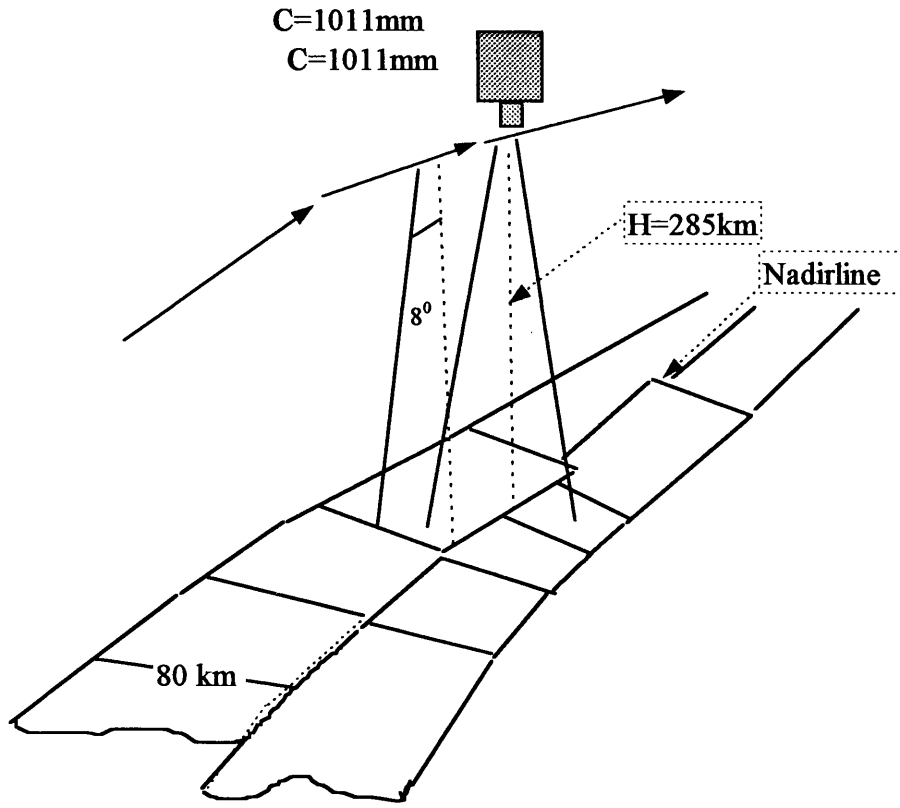

Figure 2.8: Geometric imaging arrangement of the KFA-1000
(after Almer and Buchroithner, 1990).

which can be correlated directly with the boundaries of geomorphological and pedological units. Aerial photographs are considered to be a data collecting and analytical tool (Lo 1976), which provide a basis for mapping soil erosion and evaluating soil erosion potential. Most erosion features are visible in stereoscopic images, and those which are not can be inferred from tonal variation (Bergsma 1974).

2.5.1 Soil Characteristics

Kristof et al. (1980) have shown that variations in soil reflectance can be affected by the relative proportion of clay, silt and sand in the soil. Spectral data showed a distinct decrease in reflectance with increasing clay content. On the other hand, there were significant increases in reflected energy when the amount of silt and sand increased. Seubert et al. (1979) revealed that despite of differences in soil parent material or in geographic locations, certain soil properties relevant to soil erosion may give similar spectral responses. Cihlar et al. (1987) considered three aspects of remotely sensed data for soil erosion assessment in southern Ontario: optimum spectral bands, optimum spatial resolution, and the feasibility of organic matter estimation. It was found the best three bands were centered at wavelengths 0.487nm, 0.650nm, and either 0.664nm or 0.843nm. A statistical approach to selecting the optimal bands is preferable, particularly since it permits optimization for a particular group of soils. Organic matter concentration, could be estimated using a band centred at 0.573nm with an average absolute residual error of 1.4% over the entire range of 1.1% to 50%. This relationship was not highly wavelength-sensitive, although some bands were better than others. Pixel sizes between 6.25 m. and 12.5 m. appear adequate to provide within-field information on the soil.

Soil scientists have used remote sensing data to map different soil classes (Cipra 1973, Eara et al. 1984, Kirschner et al. 1978, Weismiler 1978), and for the identification of soil types and soil properties (Al-Abbas et al 1972, Kristof and Zachary 1974, Kristof et al. 1974, Mathews et al 1973, Zachary et al. 1972).

Abdel-Hady et al. (1989) utilized MSS for soil survey, in the SW Sinai, Egypt. The first step consisted of a visual analysis of context and colour on Landsat images. Data processing consisted of several parts: (a) selection of the optimal channels for a

multispectral classification of Landsat digital data; (b) determination of the thresholds, by different methods, (frequency histograms, radiometric transits and radiometric characterization of the zones of 10×10 pixels); (c) multispectral classification of digital data represented by a computer-assisted multicoloured thematic map; and, (d) drawing of a remotely sensed map of the soil surface. The computer map provided a basis for mapping the soil surface conditions of the study area. Soil profiles and their surface conditions were described in the field with particular attention to the presence or absence of crusted surfaces, sandy surfaces and surfaces covered with coarse particles. The diagnostic values of FAO (1975) were used to determine the different textural types. These analyses allowed the grouping of the soil surface condition classes into phases (Abdel-Hady, 1987). This study concluded that the visual interpretation of remotely sensed images enables us to identify the principal geomorphologic units and is also a good means of locating the subimages. Processing remote sensing digital data facilitates soil surveying, supplying: remotely sensed maps for soil sampling that are efficient guides for pedological prospection; computer assisted maps as bases for the mapping of soil surface conditions of the arid regions; and, radiometric characterizations of selected areas, important for the study of relationships between remote sensing digital data and soil surface conditions.

2.5.2 Soil Erosion

Certain limitations are inherent in the use of aerial photography for erosion mapping. The effects of erosion may have been masked by vegetation cover at the time of over flight. Recent aerial photographs at a suitable scale are not always available for the area in which erosion is to be assessed. Correlating the grey tones of black and white photography with the soil properties is sometimes difficult. Variation in film exposure and development can also cause interpretative problems. To overcome the vegetation masking an eroded area, colour infrared photographs have been used with reasonable success (Totterdal and Mehauer 1973, Tueller and Boott 1975, Pihan 1980, Morgan et al 1979). Such photography was used to delineate homogeneous erosion mapping units, crop rotations, and management practices in a potato farming area in New Brunswick, Canada by Stephen et al. (1982). This approach produced accurate soil-loss estimates when combined with slope data taken from a topographic map, and

improved the soil erodability map. In addition, the use of air photos allows a year-round analysis which had been limited to about 120 days by traditional methods. In the above cases soil erosion has been identified by remote sensing techniques. In all cases, a surrogate of erosion related to land use has been determined. The available spatial resolution limits its use in this type of application, but for most surveys of large areas it is adequate.

Schecter (1976), Oki (1975), and Rangan and Rogers (1978), have used Landsat data to estimate land cover. The Oki model estimates the erosion and sediment contribution from sub-catchments and uses the universal soil loss equation.

Soil erosion can also be measured directly using close-range stereopairs. Welch et al. (1984) report on a method of registering digital data from the stereopairs from two dates to measure soil loss. This method can provide the spatial data necessary to develop and calibrate physically based erosion models. These data are predominantly obtained from ground-based systems that can permit millimeter accuracy to be obtained.

Poodle (1969) utilized aerial photography for erosion and slope analysis. The basic premise of this study is that aerial photography can supply detailed information about slope failure forms, including sheet wash, rills, and gullies which result from sheet or channelized flow, and creep, flow, slide, and fall which result from gravitational movement. This study shows that aerial photographs are useful for identifying erosion patterns and their sources especially for limited areas of large scales.

In recent years remote sensing data have been used to derive a number of coefficients of the USLE (equation 2/2). In particular the crop management factor has been successfully estimated using remote sensing data for a variety of environments in the USA (e.g. Berger and Jensen 1980, Degane et al. 1979, Morgan et al. 1978, 1979, 1980, Morgan and Nalepa 1982, McAdams 1980, Singher et al. 1982). For these studies the cropping management factor, C, and the erosional practice factor, P, were combined into one parameter estimated from Landsat data. A similar approach was used for an eight-county study group in Central Indiana (Campbell 1981). In this study a non-point pollution potential (NPP) index was defined as: NPP=f (soil

characteristics×agricultural land use intensity×proximity to water). This index was applied to cells of approximately 25ha (35 Landsat pixels). The agricultural land use intensity data were derived from the geocorrected Landsat data. Soil characteristics were determined from erodibility data in soil surveys, and proximity to surface water was measured by cell counting from water bodies identified on topographic maps. A GIS system was utilized to combine the data from the different data sets and assess the NPP index. Pelletier (1985) describes a GIS adaptation of the universal soil-loss equation which uses data from either the Landsat (MSS 79m resolution) or Landsat (TM, 30m resolution) to determine the land cover, and subsequently the cropping management factor. He provided a good discussion of some of the accuracy limitations that may be encountered by automating the procedure with satellite and digital elevation data. Figure 2.9 shows the various data sources and data files managed by the GIS. In the case cited above, soil erosion has not been measured directly by remote sensing techniques. In all cases, a surrogate of erosion related to land use has been determined. The spatial resolution available from common remote sensing products limits its use to this type of application and for most large area surveys and inventories it is quite adequate. However, soil erosion can be measured directly using close range stereopairs. Welch et al. (1984) report on a method of registering digital data obtained from the stereopairs from two dates to measure the soil loss. This method can provide the spatial data necessary to develop and calibrate physically based erosion models. These data are prodominatly obtained from ground based systems that can permit millimetre accuracies to be obtained.

Morris-Jones et al. (1979) estimated soil erosion potential in a 6136 ha watershed in Wisconsin. Comparison of the experimental 1977 USLE study, which employed remote sensing data collection methods, with the traditional 1975 USLE study based primarily on field survey methods yields the following results: air photo interpretation was successful in gathering all of the basic land use/land cover data needs associated with the erosion factor; remote sensing data collection techniques were less labour intensive than the traditional methods based primarily on field studies. Approximately 50 hours were required to compete the study with remote sensing methods while 93 hours were required with the traditional methodology.

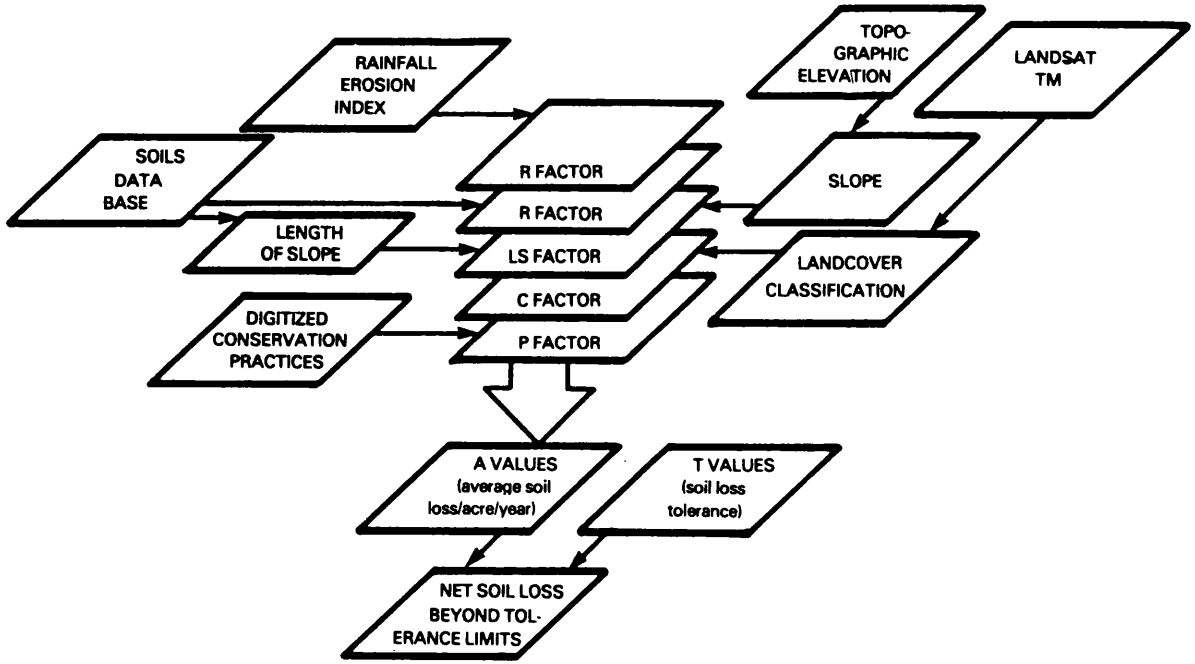

Figure 2.9: A schematic of the universal soil-loss equation database as managed by the GIS (after Pelletier 1985).

A model for estimating splash and sheet erosion on a regional scale has been developed by Mueksch (1984). This approach, based on an empirical equation, uses slope areas and lengths from Landsat imagery. The method has been tested in the East Africa coastal zone. Application to other climatic and geographic areas should be carried out with caution but the method demonstrates how remote sensing data may be used in areas where other data may not be available.

Alam and Harris (1986) studied moorland soil erosion by spectral reflectance. The study area was divided into three pedological groups based on the Soil Survey of England and Wales map, each of which was further subdivided into five substrata on the basis of tonal characteristics on the aerial photography. A stratified random sampling scheme was then used to identify sites at which a number of soil characteristics were measured in May 1985 (soil texture, moisture, organic matter, biomass and slope). At each of 70 field sites the reflectance of the surface was also measured with a Milton Multiband radiometer equipped with 4 wavebands comparable to those of the Landsat MSS (0.5-0.6, -0.6-0.7, 0.7-0.8 and 0.8-1.1*m*m). Although the discrimination analysis did not give clear results it indicated that the best band for overall discrimination is channel 4, followed by channels 1 and 3. Thus any conclusive remarks about the discriminating power of the ground radiometer data cannot be made without reservation. There was no clear relationship between individual wave bands and single ground variables, but grouping and stratification have shown that aggregate effects can be determined.

Palylyk et al. (1992), utilized multidata Landsat TM digital imagery and digital soil survey information integrated within an ARC/INFO GIS to monitor temporal soil erosion risk for a portion of the county of Flagstaff, Alberta. Land cover classifications derived from each data of Landsat imagery were converted to vector format as GIS data layers. Soil erosion risk was analysed spatially through selective query and overlay of temporal land cover and soil information. The resulting temporal-sequential soil erosion risk assessments have considerable potential for county-level conservation applications, while GIS capabilities can enhance their utility for conservation planning.

Wind erosion is usually one of the major erosional process in semi-arid areas, however it has a limited role in soil erosion in the Lar basin mainly because the area is surrounded by mountain ranges. Aeolian transport of sediment is thus insignificant in the Lar basin.

2.5.3 Land Use and Land Cover Changes

Aerial photographs, have been used extensively in the mapping of eroded areas (Stallings 1957, Buringh and Vink 1961, Emer, 1975, Jordan 1984) as well as for other qualitative assessments of landuse changes which may affect soil erosion (Ishaq and Huff 1974, Williams and Morgan 1976). Some attention has also been directed at quantitative evaluation of soil loss using aerial photographs (Buringh 1961, Jones and Keech 1966, Keech 1972, Atukum 1976, Welch et al 1984, Thomas et al 1986, Aniya 1985). Sequential aerial photographs have been used to determine the nature, location and timing of soil management changes and how those changes effect soil erosion on cropland (Stephen et al 1982). This information used in conjunction with detailed topographic maps and the USLE, permits the estimation of past and present rates of erosion and how these relate to present landuse (Stephen et al 1982).

Biswas and Singh (1990) utilized TM data for evaluation of soil resources in the Malwa plateau, India. They attempted to prepare soil resource maps by visual interpretation of a false colour composite from the TM at an average scale of 1:250000 in conjunction with field checks covering an area of 340 000 ha. Nine soil mapping units were established as well as four physiographic units, seven land use units and three waste land mapping units. This study showed low Landsat TM data can be useful for general identification of the land surface over large areas.

Sharifi (1978) applied remote sensing to the study of the agricultural and natural resources in the Qazvin area of Iran. He prepared land use maps, developed a crop yield forecasting system, and predicted the quantity of water available from melting snow and vegetation. Boundaries were determined using 4 different bands as well as the colour composite of these bands. Then a map was prepared at 1:500 000 on which the following levels were distinguished: agricultural land, forest, barren land,

hills, snow, surface water and settlement area. The result was succesful when combined with large scale aerial photos at 1:5000.

Morris et al. (1979) investigated methods for gathering the land use and land cover information required by the USLE from medium altitude, multi-date, colour and colour infrared positive transparencies, using both human and computer-based interpretation techniques. Successful results which compare favorably with traditional field study methods were obtained within the test watershed. Computer-based interpretation techniques were not capable of identifying soil conservation practices, but were successful to varying degrees in gathering other types of desired information.

In the English Lake District, Anderson and Tallis (1981) successfully mapped land cover changes and the aerial extent of erosion features from aerial photographs. Singh (1986) has identified three aspects of using aerial photographic data in relation to the assessment and mapping of landcover changes. The first is that of detecting changes in landcover; the second lies in the identification of the nature of the change, and the third involves mapping the aerial extent of the changes.

Acton and Stonehouse (1972) used 70mm photography in conjunction with the 1971 program of the Canada Centre for Remote Sensing in a soil survey program. The photography included green (0.39-0.52μm) and red (0.56-0.70μm) bands on panchromatic black and white film as well as infrared on black and white and colour film. This imagery was evaluated for suitability for soil resource mapping in comparison to conventional panchromatic photography. Low reflectance from bare soils restricted the usefulness of infrared black and white to vegetal and drainage interpretations. There was no significant difference between the red, green and colour infrared for general soil interpretations and none of these was of equal suitability to the panchromatic black and white, especially for topographic evaluation. Infrared photography, either black and white or colour, appears to be more meaningful later in the season, such as mid to late July and into August when native vegetation or crops are more advanced and likely to be reflected by soil features. From 70mm images it was difficult to single out any one of the red or green visible or colour infrared bands

as being generally superior to the onothers. Black and white infrared was suited only for distinguishing drainage and vegetation features.

Prasad et al. (1988) used Landsat data for mapping soil and land resources in northern Karnataka, India. They prepared a false colour composite of Landsat imagery at 1: 250 000 supplemented by field investigation. The soil and land resources map thus prepared formed the basis for determining land capability, land irrigability and suggested land use. A false colour composite was visually interpreted for physiography, based on differences in tone, texture, or a combination of these, and a pre-field physiographic map was prepared. For each Landsat scene of 185×185 km, about 15-20 sample strips were selected and 30 soil profiles were recorded in each, giving about 500 profile observations per scene. They concluded that by adopting remote sensing techniques supplemented by adequate field investigations, a reasonably accurate soil and land resource map at 1: 250 000 scale could be prepared speedily and economically. For the Lar basin SPOT (20m) , KFA-1000 (5m) and aerial photographs with Landsat TM were used to increased the results accuracy. Thus, against this background, aerial photographs have been employed in this research to obtain precise information on the extent of landcover changes in the Lar Dam Basin. The approaches described above show low high resolution space imagery in combination with conventional aerial photographs provide useful, fast and inexpensive means of classifying and forecasting changes in large watersheds.

2.5.4 Fluvial Features

Stream flow is one of the most prominent agents of landform sculpturing, whose effects are seen almost everywhere large quantities of sediment are removed, transported and deposited by rivers, thus modifying the land surface configuration (Baker 1986). The fluvial landscape comprises valleys, channelways and drainage networks.

Gugan and Dowman (1988) demonstrated, using maps at 1: 50 000 and 25m contours, that the enhanced spatial resolution available from TM and SPOT data allows significantly greater geomorphic information to be obtained than from the Landsat MSS. Frances and Hedges (1986) compared MSS and TM data and showed

that the latter provided much more information. Table 2.2 shows a comparison of channel lengths and drainage densities discernable from TM and MSS data when compared to black and white aerial photographs and maps in North Wales, UK.

Table 2.2: Comparison of channel lengths and drainage density from different data *(after France and Hedges, 1986).*

Type	Scale	Total channel length (km)	Drainage density (km/km^2)
MSS	250000	22.2	0.11
TM	100000	88.8	0.38
Photos	1:50000	121.5	0.52
Map	1:50000	272.2	1.15

Rahn (1979) used aerial photographs and satellite imagery to determine areas of bank erosion along the Missouri River, USA. Cloud-free Landsat images were obtained in 1973 and 1976 and in an 88 km reach, total erosion of 890 hectares and total accretion of 810 hectares were estimated. Imagery was enlarged to 1:62500 for determination of temporal changes. In order to quantify the eroded area it was required that discharge was about the same at the time of both aerial surveys. This study concluded that it is possible to periodically assess areas of erosion and deposition and it is anticipated that more researchers will be able to utilize satellite imagery for temporal fluvial studies as more data become available. Holz and Baker (1979) utilized Apollo photographs for a study of the fluvial morphology of western Amazon streams. Imagery from the ASTP Earth observations and photography experiment MA-136 was found to be useful for a variety of morphological measurements. They were able to distinguish three major river types on the basis of sinuosity (P) and other properties. Channel widths and meander wavelengths were also easily determined.

Barber et al. (1990) measured historical sediment concentrations from archived Landsat MSS imagery. The study site chosen for this investigation was Southern Indian Lake, located in northern Manitoba, Canada. Three satellite images were used, two acquired on July 1, 1988 and one on May 24, 1977. Their results show that

standardization of tonal distributions between different image dates, within a single band, do not meet their requirements of the concept of universality. However, standardization combined with a transformation to spectral radiance provided a technique which could be considered statistically universal.

Somma and Francois (1987) used remote sensing from a geomorphological reconnaissance of a semiarid mountainous region in northern Canada, including deposits and erosion features of glacial, periglacial, marine and fluvial origin. They present the results of a supervised classification with twenty one themes. It was a preliminary stage before trying to correct for topographic effects. In fact, the rugged relief of the region presented numerous problems for the automated analysis which could be minimized.

Roberts and Liedtke (1985) used colour and colour infrared photography to identify digitally, with an Eseco transmission densitometer, suspended surface sediment concentration in the Fraser River plume Canada. The photographic resolution of sediment concentration was satisfactory providing good separation of sediment differences as small as 30 mgl^{-1}. Liedtke et al. (1987) used a video system to provide separation for sediment values to within 5 mgl^{-1}.

Franklin et al. (1987) interpreted the geomorphology of a high relief, glaciated environment in the southwestern Yukon. A discriminant procedure was used and the results compared between a Landsat MSS classification, a geomorphometric (variables were elevation, slope, aspect, relief and convexity) classification, and an integrated classification. Overall classification accuracies were 60%, 75% and 85% respectively, based on 650 pixels from control areas. These results support and confirm the important role of ancillary data sources such as elevation models in the analysis of complex terrain using satellite imagery.

Royer et al. (1984) utilized Landsat images for geomorphological interpretation of an area of southern Quebec, Canada. For all of the area there was a Landsat image geometrically corrected to a scale of 1: 50000, a multispectral and panchromatic simulation of the SPOT HRV detector, a thermal inertia image generated from an albedo image, two thermographs (diurnal and nocturnal), and 20 high-resolution

synthetic aperture radar images in the X and C bands (H polarization). A digital comparison of the spectral signatures is given for 15 test sites defined by the type and nature of the loose deposits, and by their physical characteristics. Variations in the signature obtained with a Transformed Vegetation Index (TVI), thermal inertia and the radar return echo in the X and C bands were examined with respect to water content and /or drainage and relief parameters. Thermal inertia allowed bare ground having a high water content to be distinguished, but in areas of vegetation cover it seemed to be more closely related to the total biomass or the water content of the plants. Low amplitudes, which were due to saturation, did not allow indirect analysis of drainage conditions related to granulometry.

Pickup and Chewings (1987) used Landsat MSS data for forecasting patterns of soil erosion in central Australia. They presented a model based on the erosion cell mosaic approach, which exploits the high degree of temporal and spatial autocorrelation in the erosion process on flat alluvial plains. This model expresses each pixel value as a function of those of its neighbours plus a noise term. Testing of the model against observed change indicates that it is reasonably accurate as long as the underlying pattern series is obtained from imagery in which there is sufficient vegetation cover for the soil stability index to be a sensitive indicator of the state of the landscape. This study has shown that predictable changes occure in the variance and spatial autocorrelation function of soil stability index values derived from Landsat MSS data as a landscape degrades or recovers. The changes do not occur randomly in space. Instead, they accentuate existing erosion and deposition structures in the landscape. These processes can be simulated and forecasted using simple simultaneous autoregressive (s.a.r.) models making it possible to identify areas most susceptible to change.

Biwas (1978) utilized a Landsat false colour composite at 1: 250 000 to obtain data on catchment and land resources in the Rengali river catchment, India. Visual analysis was used to delineate the easily distinguishable land units and the most important image characteristics in conjunction with field validation. Visual analysis was also used with field checks of the Landsat FCC (band 4, 5 and 7) at 1:1 000 000 scale for the delineation of physiographic units, and the area was interpreted on the basis of image characteristics to produce the recognition keys and their corresponding

geomorphic units, and soils were examined in the field to prepare a soil map. This study was useful for classification of various geomorphic units for a large area (about 168 000 hectare).

Chidley and Drayton (1986) used simulated SPOT imagery in hydrological mapping in Wales. Imagery with a variety of landscape unit characteristics alone was found to be inefficient, and the use of the thematic information was found beneficial. The sites were over flown on several different times and days. Subscenes of 512×512 pixels of particular areas of interest were then extracted and enhanced. Streams were drawn directly from the SPOT photoprints at 1:50 000 (10m resolution). The images were sufficiently clear for cultural features to be easily recognized and for the interpretation to be similar to that for aerial photography. Drainage maps were drawn for the three spectral ranges independently. One major catchment boundary was drawn using drainage and topographic details interpreted from the images. The drainage network for each catchment was compared with the network extracted from 1:50 000 Ordnance Survey maps. They found that the technique of density slicing in band 3 was extremely effective for identifying bodies of open water. The most efficient approach was to do this interactively, roaming through the image in zoom mode, noting the line and row numbers and the bodies of water which were identified. Using this method they could map bodies of water of less than 0.5 ha. in area, which compares favorably with the figure of 24 ha. achieved using Landsat MSS (NASA 1977). The SPOT system could map drainage networks to an order of magnitude better than the Landsat MSS, mapping better at 1:50 000 than Landsat at 1:250000 but the percentage of the network mapped by SPOT was lower than expected.

Chidley and Drayton (1985) observed British catchments and found that drainage networks could not be mapped reliably from Landsat data at 1:250 000. Nevertheless, they found that main rivers could be mapped with an acceptable level of confidence, and that catchment areas and stream frequencies could be estimated to an accuracy appropriate to simple hydrological models based on geomorphic parameters. In contrast to earlier work they found that although winter imagery gave the greatest detail of stream networks, the detail was not consistent over the whole area and could not be relied on to give good estimates of drainage density. Summer

images showed far less detail, but provided much improved correlations with accepted values.

Govindarjan (1985) used remote sensing for identification of hydrogeological conditions in the southern part of Tamil Nadu, India. His method includes two phases. In the first, a satellite remote sensing survey was carried out during 1977-79. This was followed by systematic ground water investigations in the above area. The satellite remote sensing survey was carried out using 1:250 000 Landsat data. Landsat images of 1:250 000 scale in bands 4, 5, 6 and 7 and false-colour composites were analysed visually. Using the results of Landsat analysis and ground data, thematic maps (such as land use, soil, geomorphology) were prepared. Using the above results, hydrological conditions were evaluated for the different geomorphic units and potential groundwater zones were delineated. The second phase was carried out for 4 selected test sites, and involved mapping of the microlevel hydrological features, which were correlated with the findings from the first phase. Aerial photo interpretation was made at 1:60 000 scale. Geological and geomorphological maps were prepared and detailed field checks and collection of ground data were made. By integrating the above results, hydrological conditions were evaluated for the different geomorphic units and the potential groundwater zones were identified. The field check supported the remote sensing data and produced satisfactory results after their combination.

Astaras et al. (1990) carried out a drainage system analysis and compared Landsat-3 RBV (Return Beam Vidicon), Landsat-5 TM and SPOT PA (Panchromatic) imageries covering the central Macedonian district, Greece. The main findings were: (A) SPOT PA stereopair diapositives at 1: 20 000 can be used to map drainage systems to within an order of magnitude, slightly more readily than TM imagery at 1: 125 000, but significantly more than RBV imagery at 1: 25 000 scale. This slight superiority of SPOT imagery over TM implies that the greater spectral range of TM, vastly outweighs the advantage of SPOT's superior resolution, but not the superiority of it's stereoscopic view; (B) TM imagery can be used to map drainage systems to within an order of magnitude significantly better than RBV imagery; and (C) RBV imagery can be used to map drainage systems to an order of magnitude, less than topographic maps at 1: 50 000 but better than those at 1: 100 000. The interpretation

of the RBV, TM and SPOT images was accomplished by the incorporation of a technique similar to that used in photointerpretation. The near-infrared band 7 was used as this offers the best detection of drainage lines.

Gardner et al. (1988) used SPOT PA data for fluvial network analysis. Euclidian distance classification of the data was used to delineate ephemeral fluvial networks on low-relief, alluvial fan surfaces in an arid basin in the SW U.S.A. The SPOT classified channel network was registered to a universal transverse mercator (UTM) projection and compared to data extracted from US soil survey topographic maps and black and white aerial photographs. One-pixel and two-pixel proximity searches of the SPOT classified image correctly classified over 8% of the area of channelized flow, 77% of the second order and greater channel network, and 98% of the fourth order and greater channel network. The SPOT channel network was simplified by elimination of lower-order channel segments to produce a network closely resembling (in terms of number of channel segments and total channel length) a network created for hydrological modeling from topographic maps or aerial photographs.

Sgavetti and Ferrari (1988) utilized TM data, in the Po and Adige rivers, Italy for investigation of a deltaic depositional system. Several interactive processing techniques were applied to a large volume of TM data relative to different spectral bands and acquisition dates, to enable identification of sedimentary bodies. The results showed association of genetically related depositional elements, so allowing the interpretation of developmental stages of depositional environments.

Ali et al. (1988) utilized Landsat MSS at 1:50 000 and aerial photographs (1:70 000) for water resources investigations in Tone river basin, India. Stream networks were clearly picked up in the mountain region and to some extent in the piedmont zone. This information can be better extracted from aerial photographs because of stereo viewing capability. Digital analysis of CCT data provides discrimination of landuse and landcover types along with estimation of their areas.

An important consequence of identifying fluvial features is investigation of erodible areas in a basin. Drainage networks, slope, channel characteristics and physiographic

conditions are significant features for this assessment. This information can also be useful in estimation of depositional areas and volumes.

Hutton and Dincer (1979) used Landsat imagery to study the Okavango Swamp, Botswana. This was used to calibrate a mathematical model of the area and the flow distribution. By using the imagery to measure the area and observe the shape of the Swamp and its subsystems, it was possible to estimate the depth and flow rates, since these were correlated with the horizontal dimension of the Swamp. The imagery was also useful in assessing the relative importance of evaporation from surface water and transpiration from Swamp vegetation.

2.6 SUMMARY

This section has demonstrated that, by using imagery and available large scale topographic maps, estimation of sediment delivery can be made some extent with a limited amount of field checking for assessment of soil loss and prediction of depositional and eroding areas, SPOT and TM can be particularly useful when combined with aerial photographs or any high resolution (<10m) satellite data.

Remote sensing data including aerial photographs have been reviewed for the different types of land surface features and changes which are found in the Lar basin. Aerial photographs are of most use for mapping soil erosion because most geomorphological features were visible in stereoscopic images. Sequential aerial photographs, can also be used to determine the nature and location of land surface changes. This information can be used in conjunction with field observations and old topographical maps from the study area. For soil characteristics the major problem of using aerial photographs lies in correlating the various colours found on the images with soil conditions. Variation in film exposure and development, and vegetation masking of eroded areas can cause interpretative problems.

This literature review has identified significant gaps which it is aimed to address this research. This suggested that a successful way of estimating sediment erosion can be from plotting from conventional aerial photographs, which need ground control points and sequential photographs for selected sites. Classification of land cover is

not successful unless combined with high resolution data and field checks. Thus, for achieving this aim for vegetation, morphological changes and soil characteristics high resolution satellite data, aerial photographs and field checking are all required.

By using image processing techniques the maximum use is made of the available information. The accuracy of the classified image affects the final estimatès which depend on image resolution and the technique. All of the techniques described above showed that remote sensing data processing can be useful for appraisal of physical characteristics, especially in inaccessible and large areas. Both SPOT and TM are useful for preparing management plans for these relatively remote upland areas. It is important to emphasize that, for successful identification and discrimination of vegetation, bare soil, deposition area and erosion, digital images need: i) more integration of spectral information with spectral class so that internal variations remain at minimum, which would enhance the class variation and hence improve the classification accuracy; ii) more spectral bands at the longer wavelength, such as the Landsat TM band 5 and 7 and SPOT wavebands 1 and 2 are essential. Therefore increasing the number of spectral bands would increase the possible number of band combinations that might help in better identification and delimitation of morphological units and hence would reduce the misclassification between them. In the second stage aerial photos can be useful, following remote sensing data for deriving physical characteristics, and assessing their magnitudes, (eg. Volumes of erosion) which seems to be a significant gap in the reviewed literature. The best analytical method for the purpose of mapping and quantifying deposited soil is field survey and stereoscopic analysis on remote sensing data, which gives useful information of alluvial features. Although these techniques are perhaps adequate from remote sensing, field work is necessary and can complement them and ensure reliable results.

2.7 PREVIOUS WORK IN THE STUDY AREA

2.7.1 Geology and Petrology

The Alborz Mountains (Figure 2.10) are a continuation of the Alpine-Himalayan mountains, which are complex, asymmetric belts of folded and faulted rocks. The

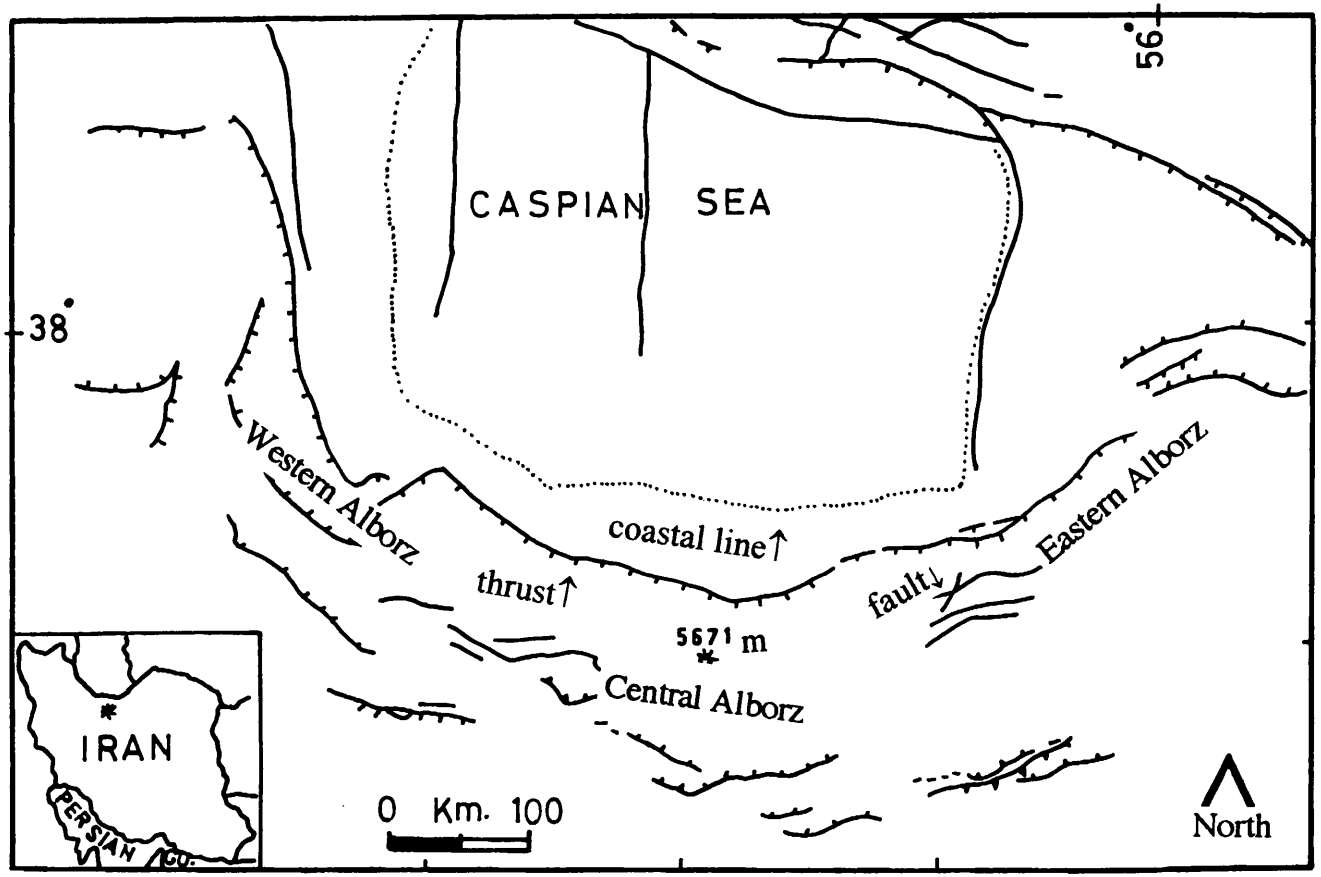

Figure 2.10: Location of Central Alborz *(after: Geological Survey of Iran, 1973).*

Alpine orogeny of the Iranian Ranges is characterized by the absence of nappes present in the European Alps (Stoklin, et al 1964). The compressive stress of Alpine orogeny resulted in thrusts and high angle reverse faults in the Central Alborz and a wide range of fold systems throughout the mountain chain.

Gansser and Huber (1962) produced a scheme for the broad tectonic subdivision of the Alborz which was subsequently adopted by later workers. The study area was 50 km northwest of the Lar basin, within which Cambrian formations overlying a Precambrian metamorphic base were recorded. They also published a structural stratigraphic subdivision of the Alborz Range.

There has been a little geological work in the study area but no previous geomorphological study has been conducted. Early investigations of this region including those of Tietze (1887) into the area of Damavand volcano, and several geologists, especially Stahl (1897, 1911) have provided descriptions of traverses along the Jajerud and Lar valleys, and an initial stratigraphic outline of northern Iran. Further stratigraphic information was provided by Morgan (1905), but it was not until Riviere (1934) that the first detailed stratigraphic framework for the Central Alborz was proposed. These early workers, recognized the influence of Damavand in controlling the creation of a lake in the upper Lar valley and the development of the modified drainage pattern in the area. Baily et al. (1948) reported some geological observations on Kuh-e-Areh, around Ab-Ali and within the Lar valley.

Assereto (1966) produced a detailed map at 1:50 000 showing the geology of the entire area covered by this present study, and the associated notes described the geological succession in some detail.

The area studied by Allenbach (1966) included Damavand and the area toward the south and east, totaling 2000 km^2 immediately to the east of the area covered by Assereto (1966). The geological history of the area was described and much detailed work on the petrography and petrology of the Damavand volcanic rocks was reported. C^{14} dating on a sample of plant debris from the terraces in the lower Lar valley suggested a minimum age of 38500 years which was said to indicate a

probable age for the Lar terraces. Sussli (1976) gave a detailed account of the lower Haraz valley.

2.7.2 Stratigraphy

From 1905 to 1930, only palaeontological studies were published on the region, and these dealt mainly with the Mesozoic (Douville, 1904; Fischer, 1914, 1915; Krumbeck, 1922; Erni, 1931). Ovcinnikow (1930) described the region between Ab-Ali and Damavand, particularly emphasizing the lithostratigraphic sequence, but with inaccurate structural interpretation. Bohne (1932), described the Shemshak region, and produced a 1:100 000 geological map with two accurate geological sections. The geological succession established by the above authors is reported in Figure 2.11.
The stratigraphy of the area owes much to Stocklin et al. (1964) and the palaeontology of the formations is provided by several authors especially, Fantini-Sestani (1965) and Assereto (1966). The overall structure of the region has been described by Stoklin (1986).

Dellenbach (1964) studied the area lying to the immediate south of the region under investigation. The time-stratigraphic subdivisions adopted in his work are shown in Figure 2.11.

2.7.3 Sedimentology

Bout and Derruau (1961) developed the concept of there being two main periods of sedimentation in Lake Lar. A brief description was given of the sediments within the basin, which are not typically lacustrine in character, laminated and varved deposits not having been observed. They interpreted the upper part of the sedimentary succession as being of fluvial origin. Associated work, reported in the same paper on the pollen from the clays in the Lar Dam Basin indicated that at the time the sediments were being laid down the climate in the area was a little drier, and possibly a little colder, than at present.

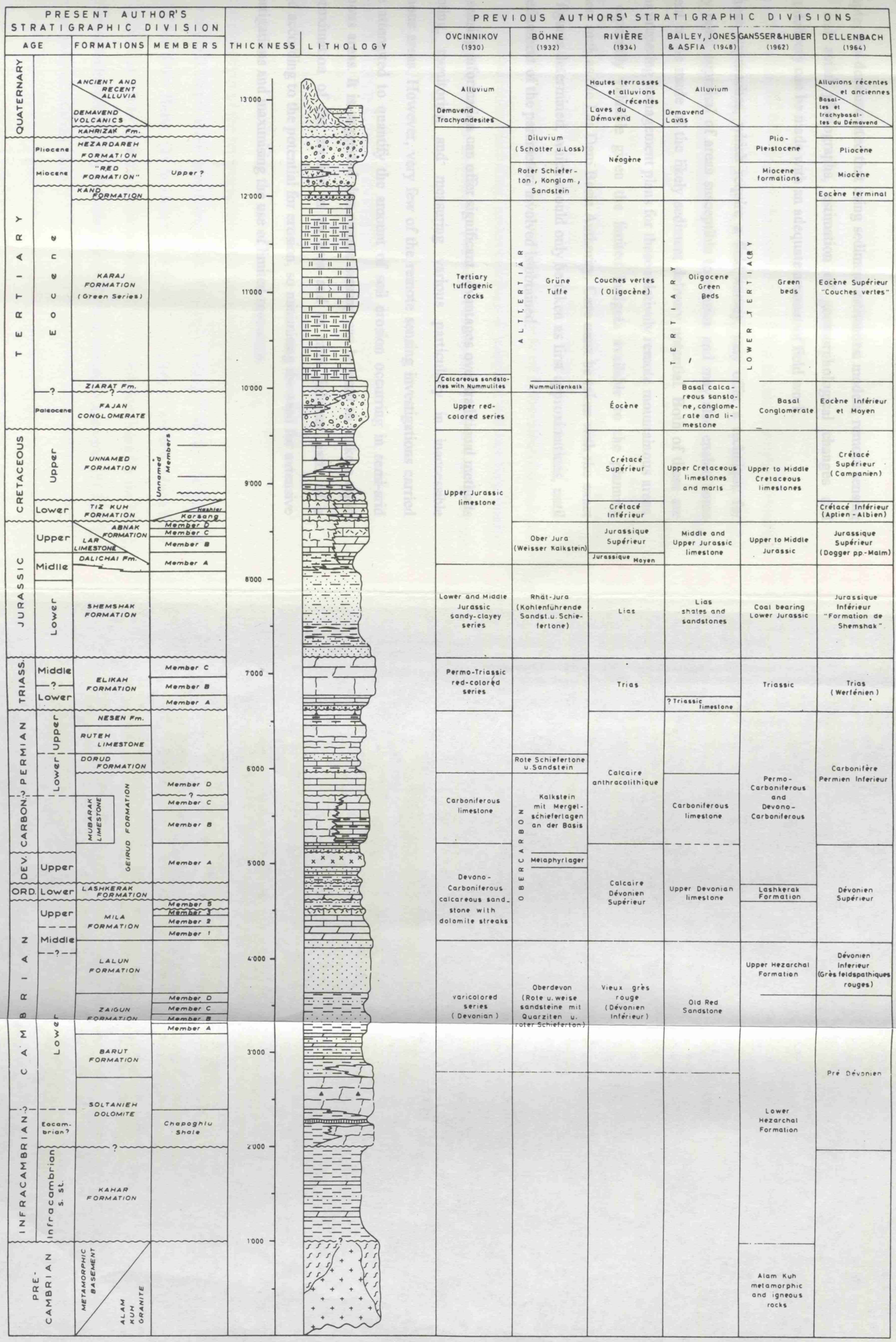

PREVIOUS AUTHORS' STRATIGRAPHIC DIVISIONS

OVCINNIKOV (1930)	BÖHNE (1932)	RIVIÈRE (1934)	BAILEY, JONES & ASFIA (1948)	GANSSER&HUBER (1962)	DELLENBACH (1964)
Alluvium / Demavend Trachyandesites		Hautes terrasses et alluvions récentes / Laves du Démavend	Alluvium / Demavend Lavas		Alluvions récentes et anciennes / Basaltes et trachybasaltes du Démavend
	Diluvium (Schotter u.Loss)	Néogène		Plio-Pleistocene	Pliocène
	Roter Schiefer-ton, Konglom., Sandstein			Miocene formations	Miocène
				LOWER TERTIARY	Eocène terminal
Tertiary tuffogenic rocks	ALTTERTIÄR Grüne Tuffe	Couches vertes (Oligocène)	TERTIARY Oligocene Green Beds	Green beds	Eocène Supérieur "Couches vertes"
Calcareous sandstones with Nummulites	Nummulitenkalk	Éocène	Basal calcareous sanstone, conglomerate and limestone	Basal Conglomerate	Eocène Inférieur et Moyen
Upper red-colored series					
Upper Jurassic limestone		Crétacé Supérieur	Upper Cretaceous limestones and marls	Upper to Middle Cretaceous limestones	Crétacé Supérieur (Campanien)
		Crétacé Inférieur			Crétacé Inférieur (Aptien-Albien)
	Ober Jura (Weisser Kalkstein)	Jurassique Supérieur	Middle and Upper Jurassic limestone	Upper to Middle Jurassic	Jurassique Supérieur (Dogger pp-Malm)
		Jurassique Moyen			
Lower and Middle Jurassic sandy-clayey series	Rhät-Jura (Kohlenführende Sandst.u. Schiefertone)	Lias	Lias shales and sandstones	Coal bearing Lower Jurassic	Jurassique Inférieur "Formation de Shemshak"
Permo-Triassic red-colored series		Trias	? Triassic limestone	Triassic	Trias (Werfénien)
	Rote Schiefertone u.Sandstein	Calcaire anthracolithique		Permo-Carboniferous and Devono-Carboniferous	Carbonifère Permien Inferieur
Carboniferous limestone	OBERCARBON Kalkstein mit Mergelschieferlagen an der Basis		Carboniferous limestone		
	Melaphyrlager				
Devono-Carboniferous calcareous sandstone with dolomite streaks		Calcaire Dévonien Supérieur	Upper Devonian limestone	Lashkerak Formation	Dévonien Supérieur
varicolored series (Devonian)	Oberdevon (Rote u. weise sandsteine mit Quarziten u. roter Schieferton)	Vieux grès rouge (Dévonien Inférieur)	Old Red Sandstone	Upper Hezarchal Formation	Dévonien Inferieur (Grès feldspathiques rouges)
				Lower Hezarchal Formation	Pré Dévonien
				Alam Kuh metamorphic and igneous rocks	

Figure 2.11: Reconstructed and simplified lithological sequence in South Central Alborz and relative stratigraphic classification employed by previous studies and in the present work, *(after Assereto 1966).*

2.8 GENERAL SUMMARY

This chapter has demonstrated that using sediment estimation models, remote sensing imagery and aerial photographs, estimation of geomorphological changes and sediment delivery can be made with an adequate amount of field work.

Thus, these approaches, which require a field survey, may offer a technique for relatively rapid appraisal of areas susceptible to erosion and may also enable some assessment to be made of the likely sediment delivery potential. Both of these are useful for preparing management plans for these relatively remote mountainous areas. This is especially valuable given the limited budgets available to the planning authorities, such as the Lar Dam Basin Authority. Care must be taken with the exact soil loss figures determined, which should only be taken as first approximations, until further refinement of the parameters involved is obtained.

Remote sensing information can offer significant advantages over traditional methods in detecting, monitoring and measuring various particularly in inaccessible mountainous areas. However, very few of the remote sensing investigations carried out have attempted to quantify the amount of soil erosion occurring in semi-arid mountainous areas. It is suggested that remote sensing can be used to make a rapid first approximation of the erosion in an area and to rank different parts of a watershed according to the potential for erosion, so minimising the need for extensive field investigations and maximising the use of limited resources.

CHAPTER 3: INVESTIGATION TECHNIQUES

INTRODUCTION

The aim of this chapter is to explain the methods employed in this research. Estimating changes in sediment supply within the Lar Dam Basin formed part of a more extensive investigation into the deposits downstream of the confluence of the Lar with the Dalichai and Sefid-Ab Rivers and the Lar Lake. The investigation techniques utilized were developed and modified during the study and their success is reflected by the detail with which it has been possible to estimate the morphological changes and sediment classification within the study area. In general terms, the investigations consisted of:
(a) Remote Sensing interpretation; **(b)** quantitative analysis of hydroclimatological data; and, **(c)** field observations including, geomorphological mapping, echsounding, control point survey, and vegetation assessment. These various aspects of the overall study are described below.

3.1 REMOTE SENSING DATA INVESTIGATION (RSDI)

3.1.1 Objectives

The precise objectives of the remote sensing data interpretation were:
(1) to identify hill slope, river morphology and vegetation changes during the past 50 years in the Lar Dam Basin; **(2)** to identify the nature and types of erosion which have occurred in the area; **(3)** to produce geomorphological, and vegetation maps for the basin; **(4)** to estimate sediment delivery volumes using photogrammetric analysis; **(5)** and, to assess the accuracy of existing maps.

3.1.2 Aerial Photographs

The first remote sensing technique employed was stereoscopic analysis of air photographs taken at different times, including pre and post-dam construction. Three sample areas with different physical conditions were selected for study: (1) Dalichai, which is a volcanic area of 196.3 km^2 (2) Sefid-Ab (119.3 km^2) as a middle sized sub-basin; and, (3) Lar (414.4 km^2 at Gozaldarreh) as the main stream in the basin transporting the most sediment. Air photos from the following dates have been used:

1955 at 1: 55 000, 1970 at 1:20 000, 1983 at 1: 5 000, and 1991 at 1:10 000 scale. Two pairs of stereo KFA-1000 photos (1990) for the whole of the Lar Dam Basin were also used at 1:270 000 scale. All of these photographs were taken in September and so are comparable. The photographs of 1955, 1991 and KFA-1000 (1990) were provided by the Iranian Army and 1970, 1983 photographs were obtained from the Iranian National Cartography Centre (N.C.C).

In order to identify the erosional features, the classification followed by Leuder (1959), Sharp (1960) and Poole (1969) was applied. The main erosional forms identified were sheet wash, and gulling. Sheet washes as defined in this study includes slope wash where no significant channelization by natural overland flow has occurred. The major type of soil erosion in the Basin includes sheet wash, rill, gully, and stream channel erosion. Both sheet and rill erosion are widespread on the photos of the Sefid-Ab, Lar and the south side of the reservoir. The interpretation of erosional forms on the air photographs of the Lar Basin was as follows:

Bare soil exposures depicting sheet erosion registered from white to light grey and there was also frequently a sharp tonal contrast between the areas affected by sheet erosion and these adjacent areas which showed no effect at all. Rill erosion was reflected in several patterns depending on slope conditions and on the stage of rill development. Occasionally it was difficult to determine from the photographs precisely when the rills become gullies. Gullying includes those deeply incised channels which have exposed or completely

removed the overlying sediment. The criteria developed and used to recognize and distinguish gullies from rills are:

gullied channels are deep and wide in comparison to rilled channels; tributary channels are numerous; channels are generally intermittent, but seepage may occur in some channels and where this occurs the moistened sections of the channel register a dark grey tone in contrast to the background. Considerable rill wash was usually associated with gully development. The channels of gullies register in grey tones from moderately dark to light especially where the channels have water in them. Rills usually form parallel to sub-parallel channels and sometimes have an anastomosing pattern. Sheet wash was associated with rill wash, confined to the areas between channels.

In order to estimate the amount of sediment contained within the depositional features of the rivers (Dalichai, Sefid-Ab and Lar alluvial fans), the height and location of control points were surveyed using known and heighted points on the maps. For each area of overlapping aerial photographs including each selected river delta), at least 4 control points were extracted. For Dalichai and Sefid-Ab sites, contour lines provided by photogrammetry from aerial photographs of 1955 and 1970 were compared with 1945, 1:25 000 topography maps in order to quantify sediment delivery in the selected areas.

3.1.3 Satellite Remote Sensing Techniques

As well as aerial photographs, satellite remote sensing was used in order to classify and map the major land surface types of the Lar Dam Basin. The data sources used were: Landsat MSS and TM, SPOT Xs and KFA-1000 in black and white and colour. Information obtained from these in conjunction with the air photos were used to estimate sediment supply within the study area. SPOT images were used for selected sites where they are especially useful for identifying geological features (such as intrusive bodies and faults), the drainage network, depositional areas and vegetation. The SPOT scene of the study area was acquired in June 1987. As there were no detailed geomorphology or erosion maps of the area in order to provide reliable surface reference data (SRD), air

photo and stereo pairs of KFA-1000 images were used prior to the analysis of the SPOT images. The following maps were produced from this interpretation:
geomorphology; vegetation; topography and hydrography; and slope maps at 1:50 000; and lithology and morphotectonic maps at 1:100 000 scale.
It is recognised that the spectral characteristics of land cover types are mainly controlled by energy-matter interactions. The proportion of energy reflected, and transmitted for each land cover type varies depending on material type and condition (Lillesand and Kiefer 1978). Some physical factors like geology, landforms, soil characteristics, climatic conditions, vegetation cover and topography influence the spectral reflectivity of land covers (Smedes 1975; Curran 1980).

Any effective use of remote sensing data closely depends on the relationship of pixels to object sizes and the spectral and spatial resolution of data. Morphologic changes in the Lar basin are mostly of small size. Therefore, for proper identification and delineation of this area it was apparent that the sensors with higher spatial resolution or a small field of view would be the most useful. For example, Landsat Multispectral Scanner (MSS), with 79 metres spatial resolution would be of less use than the Landsat Thematic Mapper (TM) and SPOT Multispectral, both which have higher spatial resolution, 30 metres and 20 metres respectively. Thus, in this research Landsat TM, airborne SPOT Multispectral and KFA-1000 data have employed as the main remote sensing data sources. These remote sensing data were supplemented by sequential air photographs and field work.

At the time of the photography (September) most of the land was being grazed; this is suitable for interpretation of geomorphology but made identifying vegetation difficult. Precision photography was used to enlarge a 1:270 000 KFA-1000 of the Lar Dam Basin to 1:100 000. This enlarged photo then acted as a base map for one-to-one transfer of the interpreted phenomena from SPOT and air photos. The resulting maps were used as surface reference data (SRD) for the subsequent analysis of the SPOT data. Interpretation of some features and some areas was difficult and so field checks were undertaken in the summers of 1993 and 1994. SPOT Xs images of the area acquired on

June 1987 were obtained from the Agriculture Ministry of Iran on floppy disks. Three sub-scenes of 512×512 pixels each were selected for analysis covering the area of Dalichai, Sefid-Ab and Lar. The scenes were processed and analysed using Dragon image processing software (Goldin-Rudahl Sys. 1992).

Both visual interpretation and digital analysis of the images were used. Digital analysis was carried out by both supervised and unsupervised classifications using sequential clustering. In supervised classification the image analyst *"supervises"* the pixel categorization process by specifying, to the computer algorithm, numerical descriptors of the various land cover types present in a scene. Like supervised classifiers, the unsupervised procedures are applied in two separate steps. The difference is that supervised classification involves a training step followed by a classification step but in the unsupervised the images are first classified by aggregating them into the natural spectral groupings, or clusters, present in the scene (Lillesand and Kiefer 1994).

Different enhancement techniques such as filtering, band ratio, and histogram stretches were carried out for visual interpretation. Overlays of filtered bands 1 and 2 and those of linear stretches of bands 2 and 3, as well as the composite images of filtered bands 1, 2 and 3 were also used for visual interpretation (Figures 3.1 and 3.2). In the remainder of this chapter the techniques of image processing which are directly used in this research are described.

3.1.4 Digital Image Processing

In order to map landcover changes this method is best, especially for inaccessible areas in the Lar basin. In the following pages the principles of Image enhancement and Image classification which are used are discussed. These are useful techniques for identifying land surface changes in the Lar basin.

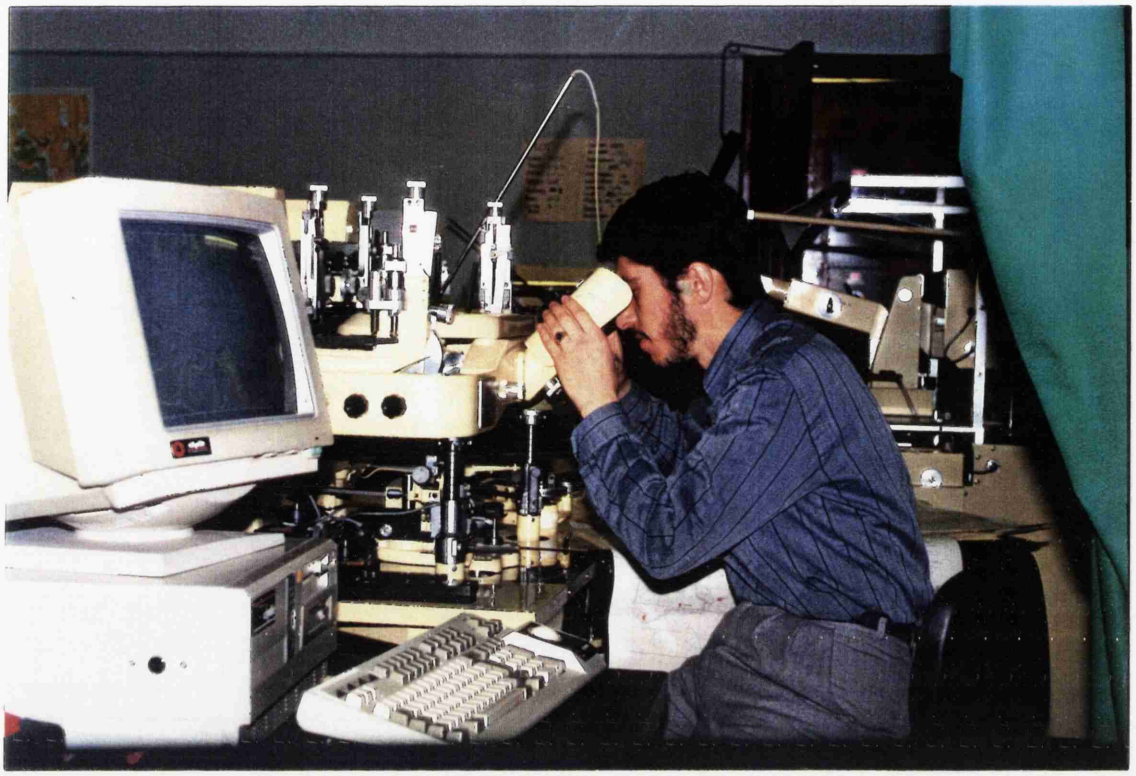

Figure 3.1: Aerial photographs plotting sediment volumes.

Figure 3.2: Digital image processing of satellite data.

3.1.4.1 Image Enhancement

The purpose of image enhancement is to render the images more interpretable, i.e. some features should become better discernible, which generally occurs at the cost of some other features which may be relatively unimportant in that specific context. It must be emphasized that the digital image should be corrected for radiometric distortions, prior to image enhancement, otherwise the errors also become enhanced. It is also possible to convert DN-values into absolute radiance or reflectance (physical) values before processing, enhancement and interpretation. The original satellite data, however, are generally poorly calibrated, and it is not considered worthwhile to attempt deduction of absolute physical values in most cases, as only relative DN-values are quite sufficient. There are no rules for producing the single "best" image for a particular application. A variety of digital filter (smoothing and enhancing) both in the space domain and in the frequency domain can be applied to data. The enhancement is successful if the analyst judges image appearance to be satisfactory. Secondly, image restoration is applied as a preliminary to digital analysis, but image enhancement prepares an image exclusively for subsequent manual interpretation. Thus when the analyst applies image enhancement procedures, there need be little concern for its statistical effects upon image data, a concern that should always be present when image restoration is attempted. The area of the ground represented by a multispectral SPOT pixel over a 60 kilometre swath requires an array of 3000 detectors per spectral band, sampled every 3 milliseconds, while a panchromatic pixel over the same swath width requires 6000 detectors per line, to be sampled every 1.5 milliseconds, thus producing a formidable amount of data which can only be successfully analysed by electronic image processors. Image enhancement can be divided into four main groups as: Single image manipulation, Multiple image enhancement, Enhancement by using colour, and Enhancement by synthetic stereo. The techniques used below were those which enabled identification of different morphological changes in the Lar basin.

3.1.4.1.1 Single Image Manipulation

The techniques developed over many years in the field of classical signal processing (e.g. Pratt 1978, Castleman 1977, Rosenfeld and Kak 1982) can also be advantageously applied to individual band/channel remote sensing images. The main types of these are as follows:

Contrast stretching (Fig.3.3-a and b), linear contrast streching or enhancement (Fig.3.3-c and 3.4-a,c), histogram stretch (Fig.3.3-a), special stretch (Fig.3.3e); multilinear stretching or piece-wise linear stretch (Fig.3.4-b); gaussian stretching; histogram equalization (Fig.3.4-d); density slicing (Fig.3.4-e); edge enhancement (Fig.3.5-a,b,c); and image smoothing (Fig.3.3, 3.4 and 3.5).

From the above techniques (used in this research) only those which were most useful are described below. For more detail on the others see Jensen, (1986), Richard, (1993) Lillesand and Kiefer, (1994).

(I) Gaussian Stretching

Another scheme of grey scale manipulation is gaussian, in which, the new grey scale is computed by fitting the original histogram into a normal distribution curve. It renders greater contrast in the tails of the old histogram, so that the cut-off limits of the old histogram are more critical in such a scheme. Gaussian stretching was useful for identification of bare soil and landslide areas in the Lar basin.

(II) Histogram Equalization Stretching

This is also called ramp stretching, cumulative distribution function stretching or uniform distribution stretching. In this method, input data are assigned to the display levels on the basis of their frequency of occurrence. Following a normal distribution, the pixels in the middle range happen to be most frequent. This approach to stretching makes all digital numbers equally frequent, i.e. the middle range is substantially expanded and made to occupy a larger of DN values in the new grey scale (Fig.3.4-d). It can be said here that this is a good transform when an individual image is to be displayed in black and white, but is not particularly recommended for making colour displays. Stream flows, fault lines, bare soil, and depositional areas (e.g. alluvial fans) were clearly identified using this technique in the Lar basin.

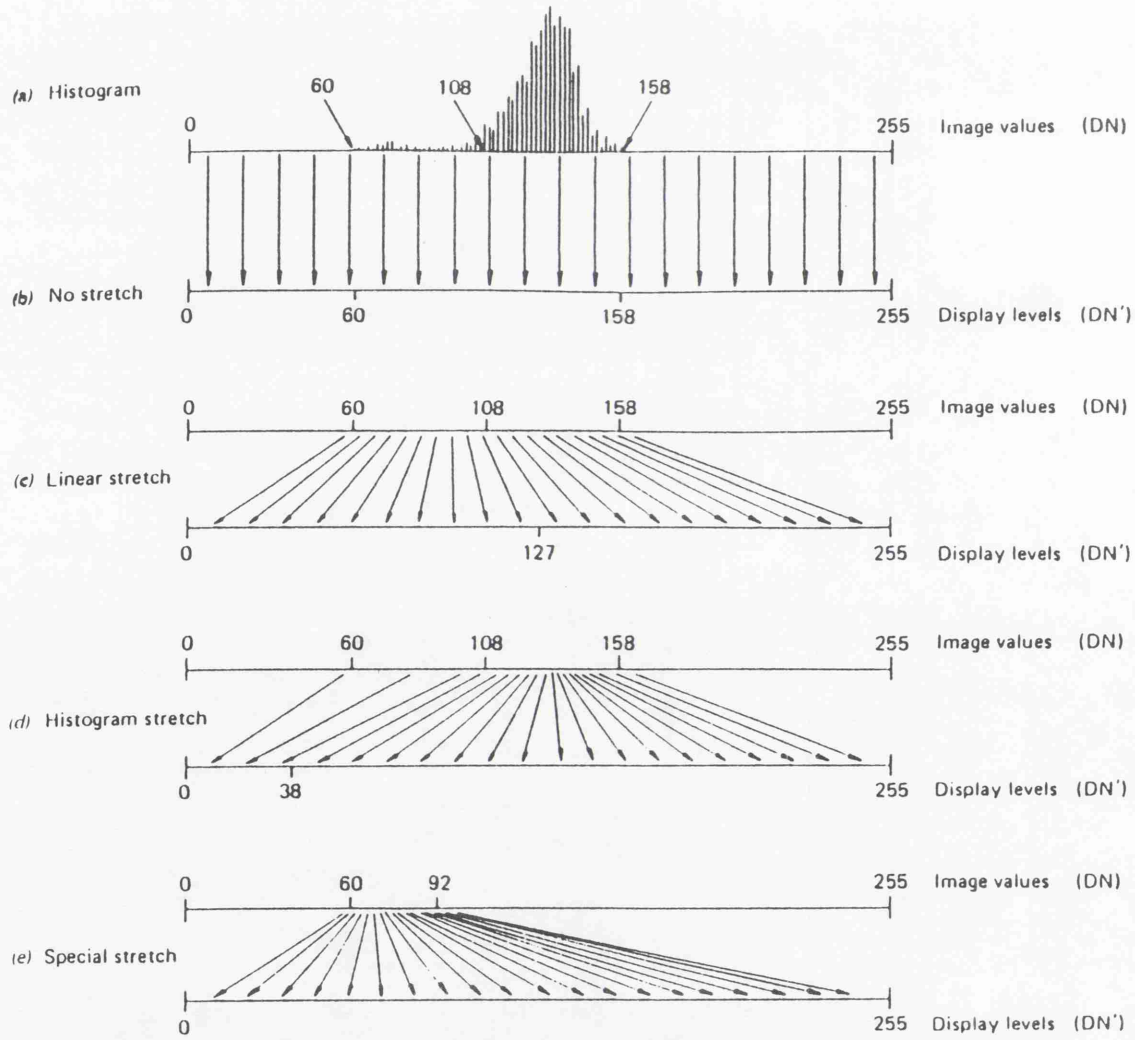

Figure 3.3: Principle of contrast stretching or enhancement, *(after Lillesand and Kiefer, 1994).*

(III) Edge Enhancement

Edge enhancement is an effort to reinforce the visual boundaries between regions of contrasting brightness. Typically the human interpreter prefers sharp edges between adjacent parcels, whereas the presence of noise, coarse resolution, and other factors often blurs or weakens the distinctiveness of these edges. Edge enhancement is in effect the strengthening of local contrast (Campbell, 1987). Rohde and Pohl (1978) describe an edge enhancement procedure used at the EROS data center. Output data is calculated using the original input value and the local average of five adjacent pixels.

Digital number plotting of a profile from one end of an image to another, could show that the profile consists of a complex combination of waveforms (Fig.3.5-a). It can be divide into: (1) high frequency variations (Fig.3.5-b), and (2) low-frequency variations (Fig.3.5-c). The high-frequency variations show local changes (e.g. from pixel to pixel), and low-frequency ones show regional changes, from one part of the image to another. The high-frequency variations which also called edges will be discussed. The edges in a remote sensing image are influenced by factors including terrain properties, vegetation, solar elevation, and season. This approach is a typical local operation in which the DN-values at a particular pixel in the new image depend also on the DN-values at neighboring pixels in the old image.

For computing of data in edge-enhancement, boxes or kernels, also called filter weight matrices are used. Figure 3.6 shows some oft-used kernels. There are no defined kernel sizes that would provide the best results in all cases. Dimensions of kernels are arbitrary and can be suitably chosen, the most common being 3×3, 5×5, 7×7 and 9×9. Odd-numbered kernel sizes are used so that the central pixel is evenly weighted on either side. Often the dimension of the kernel size is based on trial and error. It could be also be based on some statistical measure of the image, like the standard deviation of the first difference value in the horizontal direction (Chavez and Bauer 1982). The Dragon Image Processing System (DIPS), which is employed in this research, uses 3×3 filters. This means that the filtering algorithm considers the 8-pixels surrounding the "current" pixel as the spatial neighborhood:

n	n	n
n	x	n
n	n	n

Figure 3.6: Diagram of filter kernel (3×3).

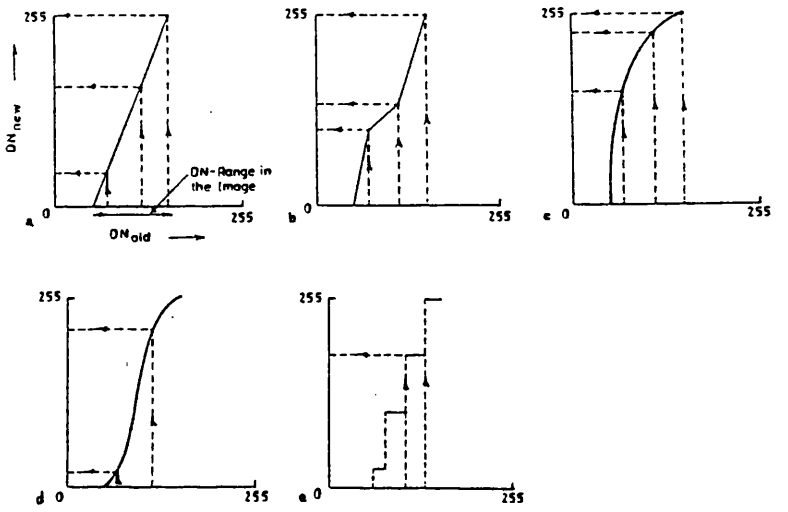

Figure 3.4: Transform for contrast stretching: **(a)** Linear contrast; **(b)** Multiple linear stretch; **(c)** Logarithmic stretch; **(d)** Histogram equalisation and **(e)** Density slicing *(after Gonzalez and Wintz, 1987).*

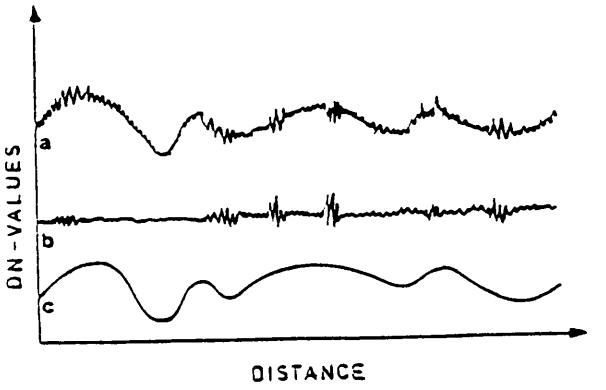

Figure 3.5: High frequency and low frequency components in an image: **(a)** A typical profile of DN-values is a complex combination of sine wave forms which can be split into **(b)** High frequency and **(c)** Low frequency components *(after Chavez and Bauer, 1982).*

X=current pixel whose value is being calculated, and n= denotes a neighborhood pixel, whose value contributes to calculations for the current pixel. Also, in the smoothing option, Dragon uses a kernel of all ones, as show in Figure 3.8.

1	1	1
1	1	1
1	1	1

Figure 3.7: An example of smoothing option (3×3).

To calculate the filtered value of the "current" pixel, this system multiplies each value in the filter function by the value of the neighborhood pixel in the corresponding position. It also multiplies the "current" pixel's value by the value in the center of the filter. These are added together and then divided by a scaling factor, which Dragon calculates as the sum of all nine values in the filter, but if the sum of filter values is zero, Dragon sets the scaling factor to 1. Therefore, the smoothing filter adds together 1 times the value of each of the nine pixels covered by the filter, and then divides the resulting sum by nine. In other words, it has the effect of replacing the "current" pixel's value with the average of that pixel's value and it's 8 neighbours, values. Figure 3.8 shows how the edge enhancement kernel is defined:

-1	-1	-1
-1	+9	-1
-1	-1	-1

Figure 3.8: The edge enhancement kernel (3×3).

There are several approaches of designing filter weight matrices and enhancing edges in digital images (Davis 1975, Shaw 1979, Peli and Malah 1982, and Jensen, 1986). The edge enhancement technique was very useful in detecting terraces, gullies, scree and landslides in the Lar basin especially on the SPOT and Landsat TM grey images.

(IV) Edge Enhancement Application for Geomorphological Investigation

As earlier described, the edge enhancement technique involves obtaining variations in Digital Number Values (DNV) in neighboring pixels. It is also called high-pass filtering or textural enhancement. The main aim of high-pass filtering as applied in the study area was as follows: **(1)** To access a sharper image containing more details that could be related to differences in topography, local vegetation, soil type, and morphology, to complete the related maps; **(2)**

Linear systems (edges) enhancement (microfractures, joints). Linear enhancement in specific directions can also be achieved using suitable anisotropic filters, although interpretation of such data has to be done very carefully; (3) Gross difference effects reducing illumination. Microvariations on an edge-enhanced image become important and large patches of any lithological unit under either bright or poor illumination are shown in similar tones. Thus it can help in bringing out more details within a larger shadowed or uniformly illuminated zone. A disadvantage of the high-pass filtering was that only local variations with respect to adjoining pixels were important and absolute DN-values had no significance, e.g. uniform large stretches of dark-toned basalt rocks and light-toned granites would show up in similar tones in the eastern side of Dalichai catchment (Fig. 3.9).

(V) Image Smoothing

Smoothing operations are used primarily for diminishing spurious effects which may be present in a digital image as a result of a poor sampling system or transmission channel. There are several ways of smoothing, like neighborhood averaging which is a straight forward spatial-domain technique. Given an N×N image $f(x,y)$, the procedure is to obtain a smoothed output $g(x,y)$ whose grey level at every point (x,y) is generated by averaging the gray-level values of the pixels of f contained in a predefined neighborhood of (x,y). The relation as below is involved the smoothed image, (for more datail see Gonzalez, et al., 1987; Richards, 1993; Lillesand and Kiefer, 1994).

$$g(x,y) = \frac{1}{M} \sum_{(n,m)\in s} f(n,m) \qquad [3/1]$$

In fact, the basic problem in employing this method is in being able to register the images so that corresponding pixels line up correctly. Low-frequency filtering of the spatial data is the main aim of image smoothing. In effect, its output is the reverse of edge enhancement. An example of image smoothing is given in Figure 3.10 from the Lar dam catchment. As image smoothing suppresses local variations, it is particularly useful when the aim is to study regional distribution over large geomorphological domains but in Figure 3.9 from same area shows that be useful in micro mrophological study. This method was also very useful for identification of limestone, bare soil, lineaments, lithology and deposition areas required to complete the related maps.

Figure 3.9: Edge enhancement from Landsat TM band-1, Lar basin.

Figure 3.10: Smoothing image from Landsat TM band-1, Lar basin.

3.1.4.1.2 Multiple Image Enhancement

The enhancement methods have been discussed for single images so far. Their classification was from the field of classical signal processing. One of the exceptional features of remote sensing is that it prepares data in multiple spectral bands, which allow bands to be superimposed over one another to identify information not readily seen on a single image.

Additionally, different sensor images, and platforms, or times can also be superimposed over each other with geometric congruence. In order to conceptually understand the results of combined multespectral images, it is necessary to know that two series of image data can be statistically represented through a two-dimensional plot as feature space: the feature axes here are the two spectral channels. In this space, any pixel location is controlled by the DN-values of the pixel in the two features, which can be repeated on, a scattergram. The scattergram can be approximated by a line when two channels are highly correlated (Figure 3.11-a), but two noncorrelated features produce a feature space plot in which points are scattered isotropically (Figure 3.11-b). The concepts of feature or cluster diagrams can be adapted to understand and discuss the various multiple image enhancement techniques, using simplified conceptual projection diagrams. In general the SPOT spectral channels used provide data which is generally corrected. This is shown by the pronounced elongated shape of the data points in a scattergram of SPOT bands 1 and 2 at Kamardasht, that is discussed in chapter 7.

3.1.4.1.2.1 Ratioing

Ratioing is the combination of one band with another and can be shown as various arithmic combinations of the data in an image as, grey-tone images of single bands, or as three-band colour images. This method was a useful operation for enhancing features on the SPOT multispectral images in the Lar basin. It is used to reduce the variable effects of topographic conditions, shadows, or seasonal changes in sunlight illumination angle and intensity. Transformations of the remote sensing data can, in certain instances, be applied to reduce the effects of such environmental conditions (Friedman, 1978). The output image is constructed by computing ratio of DN-values in two or more input images, pixel by pixel. The mathematical expression of the ratio function is:

$$DN_{output} = m\,[(DN_A \pm K_1)/(DN_B \pm K_2)] + n \qquad [3/2]$$

where DN_A and DN_B are the DN-values in A and B input images, K_1 and K_2 are factors to compensate for path radiance present in the two input images, and m and n are scaling factors for the grey range. The above form of the equation would squeeze the range when DN_B is greater than A and in this case, a better alternative is to use the logarithm (Moik 1980) or arctan functions of the ratios (Hord, 1982). Image for complex ratio parameters including additions, subtractions, multiplications and double ratios, can be produced similarly. The ratioed image can again be contrast-stretched or used as a constituent for other enhancements. Figure 3.12-a shows a two-channel plot in which lines of equal slopes have been drawn. The points have the same grey tone in the output, because all points on a single line have the same ratio value.

These ratioed data can not have information on the absolute or original values, as it depends on the relative reflectance in the channel considered. Principally, the ratio images enhance features when there are differences in spectral slopes (Figure 3.12-b). In this view, a ratio image can also be considered as a representation of spectral/colour information. The ratio values are actually influenced by path radiance including the sky-light component. If one takes the ratio values with shorter wavelength in the numerator and proceeds from poorly illuminated to well-illuminated topographical slopes of the same surface material, the ratio values are found to decrease with distance, i.e. in poorly illuminated areas, the ratio values with shorter wavelengths in the numerator are higher in comparison to those in well-illuminated areas (Kowalike and Lyon, 1983). For geomorphological applications the advantage of ratioing is that of providing a result which is quite independent of illumination conditions. The pixels acquire the same DN-output value if the earth surface has the same spectral ratio, irrespective of whether the ground happens to lie in a well or poorly illuminated zone. However, a properly made ratio image significantly reduces physiographic effects. SPOT bands 1 and 3, 1 and 2 and 1 and 3 have been combined by this technique which was useful for compositional discrimination of the land cover in the Lar upstream as is discussed in more detail in Chapter 7.

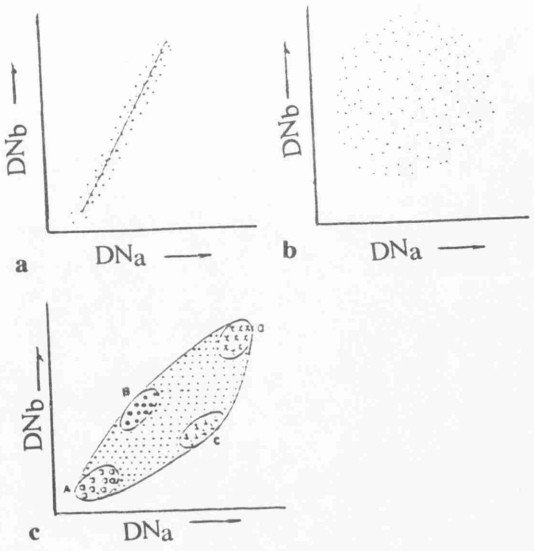

Figure 3.11: Concept of scattergrams: **(a)** extremely correlated feature axes; **(b)** non correlated feature axes, and **(c)** typical scattergram using two Landsat MSS bands *(after Drury, 1987).*

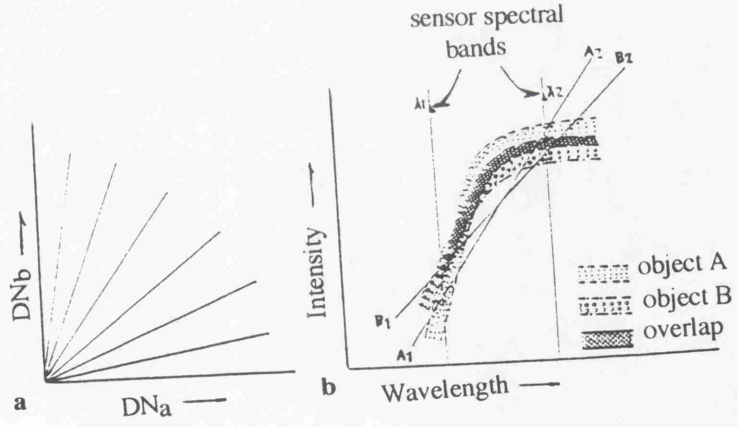

Figure 3.12: a Ratioing concept-figure shows a two-band plot in which lines of equal slopes have been drawn. All points lying on any single line have the same ratio and therefore acquire the same grey tone in the new ratio image. Therefore a ratio image depends on relative reflectance values in the component bands and is independent of the absolute albedo values. B shows spectral curves of two objects A and B, λ_1 and λ_2 being the two sensor spectral channels. The object A and B have overlapping spectral responses in both channels λ_1 and λ_2 and no single band is able to give unique results. However, if the ratio of the two bands is taken, the spectral slopes would be given by A1-A2 and B1-B2 lines, which makes discrimination between the objects A and B possible (after Drury, 1987).

3.2 HYDROLOGICAL AND SURVEY METHODS

Sediment and water discharge analysis can show the erosion rates in a basin, and be used to estimate the amount of the soil surface that is delivered down stream over time. The data interpreted in this research include water discharge and sediment concentration (daily, monthly and annual) from the Lar basin, Polour and Karesang stations; all obtained from the Ministry of Energy, Agricultural Ministry and Forest and Range Organization in Iran.

The aim of this approach was to have stations inside the selected study area and control stations outside. Sediment yield estimation from remote sensing data and from echosounding might well have no satisfactory accuracy, so the results of this analysis assist in reaching reliable results and assessing errors.

Regression analysis of sediment and water discharge was employed as a statistical tool. It was first used for filling in missing data and extending short records at selected stations by relating the available data at this station with that at adjacent stations. However it's application was broadened to cover the study of the relationship between two or more hydrologic variables and also the investigation of dependence between the successive values of sediment and water discharge. Therefore it was assumed that for two neighbouring stations there should be close correlation for total annual hydroclimatic data. For this purpose the daily suspended sediment discharge were interpreted at Polour station, (an outlet point for the present Dam basin) over a period of 18 years together with the discharge record for 46 years. In order to establish an estimate of these data over 43 years, the correlation between monthly average suspended sediment and water discharge was used to extend the record.

Sefid-Ab station in the middle area of the Dam basin, Gozaldarreh on the western side of the Lar Lake, and Dalichai station downstream have been extended by correlation with Polour station because of their limited discharge and sediment data. Finally, Karehsang

station some about 80 kilometres downstream of the Dam toward the Caspian Sea was selected as a control point for estimating sediment load (Figure 3.13). From this station the annual data for 28 years and the daily data for sediment concentration and discharge water were extracted. Then correlation between sediment concentration and discharge were applied to compare the different periods, before and after dam construction. The purpose of this was to compare how the blocked Lar basin affected sediment delivery downstream to Polour station. The same method was used for Karehsang station in order to show any dam-influenced control on sediment supply downstream. The annual average data of the sediment supply at Polour station was analysed to assess and compare the accuracy of the sediment supply derived by remote sensing data. Significant changes before and after the dam were shown by this method.

3.3 FIELD AND LABORATORY TECHNIQUES

The remote sensing interpretation of the geomorphological changes of the Lar Dam basin deposits formed a part of an extensive investigation in the field. Many morphological changes in the Lar basin are influenced by palaeo-sedimentation conditions. Therefore, field investigation of landforms and sediments was an important part of this work. These field investigation techniques were developed and modified over two summer seasons in 1993 and 1994. The selection of field sites follows those used for remote sensing techniques to allow direct comparison be attempted.

The selected sites were: (1) in the vicinity of the reservoir/Dalichai confluence; (2) Sefid-Ab/reservoir; and (3) Lar/reservoir (Figure 3.14). Detailed mapping was carried out to a scale of 1: 50 000 and the final maps present all surface observations. The geomorphology of the basin was also investigated on a more systematic basis by the production of a slope map. Figure 3.14 shows sampled areas at Dalichai, Sefid-Ab, Kamardasht, Chehelcheshmeh, Cheshmehkhooni and Asbkalak in the Lar basin where sediment characteristics were sampled.

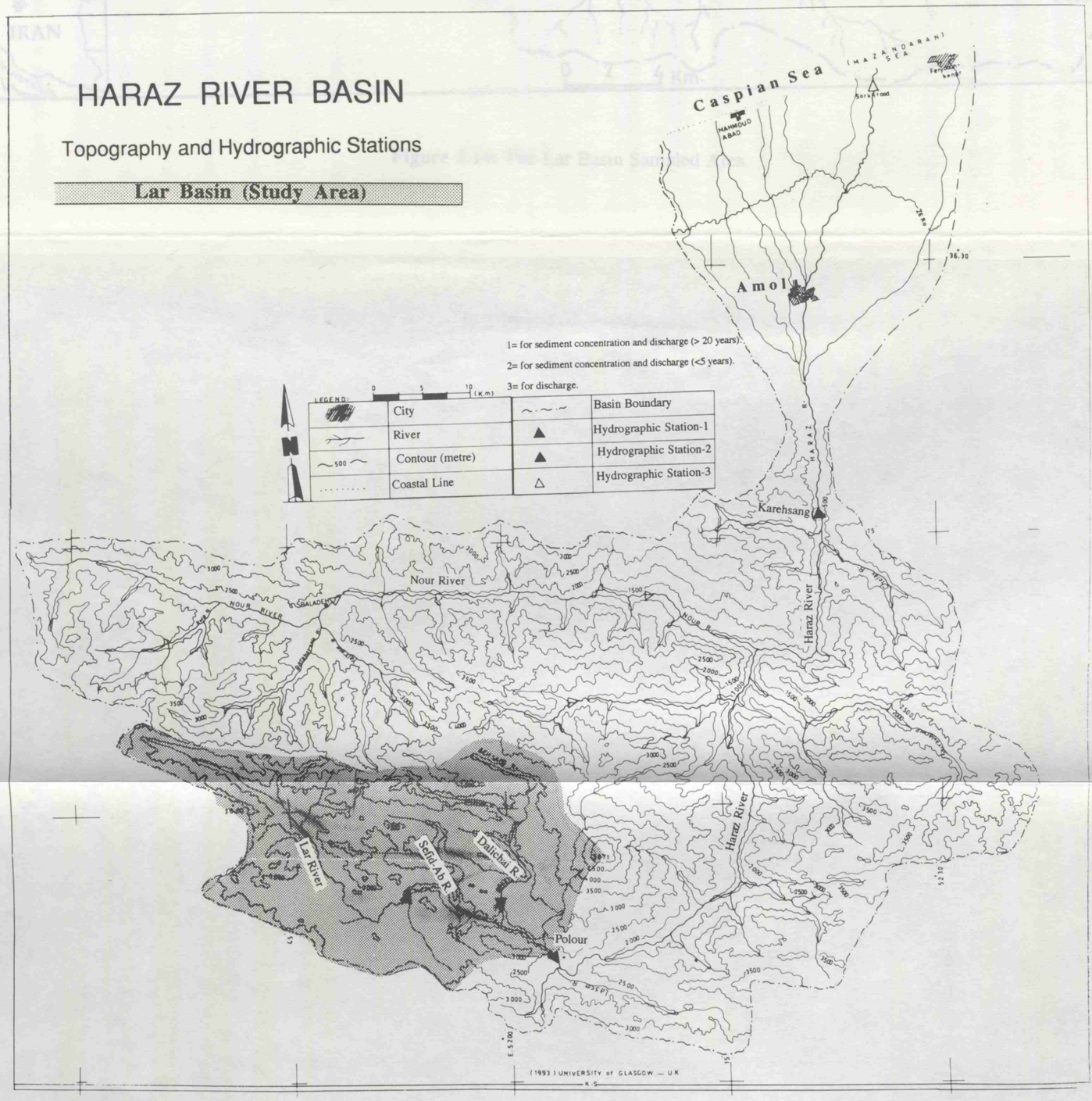

Figure 3.13: Location of the study area in relation to Haraz basin.

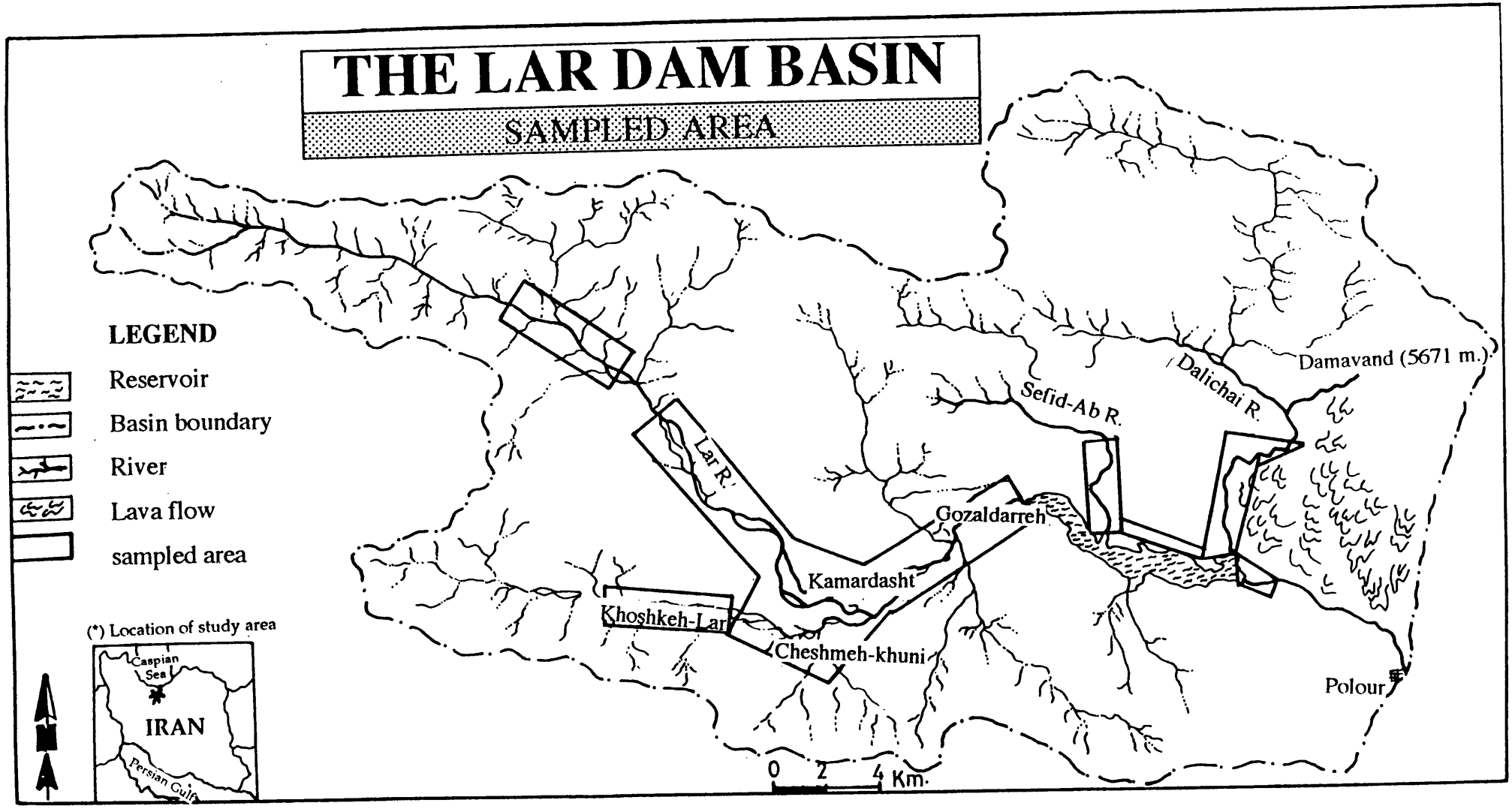

Figure 3.14: The Lar Basin Sampled Area.

3.3.1 Particle Size

The particle-size distribution is amongst the basic physical properties of geological materials. The determination of these parameters is therefore essential in any attempt to characterise fully the lithology of unconsolidated rocks (Gale and Hoare, 1991). This was carried out to help identify where the sediments come from and how they were distributed in the Lar basin by particle-size classification.

In the study area particle size of boulders and cobbles were measured directly in the field, granular and sand size were measured using sieves in the laboratory and finer sediments were measured using a variety of methods, including pipette analysis and hydrometry. This method was used to 100 particles from each site in 7 different sample areas in the Lar basin, were picked by a random selection procedure, from upstream to downstream including; 2 sites in Dalichai upstream and downstream, one site in Sefid-Ab, one in the Asbekalak, one in Khoshkehlar-Galehsardab and one in Imamzadeh Yorghidar (Figure 3.15-b, see also Figure 3.14 and Appendix Chapter 5).

3.3.2 Sieving Analysis

As mentioned above, some terraces were sampled to identify their characteristics and origins, from Cheshmeh-khooni, Sefid-Ab, and Dalichai. Samples were analysed by sieving and hydrometry (clay sizes). The samples from lower Lake deposits consisted basically of grey silts with some sands and gravels. A frequency histogram of the mean particle sizes of 38 sampled soil shows a marked peak in the fine to medium silt sizes. The upper Lake sediments are overlain almost entirely by more recent river and reworked colluvial fan deposits as terrace gravels. The frequency histogram of the distribution of mean particle sizes plotted from 42 sampled soils indicates that there is a slightly wider spread than with the Lower Lake sediments (Figure 3.15-a).

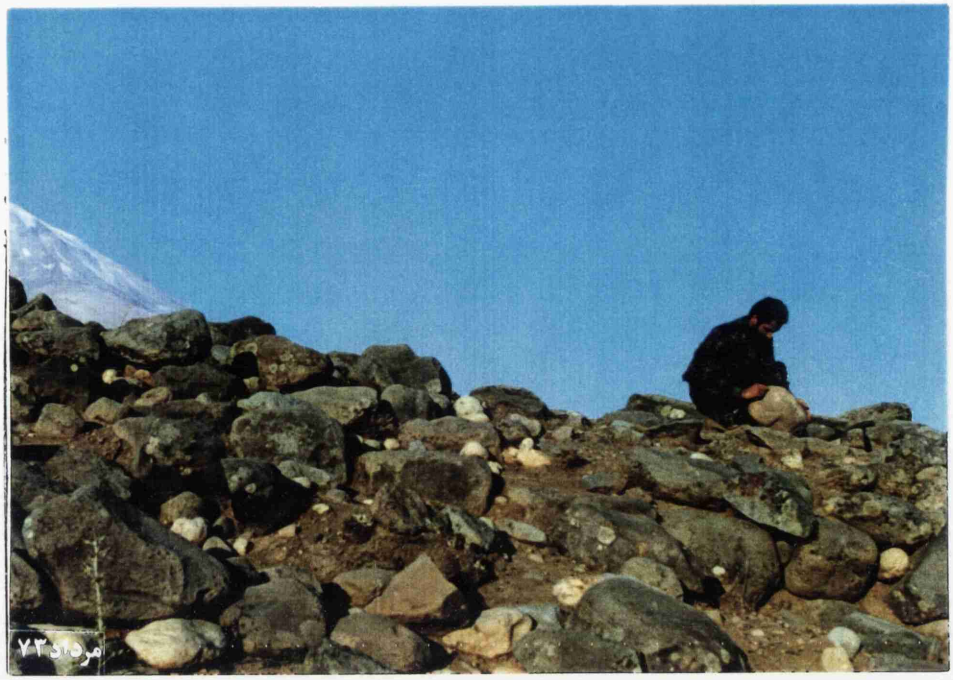

Figure 3.15-a: Surface observation in the field, (Dalichai basin, size measurement).

Figure 3.15-b: Analysis of sampled material after field work.

The location of sampled areas is shown in Figure 3.14. Sediment samples were selected to be as representative as possible of the entire deposit; where there was considerable variability in a deposit more than one sample was collected, e.g. Lar upstream at Cheshmehkhooni. From this site 7 samples were collected with fine sediments and at least 200g for each sequence. One soil sample was collected at Chehelcheshmeh in the Lake Lar west end and also one between Gozaldarreh and Sefid-Ab which were identified on remote sensing data as deposition areas. Except for the soil sample from Chehelcheshmeh all samples from Lar upstream and downstream as well as those collected from terrace sections are described in chapter 5. The collected sediment samples were returned to the laboratory for sieving analysis. They were washed, dried and split according to the method outlined by Buller and MacManus (1973).

Each sample was sieved at 0.25∅ intervals and the resultant data plotted up as cumulative percentage curves which are described in chapter 5. Particles were grouped into size related categories of sand, silt and clay. This scheme was developed by Udden (1898) and expanded by Wentworth (1922), but since most sediments have a log-normal particle size distribution, a transformation is commonly used called the phi-scale (Table 3.1). This has an origin at 1.00 mm and dimensionless units (phi-units) which are given by;

$$\varnothing = -\log_2 (D) \text{ and } D = 2^{-\varnothing} \qquad [3/3]$$

where ∅ is the particle size (phi-units);

D is the particle size (mm),

Table 3.1: Phi-unit to millimeter conversion table and the size ranges.

Sediment type	Size/mm	Size/∅ units
boulder	>256	<-8
cobble	64-256	-6 to -8
coarse gravel	16-64	-4 to -6
medium gravel	8-16	-3 to -4
fine gravel	2-8	-1 to -3
very coarse sand	1-2	0 to -1
coarse sand	0.5-1	1 to 0
medium sand	0.25-0.5	2 to1
fine sand	0.125-0.25	3 to 2
very fine sand	0.0625-0.125	4 to 3
coarse silt	0.0312-0.625	5 to 4
medium silt	0.0156-0.0312	6 to 5
fine silt	0.0078-0.0156	7 to 6
very fine silt	0.0039-0.0078	8 to 7
clay	<0.0039	>8

In the study area three different methods used for particle size: for boulders and cobbles size was measured directly in the field as mentioned above, granule and sand sizes were measured using sieves; silt sizes and finer were measured using a variety of methods, including pipette analysis and hydrometry. Once plotted the median and mean grain sizes could be extracted from the graphs. These values were obtained using the formulae given by Leeder (1982).

$$\text{Median grain size (Md)} = \varnothing_{50}=2^{-\varnothing}\ \text{mm} \qquad [3/4]$$

$$\text{Mean grain size } (\mu) = [\varnothing_{16}+\varnothing_{50}+\varnothing_{84}]/3$$

$$\text{Sorting } (\sigma) = [(\varnothing_{16} - \varnothing_{84})/(4)] + [(\varnothing_{25} - \varnothing_{95})/(6.6)] \quad [3/5]$$

$$\text{Skewness (sk)} = [[\varnothing_{16} + \varnothing_{84} - 2\varnothing_{50}]/[2(\varnothing_{84} - \varnothing_{16})] + [\varnothing_{5} + \varnothing_{95} - 2\varnothing_{50}]/[2(\varnothing_{95} - \varnothing_{5})] \quad [3/6]$$

3.3.3 Particle Shape

Shape, together with size and composition is one of the fundamental properties of particles. The determination of the shape of particles is therefore essential to the overall characterization of geological material (Gale and Hoare, 1991). This method is an important element of sediment populations since it is related to the dynamic conditions under which sediment transport and deposition occurs. The relative lengths of the three major orthogonal axes of the particles were measured. For this aim any particle is considered to have an *a*-axis, the longest axis, a *b*-axis, the longest axis at right angles to *a*-axis, and a *c*-axis, the shortest axis which is orthogonal to both the *a* and *b* axes.

Zingg (1935) gives an index of the shape of the particle and how it approximates to a Sphere, (all three axes nearly equal in length) to a Disc or Plate (with one axis much shorter than the other two) to a Blade, (with one axis much longer and one axis much shorter than the *b*-axis) or to any intermediate form. The Zingg system (1935) divides particles into four categories are as follows;

Bladed, for which both axial ratios are less than 0.667; Discoid, for which the b/a ratio is greater than 0.667; Roller or Prolate, for which the c/b ratio is greater than 0.667; and Sphere or Equant, for which both axial ratios are greater than 0.667 (Figure 3.16).

3.3.4 Echo-Sounding

Because there is no sedimentation record for Lake Lar, field survey was required. Therefore, a Radio Echo Sounder (Sea Farer-700) was employed, concentrating on the

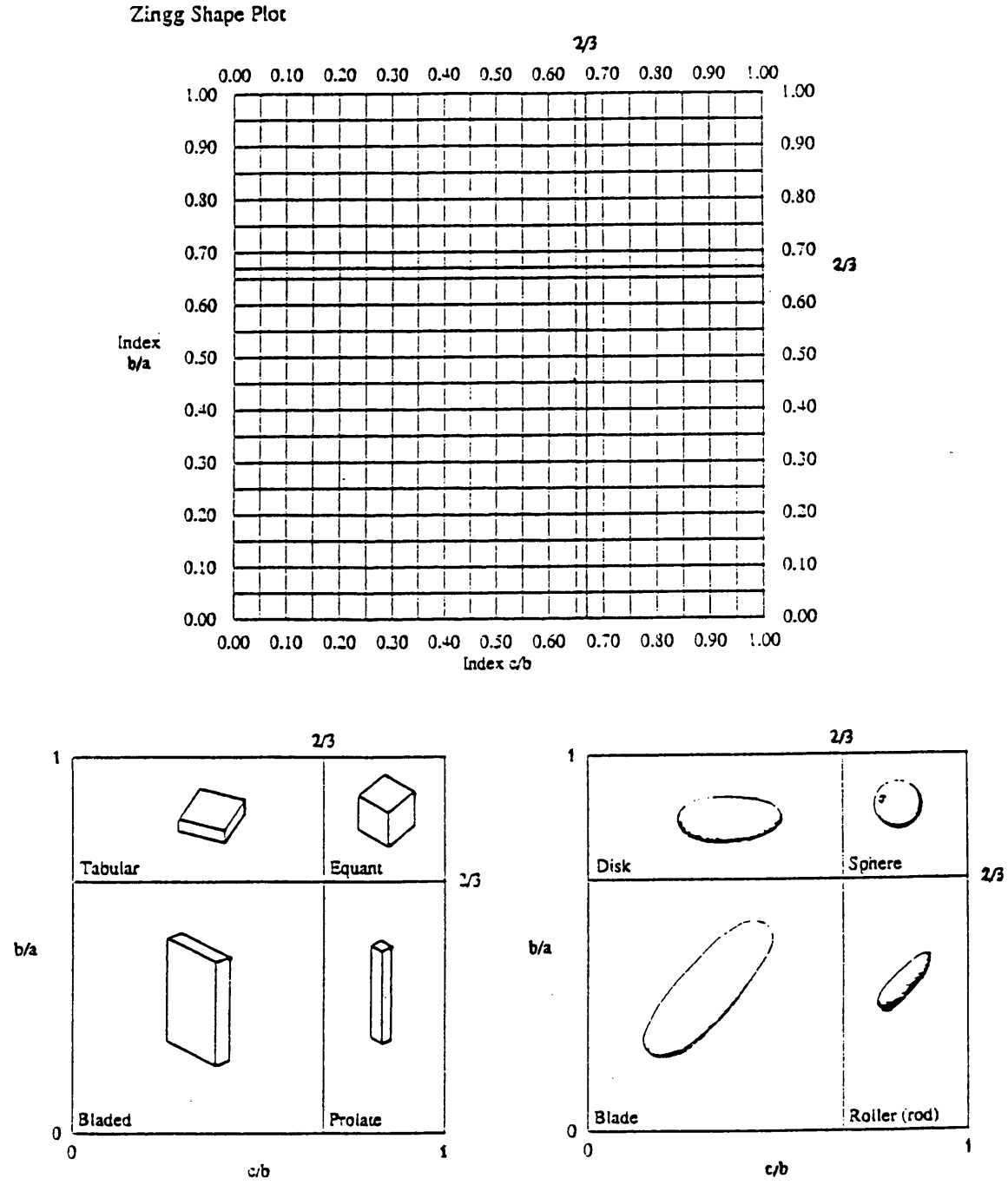

Figure 3.16: Zingg Shape Plot and Particle Shape Analysis.

deltas of the Dalichai, Sefid-Ab and Lar rivers into the Lar lake. Positions were identified by boat path surveying on the shoreline of tributary streams and by using a compass on the boat. For more accuracy of bathymetry the surveys were related to absolute heights at the Dam site.

The start and end points of each echosounding run together with intervals across the deltas were selected and surveyed and linked to the height and location of the control points. The equipment for this method included an echosounder, boat, compass, map and theodolite.

(a) for each delta area, selected survey lines radiated out from centre of the delta into deep water. With different delta conditions, nine lines at Dalichai, 11 lines at Sefid-Ab and 10 lines at Gozaldarreh were selected to define the extent and depth of the delta limits (Figure 3.14).

(b) in the boat, the start point was fixed by compass bearings on prominent land marks that were clearly identifiable from the boat and on map. A start reading was taken on the echosounder.

(c) the boat then moved along fixed compass bearing out into the lake keeping at a constant speed with the depth recorded at fixed time intervals of about 30 secs.

(d) the end point of the survey line was fixed by three compass bearings as before.

(e) for each delta a topographic map was produced to be used for sediment volumetric estimation in combination with topographic maps and aerial photography.

3.3.5 Control Points for Aerial Photos Stereo Model

Control points were surveyed in the field for control areas and transferred on the air photos for the purpose of making stereo models of the Dalichai, Sefid-Ab and Lar mouth areas. These sites were selected in and near the valley bottoms, as areas of deposition. They were precisely located and their heights accurately surveyed relative to absolute benchmarks in the Lar Dam Basin. For each overlap area of photographs about 6 points were surveyed as they were needed to ensure the accuracy of photogrammetry. These

points were then transferred to aerial photographs from 1955 and 1970 from which were derived topographic maps for sediment volume estimation.

3.3.6 Vegetation Survey

Vegetation characteristics were mapped in selected areas as controls for remote sensing data, along with the relative erosion state of the ground. For each of the sub-catchments of Dalichai, Sefid-Ab and Lar a small control area (maximum 10×10 metres) was chosen for more detailed mapping of species type, percentage vegetation and bare ground cover. As described before the Lar basin is mostly inaccessible, therefore the best technique for land cover assessment was remote sensing data. Different classification techniques were used to identify vegetation cover which will be described in Chapter 6. To increase accuracy, ground control in the field and on aerial photographs were very useful. According to type and density the vegetation was classified into four main groups. The areas of these four groups were calculated on aerial photographs for whole basin. Finally vegetation condition was assessed for 7 catchments including; Lar, Khoshkehlar, Alarm, Sefid-Ab, Imampahnak, Siahplas and Dalichai, then integrated on a vegetation map of the Lar basin. For comparison of vegetation changes between 1945 and 1994 (obtained from old maps and sequential aerial photographs) two different vegetation cover maps were derived which will be described and discussed in Chapters 6 and 7.

3.3.7 Volumetric Calculation of the Lar Basin Sediments

To provide a link between morphological changes and sedimentation, three methods were used. As mentioned before, sediment concentration data covered the whole dam basin at Polour, plus an estimation of bedload percentage for the study area. This method can be used for a comparison of sediment budget and its fluctuation before and after dam construction and also as a control point for the volumetric sedimentation data from the basin. For river deltas, deposition features and terraces, echosounding data and aerial photographs, maps and borehole data were employed to establish the upper and lower

limits of the sediments within the various postulated contour lines, therefore an estimate can be produced of the volume of sediment deposit in selected sites. For this purpose the approach from Smith et al (1960) was used as follows;

$$V = h\,(A+B+\sqrt{AB})/3 \qquad [3/7]$$

where V=volume of sediment (m^3).

A, B= the areas enclosed by two contour lines (m^2).

3.4 PROBLEMS

The main aim of using remote sensing data was to overcome the problem of inaccessibility of the Lar basin. However, there are problems related to the use of remote sensing data for this kind of discrimination. The main shortcoming was ground resolution, 79×79, 30×30 and 20×20m respectively for Landsat (MSS), (TM) and SPOT data. A second problem in the study area was the effect of shadow due to the mountainous terrain, especially in the Dalichai, Sefid-Ab and Lar upstream areas. Other limitations relate to differences in the vegetation cover, which produced overlapping classes in the classification process.

3.4.1 Topographic and Atmospheric Effects

Uneven topography leads to a varying local angle of incidence of light, so that ground illumination and intensity of back-scattering also vary accordingly. The local landscape position and orientation with respect to sensor and the sun are important factors in controlling this. Slope (direction and magnitude) is thus one of the most important single factors affecting the intensity of back scattered radiation (Stohr and West, 1985). The reflected radiance may also vary at different times of the day. Topographical effects on reflected radiance data can be so severe, especially in the Lar high relief area, that correlation and extrapolation of photo units on the basis of simple tonal signatures may some times be impossible. The Lar basin slopes are extremely steep and altitude varies from 2200m to 5671m within a few tens kilometres. The major problem created from this factor is that shadow is often misclassified with low reflective, features, particularly with

the poorly reflecting dark layers of the formation and the river channels in the northern parts of the study area, (e.g. in TM and SPOT maximum likelihood classification, shadow from high relief areas has got the highest error of omission respectively 58% and 44%).

Haze, aerosols and suspended particles in the atmosphere increase scattering and path radiance and should be considered at the time of interpretation of image data (Nelson, 1985). Atmosphere conditions prevailing at the time of observations play an important role e.g. cloud cover blocks the solar radiation and casts shadows on the ground, limiting the effective ground area to be sensed and also possibly increasing the atmospheric path radiance to some extent. For overcome these effects on the imagery different type of data acquired at different times and sensors were used by visual and image processing techniques. One effective method for enhancing the suppressed detail of heavily shadowed valley sides incorporates a "mirror type principle" which accentuates the subtle differences of shadow areas according to their degree of contrast with brighter adjacent slopes. Unfortunately the software for this process was not available in Glasgow.

3.4.2 Geometric Correction

Raw digital images usually contain geometric distortions so significant that they cannot be directly used as maps (Lillesand and Kiefer, 1994). There are a large number of combinations of effects due to different kinds of platform instability, optical and mechanical distortions in the radiation-gathering set up, earth curvature, atmospheric refraction, and both parallax and scale effects resulting from topographic relief. Apart from the last two effects, these are amenable to quite simple corrections. Where precise information about platform attitude and track relative to the Earth's rotation is available, this can be built into automatic correction programs.

The digital image data used in this study was geometrically corrected, and matched against a reliable 1:25 000 base map (British Army, 1945) for the Lar basin. This map was also helpful for correcting aerial photographs and KFA-1000 images. In order to evaluate the geometric performance of the KFA-1000 image data, ground control points were selected for a test area covered by aerial photographs and the 1:25 000 topographic map. These control points were surveyed in field and after transformation to aerial photos and topographic map then used to determine the land mapping for individual images and, on

the other hand, to investigate the accuracy of single images and of KFA-1000 stereopairs of the Lar basin.

It should also be noted that KFA-1000 imagery is suitable for stereoscopic analysis, in that adjacent scenes have an overlap of 60%. In this study four overlapping images acquired in June 1990, in order to observe topographic effects qualitatively, but have not gone on to produce stereo models of the terrain. The following simple expression used to calculate the heightening accuracy (Δh) of this stereoscopic imagery (Rees, 1990):

$$\Delta h=(2H\Delta h')/s \qquad [3/8]$$

Where H is camera altitude, $\Delta h'$ is the accuracy of measurement of relief displacement on the film, and s is film width with a normal camera altitude of 270km, an estimate of 25 μm for film measurement accuracy, and a film width of 0.3m, focal length of 1m., the accuracy of height determination from KFA-1000 can be calculated as 45m (G. Petrie, personal communication, 1994). Film measurement accuracy can be defined by analyst choice of digital interval and take no account of film instability. This suggests that high relative accuracies should be obtained for local areas, but absolute errors will increase over larger regions due to the increasing effects of film distortion. Film distortion errors are likely to dominant over these associated with optical errors in the lens, (Dowdeswell, et al. 1993).

3.5 MAP PRODUCTION

As described earlier, some parts of the Lar basin are extremely inaccessible so remote sensing data were used in map generation. Aerial photographs are the most appropriate for spatial assessment of surfaces, but are not always good enough for discrimination of different ground cover types. However, because of poor spatial accuracy from the SPOT and Landsat and the better quantitative accuracy from aerial photographs, it seems that a combination of these two methods represents the best solution for identifying boundaries and characteristics of different classes of surface for mapping.

The primary data source for mapping the land cover was corrected aerial photography, and colour KFA-1000 obtained by Iranian Geographical Organization at 1:50 000 and

1:270 000 respectively. KFA-1000 coverage was obtained in June 1990 (high vegetation season), and aerial photographs in September 1955 (early snowing season). Growing season SPOT and Landsat from June 1987 and September 1988 were also available for the Lar basin. All KFA-1000 images were of good to excellent quality but because of (1:270 000), enlargement was needed to aid the land cover interpretation. Thus they were to enlarged to at 1:100 000, and used with the base maps at 1:50 000 (vegetation, soil erosion and geomorphology) and a 1:100 000 soil map.

A mapping scale of 1:50 000 was selected for several reasons. The interpretable limit of 1:50 000 aerial photos with high quantitative accuracy presents larger scale mapping. The small size of some areas of particular land cover classes (e.g. gully or slope scree) necessitated a large mapping scale. The 1:50 000 topographic and geology maps of the basin cover all of the sample test sites in a reasonable number of map sheets, and includes other data including topography, morphological features, vegetation, soils and surrounding drainage patterns. These established maps series meet the national map accuracy standards and provide reliable a geometric control for the Lar basin and its land surface classes.

The land cover classes delineated on the SPOT and Landsat images were also identified manually on the KFA-1000 imagery, by using field checking in the accessible areas and aerial photograph control for the more inaccessible parts of the study area. This assisted in modifying the selected sites (classes) to maximise the information derived from the remote sensing data. Interpreted data were then transferred to the appropriate 1:50 000 map. The registration of the land surface data was accomplished by the use of visual interpretation and co-ordinate locations. For the less detailed SPOT and Landsat images, colour KFA-1000 was helpful, because it was up to date (June 1990). A KFA-1000 stereoscopic interpretation key was developed for each test site and was especially useful for plotting vegetation and geomorphology in the Lar basin. In addition, a morphotectonic map derived from KFA-1000, with aerial photographs and field checking was produced. A 1:50 000 slope angle map was also produced from the topographic map.

3.6 SUMMARY

In general terms, the field investigation consisted of surface observations in natural and artificial exposures, sub water surface investigations, utilizing Echosounder and sinkholes, laboratory testing of selected samples, and field surveying in three sites of Dalichai, Sefid-Ab and Gozaldarreh. The holes, both natural and drilled, before and after the Dam were very helpful for interpretation of morphological changes and sedimentation in the Lar basin. Remote sensing techniques including aerial photographs were very useful in identifying land surface characteristics and morphological changes which were combined with field on the and completed morphology, lithology, vegetation and morphotectonic maps. For sediment volumes, combined data from aerial photographs, topography maps and echosounding surveys provided significant results for comparison with hydrometric results. Finally sediment concentrations and water discharge correlation show significant reduction in sediment load after the dam construction on the Lar river, which is being deposited in the reservoir.

CHAPTER 4: PHYSICAL CHARACTERISTICS

INTRODUCTION

In order to identify geomorphological changes, monitoring of physical environments are of considerable importance and records of the landcover at appropriate time scales are essential (Crapper and Hydson 1983). The aim of this chapter is to review the characteristics of the physical environment of the Lar basin which influence land surface changes. The chapter format will be as follows:

(1) Climatic characteristics (temperature and precipitation) of the Lar basin; **(2)** Physiographic analysis at different sites; **(3)** Geology, stratigraphy and lithology; **(4)** Vegetation characteristics, and Linkage between the physical factors and surface processes of the study area.

4.1 CLIMATE

Climatic conditions, in respect to amount and type of precipitation, temperature and also their seasonal distribution, can influence both the morphological changes and sediment delivery ratio of river basins. Where high intensity storms occur on watersheds at a time when cover conditions offer minimum protection against erosion, the rate of gross erosion will be high. Where maximum rainfall energy occurs during periods when the ground surface is frozen, lower rates of erosion prevail. Where such precipitation occurs in sufficient amounts to create runoff, sediment is transported in varying amounts, depending upon the nature and frequency of the runoff.

The Haraz River basin is 4000 km^2 in area and lies between the altitude of -24 metres (the Caspian Sea) and 5671 metres (Damavand summit). One hundred kilometres lie between the Lar dam and the Caspian Sea but there is a very varied environment. Air masses from the northwest come across the Caspian Sea, reach the Alborz Ranges and rise with the resulting orographic precipitation. The northern part of the Haraz basin is wet (over 1000 mm precipitation annually) and the southern parts, including the Lar Dam basin, are semi-arid (Table 4.1&2 Appendix Chapter 4, enclosed floppy at back). The climate stations used in this thesis are inside the Lar basin, at Polour and at Panjab, Razan, Nemar, Karehsang, Amol stations (Figures 4.1-4.6, see also Figure 3.13).

4.1.1 Temperature

Temperature and statistical data for the Lar basin were analyzed from Polour station from 1956-1985. The data show that July is the warmest month (average of 18.2 °C) and January is the coldest month (average of 5.4 °C). Minimum temperature is recorded at -40 °C in January and maximum was for July at 42 °C. The main feature is the long cold season from November to April. The temperature regime for Polour shows a sinuous form that suggests a comparatively arid area with about five months of drought (Figures 4.1 and 4.2).

4.1.2 Precipitation

The mountainous nature of the Lar dam basin means that both snow and rainfall occur. The mean annual rainfall in the Lar basin is generally between 430 and 600 millimeters but over the period of maximum precipitation, it falls mainly as snow.

For the 20 year period at Polour station (Figure 4.3) an annual rainfall of 180 millimeters is exceeded with a 95% probability. The Lar basin upstream compares with the Haraz river basin, the Middle area and Downstream rainfall data as follows;

On the Haraz, the annual average rainfall at Panjab is 211.5 millimeters over a period of 18 years, at Nemar 411.1 millimeters over 23 years, and at Razen 345.7 millimeters over 16 years, Karehsang 907.2 millimeters for 20 years and Amol has 676.8 millimeter over 11 years. In the Lar, Polour has 437.4 millimeters for a period of 20 years (Figure 4.4 & Table 4.1).

Table 4.1: The Lar Basin annual Average Precipitation in Relation to the Haraz Basin.

Station	Rainfall/mm
Polour (upstream, Lar)	437.4
Panjab (middle Haraz)	211.5
Nemar (middle Haraz)	411.1
Razen (middle Haraz)	345.9
Karehsang (downstream)	907.2
Amol (downstream)	676.8

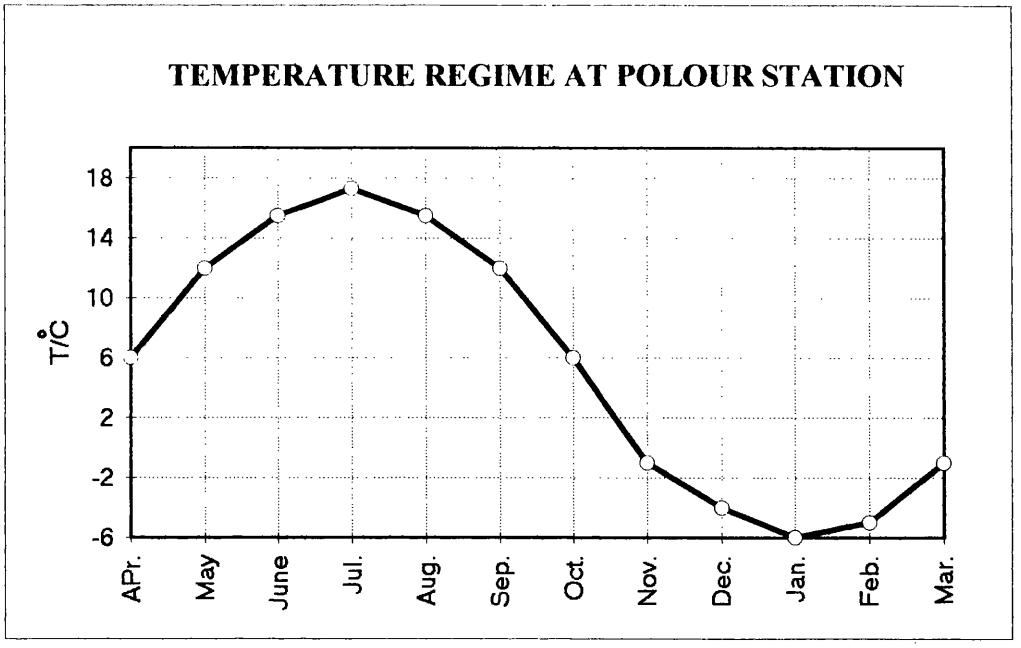

Figure 4.1: Average monthly temperature at Polour.

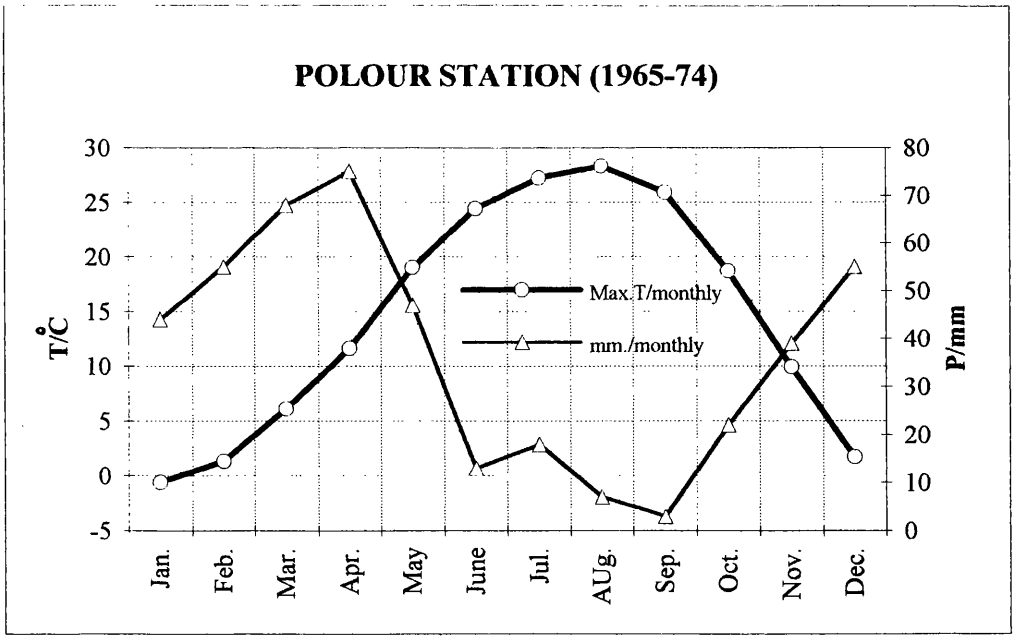

Figure 4.2: Precipitation and maximum monthly temperature at Polour.

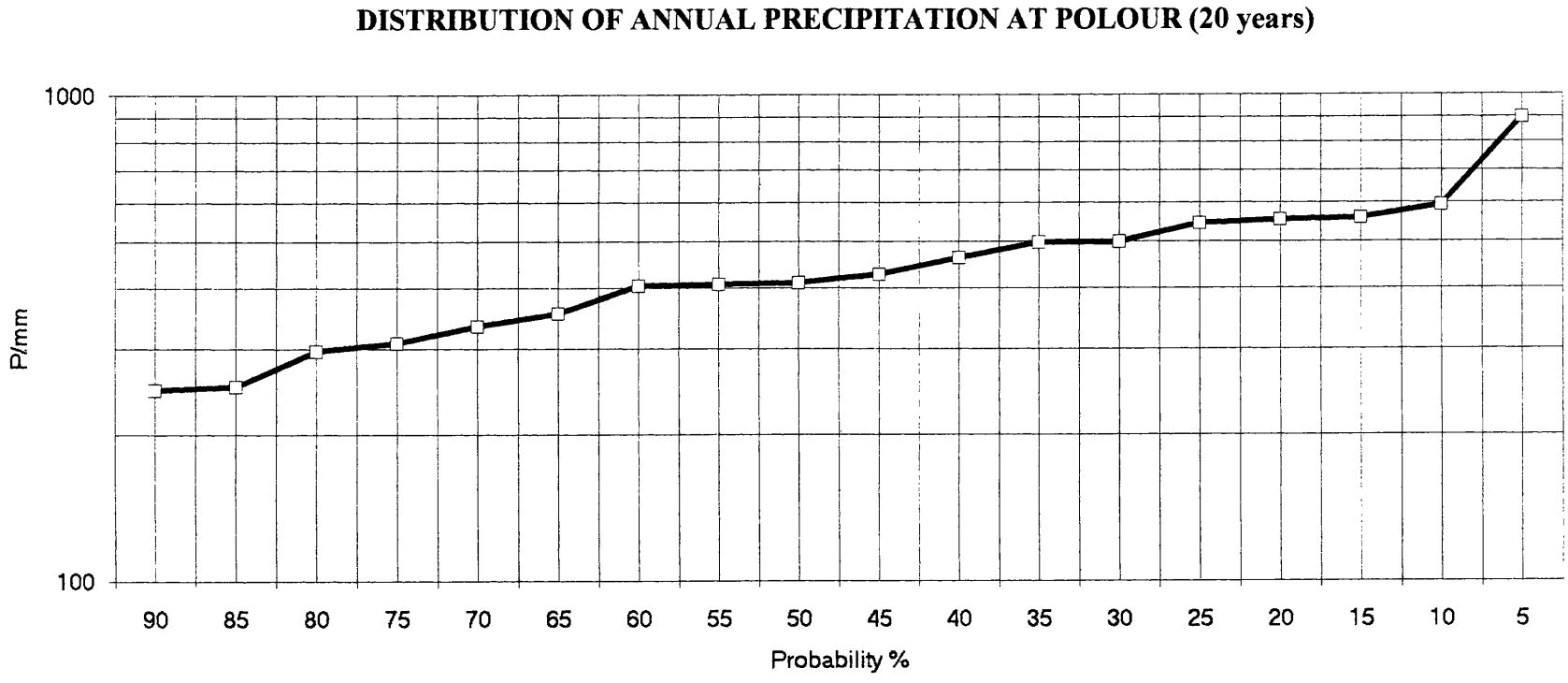

Figure 4.3: Annual precipitation at Polour station.

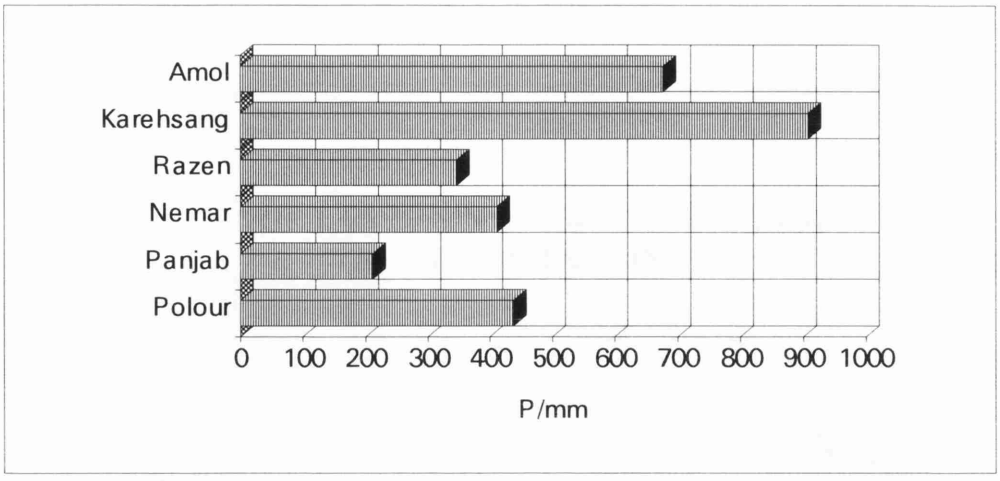

Figure 4.4: The Lar Basin Precipitation in Relation to the Haraz Basin.

The results show significant patterns in the precipitation related to **a)** the physical conditions of the upstream parts which include orographic conditions and **b)** the influence of the Caspian Sea which produces frontal precipitation. The Lar dam basin precipitation and temperature analysis at Polour station also shows that this area has a Mediterranean climate. In this type of climate maximum precipitation is related to the winter season with a dry season in the summer. In different parts of the basin, short period climate data have extended the precipitation record (Figures 4.4 and 4.5, see also Figure 4.6-a and Appendix Chapter 4, enclosed floppy at the back). This shows that precipitation in western part of the Lar (Khoshkehlar and Lar sub basins) is more than other parts, although eastern Dalichai with active orographic conditions is mostly covered by snow.

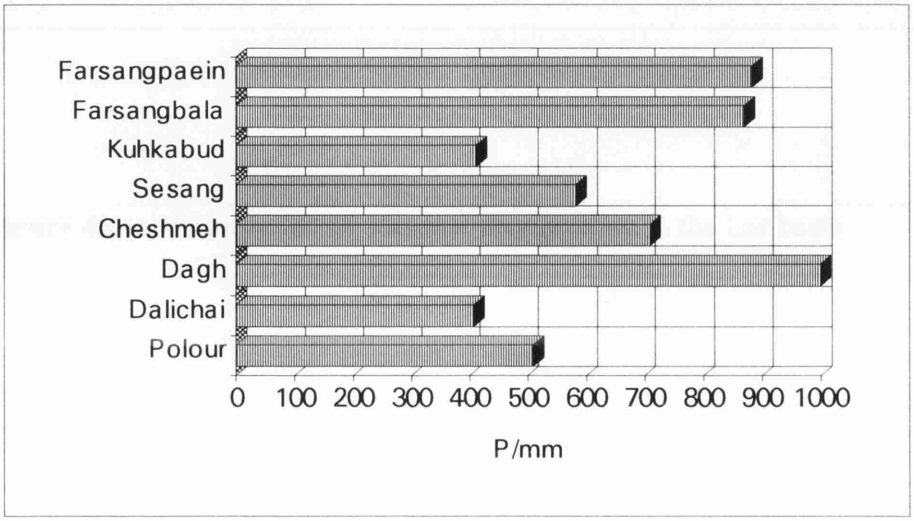

Figure 4.5: The Lar basin Annual Average Precipitation.

4.1.3 Annual Precipitation

For the most part, geomorphological studies require knowledge of precipitation over a definite area, the size of which may vary from a small parking lot to the drainage basin of a major stream. Because precipitation information collected with a raingauge represents conditions at a point, methods are required to transform point precipitation into information representative of the entire area.

The simplest method of calculating annual precipitation is to use the arithmetic mean of all the raingauge totals in the area by *station average* method, a technique which may give adequate results if there is an even distribution of gauges and if the area is fairly flat. In other situations, however, and particularly in mountainous area, where rainguge sites may be rather unrepresentative, the results obtained may be substantially in error.

$$\text{(station average) } P_{avg} = \left(\sum_{i=1}^{N} P_i / n\text{-}1 \right) = 689.7, \text{ Lar \& } 668.5, \text{Haraz}$$

Another method using *Thiessen* polygons makes some allowance for the uneven distribution of gauges throughout the area, and also enable data from adjacent areas to be incorporated in the mean. The Thiessen method weights each station in direct proportion to the area it represents without consideration of topography or other characteristics (Movahhed, 1983). This method employs perpendicular bisectors through the straight lines joining adjacent gauges, leaving each gauge in the centre of a polygon which will vary in size according to the spacing of the gauges. The percentage of the total area of the Haraz basin represented by each polygon or part of a polygon is calculated and applied to the appropriate raingauge total. These are then added to give the average precipitation which, in the case of the Lar catchment shown in Figure 4.6-b is 665.4mm and for the Haraz is 556mm.

$$*P_{avg} = \sum_{i=1}^{N} P_i A_i \div \sum_{i=1}^{N} A_i$$

*(annual average precipitation)

If used with skill, the third *isohyetal* method provides the most accurate determination of average precipitation, since it enables a large number of factors such as relief, aspect, and direction of storm movement to be taken into account. Contours of equal precipitation depth are constructed for the Haraz basin and adjacent areas as illustrated in Figure 4.6-b. Sometimes the average precipitation in each inter-hyetal zone is taken to be the mean of the bounding isohyets. The value for each zone is then weighted according to area, totaled, and finally divided by the total area of the catchment, giving a value of 649.3mm for the Lar and 540mm for Haraz.

$$P_{avg} = \sum_{i=1}^{N} m\,[(P_j+P_{j+1})\,(A_j/2)] \div \sum_{i=1}^{N} A_j$$

Where P_j is the precipitation value, Aj is the area between the isohyets, m is the total number of different contours (isohyets are lines of equal precipitation depth).

Table 4. 2: Summary of annual average precipitation (mm) in study area.

Basin	Method		
	S.A.M*	Thiessen	Isohytal
Lar	689.7	665.5	649.3
Haraz	668.5	556	540

* (Station Average Method).

It will be seen from the results, however, that the mean rainfall calculation produces values of 689.7mm (Lar) and 668.5 (Haraz) but these are not close to values produced by other methods.The Thiessen and Isohyetal method produce for the Lar values of 665.4mm and 649.3, and for the Haraz 556 and 540mm. (see Figure 4.6-a,b).These calculations show that the Thiessen method and arithemetic mean are in close agreement and are useful for calculation of the Lar basin annual precipitation. On the other hand the Isohyetal map of the study area shows the precipitation pattern important in assessing varying erodibility of the area.

The Upstream area has 350-400mm of precipitation and thus the bare soils and former Lake deposits are easily eroded. Along the Lar and Khoshkehlar rivers depositional material shows the effect of over 400mm precipitation producing erosion features and

removing material from limestone formations. Figure 4.5 shows Lar upstream at Absefid, Khoshkrud and Sefid-Ab with over 600mm, but in Dalichai and Kamardasht about 500mm annual precipitation may provide different erodibility. It seems that the high discharges and sediment delivery of the Lar tributaries, especially the Dalichai, increased in response to a period of heavy rainfall in autumn or snow melting in summer. The amount of sediment also depends on the physiographic and geological conditions. These relationship show that sediment delivery in the western parts of the Lar parts is greater than other areas because of large size of this catchment.

4.2 GEOLOGY

Geologic factors act to control morphological changes and sediment supply in any basin. In the Lar basin these can be classified as lithologic, depending primarily on the composition, texture, sequence of rock types and structure including chiefly faults and folds that interrupt the continuity or uniformity of occurrence of a rock type or sequence of rock type. Differing geology combined with other processes, control the development of morphological changes and sediment production which in turn profoundly affects the distribution and movement of sediment in the Lar basin. Together the geologic, pedologic and topographic features influence stability, form, and distribution of sediments and other landsurface characteristics in the study area.

4.2.1 The Geological History of Study area

From the Cambrian to the Middle Triassic, continental deposits covered the whole Iranian region including the Alborz. The epicontinental marine conditions which resulted in thick-bedded carbonates were ended by early Kimmarian movements. In the Central Alborz differential uplift allowed a depression to form to the north of the Central Alborz. During the Upper Triassic and Jurassic, folding resulted in the development of swell and trough structures. Continental sedimentation including coal-bearing horizons were deposited in the northern trough, but in the upper Jurassic, uplift and southward thrusting of the Central Alborz occured. During the Cretaceous a southern trough deepened south of Central Alborz, while the northern trough survived. The Alborz began to form in the Laramian orogeny as the northern trough reversed to form the range in the Tertiary (Stoklin 1974). The south Caspian Block then began to subside,

while its eastern part, the Neka uplift, continued to remain as an elevated block. In the Eocene huge amounts of submarine volcanic materials filled the depressions which formed south of the Central ridge and widening towards the west but no volcanic activity occurred north and east of the Central ridge in this time. The early Alborz Range uplifted strongly in the Oligocene. The last and most intense tectonic phase was in the late Pliocene and continued into the Quaternary. In this tectonic phase the thrusts reversed in the north (Rassekh et al. 1974).

4.2.2 Damavand Lavas

The volcanic cone of Damavand, rising to an altitude of 5671 metres above sea level, not only dominates the Lar downstream but also has exerted a major influence on the development of drainage patterns and sedimentation in the basin. It was the early eruptions of the volcano, some 60 000 years BP, that resulted in the blocking of the original channel of the Lar and first led to the creation of a natural lake. Although no volcanic eruptions from Damavand have occurred during recent geologic times, the volcano is not completely extinct. Sulphur emanations are still found within the summit crater and impart a characteristic yellow colour when free of snow. At Ab-Garm village on the eastern slopes of the Damavand, and at Ab-Ask, warm water springs are found. A further reminder is the comment of De Morgan (1905) who stated that parts of the cone were warm enough to melt snow in midwinter 1889. The recent nature of Damavand can clearly be interpreted from the presence of many primary volcanic structures preserved around the cone, effectively unmodified by sub-aerial erosion. Individual lava flows can be identified in plan, particularly by the use of KFA-1000 and aerial photographs, as can remnants of numerous lava tunnels. The upper surfaces of the lava flows undulate extensively (Figure 4.7) as can clearly be seen along the left bank of the River Lar and has also beneath the thin sedimentary cover. Adjacent to the limestone gorge through which the Lar river flows, the undulations in the lava flows appear to reflect similar undulation in the underlying bedrock surface. However, elsewhere the undulations are apparently unrelated to the form of the bedrock surface and to a large extent simply reflect the irregular way in which succeeding tongues of lava were deposited on top of each other. The undulations in the upper surface of the lava are likely to be largely primary depositional features, although at least some modification of the surface is likely to have occurred as a result of movements in the lacustrine

sediments, where these underlie the lava. The base of the trachyandesite lavas to the north of the Lar gorge has acquired a dip to the north of between 9 and 10 degrees.

4.2.3 Tectonic Structure of the Lar Basin Using KFA-1000 Imagery

Damavand volcano affects its surrounding area via the production of morphotectonic forms which have influenced sediments in the study area. The region is characterized by several broad, very regular structures extending in an E-W or ESE-WNW direction from the slopes of the Damavand Volcano as far as the course of the upper Lar where this river, having made a large bend, flows southward. A brief description of the principal structures, working from the north to the south is given below:

- *Sefid-Ab overthrust,* is a large dislocation extending from the southern slopes of Kuh-e-Namakkusar along the Sefid-Ab valley as far as the upper Lar valley, where it joins with the Garmabdar overthrust. It has a WNW-ESE trend and a some what north-sloping fault plane. The northern block, whose base is constituted by the Shemshak formation, moved over this fault, bending slightly in an anticline. North of the Dombak-Kuh and between the Alarm and Sefid-Ab valleys, occurs a system of elongate dislodged slices predominantly consisting of Jurassic and Cretaceous limestones. The Sefid-Ab overthrust may have been originated by a fracture formed at a high angle to the bedding across one limb of slightly folded anticline and by movement over the strata of an adjacent syncline; in this instance, the dislodged slice would represent the stretched southern flank of the fold.

- *Piazak overthrust,* is a minor dislocation which diverges from the Garmabdar overthrust at the Lar - Sefid-Ab confluence, near the Chehel-Khaneh of the upper Lar, joining the Sefid-Ab thrust, at the Alarm-Bozorg, after a WNW-ESE trend. The fault plane is subhorizontal or slightly inclined northward. The tectonic movements caused the Jurassic limestone of the Lar formation cropping out to the north of the fault to overlie the south-aligned Eocene tuffs of the Karaj formation.

- *Chehel Cheshmeh - Tiz Kuh syncline:* Crosses the whole of the Lar valley from Takht-e-Shekarak Kuh to Polour, extending over an area more than 30 km long and exceeding 6-7 km in breadth. It is a mostly symmetrical syncline with WNW-ESE trending axis and

very steep flanks. Eocene or Upper Cretaceous sediments are exposed in the core of the structure, the flanks are, on the other hand, comprised of Jurassic sediments. The uniformity of this structure is interrupted along the northern slope of Kamar-Dasht by a fault with a steeply south-dipping plane, which cuts the southern flank of the syncline, that has moved relatively up over the younger core. From the geometric point of view , this is a reverse fault, whose northward movement contrasts with the trends of the other structures occurring in the neighboring zones. In Asserto's opinion (1966), this dislocation is not due to any south-north stress, but it is rather related to the collapse of the core of the Chehel-Cheshmeh syncline, as a consequence of the southward movement of the Sefid-Ab thrust (Figure 4.7).

4.2.4 Stratigraphy

The formations cropping out in the area surveyed are briefly described below. Gansser and Huber (1962) divided the Central Alborz into structural and stratigraphic elements, and other authors used similar subdivisions (e.g. Stocklin, 1974; Rasekh et al, 1984) from north to south:

The Caspian Plain, coinciding with the southern border of the Caspian basin, is characterized by a thick sequence of Miocene to Quaternary, mostly marine sediments belonging to the eastern Paratethys. *The Northern Mesozoic Border Zone* forms the northern foothills of the Alborz. It is characterized in the northern part by Cretaceous rocks typical for this region and in the southern part by several slices, some of them slightly overthrust to the south, comprising mainly Triassic dolomites. The Cretaceous sediments are considered to belong to the Northern Mesozoic Border zone and not to the Caspian Plain, because, in contrast to the Tertiary deposits, they exhibit similarities with the Cretaceous sediments in the south. *The (Paleozoic) - Mesozoic* Central Range represents the main depression between the structural high of the Paleozoic central Range in East Mazandaran and in the west in Alam-kuh. In this depression the (Paleozoic) - Mesozoic Central Range consists mainly of Mesozoic rocks, with Late Paleozoic formations exposed in the Nour valley. The Pre-Tertiary zone consists of Mesozoic and Paleozoic rocks, the latter thrusting to the south over the adjacent Tertiary tuffs. The whole region is dominated by the great cone of the Quaternary

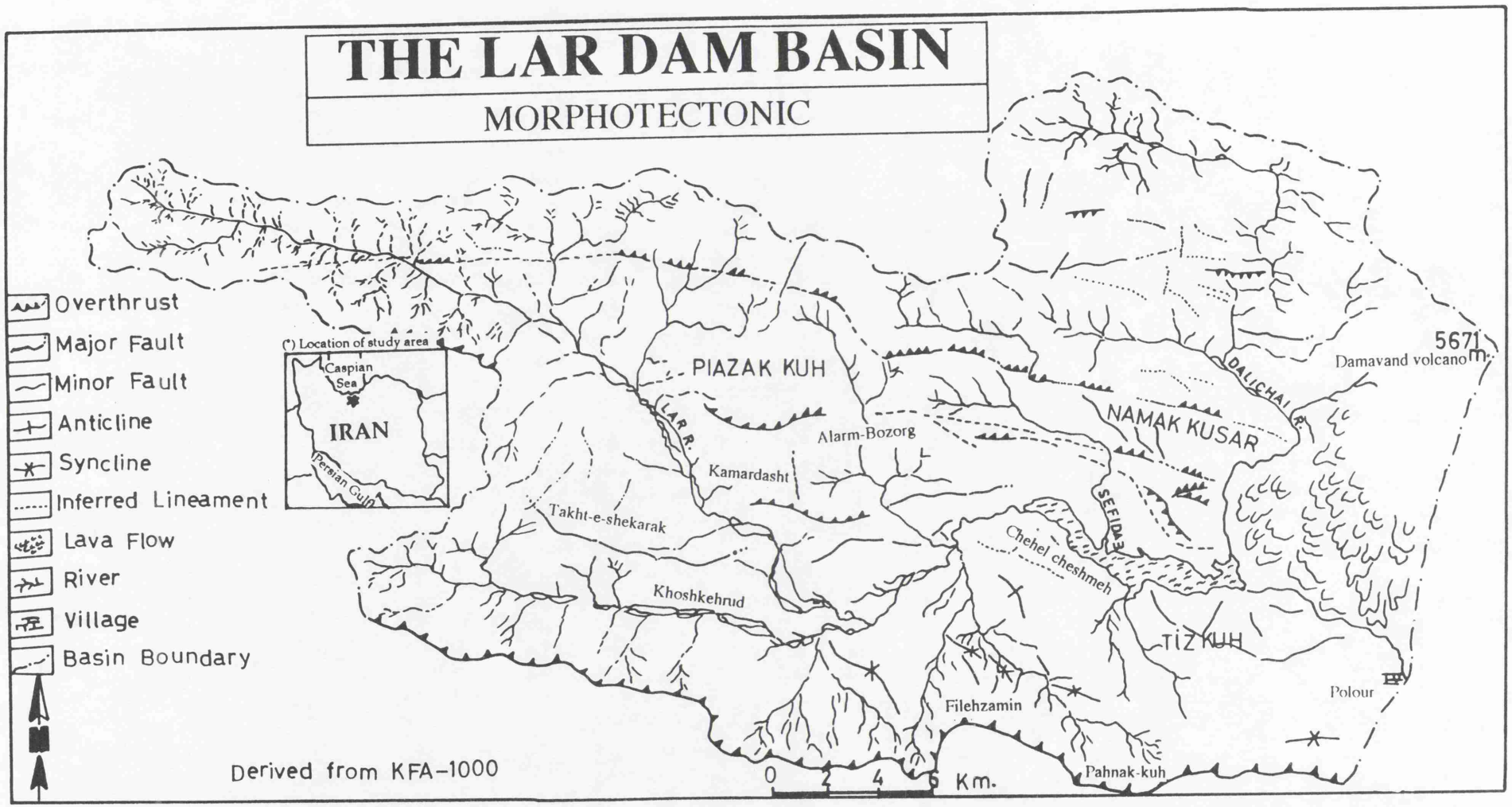

Figure 4.7: The Lar Dam Basin Morphotectonic Map.

Damavand volcano which occurs at the boundary between the Tertiary Central Zone and the Southern Paleozoic/Mesozoic Zone.

The stratigraphy of the study area is dealt with only summarily. The sediments range from young Precambrian to the Eocene, but several stratigraphical gaps, some of long duration, break the succession. Miogeosynclinal, shelf type depositional environments occur throughout the whole interval, but Eugeosynclinal sediments are completely missing. Compared with other areas of the Alborz, the Paleozoic formations show a strikingly thin development. The formation of the Lar basin which are influence the morphological changes will described below;

- Jurassic: Shemshak formation: *[green-grey and black shale and sandstone with coal streaks, many plant remains and some molluscs],* (Lias and Lower Dogger). The oldest rocks encountered extensively within the Lar Basin Belong to the Shemshak formation which is largely Liassic in age. Allenbach (1966), who worked predominantly to the east of the Lar basin, described two main sedimentary cycles prior to the deposition of the Shemshak formation, this latter deposits introduce the third cycle. Within the Lar basin, the Shemshak formation outcrops extensively in Imam- pahnak and to the west towards Siahpalas on the south side of the lake. In the north of the basin Shemshak formation rocks again outcrop and here they appear to have been faulted up against younger Jurassic Limestones. The Shemshak formation has been measured by Assereto (1966) in the Jajerud valley as approximately 1000m. thick. This formation is mostly limited to high altitude, unvegetated and first order drainage basins. The major erosion pattern is weathering and gullying which delivers eroded material via surface streams. These erosional features are visible in Vala-Rud, Dalichai, Divasiab and Sefid-Ab upstream sections.

Dalichai formation: *[grey or light green, thin-bedded, marly limestone with Ammonites],* (Upper Dogger-lowest Malm). The formation was discovered by Steiger (1966) near the Dalichai river and it is exposed only in small outcrops; in most places it is concealed by talus from the overlying calcareous cliffs of the Malm. It crops out in the Lar valley, south of Kamar-Dasht, near Alarm-Bozorg, and on the southern flanks of Kuh-e-Namak-Kusar, Fil-e-Zamin and Tiz-Kuh. Also, the formation outcrops in several places along the Haraz river. It separates the Shemshak and Lar formations and varies

from 50-120m. thick. Although the formation is not very thick some rock slides occur in the outcrop areas. Mechanical action is one of important factor influencing this formation, but the amount of sediment supply is as great as in other formations.

- Lar Limestone formation, (Malm): *[light grey, thin-bedded to massive limestone, locally with chert concretions with Ammonites],* (Upper Jurassic). The formation was measured by Assereto (1966) in the Lar valley as approximately 250m. thick. Upwards the limestones become increasingly thick bedded, hard, compact and with frequent chert nodules and bands, and thus contribute to forming the topographically spectacular limestone ridges. In the eastern part of the Lar valley it is overlain by the Tiz-Kuh formation, a thin conglomerate horizon generally marks the unconformity. Farther east, from Chehel-cheshmeh as far as the Ruteh valley, the Lar limestone is unconformably overlain by pale grey, thin-bedded, marly limestones of Upper Cretaceous age. This formation is mostly unvegetated, cliffs, scree slopes and high land. Weathering is very common and seems to have a significant role in sediment supply on this formation.

Cretaceous: Tiz Kuh formation: *[white massive Orbitolina limestone],* (Aptian-?Albian). This formation is again characterized by fine grained limestone, the deposition of which were initiated by a partial flooding of the area, from the north, during Aptian times. In the Lower Lar valley, the lower part of the unit consists of yellowish or reddish, medium bedded detrital limestones, overlain by fine grained white or pinkish, indistinctly bedded biogenic limestones with conchoidal fractures.

The Tiz-Kuh formation exhibits throughout the Lar valley a thickness varying from 0 to about 200 m. The Upper Cretaceous deposits are again calcareous in nature. Four units were distinguished by Assereto (1966), all of which rest unconformably on either the Tiz Kuh formation, or to the east and south of the confluence of the Lar and Sefid-Ab, on the Upper Jurassic Lar limestone. With the Upper Cretaceous, the third sedimentary cycle came to its close. The Tiz-Kuh formation covers only a limited area in the Lar basin but it is crossed by fault lines. Erosion of this formation, and its faults, result in mass movements, screes and gullies on the lowlands especially in the Dalichai and Sefid-Ab upstream sections.

- *Karaj formation*: The formation was examined by Lorenz (1964) in the Karaj valley. It is characterised by its green colour, and hence, is often referred to as the Green Bed. The dominant lithology is a very fine grained, green, regularly thin bedded tuff with some bedded mudstones, cherts and minor volcanics. The tuffs consist of irregular masses of finely crystalline chalcedony and very fine acicular glassy remains in an amorphous matrix. Dellenbach (1964) described three main faces within the *Karaj formation*. The basal volcanic facies were generally poorly developed except in certain localities where they reach up to 700 meteres in thickness. They consist of basalts, trachyandesites, with some associated tuffaceous sediments. The complex lithology of the Karaj formation, including as it does at least some Pillow Lavas, and its association with the postulated vicinity of possible plate margins suggest that the rocks of this area could correspond in some way to the opholites found elsewhere in the world associated with plate margins. The Karaj formation outcrops extensively upstream of Chehel-cheshmeh and also occur as small outliners, often fault bounded, within the older Mesozoic sediments. A large area of the Lar basin is covered by this formation and extreme gully erosion dissects in the formation at Barreh-Kuh and Gorgore-Kuh and in some parts of the Lar upstream.

- *Quaternary Sediments:* Quaternary, post-orogenic deposits are fairly widespread in the area, both in the Lar valley and in the Haraz valley. The origin of these is directly related to the southern lava of Damavand volcano, which blocked the drainage channels in the Lar area to form a natural Lar lake. Over a long period, continued eruptions raised the level of the lava dam and hence the lake level in the Lar valley up to a maximum elevation of 2700 metres (Solaimani, 1994). The general sequence of sediments deposited in the lake consisted of fine lacustrine silts and clays which were succeeded by silts and sands, topped by coarse sandy gravels. Intermediate periods of drainage of the lake were marked by the deposition of alluvial gravels within the fine grained sediments. The ancient alluvial deposits shown on the geologic map (Figure 4.7-a) are particularly well developed, both in extent and thickness, in the vicinity of Kand, in the Lar basin, and to the west of Polour. These ancient alluvial sediments of the Lar basin and Polour area have different characteristics and are connected with variations in local base level, caused by damming of the valley by the lava flows of the Damavand. The greatest and most characteristic system can be seen in the Lar valley and consists of extremely thick deposits (at Chehelcheshmeh it exceeds 60 m; Bailey et al. 1948). The upper portion

consists predominantly of medium coarse gravels, whereas the lower part is composed mostly of clays with silts and thin beds of sand. These deposits are related to the filling up of an ancient lake with the wandering river subsequently cutting a complicated series of terraces. South of Dombak-kuh 11 younger terraces are distinguishable grouped into 5 systems, differentiated on the map with progressive numerals, ranging from the highest to the lowest. The alluvial deposits developed at the Vararud-Dalichai conjunction are identified as Lar deposits related to damming of the Dalichai valley by Damavand lava flows. It seems this lake reached a height of about 3050 m and extended for about 7 km as far as the northern slope of Zandkuh. Terraced alluvium is also widely developed the south of Tizkuh, to the immediate west of Polour. These deposits rise along the flank of the valley to a height of about 1700 m.

Ancient scree slopes and landslide deposits, commonly cemented and terraced, are locally developed in the most easterly part of the area surveyed. These deposits are most widely distributed along the east-west trending valleys, specifically on the northern flank of Pahnakkuh, along Sefid-Ab and Vararud. Some of these deposits are developed at great altitude, 3500-3700 m and were certainly laid down on the flanks of old Pliocene valleys which followed the east-west striking structural axes in this area. The other deposits are younger, and seem to be related to the base level of the Dalichai and Lar Lakes. In the Sefid-Ab valley the old talus slopes are slightly terraced, and permit reconstruction of the ancient valley floor altitude.

Colluvial deposits and residual soils generally occur at the heads of valleys and on the slightly sloping mountain flanks and consist of fine clayey-silty, redish, rather compact mud. In some places they exhibit a thickness of about 15 metres. The limit between these deposits and alluvium is commonly uncertain, as they do not exhibit marked differences. Recent and modern alluvial deposits are limited to the recent flood plains. In the Lar valley they are developed as a result of the braided deposition of the river and the consequent greater breadth of the bed. Also the wide alluvial fans are widespread chiefly in the Lar valley, where the formation of the Quaternary Lake Lar, now alluviated, caused an appreciable uplift of the local base level and the flooding of the lower parts of the confluent valleys. These deposits constitute impressive sloping planes, in some places extending for about 2 km. They consist essentially of very coarse muddy gravels lying at the top of the fans and of finer material below (see Figure 4.7-a).

Figure 4.7-a:

GEOLOGICAL MAP OF THE LAR BASIN

(Source: Assereto, 1966, Ap. Scale 1:100000)

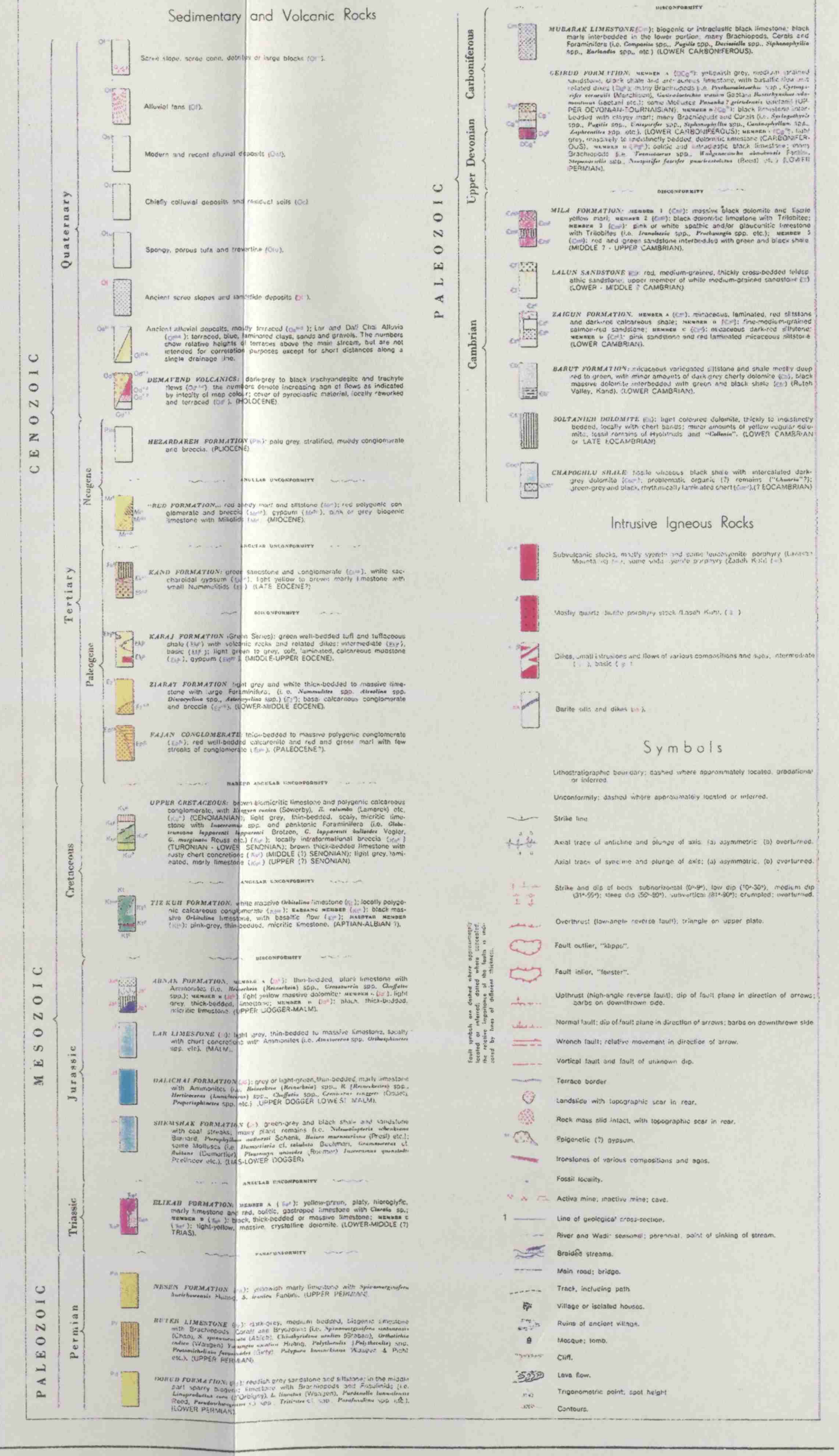

4.2.5 Soils

From the standpoint of land surface changes, one of the most important aspects is the classification of soils into major classes and subclasses which cover the land surface. This section aims to report the ways in which climates parent materials and landforms are linked with the distribution of types of soils in the Lar basin. It is also emphasises the kinds of natural vegetation associated with each of the major soil types. The soil groups in the Lar basin are mainly regosols-lithosols, lithosols, calcaric regosols in the mountain and hill units; regosols-calcic cambisols, eutric regosols-cortic luvisols on flat surfaces; and fluvisols on the gravelly river alluvial fan (see folded map no.3 in folder at back).

- *Mountain Unit:* The mountainous units possess very shallow to shallow soils on limestone and scree. The majority are dark brown soils covering about 90% of the Lar basin. These are prone to erosion and morphological changes. Scree is one of the most common morphological units in the area on the geomorphology map and is probably a main factor in sediment transport from these units. On the eastern side of the basin, Damavand volcano has two soils of volcanic origin: the lithosols and the volcanic slopes which are generally bare soil with rock outcrops; the volcanic cone with extensive basic rock and tuffs on slopes. Fractions from this formation form a significant proportion of the coarse material in the Dalichai catchment.

- *Hill Unit:* This unit possess of shallow to moderately deep soils with conglomerate, limestone rock and tuff, volcanic rock. Except in the south east part of Dalichai catchment, this unit is mostly covered by the Lake Lar and thus does not contribute to erosion or sediment delivery.

- *Flat Surfaces:* This unit includes terraces with deep soil cover and shallow to moderately deep soils on the Pleistocene rocks. This unit mostly covers the river banks at Gozaldarreh, Kamardasht, Sefid-Ab and Dalichai downstream. Very gentle slope and high vegetation density protects this unit from surface erosion but bank erosion along the river is serious.

- *Gravelly River Alluvial:* This unit is limited to between 2890-3000m. With moderate slopes and mostly river alluvium with gravel beds and very shallow soils (fluvisols) it is subject to moderate soil erosion.

According to the remote sensing data and field checks the soil condition in the Lar basin relation to vegetation, slope, geology, climate and other factors can be summarised as follows;

(1) The high mountain units are mostly very shallow soils over limestone and sandstone, with steep slopes and moderate erosion (see Aa on fold map no.3). These units are limited to between 3000-4800m. and covered with a variety of vegetation. (2) very high mountains with shallow soil cover, possess soft sandstone, limestone, shale, steep slopes and severe erosion (Ab on soils map). These units are limited to between 3000-3300m. with moderate vegetation. (3) high mountains with no soil cover or very shallow, very steep slopes and with very severe erosion, (Ac). Units limited to between 3000-3500m., and in some parts covered with moderate vegetation.(4) high mountains and cliffs are mostly without soil cover with rock outcrops, and very severe erosion (Ad). These units are limited to between 3400-4400m., with moderate vegetation in some parts. (5) high mountains with shallow soil on limestones with steep slopes and severe erosion (Ae). This unit is between 3400-4800m. (6) Damavand volcanic cone, generally without soil cover or bare soil and very shallow soil, extensive basic rocks and pyroclastic, trachyandesite formation, steep slope with tuff, very severe erosion (Af) and limited between to 2900-5671m. (7) high mountains, shallow to moderate soils in some parts with rock outcrops or soft sandy marls and limestone, steep slope with moderate erosion (Ai,j,k) and limited to between 3040-3600m., with moderate vegetation, low density or very poor vegetation. (8) hills with shallow to moderate soil cover with sandstone, limestone and conglomerate and rock outcrops, steep slope and moderate erosion (Ba,b,c), limited to between 2900-3000m., with moderate vegetation. (9) high flats and terraces with shallow to moderately deep soils, moderate topography, in some parts with gravel and old gravelly alluvial fans, in some parts of alluvial fans with severe erosion (Ca,g). This unit is limited between 2850-3100m. with moderate to high density vegetation. (10) river alluvial fans with moderate soils, gentle slopes and slight erosion (Da) but in some parts with deep soils. Moderate slopes have severe erosion (Db).

4.3 VEGETATION CHARACTERISTICS

Natural vegetation cover in the Lar basin is distributed in relation to soils, altitude, and climatic conditions. The vegetation cover ranges from high density in plateaux areas, to extremely sparse at high altitudes. Just 6% area of the Lar basin is covered with high density, 80% between 20-80% density vegetation and 13% of the area is unvegetated. Field investigations together with interpreted images of the Lar basin indicate that vegetation cover can be classified into four types with different erodibility on soils as follows;

4.3.1 Herb Type

This type of vegetation is distributed in the central basin, on gentle slopes and terraces. Estimate of cover extends to 6% (about 43000 ha) of the basin, but at a high density. In some areas it can been seen to be 100% density (see folded map no.2 in folder at back and Tables 4.2 and 4.3).

4.3.2 Shrub-perennial and Grasses-perennial Forbs

A large area of the basin is covered with this type of vegetation, its area estimated to be 50% (about 36000 ha) of the basin. Subtypes of this vegetation with ecological changes have different percentages between 20% to 80%.

Table 4.2: Distribution of vegetation type in the Lar basin.

Type of Vegetation	Area (hectare)	Area (%)	Cumulative Area (%)
Herb	4332	6.12	6.12
Shrub-Peren., Grasses & Forbs	36622	51.77	57.89
Shrub & Perennial Grasses	15664	22.14	80.03
Shrub & Forbs	3638	5.14	85.17
Rocky Land and Cliff	9256	13.08	98.25
Cultivation Land	156	0.22	98.47
Volcanic Slopes	1069	1.53	100

4.3.3 Shrub and Perennial Grasses

This type is mostly shrub plants with an area of about 15600 hectare. The percentage of vegetation cover for these types depends on different ecological factors and varies between 20% and 85% although it is usually 30% to 40%. The grasses show decreasing cover in some areas such as Sefid-Ab and Dalichai upstreams and this causes erosional activity.

4.3.4 Shrub-forbs Types

This type of vegetation is sparse and can be extremely damaged by animal grazing which has in some areas, created erosion problems. Its area is about 5% (about 3630 ha) of the basin and is very poor grassland, (see folded map no.2 in folder at back and Tables 4.2 and 4.3).

4.3.5 Rocky Land and Cliff

Due to the inaccessible nature of the Lar basin the best method for investigation and surveying of rocky land and cliff was to use remote sensing data. The area detected on the images is about 13% (about 1250 ha) of the whole basin. Such areas have little or no vegetation and a significant geomorphological feature of this area in the field and on aerial photos are extensive screes (Figure 4.8).

Table 4.3: Vegetation cover characteristics in the Lar basin.

Study Area (hectare)	Area (hectare)	Very Sparse Vegetation	Rocky Land	High-Medium Cover
Lar	21139	3232	3438	13644
Khoshkehlar	9337	2144	406	6787
Alarm	3787	713	912.5	2162
Sefis-Ab	5306	1319	962	3012
Imampahnk	2325	-	300	2025
Siahplas	4944	-	62.5	4881
Dalichai	20203	7238	2144	10821
Total Area	73081	15333	9257	45991

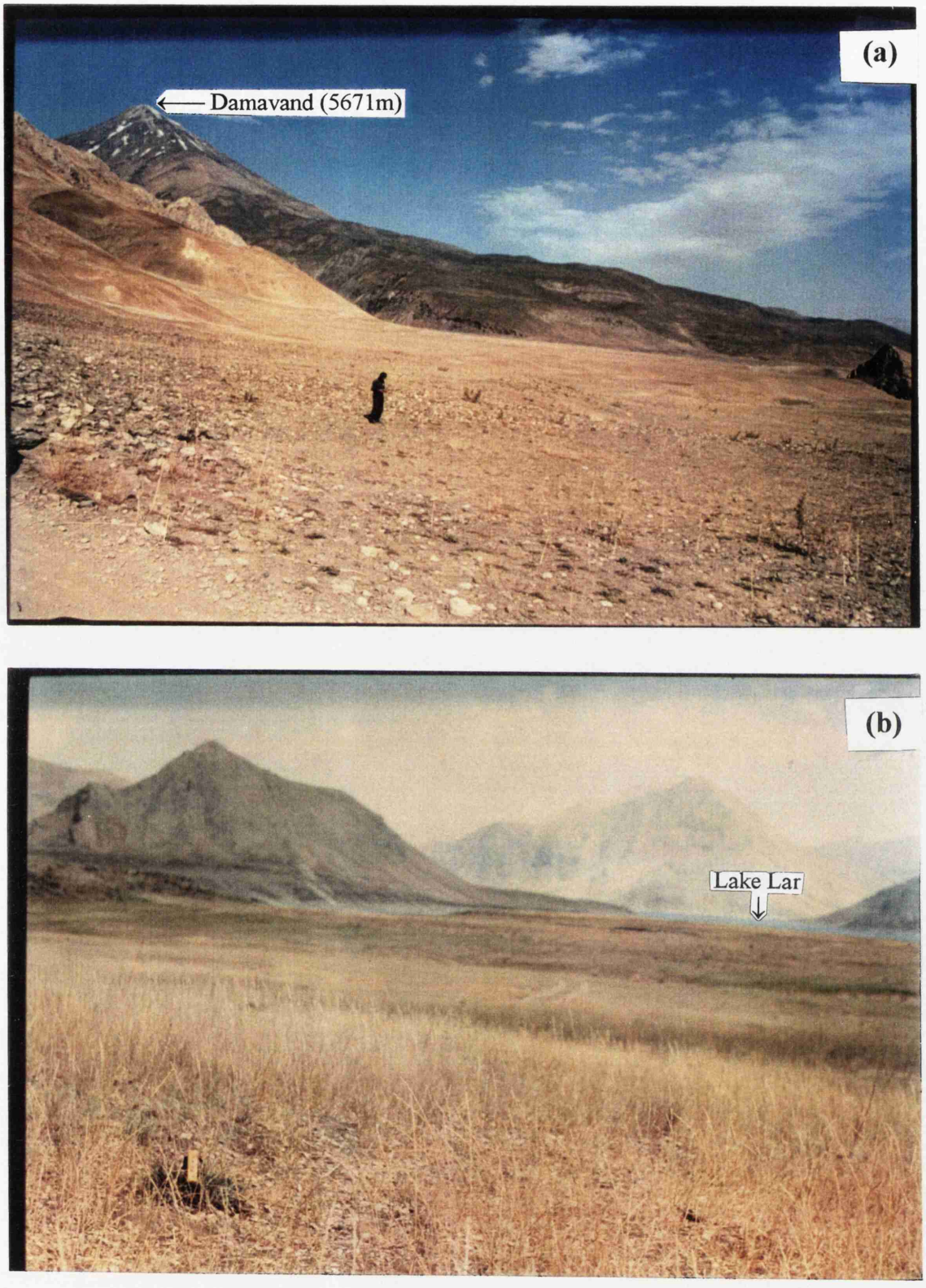

Figure 4.8: Two different kinds of vegetation cover: **(a)** Sparse and low density at Dalichai upstream; **(b)** High density, Lar downstream at Kamardasht *(looking east, Aug. 1994).*

4.4 PHYSIOGRAPHIC ANALYSIS

This section describes quantative physiographic analysis as it applies to normally developed watersheds in which running water and associated mass gravity movements, acting over long periods of time, are the chief agents in developing surface geometry. The emphasis is upon the geometry itself rather than upon the dynamic processes of erosion and transformation which shape the forms.

The efficiency of a stream system in moving eroded materials from their sources to a downstream point of measurement is dependent upon a complex array of physiographic conditions. The physiographic characteristics which appear to be significant are size of drainage area, watershed slopes, and degree of channelization. The size of a drainage basin influences the water yield; the length, shape and relief of the basin affect both water and sediment yields; and the nature and extent of the channels affect sediment availability and yield from the drainage basin.

4.4.1 Ordering the Network

Regardless of scale, or type of network, the first essential for morphometric studies is to order the network. Various ordering schemes have been suggested but for most purposes the method proposed by the Strahler (1952) is the simplest and most effective. By this scheme for ordering the network, all the 'finger tip' tributaries are designated as first order streams. When two first order streams join they form a second order stream and so on with streams of higher order. However, any second order stream which is joined by a first order stream remains a second order and so on. This ordering system is applied to the Haraz basin, a fifth order basin (Figures 4.9 and 4.10).

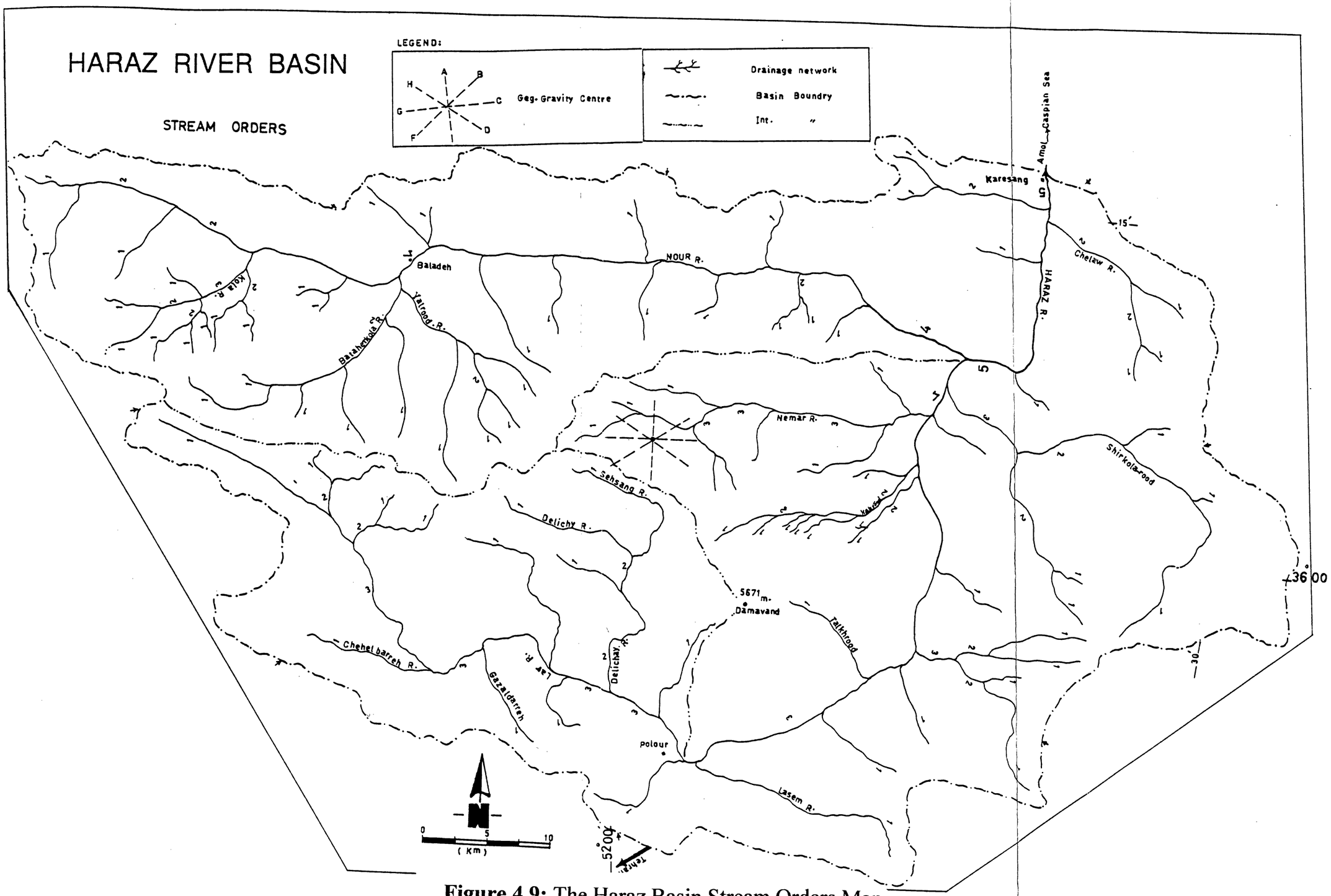

Figure 4.9: The Haraz Basin Stream Orders Map.

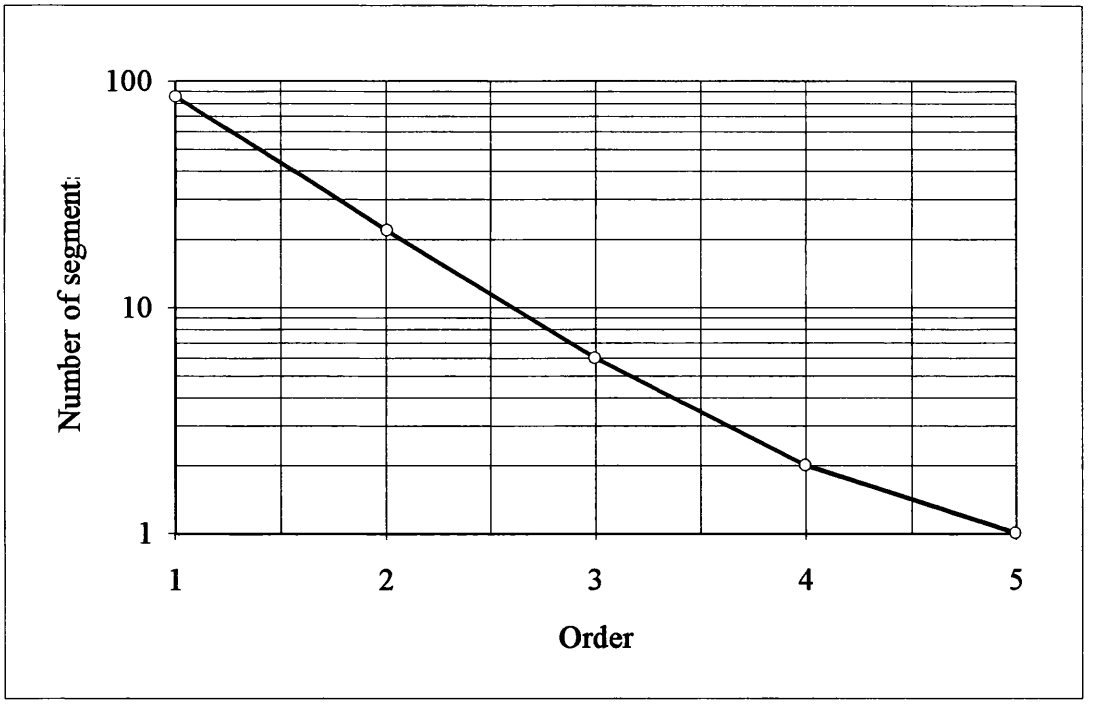

Figure 4.10: Network order at Karehsang station Haraz.

4.4.2 Basin Area and Elevation

The area of the Haraz basin at Karesang station is 4601 km^2, ranging from 220-5671 metres, of which 50% lies above 2750 metres. The average slope of the basin from the topography map is estimated to be 307.2 m/km *[S= L×H÷A]* and the channel slope according to height difference between mountainous and plain units is calculated of 37.2 m/km or 3.7% *[P= H/m÷L/km]*. Hypsometric analysis, or the relationship of horizontal cross-sectional drainage-basin area to elevation, was developed in its dimensionless from by Langbein (1947), who applied it to a large basin. Taking the drainage basin to be bounded by vertical sides and a horizontal base plane passing through the mouth, the relative height [y] is the ratio of height of a given contour [h] to total basin height *(relief)* [H]. Relative area [x] is the ratio of horizontal cross-sectional area [a] to entire basin area [A]. Results of this analysis can be useful in showing how a catchment with particular physiographic conditions can be prone to erosion.

Hypsometric and classic hypsometric curves at Karehsang station both show that over 50% of the basin is eroding (see above 'A' on Figure 4.11). The Lar basin lies between 2400-5671 m. above sea level with maximum area between 2400-3000metres (Table 4.4 and Figure 4.12). According to the topography the Lar basin slopes are classified into

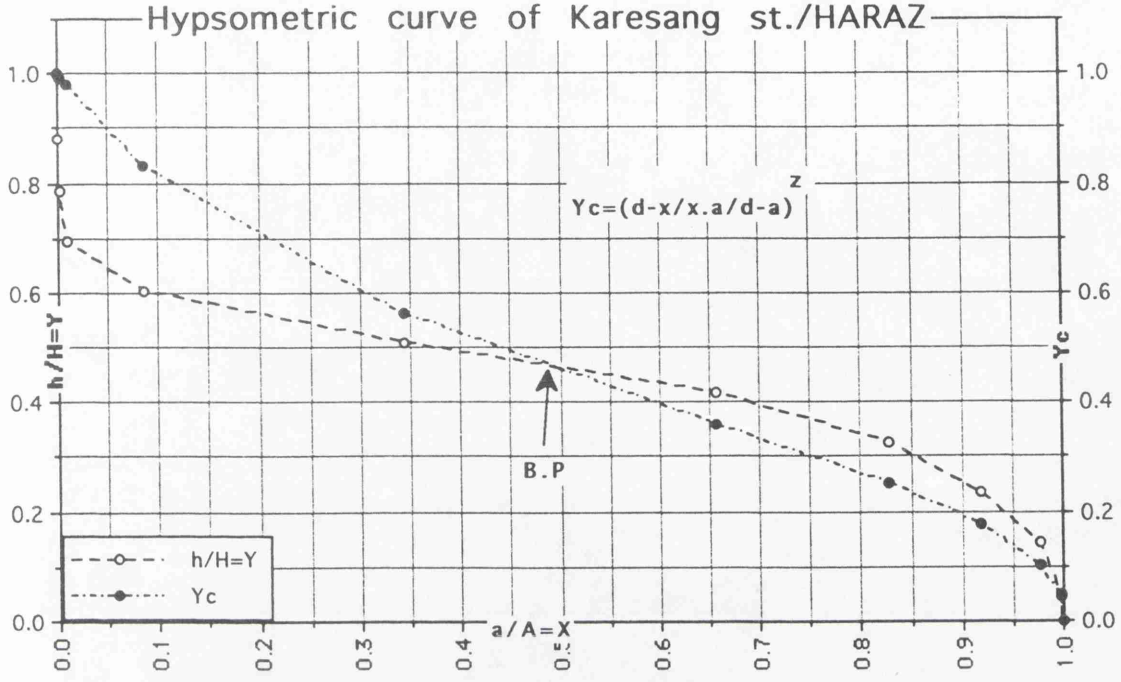

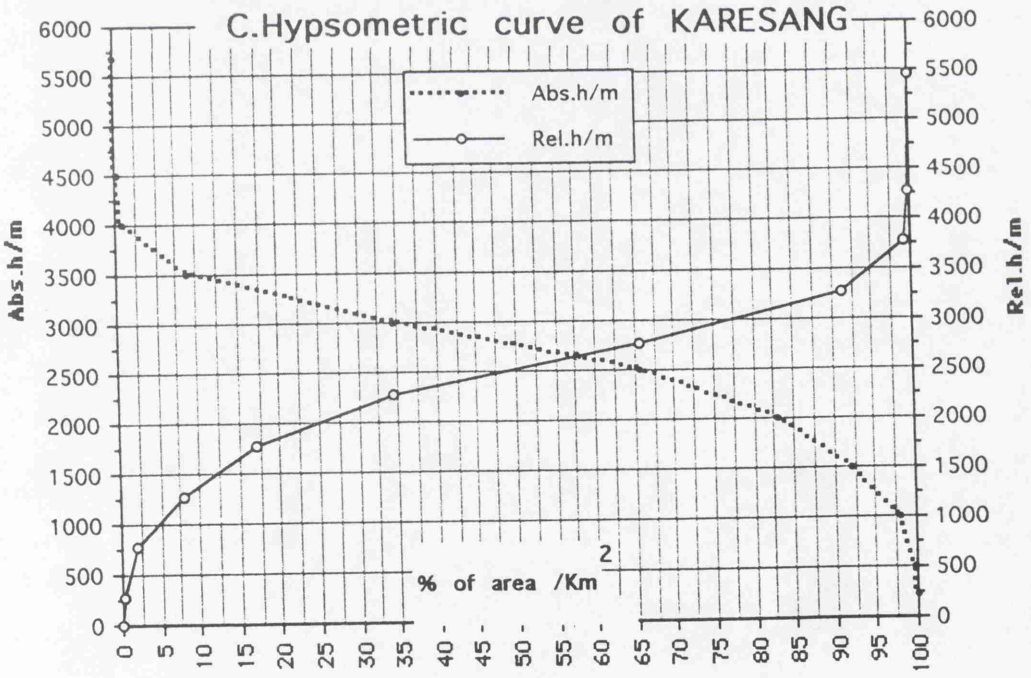

Figure 4.11: Hypsometric curves of Karehsang station, Lar (BP=balance point, to its left side are erosion area and to its right are sedimentation areas).

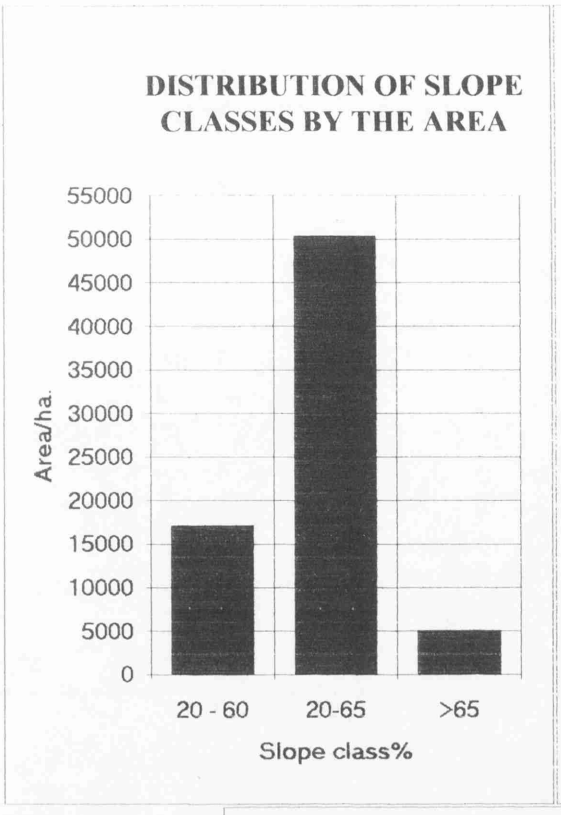

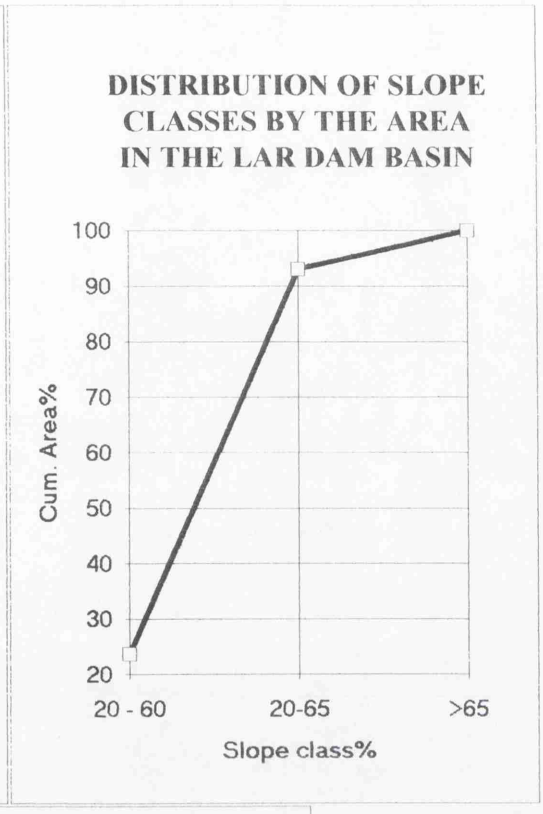

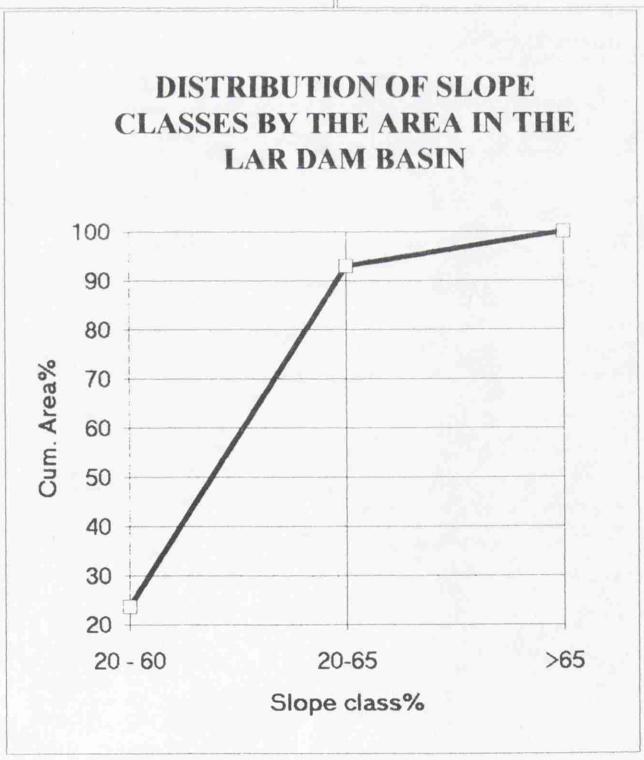

Figure 4.12: Topographic characteristics of the Lar basin.

three categories, 0-20%, 20-65% and over 65%. (Table 4.4 and Figure 4.12). At Polour station (below the Lar basin) about 60% of the area is above 3000 metres which shows a very young catchment prone to high erosion (Figure 4.13). In the Lar basin, hypsometric curves from Dalichai station show 68% of the area is above 3250 metres with high gradients (see folded map no.1 in folder at back) and probably a young catchment (Figure 4.14). On the contrary the Lar and Khoshkeh-Lar catchments at Gozaldarreh seem to be more mature basins because the areas are relatively gentle slope and 45% of the area is under erosion (Figure 4.15). Finally it can be concluded that hypsometric curves from the study area can show the parts of the catchment that are prone to morphological changes and high sediment delivery. Other physical factors can then be assessed.

Table 4.4: Distribution of area by altitude in the Lar basin.

Altitude	Area/ha.	Area%	Cum. Area	Cum.%
2400-3000	30840	42	30840	42
3000-3500	28380	39	59220	81
>3500	13780	19	73000	100

Table 4.5: Distribution of the slope classes by area in the Lar basin.

Slope class (%)	Area (%)	Cum. Area (%)	Area (hectare)	Cum.Area (hectare)
2-20	23.6	23.6	17164	17164
20-65	69.4	62	50389	67557
>65	7	100	5081	72628

The total length of the river Lar is 148 km. and its next longest tributary is 88.5 km. The Nour joins the Haraz at 750 m. at a distance of 34 km., the Shirkolarud at 820 m. at a distance of 37 km. and the Nemarestagh at 880 m., located at 40 km. The extremity length of each tributary is calculated in the tables (Figure 4.16). The Haraz basin cardinal tributary stream possess a northern orientation to the Caspian sea and the tributaries of Nour, Lar, Nemarestagh, Talkh-rud come from the West whereas the tributaries of Shirkolarud, Lassemrud arrive from the East. The basin gradient is generally from West to East and from South to North.

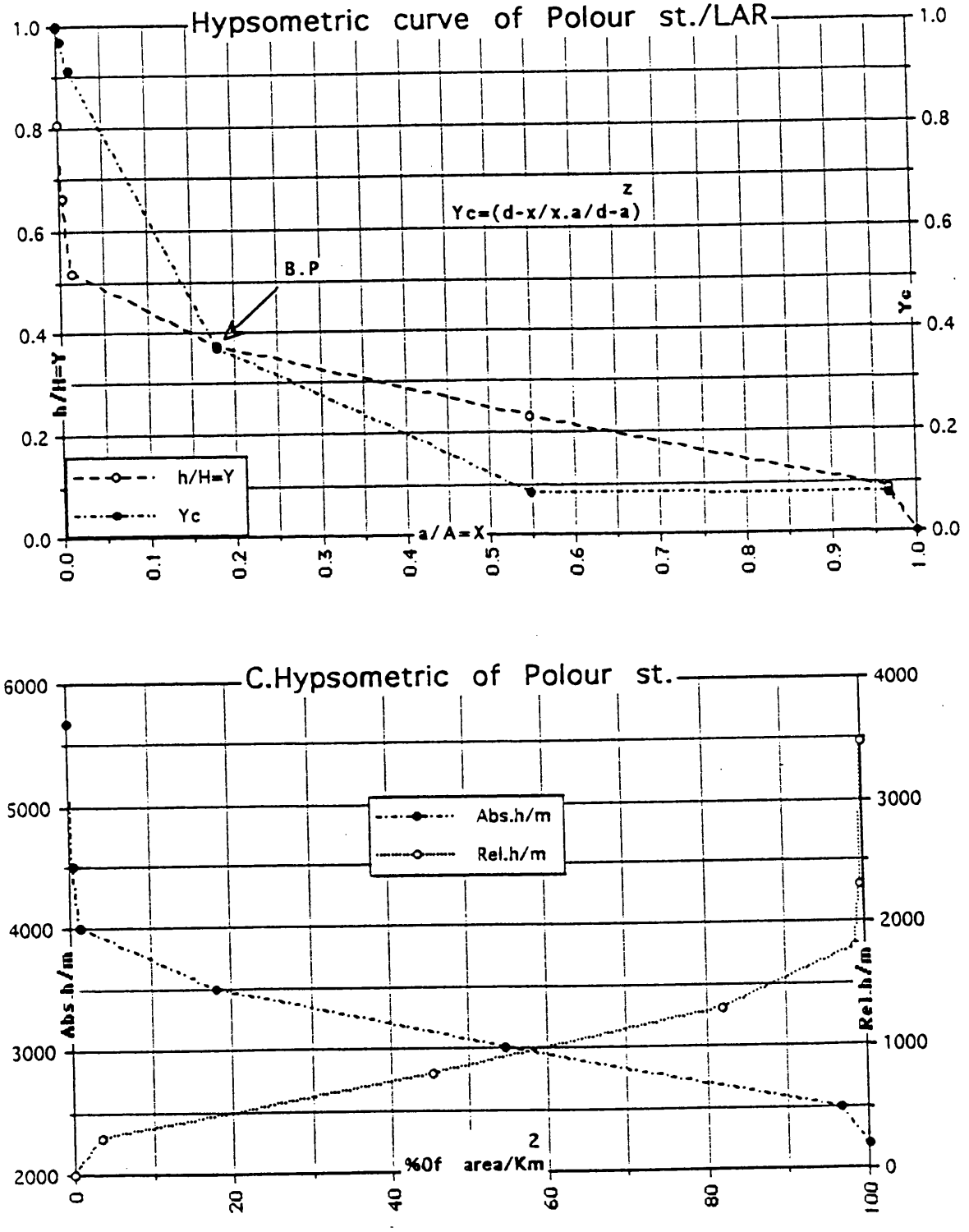

Figure 4.13: Hypsometric curves of Polour station, Lar (BP=balance point, to its left side are erosion area and to its right are sedimentation areas).

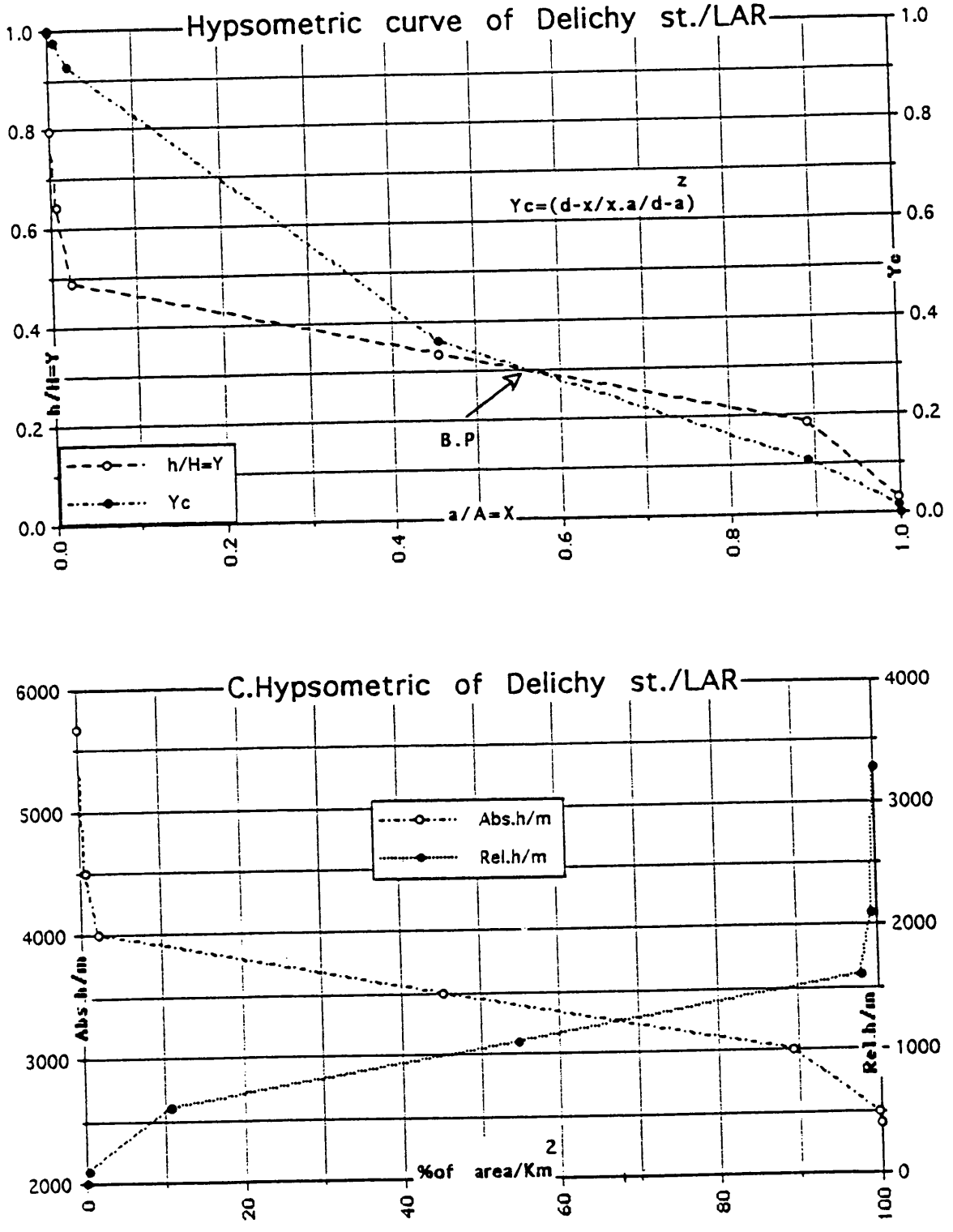

Figure 4.14: Hypsometric curves of Dalichai station, Lar (BP=balance point, to its left side are erosion area and to its right are sedimentation areas).

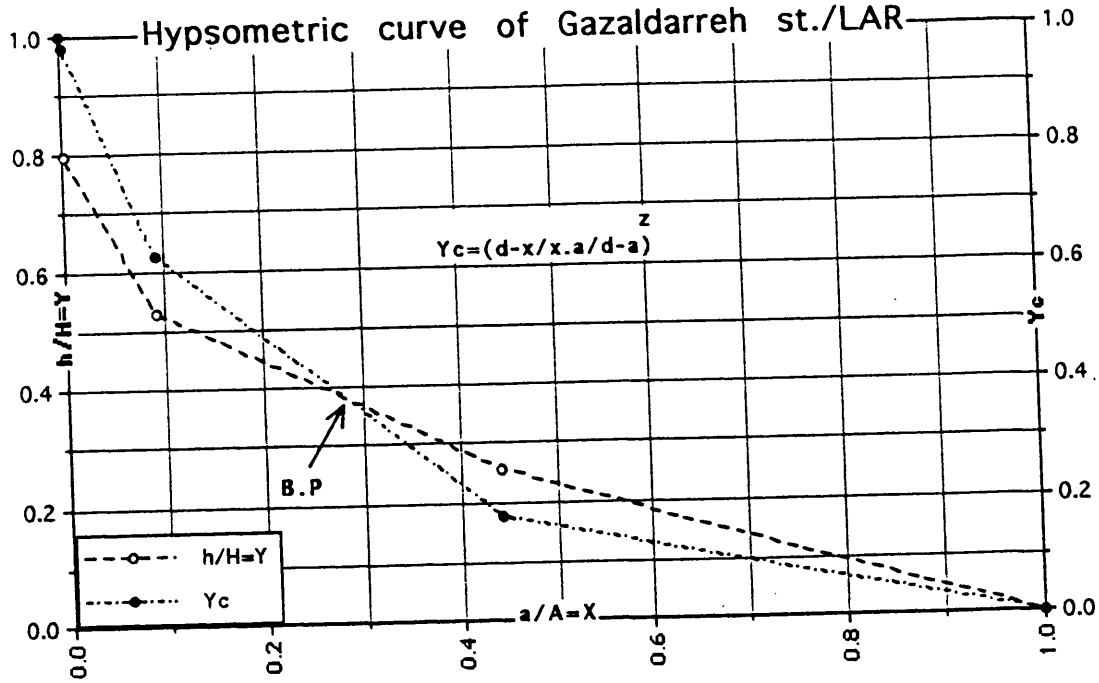

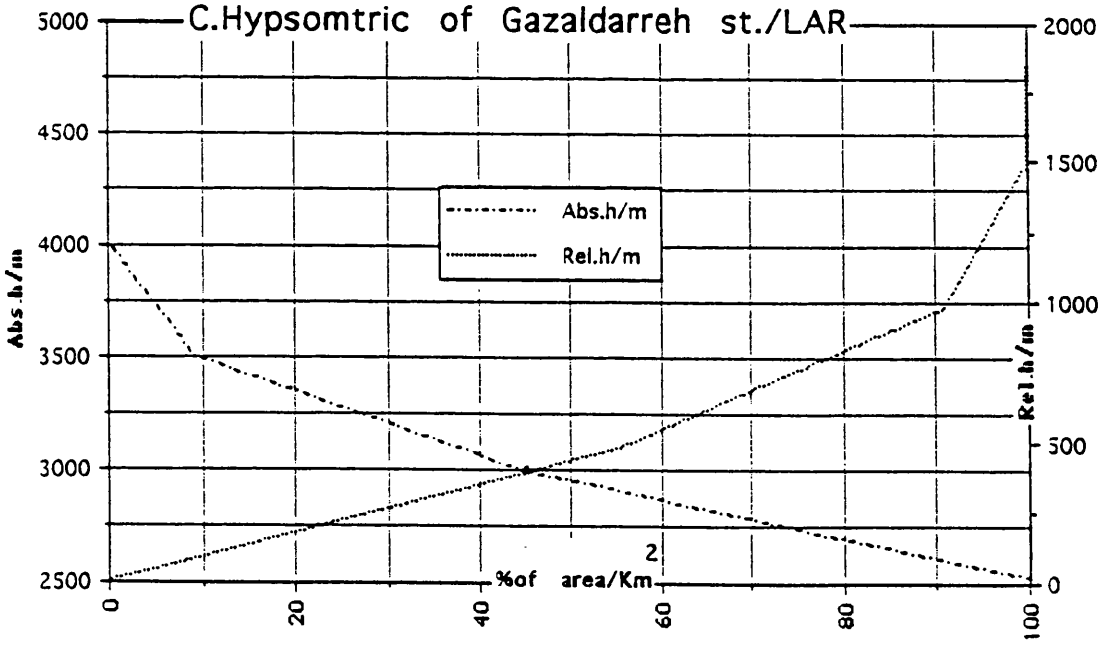

Figure 4.15: Hypsometric curves of Gozaldarreh station, Lar (BP=balance point, to its left side are erosion area and to its right are sedimentation areas).

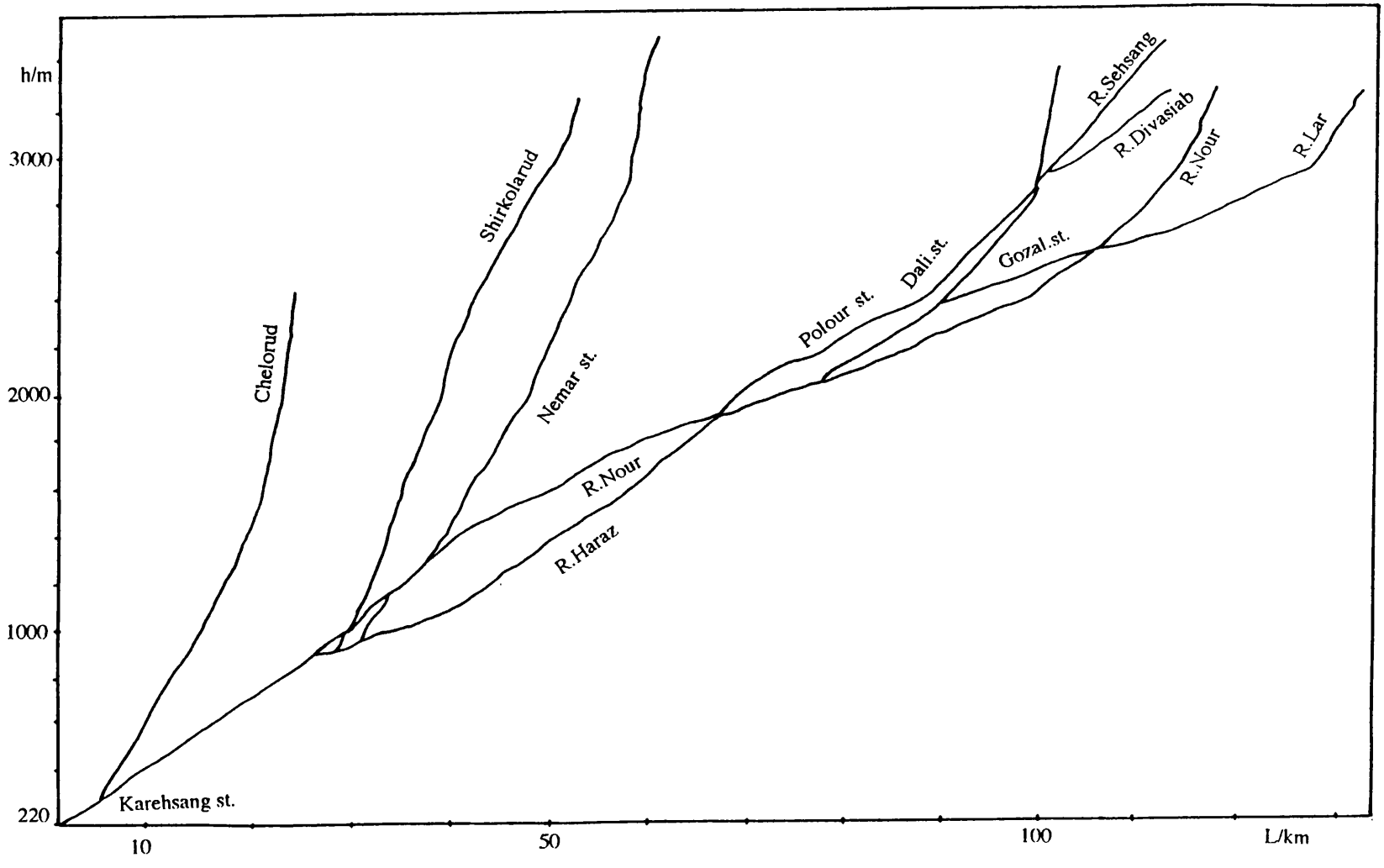

Figure 4.16: Long Profile of the Haraz River.

4.4.3 Hypsometric Analysis of Basin

As shown in Figure 4.17 (*lower right)*, the shape of the hypsometric curve varies in early geologic stages of development of the drainage basin, but once a steady state is attained, tends to vary little thereafter, despite lowering relief. Certain these attributes of the hypsometric curve are useful for comparative purposes, and include the integral or relative area lying below the curve, the slope of the curve at its inflection point, and the degree of sinuosity of the curve (Strahler, 1952).

Many hypsometric curves seem to be closely fitted by the model function shown in Figure 4.17 (*lower left*), although no rational basis is known for this. Hypsometric curves plotted for small basins for a wide variety of regions and conditions show generally stable curve properties where the rock masses are homogeneous; the erosion stage is conventionally described as mature. Small but distinct differences in curve form exist between regions.

4.4.3.1 Drainage Density

The evolution and incision of a drainage network creates the essential framework which integrates the processes of water and sediment transfers in a fluvially eroded landscape. The network consists of a hierarchical system of 'links' classified by Strahler order (Strahler, 1952) or Shreve magnitude (Shreve, 1966,1967), and connecting nodes which are 'sources', 'junctions', or the basin outlet. A high drainage density reflects a highly dissected basin, and this should respond relatively rapidly to a rainfall input, while low drainage density reflects a poorly drained basin with slow hydrologic responses. Low drainage densities are observed where soil materials are resistant to erosion or very permeable and where slopes are low. High values may be expected where soils are easily eroded or relatively impermeable, slopes are steep, and vegetation cover is limited. In this section of the Haraz basin total channel-segment lengths in the basin area (km/km^2 were calculated) as follows;

$$D = \frac{\sum_{i=1}^{n} Li}{A} \qquad [5]$$

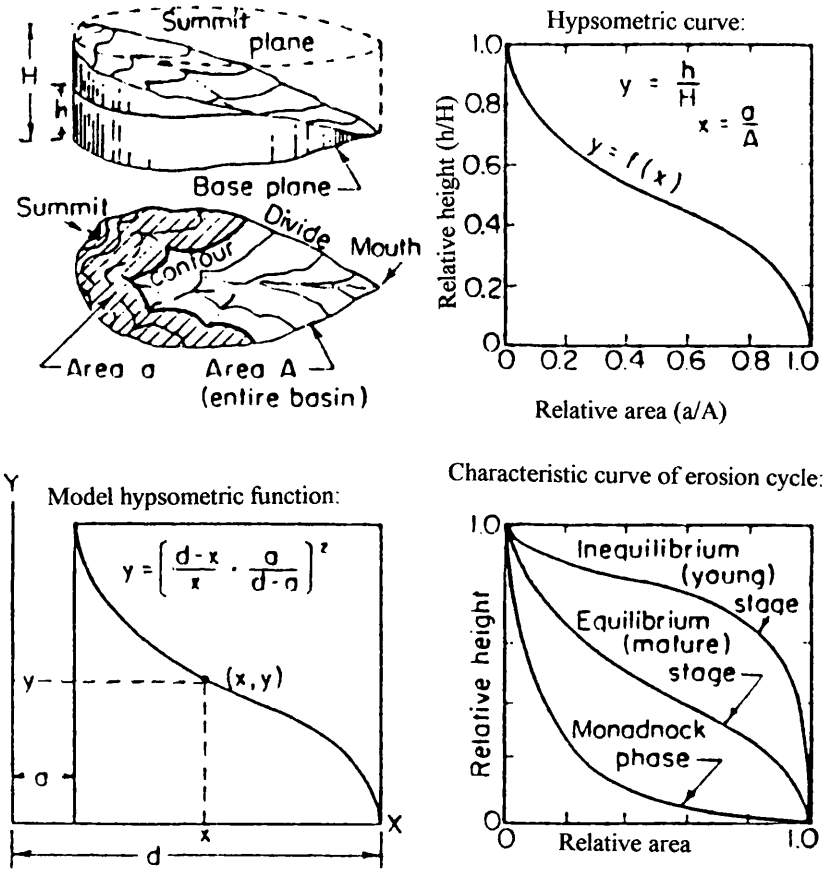

Figure 4.17: Definitions and functions in hypsometric analysis of small drainage basins, *(after Strahler, 1957).*

in which Li = Length of each channel in km., A= the area of the basin in square kilometres and D is network of rivers in km/km^2. The value of the drainage density for the whole basin at Karehsang station is calculated at 0.20 (Table 4.6). This value indicates how frequently streams occur on the land surface. In upland areas with impermeable rocks, high rainfall totals and steep slopes, drainage densities are high. Conversely, low values of drainage density are found where slopes are gentle, rainfall low and the bedrock permeable.

Table 4.6: Order and segments at Karahsang station.

Order	1	2	3	4	5
Number	86	22	6	2	1

$$BR = [(n1 \div n2 + n2 \div n3 + \ldots . n\,(i-1) \div ni)]/(i-1) \qquad [6]$$

$$BR = \text{Antilog}\ \frac{\log 1 - \log ni}{n-1} \qquad [7]$$

Where *BR* is bifurcation ratio and *n* is number of order and their number, therefore for the Haraz basin this value is calculated at 3.14 [6] and 3.04 [7].

According to hydrological studies the value of *BR* for a normal basin is usually between 3 and 5. The Haraz basin is in this group. The theoretical minimum possible value of 2 is rarely approached under natural conditions. Because the bifurcation ratio is a dimensionless property, and because drainage systems in homogeneous materials tend to display geometrical similarity, it is not surprising that the ratio shows only a small variation from region to region. Abnormally high bifurcation ratios might be expected in regions of steeply dipping rock strata where narrow strike valleys are confined between hogback ridges. Basin A in Figure 4.18 shows such an elongate basin compared with an normal basin (basin B) and one approaching the theoretical minimum value of 2 (basin C). The effect of such distortions upon maximum flood discharges, assuming precipitation and other controls to be the same throughout, are suggested by hydrographs (Figure 4.18). Where the elongate basin with high *BR* would yield a low but extended peak flow, the circular basin with low *BR* would produce a sharp peak. Basin B would lie somewhere between these two extremes.

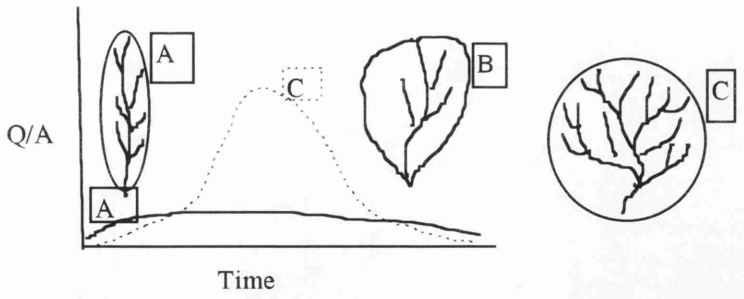

Figure 4.18: Hypothetical basins of extreme and moderate bifurcation ratios, with schematic hydrographs.

4.4.3.2 Geometry of the Basin

The geometry of the basin is very important. Very long basins need longer to achieve a through flow of water or sediment. The most efficient basin would be one in which the watershed is circular and all the water disappears down a hole in the middle. This would minimise the channel length in the basin. There are a variety of ways that the basin shape can be assessed e.g. Shape index, Gravelus coefficient, Circularity, Elongation and etc.

4.4.3.2.1 Form Factor: The shape, or outline form, of a drainage basin, affects stream-discharge characteristics. As explained above long narrow basins with high bifurcation ratios can be expected to have attenuated flood discharge periods, whereas circular basins of low bifurcation ratio would be expected to have sharply peaked flood discharges (Strahler 1964).

Horton (1941) described the outline of a normal discharge basin as a pear-shaped ovoid. He depicted the average outline of six great rivers of the world by a composite of their perimeters reduced to equal basin area and superimposed on one another. Horton regarded the pear shape as one proof that drainage basins are formed largely by sheet erosion processes acting upon an initially inclined surface. Values of the coefficient for a circle where its diameter is the flow path is;

$$\text{(form factor) } R_f = \pi r^2 \div 4r^2 = 0.79 \qquad [8]$$

While for a square where the flow path is along its centre and parallel to the sides, it is;

$$Rf = L^2 \div L^2 = 1 \qquad [9]$$

Finally, for square with a flow path along of its diameters or as bisector of angle is;

$$Rf = L^2 / 2L^2 = 1/2 \qquad [10]$$

All the Haraz basins elongations are higher than the above values, as shown in Figure 4.19.

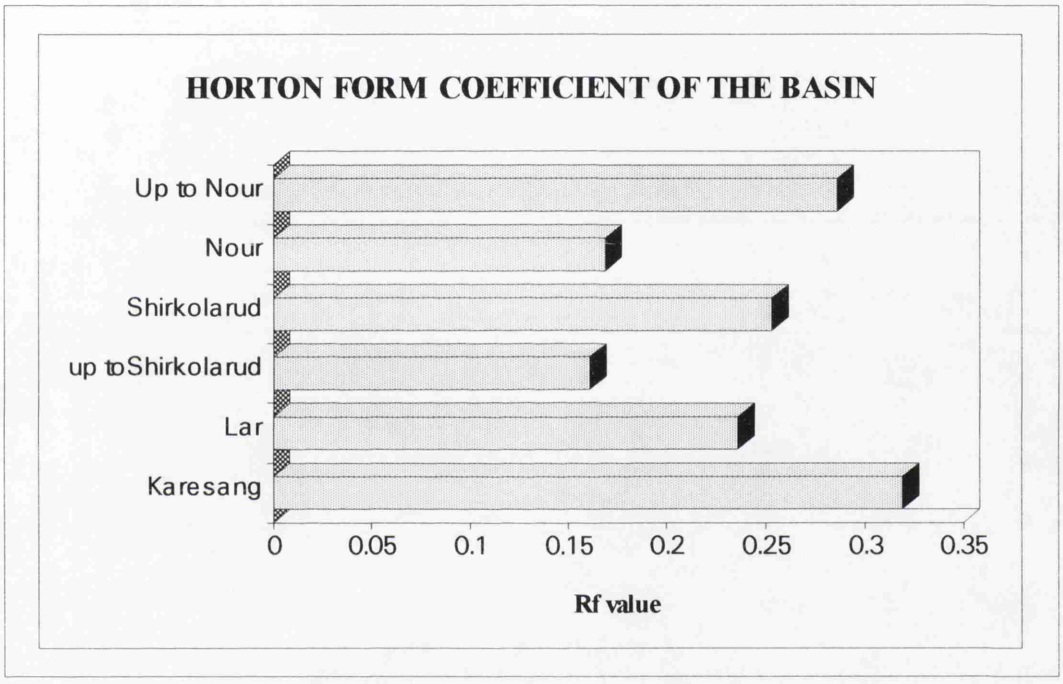

Figure 4.19: Form value of the basin

4.4.3.2.2 The Shape Index: This coefficient differs from Horton's form (*which was the dimensionless ratio of basin area*) since this index utilizes L which is longest length of the basin;

$$\text{(shape index) } Sw = L/w = L^2/A \qquad [11]$$

in which L is the length of the watershed along the mainstream in km.(measure the valley length and not the length of the meandering river), w is the average width in km. (=A/L), and A is the watershed size (area) in km^2 (Horton, 1945) see Figure 4.20.

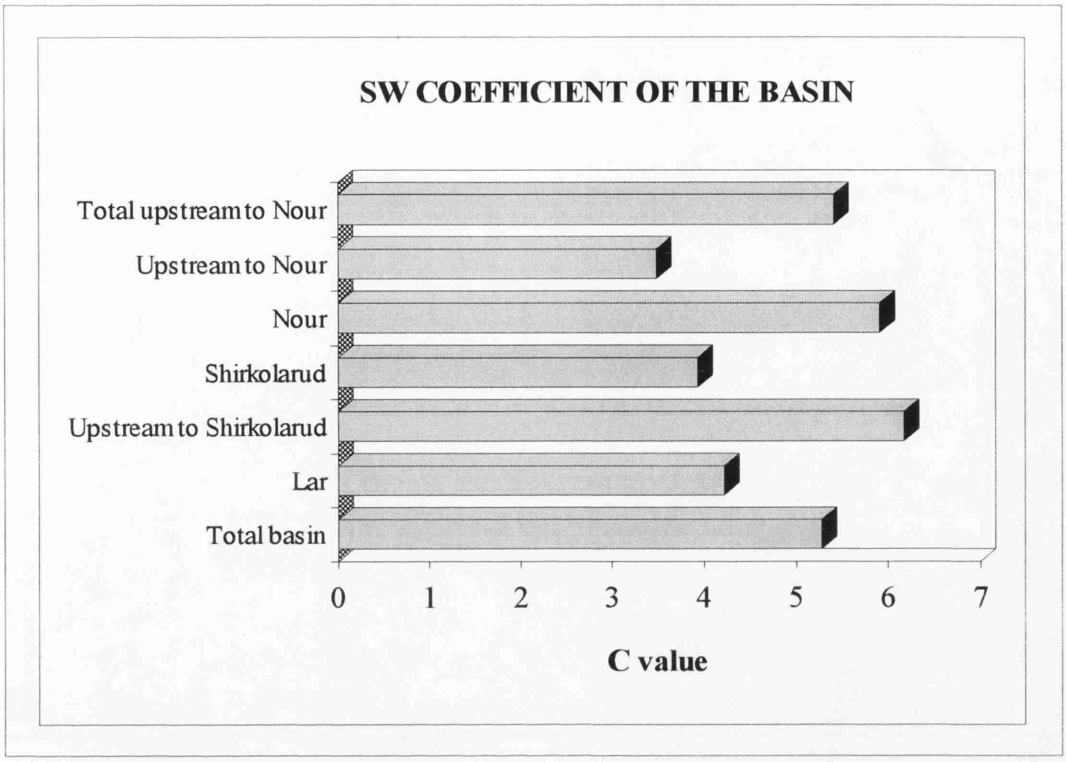

Figure 4.20: Shape (Sw) coefficient of the Lar basin in relation to Haraz basin.

*4.4.3.2.3 **Gravelus Coefficient:*** This coefficient compares the basin to the area of a circle as follows;

$$A = \pi R^2 \qquad [12]$$

in which A is surface of basin, π is 3.14, and R is the circle radius. Therefore the Gravelus calculation of the basin is as follows;

$$Kc = 0.28P / \sqrt{A} \qquad [13]$$

The value $Kc = 1$ indicates that the form of basin is circular. However if this value exceeds 1, the basin will be elongate. For the whole basin, this value is 1.75, which shows an elongate basin. Kc coefficients for the study area are shown in Figure 4.21.

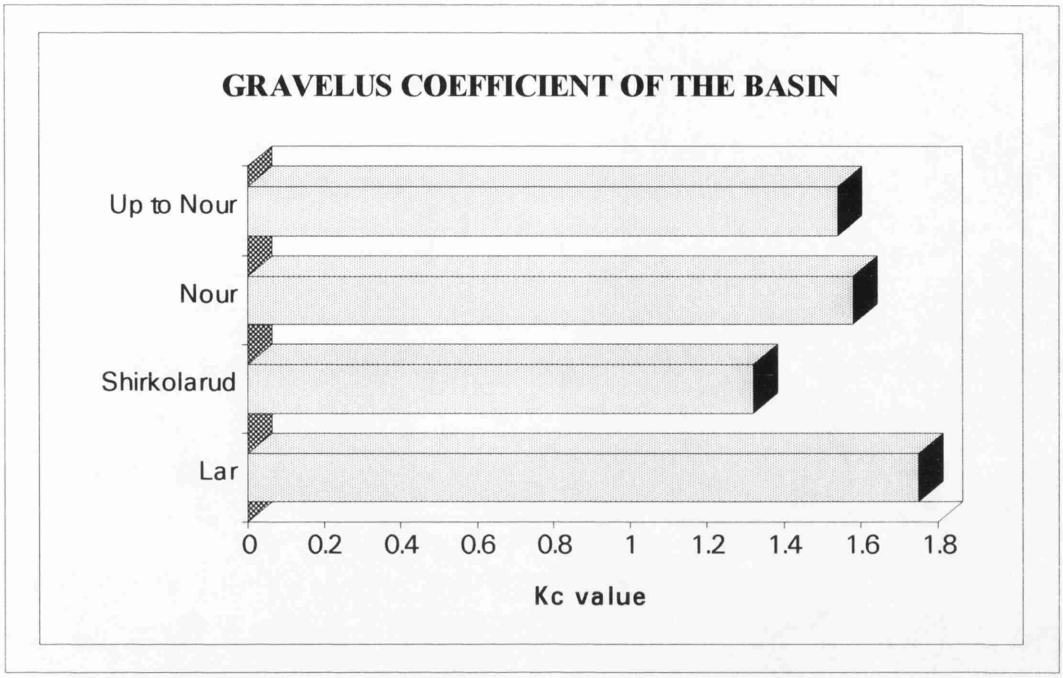

Figure 4.21: Kc value of the study area.

4.4.3.2.4 The Circularity Ratio: Miller (1953) used a dimensionless circularity ratio *Rc*, defined as the ratio of basin area *AD* to the area of a circle *Ac* having the same perimeter as the basin. He found that the circularity ratio remained remarkably uniform in the range 0.6 to 0.7 for first-and second-order basin in homogeneous shales and dolomites, indicating the tendency of small drainage basins in homogeneous geologic materials to preserve geometrical similarity. The Haraz basin produces ratios of less than 0.7.

$$\textit{(circularity ratio)}\ Rc = 12.566.AD/Ac \qquad [14]$$

4.4.3.2.5 The Elongation Ratio: Schumm (1956) used an elongation ratio Re, defined as the ratio of diameter of a circle of the same area as the basin to the maximum basin length. This ratio runs between 0.6 and 1.0 over a wide variety of climatic and geologic types. Values near to 1.0 are typical of regions of very low relief, whereas values in the range 0.6 to 0.8 are generally associated with strong relief and steep ground slopes (Figure 4.22 and Table 4.7).

$$\text{(elongation ratio)}\ Re = 1.128(\sqrt{A} / Lb) \qquad [15]$$

where A is the basin area and Lb is longest length of the basin.

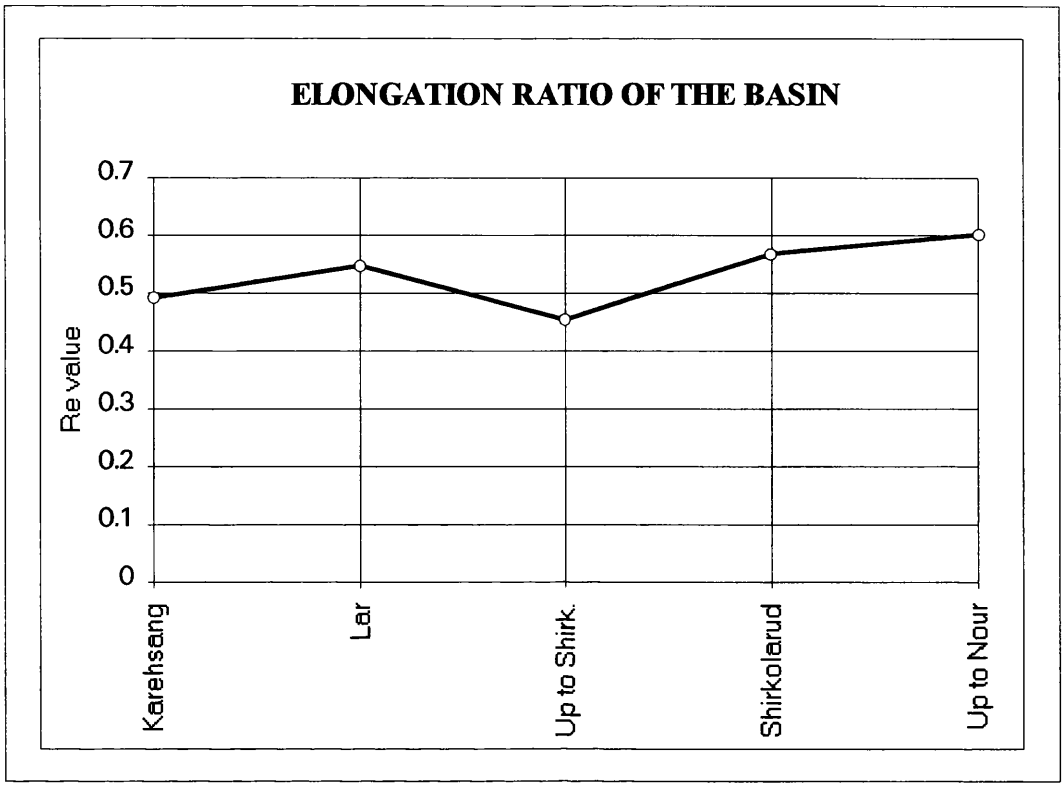

Figure 4.22: Elongation ratio of study area.

4.4.3.2.6 The Time of Concentration (Tc): Tc, which is the time required for the surface runoff from the remotest point of the drainage basin to reach the point being considered. For uniform rainfall intensity, this would be the time of equilibrium at which the rate of runoff is equal to the rate of rainfall supply. For natural drainage basins of large size and complex drainage pattern, runoff water originating in the most remote portion may arrive at the outlet too late to contribute to the peak flow. Accordingly, the time of concentration is generally greater than the lag time of the peak flow. For small drainage basins with simple drainage patterns, the time of concentration may be very close to the lag time of the peak flow. An empirical formula for the time of concentration in hours determined by Kirpich (1940) after same changes is;

$$Tc = (0.95\ L^{1.155})(H^{-0.385}) \qquad [16]$$

Where L is the length of the watershed along the mainstream in km, and H is ($H_{max.}$-$H_{min.}$) in metres, from the farthest point on the basin to the outlet of runoff, or approximately the average slope of the watershed in dimensionless ratio. Figure 4.23 shows time concentration for the study area.

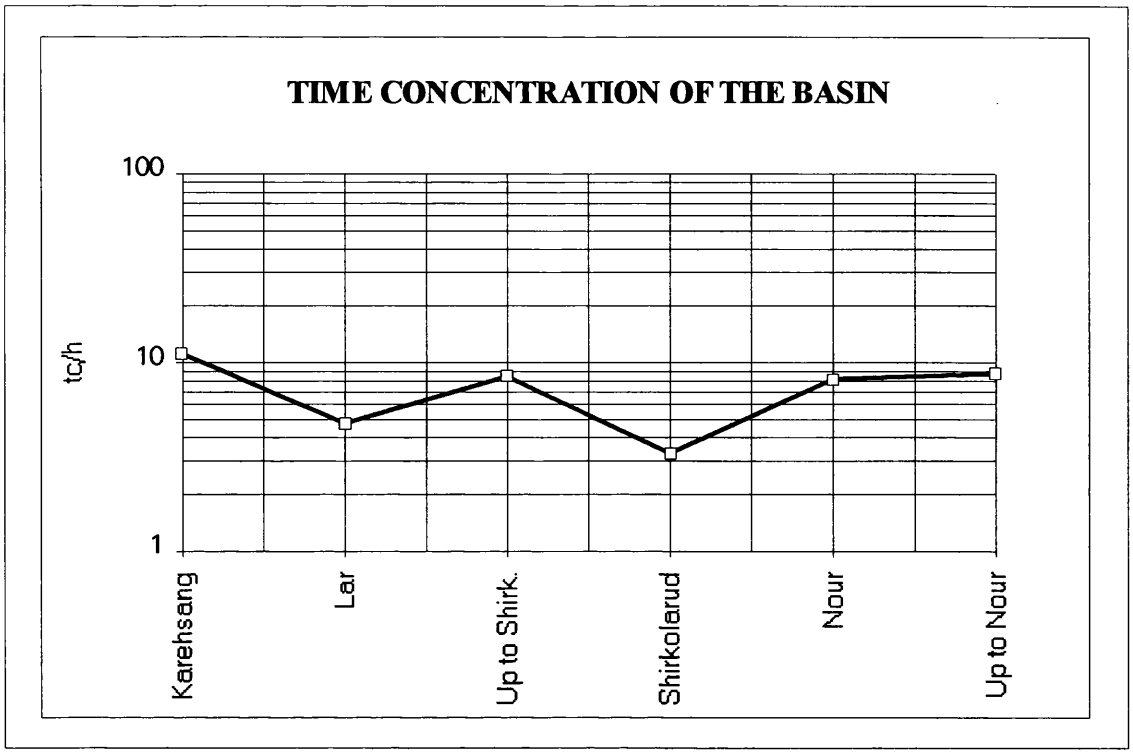

Figure 4.23: Time of concentration of the Lar basin in relation to the Haraz basin.

Evidently, differences in values are introduced by physical characteristics of the study area, e.g.; values of lesser than 5 mostly show sub basins in the study area which have pasture cover and more drainage density. But the value of *Tc* confirms the higher density forest cover, e.g.; in the middle-stream of the Haraz basin. In Chapter 5 it will be shown that physographic factors influence sediment concentration and discharge at two different stations. Thus, it seems that in the Lar, discharge and sediment concentration are subjected to more fluctuation than at Karehsang station down stream because of it's high elongation ratio, steepness, high Kc value, bifurcation ratio, geology and poor vegetation cover (Table 4.7).

Table 4.7: Summury of physiographic characteristics of the study area.

Basin	Kc	Rf	Sw	Re	Tc	Rc
Lar	1.57	0.24	4.22	0.55	4.8	0.4
Nour	1.6	0.2	5.9	0.5	8.2	0.39
Haraz	1.57	0.32	5.27	0.49	11.1	0.4

4.5 SUMMARY

Polour is located at the lowest altitude in the Lar basin, where the climatic type is semi-Mediterranean. The maximum rainfall occurs during winter but summer is dry and semi-arid, similar to much of Iran. Amberjeh's classification is based on annual rainfall and seasonal temperatures. The data from the Haraz basin including the Lar Dam sub-basin, can be summarised as follows:

The precipitation in downstream areas is considerably higher than in the mountains. Downstream the adequate precipitation and relative humidity supports relatively high density vegetation cover. The major rainfall is in March/April. In the mountainous areas, especially the Lar Dam basin, the main climatic feature is the long cold season from November to April. This coincides with the period of maximum precipitation which falls mainly as snow. The summers are warm to hot, depending on altitude, and are generally dry although some convective storms do occur, particularly during the spring and autumn. The temperatures at Polour range from a maximum of around +42°C (July 1958) in summer to a minimum of around -40°C (January 1969) in winter, and monthly temperature is from an average +18.2°C in July to an average coldest months in January -5.5°C (see Appendix Ch.4, enclosed floppy at the back). These conditions, related to other physical factors (e.g. geology, vegetation), provide different kinds of erosion in the Lar basin. The Dalichai catchment with volcanic rocks and cold weather, is prone to weathering which produces scree and talus formation on slopes which are eroded by stream flow and rainfall (see folded map no.4). In the Sefid-Ab catchment, with limestone formations, weathering conditions also produce extensive scree forms on slopes which are mostly covered by vegetation. High drainage densities in this area allow erosion of the base of the formation. In the Lar and Khoshkehlar catchments seasonal precipitation erodes river banks and bare soil areas.

The physiography of the area studied is strongly influenced by the regional structure and by the lithological nature of the outcrops. It is an area with strong relief, in which intense vertical tectonic movements operated until the Pleistocene, giving a clear trend to the morphology of the range. From the western side to the eastern side of the Lar basin, one can distinguish the following physiographic regions, all of which are aligned east to west.

* *Lar valley alluvial flats:* Along the course of the Lar River, just across the central zone of the ridge, are wide alluvial flats, originated by the volcanic damming of the Lar valley north-west of Polour. The flats have been successively eroded by the meandering Lar River which has engraved a very complicated series of large terraces.

* *Damavand volcanic cone:* Between the Haraz valley and the Lar valley the Quaternary volcanic cone of the Damavand is a massive structure superimposed on a intensely folded and faulted Mesozoic basement. The western portion of the Dalichai catchment is covered by volcanic rocks. Destructive action is mostly mechanical and due to the high velocities of the stream, the catchment supplies large sizes of volcanic rocks. This portion of the basin possesses steep slopes and is semi-active tectonically; landslides, rockfalls and their delivery of sediment to down stream are very common.

In addition to broad structural influences, the indirect effect of the Damavand volcanic eruption was that of a lava dam created on the Lar. This geological occurrence also formed a large depositional area along the Lar valley of lacustrine formations that caused later morphological changes in the study area. Terraces, landslides and sinkholes are related to this formation which have created problems for the recent artificial Dam. On the other hand Damavand volcano blocked this portion of the basin in the past resulting in completely different surface changes than those in the western Lar. The mophotectonic map of the basin shows that the influences of morphotectonic activity are considerable and will affect sediment delivery to this area. Thus erosion is influenced by different geological characteristics and climate conditions in the Lar basin. In the Dalichai, which possesses volcanic and sedimentary formations, two kinds of erosion will be described in the follow chapters. In the Sefid -Ab catchment the only formation is limestone and this is very prone to weathering, forming talus, scree and landslides. In the Lar and Khoshkehlar catchments, former Lake formations are easily erodible.

The physiography of the Lar basin shows that western sideof the Dalichai catchment can be more prone to erosion because of its high drainage density and circular form than the two other catchments which were described. The western side of the elongated Lar basin has low erosion but lithological, vegetation and climatic conditions accelerate erosion in this area. In the middle Sefid-Ab catchment, physiographic characteristics make this catchment a normal basin.

The majority of vegetation in the Lar basin includes shrub-perennial grasses and forbs (51.8%) and a minority is cultivated land (0.2%). Measurement on the aerial photographs, KFA-1000 and remote sensing data show that 15333 ha. out of 73086ha. (whole area) is covered by very poor vegetation, 92567ha. is rocky land and 45991ha. covered with grassland. 33.6% of the basin is subject to surface erosion. This estimation of surface erosion is considerable for Khoshkehlar, Dalichai, Sefid-Ab, Alarm and finally the Lar subcatchments. In Dalichai catchment climate and geologic characteristics are a major factor in erosion especially on the volcanic rocks influenced by mechanical weathering. In the Sefid-Ab, the upstream and downstream sections are vegetated but the middle is characterised by bare soil which supports scree and talus features on slopes. In Lar and Khoshkehlar, river bank and terrace areas are covered by vegetation, but the bare soil of the limestones are prone to erosion especially in the western Lar and Khoshkehlar catchments.

CHAPTER 5: MORPHOLOGICAL CHANGES AND DEPOSITION

INTRODUCTION

In pre-Pliocene times the Lar River eroded its valley into the Cretaceous and Jurassic limestone rocks of the area. Upstream of Chehel-Cheshmeh, in Imampahnak and in the valleys of the Sefid-Ab and the Dalichai, the rivers also cut into Liassic formations and Eocene Green Beds. Eruptions of Damavand in the Pleistocene caused a blockage of the valley and the creation of a lake within which large amounts of sediments were deposited. Subsequently there was a complex phase of lake drainage and the lake deposits were partially removed by river action to form the terraces now seen in the valley.

The aim of this chapter is to assess the history of erosion and sedimentation, the influences of the Damavand lava flows on sedimentation and morphogenesis, and the linkages between the deposits and contemporary geomorphological processes in the Lar Dam Basin.

5.1 SEDIMENTATION CYCLES IN THE BASIN

The initial eruption of Damavand in the early Weiselian, about 58000B.P. (Allenbach 1966) blocked the Lar stream and resulted in the formation of a palaeo-lake which extended more than 25 kilometres upstream. Within this lake large amounts of sediment were deposited. After a prolonged period of accumulation of lake deposits, a further phase of volcanic eruptions occurred and large quantities of trachyandesite lava flowed out over the existing Lake sediment.

Surface observations throughout the Lar basin and subsurface investigations (borehole data from Dam Authority 1994) around the Dam wall area have indicated that the Lar Basin deposits can be subdivided into a series of relatively well defined units. In order to obtain a better understanding of the sediments it was considered desirable to attempt a more detailed subdivision of the deposits. Therefore the sediment were initially subdivided into the Lower and Upper Lake deposits.

The lower Lar valley is dominated by the volcanic cone of Damavand and the associated effusive rocks. The earliest Damavand lavas are probably post-Pliocene in age since they do not show signs of deformation and hence must post-date the most recent tectonic phase (Allenbach 1966). The basaltic flows at Polour almost certainly belong to this early phase. At Polour these rest directly on river gravels and it is likely that this series of flows caused the initial damming of the old course of the Lar and first initiated lake Lar. The first stage of lake deposits are referred to as the Lower lake deposits and consist of stiff grey, (brown) silts and sands. Following their deposition there was a second major phase of vulcanicity, marked by thin bands of tuffaceous material in the upper part of the Lower lake deposits. This second phase of activity produced the large amount of intermediate lava, (generally trachyandesite) which is bounded to the south and east by the Lar and Dalichai rivers. The outflowing of these lavas re-initiated lake Lar, since it is thought likely that either partial or complete drainage of the lake had occurred prior to this stage (Allenbach, 1961). In the first stage of the lake deposits when the lava dam was breached. Within the second lake, silts and sands were again deposited. These are overlain by large quantities of coarse sandy gravels which are thought by Assereto (1966) to represent reworked alluvial or colluvial fan deposits. Subsequently the lake was drained and the rivers incised in a series of phases to produce the prominent set of terraces now found in the Lar valley. One anomaly here is the fact that the valley of the Lar is a steep sided gorge, possibly formed by the sudden collapse of some sort of cavern system, whereas the presence of terraces suggests that the river had gradually cut down its course in a series of phases, each phase being represented by a terrace level upstream.

Allenbach (1966) has reported that C^{14} dating of plant remains from the terraces of the lower Lar give a minimum age of 38500 B.P., indicating a probable late Pleistocene age (early Weiselian) for the lower Lake deposits. The origin of these is directly related to the southern lavas of the Damavand volcano, which dammed and caused the infilling of the lava lake. In contrast, the most recent volcanic deposits of Damavand are Holocene and the volcanic cone shows no sign of Pleistocene glaciation.

The present topography of the lower Lar valley is a combination of both erosive and depositional features. The Jurassic and Cretaceous limestones were eroded into their present form during Pleistocene times. Subsequently the valley of the Lar was blocked by the Damavand lavas which still retain many of their primary features and so can be quite

easily recognised on the ground. The old course of the Lar River is thought to flow under the southern side of Damavand and to emerge in the present Haraz valley in the vicinity of Ab-Ask village.

5.2 GENERAL OBSERVATIONS ON SEDIMENT DISTRIBUTION

The aim of this section is to identify the main sedimentary units in the Lar basin. Examination of the morphology of the study area using aerial photographs and KFA-1000 images reveals the influence of Damavand on drainage patterns. The prominent east-west limestone ridges which pre-date the Damavand eruptions can be seen to disappear beneath the volcanic deposits and to emerge on the opposite site of the cone. The major rivers, in contrast, have all been diverted around the volcano; the Dalichai to the west, the Lar to the south and the Haraz to the east.

This diversion of the rivers occured after large quantities of sediment and detritus accumulated in the former valleys upstream of natural lava dams. The largest of these accumulations is in the Lar where the sediments can be traced upstream to Ab-Sefid and beyond Asb-Kalak (Figure 5.1) outside the limits of the volcano. Smaller accumulations can also be recognised in the upper valley of the Dalichai in the east of study area, downstream of the Lar gorge at Polour village, and in a tributary valley about 12 km. farther downstream (Figures 5.1). The various groups of sediments, whilst they share a common origin in that they accumulated upstream of lava dams, were not interconnected.

The maximum elevation reached by the sediments varies from sub-basin to sub-basin. The maximum elevation reached was in the Dalichai catchment upstream where sediments accumulated up to about 3500 metres altitude whilst at Polour a maximum height of sediment of only 2260 metres was attained. These various elevations represent the spillway levels in the lava flows responsible for damming the individual valleys. The present Lar-Lassem conjunction was dammed at about 2300m where a spillway accures and in the Dalichai-Lar at about 3500 metres.

The elevations of the top of the deposits also varies within sub-basins. Within the main portion of the Lar Basin, the top of the sediments attain a height of 2600 metres in the Kamardasht area. However, on approaching the main tributary valleys which provide

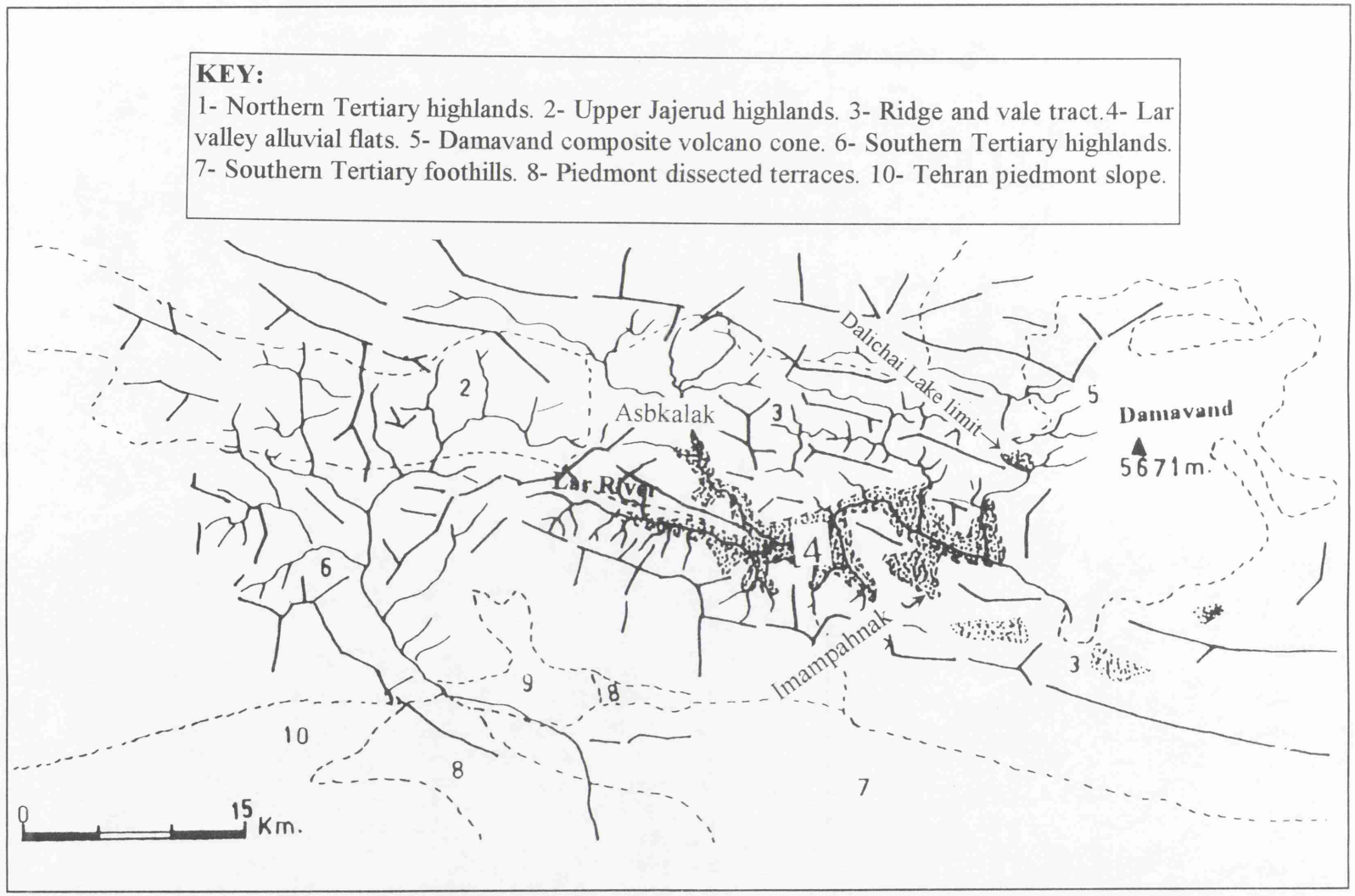

Figure 5.1: Tectonic Sketch Map of the Lar Dam Basin
(the coloured area shows alluvial deposits; *after Assereto, 1960*).

major sediment sources, the elevation of the top of the sediments begins to rise quite sharply with slopes of between 1 in 50 and 1 in 100 (see folded map no.1 in folder at back). This change in slope marks the boundary between the main basin sediments and the subaerial alluvial fans built up by the tributary rivers as they entered the basin.

The distribution of the Lar Basin sediments for 15 km below Chehelcheshmeh is shown on Figure 5.2-a. They are capped by a thin bouldery surface layer and are consequently not particularly well exposed, except in limited river cliffs where the top 100 metres or so of the succession is visible. Neverthless, it is clear from the limited exposure of the deposits and the borehole data in Figure 5.2-a that considerable vertical and lateral variability occurs within them. It is also clear that the upper sediments overlie the bulk of the Damavand lavas and so post-date them.

Assereto (1966) reported a general vertical sequence of predominatly medium to coarse gravels overlying a sequence of clay and silts with thin beds of sand. In detail the sequence is more complex than described by Assereto. The gravels are horizontally bedded, weakly cemented, well rounded and rather sandy. They are normally covered with rounded boulders, the composition of which varies throughout the basin. Lava boulders are found around the Dalichai river (Figure 3.15-a), and extend a considerable way up the Lar valley towards the Sefid-Ab. Elsewhere, lava boulders are absent and the cover layer consists largely of rounded limestone boulders. The gravels are locally underlain by finer grained deposits of interbedded silts and sands. These are particularly well exposed on the left bank of the Lar near the Lar Gorge. Elsewhere, these have been largely eroded and the reworked gravels rest uncomformably on eroded surfaces of silts and clays.

Silts and clays infill the majority of the Lar basin. They occur beneath the sands and are only very locally exposed in river cliffs. Their presence elsewhere can be deduced from the presence of damp ground marked by concentrations of green vegetation on aerial photographs and local minor slope instability. These fine grained deposits consist largely of thin bedded to laminated, low plasticity silts and silty clays with minor sand bands. Some variation does occur in composition, as for example on the left bank of the Lar at Chehelcheshmeh where they consist almost entirely of high-plasticity silty clays; the higher

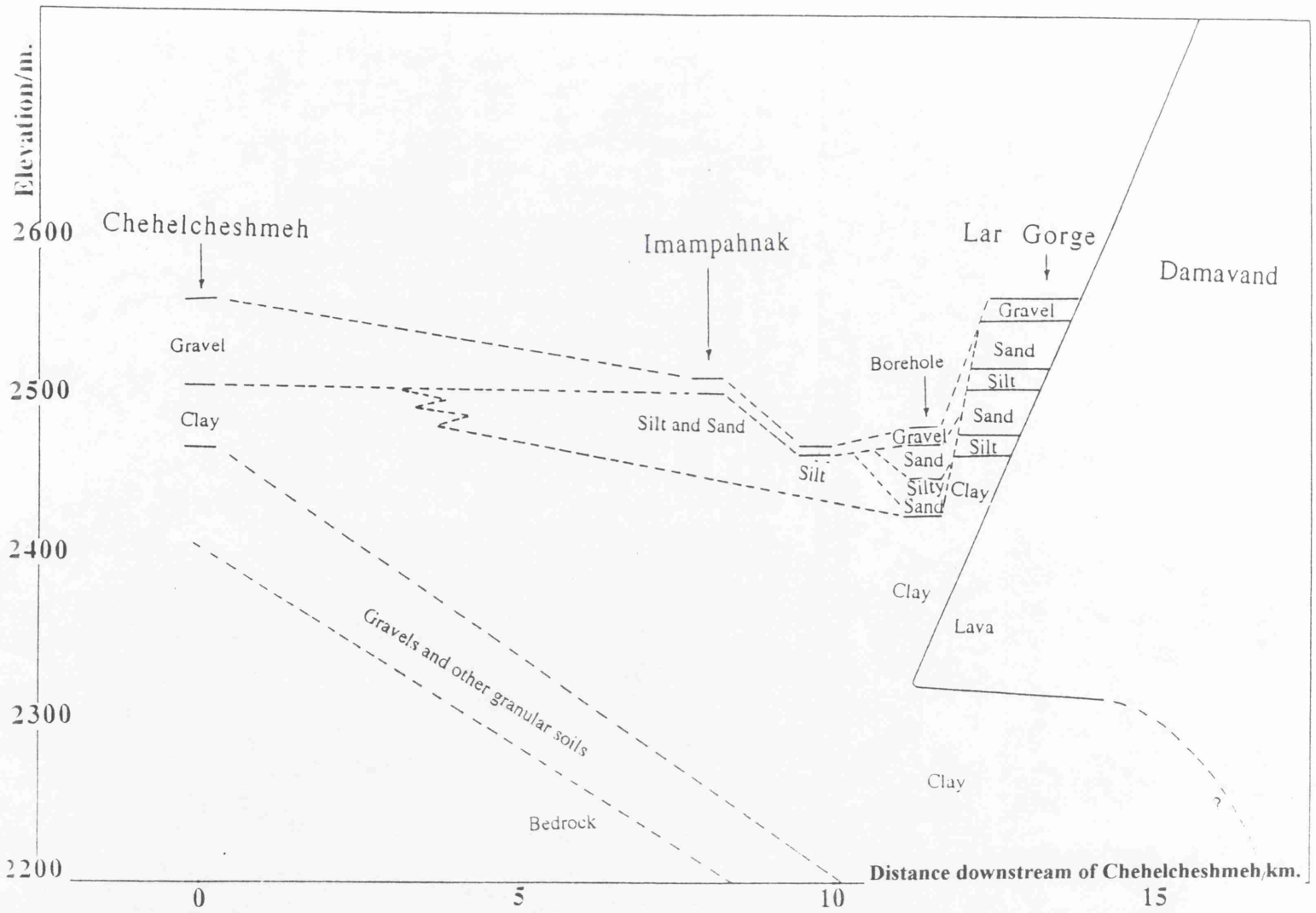

Figure 5.2-a: Distribution of sediments in the Lar basin
(source of borehole data; Lar Dam Authority, 1973; see geology map for location).

plasticity reflecting the derivation of the soils from the argillaceous tuffs of the Karaj formation exposed on the valley sides upstream.

5.2.1 Great Lake Lar

The Damavand lava flows blocked the Lar valley at 2200m altitude in the south and resulted in the formation of a lake which extended up the valley for more than 25km. The important sediments in the Lar catchment valley, consist of extremely thick deposits (borehole at Chehelcheshmeh) which extend for more than 60m below the present level of the Lar without encountering bedrock (Bailey et al., 1948). The upper portion consists predominantly of medium coarse gravels, whereas the lower part is composed mostly of clays with silts and thin beds of sands. These deposits are related to the filling up of the former Lake Lar as a result of lava damming of the valley south of the present volcano. These lake dedopsits were subsequently eroded and the wandering river incised a very complicated series of terraces whose geomorphology has been mapped in detail (see Figure 5.2-b).

5.2.2 Small Lake of Dalichai

North of Kuh-e-Namakkusar in the upstream section of the Dalichai (Vararud) there are deposits related to infilling of an ancient small lake which also originated by volcanic damming of the valley (see Figures 5.1 and also 4.7-a). The surface of the infilled lake appears subhorizontal in the centre of the basin and lies at about 3200 m. At the edges the deposits lie higher and are slightly inclined. These lacustrine deposits were subsequently eroded by a wandering river which has incised a series of terraces (see folded map no.4, back pocket). The alluvial deposits developed at Vararud are identified on the map with the same symbol as the ancient deposits in the Lar and are analogous to them, although they are not directly connected. (see Figure 4.7-a). It seems, at one time the Dalichai Lake reached a height of about 3500 m, and extended for about 7 km, as far as the northern slope of Zand Kuh (see Figure 4.7-a). In Figure 5.2-b the limits of this lake are shown as ancient deposits. On account of it's smaller size and the steepness of the flanks of the surrounding mountains, the Dalichai Lake has been infilled with coarser material than that of the Lar Lake (see Figure 5.2-b).

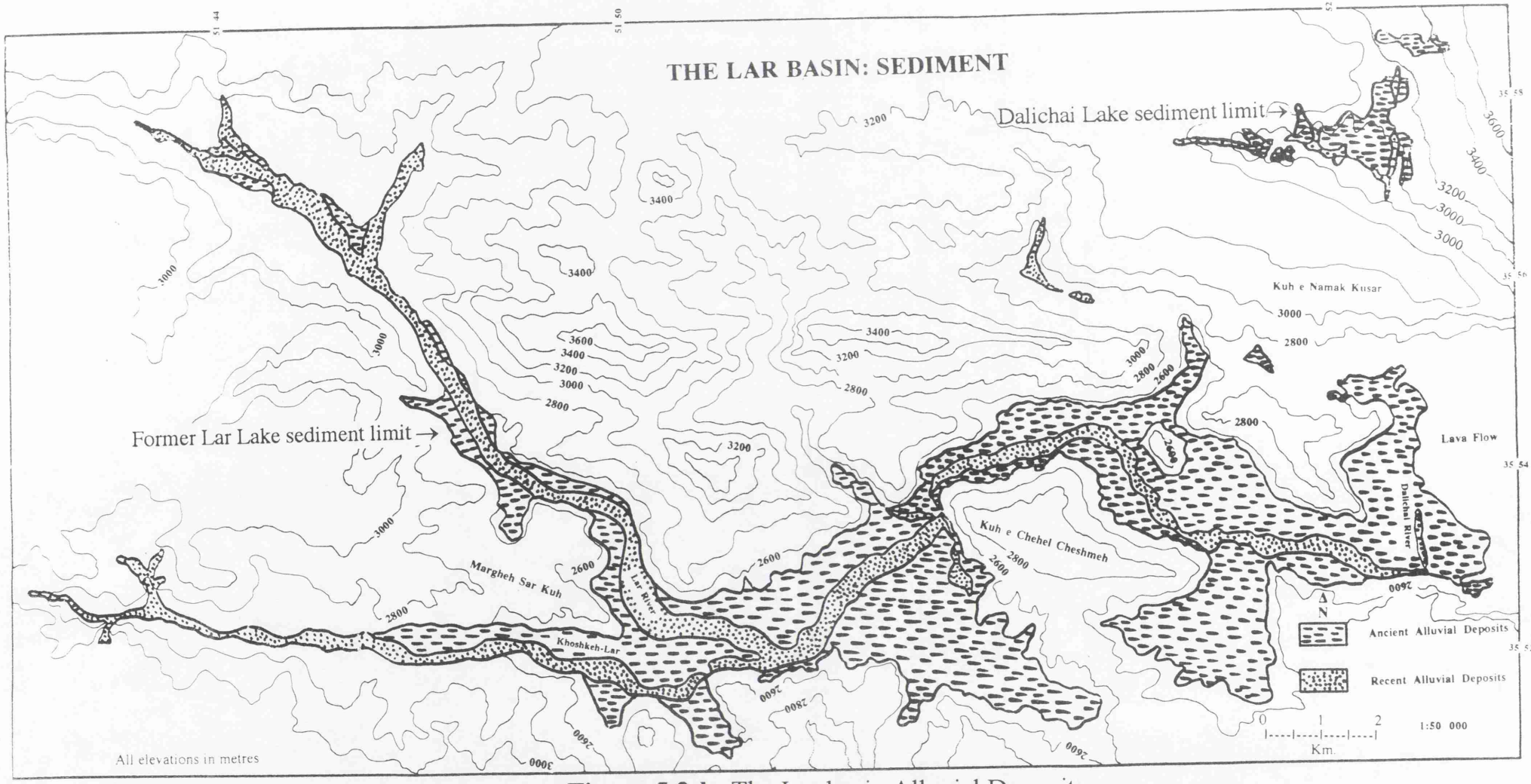

Figure 5.2-b: The Lar basin Alluvial Deposits.

5.3 SEDIMENT IN THE IMAM-PAHNAK AREA

On the southern side of present Lake, Imampahnak is a depositional area which shows sequences of terraces that are largely composed of horizontally thin bedded to laminated silt and sand. The terrace surfaces are formed of a variable thickness (1.5-5 m) of reworked, well graded sandy gravels which rest unconformably on an irregular erosional surface cut into the underlying fine grained deposits.

Within the silt horizons, coarse silt and fine sand dustings occur on the bedding planes. Some of the beds are graded whilst others are occasionally fissured. The noncohesive bands are generally of silty fine and fine to medium sand and at scattered localities erosional surfaces can be recognised at the base of sand horizons. These are characterised by the presence of reworked silt pellets immediately above the erosion surface. The sands then tend to pass gradationally up into overlying silts. Cross bedding is also locally developed in the sands. On the eastern margins of this area, approximately 500 metres upstream of the Dalichai confluence, a sequence of loose uniform fine sands have been exposed in a road cutting beneath a thin (0.5 metres) cover of topsoil and deposits, the deposits lying some 10 - 20 metres higher than the silts exposed upstream. The sands are cross-bedded and contain abundant rounded gravel sized fragments of light porous lava derived from Damavand. Some thin irregular, subhorizontal horizons of brown silt occur within the sequence and are characterised by the presence of small calcareous nodules and small root hollows; features typical of fossil soil horizons.

5.4 MORPHOLOGICAL CHANGES IN THE LAR BASIN

Morphotectonic characteristics of the Lar Basin were explained in Chapter 4 (Figure 4.7). The terrace gravel bands on the left bank of the Lar near the entrance to Imampahnak have been displaced about 2 metres by fault movements, and on the right bank of Dalichai, some 4 kilometres upstream of the Lar confluence, a second fault has displaced by the terrace gravels about 5 metres. This displacement is clearly visible on the aerial photographs and KFA-1000.

On the left bank of the Lar river, in the area which has been intensively studied, undulations have been noted in the boundaries that separate the various members of the

Upper Deposits. Marwick (1972) suggested that these undulations were the result of faulting. However a second possible explanation is that the undulations have developed as primary sedimentary features caused by variations in the amounts of material deposited at different positions in the basin. In order to demonstrate whether or not faulting of the Upper deposits has contributed to the production of the undulations in the boundaries of the members the available evidence has been re-examined in the light of Marwick's interpretation. A correlation between facies changes and the undulations would tend to suggest that some at least of the undulations had resulted from primary depositional processes.

According to aerial photo interpretation and field observations the following can be concluded: faulting of the upper deposits in the upper Dalichai is observed in surface exposures. On the right side of Dalichai the only feature that could be reliably interpreted as a fault scarp is the line bounding the lava outcrop to the north of the horseshoe form. This line trends in an east west direction and to the west joins up with a fault line which is clearly visible on the remote sensing data especialy on KFA-1000 (Figure 4.7). There is a distinct E-W trough in the upper surfaces of the lower and middle silts and sands centered at about the same location as the faults postulated by Marwick. The organic silts and clays occur in two basin shaped depressions on the lava surface. In the westerly trough the upper surface of the deposits lies at an elevation of about 2455 metres whilst in the easterly area the upper surface of the deposits is generally 8 metres higher. The level of the top of the lower sands is virtually constant over the part of the site under consideration.

It would appear that the most recent period of movement on these faults occured after the end of deposition of the upper deposit but prior to the formation of the river terraces. On the downstream side of the Dalichai the top of the lower sands is effectively horizontal and hence any faulting of these sediments ceased prior to the end of the deposition of the lower sands i.e. much earlier than the final movements on the faults just upstream.

It is most likely that the undulations in the boundaries of the upper deposits were produced by variations in the thickness of sediments laid down around a river channel and by the effects of scour along the length of the channel. Nevertheless it is still possible that some faulting of the sediments has occurred either as a result of movements of faults in

the underlying bedrock, which are known to extend beneath the site. Alternatively faulting could have occurred due to movements in the lava caused by differential gravity compaction of the underlying lower lake deposits (Figure 4.7).

5.5 CLASSIFICATION OF DEPOSITS IN THE LAR DAM BASIN

Field inspection throughout the Lar Dam Basin, and of the subsurface data from the Dam Authority around Lar Gorge, indicate that the Lar Basin deposits can be classified into a series of relatively well defined units as follows:

Present deposits: Coarse granular deposits often resting unconformably on older finer grained deposits. Interbedded silts and sands. Clay with some intercalated silts, sands and gravels. Coarse granular deposits resting directly on the eroded, largely Mesozoic, bedrock surface. This class of deposits represents the youngest formations in the Lar basin.

Past deposits: The general distribution of these sediment types throughout the basin is shown in Figure 5.2, and can be identified as the oldest deposits. In order to obtain a better understanding of the sediments it was considered desirable to attempt a more detailed subdivision of the deposits. The initial eruption of Damavand volcano in Pleistocene times resulted in basic lavas blocking the valley of the old Lar river. This river is believed to have flowed beneath the present southern slopes of Damavand volcano and to have emerged in the present Haraz valley in the vicinity of Ab-Ask village (Figures 5.3 and 5.4).

The blocking of the Lar valley resulted in the formation of a lake which extended up the valley for more than 25 kilometres. Within this lake large amounts of sediment were deposited, consisting basically of grey (weathered to brown) silts and sands; minor amounts of gravels were also deposited. After these lake deposits had been accumulating for some time a further major phase of volcanic eruption occured and large quantities of trachyandesite (intermediate) lava flowed onto the existing lake sediments. The lake sediments deposited prior to this major volcanic phase are hereafter referred to as the "Lower lake deposits".

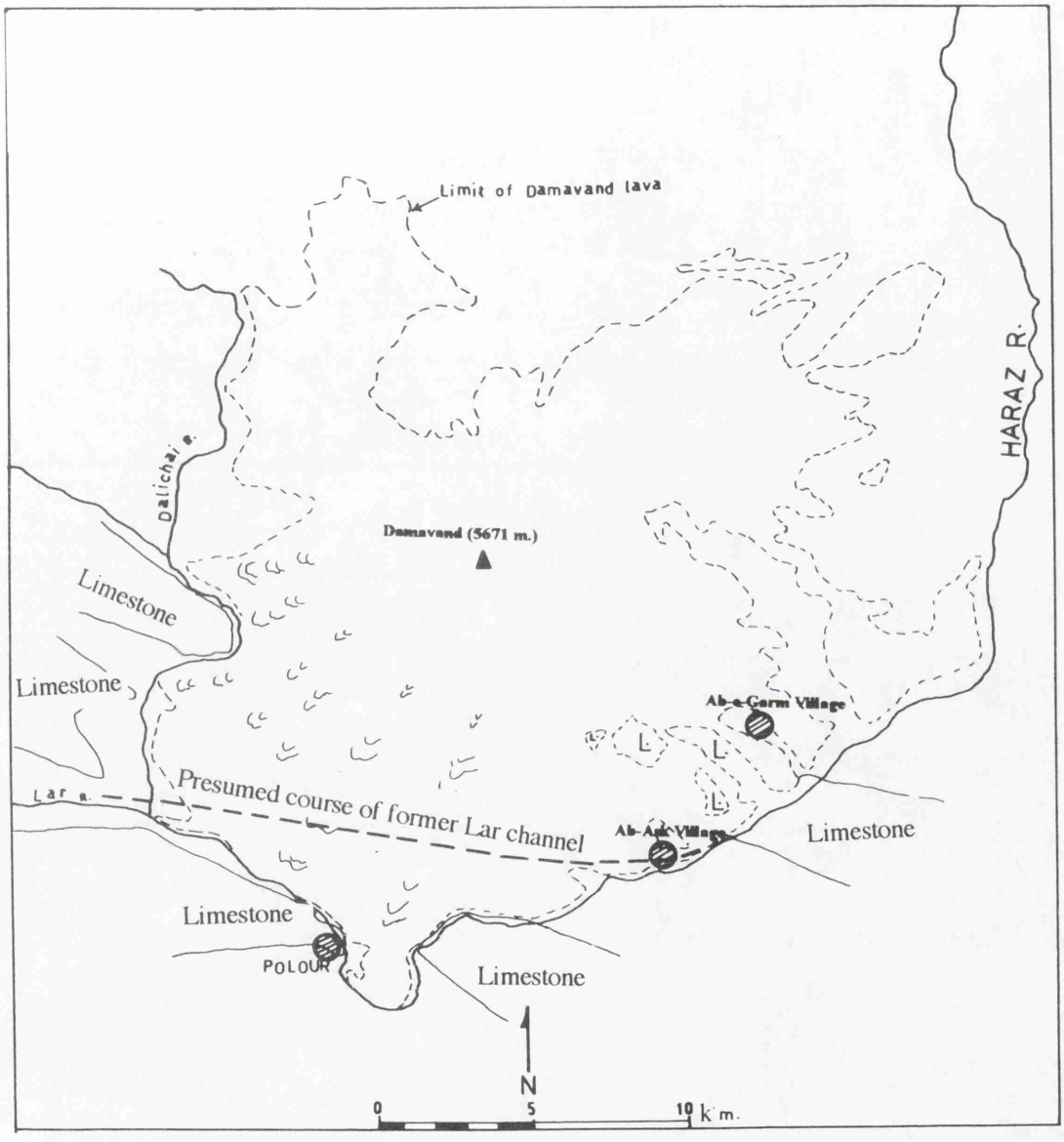

Figure 5.3: Presumed Course of the Former Lar Channel.

Figure 5.4: Former Lar River terraces at Ab-Ask village, looking Northwest
(Approx. Scale 1:200; July 1993, see also Figure 5.3).

Further lake sediments were then laid above the lavas. These are referred to as the "Upper lake deposits" and again consist of brown and grey silts and sands. These in turn are capped by coarse sands and gravels which appear to represent a sequence of river deposits, together with some reworked fan debris. These deposits are thought to have been formed after the drainage of the lake, during the period when the rivers were down-cutting their beds to form the prominent set of terraces now seen in the Lar valley (Figure 5.5).

The lithologies of the upper and lower lake deposits are basically similar. Downstream of the Dalichai confluence, upper and lower lake deposits are separated by many tens of lava beds, and hence the subdivision is useful in defining the position of samples and soil types within the overall succession of the area. A major difference between the upper and lower deposits lies in their deformational history. The upper deposits are normally horizontally bedded and undeformed. In contrast the lower lake deposits, when they occur beneath the lavas, have taken on a dip, in some cases they are nearly vertical. This is partly due to differential gravity compaction of the sediment and partly due to the squeezing up of the sediments between advancing tongues of lava.

Upstream of the Dalichai, beyond the limit of the Damavand lavas, the subdivision between the upper and lower lake deposits becomes difficult to define as the entire sequence of sediments are horizontally bedded and undeformed.

5.5.1 Lower Lake Deposits

The lower lake deposits rest directly upon the floor of the ancient valley of the Lar river. Their maximum thickness is 120 metres although the original maximum thickness could have been much greater since a large degree of consolidation of the deposits has occurred under the influence of the loading imposed by up to 100 metres of overlying lava. On moving north from the present Lar river, the lower lake deposits increase in thickness by about 50 metres towards the centre of the old valley.

Subsequent changes in sediment thickness have occured, largely due to the influence of the overlying trachyandesite lavas. The vertical loading imposed by the lavas has resulted in the consolidation of the sediments especially in the centre of the valley. In addition to

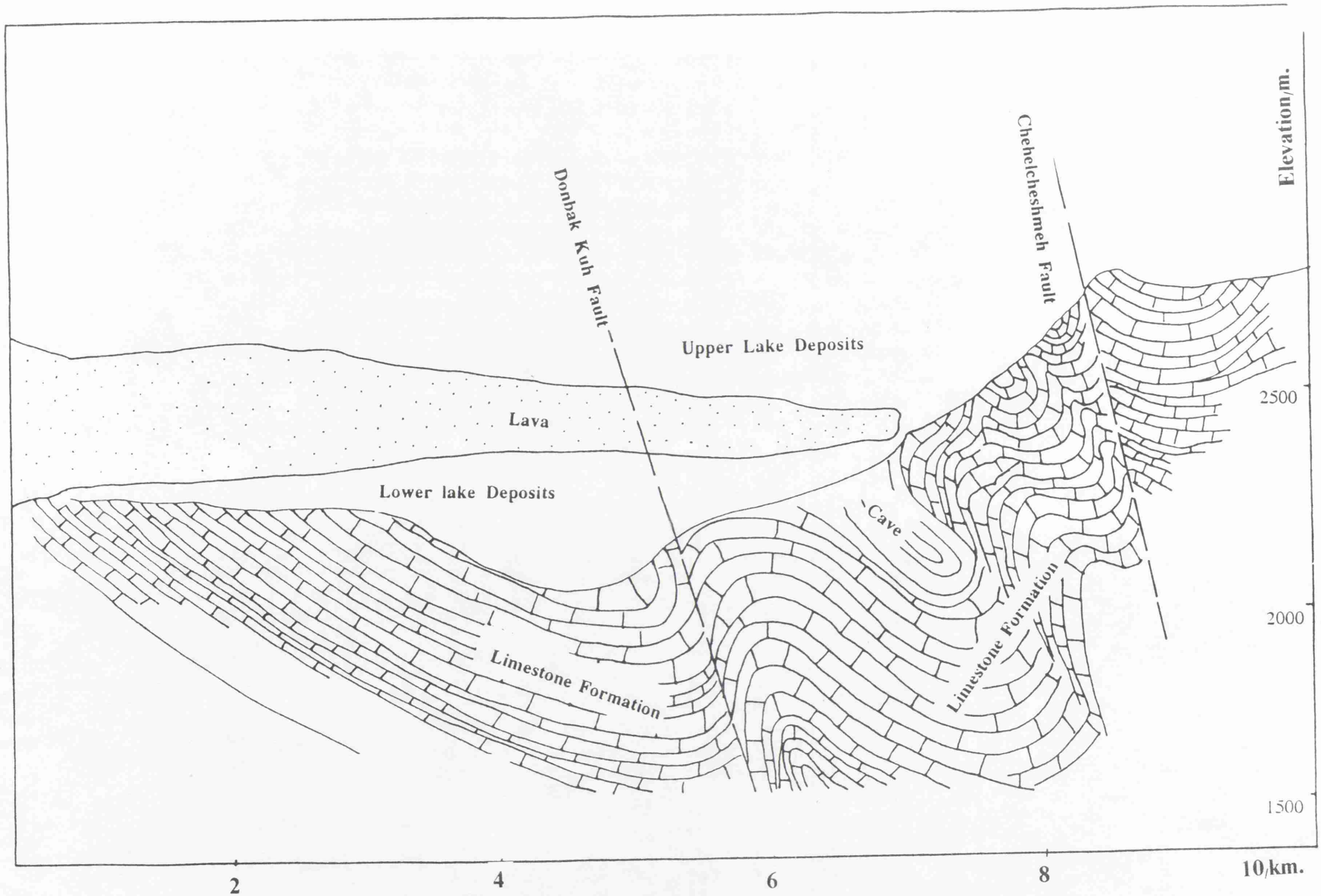

Figure 5.5: Presumed Upper and Lower Lake Deposits
(source; exploration data from Lar Dam Authority, 1994).

the vertical loading imparted by the lava, horizontal shear stresses are thought to have been produced by the lava tongues advancing over the lake sediments. These stresses, combined with the effect of the vertical loading, have resulted in the forcing up of the sediments between the advancing tongues of lava. Abundant small scale faulting within the lake sediments also occured at the flanks of the lava outcrops. Evidence of the forcing up of the lake sediments between advancing lava tongues has been found on the right bank of the Lar. Here, brown silts and sands can be seen in direct contact with the lavas. The silts immediately adjacent to the lava have been subjected to contact metamorphism as they are now hard and brittle and contain much sand sized lava debris.

Beyond a thin disturbed zone, of the order of 0.1 metre thick, a 1 metre band of brown silts and sands occurs, again showing signs of contact metamorphism, but containing no lava debris. The margins of this horizon are parallel to the lava contact and are not controlled by the bedding within the sediments, which can still be clearly distingushed. Beyond the metamorphosed zone the silts and sands retain their steep dip, and a series of planar structures, apparently a form of cleavage, are developed.

Deformation within the lower lake deposits largely takes the form of small scale faulting. Some minor movements appear to have taken place along 'joints' as displayed by the presence of slickensliding. However, where these shear joints cross a distinct marker horizon, virtually no displacement can be distinguished. No small scale fissures have been recognised within the lower lake deposits except immediately beneath a zone which is believed to represent the contact between the upper and lower lake deposits. At this locality the lava is absent but the contact is marked by thin grey bands of tuffaceous material. There is a marked angular discordance between the horizontally bedded sediments above, and the grey silty clay below this band. The lower deposits dip to the north about 5° - 10° and are characterised by abundant small scale fissuring. Occasional dessication cracks can be recognised and it is tentatively assumed that the fissuring is to a large extent the result of dessication. The type of faulting developed within the lower lake deposits is related to the loading produced by the lava. When the lake deposits lie ahead of the lava front reverse faults, dipping to the north, are dominant, whereas beneath the lava front normal faults also dipping to the north predominate.

The lower lake deposits consist of grey silts with some sands and gravels. A frequency histogram of the mean particle sizes of soil samples shows a marked peak in the fine to medium silt sizes (Figure 5.6). A frequency histogram of the uniformity coefficient of soil samples has similary been plotted and shows a marked peak in the range of 3 to 10 (Figure 5.6). Thus the dominant soil type consists of well graded silts. The sand horizons were of two types. Beyond (at the Lar downstream) 50 metres below the dam, the dominant variety consisted of a brown silty fine to medium sand which was regularly inter-bedded with brown silts. The second sand is found predominantly upstream of this. It is generally coarser grained and is characterised by the presence of white mottling. This latter lithotype is thought to represent a reworked, partly tuffaceous deposit. Graded bedding was completely absent from the succession and cross bedding was only very locally developed indicating the relatively quiet and stable environment within which these sediments were laid down. It would be expected that, had traction currents been operating within the lake at the time of deposition of these sediments, then associated structures would have been developed, such as extensive cross bedding, graded bedding and possible ripple structures. The investigations have failed to discover any extensive development of such structures and therefore it is assumed that the waters of the lake were very quiet during this initial period of deposition.

The gravels occuring within the lower lake deposits appear to be water-lain as the fragments are all rounded. The gravels consist predominantly of limestone, but some fragments are derived from the Green beds and basic Damavand lavas. The significance of these latter fragments is that pre-existing lavas erupted from Damavand were undergoing active erosion prior to the major volcanic phase during which the large amounts of intermediate lavas were outpoured.

The lower lake deposits appear to be almost completly devoid of organic material, other than some small scattered mollusc shells. Also the sediments have failed to reveal any evidence of dessication or sud-aerial exposure other than at the extreme top of the succession, and then only very locally. The major horizons are generally thin and this rapid variation in soil types within the succession is also demonstrated from sinkhole exposures. However some significant sub-surface morphological changes which are discussed later in this chapter can be directly related to the Lower Lake deposits.

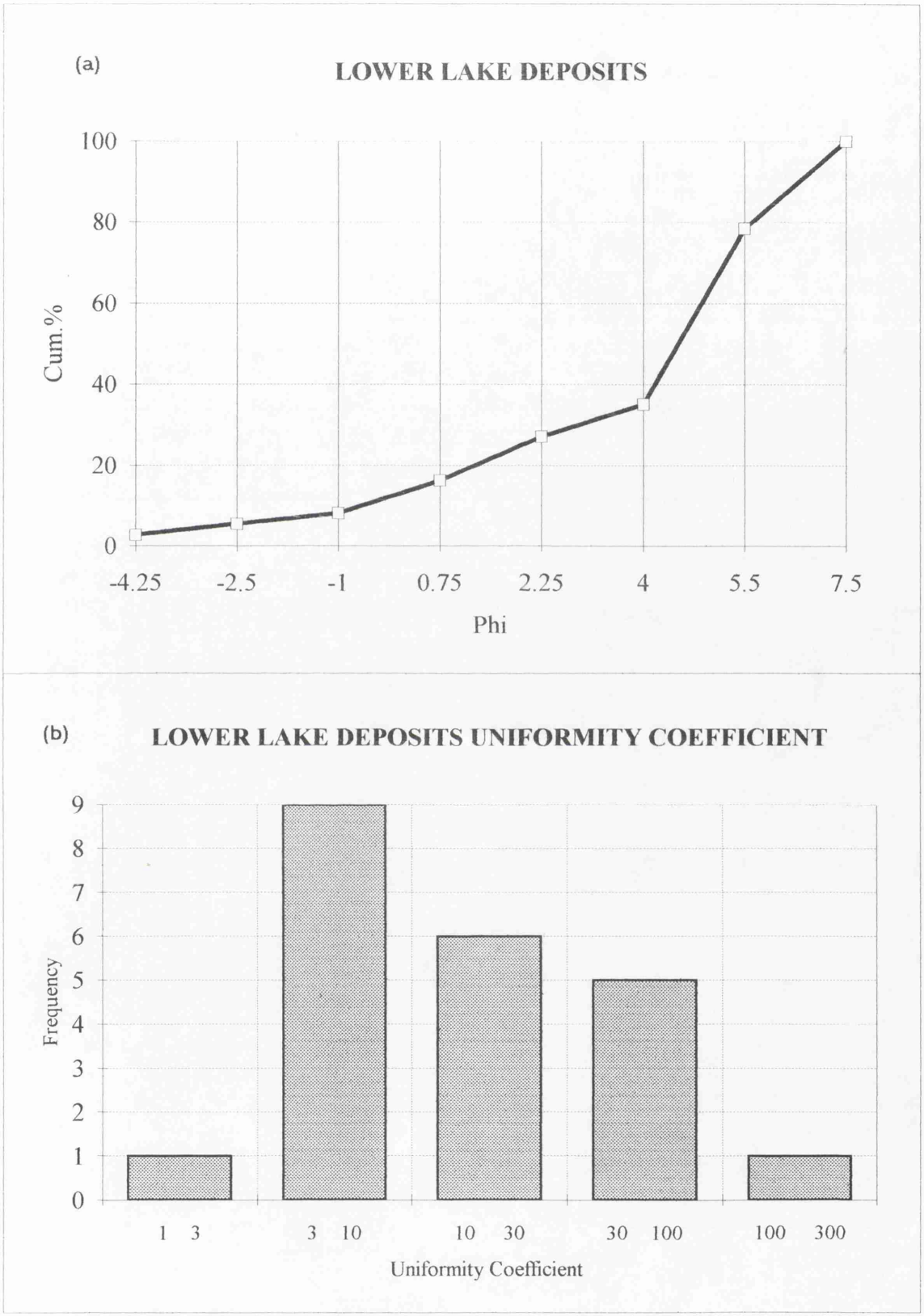

Figure 5.6: (a) Cumulative frequency curve of mean particle size from 22 samples from the Lower Lake deposits; **(b)** uniformity co-efficient from the same 22 samples.

5.5.1.1 Mode of Deposition and Subsequent History of Sediments

Several factors are relevant in the determination of the mode of deposition and subsequent history of the lower lake deposits, as follows:
there is rapid vertical variation in soil types; within the succession, silts are dominant, with some sands and gravels, but with virtually no clay; grading and cross bedding are virtually absent; other than small mollusc shells, virtually no organic matter is present; only at the very top of the succession do dessication features and traces of organic matter occur; tuffaceous sediments occur near the top of the succession; the mode of deformation of the sediments due to the stresses imparted by the overlying lava are partly brittle in nature; and the present water table in the rocks surrounding the lake basin is depressed well below what have been the former level of the lake.
The main issues concerning the development of the lake and its sediment fall into the two categories discussed below:
(1) the nature of the sedimentation conditions prevailing in the lake; and
(2) whether drainage occurred at any stage during the deposition of the lower lake deposits?

5.5.1.2 The type of sedimentation conditions

The lacustrine origin of these sediments is confirmed by the nature of the stratigraphy and characteristic of the sediments and by the physiography of the area and presence of a valley blocking agent. The rapid variation in sediment types may reflect a variation in the rate of inflow into the lake basin of the sediment-laden rivers. The cycles developed in the lower lake deposits do not have the same degree of regularity as fluviglacial varves, nevertheless a series of imperfect cycles does exist producing the problem of determining the causes of this cyclic sedimentation. The present day rivers exhibit an annually cyclic variation in flow: the peak flow occurs in the spring due to the melting snow and the minimum flow occurs in late summer. The lower lake deposits are Pleistocene in age and since a Pleistocene glaciation is known to have affected this area it is possible that during the winters the rivers were completely frozen so that no sediment entered the lake. The thickness of the individual bands of silt and sand is often in excess of 0.2 metre which may be excessive for an annual deposit. However, varves have been reported from Finland (Jones, 1970) which have a mean thickness of 0.3 m., near to the rivers source. In a lake

of the size of Lake Lar, most localities would have been relatively near to their sediment source and hence bands of 0.2-0.3 m. in thicknessmay be of seasonal origin.

It is clear that further data is required on the nature of the lower lake deposits before a clear picture as to their mode of origin is likely to appear. A detailed study of the sediments, together with the minor structures contained within them is clearly necessary. A study of the micro and macro fauna and flora may prove useful in establishing the climate of the area during the period of deposition of the lower lake sediments, and hence help to establish whether ice is likely to have exerted any influence on the sedimentation within the lake.

5.5.2 Upper Lake Deposits

Following the major eruption of Damavand, further lake sediments were deposited within the basin on the top of the lava and, presumably therefore, upstream of the lavas also. It is these sediments which occur above the lavas that are referred to as the "upper lake deposits". If the tuffaceous horizons are recognisable upstream of the lava output it will then be possible to extend the distinction between the upper and lower lake deposits well upstream into the main lake basin.

The upper deposits are currently defined as those lacustrine sediments which occur above the trachyandesite lavas in the vicinity of the Lar Gorge. The sediments occur as basin-infillings upon the irregular top of the most recent lava flow, and upstream they apparently spread out over the older lower lake deposits.They are overlain almost entirely by more recent river and reworked colluvial fan deposits (terrace gravels).

The distribution of the mean particle sizes of soils indicates that although there is a slightly wider spread than with the lower lake deposits, there is again a marked peak within the silt range spreading out into the fine sand range; minor gravels and clay also occur. The sediments are generally grey in colour when they are in the unweathered state but they appear to weather rapidly to a brown colour when exposed to the atmosphere, provided adequate moisture is present. The grey colour is retained after exposure if the material is retained in a dry condition (Figure 5.7). The upper lake deposits are

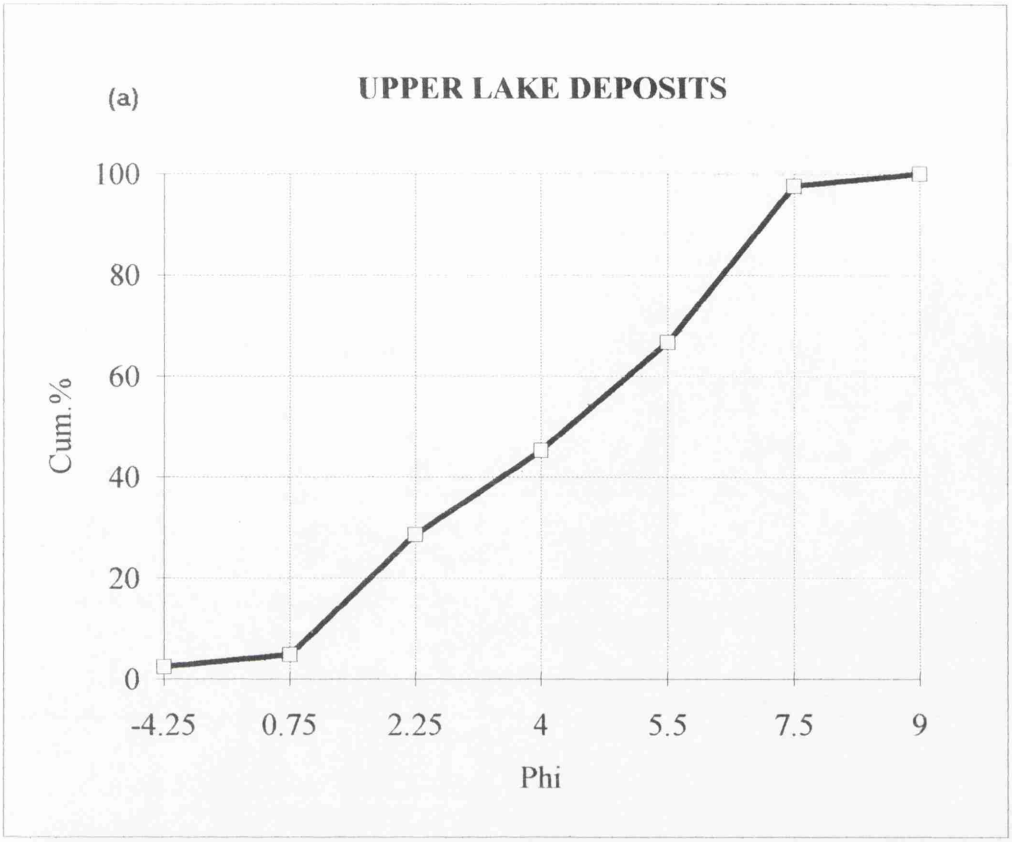

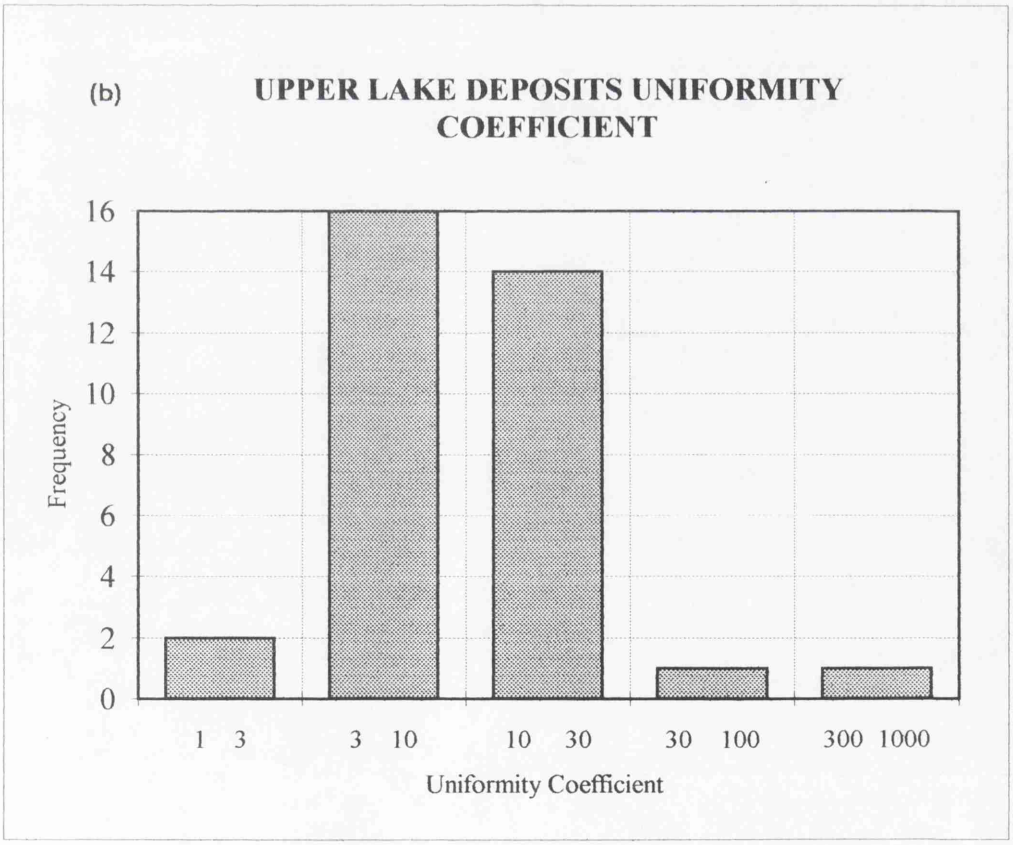

Figure 5.7: (a) Cumulative frequency curve of mean particle size from 34 samples from the Upper Lake deposits; **(b)** uniformity co-efficient from the same 34 samples.

horizontally bedded throughout. Small scale sedimentary structures are much more abundant than within the lower lake deposits (Figures 5.7-a and b).

5.5.2.1 Lithology

The upper lake deposits consist largely of grey silt, with some sands and very occasional gravels and clays. The most pronounced lithological difference between the upper and lower lake deposits lies in their distribution of particle sizes and clay fractions. The upper lake deposits consist of a sequence of horizontally bedded silts and sand with minor clays and gravels. Evidence has been obtained (Dam Authority, 1975) that these deposits were formed in a relatively shallow lake by a form of rather imperfect cyclic sedimentation. This appears to have been relatively unstable, as shown by structures produced by traction currents. Numerous fossil soil horizons have been identified, indicating that at frequent stages during the period when the upper lake deposits were being laid down, the lake was sufficiently shallow to allow vegetation to thrive on its bed. The various sedimentary structures discovered within the upper lake deposits will be described and their significance will then be discussed.

5.5.2.1.1 Penecontemperaneous Slump Structures

Highly irregular contorted bedding occurs in the upper lake deposits within a sequence of thin bedded brown silts and clays on the left bank of the Lar river (Figure 5.8-a). These structures are belived to result from the movement of incoherent masses of sediment on the lake bed, and can be attributed to instability (e.g. landslides) in the environment of sedimentation.

5.5.2.1.2 Cross Bedding

Abundant evidence of cross bedding, often associated with reworked silt pellets, has been found in the sandy horizons of the upper lake deposits. Again, the presence of these structures, of which appear to be ripple structures, indicates, a relatively shallow and dynamic environment of deposition (Figure 5.8-b).

Figure 5.7a: The Lar Lake Northern side lacustrine terraces (Approx. scale 1:100)

Figure 5.7b: Erodible lacustrine terrace formation (sand, silt and clay) at Gozaldarreh, looking Southwest (Aug. 1994).

5.5.2.1.3 Fossil Soil Horizons

Thin horizontal bands of brown sandy silt have been located, within the sequence of upper lake deposits, which appear to represent fossil soils. They also display some degree of horizontal colour lamination and invariably contain root hollows and white, decomposed root debris. Some infilled worm burrows were also discovered. Horizontal planes containing elongated, cream coloured calcareous concretions were also characteristic of these silt bands. A close examination of the silts and sand containing these fossil soil horizons indicates that their deposition has been approximately cyclic. A regular silt/sand cycle is rarely developed since thin sand bands tend to occur within the main silt horizons and, likewise but more rarely, silt bands occur within a predominantly sandy horizon. It is likely that the sands were deposited during periods of high river flow; this is indicated by the fact that such sands are often cross bedded. During this time of high flow some of the underlying silts were reworked and incorporated into the sand as pellets. As the traction currents decreased in velocity, successively finer grained sediments would settle out from the water. It is thought that this water gradually became shallower until the bed of the lake was invaded by plant life and disturbed by burrowing organisms. These conditions would then persist until a subsequent period of high river flow caused the inundation of the area. This process must have been repeated many times, as shown by the number of silt horizons which display the signs of having supported plant life.

It is difficult to estimate the period of time involved in the formation of the cycles described above. An annual cycle is perhaps the shortest possible time period, the period of high flow corresponding to the peak river flow in the spring caused by the melting of the snow. At the time of deposition of these sediments it is likely that the temperatures were lower than at present and hence the supply of sediment to the lake during the winter is likely to have been virtually cut off by freezing of the rivers. The relative scarcity of organic matter in the sediments could also be accounted for by the low temperature prevailing during the Pleistocene (Figure 5.8-c).

5.5.2.2 Environment of Deposition of Upper Lake Deposits

Again it is assumed that the sediments under discussion were deposited in a lake on the basis of the physiography of the area and the low activities of the cohesive members of the

PENECONTEMPERANEOUS SLUMP STRUCTURE:

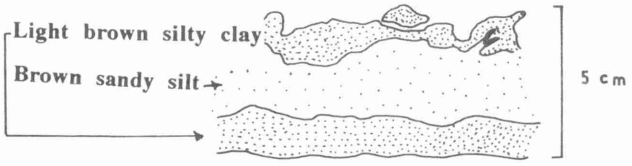

a)

CROSS BEDDING

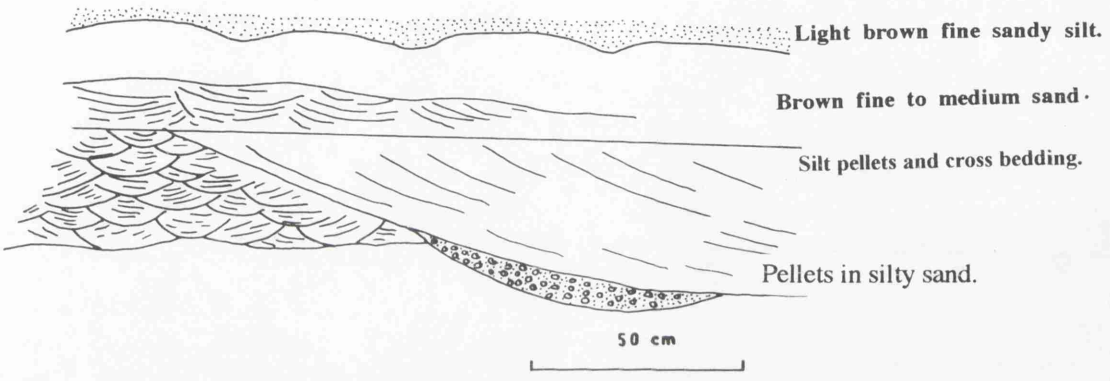

b)

CYCLIC SEDIMENTATION

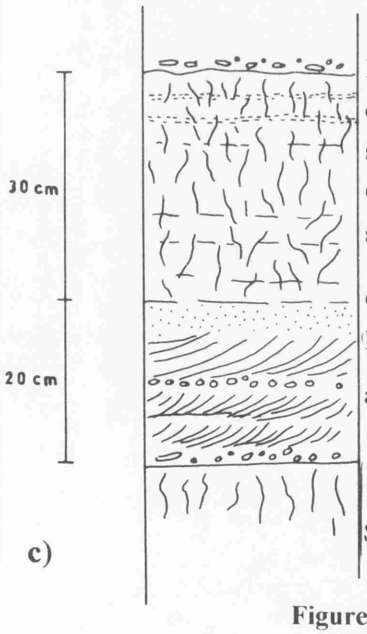

Sharp boundary:
Brown fine sandy silt with layers of elongate cream coloured calcareous concretions and occasional thin bands of brown silty fine to medium sand. Root hollows throughout. Occasional burrows and white, secondary material infilling some root hollows.

Gradational boundary:
Brown fine medium sand, cross bedded with two layers containing a little fine to medium gravel including pumice and silt pellets.

Sharp boundary:
Silt with root hollows.

c)

Figure 5.8: Upper Lake deposits sedimentary structure.

succession. The presence of slump structures, cross bedding and reworked silt pellets all indicate the a high dynamic depositional environment whilst the cyclic sequence of sediments suggests periodic, probably annual, variations in sedimentation conditions.

Fossil soil horizons contained within the succession suggest a shallow water environment with fluctuating water levels. This is further substantiated by the presence of ripple bedding. No direct evidence, such as dessication phenomena, for the complete drainage of the lake have been found. To sum-up, the upper lake deposits appear to have been laid down in an unstable relatively shallow water lacustrine environment, into which the flow of sediment varied in some periodic manner.

The upper lake deposits are nearly everywhere overlain by coarse gravel sized materials. These appear to be a combination of reworked colluvial fan deposits and river gravels deposited as the rivers incised through the lake sediments after the drainage of the lake. The period of erosion of the lake deposits and the deposition of the gravels must have occurred after the drainage of the lake since river erosion could not have occurred much below the level of the standing water in a lake.

5.5.3 The Lar Dam Basin Terrace Gravels

Throughout the lake basin the lake deposits are covered with a varying thickness of coarse, rounded gravel sized, sediments. These cap the prominent terraces and hence will be referred to as "Terrace gravel". Some sand and occasional silty horizons occur within these deposits. The gravels are invariably horizontally bedded except where they have been washed over terrace slopes and redeposited as colluvial deposits with a primary dip roughly parallel to the terrace slope.

The coarse gravels are thought to represent channel deposits whilst the finer members of the sequence would appear to represent overbank flood plain deposits. Some of the silt horizons contain evidence of having supported plant life. The gravels tend in general to be well graded. However, some horizons occur which consist almost entirely of rounded coarse gravel and cobbles with no fines. Because of the lack of fines these deposits are highly porous and permeable. Their mode of origin is not understood and their presence

may be due to initial deposition without fines or to the subsequent removal of fines from an originally well graded deposit (Figures 5.9-a and b).

5.5.4 Lacustrine Terraces

The basin of the former lake Lar contains a very prominent set of terraces formed by the gradual downcutting of the rivers into the plain formed by the lake sediments. The effects of these wandering rivers are in part erosional and in part depositional. Thus, the current river cliffs display a sequence consisting of river gravels resting on an eroded surface of lake deposits. Similarly the present bed of the river consists of recent river gravels resting on an eroded lake deposit surface.

The individual terrace levels must be related to former base levels of the river. It may be possible to relate these terrace levels to topographic features on the river banks downstream of the lake basin. However, since river erosion and deposition of the type found in the Lar valley could not have occured much beneath a standing body of water, it must be assumed that drainage of the lake had occured prior to the formation of the terraces.

The lake basin is known to have been gradually filling with sediment, and water from the lake must have at the same time been escaping either by overtopping of the valley barrier or by leakage through the margins of the basin. Some overtopping is thought to have occured as topographic features exist such as spillways and terraces whose altitudes match with overtopping altitudes. However, although it is not known what caused the final drainage of standing water from the lake, it is thought that the terrace levels must be controlled by successive downcutting of the present Lar valley (Figures 5.9-a and b). A preliminary survey of the Lar terraces has been made in order to establish the dominant terrace levels. Initially the survey has been carried out by noting all the prominent terraces on the maps of the lake basin between Lar and Chehel-Cheshmeh. Levels have been obtained for all the terrace tops, and plotted as a histogram (Figure 5.9-c, d and 5.10-a, b,c, 1 and 2). As was expected, a marked peak has emerged at just above the 2700 metres level. Secondary peaks also emerge at around 2365 metres and 2450 metres (all levels from the Lar valley datum). A preliminary study of the topographic maps of the lower Lar valley suggests that the base level corresponding to the 2450 metres terrace level is likely

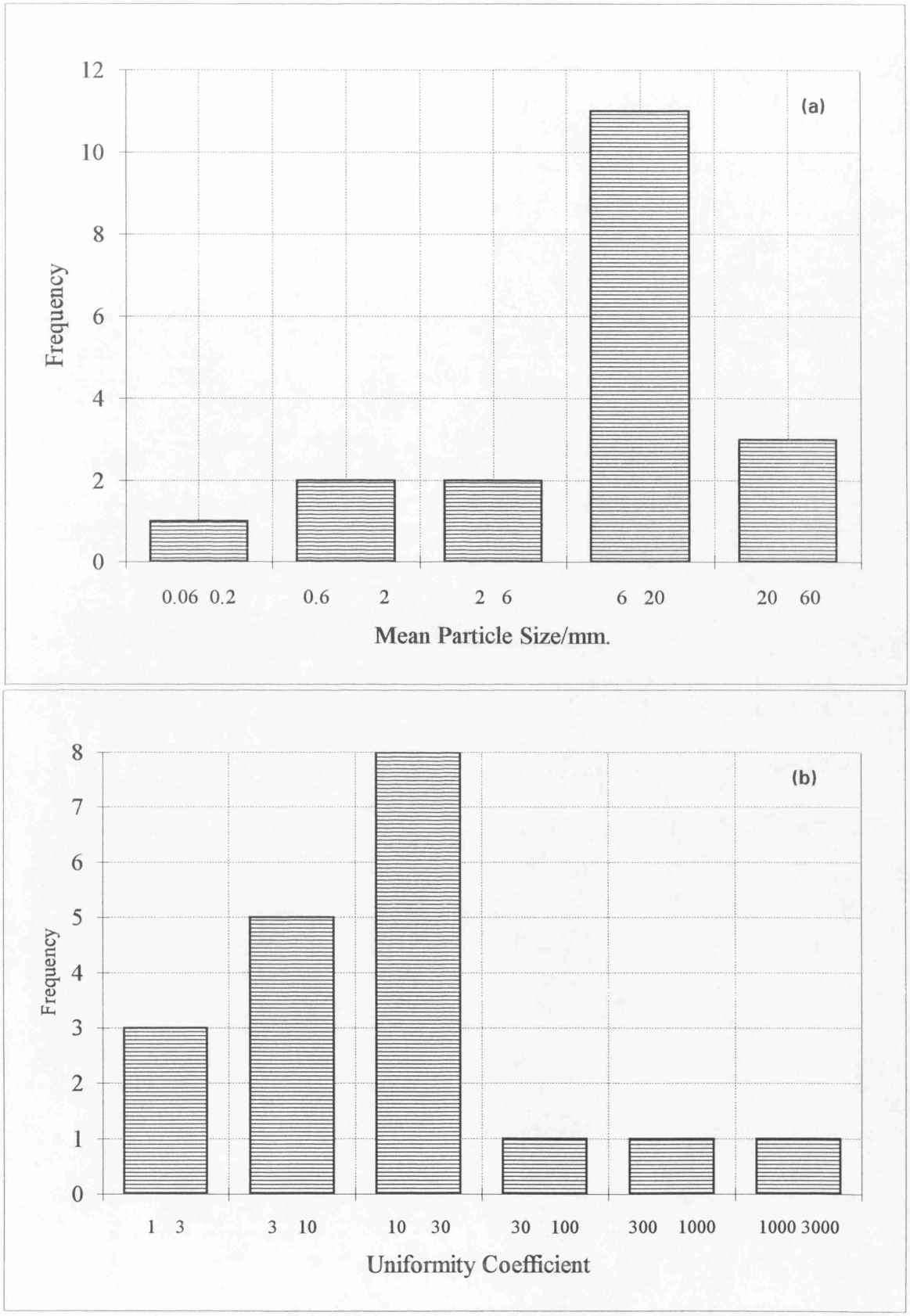

Figure 5.9: The Lar basin terrace gravels; **a)** Mean particle size and **b)** uniformity coefficient.

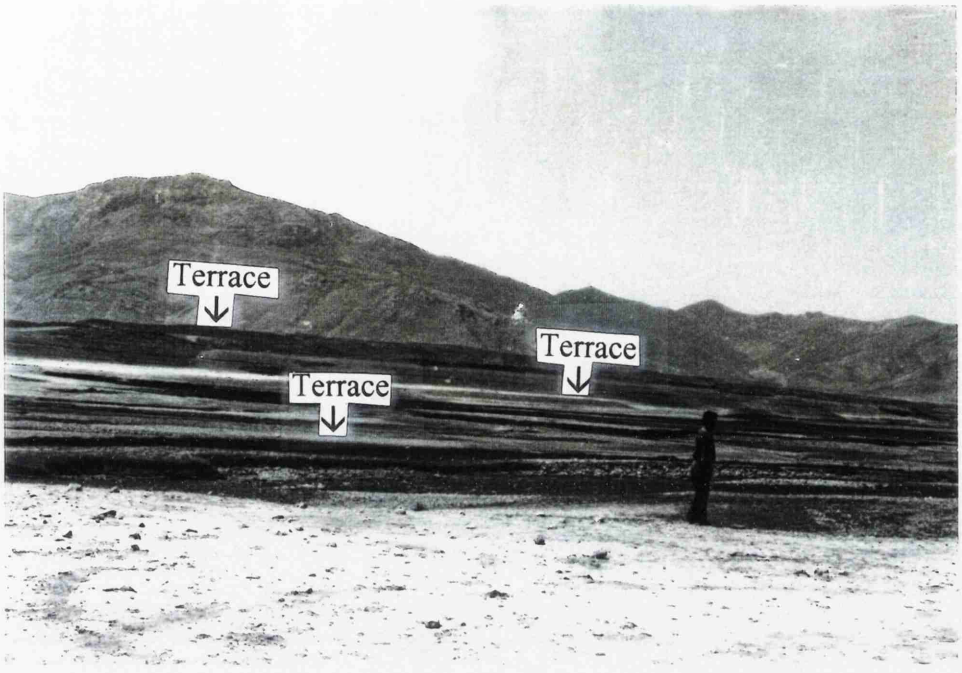

Figure 5.9c: The Lar upstream terraces about 2650m, looking South (Approx. gradient <5%, Aug. 1994)

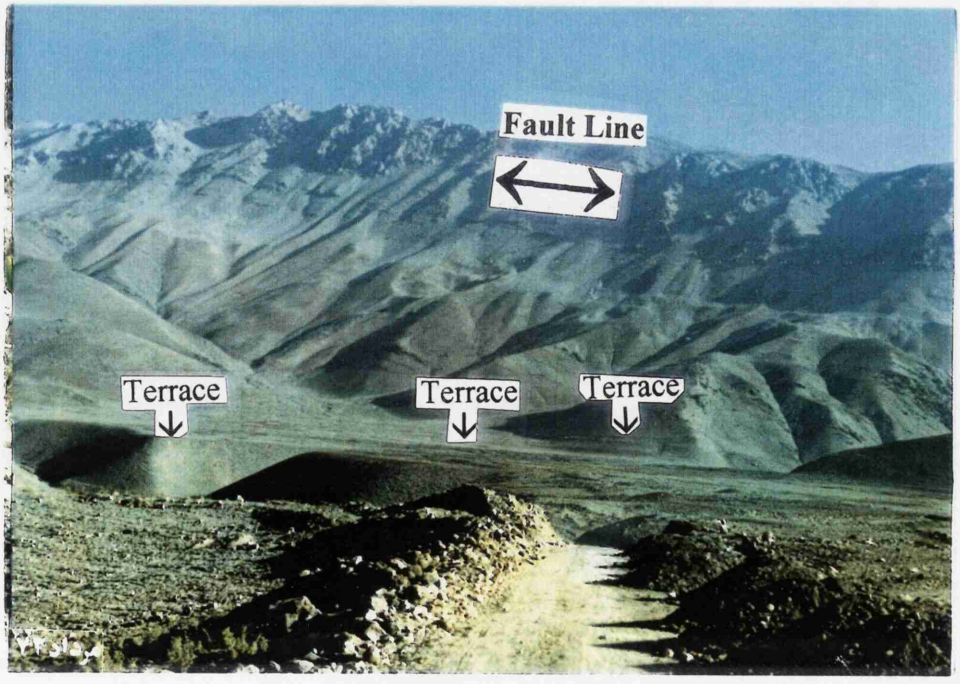

Figure 5.9d: Lower Dalichai terraces, about 2450m, looking Northwest (Aug. 1994).

to been produced by the top of the lava mass prior to the formation of Lar downstream (see Figure 5.10-a). The 2400 metres level corresponds approximately with a small waterfall at co-ordinates 79400 E, 41080 N. The 2365 metres level is more difficult to explain since it could have been due to several factors. The top of the limestone in Lar gorge and the top of the lava landslide debris in Lar downstream both correspond to the expected base level.

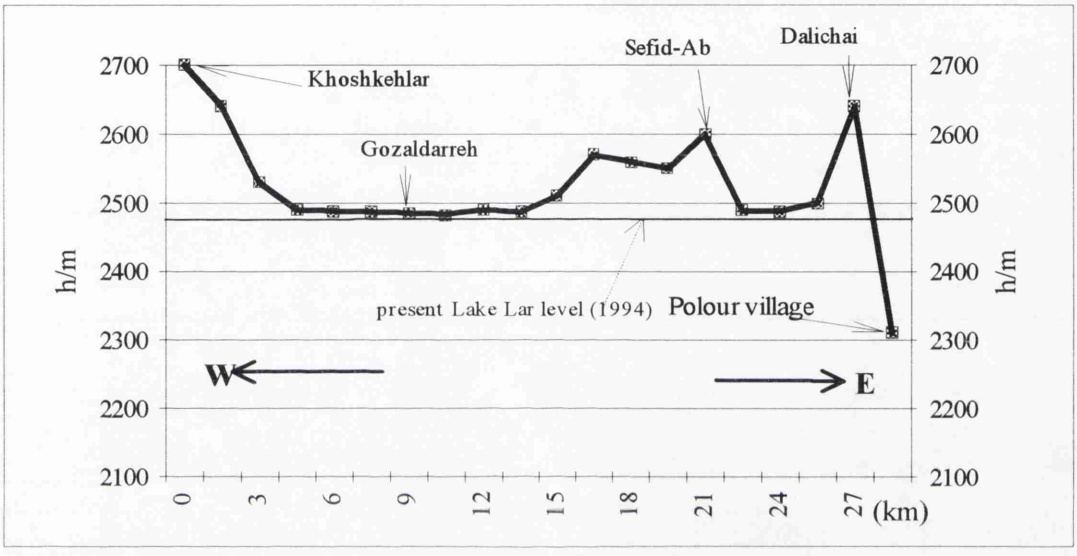

Figure 5.10-c : The Lar basin terrace section from west to east. The curve shows the upper limit of lacustrine terraces.

Hence, at this stage it would appear that the terraces were formed by the river overtopping constrictions in the Lar Gorge area. At some subsequent stage, major collapse of these barriers occurred and a new base level was defined by a lower level obstruction.

5.5.1.3 Drainage of the Lake

No direct evidence has, as yet, been obtained to indicate with any certainty, whether or not the lake was drained at any time prior to the eruption of the large quantities of intermediate lava from Damavand. The apparent absence of dessication phenomena and organic remains within the lower lake deposits, except for at one locality high on the right bank of the Lar river, would tend to suggest that at no stage prior to the major eruption of Damavand was the lake drained.

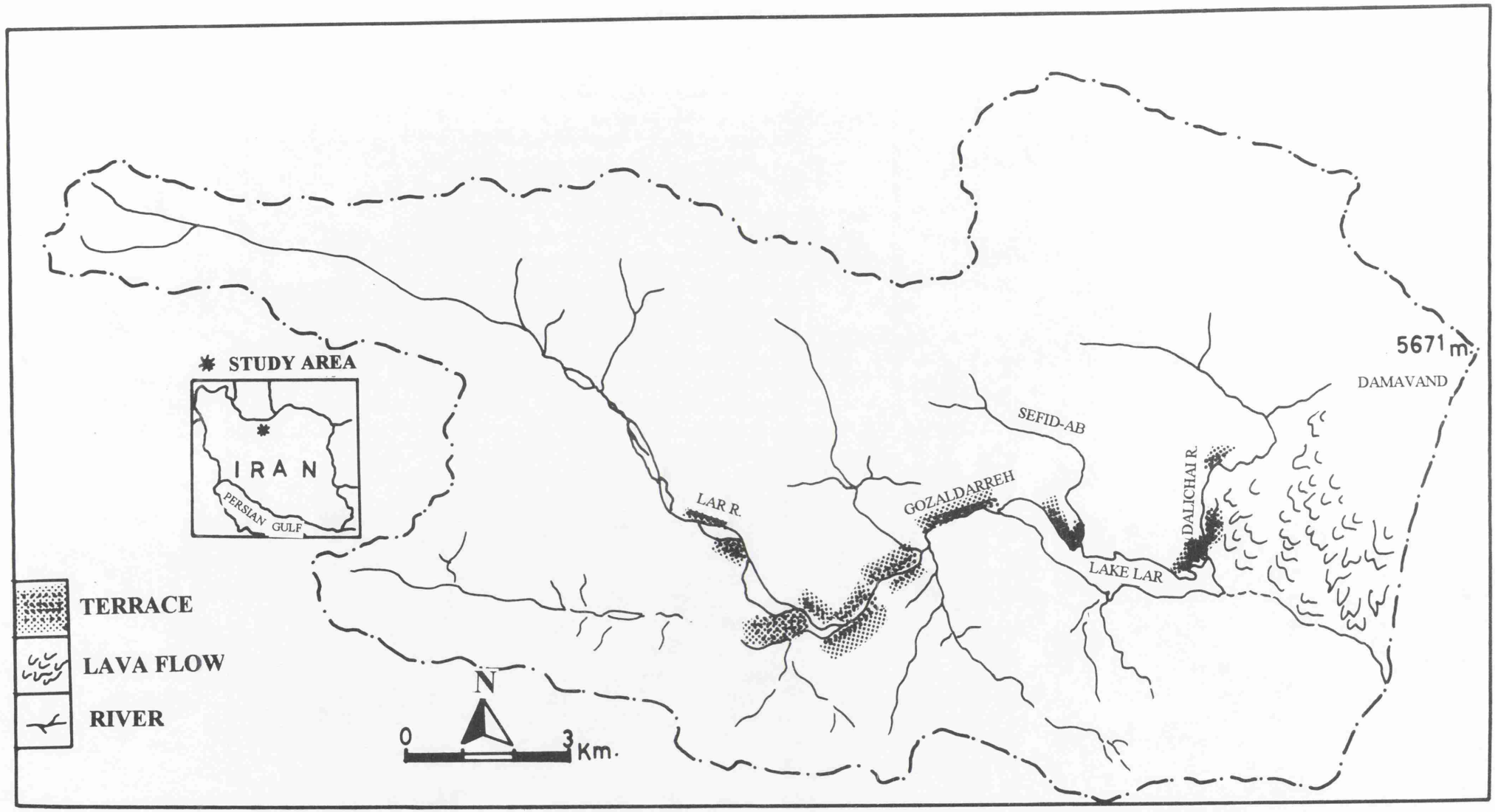

Figure 5.10a: The Lar Dam Basin Terraces (source; KFA-1000, June 1990).

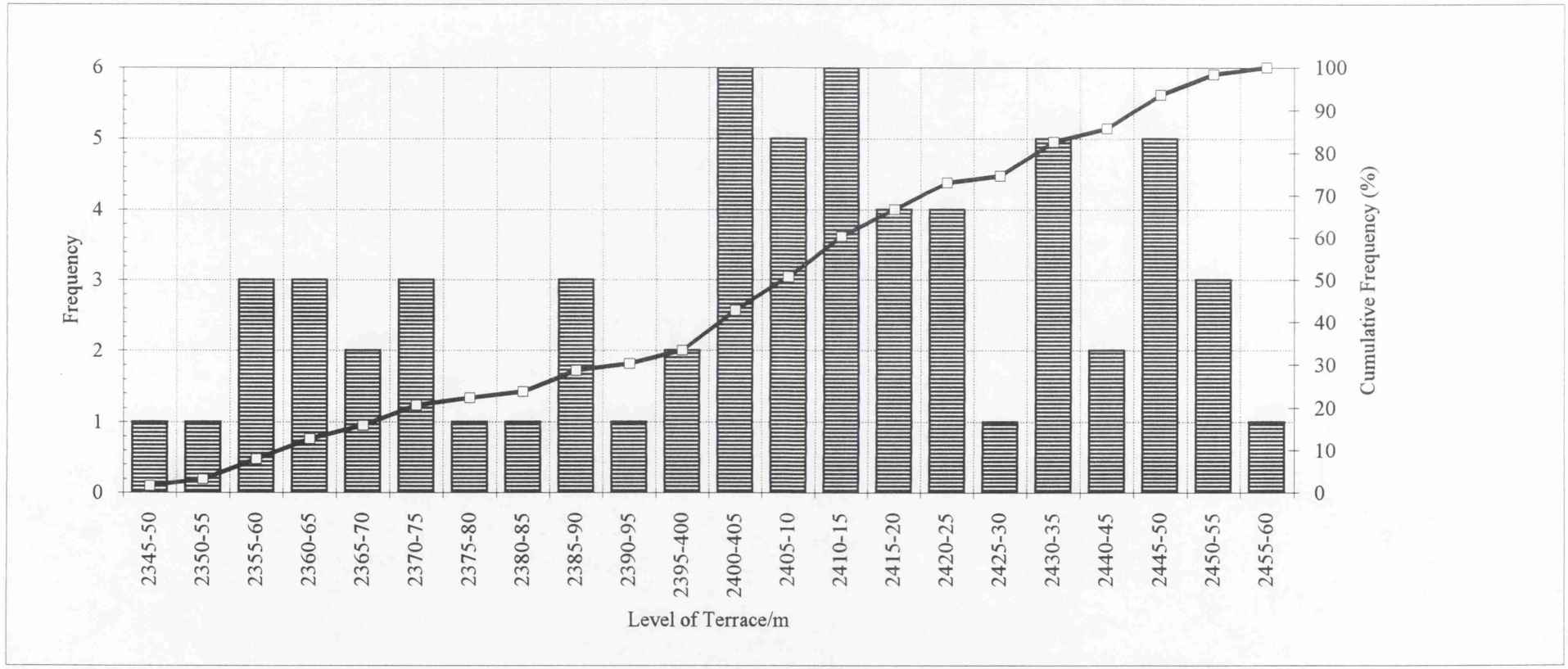

Figure 5.10-b: The Lar Valley Terrace Frequency.

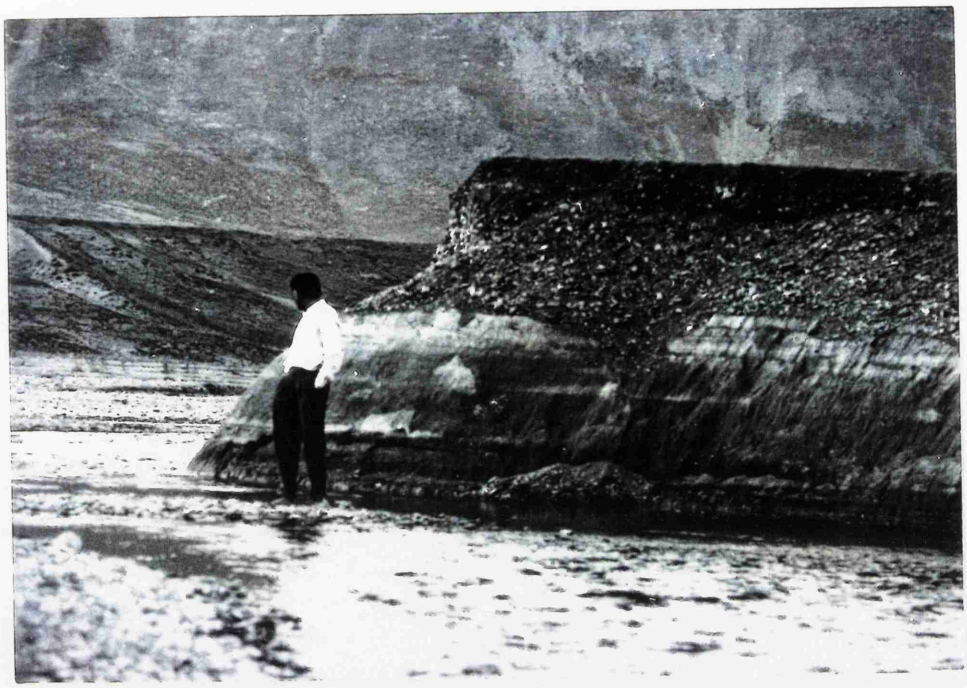

Figure 5.10-1: Former Lake Lar terraces at Kamardasht looking Southeast (from top to bottom: clay, gravel, sand, silt and clay and gravel; Aug. 1994).

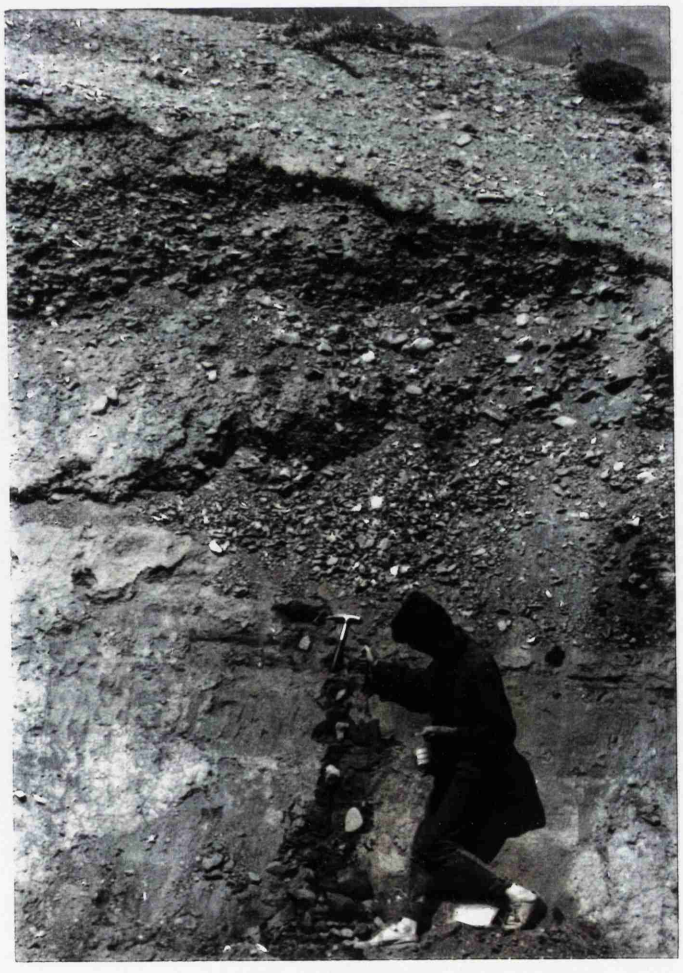

Figure 5.10-2: Cheshmehkhooni terraces, about 2700m, looking Southwest (from top to bottom: clay, gravel, sand, silt and clay; Aug. 1994).

On the other hand indirect evidence that the lake had been drained, prior to the major volcanic outpourings, is given by the mode of deformation found within the lake sediments. A certain degree of semi-brittle failure appears to have occured within the lake sediments as a result of the additional loadings applied by advancing lava. Thus faulting and jointing seem to have been the predominant deformation structures produced by the lava. On the right bank of the Lar, where lake deposits have bulged up between adjacent lava tongues, the silts and sand have retained their primary bedding, and have even developed a pseudo-cleavage.

The arguments for or against drainage of the lake are inconclusive and further work will be required before a final answer emerges. It is not yet clear what, if any, influence the present depressed water table at Lar had upon the stability of the lake. The upper limit of the lake deposits is defined by the eruption of Damavand to produce the large quantities of intermediate lavas which now dominate the lower Lar valley. The most recent eruption from Damavand is thought to be post-Pleistocene since the volconic cone shows no signs of Pleistocene glaciation. However, Allenbach (1966) reported on a C^{14} - dating of plant remains from the "terraces of the lower Lar" which gave a minimum age of 38,500 B.P., indicating a probable Pleistocene age for the sediments within the Lar basin. It is probable that Allenbach is reporting a dating for the lower lake deposits.

From the evidence obtained by the Dam Authority (1975) in the adits and trenches around the Lar Gorge (lower) and Chehelcheshmeh (upper), it would appear that the onset of the volcanic eruption was marked within the lake succession by a thin sequence of tuffaceous sediments. Whether it is be possible to locate this boundary upstream of the lava limit is not yet known.

5.6 DETECTION OF LANDSLIDES AND SINKHOLES

As described in chapter 1, one of the aims of this research is to investigate morphological changes which influence sediment delivery in the Lar basin. In chapter 4 the physical characteristics important for sediment supply in the Lar basin, such as former lake deposits, limestone bedrock, unstable slopes, sinkholes and landslides were described. The sinkholes are important for sediment delivery and water loss, although it is difficult to estimate sediment loss from them because of lack of data. Four years of monthly records

of water leaked from sinkholes at Ab-Ask shows their effect on the Lar reservoir water loss, and is described later in this section.

The mass movement of debris downslope occurs when stress on the material exceeds it's resistance to movement. Wherever slopes are oversteepend by glacial or fluvial action the result may be slope failure. Movement may also take place when the soil or bedrock materials become saturated with water and are burdened with an increased load or experience a shock such as an earthquake.

Sinkholes occur in karst landscapes where solution has created an internal drainage hole. Some may subsequently be filled, others remain steep sided deep holes, like those in the Lar basin. The number of holes has significantly increased after construction of the artificial dam, and they are able to deliver water and sediments to the Lar River via subsurface channels.

At present, solution is active in the Lar Lake limestone areas and is detected on aerial photographs and in the field. Three large holes occurred downstream of the dam and four more exist within the area of the new lake. Two old sinkholes occurred between Dalichai and Sefid-Ab and 6 recent and curently active holes were identified in the terraces above and below the water (Figure 5.13 and see also folded map no.4 in folder at back). Two recently formed sinkholes were detected on KFA-1000 and aerial photographs and field inspection gave following information:

Sinkhole 1 on the west side of Dalichai formed in 1988 some 1 kilometre from the Dam crest and about 30 metres from an old hole. The second sinkhole occured on the east side of Sefid-Ab in Arab-Davood area and formed in spring 1986 (Table 5.1, Section 1, 2 and Figures 5.11, 5.12).

Table5.1: Geometric characteristics of sinholes no. 1 and 2.

Sinkhole No.	Diameter/m.	Depth/m.
1	27.7	15.5
2	16.9	12.3

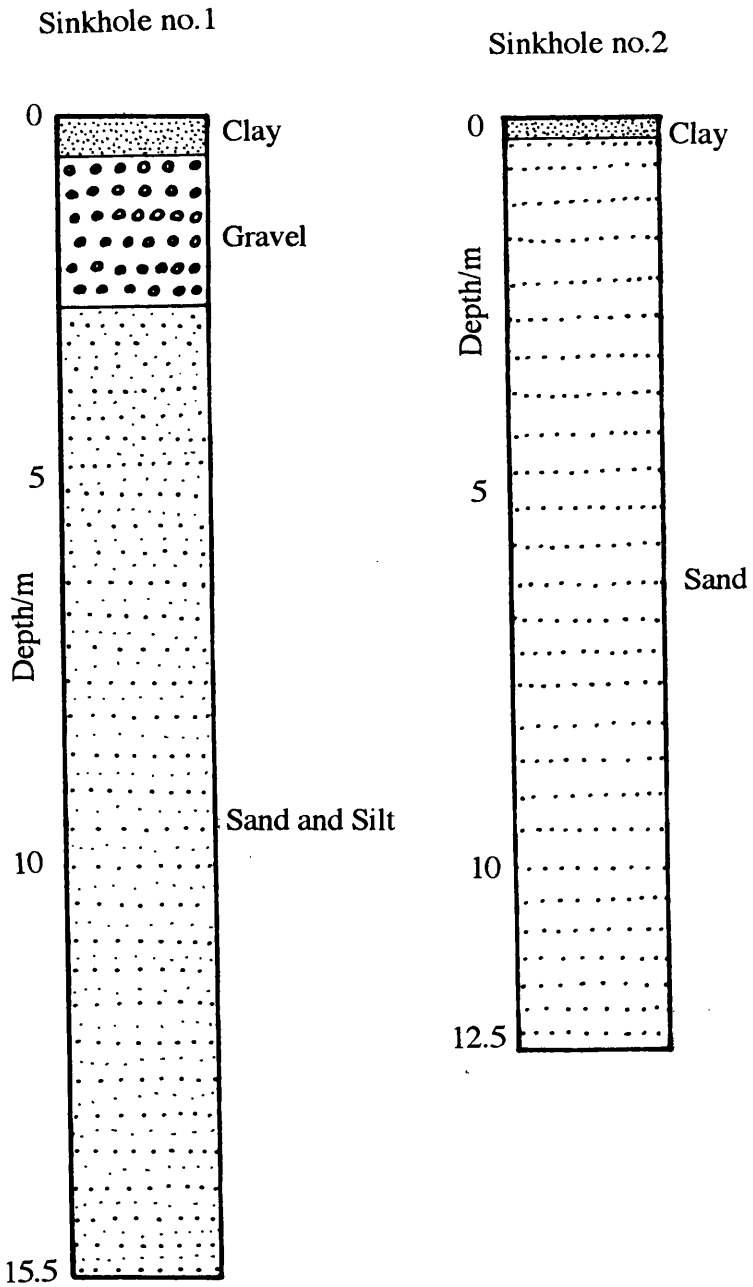

Section 1 and 2: Schematic diagram of sinkholes 1 and 2 to illustrate the Lake Lar deposition *(Scale; 1:100).*

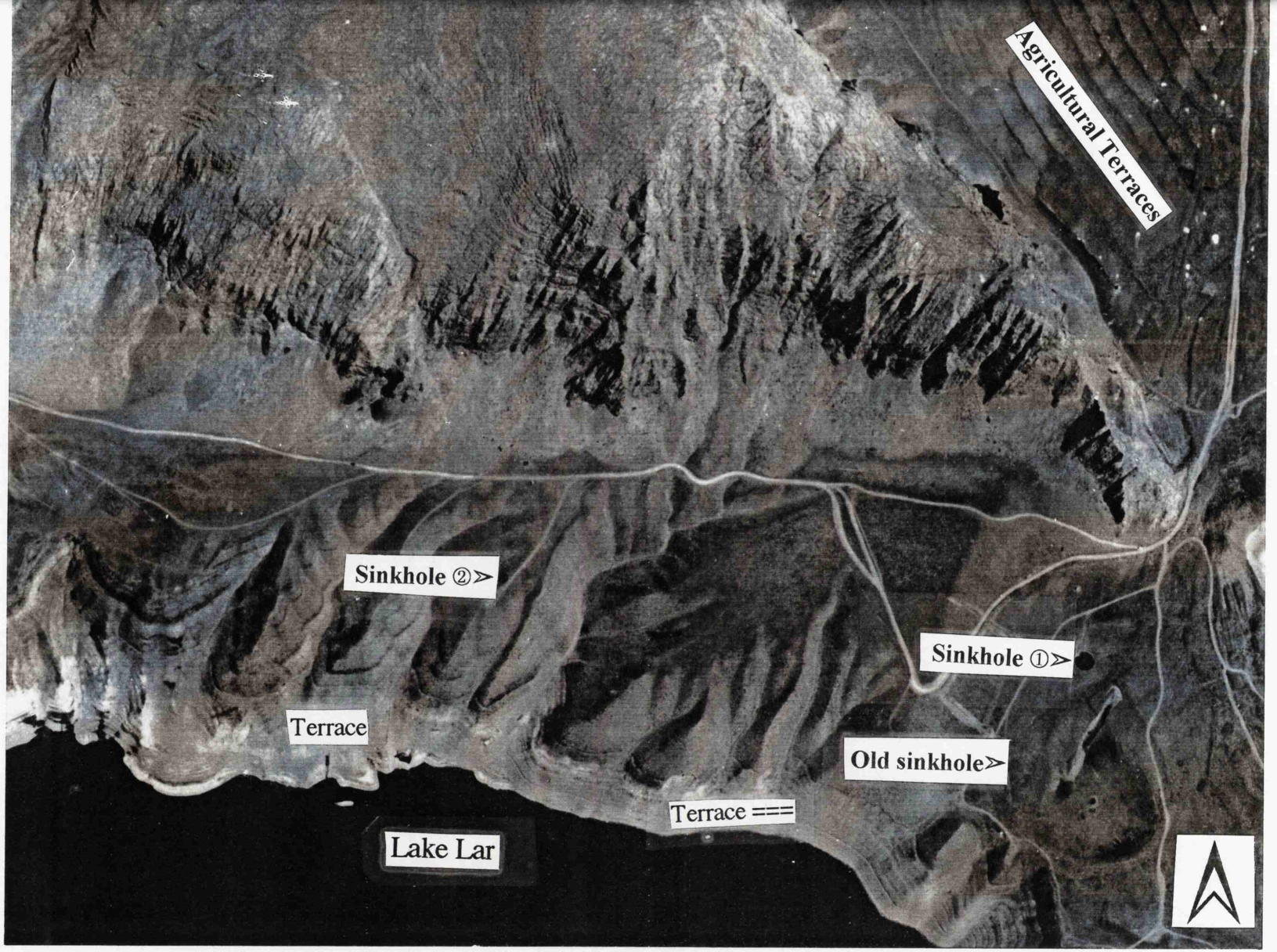

Figure 5.11: Sinkholes and terraces on aerial photo in Lake Lar area (Approx. scale 1:3000; Sept. 1990, see also Figure 5.12).

Figure 5.12a: Sinkhole no. 2, looking South (Aug. 1994).

Figure 5.12b: Lake Lar and Sinkhole no. 1, looking South (Aug. 1994, see also Figure 5.11).

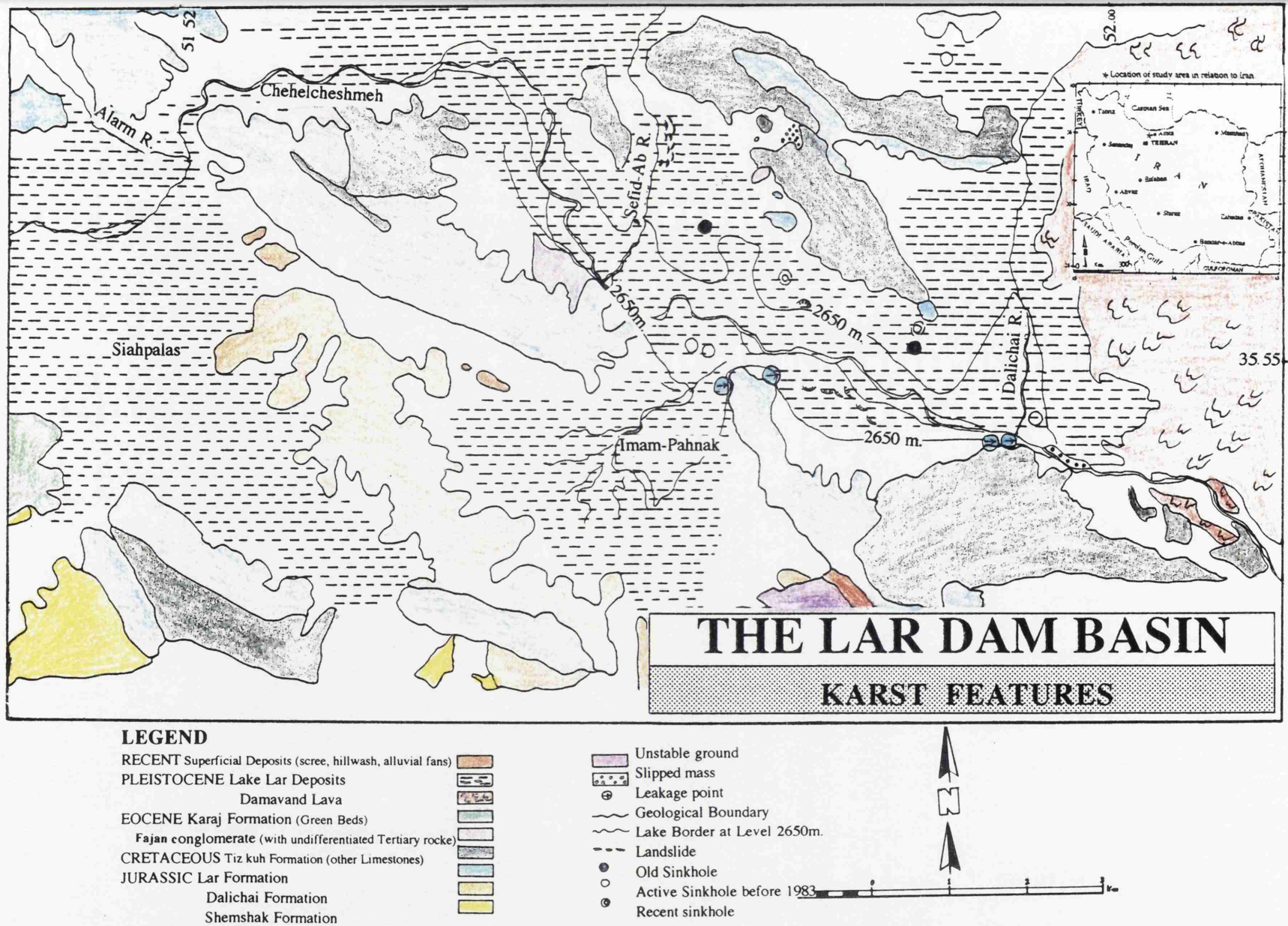

Figure 5.13-a: The Lar Dam Basin Karst Features.

In addition to the recently formed sinkholes several large older sinkholes exist within the Lar basin. These vary quite appreciably in nature from the shallow flat bottomed type that occurs in the southern side of the Lar river at Siah-Palas, and at 43550 N., 74250 E., to the large deep, flat bottomed sinkhole at 42200 N., 76700 E. This latter sinkhole is situated on the terrace top and is 160 by 140 metres across, and about 12 to 15 metres deep. It appears to be completely inactive at present and its base appears stable. In direct contrast to this, at 45370 N., 77120 E. there occurs a conical shaped sinkhole with active collapse occurring in its base. This sinkhole is circular in plan with a diameter of about 30 - 40 metres and a depth of 12 -15 metres. Although these sinkholes vary somewhat in size and form, they are all situated along the lines of major faults which affect the underlying bedrock and in some cases the overlying sediments also (Figure 5.13-a).

The seasonal recorded leakage at Ab-Ask and the Lar gorge (Figure 5.13-b) shows that the 6-monthly loss during 1983-93 varied between 95.2 and $212.2\times10^6 m^3$, respectively in the winter and summer of 1992. The graph shows a general correlation between the rate of loss and the volume of water in the reservoir (r=0.94).

The percentage of annual water losses during the winter season are between 44% and 55% exept for winter 1992 (31%). The average seasonal loss for this period is $144\times10^6 m^3$ against $958\times10^6 m^3$ total reservoir volume which shows significant leakage through the sinkholes. Finally Figure 5.13-b shows that leakage fell from 1983 to 1986 increased between 1986-88, and decreased again from 1988-91 and then rapidly increased from 1991 to 1993. This is related to the reservoir input volume fluctuation, which influnces the leakage of water via sinkholes in the Lar basin.

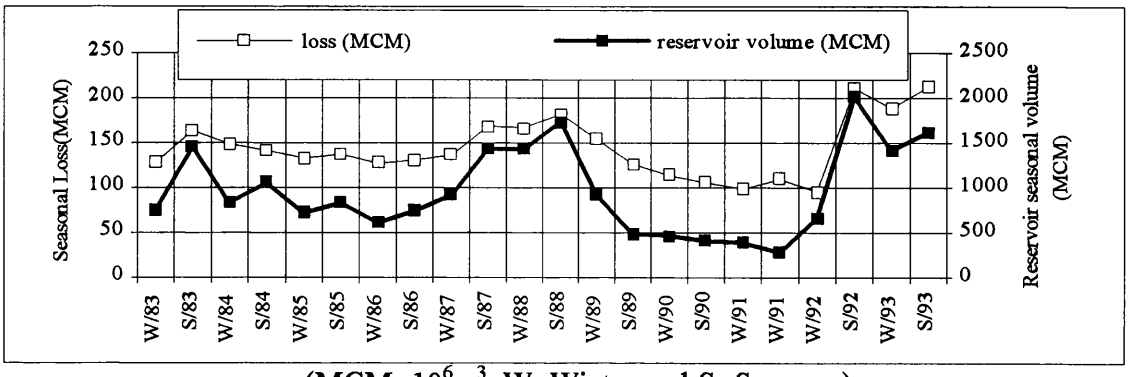

(MCM=$10^6 m^3$; W=Winter and S=Summer)

Fifure 5.13-b: The Lar reservoir volume and seasonal water loss from sinkholes.

5.6.1 Lassem Landslide Area

Lacustrine terrace deposits in the Lassem tributary extended some 6.5 km. from the Haraz confluence with the Lassem. There is no gauging station close to this area to show its effects on sediment delivery. The nearest station is 90 km downstream at Karehsang (for location see Chapter 3 Figure 3.13). The origin of these deposits is directly related to the southeastern lava flows from Damavand, which caused the daming and infilling of the Lassem Lake, at the same time on the Lar Lake was forming. Aerial photographs from 1955 show that occurence of landslides in this area is common and has increased sediment delivery via the Lassem tributary to Haraz River. A landslide in May 1985 moved a large mass across the Lassem stream, some 1 kilometre from Polour (Figures 5.14 and 5.15) producing a natural lake some 1 kilometre long and 100 metres wide. The landslide material is mostly from the youngest alluvium, marls, sands together with a small amount of old alluvium from the remains of a terrace of the natural old lake of the Lassem (38500 years B.P. Allenbach, 1966).

From May 1985 to the present, the surface of the Lassem landslide shows significant changes. Water infiltration from snow filled cirques on the southern side is this thought to be the main factor affecting the stability of the Quaternary deposits and their eventual failure in the Lassem landslide (Figures 5.16, 5.17 and 5.18).

5.7 SEDIMENT CHARACTERISTICS IN THE LAR BASIN

As mentioned in Chapter 4 only limited information concerning the lacustrine formations in the upper Lar existed prior to this study. From analysis of both remote sensing data and field inspection it was confirmed that extensive former Lake deposits exist in the Cheshmeh Khooni, Gozaldarreh and Chehelcheshmeh (see Figure 3.14) areas.

A knowledge of the sediment characteristics of the basin, primarily the grain size distribution, is important for relating sediment transport to discharge over time and for estimating the sediment yield from the basin. It would be of use to have an estimate of the bed load percentage in the absense of other data.

Figure 5.14: Lassem Lake Landslide on aerial photo (September 1990, Approx. Scale 1:7000).

Figure 5.15: Lassem Lake and Landslide looking South (Aug. 1993).

Figure 5.16: The Lar Basin Sinkholes, Landslides and Surrounding Geomorphology on KFA-1000 *(June 1990, Approx. Scale 1:270 000).*

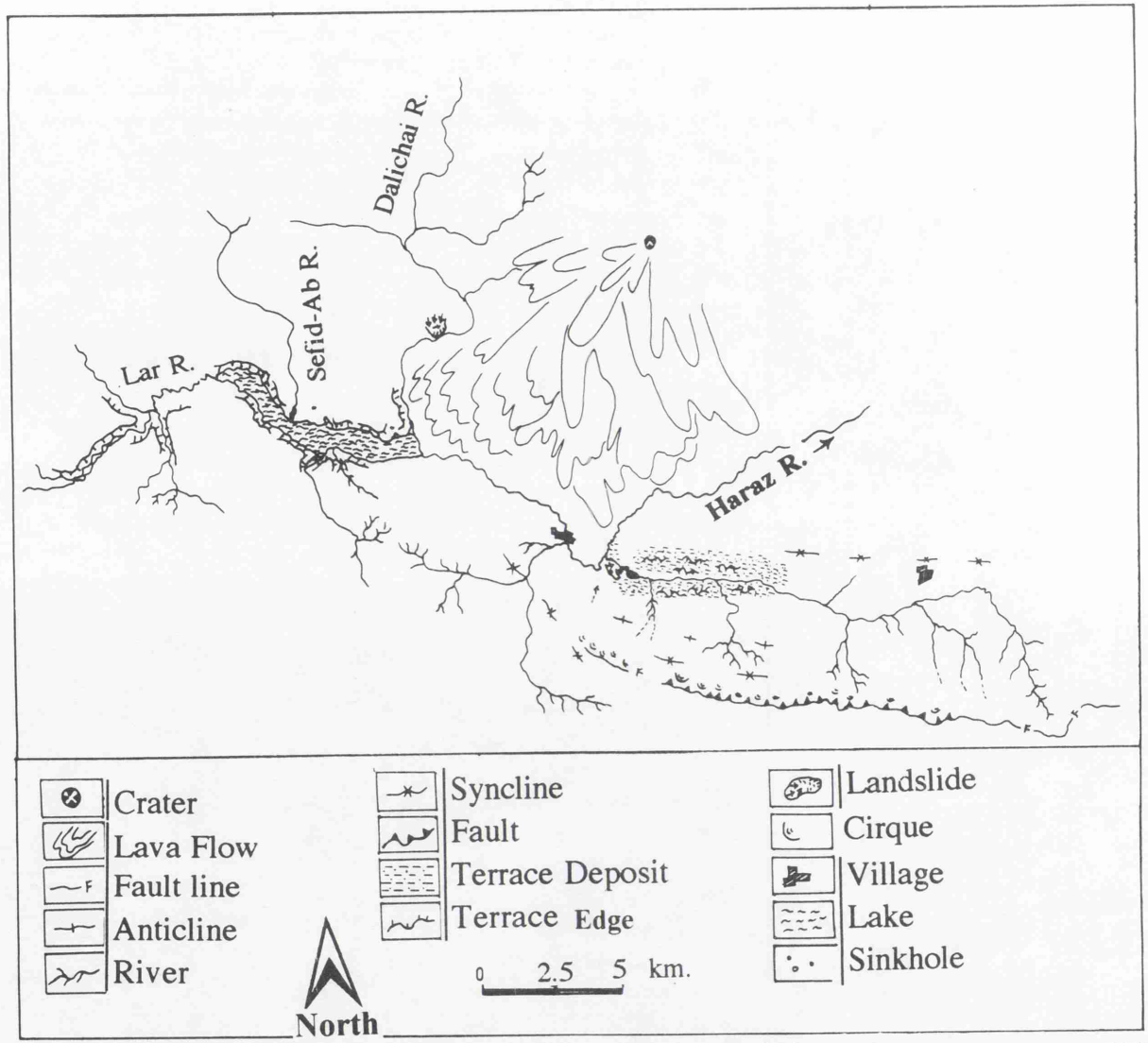

Figure 5.17: The Lar basin Sinkholes, Landslides and Surrounding Geomorphology *(source: KFA-1000, June 1990).*

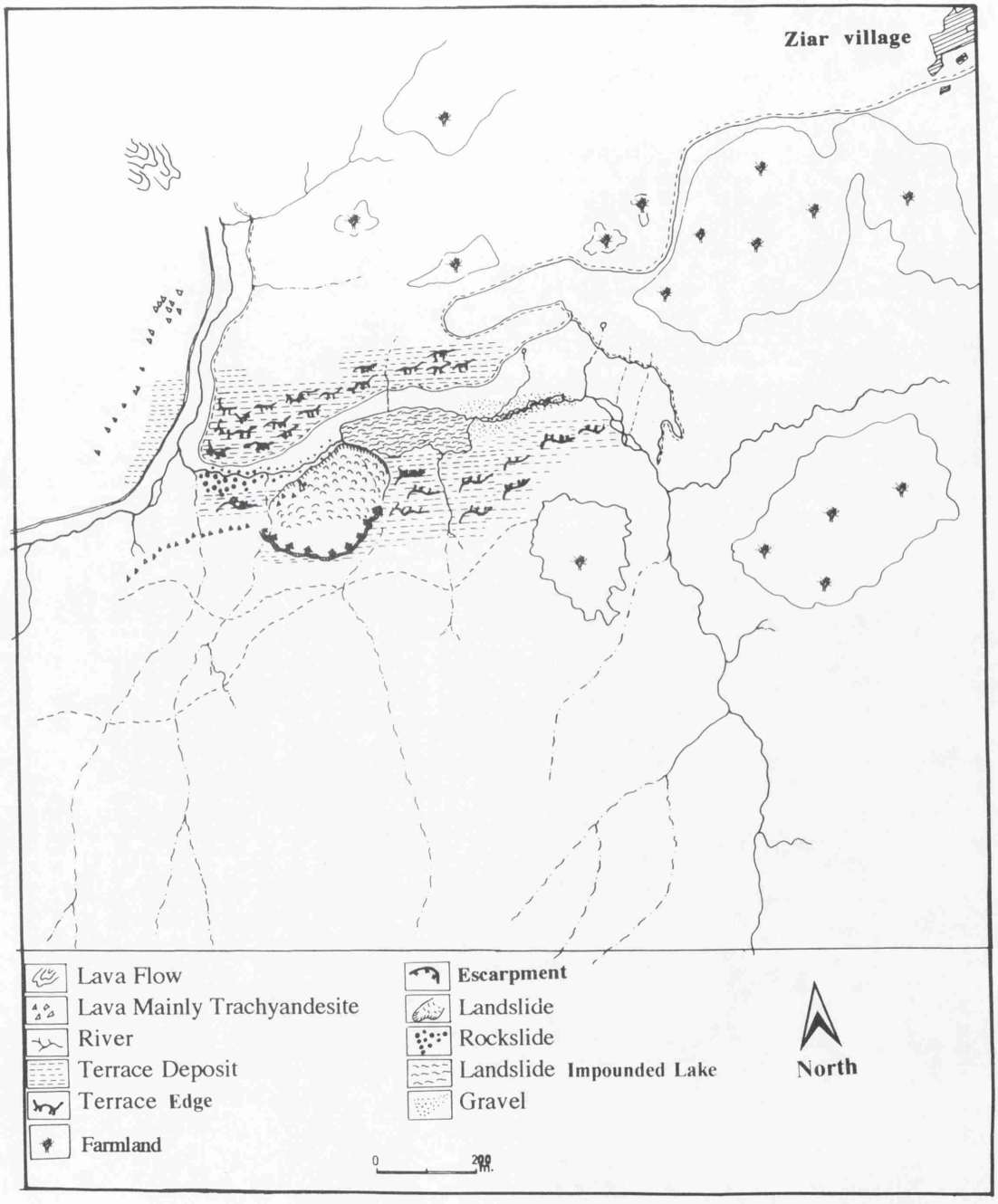

Figure 5.18: Lassem Landslide and Surrounds (source; aerial photo, 1990).

5.7.1 Particle Characteristics

Sedimentary particles in the Lar basin consist of a large variety of volcanic rocks in the Dalichai basin and sedimentary or metamorphic ones in the Lar and Sefid-Ab basins. The finer clay size particles (< 0.004mm) normally consist of a separate group of clay minerals with specific structure, and are usually found in the lake deposits. The mineralogy of the original source rocks, together with chemical weathering processes and mechanical weathering, including abrasion due to transport, determines the ultimate size, weight, and shape of sediment particles. On the frequency diagrams sizes between 0.002mm and 0.06mm (Figure 5.19) are fine, medium and coarse silt; less than 0.002mm is clay; between 0.06mm and 2mm is sand; 2mm-60mm is gravel; and, 60-200mm is cobbles. Most particles in the lake deposits are clay and silt, but in terrace formations are generally greater than 0.6mm (sand and gravel sizes).

5.7.2 Size

Sample areas for particle size and shape were selected to represent the distribution of sediments in the Lar basin. Therefore, for the purpose of characterizing the depositional areas, the sites were selected as follows; Lar upstream, Khoshkehlar junction to Lar, Gozaldarreh, Dalichai and Sefid-Ab (see Figure 3.14).

The most important physical factor related to sediment transport and deposition is the particle size. Broadly, this factor determines how and when a particle will move or deposit with a given set of flow hydraulic characteristics. Particle size exerts an important influence on the amount of sediment trapped and the distribution and ultimate volume of sediment in the Lar dam basin.

Bulk characteristics: The grain size distribution and the specific weight of deposited sediment are of particular concern in basin sedimentation problems. Sediments with more than 50% of the particles larger than 0.062mm are hereafter referred to as coarse-grained sediments, while those with more than 50% in grains of less than 0.062mm are designated fine-grained sediments. As shown in the terrace particle size diagrams (Figure 5.9-a) more than 50% of the sediments are coarse grained and other two samples contained >50% less than 0.06 and are designated as fine-grained sediments. Also analysis of six samples from

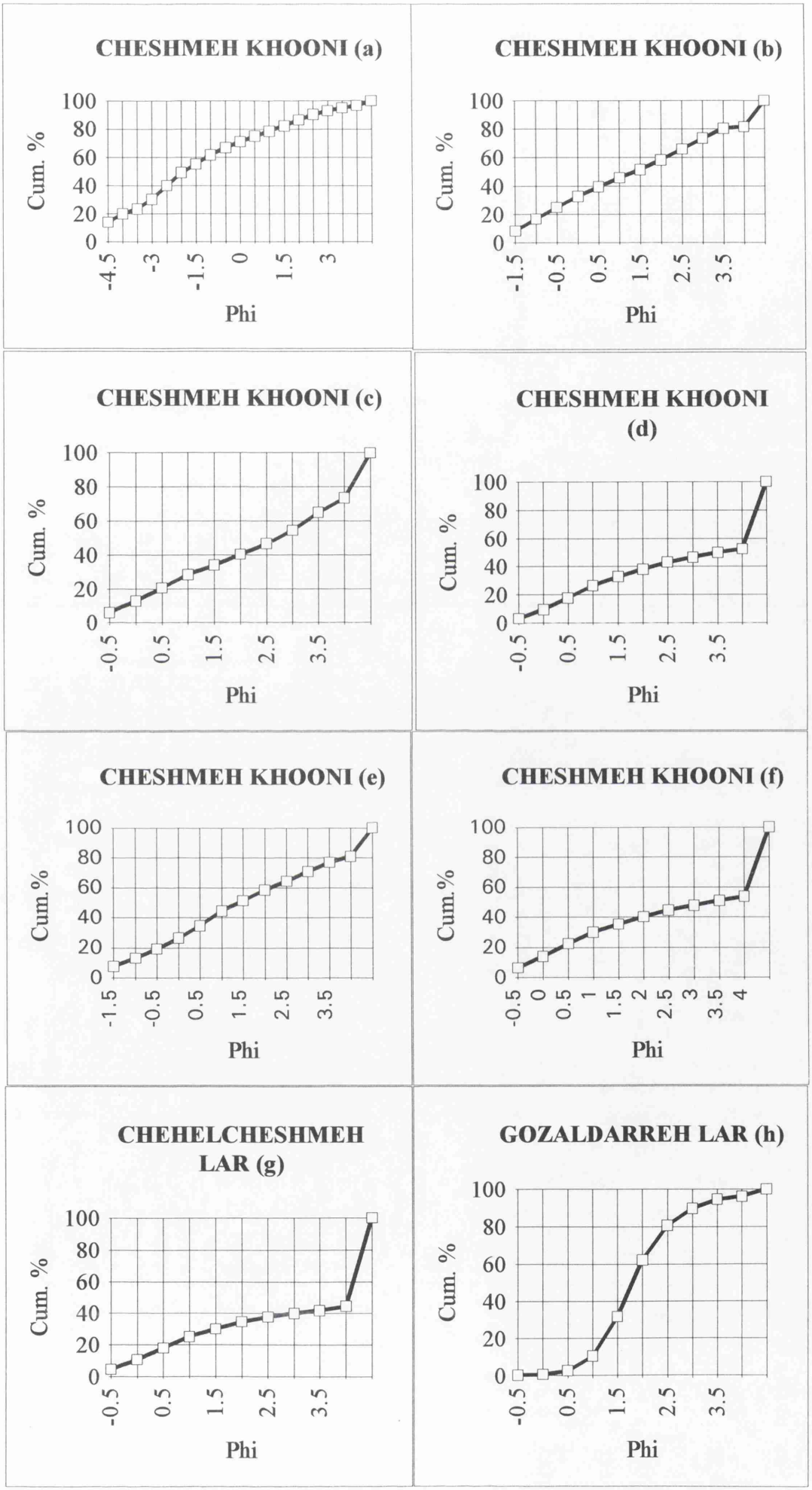

Figure 5.19: Grain-size distributions at Lar Upstream.

Cheshmehkhooni at Khoshkehlar show that 50% of one sample is less than 0.06mm, but the other five samples from same section have more than 50% of grains larger than 0.062mm (coarse-grained sediments). All size classes of sediment fill parts of the basin space upon deposition and therefore are of concern.

In Figure 5.19, Cheshmehkhooni (a) shows 55% of the particles are pebble (between 22.6-2.8mm size), 6.5% granule (2mm), 5% very coarse sand and other particles include sand, silt and clay. Sample (b) indicates that 16.5% is gravel, the others are sand, clay and silt, almost same distribution is in sample (e). In sample (c) 6% is coarse but most of this sample contains fine particles, which have the same characteristics as samples d, f, g, and h. Except for sample (g), from Chehelchashmeh, the other six samples are from Lar upstream at Chaeshmehkhooni. All of them are very poorly sorted except sample (g) which is moderately sorted.

It can be suggested that sample (a) has been deposited by the Lar river, because of its stratigraphic location and that it contains over 50% of pebble particles, and that the other samples originated from the former Lar lake. The significance of this result is that it indicates that the former Lar Lake extended up about 2700 metres at Kamardasht (see Table 5.3). Different thicknesses and particle sizes of sedimentary layers from sampled sections shows different depositional conditions in the Lar basin, which are probably related to climatic changes in Quaternary time.

Analysis of the upper deposits indicated that 2.5% of the particles are pebble, 43% sand and the rest is silt and clay (Figure 5.7). The upper lake sample is from the former lake deposits and is very poorly sorted (2.58, Table 5.4). Figure 5.6, taken from the lower lake deposits shows that 5% is pebble, 2.7% gravel, 19% sand and the remainder silt and clay. The sorting value of this sample is 2.51, a very poorly sorted lake deposit (Table 5.4). Terrace samples in Figure 5.9 shows that 15.8% of the particles are cobble, 58% gravel, 10.5% pebble, 10.5% granule and others including sand. They were taken from terraces and the sorting value of 1.7 shows that this sample is poorly sorted (Table 5.4 and see also Table 3.1 for the size ranges in Chapter 3).

For the upper and lower lake samples, clay percentage plotted in Figure 5.19-1 shows that there is generally much less clay in the upper deposits (a) than the lower (b). In the upper

Table 5.3: Sieving results from the Upper Lar.

Phi	%coarser	Phi	%coarser	Phi	%coarser	Phi	%coarser
Cheshmkhooni (a)		Cheshmkhooni (b)		Cheshmkhooni (c)		Cheshmkhooni (d)	
-4.5	13.7	-1.5	8.3	-0.5	6.04	-0.5	3.06
-4	19.98	-1	16.57	0	12.86	0	9.54
-3.5	23.52	-0.5	24.88	0.5	20.59	0.5	17.79
-3	30.48	0	32.58	1	28.37	1	26.42
-2.5	40.01	0.5	39.34	1.5	33.66	1.5	32.61
-2	48.81	1	45.67	2	40.11	2	38.01
-1.5	55.12	1.5	51.48	2.5	46.46	2.5	42.8
-1	61.65	2	58.27	3	54.5	3	46.53
-0.5	66.61	2.5	65.8	3.5	64.81	3.5	49.95
0	70.82	3	73.39	4	73.33	4	52.41
0.5	74.6	3.5	80.46		100		100
1	78.4	4	81.29				
1.5	82.15		100				
2	86.49						
2.5	90.15						
3	92.91						
3.5	95.07						
4	96.05						
	100						
Cheshmkhooni (e)		Cheshmkhooni (f)		Chehelchaeshmeh (g)		Gozaldarreh (h)	
-1.5	7.75	-0.5	6.53	-0.5	4.67	-0.5	0.2
-1	13.24	0	14.36	0	10.5	0	0.56
-0.5	19.21	0.5	22.42	0.5	17.82	0.5	2.51
0	26.27	1	30.3	1	25.24	1	10.16
0.5	34.73	1.5	35.37	1.5	30.05	1.5	31.81
1	44.48	2	40.28	2	34.61	2	62.2
1.5	51.43	2.5	44.44	2.5	37.6	2.5	80.73
2	58.68	3	47.87	3	40.01	3	89.89
2.5	64.37	3.5	51.15	3.5	42.01	3.5	94.43
3	70.85	4	53.64	4	44.4	4	96.14
3.5	76.89		100		100		100
4	80.96						
	100						

Sorting values for graphical statistics.

Sample	ϕ50	ϕ16	Sorting
a	-1.91	-4.32	very poor
b	1.37	-1.03	very poor
c	2.72	0.2	very poor
d	3.52	0.39	very poor
e	1.4	-0.77	very poor
f	3.32	0.1	very poor
g	*	0.38	*
h	1.8	1.13	Moderate
	Median size	Coarser	

*cannot be calculated.

Sampled area: a...f) see figure 2.10-2 from cheshmehkhooni terraces, 5m. higher than river bed. g) Chehelcheshmeh about 2450m. and h) Gozaldarreh sampled at 2520m.

Table: 5.4: Sieving results from the upper (1), lower (2) and terrace (3) deposits.

(1) Phi	%Coarser	(2) Phi	%Coarser	(3) Phi	%Coarser
-4.25	2.38	-4.25	2.7	-6	15.8
0.75	2.38	-2.5	2.7	-4.25	57.9
2.25	23.8	-1	2.7	-2.5	10.52
4	16.67	0.75	8.1	-1	10.52
5.5	21.43	2.25	10.8	-2.25	5.26
7.5	30.95	4	8.1		
9	2.38	5.5	43.2		
		7.5	21.6		

Sorting values for graphical statistics.

Sample	ϕ50	ϕ16	Sorting
Upper	4.33	6.25	very poor
Lower	4.56	6.06	very poor
Terrace	-4.73	-2.17	very poor

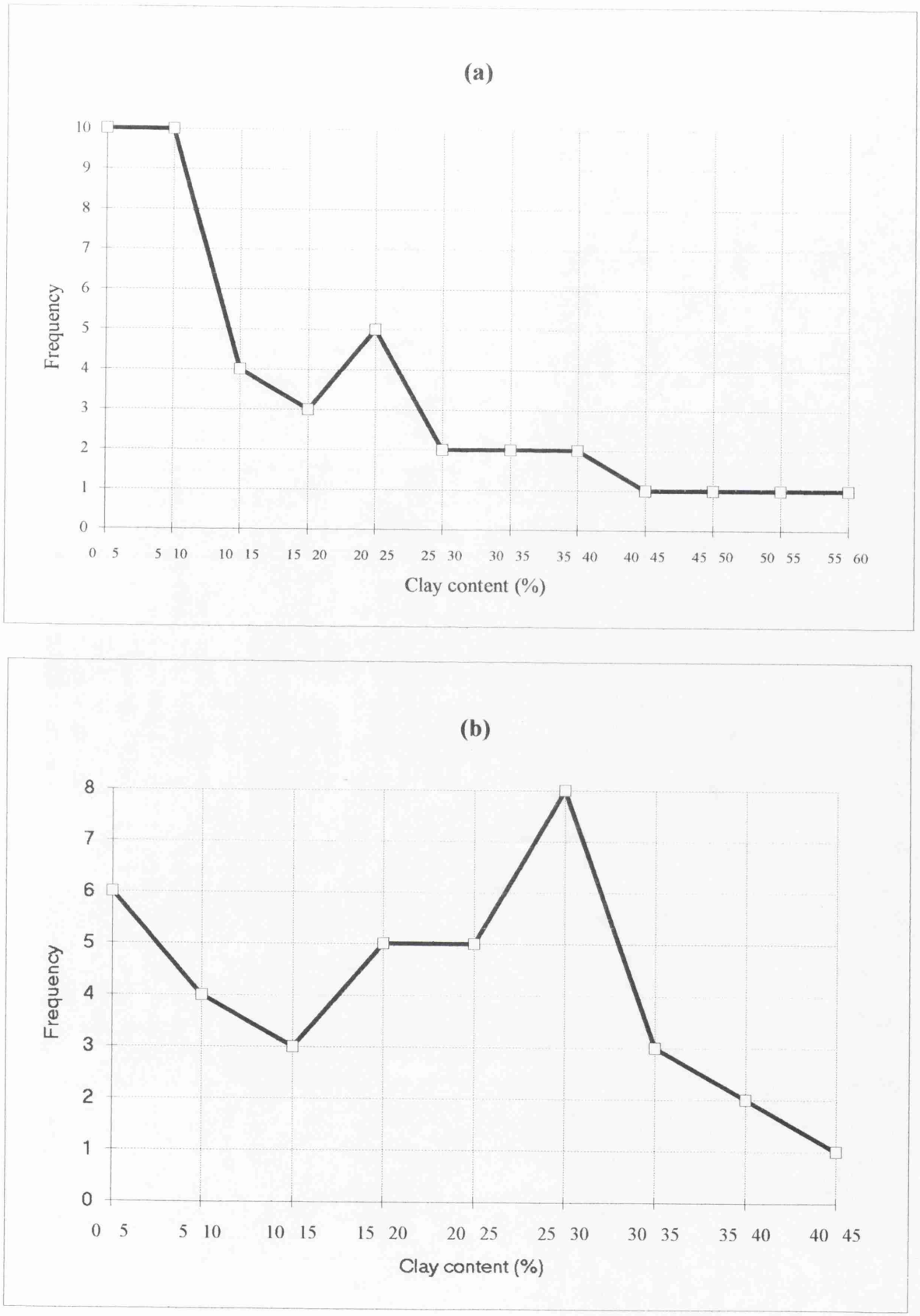

Figure 5.19-1: Clay percentage of the Lar Upper **(a)** and Lower **(b)** deposits.

deposits, the few samples have more than 10% clay. In the lower deposits, the percentage of clay is more variable (Table 5.4).

5.7.3 Shape

As previously indicated, particle shape is determined by the structure and pre-transportation deformation history of the parent rocks. Thus fractured rocks break down into angular and subangular particles and eventually, through abrasion during transportation, to subrounded and rounded particles. Fine-grained particles, such as rock flour, are equidimensional, while most clay minerals are platy. Overall particle shape, sphericity and roundness are usual measures in particle shape analysis. Overall the particle shape measure (Zingg method) used in this research is useful for alluvial interpretation. In this method the long (a), intermediate (b) and short (c) axes (defined at 90° to each other) are plotted as the b/a axis ratio against the c/b ratio (see Appendix Chapter 5, Figures particle shape analysis of the Lar dam basin). Particles are divided into four categories: Bladed (both axial ratios are less than 0.667), Tabular or Discoid (the b/a ratio is greater than 0.667), Prolate or Roller (c/b ratio is greater than 0.667); and Equant or sphere, for which both axial ratios are greater than 0.667.

Because of the logistics of working in an inaccessible mountain environment, only seven samples of 100 particles were taken (Figure 5.20). This number of samples provides a general indication of particle shape only. For full description a much greater number of samples would be required. Sample number A-1 (Dalichai downstream) shows maximum percentage spheres (63%) against a minimum (9%) at Khoshkehlar (no.D-1), because of two different physiographic conditions and different particle mineralogy with volcanic material at Dalichai and sedimentary rocks in Khoshkelar (Table 5.5).

At the Dalichai upstream, sample no. A-2 shows maximum percentage of discs (37%) and spheres (33%). In the Sefid-Ab tributary, which has a gentle gradient and mostly limestone particles, there are equal percentages of spheres and discs (35%), (Table 5.5). At Asbekalak, sample no. C-1 includes particles coming from scree sources. The particles are mostly sedimentary and were deposited because of low stream power (Appendix Chapter 5; Figure C-1 & photo). At Gozaldarreh confluence with Lar lake the modal shape is discs (49%) and the particles are mostly sedimentary types (Appendix Chapter 5;

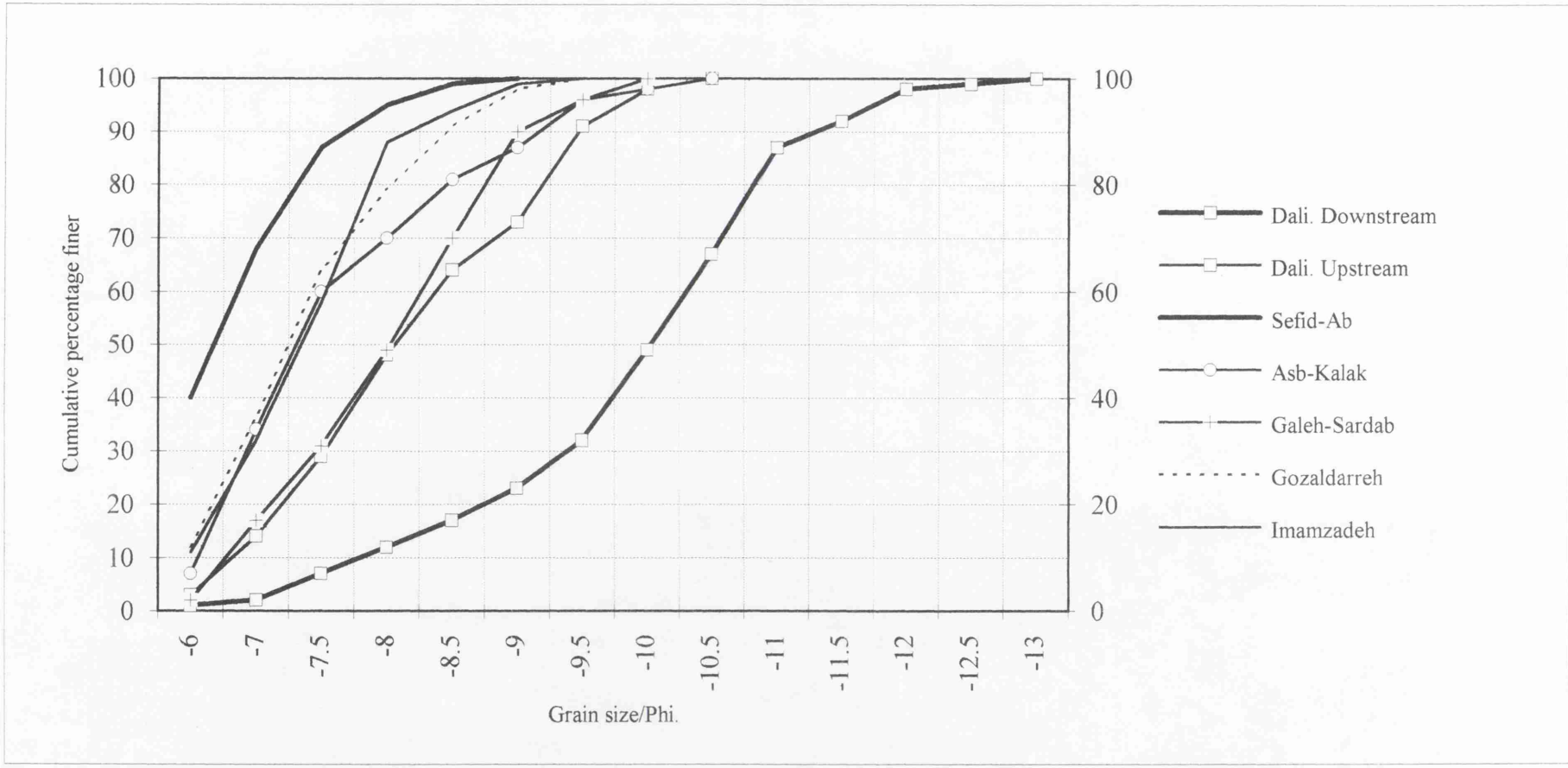

Figure 5.20: The Lar basin gravel size analysis.

Figure E-1 & photo). Finally, sample F-1 from the Lar upstream of the Khoshkelar confluence has a maximum percentage of discs (49%) that are mostly sedimentary particles derived from the upstream end of the Lar basin (Appendix Chapter 5; Figure F-1 & photo). As Damavand volcano is situated in the eastern end of the basin, the lithology of the western part of the basin is mostly sedimentary. Accordingly, with the exception of the 15% volcanics and tuff, 85% of the particle lithologies are of sedimentary origin. Particles with same sedimentary lithology, but 9 kilometres apart, shows an increase to 49% discs from 40% upstream, because of abrasion during transport (Table 5.5).

Table 5.5: Summary of particle shape results in the Lar Basin.

Station	Spheres%	Blades%	Discs%	Rollers%
Dalichai-A1	59	4	8	9
Dalichai-A2	33	11	4	16
Sefid-Ab	35	13	35	17
Asbekalak	20	24	40	16
KhoshkehLar	9	26	53	12
Gozaldarreh	11	28	49	12
Imamzadeh	10	23	49	18

The Lar river has a low energy flow and after the Khoshkelar confluence is meandering (Figure E-1). The E-1 sample taken about one kilometer from Chehelcheshmeh, which has smaller size particle than Lar upstream and accumulated in a large area. After the Khoshkehlar-Galehsardab confluence there is 16% volcanic material, and 10% at Imamzadeh Yorghidar. At sample site D-1 at Khoshkehlar, the flow is seasonal and a high volume of sediment is supplied from upstream. At Imamzadeh (sample no. F-1) the river bed changes frequently because of higher upstream sediment supply from rates. At Sefid-Ab the bed particles come from the Shemshak formation, Lar limestone, Dalichai formation and from scree slopes, and show angular shapes. At Dalichai, further downstream, except for 10% of sedimentary and metamorphic rocks, particle lithilogy is mostly volcanic and almost spherical (59%). This tributary comes from highest point of the basin. Thus large sized particles are found close to the dam.

5.8 ESTIMATION OF SEDIMENT YIELD FROM THE BASIN

Erosion, transportation and deposition of sediment are natural processes which have occurred throughout geologic time. The extent of erosion and consequently the amount of sediment which moves out of a watershed varies greatly from one area to another, depending upon geologic, climatic, physical, vegetation, and other conditions. Thus sedimentation in a reservoir created by a dam constructed accross a natural water course is inevitable. Two kinds of sediment are being and have been deposited in the Lar basin; first suspended sediment consisting mainly of clay and silt particles, and second bedload sand and gravel mixtures in terraces and deltas.

5.8.1 Sediment Volumes

Since sedimentation has occurred in terraces up to a maximum altitude of 2700 metres in the former Lar Lake and to 3500 metres in the Dalichai Lake, by measuring the area of the terraces in the basin, an estimate can be made of the total volume of sediment deposited in the former Lake (see section 5.2.1 and 5.2.2 for the limit of basin sediments). Using the equation proposed by Smith et al (1960) the sediment volume between two levels on contours, h metres apart, can be estimated as follows;

$$V = h\,(A + B + \sqrt{AB})/3 \qquad [5.1]$$

where; A and B = the areas enclosed by the two contours (m^2) and V = volume of the sediment including pore spaces (m^3). This formula represents the definite integral of the area of lake sediments over the vertical interval h (which is the interval between contour lines, for the Lar basin this was usually was 100 metres). The use of this formula is shown in Figure 5.21 allows a maximum volume, to be calculated. However, because lake deposits are not horizontal, but are lower toward the centre of the lake than near the edges, the calculation over estimates the real volume.

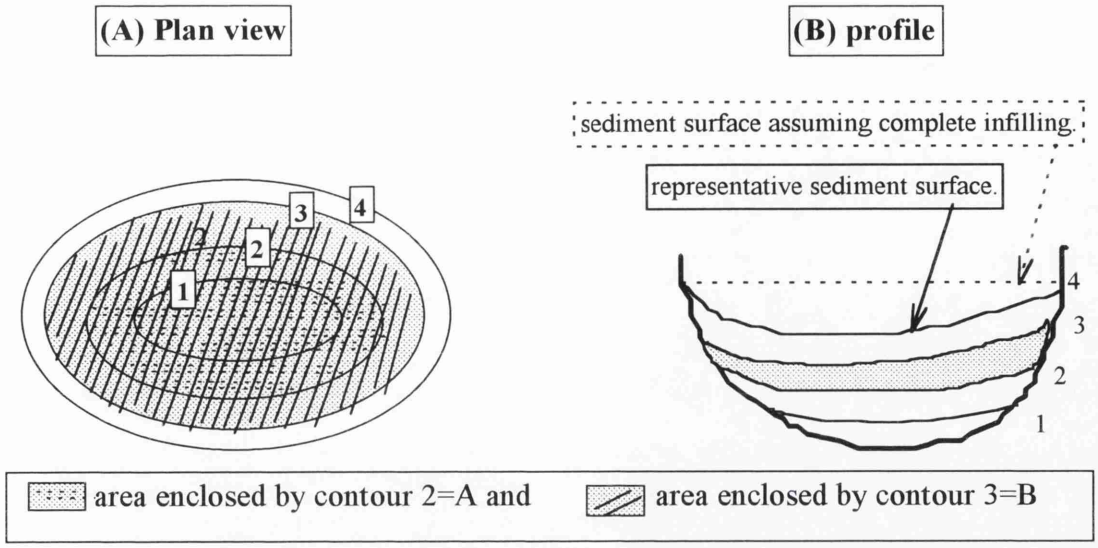

Figure 5.21: Schematic diagram of the volume calculation (A) and the area in the valley (B).

The data used for this calculation were derived from 1945 (British Army) topographic maps of the Lar basin at 1:25 000 scale with 100 metres contour intervals. This was compared with aerial photographs at different scales and times and an echosounding survey obtained in summer 1994 from three selected Lake sites. The results of echosounding data are important because they document the increasing delta volumes during the Dam period (1974-94), which are observed on the aerial photographs and also topography maps. The lack of any sediment and water discharge measurements at the main water enterances (Lar, Sefid-Ab and Dalichai) to the lake, the echosounding is useful at this stage. For each fan, contour lines were interpolated by hand and were used in estimation of sediment volumes by equation 5.1.

5.8.1.1 Sediment Estimation Using the Topographic Map

The following table presents the calculations for estimating the volume of sediment accumulated in the Lar basin from topographic map. For each delta, contour lines were used in estimation of sediment volumes using equation 5.1. This gives a maximum volume, which is an over estimate because of the unknown gradient of the bed. The time required for this amount of sediment to be carried into the Lake basin is dependent upon the quantities of sediment delivered into the lake by the various streams which feed it (Table 5.6 and Figure 5.22). Between altitudes 2200 and 2700m the topographic and sedimentological data indicate that the sediment was deposited in the former Lar Lake

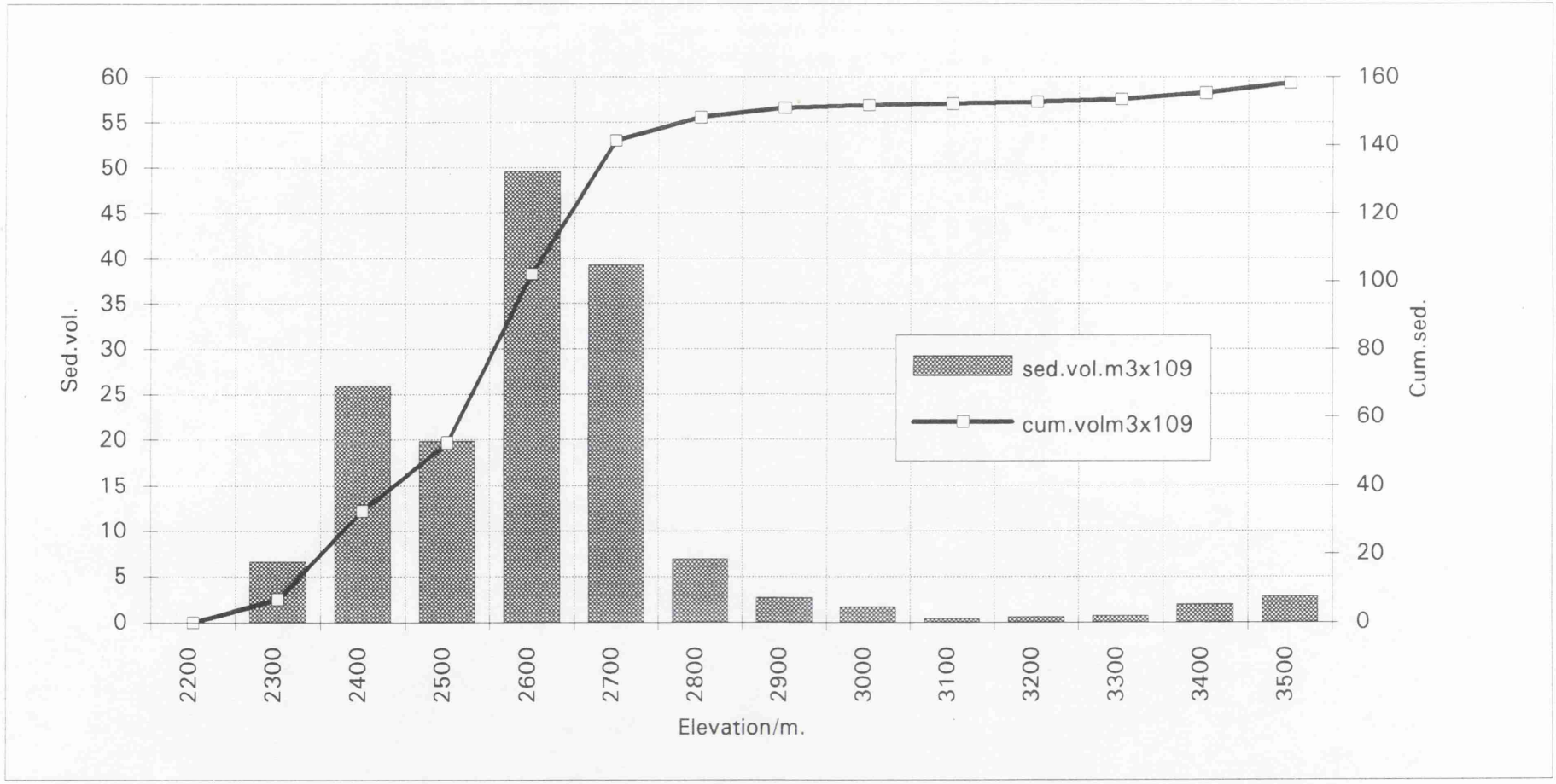

Figure 5.22: : Distribution of former sediments volumes in the Lar basin.

(Table 5.6-a). Over 2700m in altitude, deposition was in the small Lake of Dalichai and other smaller areas (Table 5.6-b; see Figure 5.2-b). It can be seen that up to 1.41×10^{11} m^3 (this amount includes the upper and lower sediment) of sediment accumulated in the former Lake Lar (without allowing for porosity). The bulk of the sediments (68%) lie at the altitude between 2500-2700m. where lacustrine and Lar valley terraces are found (see Figures 5.9-c, d and section 5.2).

Table 5.6-a: The Lar Lake sediment volumes from topographic maps (1945 1:25000).

Elevation/m	Area$\times10^6$ m^2	Sed.vol.$\times10^9/m^3$	Cum.vol.$\times10^9/m^3$
2200	0	0.0	0.0
2300	198	7	7
2400	327	26	33
2500	264	20	52
2600	773	50	102
2700	112	39	141

Table 5.6-b: Sediment volumes in the Dalichai Lake and other deposition areas, from topographic maps (1945, 1:25000).

Elevation/m	Area$\times10^6$ m^2	Sed.vol.$\times10^9/m^3$	Cum.vol.$\times10^9/m^3$
2700	0	0.0	0.0
2800	34	7	148
2900	21	3	151
3000	14	2	152
3100	8	0.4	152
3200	4	1	153
3300	12	1	153
3400	32	2	155
3500	24	3	158

5.8.1.2 Sediment Estimation from Aerial Photographs

As described in Chapter 3 (see p.59) for the pupose of making stereo models, control points were selected in and near the selected valley bottoms, which are the areas where the deposits are located. Each delta lay on one pair of aerial photographs. For each overlap area between photographs control points were accurately surveyed by theodolite in the field using absolute benchmarks in the Lar Dam site. For example, there were 9 control points at the Dalichai delta, and 8 for the Sefid-Ab. After transfering the control points to aerial photos, topographic maps were derived at a 5 metre contour interval (see Figures 5.23-a, Dalichai delta and 5.23-b, Sefid-Ab delta).

In the second stage common baselines were defined for fans and deltas, assuming that the catchments base levels are at influence with the Lar river. The confluence at Sefid-Ab is located at 42910N-730306E, at Dalichai it is located at 41140N-78060E and Gozaldarreh at 45340N-71130E. The baselines are parallel to the Lar river at 90° to the tributaries (Figure 5.24). The same baselines were used both for echosounding surveys, topographic maps, and for aerial photos analysis.

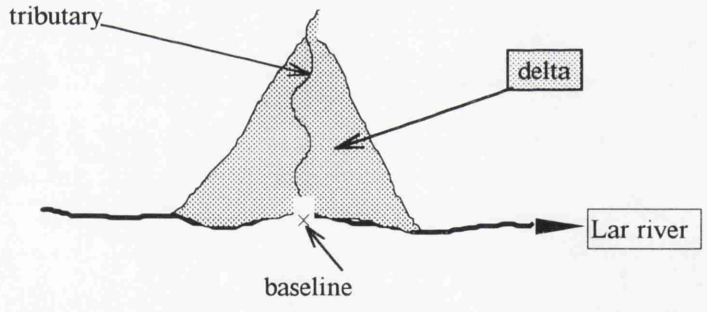

Figure 5.24: Schematic diagram of the baseline parallel to the Lar river.

Because fans/deltas grow laterally through time, common baselines are needed for the volume calculations and were taken as the location of the former confluences between the tributaries and the Lar river. These baselines can also be used with the echosounding data, to enable direct comparison between the two methods.

Photogrammetric results from aerial photographs were obtained for two selected sites at Dalichai and Sefid-Ab for 1955 and 1970, but because of a lack of aerial photographs for Gozaldarreh, only the topographic maps at 1:25 000 (British Army, 1945) and 1:10000

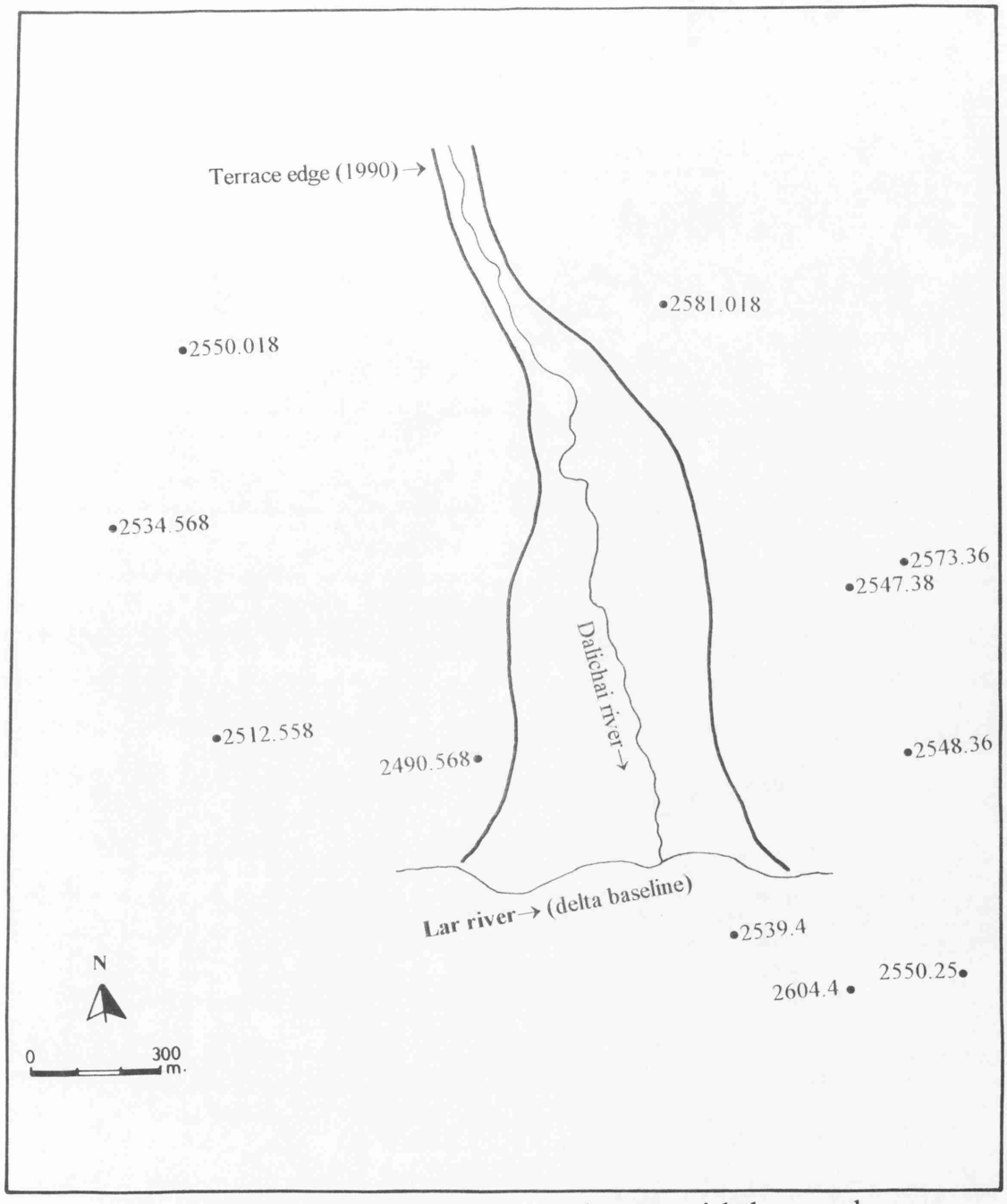

Figure 5.23-a: Dalichai delta control points on aerial photographs (all spot heights are in metres).

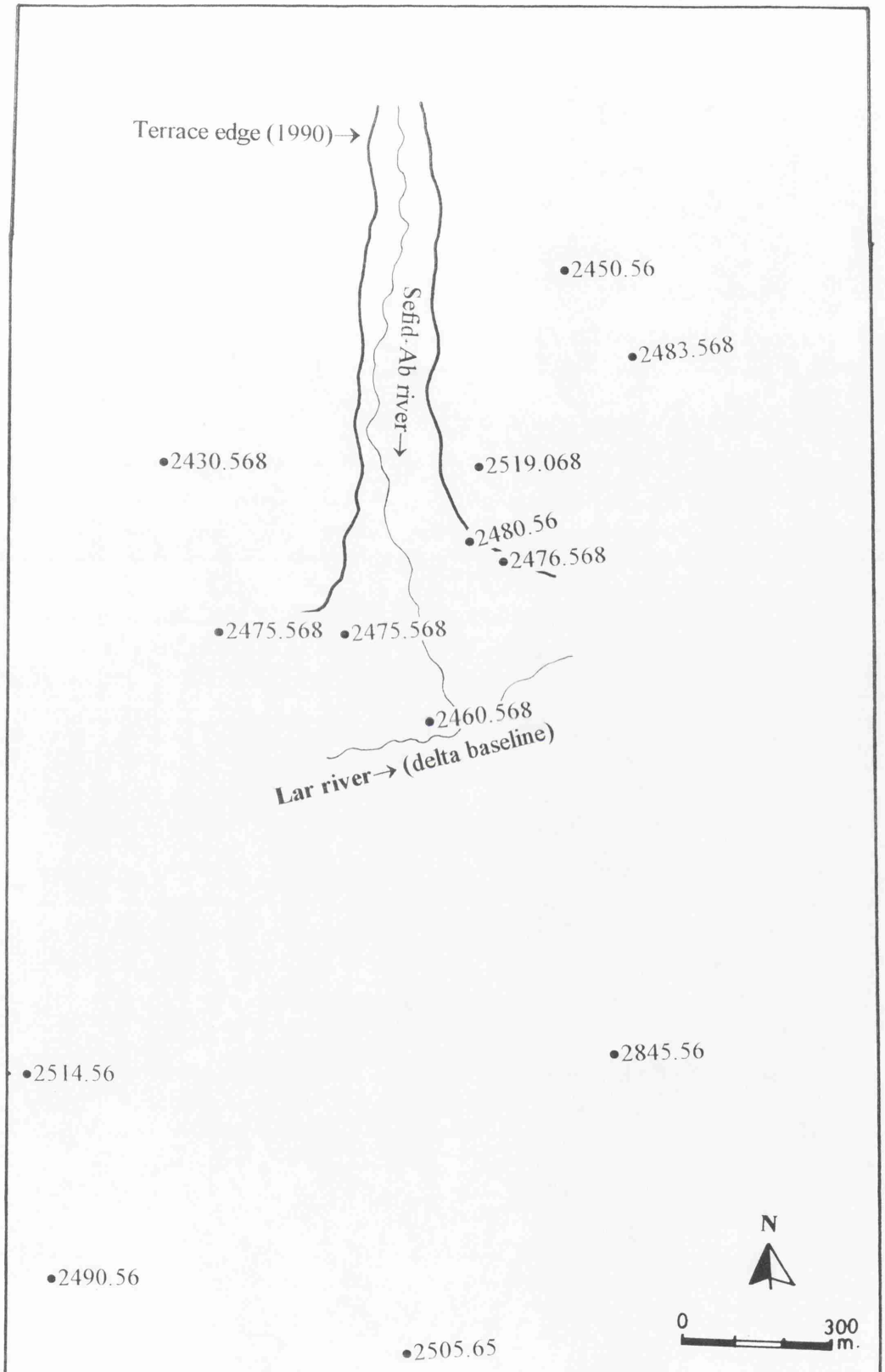

Figure 5.23-b: Sefid-Ab delta control points on aerial photographs (all spot heights are in metres).

(1962 enlarged from B.A, 1945) could be employed (Figure 5.25). Because of the photograph scale and locations of control points, absolute heights on the photogrammetric models from different times are not always identical. However, relative heights within each model are subject to much less error. Also when volumes are calculated it is change in the areas of the deposits which is the main control over the volumes of stored sediment, rather than changes in the elevations of the tops of the sediment surfaces.

Although the total sediment volume at the Gozaldarreh site is more than at either the Sefid-Ab or Dalichai sites, the specific volume (volume ÷ catchment area) value at Dalichai (1.6 and 1.96×10^3 m^3/km^2 respectively for 1955 and 1970) is greater than at either Gozaldarreh (1.08×10^3 m^3/km^2) or Sefid-Ab (1.2 and 1.9×10^3 m^3/km^2 respectively for 1955 and 1970). Annual specific yields are 0.42×10^3 $m^3/km^2/yr$ and 0.02×10^3 $m^3/km^2/yr$ respectively for Sefid-Ab and Dalichai (Table 5.7).

Table 5.7: Volume of selected depositional fans using aerial photographs (1955-70).

Site	Elevation (metre)	Area ($\times10^5 m^2$)	Sed.volume ($\times10^5 m^3$)	Specific estimate (m^3/km^2)
***Gozaldarreh**	2470-2500	0.41	4.5	1.08×10^3
1955	2450-2475	0.13	0.67	1.2×10^3
Sefid-Ab 1970	2450-2475	0.198	1.0	1.9×10^3
Change (55-70)	→	→	0.33 ($0.02a^{-1}$)	0.04×10^3 (annual)
1955	2450-2485	1.1	3.3	1.6×10^3
Dalichai 1970	2450-2490	1.28	3.85	1.96×10^3
Change (55-70)	→	→	0.55 ($0.04\ a^{-1}$)	0.02×10^3 (annual)

*(this delta calculated from 1:25 000 topography map, 1945 British Army).

5.8.1.3 Sediment Estimation Using Echosounder

Echosounding was used to estimate volumes of sediment accumulated in sub-basin deltas. As described in Chapter 3 (p.58-59) the echosounder was used from a boat which traversed the lake. Positions were fixed using a theodelite on the shore, and the surveys were related to absolute heights at the dam site. The depth was recorded at fixed time intervals of about 30 sec. which represents about a 100 metre interval (the theodolite

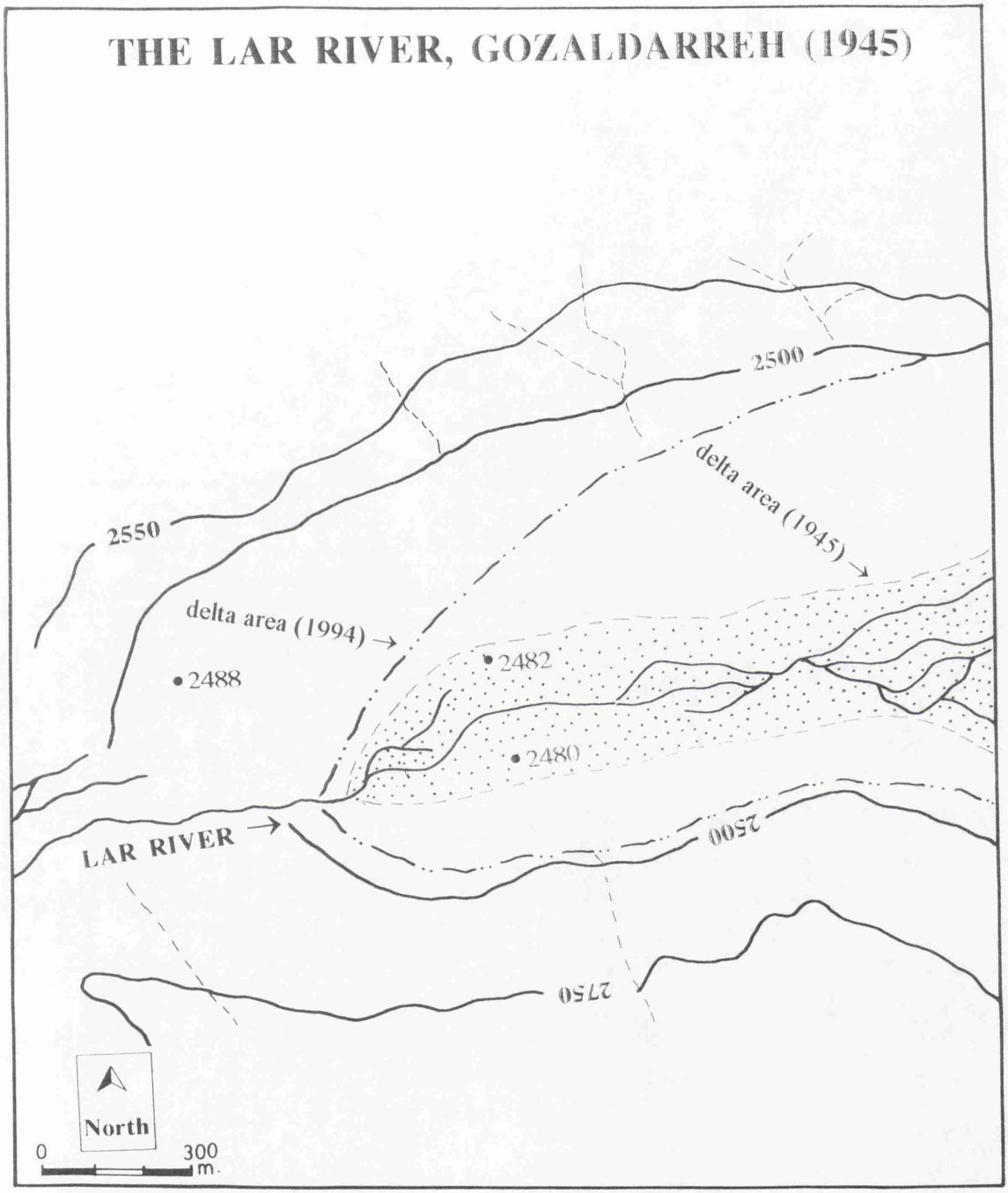

Figure 5.25: Gozaldarreh delta topography from topographic map, enlarged to 1:10 000 (*present delta from echosounding survey is around contour line 2500m.)
(source; Lar topographic map at 1:25 000, British Army, 1945).

survey gives accurate locations). Before starting surveying the echosounder was precisely calibrated, and in the shallow depths of the deltas (less than 20 metres) its accuracy is ±5 cm. To reduce the effects of waves, the internal software of the equipment records the mean of a number of readings automatically. Figures 5.26-a, 5.27-a and 5.28-a show the actual boat paths in near parallel lines. Figures 5.26-b, 5.27-b and 5.28-b show the surveyed points on the selected deltas (see Tables 5.26-b, 5.27-b and 5.28-b for raw data). Finally for each delta, contour lines were interpolated by eye and were used in estimation of sediment volumes using equation 5.1 [$V = h\,(A+B+\sqrt{AB})/3$].

The echosounding results (the sediment volumes estimated by equation 5.1) are very similar to those using photogrammetric data described above. The Gozaldarreh stream has a high volume of sediment ($6.3\times10^5 m^3$ or $0.315\times10^5 m^3a^{-1}$), with less volume of sediment in the Sefid-Ab ($1.7\times10^5 m^3$ or $0.085\times10^5 m^3a^{-1}$). The Dalichai produces $5.9\times10^5 m^3$ or $0.3\times10^5 m^3a^{-1}$ and to gether with the Gozaldarreh, both seem to have high erodibility. The production of sediment related to catchment area, shows that Dalichai with $3\times10^3 m^3/km^2$ or $0.15\times10^3 m^3/km^2a^{-1}$ [Gozaldarreh ($1.5\times10^3 m^3/km^2$ or $0.075\times10^3 m^3/km^2a^{-1}$) and Sefid-Ab ($1.4\times10^3 m^3/km^2$ or $0.07\times10^3 m^3/km^2a^{-1}$)] has higher sediment supply per km^2. The Dalichai catchment area is $77km^2$ larger than Sefid-Ab ($119km^2$) and $218km^2$ smaller than the Lar catchment area. Converted to mass for Gozaldarreh about $1.2\times10^6 t(0.06\times10^6 ta^{-1})$ is found, with 3.5×10^5 t (0.175×10^6t a^{-1}) for Sefid-Ab and 1.2×10^6 t (0.06×10^6t a^{-1}) for Dalichai (Table 5.8).

Table 5.8: Volumes of selected depositional fan deltas by Echosounding (1994).

Site	Elevation (metre)	Area ($\times10^5 m^2$)	Volume ($\times10^5 m^3$)	Estimated specific supply (m^3/km^2)	Annual specific estimate ($m^3/km^2/yr$)
Gozaldarreh	2480-2489	2.1	6.3	1.5×10^3	0.075
Sefid-Ab	2483-2488	1.12	1.7	1.4×10^3	0.035 *
Dalichai	2484-2488	2.13	5.9	3×10^3	0.1 *

*these values calculated from specific supply (estimated by 1970 aerial photographs) /20 (20 years is the period after dam construction).

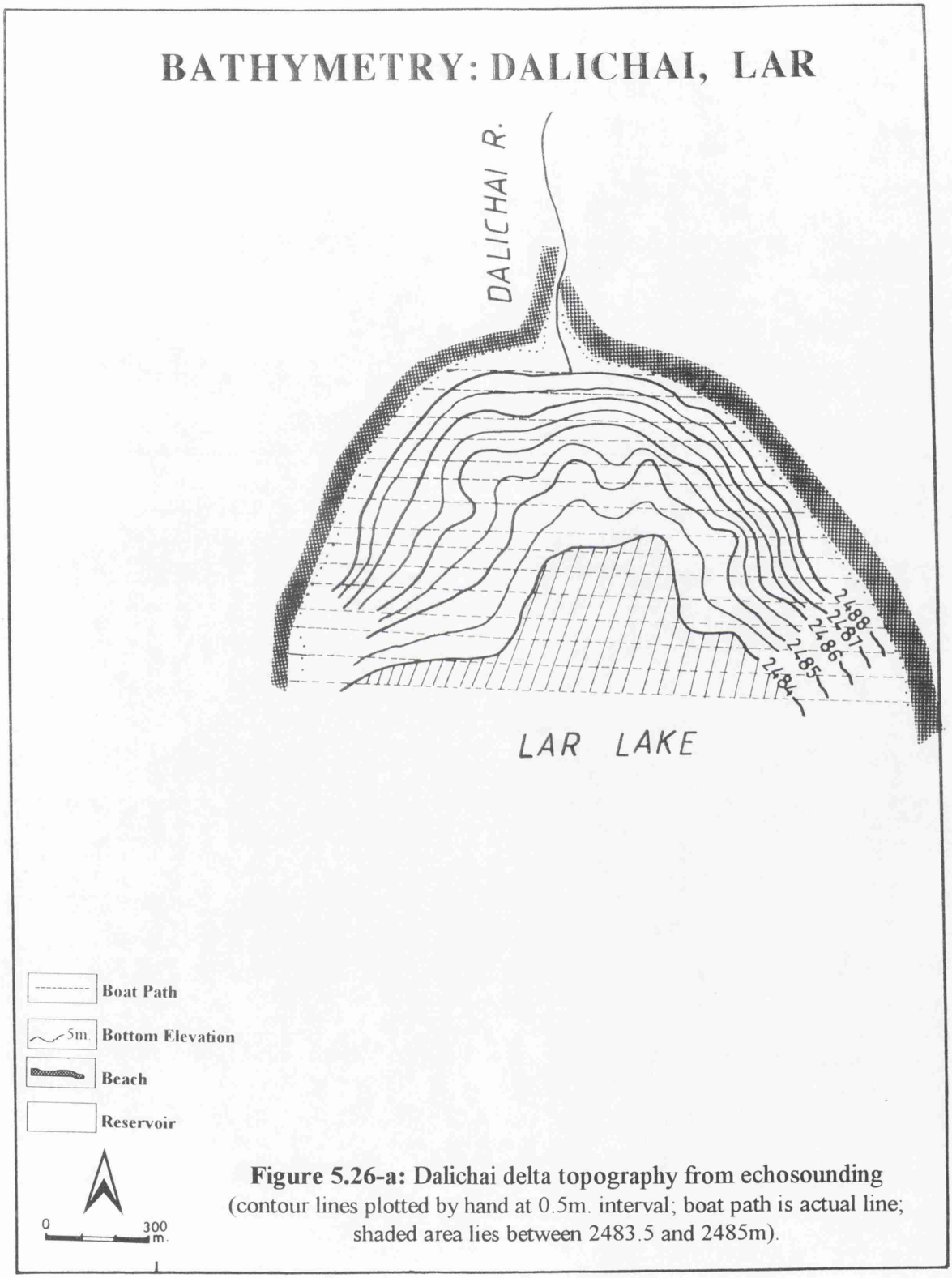

Figure 5.26-a: Dalichai delta topography from echosounding
(contour lines plotted by hand at 0.5m. interval; boat path is actual line; shaded area lies between 2483.5 and 2485m).

Table figure 5.26-b: Dalichai delta depth points (metre) from echosounding (see Figure 5.21-d for point locations).

Depth	BOAT PATH														
Points	A	B	C	D	E	F	G	H	I	J	K	L	M	N	O
1	3	0.7	1.31	0.65	0.68	0.66	0.67	0.67	0.65	0.69	0.63	0.69	0.64	9.72	0.64
2	3.3	0.81	1.15	2.2	1.23	0.69	1.75	0.8	0.8	1.3	0.79	0.76	0.78	0.75	0.71
3	3.4	3.1	2.42	2.8	2.11	1.3	2.5	2.65	1.6	2.4	1.3	1.3	0.78	0.75	0.69
4	3.4	3.32	2.81	3.15	2.75	2.82	3.3	3.1	2.5	2.6	1.8	1.3	0.79	0.75	0.71
5	3.48	3.46	3.4	3.4	3.35	3.3	3.3	2.95	2.7	2.5	1.78	0.78	0.78	0.65	
6	3.48	3.74	3.47	3.39	3.36	3.32	2.6	2.3	2.5	1.6	1.2	0.78	0.71	0.55	
7	3.47	3.45	3.5	3.1	2.79	2.33	0.87	1.6	1.3	0.8	0.72	0.63	0.6		
8	3.47	3.31	3.31	2.56	1.75	1.82	0.7	0.75	0.69	0.67	0.65	0.61			
9	3.31	3.28	3.32	1.3	0.71	1.25	0.65	0.96	0.63						
10	2.25	2.8	3.33	0.71	0.66	0.67									
11	0.71	2.28	0.69	0.65											

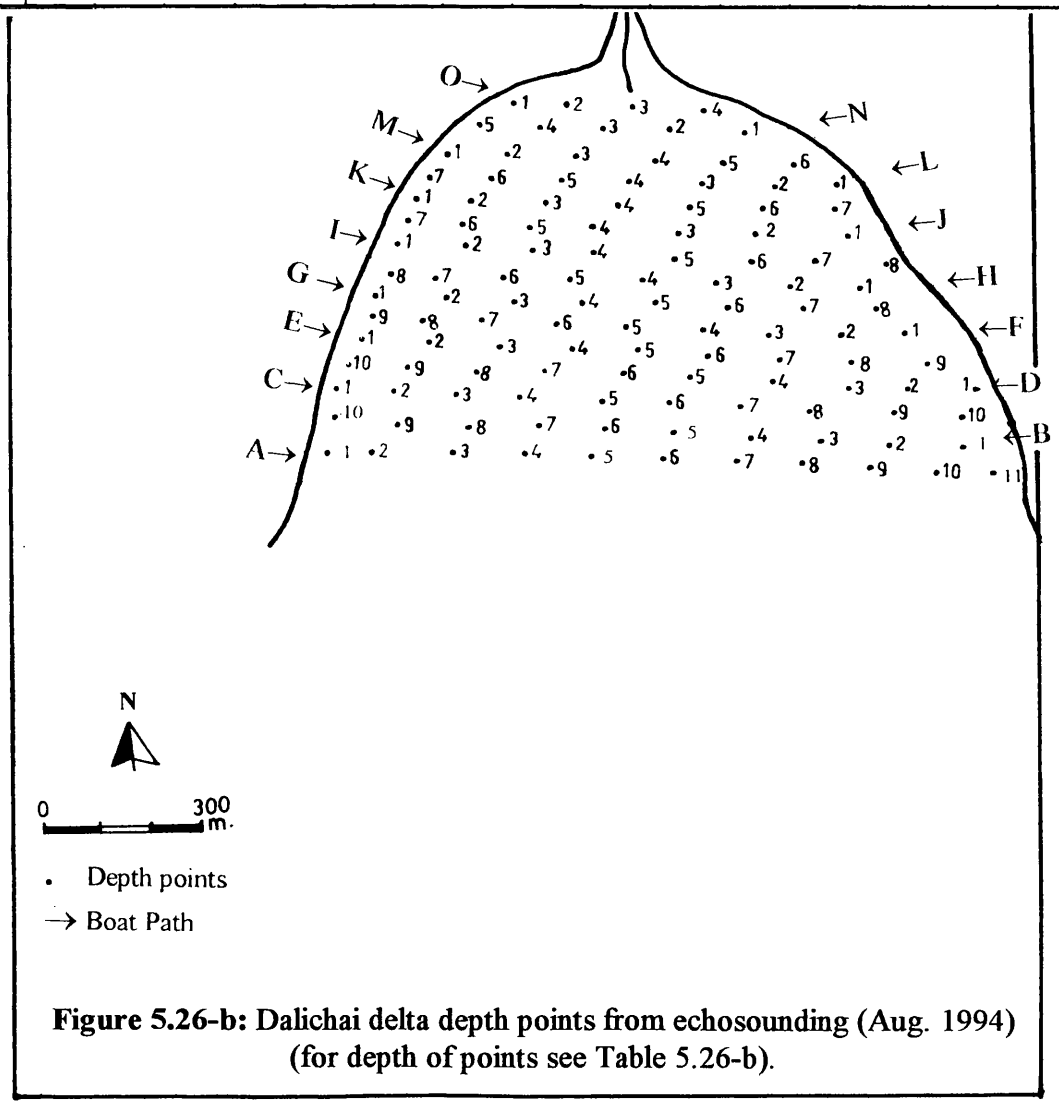

Figure 5.26-b: Dalichai delta depth points from echosounding (Aug. 1994) (for depth of points see Table 5.26-b).

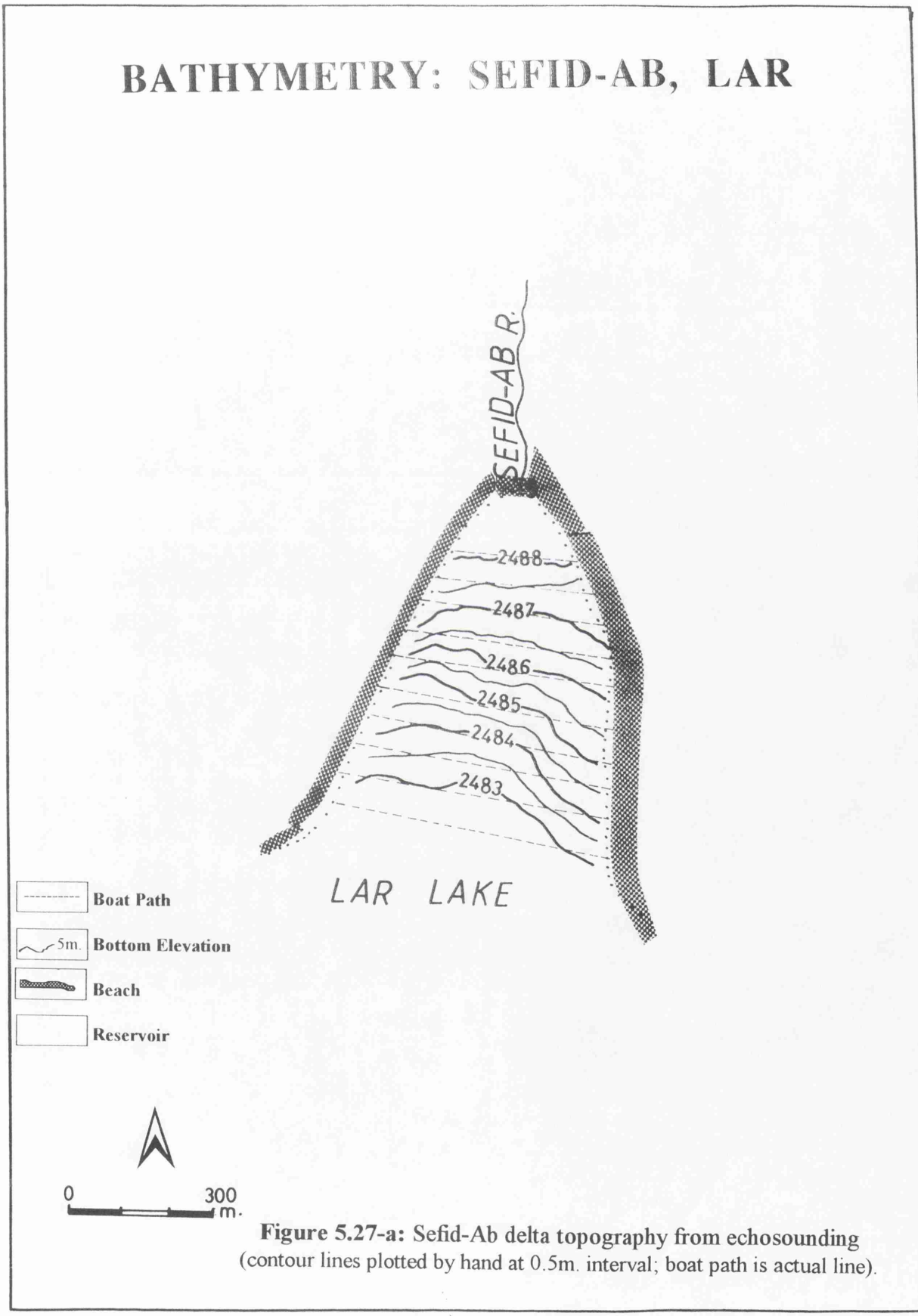

Figure 5.27-a: Sefid-Ab delta topography from echosounding
(contour lines plotted by hand at 0.5m. interval; boat path is actual line).

Table figure 5.27-b: Sefid-Ab delta depth points (metre) from echosounding (see Figure 5.22-d for point locations).

Depth	B O A T P A T H									
Points	A	B	C	D	E	F	G	H	I	J
1	4.5	3.3	3.55	2.3	2.7	1.1	0.7	0.65	0.55	0.52
2	4.7	3.8	3.85	3.5	2.1	1.3	0.89	0.7	0.6	0.5
3	5.0	4.5	3.5	3.3	2.4	1.2	0.79	0.7	0.62	
4	5.0	4.3	2.75	3.2	1.8	1.3	0.72			
5	4.3	4.0		2.76						

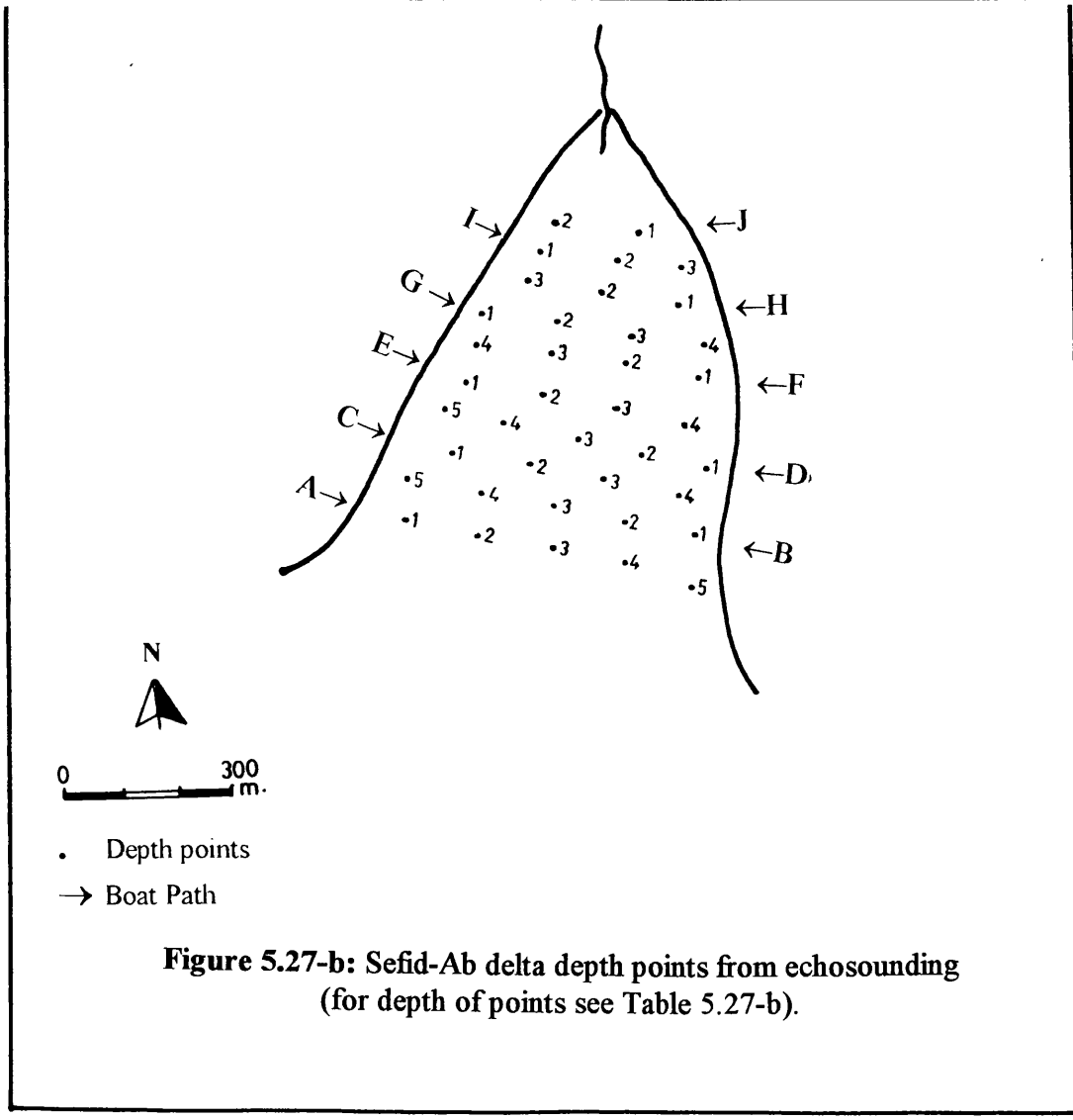

Figure 5.27-b: Sefid-Ab delta depth points from echosounding (for depth of points see Table 5.27-b).

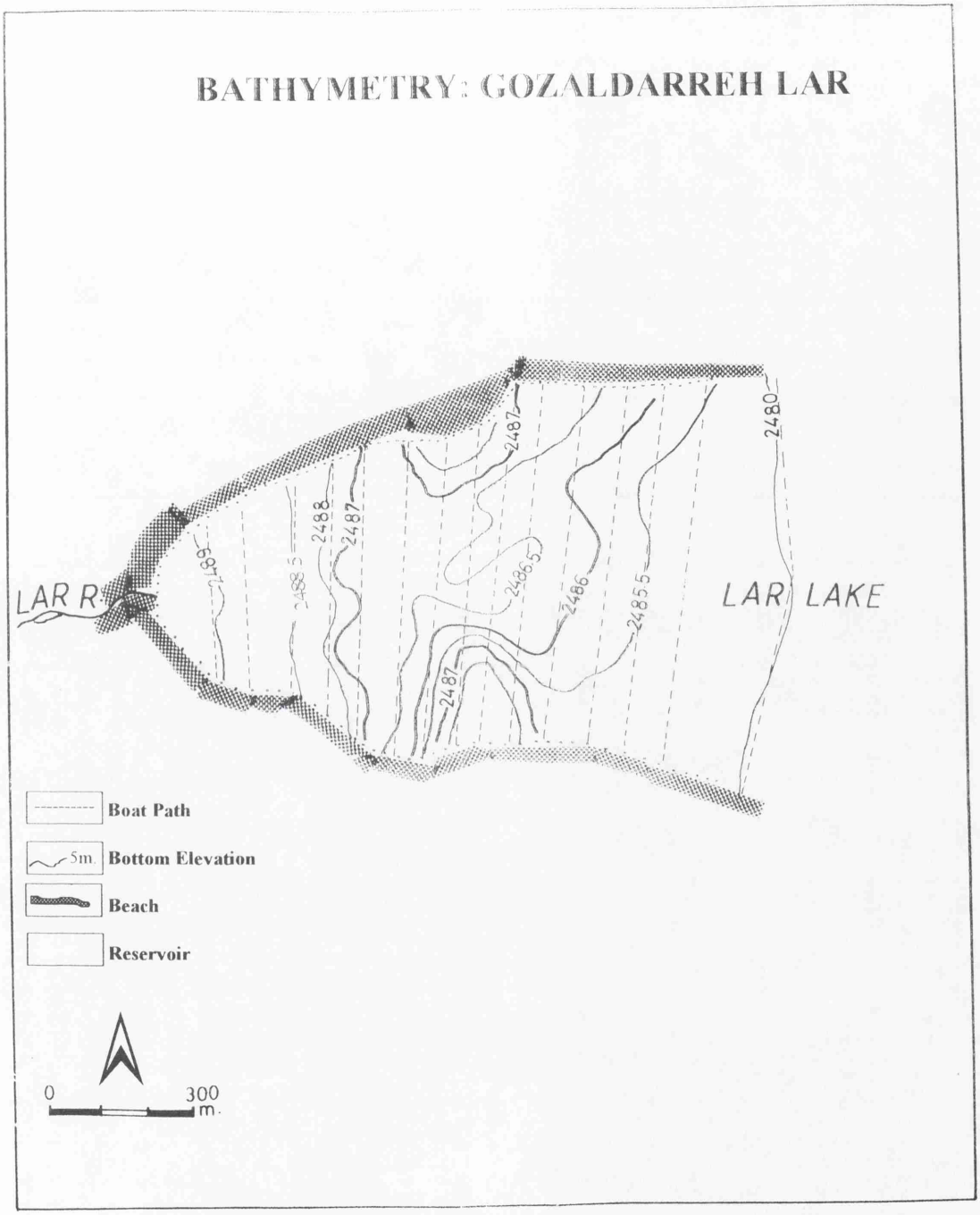

Figure 5.28-a: Gozaldarreh delta topography from echosounding (contour lines plotted by hand at 0.5m. interval; boat path is actual line).

Table figure 5.28-b: Gozaldarreh delta depth points (metre) from echosounding (see Figure 5.23-d for point locations).

Depth	BOAT								PATH							
Points	A	B	C	D	E	F	G	H	I	J	K	L	M	N	O	
1	7.29	1.72	1.67	0.9	0.8	0.79	0.69	0.72	1.75	0.78	0.77	0.69	0.22	0.23	0.18	
2	7.32	2.2	1.69	1.3	1.75	0.8	0.78	0.8	1.3	0.79	0.78	0.7	0.23	0.23	0.17	
3	7.27	2.8	1.75	1.5	1.51	0.88	0.79	0.83	1.2	0.79	0.78	0.69	0.23	0.23	0.15	
4	7.25	2.5	1.74	1.47	1.2	0.8	0.82	0.82	0.79	0.78	0.78	0.69	0.22			
5	7.32	2.3	1.75	1.48	0.9	1.3	0.78	0.78	0.78	0.8	0.79					
6	7.32	2.1	1.3	1.7	1.3	0.78	0.78	0.72	0.68							
7	7.32	1.75			0.8	0.71										

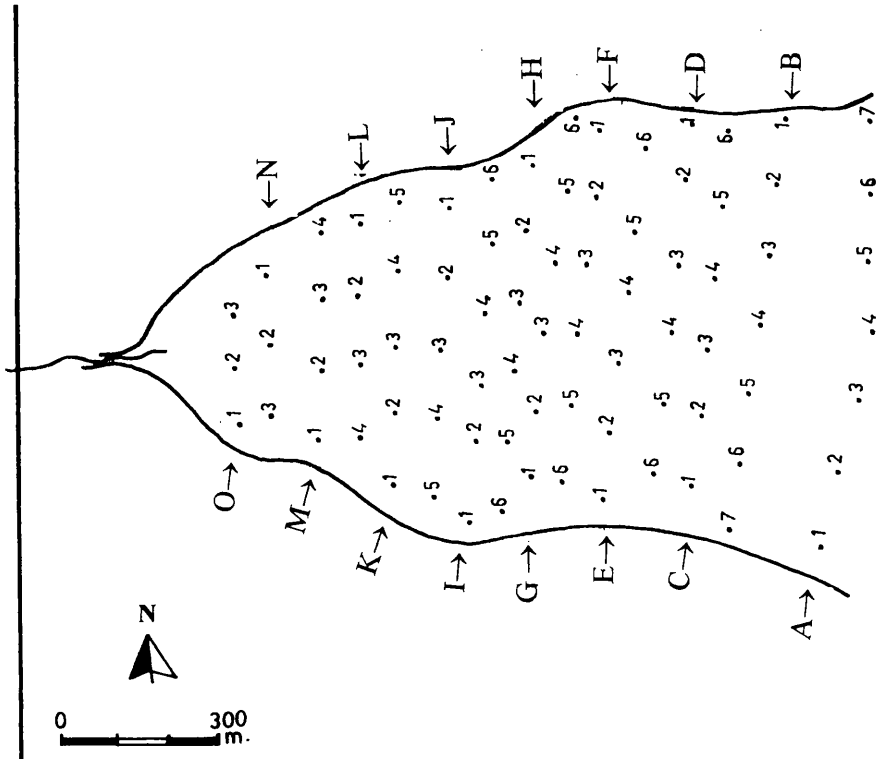

Figure 5.28-b: Gozaldarreh delta depth points from echosounding (for depth of points see Table 5.28-b).

5.8.14 Error Calculation of Estimated Sediment Volumes

Table 5.9 shows the calculated volume error from echosounding, assuming that individual points are accurate to ±5cm (the Sea Farer-700 Radio Echosounder used for this research, specified ±5cm error for surveying when water depth is less than 20 metres). The errors are calculated by assuming that the measured volume divided by the delta area gives a mean depth of sediments (D) i.e D=V/A;

$$(D=V/A) \qquad [5.2]$$

where V=Sediment volume (m^3) and A=sediment area (m^2). Assuming ±5 cm errors, maximum and minimum volume estimates are obtained as:

$$V^+ = A(D+5\ cm) \qquad [5.2]$$

$$V^- = A.(D-5\ cm) \qquad [5.3]$$

Table 5.9: Volume errors for echosounding results.

Value of error	Gozaldarreh	Sefid-Ab	Dalichai
V ($10^5 m^3$)	6.30	1.70	5.90
V^+ ($10^5 m^3$)	6.41	1.75	6.01
V^- ($10^5 m^3$)	6.20	1.64	5.79
A (m^2)	2.1×10^5	1.12×10^5	2.13×10^5
D (m)	3.00	1.52	2.77

The error ranges shows in Table 5.9 are indicative of likely uncertainties in the results. It is clear that the areas of the deposits are the main determinant of volumes, rather than their thickness. There may be greater error introduced because of uncertainty in the elevation of the base of the deposits. However, the magnitude of the errors is small compared to the differences between catchments.

Table 5.10 presents the calculated volume error for the aerial photographs of 1955 and 1970 at both the Dalichai and Sefid-Ab deltas. The errors are calculated using the above

method, with likely errors estimated as follows (J.Drummond, personal communication 1966);

$$h \div f = e \text{ (scale)} \qquad [5.4]$$

$$\text{error} = (h \div e) \times 3 \qquad [5.5]$$

where h=flying height and f=focal length of the photograph. For both 1955 (h÷e=7717÷50 000) and 1970 (h÷e=3056÷20 000) ±0.46m errors were used, maximum and minimum volume estimates are obtained as:

$$V^{+} = A(D+0.46m)$$

$$V^{-} = A.(D-0.46m)$$

For topographic maps the error in plan position (x,y) is 0.5mm×scale factor, and the error in elevation (h) is also 0.5×the vertical interval (Drummond, personal communication 1996). Therefore the error estimate for the 1:25 000 topographic map with 50m contour interval, is; V=f(x,y,h). Using propagation of variance, error in the elevation of any one point is;

$$\sqrt{(SDx)^2 + (SDy)^2 + (SDh)^2} \qquad [5.6]$$

therefore;

$$\sqrt{156.25+156.25+625} = 30.6m$$

However, the value relies on the standard error, estimated as $30.6/\sqrt{n}$, where n is the number of points involved in the calculation. Taking n=150 (on arbitrary but realistic value) suggests an error of ±2.42m. This is used in Table 5.10.

Table 5.10: Volume errors for aerial photographs and maps.

Value of error	Sefid-Ab	Dalichai	*Gozaldarreh
1955	0.73	3.81	5.49
V^+ ($10^5 m^3$)			
1970	1.09	4.44	
1955	0.61	2.79	3.51
V^- ($10^5 m^3$)			
1970	0.91	3.25	
1955	0.13×10^5	1.1×10^5	0.41
A (m^2)			
1970	0.198×10^5	1.28×10^5	
1955	5.15	3.0	10.98
D (m)			
1970	5.05	3.0	

*(this calculation is from 1:25000 topography map, 1945).

As for the echosounding data, the the calculated errors are indicative only. They suggest that aerial photographs provide estimates of slightly greater uncertainty than echosounding, but the differences between catchments are clearly detected by this method. There is greater uncertainty for the topographic map, but the volume estimate produced is realistic when compared with those from other locations.

5.8.1.5 Results Summary For Different Deltas

Because of high erodibility in the Dalichai and Sefid-Ab downstream channels there were relatively minor changes between the two aerial photograph dates (1955-1970). A sediment supply rate of $0.02\times10^5 m^3 a^{-1}$ during this period was calculated for the Sefid-Ab delta, and $0.04\times10^5 m^3 a^{-1}$ in the same period for Dalichai delta (see Table 5.7). Figure 5.26-c,d and 5.27-c,d show that derived contour lines in delta areas are very similar which confirms there are no major new deposits in the selected sites.

After construction of the artificial dam in 1974 there have been significant changes to the fans at their former confluences with the Lar river. The Lar Lake supported the accumulation of more sediment delivered from upstream, confirmed by significant changes on contour lines derived from echosounding results, about 40 years after the aerial photographs (1955-1994).

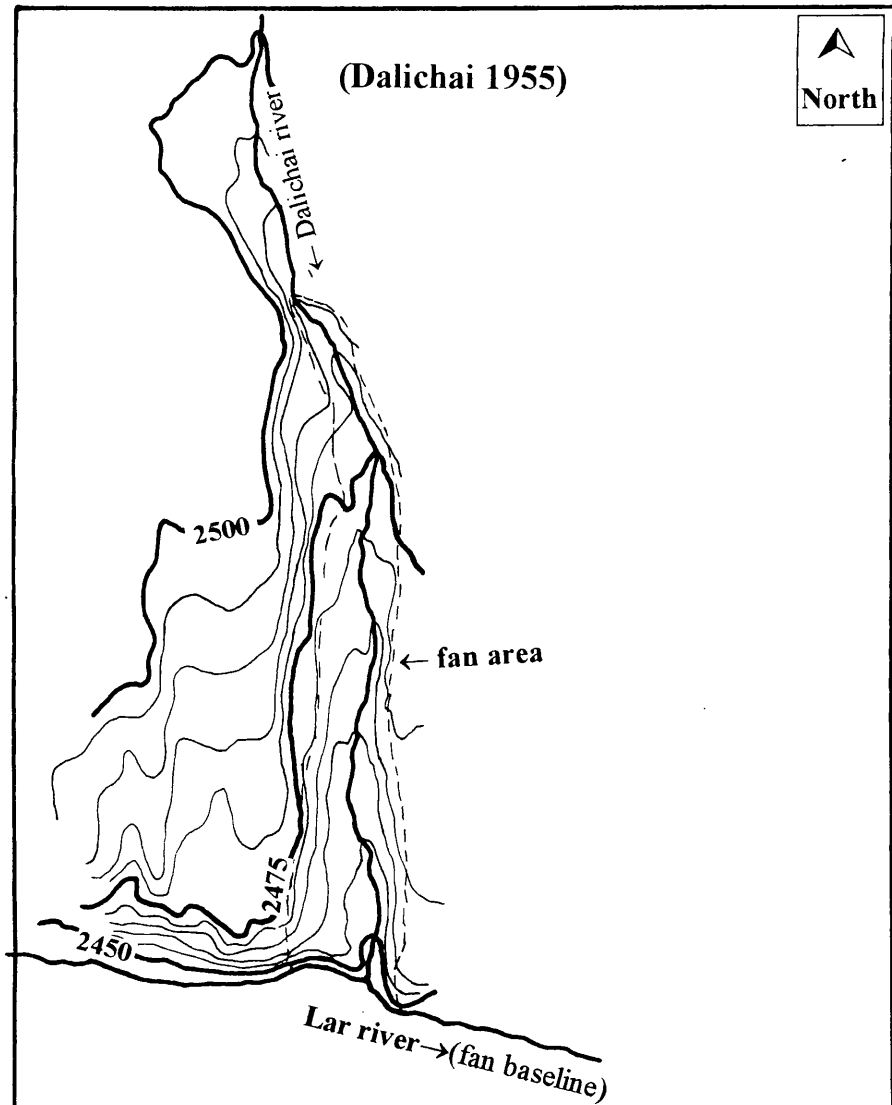

Figure 5.26-c: Dalichai fan topography from aerial photograph (Sept. 1955; Scale, 1:10 000; contour interval 5m).

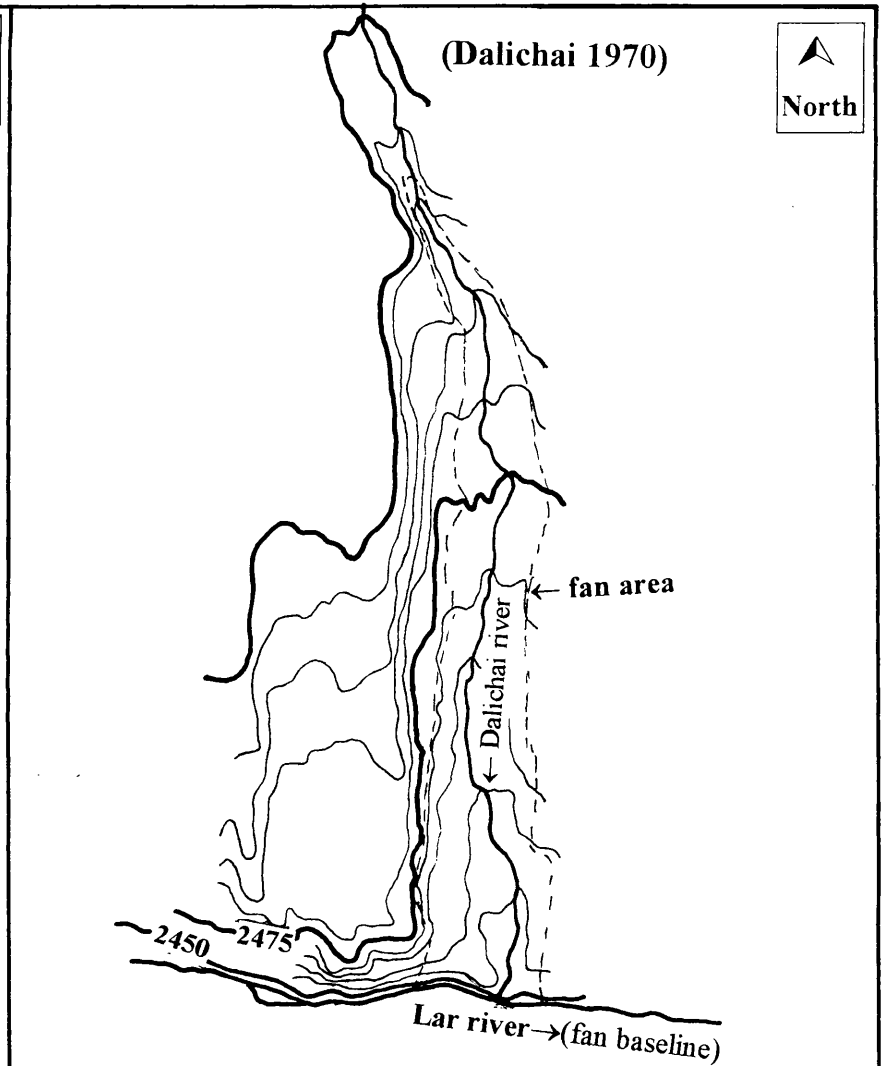

Figure 5.26-d: Dalichai fan topography from aerial photograph (Sept. 1970; Scale, 1:10 000; contour interval 5m).

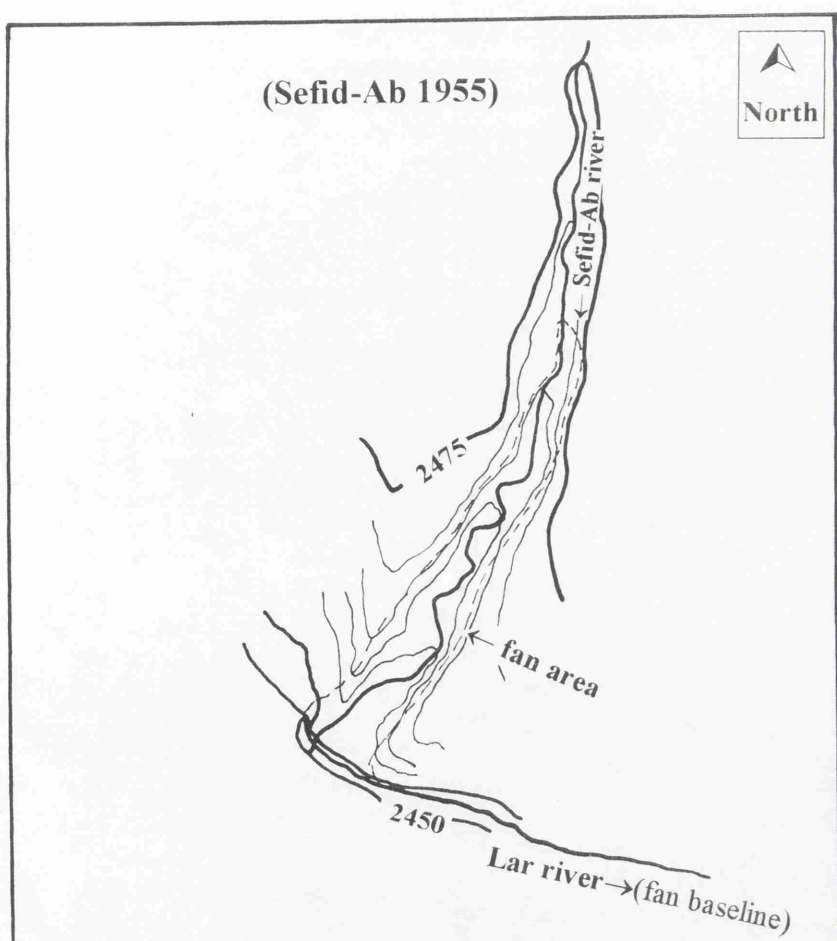

Figure 5.27-c: Sefid-Ab fan topography from aerial photograph (Sept. 1955; Scale, 1:10 000; contour interval 5m).

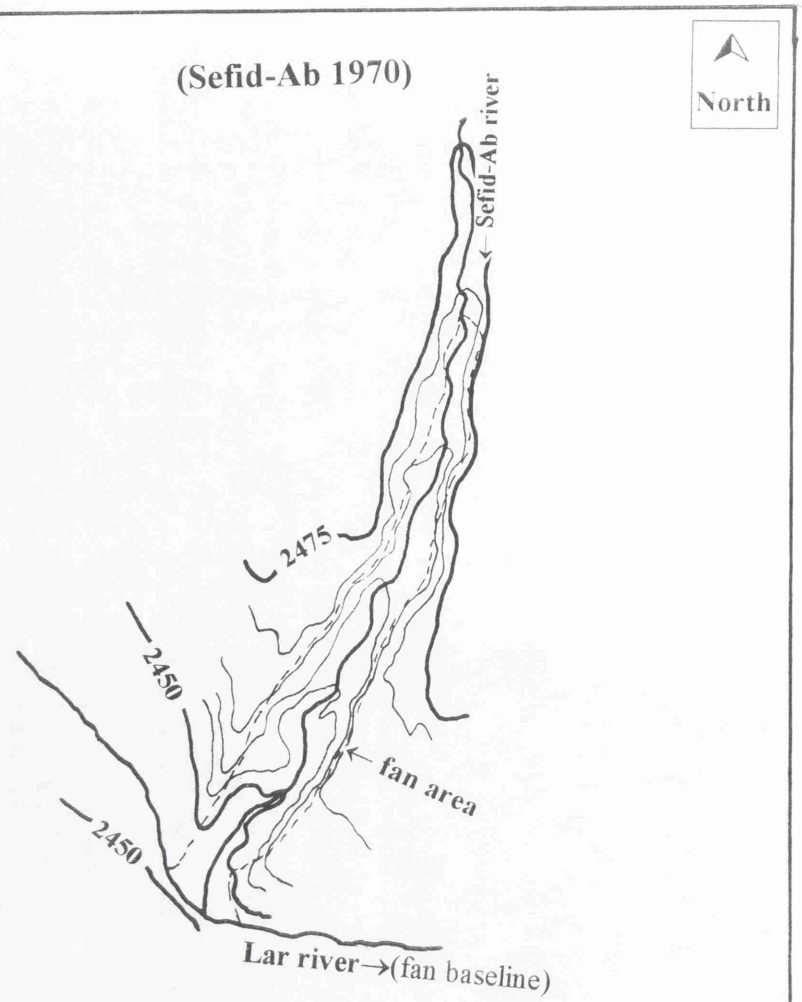

Figure 5.27-d: Sefid-Ab fan topography from aerial photograph (Sept. 1970; Scale, 1:10 000; contour interval 5m).

Finally, subtracting of the results of the 1955 aerial photographs from echosounding shows that the volume increased at Gozaldarreh by $1.8\times10^5m^3$ ($0.008\times10^5m^3/km^2a^{-1}$), at Sefid-Ab by $1.03\times10^5m^3$ ($0.02\times10^5m^3/km^2a^{-1}$), and at Dalichai by $2.6\times10^5m^3$ ($0.03\times10^5m^3/km^2a^{-1}$), (see Figure 5.29).

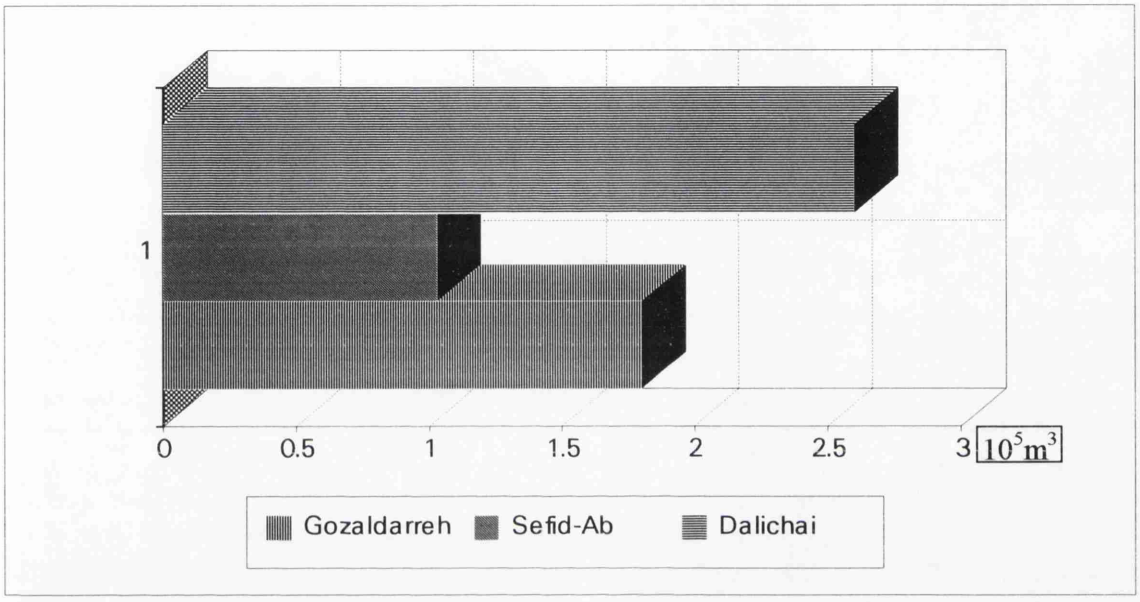

Figure 5.29: Increased volume (10^5m^3)of depositional delta fans (1955-1994).

5.8.2 Estimation From Comparative Basins

The Latian basin (see Figure 5.16, some 20 km to the southwest of the Lar basin) was the only dam basin close to the Lar basin for which data was available for comparision. The physical conditions of the Latian, with its low precipitation and poor vegetation cover, represent differences from the Lar, but lithological characteristics are mostly the same.

Comparing the Lar river with one of the Jadjerud river tributaries in the Latian basin (Hablehrud subcatchment) shows that the sediment yield of the Lar river basin is extremely low. On the Hablehrud river (Boneh-kuh station of the Latian basin) a maximum sediment concentration of 870 gl^{-1} of sediment was measured during the average flood (24 hours), an average of 447 gl^{-1} observed and a total suspended sediment discharge during 24 hours of 1037×10^6 tons. But on the Lar river over a 22 year period the average annual suspended load was only 0.115×10^6 tonnes. This is not an unreasonable amount since the Jajerud with an annual flow and area similar to that of the Lar is depositing some 1.2×10^6 tonnes of sediment in the Latian reservoir (data from

Ministry of Energy, Iran). The Latian basin area is 71×10^3 ha. and the Lar is 73×10^3 ha. at the dam sites, suggesting that this comparison is reasonable. Table 5.11 also shows that the Lar annual average sediment production is lower than in some other other reservoirs like Sefid-Rud in Iran (650 t/km^2), L.Arthur in Africa with 548 t/km^2, and Soyama in Japan (198 t/km^2), but is not unusually low.

Table 5.11: Representative data on rates of sediment deposition in reservoirs.

Country	River/reservoir	Catchment area (km^2)	Period of record (year)	Original capacity (10^6 m^3)	Annual average sediment yield (ton/km^2)
Africa	L.Arthur	5880	10	78.5	548
Africa	L.Mentz	12490	12	116.7	271
China	Yanguoxi	182800	18	222	48
China	Quingtong	285000	12	620	142
China	Sanmenxia	688421	19	9640	287
India	Pahari	7840	28	47.2	128
Iran	Sefid-Rud	56200	17	1760	650
Iran	Lar	726	43	960	198
Italy	Mont Reale	435	1	1.5	114
Japan	Soyama	1500	19	33	505
USA	Boysen	20050	13	19.7	62
USA	Mississippi	308200	15	456.3	30

(data after Toluie, 1993)

5.8.3 Sediment-Load Measuring Stations and Estimating the Sediment Delivery Ratio

In addition to calculating the volume of sediment deposited within different time periods, sediment yield from a watershed may also be obtained by installation of a stream-gauging station and periodic sampling of stream flow. This method is used for the planning of major structures on large watersheds where investigations, prior to design of the structure, allow an adequate period of sampling to obtain measurements representative of expected long-term discharges. The results of such measurements, adjusted for expected long-term sediment yield, are used directly for design purposes but may depend on sediment yield data calibration for elswhere. Seven sites in the Lar basin were selected for this purpose, mostly located on alluvial fans.

Sufficient data on sediment yield are not always available to evaluate the relative effect of the various factors influencing sediment yield. Also, sufficient time may not be available to

conduct sediment-load measurements prior to design of a structure. In such instances the sediment yield may be predicted by estimating the gross erosion in the watershed and adjusting for the expected delivery ratio of sediment to the structure site. This method is applicable to smaller watersheds and particularly useful where abnormal changes in land use and agricultural practices are anticipated in the watershed during the design life of the structure.

5.8.4 Measurement of Sediment Discharge

The measurement of sediment discharge provides direct estimation of the sediments delivered from a basin.The sediment discharge is important when a sedimentary basin like the Lar is being studied because surface water is the main agent delivering the sediment discharge.

It is possible to calculate the total sediment discharge from the Lar dam basin by using daily measurements of suspended sediment discharge at three stations within the Lar basin, and two downstream stations at Polour (the dam outlet point) and Karehsang as a control point in the Haraz downstream (data source; Ministry of Energy-Iran).

5.8.4.1 Method Applied to Suspended Sediment Discharge

The factors which are causing erosion in the basin can be divided into those which are relatively unchanging, and those which change over period of several years, depending on meteorological and climatological factors. In the first group are factors which characterize the morphology, topography, geological structure and composition, biological cover and type of cultivation in the area. In the second group are factors which change on a year by year basis such as temperature and precipitation. The hydrological characteristics of a river are a function of all of the above parameters. Over time the water and sediment discharge of streams are related and so it should be possible correlate water and sediment discharge for the observation period, and then to determine sediment discharges using the long term observations of water discharge. Rating curves between water and sediment discharges can be obtained for: average daily water and sediment discharges; average annual water and sediment discharges.

By this analysis it was found that the best correlation between water and sediment discharges are for the longer periods of average daily data. However, for four stations on the Lar dam basin relations between water and sediment discharges are given for daily water and sediment discharges.

-Dalichai Catchment

This catchment of 196.3 km^2 has a different regime from the other catchments, because of topography and geological characteristics. For interpretation of sediment concentration and discharge only 43 daily measurements were used. There is no significant relationship (r^2=0.139) between discharge and sediment concentration (Figure 5.30-a). As shown in Chapter 4, 90% of this catchment is located at over 3000 metres altitude. On the other hand due to geological characteristics (mostly volcanic rocks) most particle shapes are spheres (63%, see App. Chapter 5, Dalichai particle shape graph). Statistical parameters at Dalichai were calculated as flows;
r^2=0.14, Standard Error =0.42, F=6.62, and p<0.0001, a=9.84, b=0.63 and the equation is: $C_s=9.84\ (Q)^{0.63}$. (Table 5.12).

- Sefid-Ab Catchment

At Sefid-Ab station with 52.35 km^2 area only 2 years of effective daily discharge and sediment discharge data were available with considerable interruptions, so although measurements on this catchment were extended to 35 years, it was not possible to successfully estimate sediment yield because of the lack of data for this station (see chapter 3). Statistical parameters at Sefid-Ab were calculated as flows;
r^2=0.17, Standard Error =1.006, F=5.567, and p<0.0001, a=1.66, b=0.48 and the equation is: $C_s=16.66\ (Q)^{1.48}$ (Table 5.12 and Figure 5.30-b).

-Gozaldarreh

For the 22 year period average annual suspended sediment discharge at Gozaldarreh (including both KhoshkehLar and Lar tributaries) is 55×10^3 tonnes. If it is assumed that 20% of total sediment at Gozaldarreh is moved as bed load (FAO, 1969) then the total sediment load is about 70×10^3 tonnes. It is some what more than Polour, but is a quite

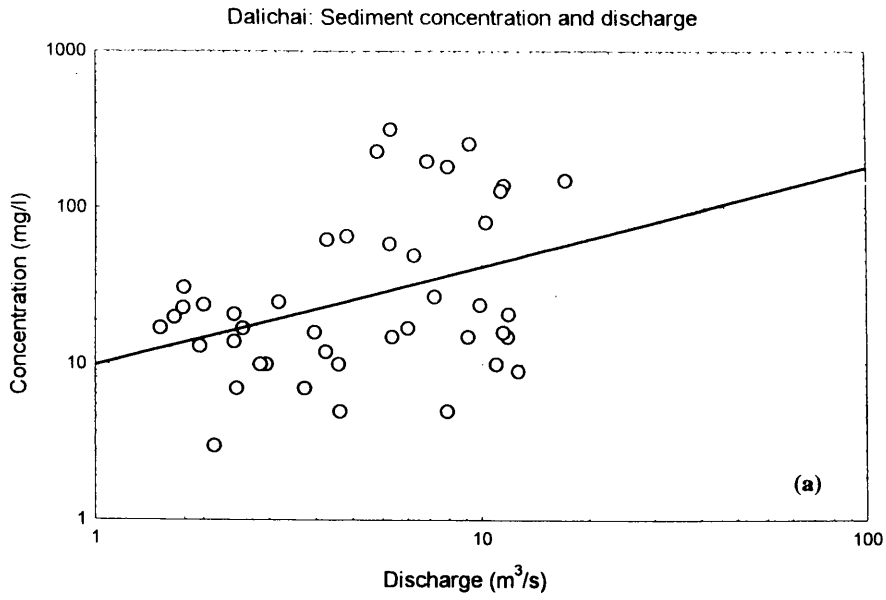

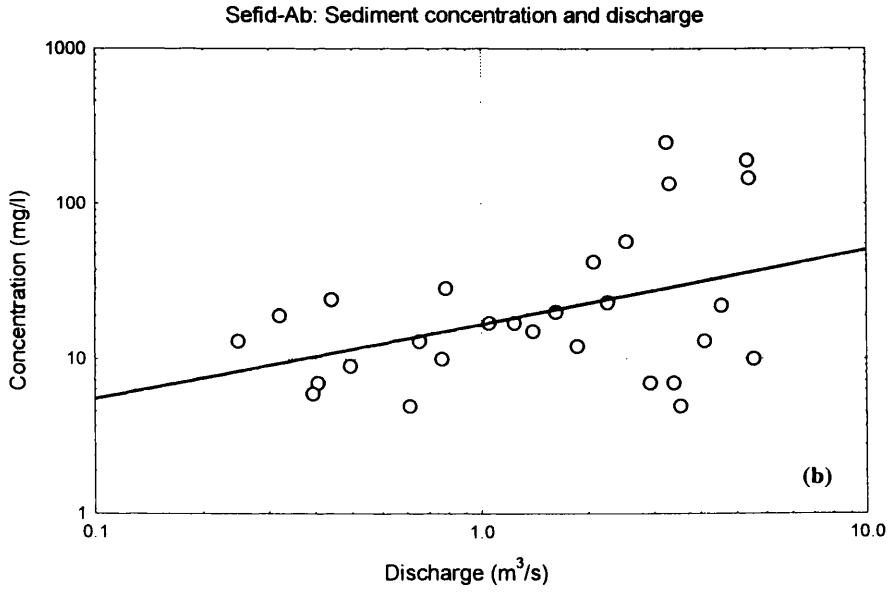

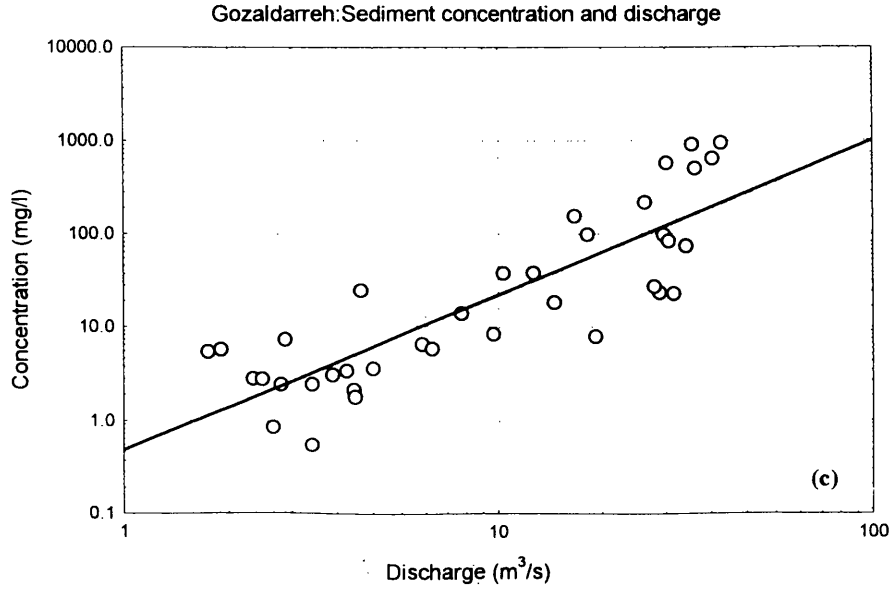

Figure 5.30: Daily sediment concentration and discharge at Dalichai **(a)**, Sefid-Ab **(b)** and Gozaldarreh **(c)**.

reasonable amount taking into account the high sediment yield from upstream of Lar and Khoshkehlar rivers. Statistical parameters at Gozaldarreh were calculated as flows; r^2=0.72, Standard Error =1.100, F=90.14, and p<0000001, a=0.48, b=1.66 which show a significant relation (Table 5.12). The equation is: $C_s=0.48\ (Q)^{1.66}$ (Figure 5.30-c).

- At Polour Station

Daily measurements of suspended sediment discharge were made at Polour station from 1968 - 1986 (a period of 18 years) and its water discharge recorded from 1946 - 1993. This provides the possibility of establishing a discharge/sediment relationship over 18 years and extrapolation of the results over the 43 years of discharge data. Daily observations of suspended sediment discharge consisted of determination of concentrations from a single sample at one point of the river cross section. At Polour station these samples represent a good estimate of sediment discharge in the full cross sectional area because of the very high turbulence of the water. During the summer months one sample of water was taken every second day and during flood events 2-5 samples during the day.

For the 43 years period, average annual suspended sediment discharge is 101×10^3 tonnes. If we accept that 70% (this amount estimated at Polour station by Dam Authority, 1972) of total sediment is suspended sediment and 30% bed load sediment, then we will have a total annual estimate of about 144×10^3 tonnes. Average sediment yield from the whole basin at Polour station is about 189 tonnes/km^2/year.

The data before dam construction for discharge and concentration show a good correlation (Figure 5.31-a). After dam construction there is significant correlation (Figure 5.31-b). Statistical parameters before the dam are: r^2=0.27, Intercept=7.50, Standard Error =0.21, F=204.9, p<0.000001, a=7.50, b=0.99 and for after the dam: r^2=0.27, Intercept=23.20, Standard Error =0.102, F=247, and p<0.00001, a=23.2, b=0.52 (Table 5.12). The equation before the dam is: $C_s=7.50\ (Q)^{0.99}$ and after the dam is: $C_s=23.20\ (Q)^{0.52}$.

To estimate sediment discharge throughout the Lar Dam basin, three stations have been chosen. Using adjacent stations for calibration, the data has been extended to a longer

Table 5.12: Sediment concentration and Discharge at different stations in the Lar basin.

Station	Area/km^2	Length of period; discharge/ sediment	Mean discharge (m^3/sec.)	Maximum Discharge (m^3/sec.)	Mean sediment concentration (mg/l)	a	b	r^2	Mean annual sediment load (×10^{3}tonne)	Load (tonne/ km^2/yr)
Dalichai	196.3	43/daily	6.1	16.5	55.1	9.84	0.63	0.14	*	*
Sefid-Ab	119.3	28/daily	2.0	5.09	40.0	16.6	0.48	0.17	*	*
Gozaldarreh	414.4	37/daily	14.4	39.4	124.4	0.48	1.66	0.72	70	169
Polour	760	43/18 year	25.5	90.7	475.8	7.50	0.99	0.27	170	223
-before dam			20.4	96.5	288.3	23.2	0.52	0.27	118	155
-after dam										
Karehsang	4061	28/year	67.2	329.1	4756.6	2.80	1.61	0.84	*	*
-before dam			51.61	704	1267.8	7.81	1.15	0.38	*	*
-after dam										

*(can not be calculated).

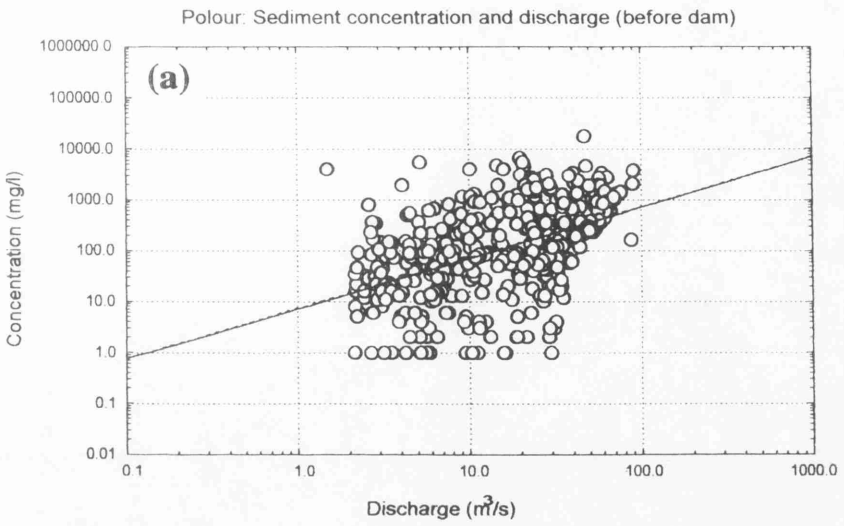

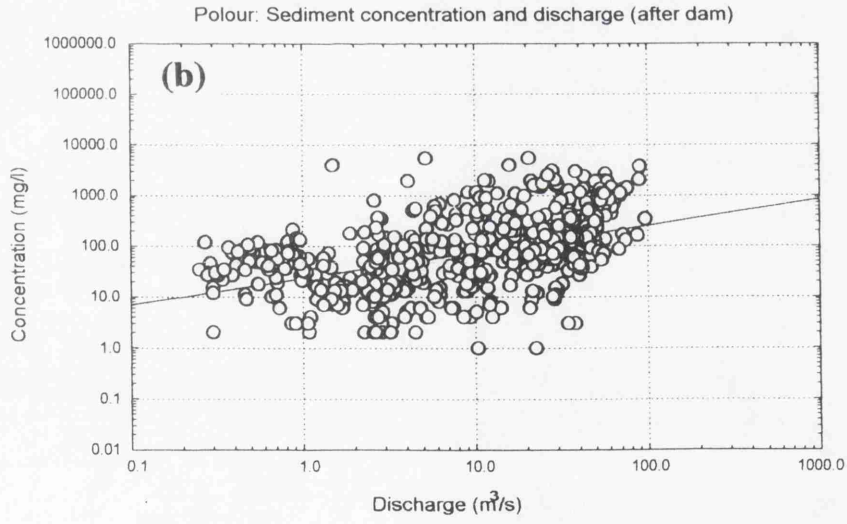

Figure 5.31: Daily sediment concentration and discharge at Polour before **(a)** and after the dam **(b)**.

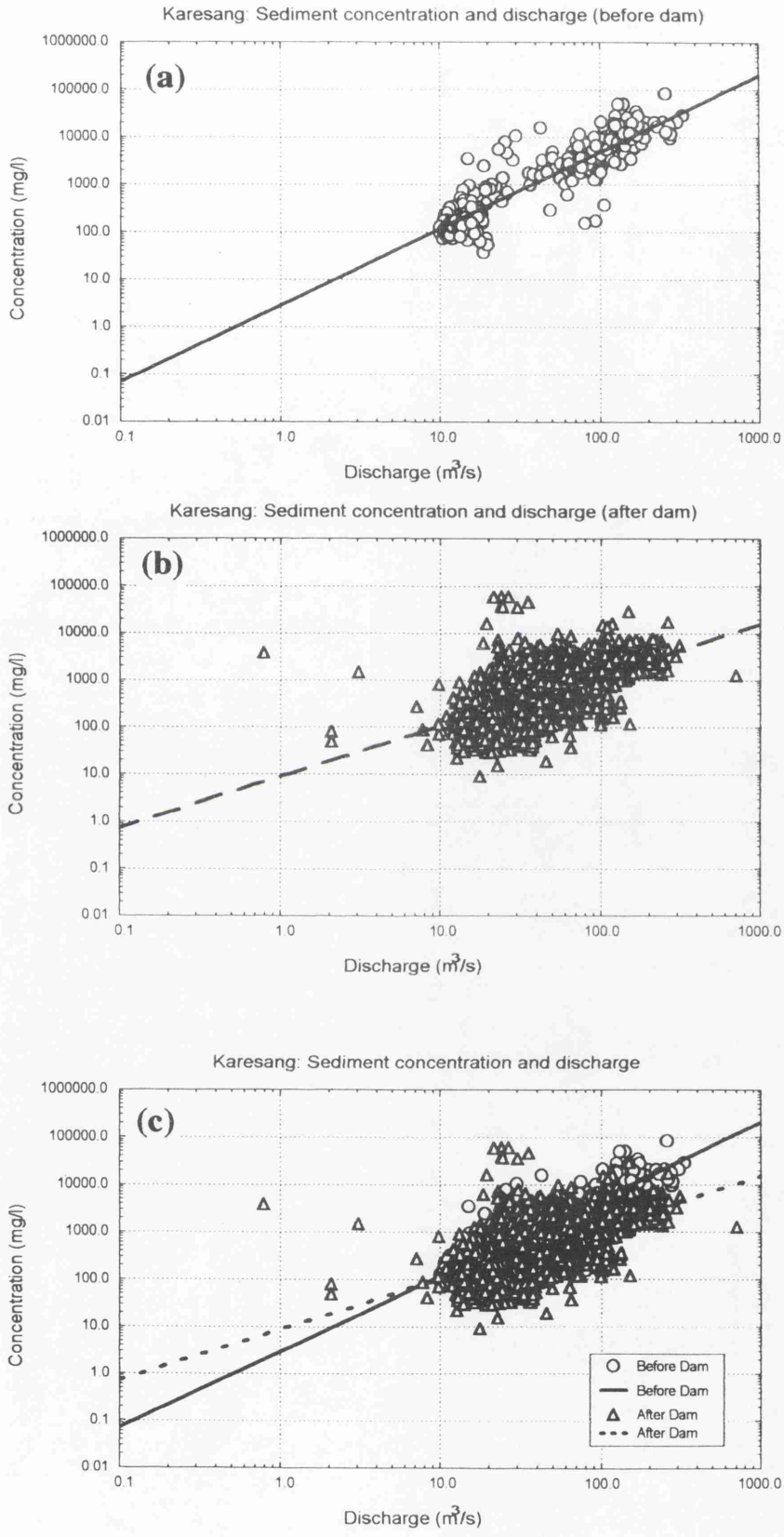

Figure 5.32: Daily sediment concentration and discharge at Karehsang, before **(a)** and after the dam **(b)** and comparison **(c)**.

period, as was conducted at Polour station. This works for Sefid-Ab and Dalichai only for discharges, but at Gozaldarreh there was adequate data.

- Karehsang Station

Karehsang station was employed as a control point at the far end of the basin for discharge (annual data for a period of 28 years) and 21 years daily data were interpreted for sediment concentration and discharge (Figure 5.32-a, b and c). For daily concentration and discharge, statistical parameters before tha dam are: r^2=0.84, Standard Error =0.76, p<0001, F=1735, a=2.80, b=1.61, the equation is; C_s=2.80 $(Q)^{1.61}$ and after the dam are: r^2=0.38, Standard Error =0.8, p<0001, F=944, a=7.81, b=1.15, the equation is; C_s=7.81 $(Q)^{1.15}$ (Table 5.12).

This station covers 4068 km^2 of the Haraz basin of which the dam basin is just 25%. Its average annual flood discharge is 1055m^3s^{-1} and the average daily discharge is 53.9m^3.sec.$^{-1}$. The average daily sediment yield is 1885 tonnes (see also App. Chapter 5).

5.9 SUMMARY

After blocking of the old Lar valley by lava from an eruption of Damavand, a natural dam with a spillway level at an elevation of about 2150 metres formed at the southern side of the present volcanic cone. The basin of this early dam has been infilled with a coarsening upward sequence of sediments before renewed eruptions of Damavand, after the first creation of the natural lake, produced basic lava flows which raised the dam in the Lar valley to about 2700 metres.

Sedimentation continued in the lake until the basin finally became completely infilled, after that water spilling over the lava dam caused it to be breached. Faulting which occurred at about this time is likely to have contributed to breakup of the dam. As the valley of the new Lar River was established the sediments in the basin began to be progressively removed, a significant set of river terraces being formed in the process. The stage of development is still operating at the present time, and is influencing sediment delivery in the basin. These conditions have produced a sensitive environment which currently is characterized by landslides, sinkholes and scree. In the Lar basin, the amount of sediment

infill estimated from topographic maps amounts to about $158\times10^9/m^3$ for the Lar basin, and represents a rate of $208\times10^3m^3/km^2/yr$. From aerial photos the sediment volume of three fan deltas (Dalichai, Sefid-Ab and Gozaldarreh) is estimated at about $8.5\times10^5m^3$ which represents $3.9\times10^3m^3/km^2/yr$. The higher value of annual sediment yield is related to Dalichai ($1.6\times10^3m^3/km^2$) and the lower value is for Gozaldarreh with $1.08\times10^3m^3/km^2$. Recent volumetric from echosounding results estimated a total of $13.9\times10^5m^3$ sediment in depositional fan deltas at Gozaldarreh, Sefid-Ab and Dalichai and showed a higher specific amount of sediment yield for the Dalichai ($3\times10^3m^3/km^2$) than for other two catchments.

Sediment concentration at Gozaldarreh suggests that mean annual sediment for Lar upstream (including 45.5% of the whole basin area) is about 70×10^3 tonnes which can be estimated as $169t/km^2/yr$. For Polour, the amount of sediment yield before and after dam construction shows a significant value about $223t/km^2/yr$ before the dam reducing to 155 $t/km^2/yr$ after it. This rate for mean annual sediment load was respectively 170×10^3 t and 118×10^3 t at Polour station. Chapter 7 will discuss the Lar Basin sediment yield obtained by different techniques.

CHAPTER 6: DIGITAL IMAGE PROCESSING TECHNIQUES AND RESULTS

INTRODUCTION

In the previous chapter, the importance of integrating remote sensing and field data was discussed. The aim of this chapter is to consider in detail the use of these approaches in the geomorphological investigation conducted here. In the study area, field investigations are severely hampered by the scale and inaccessibility of the area and so quantitative analysis by remote sensing was useful (see Table 6.1). Digital image enhancement and classification are used to assist in the identification of morphological characteristics and vegetation cover of the Lar basin.

The success of quantitative analysis in photointerpretation depends on information provided at key stages by the analyst, although much of this success depends on the availability of both images at appropriate scales and well controlled ground identification points. Aerial photo interpretation, involving direct interaction and therefore high level decisions, seems to be the most appropriate for spatial assessment of surfaces but is less good for quantitative accuracy of the nature of those surfaces. Remote sensing is the reverse, good in quantitative accuracy but poor in spatial accuracy. A combination of the two seems an ideal solution to identify boundaries and spectral characteristics of different classes of surface.

SPOT (June 1987) and Landsat-4 (September 1988) data provided a useful source of information for geomorphological investigation. All of this data had been geometrically corrected (see Chapter 3 section 3.4.2). For generalized regional studies, photographic prints in black and white or colour composite copies of Landsat images and KFA-1000 are also adequate sources of information. However, in the absence of large scale aerial photography, for more detailed interpretation of smaller areas and for specialized purposes, digital image processing is necessary to extract the detail required (Beaven, 1984; Rothery and Drury, 1984).

Table 6.1: A comparison of the two approaches.

Photointerpretation (by an interpreter)	Quantitative (by computer)
On a scale large relative to pixel size	At individual pixel level
Inaccurate area estimates	Accurate area estimates possible
Only limited multispectral analysis	Can perform true multispectral (multidimensional) analysis
Can assimilate only a limited number of distinct brightness levels (say 16 levels in each feature)	Can make use quantitatively of all available brightness levels in all features (e.g. 64, 128, 256)
Shape determination is easy	Shape determination involves complex software decisions
Spatial information is easy to use in a qualitative sense	Limited techniques available for making use of spatial data

(after Richards, 1993).

The computer-assisted recognition of surface material, commonly called classification, is based on the spectral properties of the target surface. Digital classification aims to organize thematic maps where each pixel in the scene is assigned to a particular class of objects by name, based on spectral response. The principals of digital pattern recognition form the basis of image classification and the identification of the pattern enables classification of the data point in question (Duda and Hord (1973), Addington (1975), Anuta (1977), Strahler (1980) Swain and Davis (1978), Haralick and Fu (1983). For the first part of the classification process, the computer system must be 'trained' to recognize patterns in the data. Training is the process of defining the criteria by which patterns are recognized. The result of training is a set of signatures, which are the result of setting statistical criteria for the proposed class. Examples are land cover or geomorphological changes, agricultural crop mapping, forest and rangeland change detection, and hydrological analysis (Figure 6.1).

6.1 SPECIFIC OBJECTIVES OF THIS STUDY

The primary objective here is to evaluate the spatial and spectral characteristics of the SPOT and TM data for the discrimination of morphological changes, bare soil, landslide,

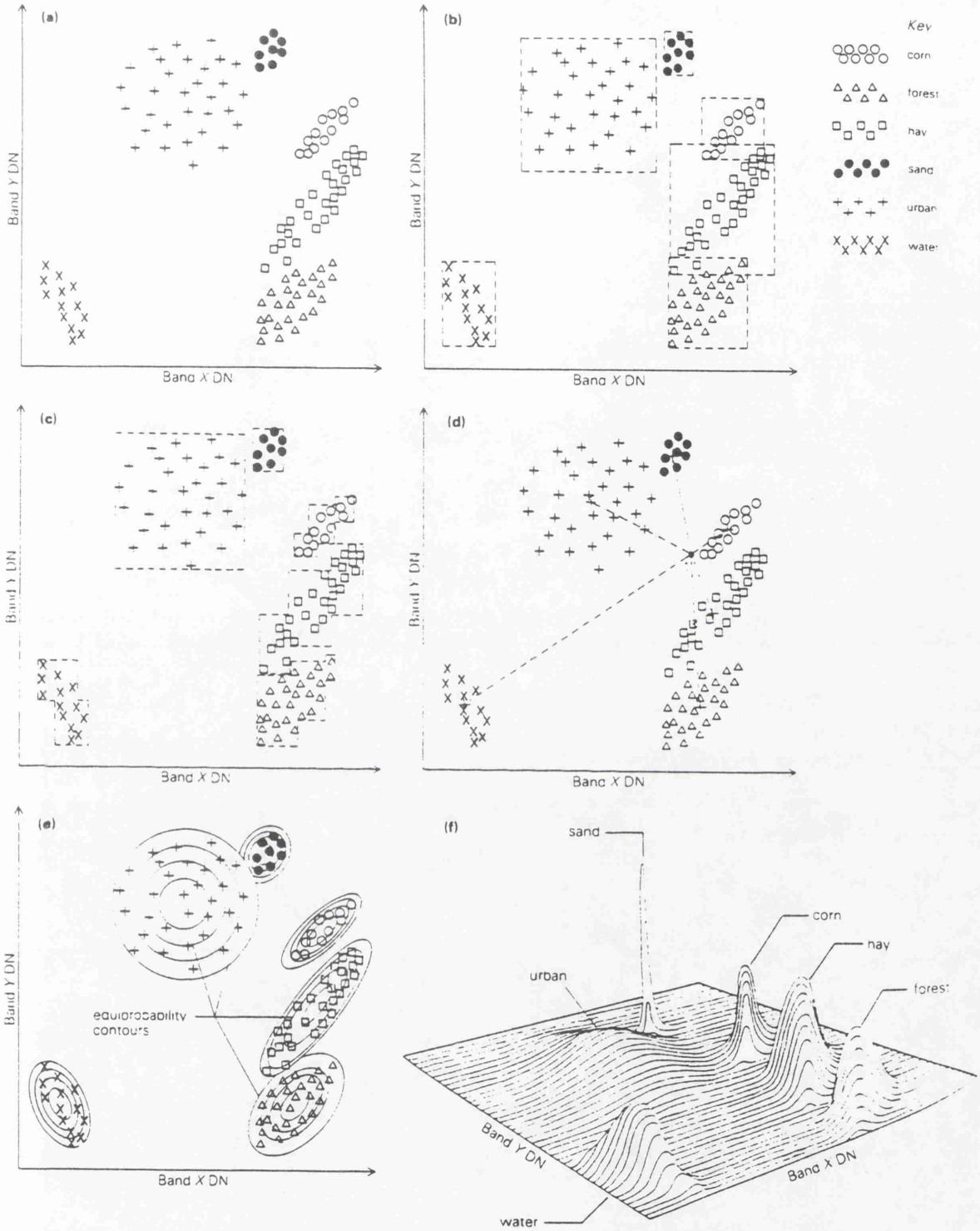

Figure 6.1 Different methods of spectral classification can be represented diagrammatically by reference to bivariate plots of two of the bands employed. In (a) several clusters in the data correspond to areas with different kinds of surface. The simple parallelpiped classification is shown in (b), that based on more precise boundaries for each class in (c), and (d) represents the minimum distance to means method. The contour in (e) express the probability that any point belongs to a particular class, which is the basis of the maximum likelihood method of classification. The probabilities are illustrated more graphically as a three dimensional topology in (f) *(After Curran, 1985; Lillesand and Kiefer, 1993).*

terrace areas and vegetation extent and cover in the Lar Dam Basin. The specific spatial and spectral related objectives are as follows: to use statistical techniques to evaluate the spectral relationship of the SPOT and TM data with the aerial photograph control and the field data; and to assess the usefulness of the multispectral SPOT bands for identifying changes in land surface types in comparison with: *a)* Landsat TM (30m ground resolution); and *b)* false colour and panchromatic data from KFA-1000 (8m ground resolution).

The first stage of this study concentrates on the analysis of pixel values extracted from the Lar SPOT and Landsat data sets for June 1987 and September 1988. In particular the aim was to determine the relationships between certain ground variables and spectral radiance on the SPOT and Landsat bands. The location of pixels within subscenes of the two different images were considered, with ground sampling points determined through cross correlation of land cover patterns in the imagery and the 1:20 000 aerial photographs on which the latter were located. DN values for each selected pixel were derived. An underlying assumption was that the extracted pixel values were representative of particular land cover units. In addition it was assumed that the ground parameters measured on a single ground sampling point were representative of the same parameter over the area on the ground covered by the pixel. There was however a problem in relating the pixel data of SPOT and Landsat with the ground variables measured in 1987 and 1988, particularly with dynamic variables such as soil and vegetation types.

6.1.1 Geometric Correction

Since the raw remote sensing data contain geometric distortions, the SPOT (XS) images used in this study were geometrically corrected for the Lar basin. The Landsat TM data (CCT format) required no additional preprocessing because the data was already geometrically and radiometrically corrected. During the radiometric correction the data is decomposed to a dynamic pixel range of 0-127 and compensated for MSS and TM

detector gains and offset changes (the details of this is included on the tape). Geometric correction of the data compensates for earth rotation, spacecraft altitude, attitude and sesor variations.

The system projection of the data used for this research was Space Oblique Mercator (SOM). This is the standard Landsat 4 and 5 MSS and TM projection (vertually distortion free). Scale and angular relations (conformality), are preserved thus allowing use of a continous parallelogram grid over the coverage area. Finally, registration of the output of a 512×512 portion of the TM and SPOT data with the 1:50 000 topographic map by means of a planvariograph, revealed that the geometric correction of TM and SPOT data are good enough for this purpose. For greater accuracy, however, ground control points were employed and this is particularly important when images were joined together to form a mosaic, in addition to when images of the same area (acquired at different times or with different sensors) needed to be compared with one another (see also Chapter 3).

6.1.2 Ancillary Data

Ancillary data consists of any sort of data which helps a user to find training sites to perform supervised classification. Ancillary data also refers to information which is used for matching the spectral classes (natural groups) with information classes (reference classes). The ancillary data available for this research of the Lar basin are:
(a) topographic maps at 1:25 000 (British Army, 1945), 1:50 000 and 1:250 000 (Iranian Geographical Organization, 1955); **(b)** 1:50 000 geology map (Assereto, 1966); **(c)** aerial photographs at 1:50 000 (Iranian Geographical Organization, September 1955), 1:20 000 (Iranian National Cartographic Centre, June 1970), 1:10 000 (Iranian Geographical Organization, August 1991), and 1:5000 scale taken in September 1985 by the Iranian Geographical Organization; **(d)** KFA-1000 photographs at 1:270 000 (Russian Cosmos Spacecraft, June 1990); and **(e)** two preliminary field seasons during summer 1993 and 1994. Black and white aerial photographs and KFA-1000 were the

main tools used to assist in the identification of the main landcover classes, along with ground truth from field work.

6.1.3 Training Area

This stage requires the application of a supervised classification. It needs close interaction between the image analyst and the image data represented as known pixels on an image (Figure 6.2). The use of a supervised classification method is affected by the classification characteristics of the classes that are to be estimated from the training sample pixels (see Mather, 1987 for more detail). Selecting the training areas was difficult because there was little data concerning the spectral response of the cover types encountered. Existing black and white aerial photographs, dated 1955, 1970 and 1991 (for only some parts of the Lar basin), were available. The KFA-1000 photograph 1990 of the study area at 1:270 000 scale is not suitable for small scale sampling. The other difficulty in selecting the training areas was that land cover units were small and also landcover types were composed of a complex mixture of vegetation types. In addition to these problems, classification of some small scale geomorphological features, was difficult on account of their size being smaller than the pixel size of the imagery and of the resolution of some of the aerial photography.

6.2 ESTIMATION OF POPULATION STATISTICS (EPS)

One of the most widely used methods of information extraction is multispectral classification. In principal, classification of multispectral image data should be straightforward. However to achieve results of acceptable accuracy care is required, firstly in choosing the analytical tools to be used. In the following, the analytical procedures of supervised and unsupervised classification are examined from an operational point of view, with their strengths and weaknesses highlighted. These approaches are successful on their own, although, often a combination of the two is necessary to attain optimal results. There are two methods of digital classification:

6.2.1 Supervised pattern recognition

In supervised classification all the various types of ground categories and locations are known (pixels already assigned to information classes) though a combination of analyses of aerial photography, maps, field work, and personal experience (Figure 6.3). Samples of known identity are those pixels located within training areas for each of which multivariate statistical parameters are known (Jensen, 1986). The accuracy of supervised classification depends upon the selection of suitable training areas with a careful choice of wavebands, e.g. in a small but representative area, determination of the relationships between DNs (Digital Numbers) and object type in the chosen wavebands, can lead to the extrapolation of these relationships to the whole image data and the display and accuracy assessment of the resultant images (Curran, 1985), as illustrated in Figure 6.2. The suitable conditions for choosing the *supervised classification* method occur when: *(a)* easily recognized, homogeneous regions are available for training; *(b)* relatively distinct classes are desired; *(c)* a minimum amount of mixed boundary pixels occur in the data; *(d)* other data sources are available from ground truth; *(e)* desired classes are known prior to classification; and, *(f)* fast processing speed is important.

As mentioned above, supervised classification involves training of the computer to identify patterns on the basis of prior knowledge of the number of spectral classes, and then using these rules to classify the rest of the image data. The underlying requirement of supervised classification techniques is that the analyst has available sufficient known pixels for each class of interest that a representative signature can be developed for those classes. These prototype pixels are often referred to as training data, and collections of them, identified in an image and used to generate class signatures, are called *training* fields.

Signatures generated from the training data will be of different form depending on the classifier type to be used. For *parallelepiped* classification the class signatures will be the upper and lower bands of brightness in each spectral band. For *minimum distance* classification the signature will be the mean vectors of the training data for each class, while for *maximum likelihood* classification both class mean vectors and covariance matrices constitute the signatures. Figure 6.4 shows the main stages in supervised

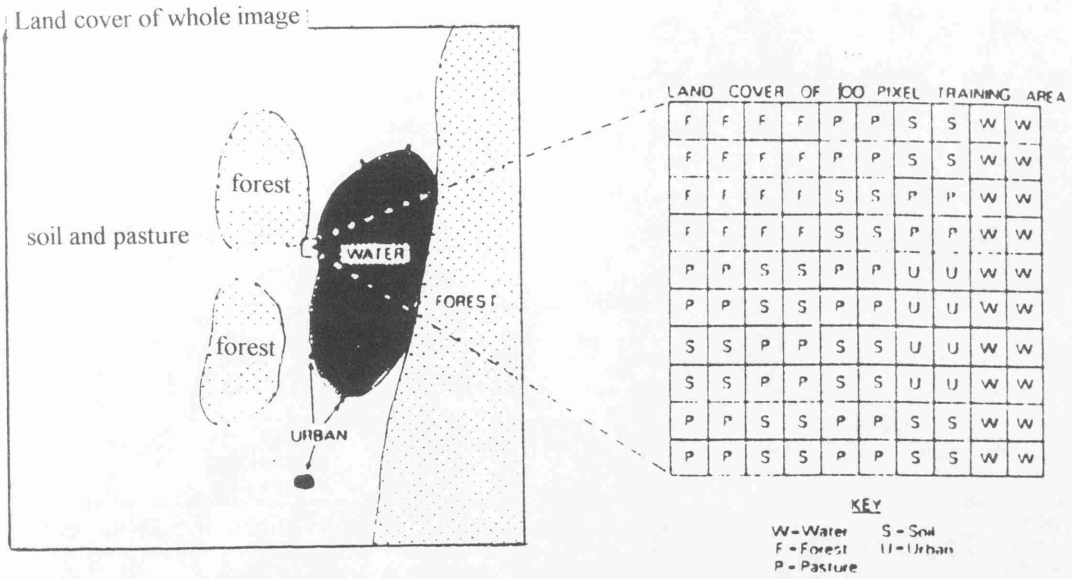

Figure 6.2: The Location of Representative Training Area (adapted from Curran, 1985).

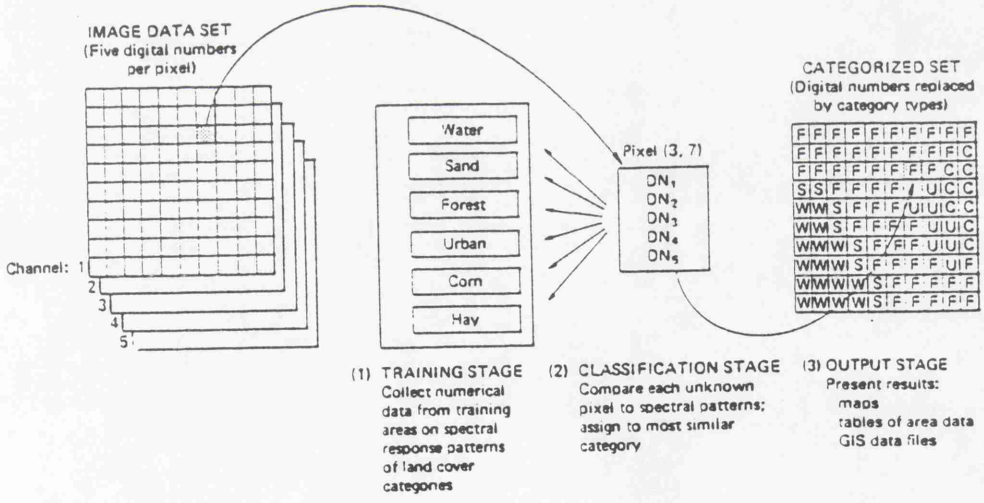

Figure 6.3: Basic steps in Supervised classification (Source: Lillesand & Kiefer, 1994).

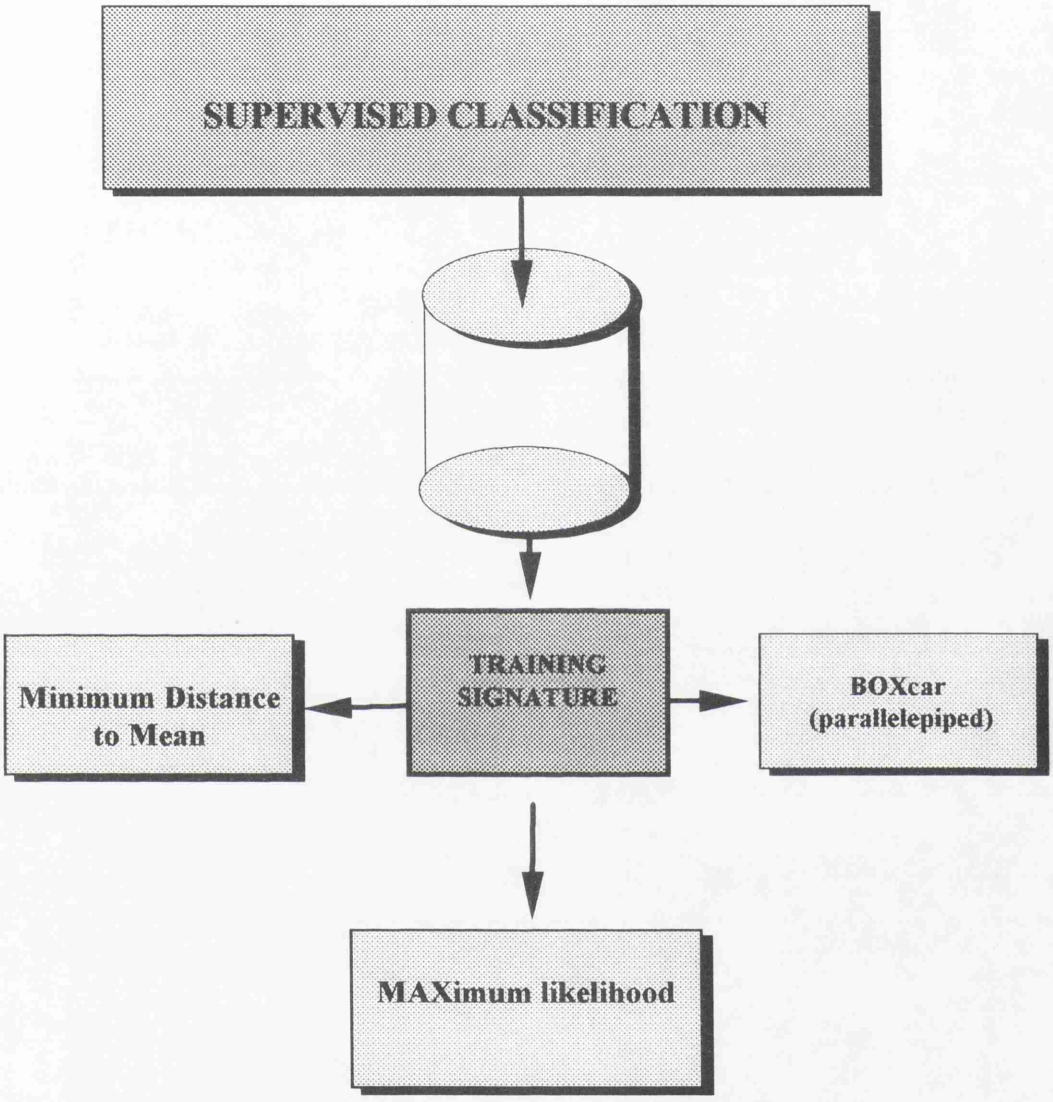

Figure 6.4: Supervised classification stages used in this research.

classification training (for more information of the main stages see Lillesand and Kiefer, 1994).

6.2.1.1 Selection of the Type of Classifier and Classification

A variety of different approaches have been designed for supervised classifications. The aim is to divide the feature space into disjoint sub-spaces by putting decision boundaries so that any given pixel or pattern can be assigned to any one of the classes. The strategy of a statistical pattern classifier can be based on geometry, probability and a discriminate function.

6.2.1.1.1 Minimum Distance Mean

In this case, the distance of a given point in DN-space is calculated from the centeroid of each cluster, and the MDM is used to identify the required cluster. This is illustrated schematically in Figure 6.1-d. The method has obvious disdvantages, notably that no account is taken of the shape of the clusters, and that the distance between two points in DN-space is generally not a quantitatively significant measure. Figure 6.5 (MDM), shows a classified SPOT image from Lar upstream using the minimum distance to mean technique, and was used to identify fresh vegetation in green, bare soil in orange and limestone in grey colour.

6.2.1.1.2 Parallelepiped or Box Classifier

The Parallelepiped or Box classification is the simplest form of multispectral analysis and the most popular classifier for remote sensing applications (Curran, 1985; Harris, 1987). Many bands may be used, and this approach can operate in one of two methods: qualitative identification from a combination of brightness in the thermal infrared and visible wavebands; and, quantitative where a range of values is plotted on each axis for any one cover type. The range defined by the highest and lowest DN (Digital Number)

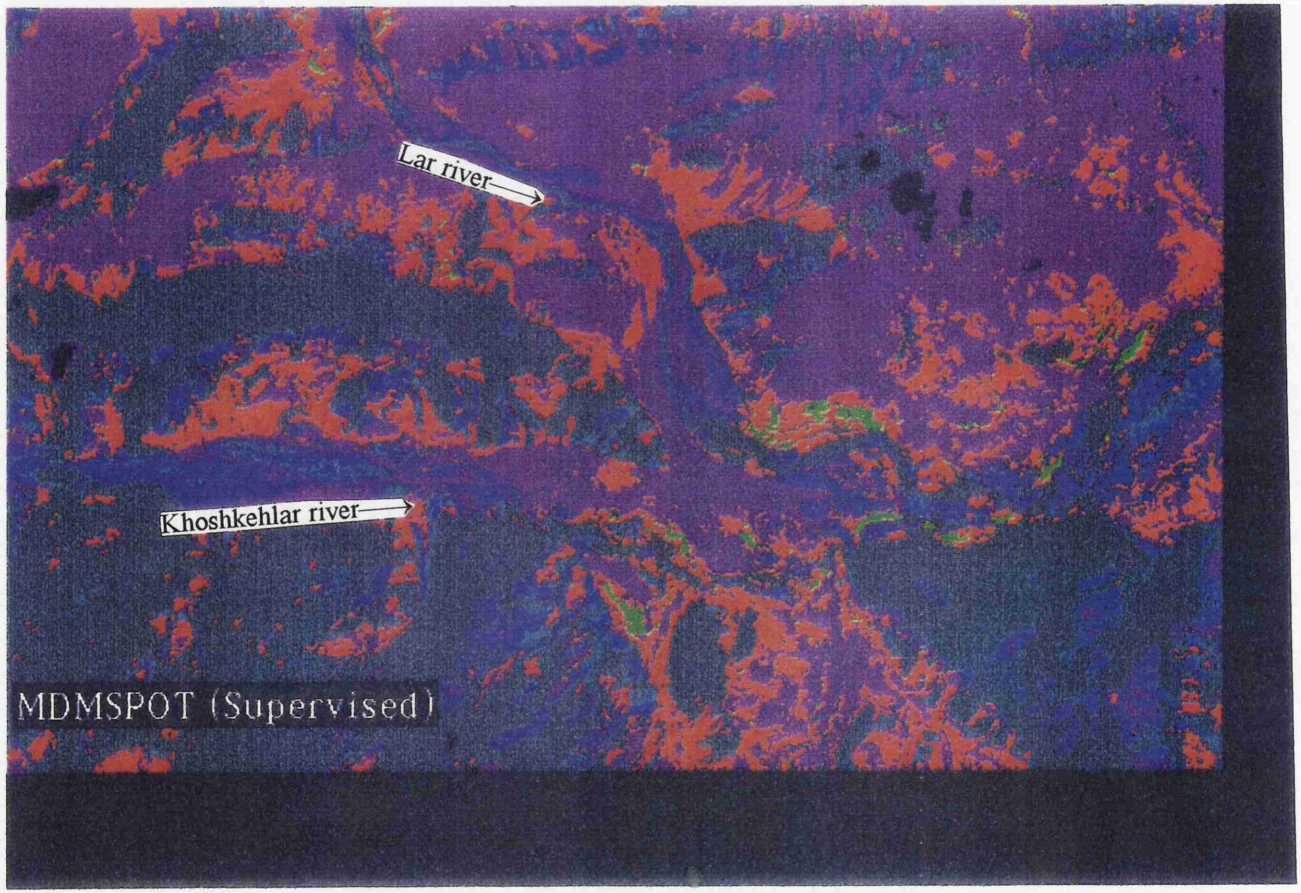

Figure 6.5: MDM of SPOT from La upstream (fresh vegetation is bright green, bare soil in orange, dark blue shows high density vegetation).

values in each band appears as a rectangular area in a two-channel scatter diagram. The ranges of digital number are plotted on the diagram (Figure 6.1). Two extreme cases in the box classifier may be considered, as pixels of unknown type may be found as the point representing a particular pixel does not lie inside any of the regions defined by the boxes. In the second case the point lies inside one of the boxes, and the corresponding pixel is therefore labeled as a member of the class represented by the box. The decision becomes more complicated because the possibility exists that a point may lie inside two or more overlapping boxes. Figure 6.6 shows box classification result from Lar upstream which classified precisly fresh grass and high density vegetation in red colour, unvegetated and exposed limestone in light blue, dried vegetation in dark grey and bare soil as light grey. Box classification was very useful for identifying high density vegetation cover and unvegetated areas.

6.2.1.1.3 Maximum Likelihood or Probability-Based Classifier

This method of classifier is usually the most accurate and is based on the principle that a given pixel should be assigned to a class to which it has the highest probability of belonging to (Figure 6.1-f). It operates by calculating the mean, variance and correlation for each land cover class in the training area (Curran, 1985). The likelihood L_k is defined as the probability of a pixel belonging to class k.

$$L_k = P(k/X) = [P(k)*P(X/k)] / [\sum P(i)*P(X/i)] \qquad [6.1]$$

where; P(k)=prior probability of class k, P(X/k)=conditional probability to observe **X** from class k. Usually P(k) are assumed to be equal to each other and the sum across all classes (I = 1, 2, 3, ...), $\sum P(i)*P(X/i)$ is also constant. Therefore L_k depends on P(X/k) or the probability density function. For mathematical reasons, a multivariate normal distribution is applied as the probability density function. In the case of normal distributions, the likelihood can be expressed as follows (Richards, 1993);

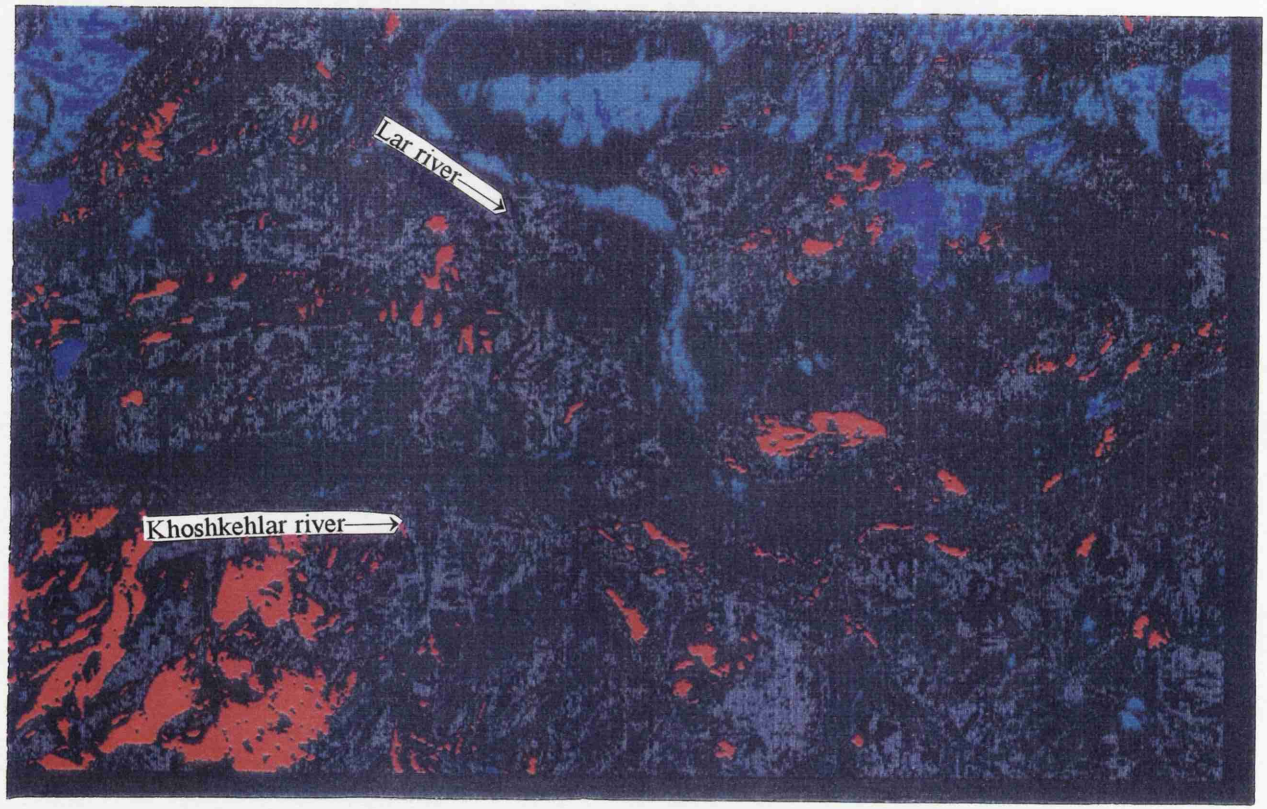

Figure 6.6: Box classified SPOT band 1, Lar upstream (red is fresh grass with high density, light blue is exposed height limestone and unvegetated area, grey is bare soil and dark grey shows dried vegetation).

$$L_k(\mathbf{X}) = \frac{1}{(2\pi)^{n/2} |\Sigma_k|^{1/2}} \exp\left[-\frac{1}{2} (\mathbf{X}-\mu_k)\Sigma_k^{-1} (\mathbf{X}-\mu_k)^t\right] \qquad [6.2]$$

where; n=number of bands, **X**=image data of n bands, $L_k(\mathbf{X})$=likelihood of **X** belonging to class k, $|\Sigma_k|$=determinant of Σ_k, Σ_k=variance-covariance matrix of class k, superscript 't' denotes vector transpose and μ_k is the mean position of spectral class (e.g. the position x at which a pixel from the class is most likely to be found). When the variance-covariance matrix is symmetric, the likelihood is the same as Euclidian distance, but if the determinants are equal, the likelihood becomes the same as the Mohalanobis distances (Richards, 1993; see Figure 6.1-e).

The assumption is made that the training data for each class are normally distributed. With this information, the distribution of the category response pattern can be completely described by the mean vector and the covariance matrix. The probability of all points in the feature space are plotted, so that each point has a probability of belonging to each of the classes identified. In this scatter diagram, the probability-based classifier delineates ellipsoidal "equiprobability contours" shown in Figure 6.7. In maximum likelihood classification it is possible to interactively weight each class to improve the accuracy of this method for particular applications (Curran, 1985). Such manipulation is justified in two situations: *(a)* if the training area is not representative of the proportion of the classes in the total scene; and *(b)* when all of the pixels in a given class must be classified as belonging to a data class.

The Bayes-optimal or Bayesian method is usually used and minimizes the error of misclassification over the entire set of data classified. It is another way of stating the maximum likelihood principle. The approach utilizes the probability density function. In practice several classes may exist, each having a different inherent probability of occurrence in the area, and this parameter may also be taken into account by considering the prior probability of accuracy of the respective classes. The technique uses more

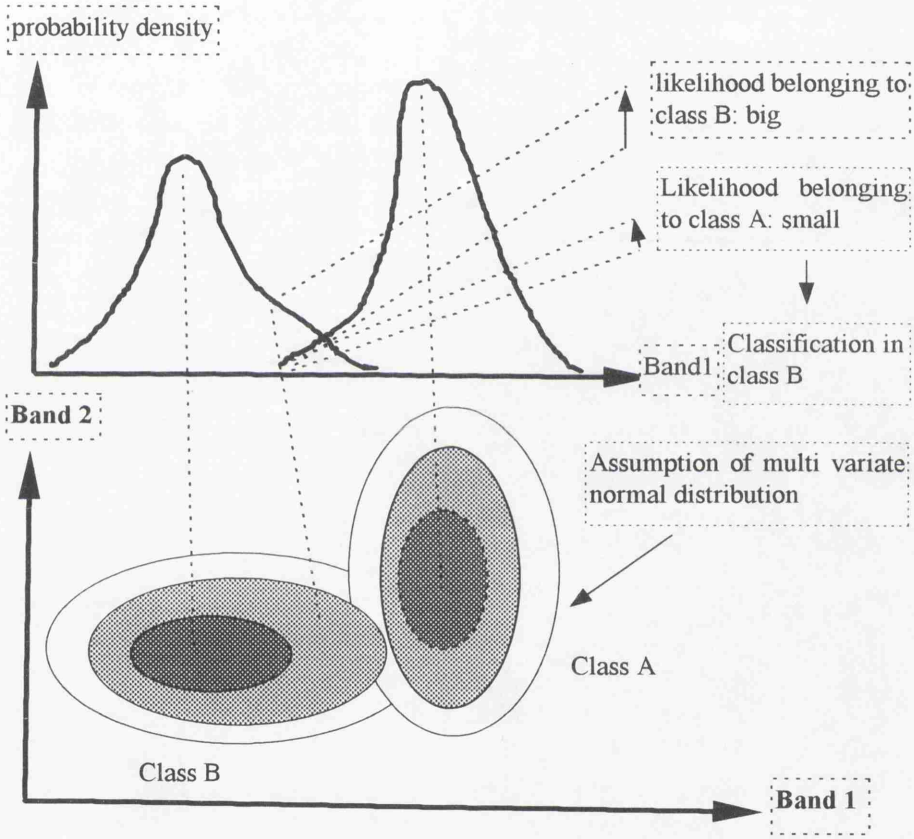

Figure 6.7: Concept of Maximum Likelihood Method.

computer time, but is most popularly used in classifying remote sensing data, as it gives minimum error.

6.2.2 Unsupervised Classification

This approach does not utilize training data as the basis for classification. It is applied in cases where a previous knowledge of the types of classes is not available and class-sets have to be determined empirically. Numerical operations are performed that search for 'natural' groupings or clusters present in the spectral properties of pixels, as examined in the image values. The user allows the computer to choose the class means and covariance matrices to be used in the classification (Lillesand and Kiefer, 1987, Jensen 1986). Once the data are classified, the analyst attempts to assign these 'natural' or spectral classes to the information classes of interest (Robinove, 1982). Unsupervised classification is useful in totally unknown areas, when it provides the operator with a means of identifying spectrally different kinds of terrain.

The method involves development of sets of unlabelled clusters, in which pixels are more similar within a cluster than with those outside. It is also termed *cluster analysis.* In practice, the distance between any two pixels is used to measure their similarity or dissimilarity. The simplest method is as follows: Start with one pixel and assign it to cluster I; then take the next, and compute it's mathematical distance to cluster I, if this distance is less than a certain threshold, group it in cluster I, alternatively put it in cluster II, then take the next pixel and classify it as a member of cluster I or II or alternatively cluster III, depending an mathematical location. In this method, all the subsequent points may be classified (Figures 6.8).

Unsupervised classification is the definition, identification, labeling, and mapping of these natural classes of land surface (Campbell, 1987). It is more computer automated, but allows specification of parameters which the computer uses as guidelines to uncover statistical patterns in the data.

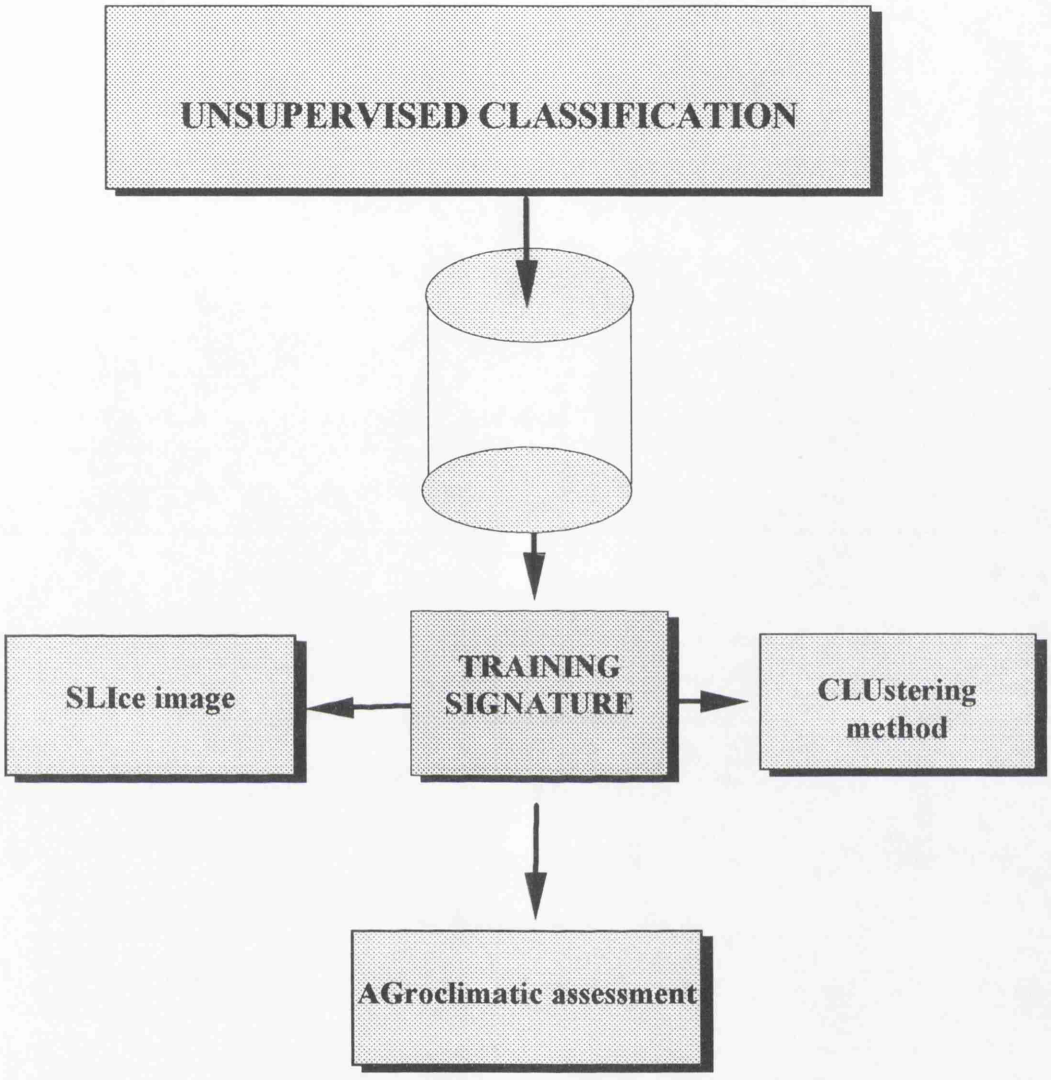

Figure 6.8: Unsupervised classification stages used in this research.

Patterns determined in unsupervised classification do not necessarily correspond to meaningful characteristics of the data, and after initial classification meaning must be attached to the resulting classes. This may be difficult with pixels of mixed landcover, but easier with homogenous areas. To increase the potential for correctly identifying classes, an understanding of the spectral characteristics of the features in the data is required. The advantages of *Unsupervised classification* related to supervised are: *(a)* no detailed prior knowledge is required, but a knowledge of the region is required to interpret the result produced by the classification process; *(b)* no detailed decisions are required; *(c)* the classes defined by unsupervised classification are often much more uniform in respect of composition than are those generated by supervised classification; and *(d)* unique areas are identified as distinct units. The disadvantages of *Unsupervised classification* are: *(a)* the analyst has very limited control over the menu of classes and their specific identities; *(b)* spectral properties of specific information classes will change over time; and *(c)* this method only identifies spectrally homogeneous classes within the data (Campbell, 1987).

Finally, where spatial discrimination and ground resolution are important, such as on complex morphological surfaces, the greater spatial resolution of SPOT (20 m. ground resolution in the three Xs bands) should allow for much better classification than the TM imagery (30 m. ground resolution).

Both supervised and unsupervised classification were applied to the Lar basin using Dragon software, but there was no good discrimination between landcover types in unsupervised classification. Due to the high relief and steep slopes, the presence of shadows, sun facing and poorly illuminated surfaces meant that unsupervised classification was not very successful in the Lar basin. On the other hand subjective assessment of the supervised classification revealed that classification of vegetated land cover types was successful, although it remained very poor within the barren land, and those areas from which the surface materials have been removed (such as the badlands and dnesly gullied areas).

6.3 REMOTE SENSING DATA CLASSIFICATION ACCURACY

In recent years, accuracy assessment of remotely sensed data has received widespread attention. Discrete multivariate analysis techniques, introduced by Congalton et al (1983), have become widely used tools for assessing the accuracy of maps derived from remotely sensed data. The importance of accuracy is now well recognized both for the information it yields (Story and Congalton, 1986) and as input into more advanced statistical techniques.

Every method of image classification using manual interpretation produces problems, usually caused by excessive generalization, errors in registration, misclassification, and variations in detail of interpretation. The errors of image classification using machine analysis come from sensor resolution, complex interactions between the spatial structures of the landscape, processing algorithms, and classification procedures.
There are two categories of classification errors, omission and commission:
(1) an error of *omission* occurs when a pixel that actually belong to class A is mistakenly classified as belonging to some other class. **(2)** an error of *commission* occurs when a pixel which actually belongs to another is assigned to class A instead. Labeling a misclassified pixel as an error of omission or commission is always relative to a particular class.

6.3.1 Selection of Sample Areas

According to Vangendaren and Lock (1977), and Jensen (1986), the smallest number in the sample should be about 20 sites (for more detail see Jensen, 1986 p.226-229). Selection of sample sites within a training area for supervised classification should be avoided unless the training area is spatially well distributed (Jensen, 1986). In addition to the number of the sample sites, their spatial distribution is also important for the assessment of classification accuracy. There are various sampling schemes which can be used. In this study cluster sampling is used for choosing the sample sites (i.e. selection of centroids randomly) subsequently sample sites should be chosen from the centroid either randomly or by spatial strategy (Congalton, 1988). The assumption heren is that this sampling pattern is be efficient with regard to the time and sources required in comparison to the sampling effort.

Data for assessing classification accuracy were selected using field checking for accessible areas, and aerial photographs and KFA-1000 images for remote areas. A map of the sample areas in the Lar basin is shown in Figure 6.9. A transparent sheet was registered on the hardcopy of the classified image, and a grid sheet (1×1mm on the image) was used to choose the sample sites. The class for each of the sample sites on the classified image and their corresponding class on the control data, (e.g. field and air photo) was then recorded. Sample sites belonging to more than one landcover group were counted in each landcover group on the control data. In spite of the fact that the error might not be precisely accurate due to both difficulty of registration and resolution limitations of the remote sensing data, this is a good way of assessing classification accuracy for a varied area such as the Lar basin.

The number of test sites sampled varied between 6 for homogeneous areas to 15 for a more complex landcover and approximately 75 sample sites were selected for each class. Again, pixel identification was aided by using control data represented by the 1:10 000 aerial photographs (1990), the 1:100 000 enlarged KFA-1000 photos (1990) and field checking. In the absence of high quality maps of the study area and because of the close coincidence of data representation on aerial photo, KFA-1000 and field checks, it is assumed that these three sources are the most accurate data available and so are used as control data. It is assumed that the control data are more accurate than the remote sensing imagery. In addition, timing of the control data was almost simultaneous with the timing of the image.

In the earlier sections the various techniques of the landcover procedure were described. An assessment of the accuracy of the results between classification techniques produced from TM and SPOT (Figure 6.10-a)(using the Dragon method) and Figure 6.10-b (produced by means of aerial photo, KFA-1000 and field checking) shows a high degree of similarity between the two plots. The only disagreement between these results is found those areas which are affected by shadow, disrupted by farming, or characterized by dead grass.

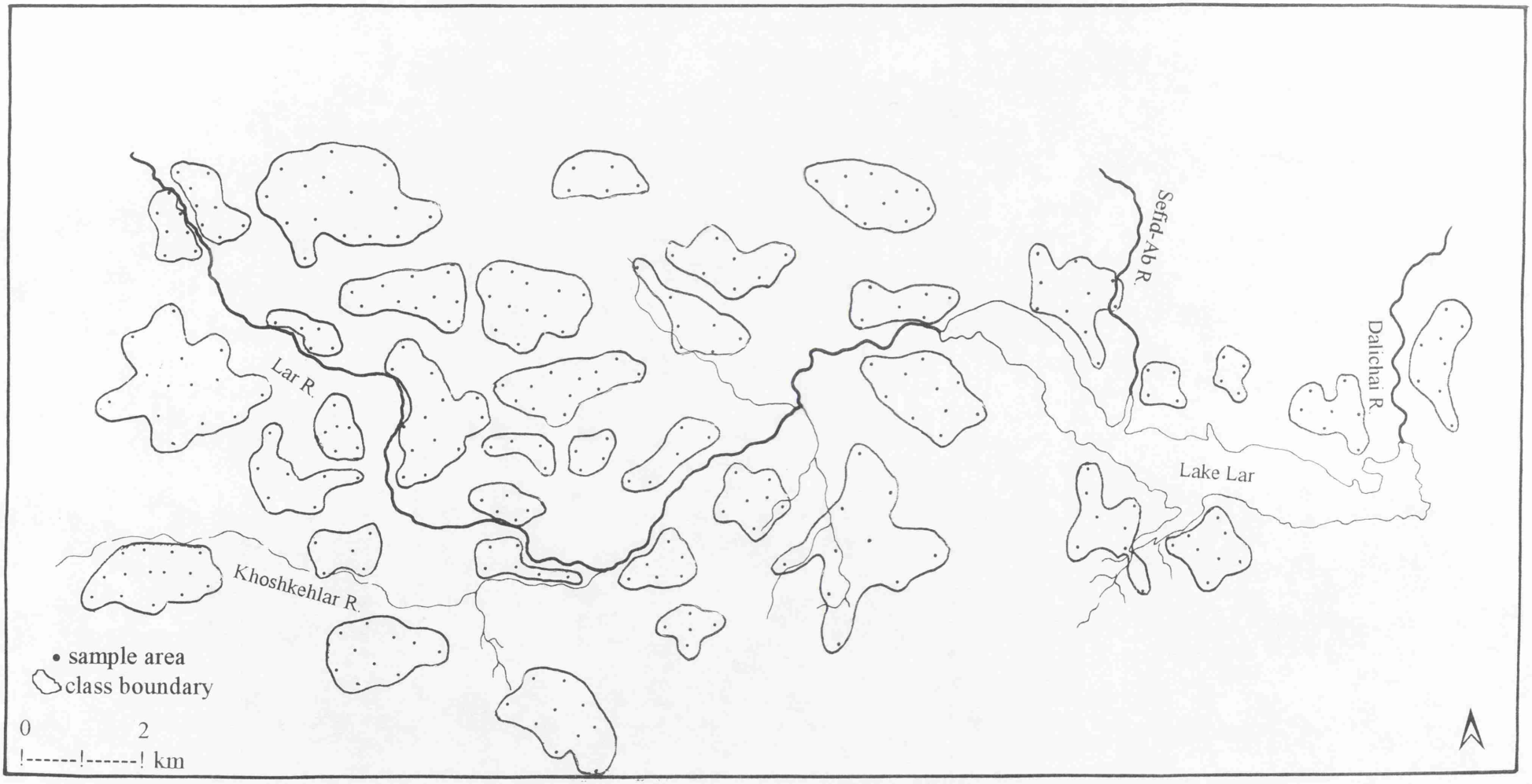

Figure 6.9: Sample areas for classification accuracy. Each dot is a sample area and approximates to the size of TM/SPOT pixels at scale 1:100 000.
(source; KFA-1000, aerial photographs and field check).

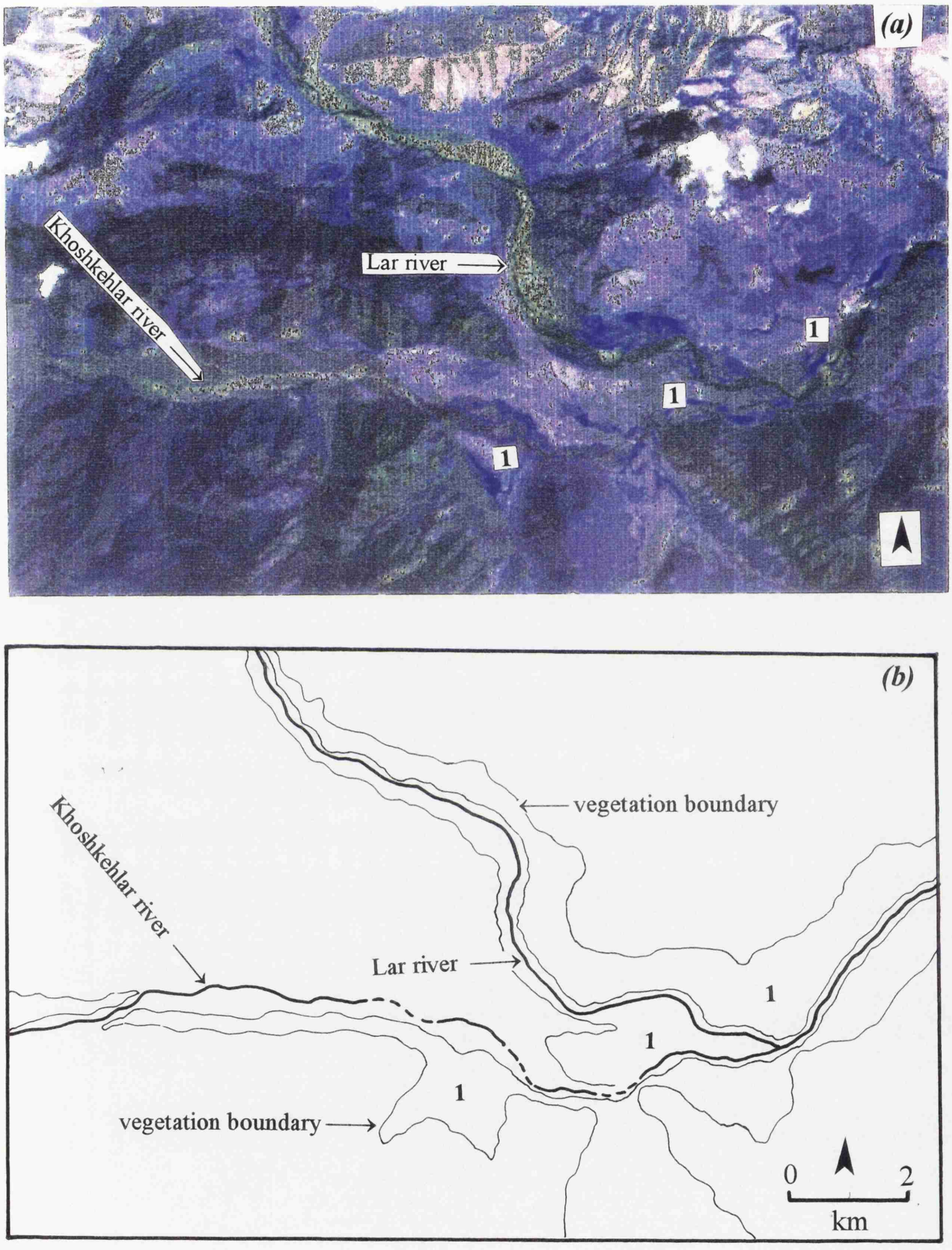

Figure 6.10: ***(a)*** high-moderate density vegetation on SPOT 3BA (blue and green colours '1') of the Lar upstream sub-catchments and ***(b)*** same area from KFA-1000 (1).

6.3.2 Image Processing and Error

The average accuracy can be calculated and displayed using the Dragon software. Average accuracy is computed by summing the individual percent correct values for each class and dividing the total by the number of classes. Overall accuracy is calculated by multiplying each percent corrected by the number of test pixels for the corresponding class, summing these weighted percents, and dividing by the total number of test pixels (over all classes).

Finally, the *Kappa coefficient* is calculated and displayed. This statistic has been recommended in the remote sensing literature as a suitable accuracy measure for thematic classification, since it considers all elements of the confusion matrix. Basically, kappa measures how far the distribution of values in the confusion matrix deviates from a chance arrangement. The larger the value of Kappa, the higher the accuracy of the classification. A perfectly accurate classification would produce a Kappa value of 1.00.

6.3.3 Result of Classification

Tables 6.1 to 4 provide a summary of the individual kappa coefficient, class accuracy and overall performance for the two classifier method used here on SPOT and Landsat (TM) images. The maximum likelihood classifier yielded 69.92 percent accuracy overall using three TM bands 1, 3 and 7, this decreased to 68.88 percent for the minimum distance mean (MDM) for the same area image in the Lar basin (Tables 6.2 and 6.3).

Table 6.2: Summary of classification error of TM (max. Likelihood) in Lake area.

Class (*)	Pixels correct	Commission		Omission	
		Pixels assigned	Percent correct	Trueclass pixels	Percent correct
1	4311	7785	55.37	7654	56.32
2	1008	2403	41.94	1831	55.05
3	1305	1905	68.5	1868	69.86
4	2140	7251	29.51	3340	64.07
5	37830	72385	52.26	62217	60.08
6	34050	34311	99.24	80432	42.33

Average accuracy: 59.45% Overall accuracy: 69.92 % Kappa coefficient: 0.54

*(1=sparse vegetation, 2=bare soil, 3=moderate vegetation density, 4=gully erosion, 5=dead grass and 6=high density vegetation).

Table 6.3: Summary of classification error of TM (MDM) in Lake area.

Class (*)	Pixels correct	Commission		Omission	
		Pixels assigned	Percent correct	Trueclass pixels	Percent correct
1	4311	23466	18.37	8383	51.42
2	1008	2396	42.07	2403	41.94
3	1305	3783	34.5	5812	22.45
4	2140	3365	63.6	4235	50.53
5	37830	71971	52.56	73232	51.66
6	34050	74536	45.68	34386	99.02

Average accuracy: 52.83% Overall accuracy: 68.88% Kappa coefficient: 0.39

*(1=sparse vegetation, 2=bare soil, 3=moderate vegetation density, 4=gully erosion, 5=dead grass and 6=high density vegetation).

Tables 6.4 and 6.5 also show the percent of overall accuracy of the SPOT classified images for the same methods as used for TM for the same area. The final rows in all Tables show the results after the two classifications. The overall accuracy of the SPOT three band maximum likelihood is 56.36%, which decreased to 55.14% in MDM for same area. Accuracy of these classified is based on the 300 field sites with a confidence interval of 55.14 on SPOT (MDM) to 69.92% on TM maximum likelihood.

Table 6.4: Summary of classification error of SPOT (max.likelihood) in Lar upstream.

Class (*)	Pixels correct	Commission		Omission	
		Pixels assigned	Percent correct	Trueclass pixels	Percent correct
1	1223	2203	5.58	1658	74.36
2	410	2561	16	735	55.78
3	648	3218	20.14	967	67.01
4	281	12165	2.31	393	71.50
5	44319	73607	60.21	55722	79.53
6	10250	25419	40.32	15071	68.01

Average accuracy: 78.11% Overall accuracy: 56.36% Kappa coefficient: 0.65

*(1=sparse vegetation, 2=bare soil, 3=moderate vegetation density, 4=gully erosion, 5=dead grass and 6=high density vegetation).

Table 6.5: Summary of classification error of SPOT (MDM) in Lar upstream.

Class (*)	Pixels correct	Commission		Omission	
		Pixels assigned	Percent correct	Trueclass pixels	Percent correct
1	123	28198	0.44	825	14.9
2	410	1835	22.34	2538	16.15
3	648	3685	17.58	971	66.73
4	281	7847	3.58	2327	12.07
5	44319	95722	46.30	80950	54.75
6	10250	41886	24.47	29624	34.60

Average accuracy: 33.2% Overall accuracy: 55.14% Kappa coefficient: 0.13

*(1=sparse vegetation, 2=bare soil, 3=moderate vegetation density, 4=gully erosion, 5=dead grass and 6=high density vegetation).

The error from the classified images shows that the maximum likelihood classification method in this study is the best for both of the Landsat TM and SPOT images especially for vegetation classification. The overall accuracy and kappa coefficient of the SPOT and TM maximum likelihood are respectively 56% and 0.65, 70% and 0.54 (Figure 6.11).

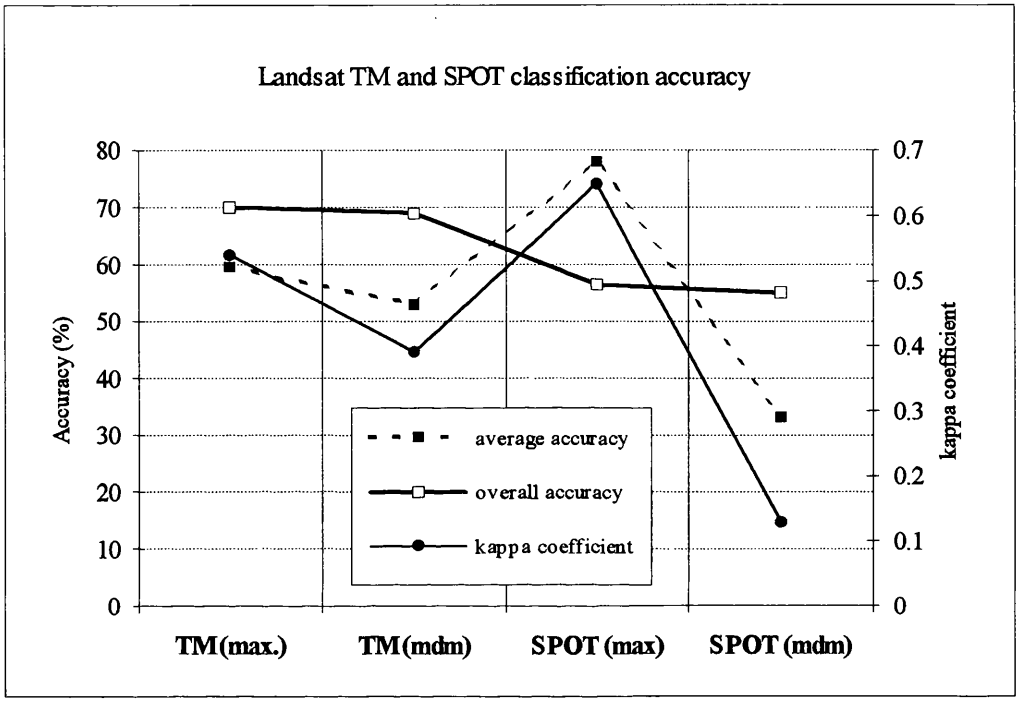

Figure 6.11: Landsat (TM) and SPOT classification accuracy.

6.4 REMOTE SENSING AND THE GEOMORPHOLOGY OF THE LAR BASIN

Multispectral remote sensing data classification methods have so far found rather limited applications in geomorphology. Most of the available satellite data (e.g. Landsat or SPOT) relate to the top few microns-thick part of the surficial cover of the earth's surface. Thermal infrared data is also related to a few cms-thick top surface layer and, although better in this respect, it is rarely available at high spatial resolution. Geomorphological studies are interested in defining a range of attributes which may influence landforms and sediment delivery. The type of soil, soil moisture and vegetation also give indirect information on the geomorphology of the area. In this research, remote sensing data was a necessary alternative to field investigation for inaccessable areas.

Elsewhere, it represents an additional source of data collection to field surveying, observation, sampling and analysis of surface and subsurface sediment.

As mentioned above, geomorphological changes in the Lar dam catchment were detected by remote sensing data as follows: *(a)* sink holes and collapse structures mark limestone terrain and lacustrine formations which existed before the dam; *(b)* recent holes, landslides, soil creep, rockfalls, lacustrine terraces, alluvial fans, river bars, all of which indicate a vigorous sediment supply environment; *(c)* deltas, beach spits and lagoons show lake processes; *(d)* and volcanic cones and lava flows characterize the igneous environment. Most of these features were directly observed on the remote sensing data, and the data collected over two field seasons. Stereopair Cosmos imagery and aerial photographs were useful for landform interpretation and digital data were also used to identify geomorphological process and forms.

6.4.1 Tectonic Landforms

Tectonic landforms may be defined as structural landforms of regional extent. Structure, e.g. the deformation pattern, has the most profound control on landform development and has laid the foundation of the concept of *morphotectonics*. In almost all cases in the Lar catchment, the structure of the rock has an intrinsic influence on landforms due to selective differential erosion and denudation along structurally weaker zones especially in the Dalichai sub-catchment (Solaimani, 1995). In the study area numerous tectonic features can be identified using the KFA-1000 and aerial photographs (see Figure 6.12). In addition younger features caused by tectonic activity occur, such as the landslides in the Dalichai and Lar upstream that are mapped on the geomorphology map. These areas are mostly steep, unvegetated and highly erodable. Figures 6.12 and 6.13 show the tectonic landforms and bare soil areas. In Figure 6.13, TM band-1 shows tectonic changes on the northern side of the Lake, which are generally directed east to west from the Dalichai valley to the Lar upstream, shown in the light colours that characterize

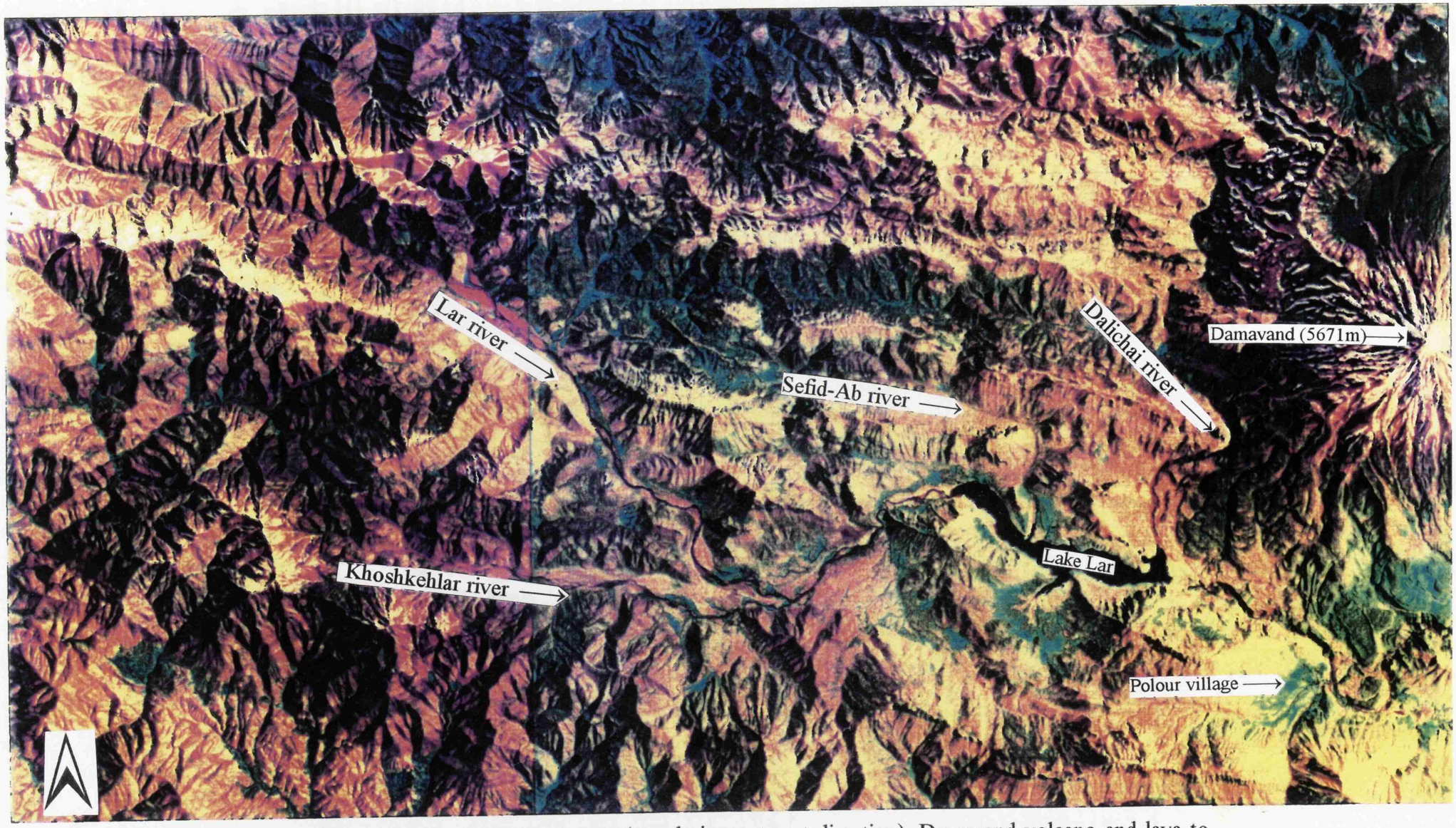

Figure 6.12: Tectonic structure (mostly in west-east direction), Damavand volcano and lava to the right side. Green is high density vegetation, light yellow is exposed limestone, light red shows medium and dried vegetation and red is bare soil, *(KFA-1000, 1990, approx. Scale is 1:200 000).*

bare soil on the image. The same colour representing tectonic features can be seen at Gozaldarreh (6.13-a) and Dalichai downstream (6.13-b).

6.4.2 Structure

The basis of deriving structural information from remote sensing data results from the concept of morphotectonics: that rocks acted upon by the deformational process result in landforms which are related both to internal characteristics (e.g. lithology, structure) geomorphological and chemical rock defects and to external parameters (e.g. types and intensity of erosion processs). The purpose of structural studies here is to interpret discontinuities in the terrain of the Lar basin and understand their disposition. Discontinuities are expressed as differences in topography, slope, relief, tone, and colour. They were visible on KFA-1000 stereo (Figure 6.12), aerial photographs and on the satellite data after processing aimed at enhancing structural features.

Remote sensing from Landsat MSS, TM, SPOT allows vertical and steep planar discontinuities to be very prominently displayed on these images and photographs. Folds in the study area were detected by tracing the bedding/marker horizon along the strike and recognition of dips on the KFA-1000 and aerial photographs followed up by field investigation. Broad, open, longitudinal folds were easy to locate on the remote sensing data, but tight overturned isoclinal folds were difficult to investigate. Such folds need to be identified at larger scales, by aerial photographs and field checking. Also delineating vertical to high angle faults or suspected faults was one of the greatest advantages of the remote sensing data (see folded geom. maps no.4).

6.4.3 Lineaments

The term lineament is defined by Siegal and Gillespie (1980) as a two dimensional geomorphological term referring to a mappable, simple or composite linear feature of a surface whose parts are aligned in a rectilinear or slightly curvilinear relationship and

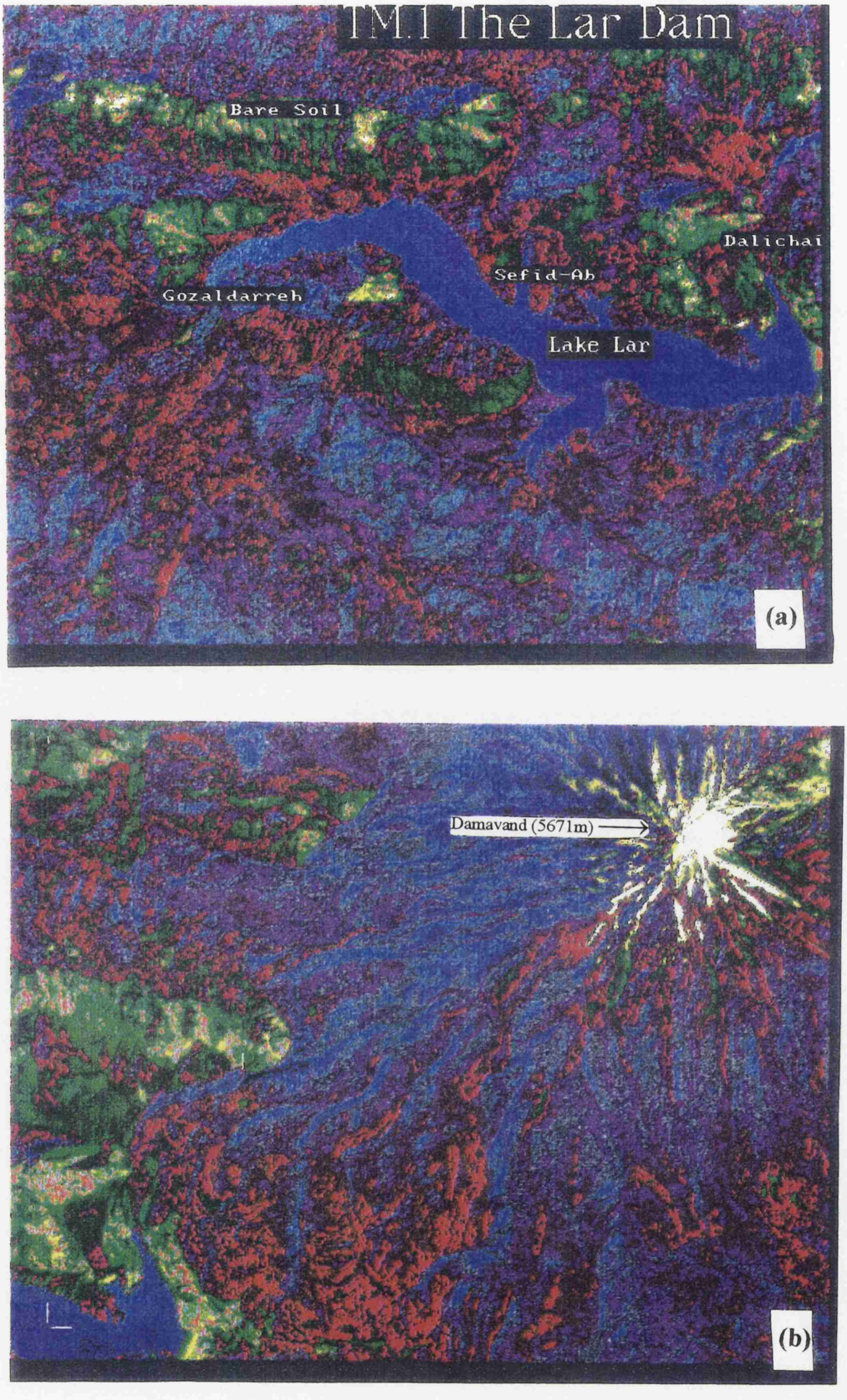

Figure 6.13: TM band 1 tectonic structure and bare soil (yellow and green colours show tectonic line mostly with west east direction and white colour is snow on Damavand, (**a**; Lar Lake area and **b**; is Dalichai).

which differs distinctly from the patterns of adjacent features and presumably reflects a subsurface phenomenon.

This term has been extensively used recently but often with differing shades of meaning. The linear alignment of landforms on photos and images are one of the most obvious features on high-altitude aerial and space images, and therefore the use of the term lineament has proliferated in remote sensing geomorphology literature recently. Hobbs (1904) first used the term lineament to define a significant line of landscape which reveals the hidden architecture of rock basement. The manifestation of a lineament is dependent on the scale of observation and dimension involved. Lineaments of a certain dimension and character were clearer on aerial photographs from the Lar Dam catchment but on the KFA-1000 images features of the size of hundreds of kilometers were equally clear.

On the KFA-1000 images and on aerial photographs the lineaments were easily identified by stereoscopic interpretation using tone, colour, texture and pattern. Alternatively, the computer digital techniques of edge detection can also be applied for lineament detection. Visual interpretation of the lineaments involves some degree of subjectivity, i.g. the result may change from person to person (Siegal 1977; Wise 1982; Burns and Brown 1978; Moor and Waltz 1983).

The lineaments mapped on remote sensing images usually exhibit spatial variations in trend, frequency and length and for statistical analysis they are often grouped in ranges of angles (commonly 10 degree intervals) in plan. Landsat spectral bands (4, 5, 6, and 7) are usually used for geomorphological interpretation although band 7 can detect linear features better than others (Figure 6.14). Figure 6.15 shows the result of enhanced image of SPOT band 3, on which regional lineaments are identified by distinguishing the continuous or closely spaced alignment of linear drainage segments, tonal contrast, or topographic features. Interpretation of the red band was also effective in deriving the

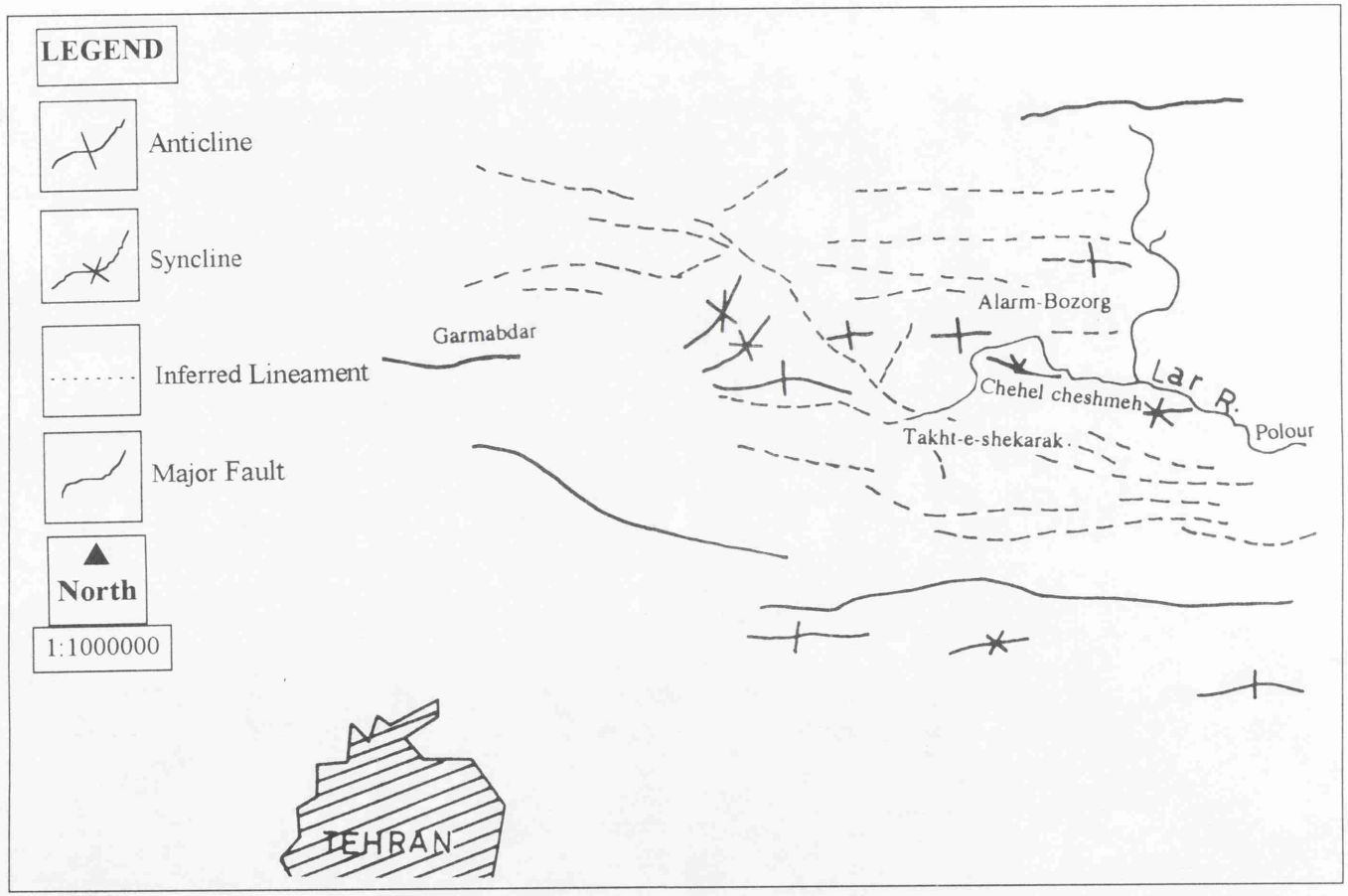

Figure 6.14: Lineament of the Lar basin from Landsat (MSS).

lineaments in the Lar dam basin and in verifying the major folds and faults that were identified from Landsat MSS band 7.

Figure 6.14, shows definite trends in lineaments interpreted from Landsat MSS. These lineaments show significant points of surface traces of zones of faulting, and also specify zones of weakness in unconsolidated sediments, which make them more subject to erosion.

6.4.4 Damavand Volcano

Volcanic landforms are primarily constructional, and result from extrusion or expulsion of magma along fractures or eruption centres on the surface. Depending upon the mode and type of eruption and magma, landforms such as volcanic cones can be produced (see Figure 6.12), from piles of flows and sheets of fragmented volcanic material. The Damavand lava flows previously blocked the valley of the old Lar stream and formed one of the largest natural lakes in Iran (see folded map no.4 and also Figure 6.15).

Volcanic rocks are characterized by the absence of bedding or foliation. Intrusive igneous rocks are massive, isotropic and homogeneous over large areas and are visible in Chehelbarreh upstream and in Laseh kuh of the Lar upstream. In the study area both on the SPOT and KFA-1000 images, they are shown as well jointed rocks which were easily mapped from moisture and vegetation differences. On the edge-enhanced SPOT data, the flow pattern of the lavas show coarse dendritic drainage patterns that are easy to identity (Figures 6.12 and 6.14).

Extrusive igneous rocks are delineated with the help of the associated volcanic landforms which cover the eastern side of Dalichai and on digital images, especially the stereoscopic KFA-1000, lava flows, cones and craters are clearly visible. The flows show a rough surface topography but some of older ones have undergone extensive weathering resulting in soil and vegetation cover on the northern and southern flanks, which renders their identification more difficult. The west and northern flanks of Damavand are wetter than the other sides, and so are more prone to weathering. The flows mostly occur as bodies of gigantic dimensions formed as extrusive volcanic rocks

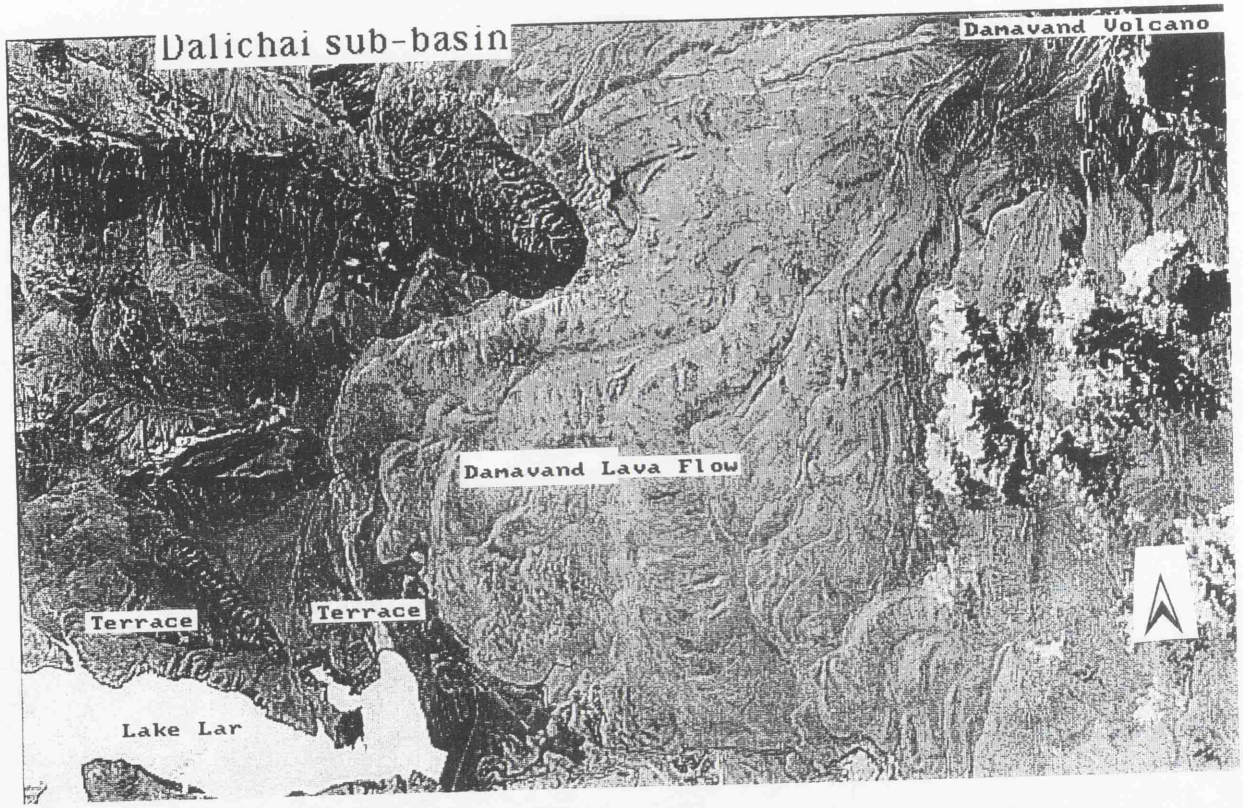

Figure 6.15: SPOT band 3 enhancement of Dalichai downstream shows terraces, lava flow and gully feature on the top of image in left corner.

which typically exhibit spheroidal weathering. From these, huge angular boulders develop, which when moved by streams in Dalichai valley produce more rounded forms (Figure 6.16). In Chapter 5 the volcanic material delivered from upstream was shown to be at a maximum percentage in Dalichai and which a higher spherity than the other selected sites in the Lar basin.

6.4.5 Fluvial Features

Drainage patterns in the Lar dam catchment can also be clearly identified from the imagery. Meandering can seen between the Lar/Khoshkehlar junction and Gozaldarreh station (Figure 6.12 with stereo view). On the stereo data this part of the channel has a sinuous shape, developing alternating bends with irregular spacing along the length. After stereo interpretation and field checking, this part of the river was found to have relatively narrow deep channels and stable banks. A distributory pattern consisting of several channel branches that originated from the same source appears close to Lar lake between Kamardasht and Gozaldarreh. This indicates the spreading of water and sediments across the depositional basin and the development of alluvial fans and deltas in this area. An anastomosing pattern comprises multiple interconnecting channels, separated by relatively stable areas of flood plain or bedrock. In the Lar downstream after Kamardasht, lower stream gradients produce braiding on the flood plain. In same area before Gozaldarreh a braided pattern is controlled by the load carried by the Lar and Khoshkehlar and is marked by a shallow channel separated by islands and channel bars (see folded Geom. map no.4 and Figures 6.17). Figures 6.17-a,b from Landsat and SPOT 3 band composite images show the channel morphology and alluvial deposits of the Khoshkehlar and Lar tributaries. The alluvial deposits on the TM 3 band composite image are identified by a light blue colour and on SPOT 3 band composite (Figure 6.17-a,b see also Figure 5.25) image, identified in light green colour. These two images show that in the Lar upstream surface erosion is active and its delivery downstream changes river channel shape.

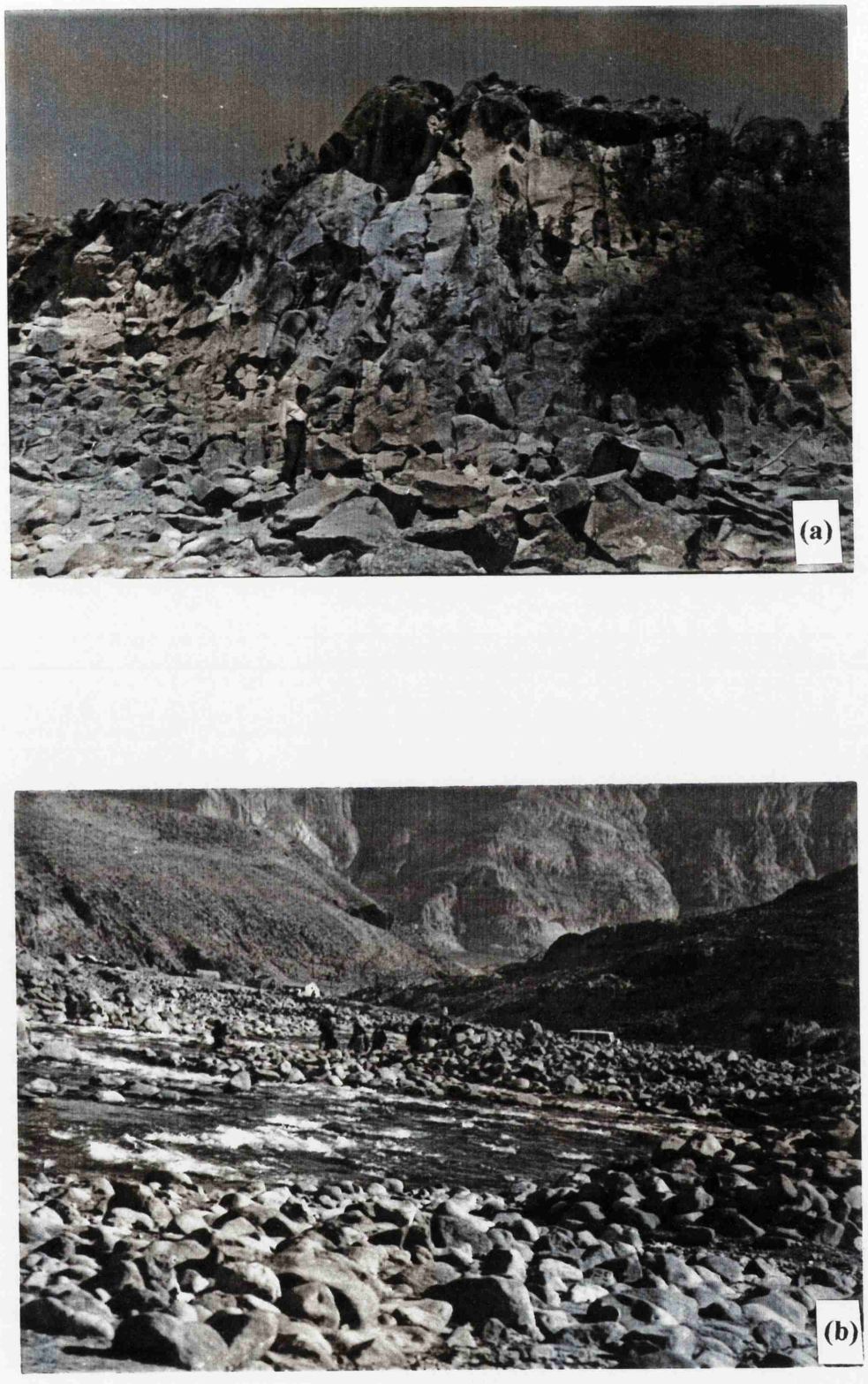

Figure 6.16: (a) Dalichai upstream sharp forms of trachyandesite and **(b)** downstream rounded shape of volcanic rocks, about 2 km from **(a)** site (Aug.1994).

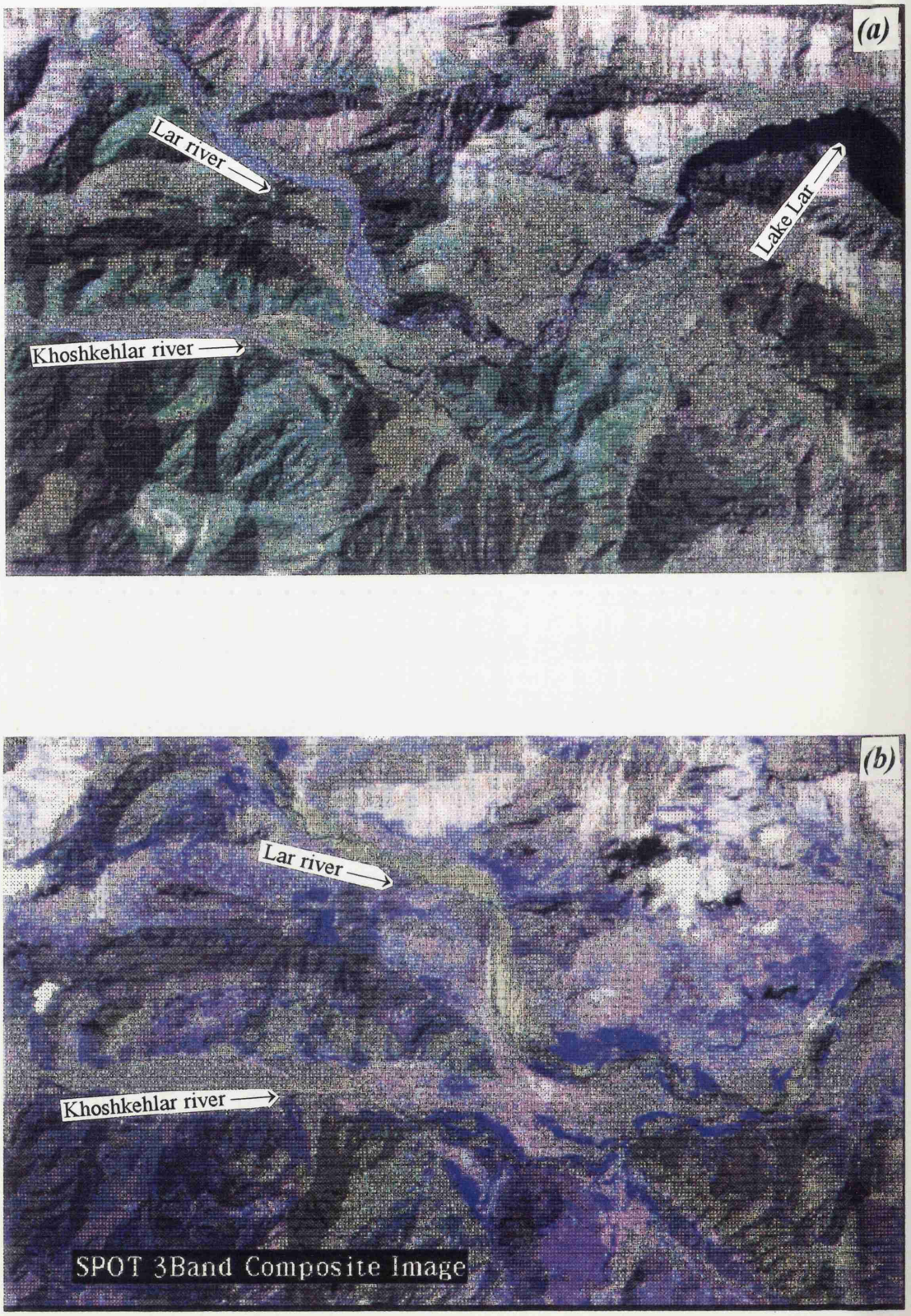

Figure 6.17: (a) Landsat (TM) (light blue is alluvial deposits, dark green is bare soil, white is limestone, light green colour shows high density vegetation over, other colour show medium or poor vegetation) and, **(b)** SPOT 3B composite image of the Lar and Khoshkehlar catchments light green is alluvial deposits dark green is bare soil, white is limestone, blue colour shows high density vegeation cover, other colour show medium or poor vegetation).

The landforms associated with fluvial erosion in the Lar are gorges and V-shaped valleys, which are identified on stereoscopic KFA-1000 (Lar down stream after Dam and the middle part of Dalichai). Typical depositional landforms including fans, alluvial plains, natural levees, river terraces and meander scars, can all be seen in the Lar and Khoshkehlar tributaries on stereo view of KFA-1000 (Figure 6.12 and see also folded Geom.map no.4). These landforms were identified on aerial and satellite remote sensing data also and finally plotted an geomorphology map (folded geom.map no.4). An important application of remote sensing data is in detection of dynamic features, such as changes in planform and migration of the rivers and delineation of paleochannels. Some significant fluvial changes occur in the Lar upstream because of the physiographic conditions described in Chapter 4. Sediment transport from the erodible surfaces upstream and also from river banks in the middle and downstream is widespread and in some areas of the Lar and Khoshkehlar, deflects stream flows (see Figures 5.15, 6.12 and also folded map no. 4).

6.4.6 Terraces

As described in chapter 1, one of the main aims in this study is to identify the morphological changes in the Lar basin and produce a geomorphology map. The most prominent geomorphological feature in the Lar and Dalichai catchments is the well developed series of river terraces formed as the river incised into its bed when the Lar lake drained. The tectonic changes as described in Chapters 4 and 5, appear to have ceased in the area shortly before these terraces were formed, as two major faults in the area can be seen to displace soil horizons in the deposits but no displacement of the terrace surfaces can be detected (see folded geom.map no.4). The local base level of the rivers appears to have been lowered sporadically during the formation of the terraces. For each terrace level some constriction in the lower valley must have maintained the base of the river at a fairly constant elevation until such time as the constriction was breached and a new local base level was established at a lower elevation. A simple survey of the terrace levels on the KFA-1000, SPOT and aerial photographs has been undertaken, consisting of recording the main elevation of every terrace flat between the Lar Dam and Gozaldarreh. A frequency histogram of the main

elevation of every terrace flat between Gozaldarreh and the Lar Dam was produced (Figure 5.10).

To obtain a quantitative appraisal of the are of terraces an attempt was made to detect the terrace levels by measuring the area on the map between contours at 10 metre intervals. Dominant terrace levels should be identified by above average areas between adjacent contours. This technique proved unsuccessful due mainly to the presence of a large number of smaller, intermediate terraces and to the general rise in elevation of terrace flats in an upstream direction. As a result of these factors the survey failed to adequately define the terrace levels even when measurements were made over a relatively small area to reduce the effects of the upstream rise in elevation. However, the field survey proved to be essential to identify and quantify terrace occurrence and areal extents.

In order to determine the accuracy of terrace detection from different remote sensing data sources, the terrace extent was mapped from aerial photographs to provide control data. The terraces were also identified from a three band composite SPOT image (which shows terraces as the light green and blue colours along the river channels. The area of these was measured using geometrical correction within the Dragon image processing system. The same operations were performed on a Landsat TM 3B composite image, which shows the light blue and green colours along the river channels as terrace areas (Figure 6.17-a,b). For automatic measurement of such areas, Dragon counts the number of pixels in a specified class. These are converted to area based on a specified pixel size (30m for Landsat TM, 20m for SPOT; see Figures 6.18-a,b,c).

Measurements from different data places the total Lar basin terrace area as follows (total area of terrace); SPOT 5.3%, Landsat (TM) 3.44%, KFA-1000 5.61% and on the geomorphology map about 6.41% of the whole basin area (780km^2). Figure 6.19 Shows that from various methods the KFA-1000 is the best match against the control data which shows also SPOT and Landsat TM respectively in second and third stage.

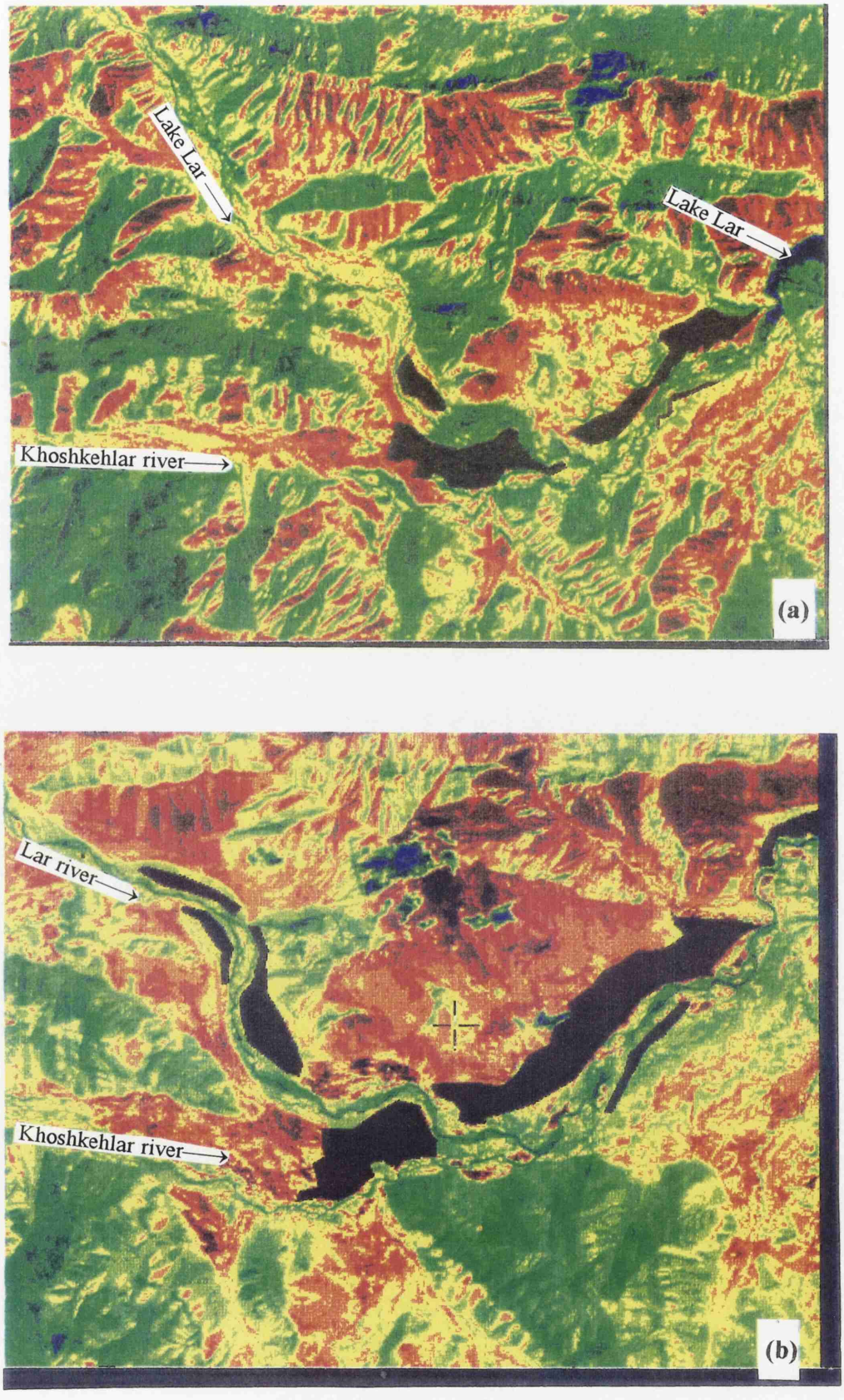

Figure 6.18: ***(a)*** Landsat TM band 7 and, ***(b)*** SPOT band 3 of the Lar upstream terraces by the Dragon geometry function (black colour, see also 6.18-**c** terrace area from KFA-1000).

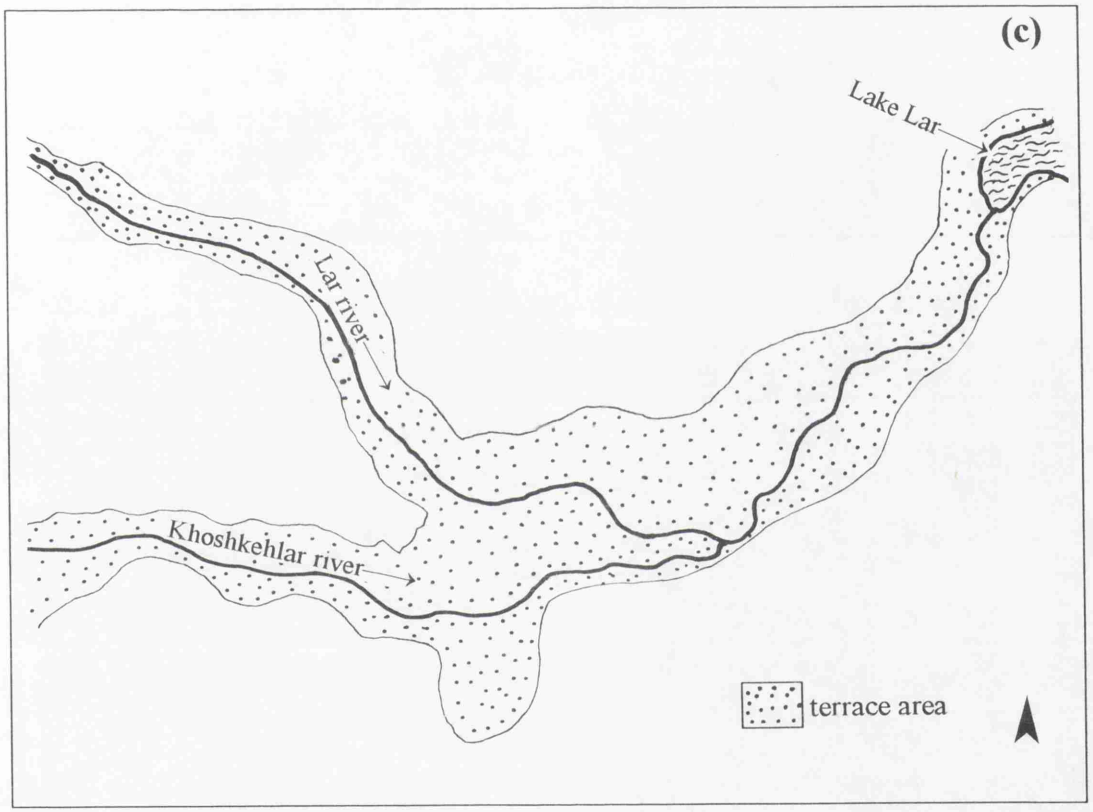

Figure 6.18-c: Terrace area of the Lar upstream from KFA-1000
(Approx. scale 1:100 000).

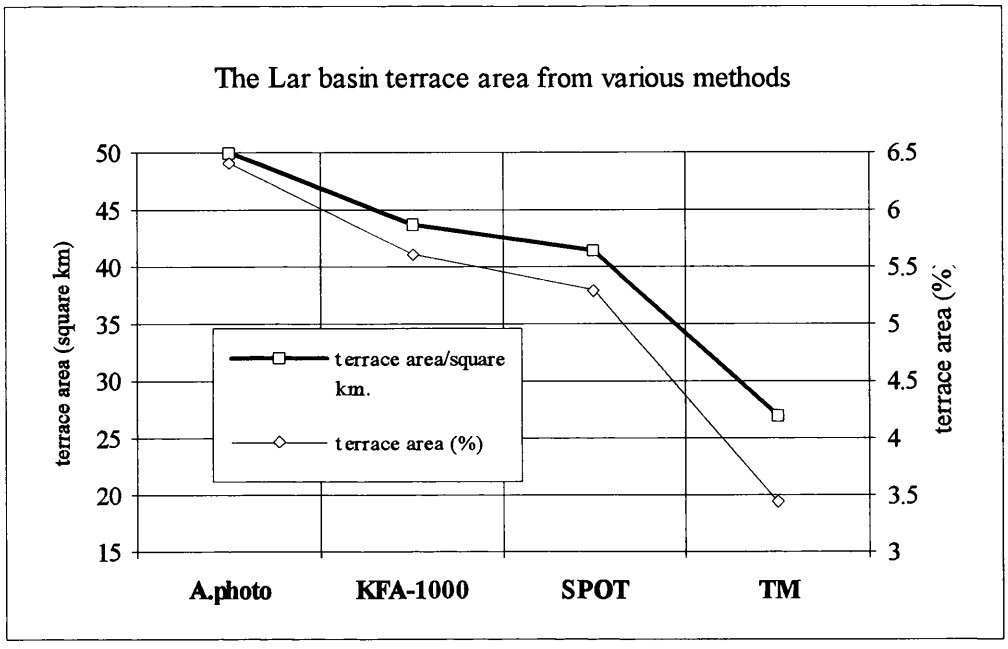

Figure 6.19: The Lar basin terrace area from different methods.

The best estimator of the terrace area is the ground verified geomorphology map in conjunction with aerial photograph data. Compared with this the KFA-1000 data has 87.5% accuracy, SPOT has 82.7% accuracy, and TM has 53.7% accuracy. Table 6.6 shows the terrace area from 13 sub-catchments where remote sensing methods are matched against the control data (aerial photographs and geomorphology map). The KFA-1000 is the best match against the control data with more than 50% of the terrace areas of the sub-catchments estimated to within ±20% of the control area (38.5% of the terrace areas is estimated to within ±10% of that of the control areas). The SPOT result also shows a reasonable match against the control data, and to estimated 38.5% and 15.5% of the terrace areas respectively within ±20% and ±10% of the control areas. The Landsat TM shows a poor match against the control data (31% and 7.7% of the terrace areas are respectively within ±20% and ±10% of the control areas). It is notable that the area in Asbe-kalak, E-Sefid, Chehelcheshmeh and particularly Ghushkhaneh with higher steep slopes do not match well with the control data. Other areas with relatively smooth topography and generally flat surfaces e.g. Sefid-Ab downstream, Gozaldarreh, Imamzadeh-1, Dalichai downstream and Sefid-R mostly match well with the control data (see Table 6.6).

It is possible that the differences in Table 6.6 are related to the resolution of the imagery e.g. 20m for SPOT, 30m for TM and 5-10m for KFA-1000. In addition, environmental

factors such as slope and topography impact on the images. Because of the high relief in the Lar basin, there is an enhanced topographic and slope effect on the reflected radiance data, so that sometimes long slopes are represented by only a small part of the pixel areas. Therefore identification of terrace units on images may sometimes be different, dependent upon topography.

Different enhancement techniques such as filtering, band ratios and histogram stretches were employed for digital interpretation with the Dragon Image Processing System. Smoothing of different bands was useful in the detection of terraced areas, which are depicted by light tones on the grey tone images. Overlaying of filtered bands one and three, and those from linear stretches of bands two and three, as well as the composite images of filtered bands one, two and three were also utilized for visual interpretation. Visual interpretation was particularly useful in separating the terraces from massive limestone beds by using the visible parallel patterns. Aerial photographs at scale of 1: 20 000, 1: 50 000 and KFA-1000 at scale 1:270 000 were used to gain a better accuracy of classified digital images from Landsat TM and SPOT multispectral data. The aerial photographs showed a prominent and well developed series of river terraces formed as the rivers cut down their beds after the drainage of the lake sediments (Figure 6.18).

Table 6.6: Summary of terrace area measurement from various methods (13 test area).

Location	SPOT Xs (area%)	Landsat TM (area %)	KFA-1000 (stereoscopic)	Control Aerial Photographs
Sefid-Ab	0.54*	0.12*	0.59•	0.65
Gozaldarreh	1.39•	0.9	1.41•	1.45
Glahsardab	0.53	0.13	0.56•	0.62
Kamardasht	0.50	0.65	0.53•	0.58
Imamzadeh-1	0.42*	0.39*	0.44*	0.51
Asbe-Kalak	0.07	0.09	0.13	0.19
Imamzadeh-2	0.097	0.2•	0.15	0.2
Dalichai	0.81•	0.09	0.82•	0.89
E-Sefid	0.09	0.37	0.11	0.15
Sefid-R	0.185*	0.12	0.19*	0.23
Sefid-L	0.105	0.03*	0.109	0.16
Ghushkhaneh	0.117	?	0.12	0.17
Chehelcheshmeh	0.40	0.25	0.43	0.61

?(no measurement was possible). [(•) means remote sensing result is within ±10% and, (*) means ±20% of aerial photo result].

Stereoscopic interpretation of the KFA-1000 images shows that the effects of meandering of the Lar are part erosional and part depositional. Therefore the current river cliffs display a sequence consisting of river gravels resting on an eroded surface of lake deposits. The terrace levels also relate to constrictions in the lower valley and there is a close match between terrace levels and the elevations of constriction and blockage. The sediment distribution, morphological changes related to geological characteristics and terrace volumes are discussed in Chapter 7 as significant factors for the sediment yield in the Lar basin.

6.4.7 Landslides

Landslides in the Lar Dam catchment were investigated at scales of about 1:5 000 - 1:30 000 on aerial photographs which provided a ground spatial resolution of about 5 meters. Stereoscopic KFA-1000 imagery was also most suitable whereas present day space-acquired data had rather limited applicability, owing to constraints of spatial resolution and 3-D viewing. On the aerial photographs landslides are marked by a number of characters (Rib and Laing 1978), e.g. sharp breaks of slope in the topography, hummocky topography on the down-slope side, abrupt changes in tone and vegetation, and drainage disruption.

When using remote sensing data for landslides, the most useful strategy is to identify situations and phenomena which lead to slope instability. As remote sensing data provides a regional view, areas vulnerable to landslide activity can be delineated for further detailed field checking (see folded Geom.map no.4). In Figure 6.20 on TM band-3 in western side of Dalichai a landslide is identified on the south-eastern flank of a fault line. This landslide was observed in the field and is still active and supplying sediment to Dalichai river. Figure 6.20-b shows the landslide from 6.20-a enlarged and shows different stages of the landslide in dark colour with west-east direction. Figure 6.20-c (photograph) shows sequences of eroded material and a fault line at the top.

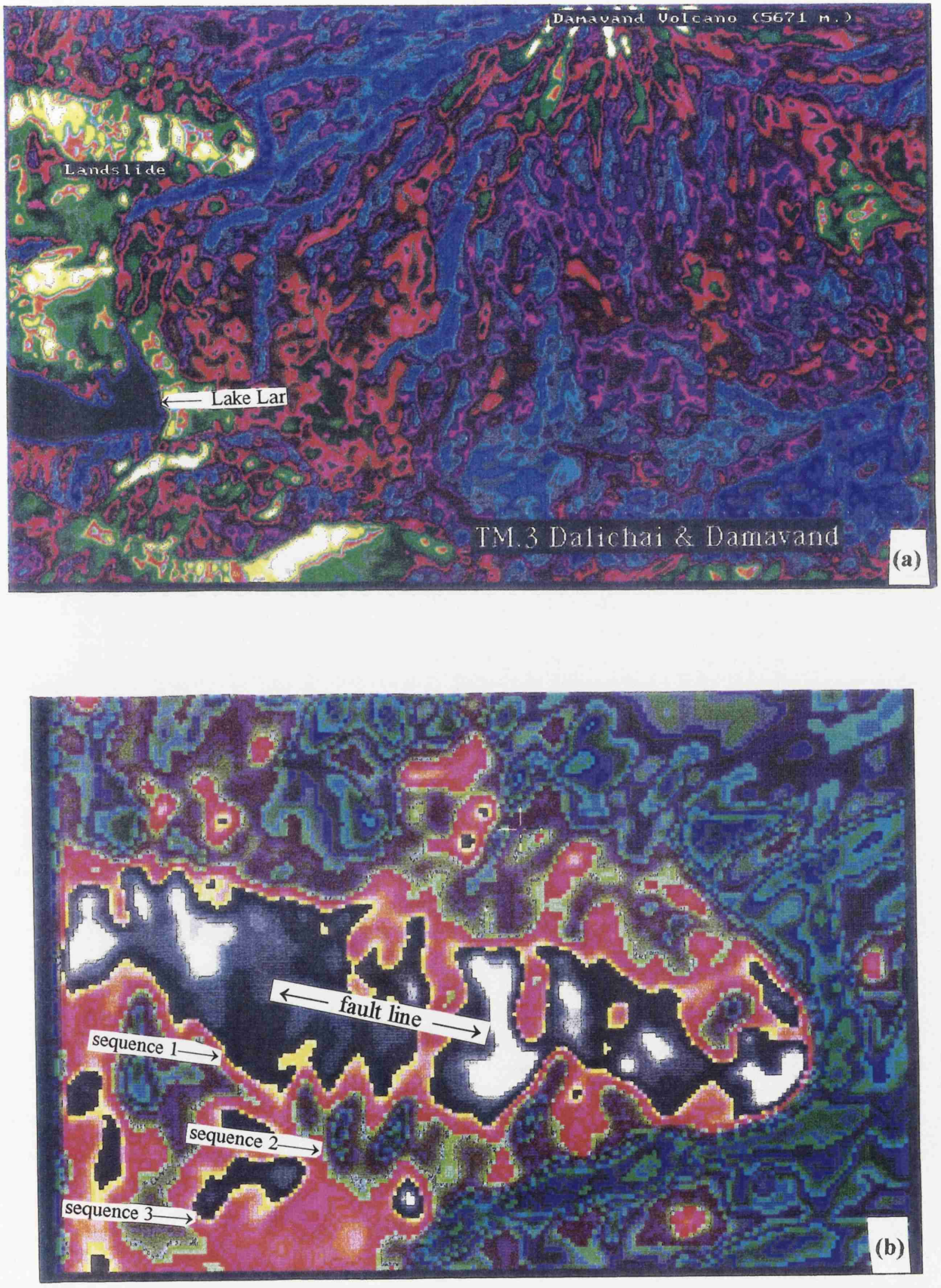

Figure 6.20: *(a)* TM band 3 Dalichai Landslide, *(b)* same area enlarged image shows sequences of Landslide in separate black and white colour (see fig.6.20-**c**).

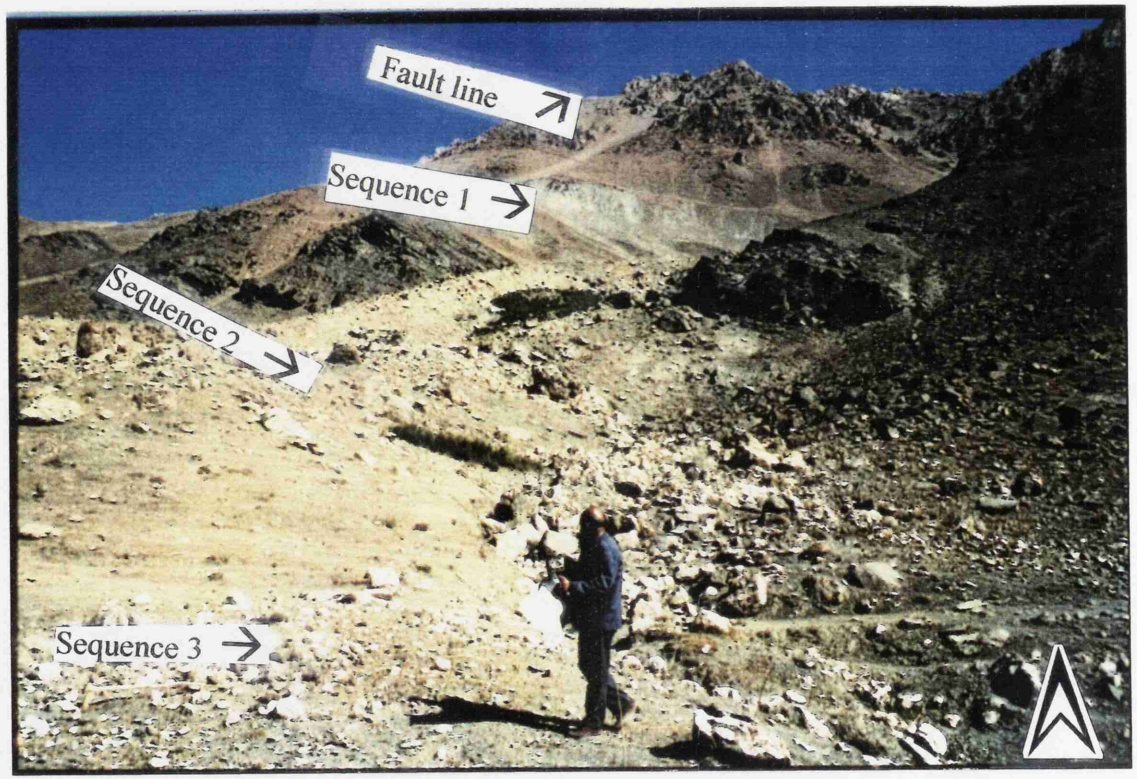

Figure 6.20-c: Sequences of Dalichi Landslide
(Aug. 1994) see same area on Figure 6.19-**b** in the right side.

6.5 VEGETATION COVER AND SOIL EROSION

Soil erosion contributes to sediment delivery to the streams and it's assessment is an important aim of this study. Topography, slopes, soil type, landcover and drainage characteristics are often required for assessment of the extent of erosion. The study area vegetation and soils reflect the local and temporary grazing of livestock during the summer. In western Dalichai, Sefid-Ab and the Lar river catchment, because of the easy access to water and grass this impact is detectable on the SPOT and Landsat TM (Figure 6.17-a,b). Figures 6.17-a,b (TM and SPOT 3BA) show that along the Lar and Khoshkehlar rivers the dark green colour show that light green colour are reflected grazing area in the Lar basin which is confirmed in the field (Fihures 6.10-a,b see also Figure 4.8-a from Dalichai upstream).

Remote sensing is useful in vegetation mapping because the spectral properties of vegetation changes in response to stress. In the study area, different types of vegetation are visible with normally strong reflectance from healthy vegetation in the near-infrared region, and decreased reflectance in the near-infrared for senescent vegetation. KFA-1000 and aerial photographs were employed together with field checks to verify this effect. Based on the classified images, the results related to vegetation and erodible areas are as follows: A global vegetation index (GVI) was calculated according to formulae developed by the NOAA National Climatic Data Centre (Dragon User Manual, 1993). The GVI calculations are intended to be applied to scaled channel 1 and 2 data acquired from the NOAA instrument. Global vegetation index images are particularly useful for multitemporal vegetation analyses because NOAA maintains archived GVI data stretching back more than a decade. This calculation first calculates a Normalized Vegetation Index (NVI) for each pixel according to the equation;

$$NVI = (Ch2-Ch1)/(Ch2+Ch1) \qquad [6.3]$$

where; NIV = Normalized Vegetation Index and Ch = image band.

Due to previous scaling applied to the channel files, the value of this index can range from -0.05 (no green) to 0.60 (maximum green). This index is then scaled to the range 0 through 255, as follows;

$$GVI = 240-(NVI-0.05)\times 350 \qquad [6.4]$$

This scaling inverts the index such that the greenest areas appear darkest in the final image, which are dark green with some close to blue colour on TM bands 3 and 7 in the Lar upstream and light green colour on SPOT bands 1 and 3 for same area. The enhancement operation VEG provides an approximation to first step of the GVI calculation (Figure 6.21-a,b). It calculates the ratio of the difference of the bands to the sum of bands, then scales the result to fill the range from 0-255, where a vegetation ratio of 0 will be mapped to an image data value 127 in the final image. Figures 6.21-a,b (GVI) and Figure 4.8-a,b (photos) show the vegetation cover in the Lar upstream. On SPOT bands 1 and 3 GVI (Figure 6.21-a) dark grey is limestone, light grey bare soil, blue is high density fresh vegetation and other green show vegetation. In TM, (Figure 6.21-b) pink is limestone, light green is bare soil, dark green is vegetation. Generally Figure 6.21-a shows that the SPOT bands 1 and 3 were successfully able to identify vegetation, but the results from TM bands 7 and 3 (global vegetation index) shows more variety in vegetation type and density than the other bands. Figures 6.21-a and b both show that high density vegetation cover is related almost exclusively to terraces and flat areas (mostly along the Lar river, Sefid-Ab and Dalichai upstream and the northern side of the Lake) where the erosion rate is very low, although bank erosion acts as an important factor in sediment delivery. So SPOT images are useful for identification of vegetation density, while TM data is more successful in identifying different types of vegetation.

The single band images of TM (Lands) show an interesting range of spectral and spatial variation within the major surface types of bare soil and erodible areas in bands 1 and 7 in white and green colours. (Figures 6.22-a, b TM bands 1,7).

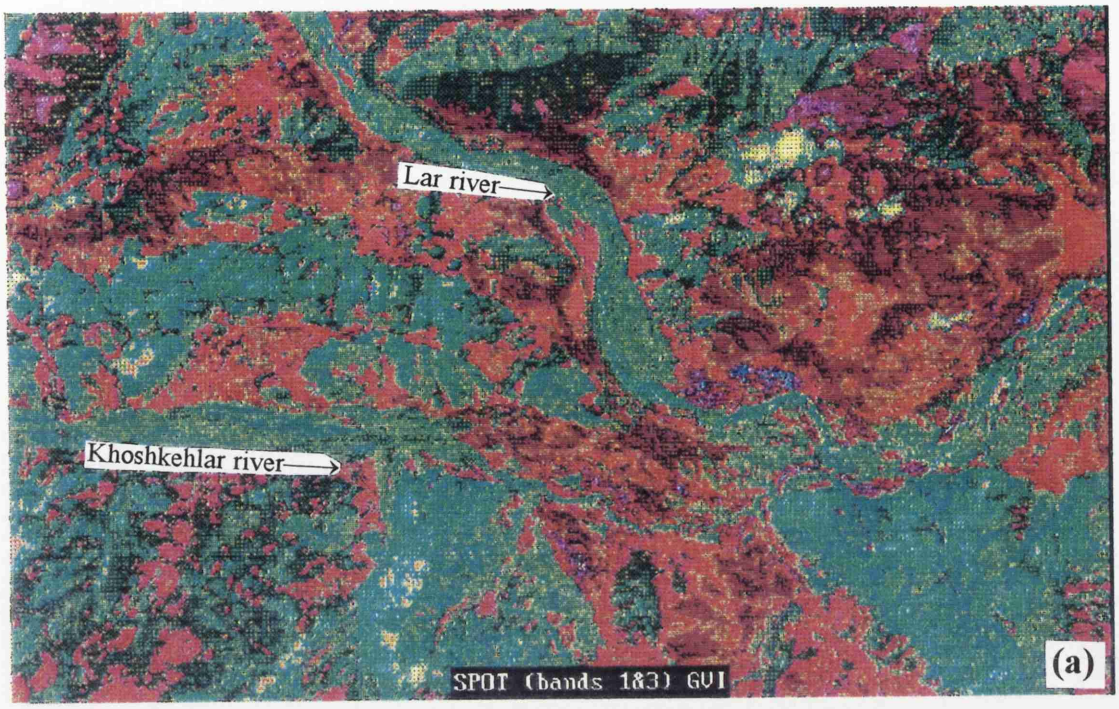

Figure 6.21-a: SPOT bands 1 & 3 Global Vegetation Index of the Lar upstream (dark grey is limestone, light grey bare soil, blue is high density fresh vegetation and other green show vegetation).

Figure 6.21-b: TM bands 3 & 7 Global Vegetation Index of the Lar upstream (pink is limestone, light green is bare soil, dark green is vegetationand blue is Lake Lar).

Figures 6.22-a and b show that TM single band 1 and 7 images are very useful for identifying erodible areas in the Lar basin. On TM band 1, all bright green, yellow, red and white colours show erodible areas which include the Lar basin from Gozaldarreh to Damavand. In the middle parts of the image a blue south-north line shows an area of gully erosion which mostly lies in the Sefid-Ab upstream and the middle part of Dalichai (Figure 6.22-a). In Figure 6.22-b for Lar upstream a similar pattern can be identified in the same colours, showing higher density gullying than the Lar downstream, especially on the southern side of the Dalichai catchment (6.22-a). Interpretation of these two figures shows that from the remote sensing data the Khoshkehlar catchment with a high density of gully features, erodible areas should have the conditions favouring higher surface erosion than other sub-catchmants in the Lar basin. However, it has only ephemeral stream and so erosion may be more limited and seasonal than first appears.

A combination of three bands from the Landsat Thematic Mapper was used to identify both fluvial and erodible areas in the Lar basin. In the three band composite of TM band bands 1, 3 and 7 of the Lar upstream (Figure 6.17-a) bright grey areas are bare soil, dark shows limestone and other colours are different types of vegetation, which can be compared with KFA-1000 images (Table 6.7).

Table 6.7: TM 3BA (1, 3 and7) land surface and inferred level of erosion in the Lar basin.

Spectral class colour code	Land cover	Inferred erosion
dark green	high vegetation density	low - moderate
blue	medium (recent deposits)	very high - high
bright grey	poor cover (bare soil)	high - moderate
dark grey	no veg. (Limestone heights)	low - moderate
black	Lake Lar	low - very low

The same bands have been employed for the Lar downstream, with limestone in bright grey, the pink colour as Damavand peak snow cover, bare soil identified in grey colour, and other colours showing vegetation. Because of individual physical conditions these

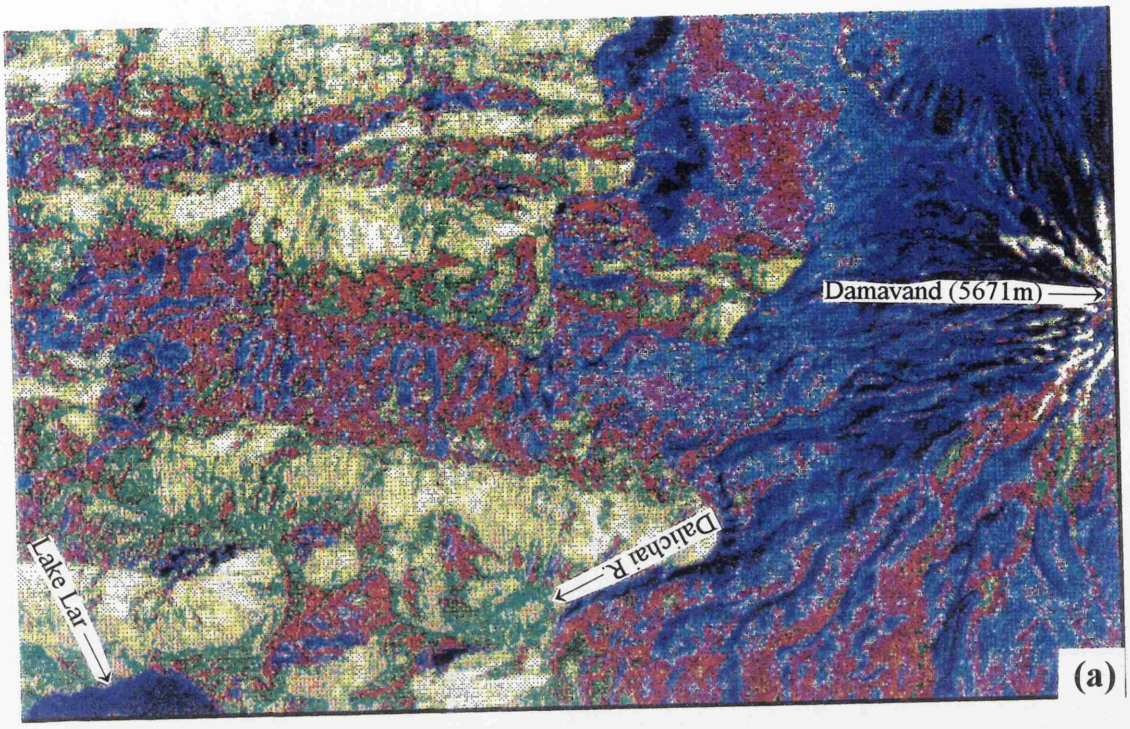

Figure 6.22-a: Landsat TM band-1 equalisation histogram of the Lar downstream catchments (all bright green, yellow, red and white colours show erodable areas).

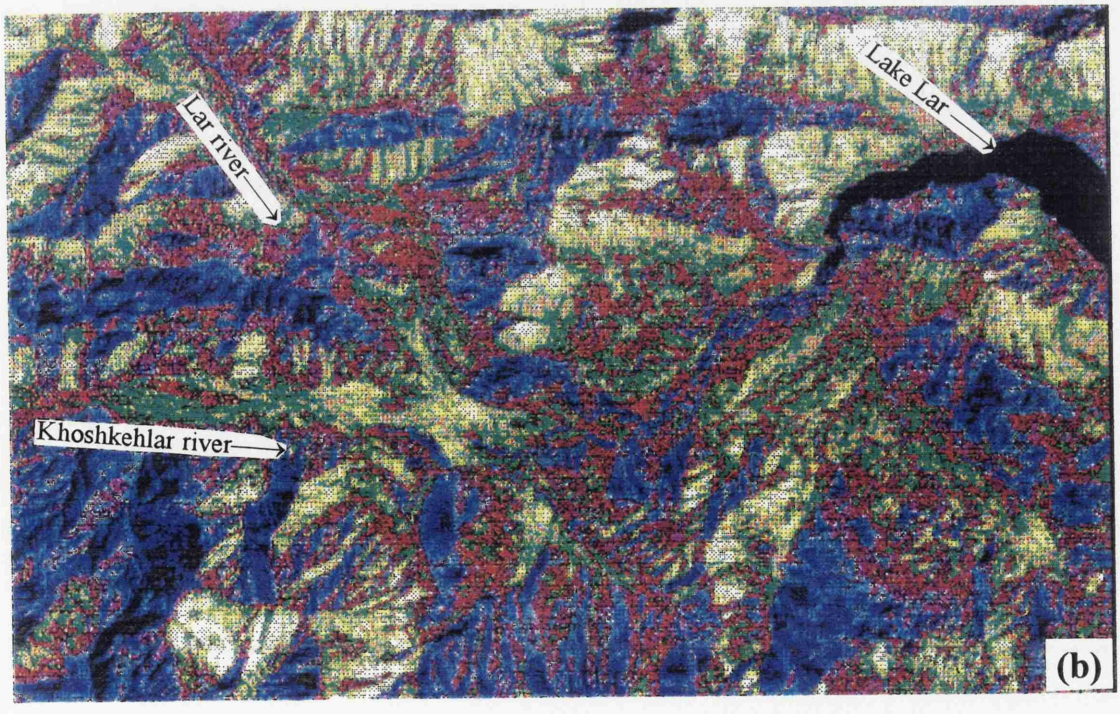

Figure 6.22-b: Landsat TM band-7 equalisation histogram of the Lar upstream catchments (all bright green, yellow, red and white colours show erodable areas).

have no conformity with KFA-1000 images. This method is useful to identify the erodible areas because erosion patterns and vegetation density are separated more clearly than with other techniques. On both of them, gully erosion and scree patterns occur in parallel lines with south-north directions. This mostly includes the northern side of the Lar, the southern flank of Khoshkehlar and the western side of the Dalichai and Sefid-Ab catchments.

Figure 6.23 TM bands 1,3 and 7 were used to produce a 3B composite with the maximum likelihood method. This shows light red as dead grass, blue colour bare soil, green is limestone and gully area, orange shows high density vegetation, and other colours show different types of low density vegetation (Table 6.8).

Table 6.8: TM 3BA (1, 7 and 3 Maximum likelihood), land surface and inferred level of erosion in Lar upstream.

Spectral class colour code	Land cover	Inferred erosion
orange	high vegetation density	low - moderate
light blue	bare soil (poor veg.)	high - moderate
green	limestone heights (no veg.)	low - moderate
dark blue	Lake Lar	low - very low

In Figure 6.17, the result of the SPOT three bands composite of the Lar upstream shows that blue colour is vegetation, dark grey as bare soil, light grey as dead grass and the white colour diagnoses limestone. A SPOT three bands composite Maximum likelihood (Figure 6.24; SPOT bands 1, 2 and 3) of the Lar upstream (Khoshkeh-Lar and Lar tributaries) enables identification of the grey and orange colours are bare soil, green as moderate density vegetation, blue as high density vegetation, and other colours as different types of vegetation which are classified precisely on the Lar basin vegetation map. In Figure 6.23 (Landsat TM 3B) the maximum likelihood technique shows that most parts of Khoshkehlar catchment are covered by low density vegetation and bare soil, especially in the southern side, which can influence sediment delivery to Lar downstream. Gully features are mostly created on limestone slopes in the northern side of the Lar where there is poor or moderate vegetation cover, but terrace areas are covered by high density vegetation and very low surface erosion. This technique is more

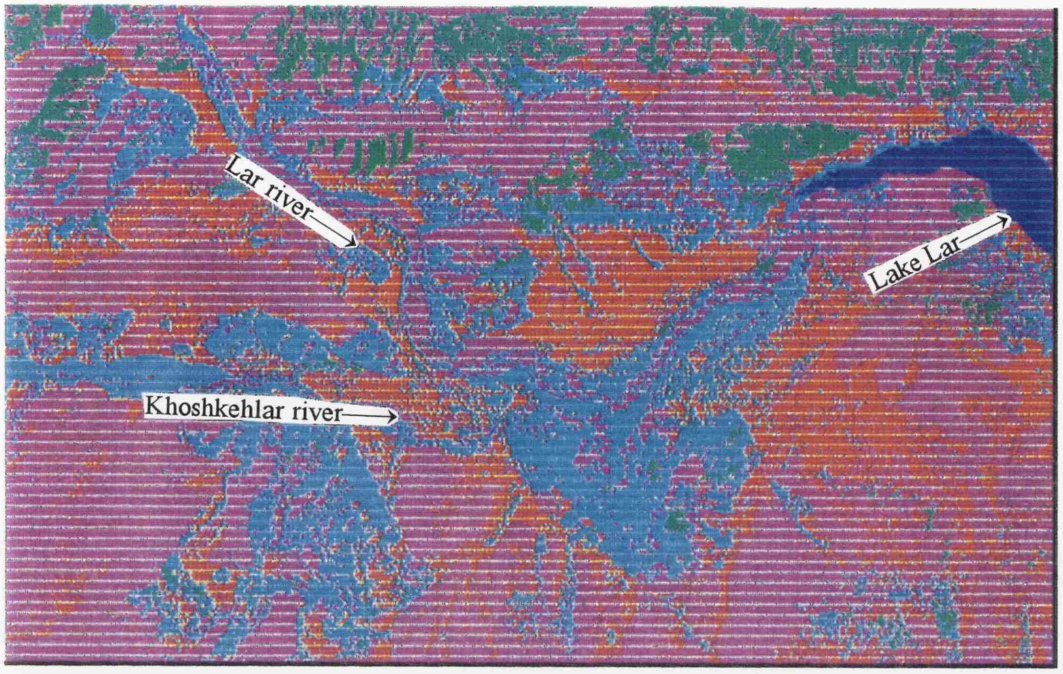

Figure 6.23: Landsat TM 3B Composite Maximum Likelihood of the Lar Upstream, (light red shows dead grass, blue colour bare soil, green is limestone and gully area, orange shows high density vegetation and other colours show different types of low density vegetation).

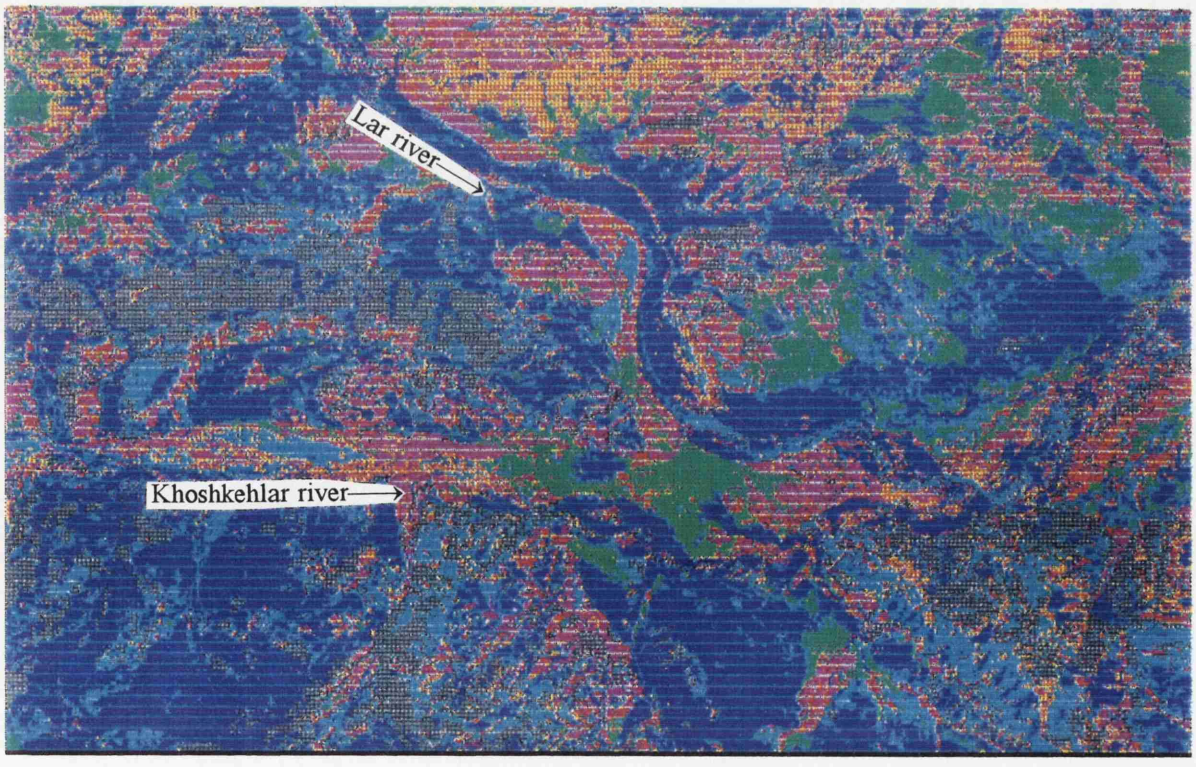

Figure 6.24: A SPOT 3B Composite Maximum Likelihood of the Lar Upstream, (Grey and orange colours are bare soil, green shows moderate density and blue is high density vegetation and other colours show different types of vegetation).

useful than other techniques for identifying both erodible and vegetation covered areas. It shows that surface erosion is mostly related to unvegetated limestone formations in the northern side of the Lar, the area between Khoshkehlar and Lar catchments and southern Khoshkehlar. Although there was some limitation to choose 3BA maximum likelihood for vegetation, but it was the most useful technique for detection of erosion features and erodible areas in the Lar basin.

Band 1/2 and 3/1 ratios were chosen to assess the spatial cover discrimination performance. Curran (1983) has used a ratio image of infrared and red to provide indications of vegetation density. The ratio is very effective in enhancing differences between vegetated and non-vegetated areas. The variations displayed in this ratio were enhanced further using density slicing to produce a colour representation of the extent and variations occurring between and within land surface types (Figures 6.25-a and b). The result of the SPOT bands 3 and 2 ratio image of the Khoshkehlar and Lar catchments in upstream diagnosed exposed limestone and bare soil in light blue and yellow colours, poor vegetation in red colour, moderate vegetation in green, white colour is high density vegetation and other colours show different types of vegetation which are classified on the basin vegetation map (see folded veg. Map no.2). SPOT bands 3 and 1 ratio of the same area (upstream) utilized for the surface cover identification which is diagnosed bare soil in light yellow and grey colours, moderate vegetation as green, white is high density fresh vegetation, blue colour shows high density vegetation, and other colors show different density of vegetation. The band ratio of SPOT 3/2 (Figure 6.25-a) and 3/1 (Figure 6.25-b) were useful to identify and delimiting the exposed limestone from dried vegetation and bare soil. So the best ratioing is between 1/2 which was moderately successful in delimiting dead grass from bare soil and vegetation.

The effectiveness of band ratios (particularly infrared/red) as an aid in image classification, and therefore in the discrimination of different land surface covers, was previously suggested by Pearson and Miller (1972) and this was later supported with similar observations by Chalmers and Harris (1981) using Landsat (MSS) data. Ratios are used to subtract out or divide out the undesirable effects of the atmosphere or variable scene illumination (Swain 1975). Such an image usually supports detail common to the two images (Sabins 1978, Condit and Chavez 1979, Townshend 1981) and

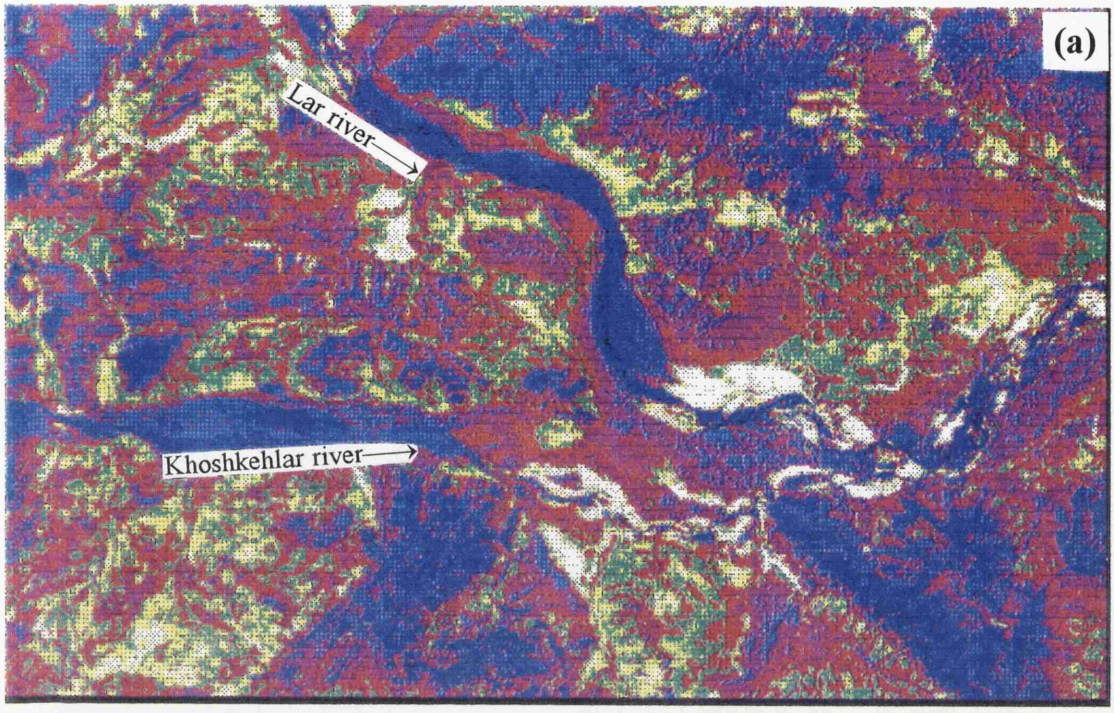

Figure 6.25-a: SPOT bands 2 & 3 ratio of the Lar upstream catchments (exposed limestone and bare soil in light blue and yellow colours, red is poor vegetation, moderate vegetation in green, white colour is high density vegetation and other colours show different types of vegetation).

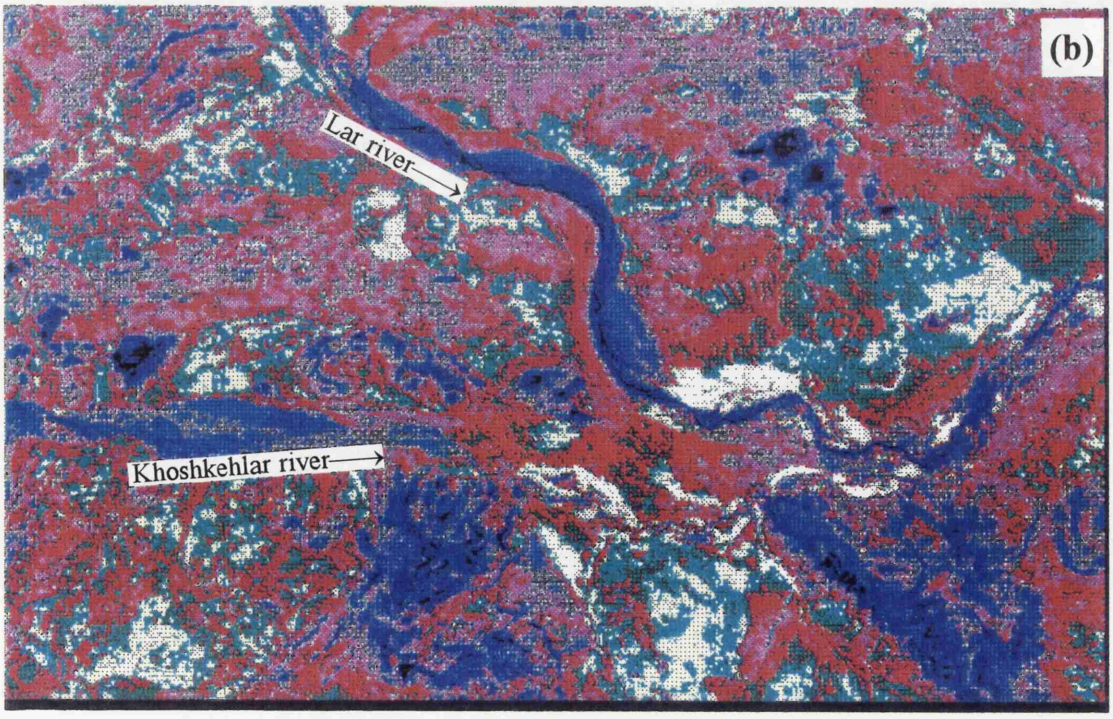

Figure 6.25-b: SPOT bands 1 & 3 ratio of the Lar upstream catchments (bare soil in light yellow and grey colours, moderate vegetation as green, white is high density fresh vegetation, blue colour shows high density vegetation and other colours show different density of vegetation).

enhance differences between the two images. Thus, band ratioing was attempted here to determine it's utility for enhancing spectral differences between land surface covers. For the discrimination by band ratioing it was essential to chose effective band combinations. Plots of all test pixels for 3 SPOT bands show that band 3 was relatively poorly correlated with both bands 1 and 2 (Figure 6.25-c). The high correlation between band 1 and 2 is apparent in Figure 6.25c-1. The band ratioing was moderately successful in delimiting dried grassland from bare soil and vegetation.

Table 6.7 summarizes the TM 3 band composite (1, 3 and 7) of the Lar basin. High density vegetation in Lar downstream (Dalichai and Sefid-Ab catchments) mostly covers terraces and flat areas in the middle parts. This area has low-moderate erosion and erodible area are mostly from scree. Although the Lar upstream possesses medium and high density vegetation in most parts especially on terraces, the erosion rate for this medium vegetation cover area is predicted to be high-moderate and very high rate for high density area, because of bank erosion in these parts. The middle and upper parts of the subbasins and unvegetated limestone heights are identified with low-moderate erosion.

Table 6.8 shows the results of TM 3 band composite in maximum likelihood classification, on which high-moderate surface erosion on bare soil and poorly vegetated areas, especially in southern side of Khoshkehlar, are identified as well as low surface erosion rates related to the Lar downstream with high density vegetation.

Table 6.9 summarizes from SPOT 3 band composite of the Lar upstream which showing high rates of surface erosion on scree slopes and gullied areas with low vegetation cover, and mostly including the Lar northern side and southern side of Khoshkehlar. Low-moderate erosion is predicted on exposed limestone with poor or unvegetated area especially in Lar upstream, Sefid-Ab and some parts of Khoshkehlar. High vegetation density which covers most southern parts and downstream of the Lar and Khoshkehlar, has low -moderate surface erosion.

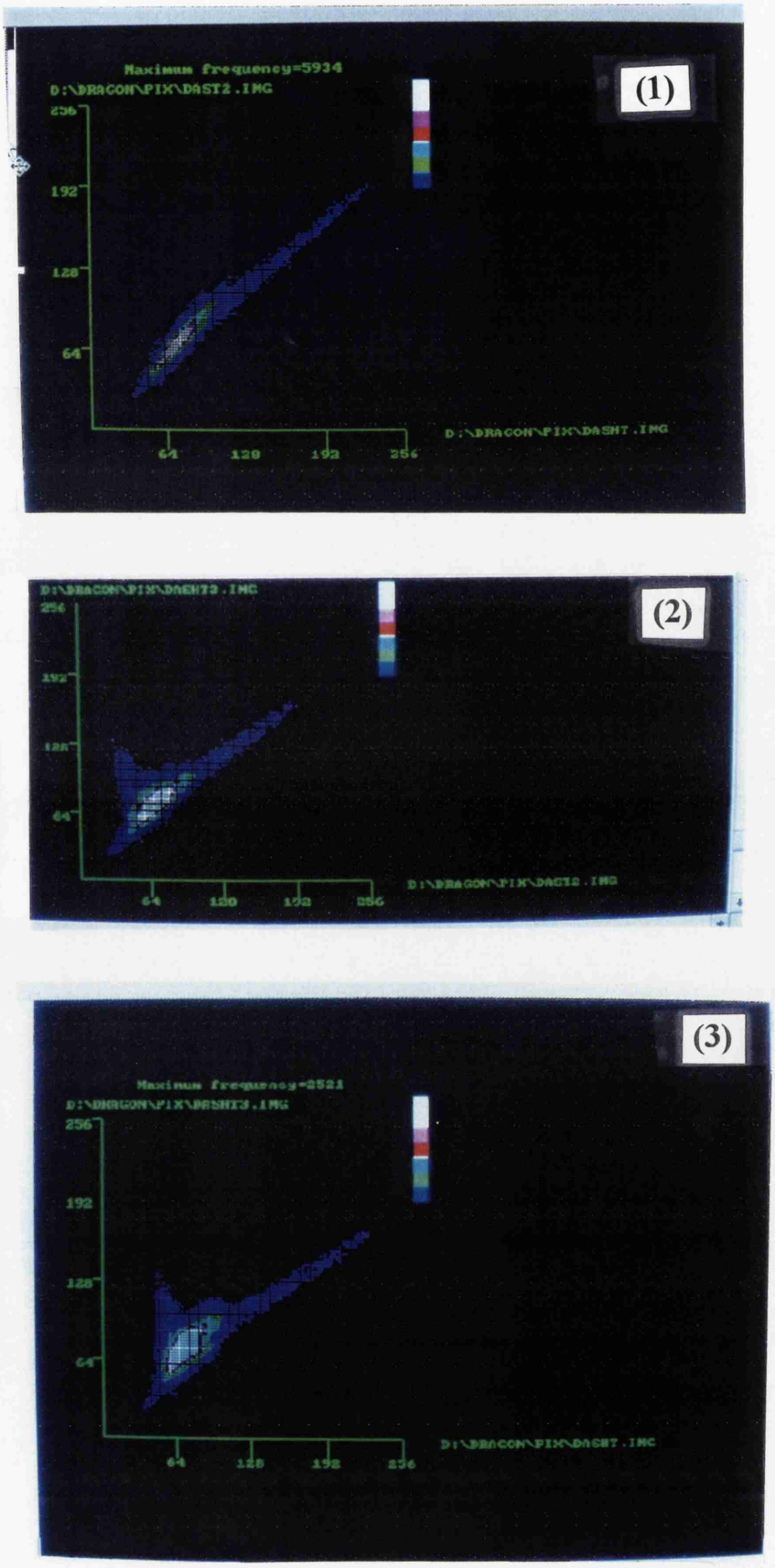

Figure 6.25-C: Scatter plot of SPOT bands 1/2 (1); 2/3 (2); and 1/3 (3) at Kamardasht Lar (the light correlation is between bands 1 and 2 and the lower correlations are between bands 1 and 2, as well as 2 and 3).

Table 6.9: SPOT 3BA, land surface and inferred level of erosion in Lar upstream.

Spectral class colour code	Land cover	Inferred erosion
dark blue	high vegetation density	low - moderate
light blue	medium veg. cover	high - moderate
light pink	limestone heights (poor)	low - moderate
light green	low cover (recent sed.)	high - very high

The distribution of erosion was mapped using the above different techniques with the support of ancillary data e.g. KFA-1000, aerial photographs and field checking in the Lar Basin (Figure 6.26). The map shows that severe erosion mostly occurs in the sub-catchments upstream whithin the Dalichai, Sefid-Ab, Ghushkhaneh Darreh, Pahnak Darreh and Chehelbarreh sub-catchments. These areas are mostly covered by gully features however they are very prone to surface erosion. Slight erosion is also irregularly distributed over the study area, especially within the high limestone relief between Lar and Khoshkehlar, Alarm and Lar doenstream Kuh e Chahelcheshmeh, Dombak kuh, Kuh e Namakkusar, Zardepashteh kuh and on the Damavand lava flows in the west. Finally, moderate erosion covers the upstream areas of much of the Lar catchment where there is only moderate protection by vegetation cover.

6.6 LAND COVER PATTERN ASSESSMENT

As described in chapter three, sequential aerial photos of the Lar basin (1955, 1970, 1983, 1990), KFA-1000 (1990), SPOT MSS (1987) and Landsat (MSS, TM) 1972, were used to identify different types of reflection characteristics. Characteristic tonal types on these images are mainly associated with the density and extent of surface vegetation cover and differences in surface soil and lithology.

For each class of the classified images at least 75 sample areas were selected in the field to cover different parts of the basin. The selected samples were then compared using aerial photographs and identified by different tones as differences in vegetation cover. Stereoscopic aerial photographs and KFA-1000 images were then used to complete (a) a base map at 1:300 000 scale to show changes between 1945 to 1995; (b) vegetation changes and other major surface changes like sinkhole, landslide and rock fall, after

identification by different methods (SPOT, Landsat TM, aerial photographs, KFA-1000 and field check) transferred to the base map, and (c) different vegetation densities identified by differences in colour on images and tones on aerial photographs. From each of these categories an estimate of vegetation density percent was made.

The highest density of vegetation (over 80%) appear as dark tones (mostly herb types) and distributed on gentle slopes or terraces. The area calculated on different images is estimated to cover 6% of the basin area. On the stereo KFA-1000 the vegetation shows as a green colour (Figure 6.9). In some parts of the basin a very high density of cover up to a 100% occurred (see folded veg. map no.2, follow legend 1.6 and Figure 4.8-b Photographs). Differences of vegetation density in the Lar Basin are related to lithologic conditions as described earlier in this chapter. Bare soil with no vegetation appears as white and is estimated to cover about 13% of the Lar basin, identified on the vegetation map as rocky land. This type of surface covers most of Dalichai upstream and some parts of the Lar on the southern side of the present Lake (R. on folded veg. map no.2 and Figure 6.9 'white colour'). Bare ground is also found high in the mountains with shallow soils and rock outcrops, on the soft limestone-sandstone formation and on steep slope gradients of greater than 65% (see folded maps no.1 and 3).

The geomorphology of the basin shows a clear relationship with other land factors which are covered by eight main types of vegetation, four main types of lithology and six types of slope gradient (see folded veg.no.2 , litho.no.3 and slope no.1 maps). Changes in these types for the fifty years of data can be measured from different maps, aerial photographs and satellite remote sensing data. The effect of the lava dammed Lake, is reflected in the surface cover changes of the study area at the Lar upstream, Sefid-Ab and Dalichai.

Moderately dark tones on the images were identified as relatively less smooth than dark tones both on aerial photographs and KFA-1000. This type of tonal category moderately dark has seriously suffered from animal grazing and the density of vegetation ranges from 20 to 80% estimated from different images to cover about 41% of the study area. These areas mostly occur in the highland flats in the Sefid-Ab, Lar and Dalichai upstream (see Chapter 4, vegetation section for more detail). The vegetation type is

mostly shrub-perennial and grass-perennial forbs and soil types, and include dissected old flats (terraces) which are tending to erode (see folded map no.3).

Moderately light tones have 30 to 40% vegetation cover density. The tonal degradation of this category was mainly due to it's poor vegetation cover. In terms of aerial photographs and digital images, this type is shrub and perennial grasses with as area of 22% and it's density, depending on different ecological factors, is changeable.

Light tones are characteristic of areas of bare ground with a very sparse, widely scattered vegetation cover of 5 to 10%. This type has been damaged severely by grazing, which as described briefly earlier is creating erosion problems in small areas. It covers mostly flat surfaces, about 5% of the basin, and is very poor grassland including shrub-forbs. White tones are associated with bare soil and exposed soil. This area has no vegetation or very poor plants, and is 13% of the basin area.

The overal tonal sequences in all the aerial photos of the Lar basin however didn't clearly develop a systematic pattern of tones, because within the dark tone there was significant irregularity which has resulted in the break of tonal texture.

Apart from the dark and white tones, tonal variations were very inconsistent and irregularly merged at varying levels between the other categories. It appears clear that since 1945, changes in surface cover of the Lar basin have occurred which are unprecedented in scale, especially in their impacts on the base soil, some geomorphological features and vegetation. Construction of the artificial Lar Dam (1974-1980) also created some unexpected morphological changes in both the land surface and subsurface characteristics, especially karst features, which are described in Chapter 5 and earlier in the present chapter (Figures 6.27-a and b).

Comparing Figure 6.27-a (1945) with Figure 6.27-b (1995) shows the worst affected areas for land surface changes relate to vegetation changes, landslide and sinkholes. In the Dalichai, Sefid-Ab and the Lar sub-catchments, vegetation density was mostly decreased from very high, moderate and high density to moderate or low-moderate density. The second major change relates to landslide activity can be related to the vegetation changes inaddition to the effect of tectonic activity in this area. Three

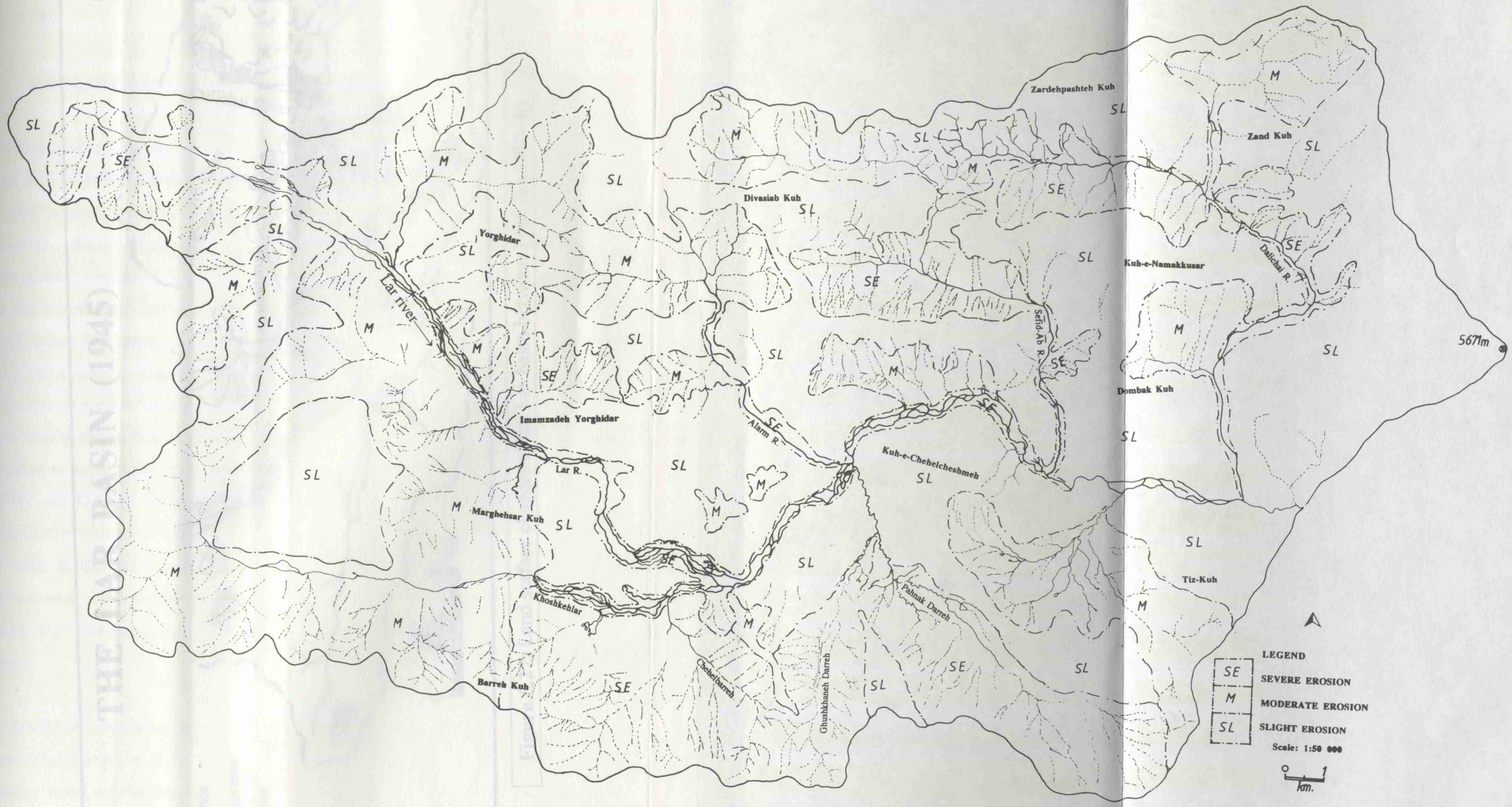

Figure 6.26: Distribution of Erosion in the Lar Basin.

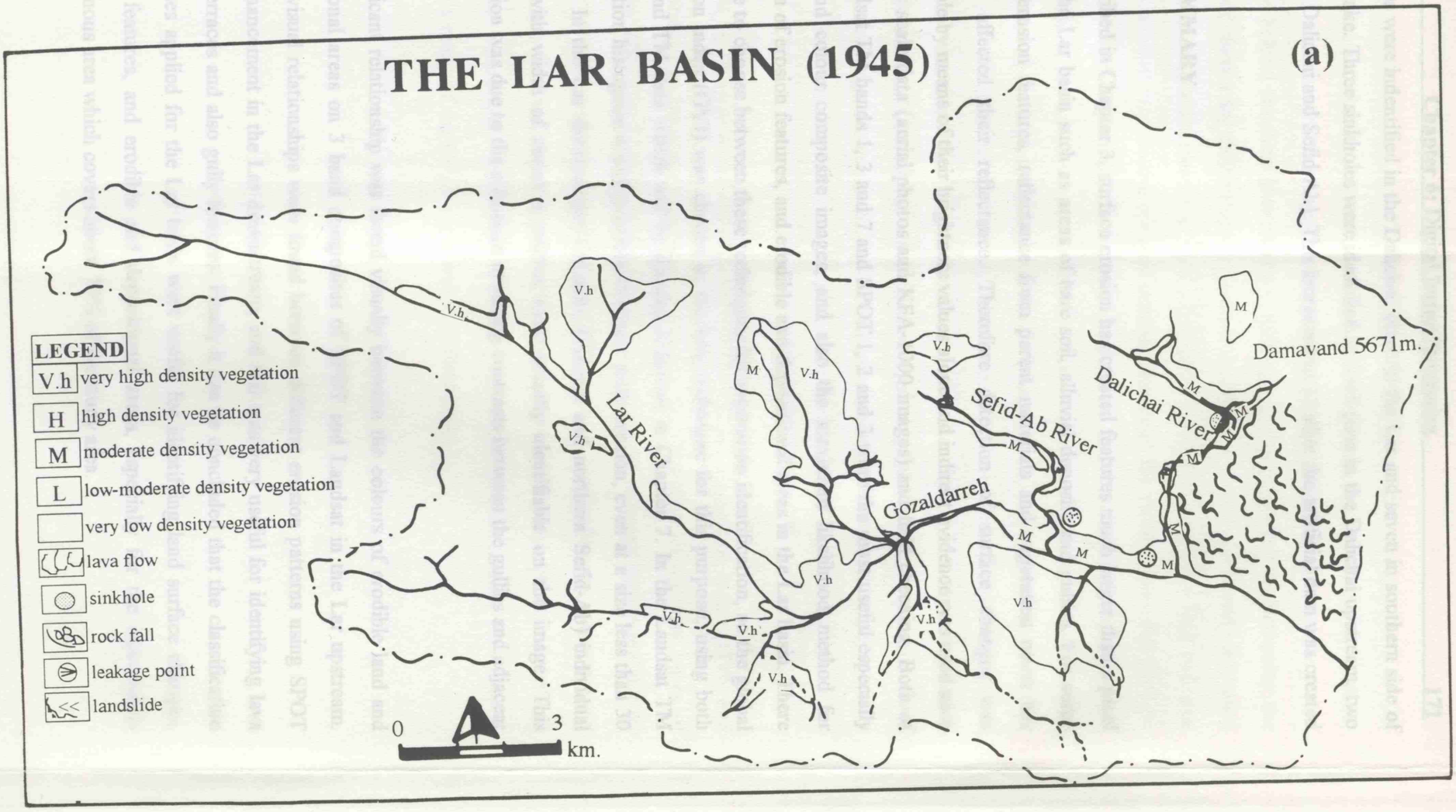

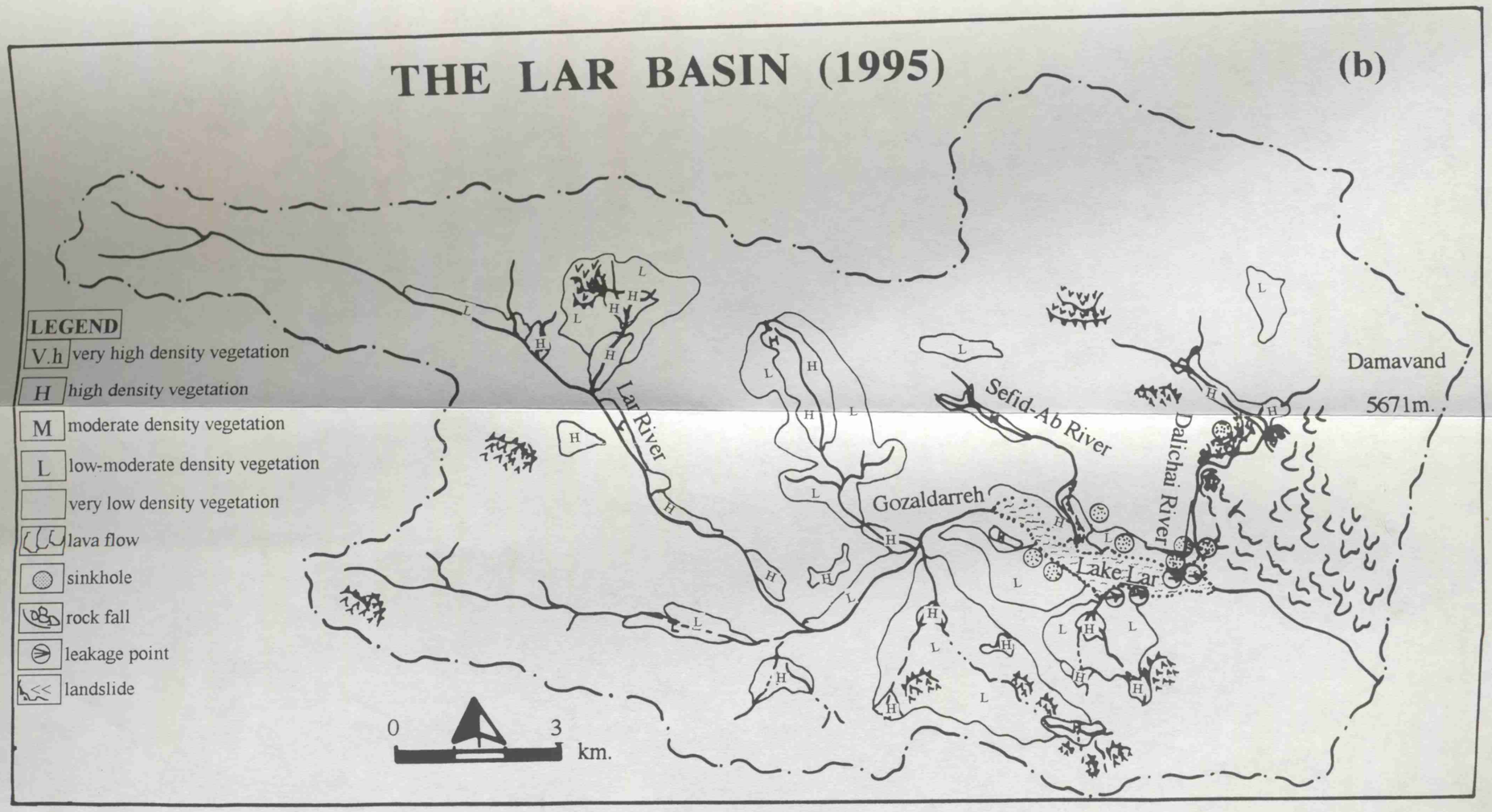

Figure 6.27: Land surface changes in the Lar basin between 1945 (a)-1995 (b).

landslides were indentified in the Dalichai, three in the Lar and seven in southern side of the Lar lake. Three sinkholes were identified in 1945 (one in the Dalichai upstream, two between Dalichai and Sefid-Ab). This increased to 12 after the artificial dam was created in 1955.

6. 7 SUMMARY

As described in Chapter 3, surface erosion has created features much larger than a pixel size in the Lar basin such as areas of bare soil, alluvial deposits and gullies. For some smaller erosion features, reflectance from parent materials and vegetation cover has severely affected their reflectance. Therefore detection of surface changes was impossible by means of their brightness values alone and indirect evidence was used such as larger scale data (aerial photos and KFA-1000 images) and field checking. Both of the Landsat TM bands 1, 3 and 7 and SPOT 1, 2 and 3 were the most useful especially in 3 band colour composite images, and also the maximum likelihood method for detection of erosion features, and erodible and depositional areas in the Lar basin. There was little to choose between these techniques for vegetation identification, so the global vegetation index (GVI) was chosen as the best technique for this purpose, using both SPOT and TM data which will be discussed further in Chapter 7. In the Landsat TM equalization histogram it was possible to detect gully erosion, even at a size less than 30 m wide. In the Lar downstream (western Dalichai and northern Sefid-Ab) individual gullies with width of about 6 metres were visually identifiable on the image. This recognition was due to the existence of strong contrasts between the gullies and adjacent areas.

A significant relationship was found visually between the colours of erodible land and depositional areas on 3 band composites of SPOT and Landsat in the Lar upstream. Similar visual relationships were found between different erosion patterns using SPOT edge enhancement in the Lar downstream, and this was very useful for identifying lava flows, terraces and also gully features. Finally it can be concluded that the classification techniques applied for the Lar basin were useful for identifying land surface changes, erosion features, and erodible and depositional areas, especially for the inaccessible mountainous area which covers about 70% of the study area.

It can be concluded that identification of the geomorphological features such as the terrace areas and the area subjected to sinkholes is difficult by means of classification. Initially it was thought that using ancillary data e.g. KFA-1000 and aerial photographs would be helpful for their identification. Although it was supported by increasing the number of classes for discriminating between landcovers, in fact this merely increased the number of spectral classes in each information class. For example a bare soil area may be classified into several spectral classes. However, the results show that high to moderate density vegetation are mostly related to the Dalichai, Sefid-Ab upstream and the area along the Lar river characterised by flat areas (mostly on terraces in the Lar basin). Most of the high relief areas in the Dalichai western and northern parts, Sefid-Ab, Lar and Khoshkehlar upstream are characterised by low density vegetation where topographic conditions are suitable, such as on terrace areas, much higer vegetation density is achieved. Initially it was expected that very low density vegetation areas would possess high erosion rates. In fact this area is also characterised by high erosion because of bank erosion of terrace along the Lar river, in spite of high density vegetation cover.

Generally, in all regions the classification and the Global Vegetation Index (GVI) had similar ability in identifying the land cover, but for extraction of different types of vegetation, GVI is preferable. Finally with a proper system of image processing and up to date ancillary data, supervised classification is preferable to unsupervised classification for landcover indentification in the mountainous conditions of the Lar basin. For mountainous basin like Lar, the GVI method provides more flexibility in mapping a range of vegetation types and is preferred here.

CHAPTER 7: DISCUSSION

INTRODUCTION

This chapter examines how the morphological characteristics of the Lar Dam Basin can be related to sediment supply by using the results of the remote sensing data together with geomorphological changes and landform processes identified in the study area over 50 years. Field surveys and the results of sample analysis described in chapters 4, 5 and 6 are linked together in order to achieve these aims.

The morphological changes and sedimentary history will be linked to the physical conditions of the Lar basin, in an attempt to understand the distribution of the sediment sources, the factors important in affecting erosion in different parts of the basin and the distribution of the sediments. This chapter first discusses the morphological changes and sedimentary history together with land cover analysis using Landsat TM, SPOT, KFA-1000 and aerial photographs. Erosion sources in the basin are then discussed and related to depositional zones. Finally a critique of the research methods used is presented.

7.1 MORPHOLOGICAL CHANGES AND SEDIMENTARY HISTORY IN THE LAR BASIN

The initial presentation of the sedimentology of the Lar Basin in this study represents an important stage towards an interpretation of its morphological evolution. The morphological changes of the study area hinge on two stages: firstly identification of the extent of sedimentation of the former Lake Lar, and; secondly the distribution of bare surfaces of present day erosion.

7.1.1 Late Quaternary Sedimentary History of the Study Area

The Central Alborz Range is an area of high topography consisting of marine sedimentary rocks of Paleozoic and Mesozoic ages and Tertiary rocks of volcanic origin belonging to the upper part of the early Pliocene, although movements were renewed in the late Pliocene or early Pleistocene (Rieben, 1955). The blocking of streams in the

study area by Late Quaternary lava flows from Damavand volcano had an important geomorphological effect on the area and an extensive lake was formed upstream of a lava blockage. At its maximum extent, the lake stretched 25 kilometres upstream of the dam, and within it a maximum thickness of over 600 metres of sedimentary and volcanic detritus accumulated before the dam was breached. Subsequently, rivers incised into fluvial and lake sediments to produce a prominent set of terraces.

If the geochronological evidence is accurate, then Lake Lar was in existence during the second period of ice advance during the Weichselian glaciation. Although the ice caps do not appear to have covered the location of the Lake at this time, Bobek (1963) suggested that the snow line was lowered by about 700-800 metres from its present position of 4000 metres above sea level. Climatic changes must presumably have recurred during the Weichselian glaciation in order to produce such an increase in size of the ice caps. It is important therefore to investigate the nature of any such climatic changes which occurred in Iran during late Pleistocene times and to assess their possible effects on the balance of water flowing into and out of the Lake.

With regard to changes in precipitation, the evidence appears somewhat conflicting. Raikes (1967) suggested that "there is some evidence that rainfall amounts in northern Mediterranean latitudes were greater during the ice ages (p.134)". Lamb (1961), has also suggested "during the ice age rainfall was presumably increased for some time in the lower middle latitudes and sub tropics, which were affected by most travelling depressions associated with the upper Westerlies (p.34)".

Bobek (1963) and Vita-Finzi (1969) investigated accumulated sediment in Iran during Lateglacial and Recent times and concluded that the changes in sedimentation which occurred could not adequately be explained by a simple increase in the mean precipitation. During the Wieslian glaciation in Iran the mean temperature was about 4 - 5 °C lower than at present and the lower limit of solifluction was 700 metres lower, at about 2300 metres (Bobek, 1963). Therefore plentiful slope material was available to overload the rivers and to force aggradation especially in the upper reaches. However the way in which this process would have helped to build up such gravel terraces in the mountain valleys is not clear.

However, archaeological studies by Braidwood (1963) in the Zagros Mountains stated that there appeared to have been "no great climatic changes from the approximate level of the Mousterian (c 40 000 B.C.)" (p.252) onwards. The consensus of opinion would therefore appear to be that during the existence of Lake Lar, there was at best a small increase in precipitation in the area, although losses from the lake due to evaporation were probably somewhat lower than under present day conditions due to the lower mean temperatures. Hence the total amount of water available for impounding was probably slightly greater than at present. Having established that the climatic conditions during the Lake were only slightly different to those of today, and that significant fluctuations probably did not occur, it is necessary to review again the possible mechanisms which could have led to the drainage of the Lake to produce the intermediate gravel beds and also the final drainage of the basin.

It seems possible that leakage of water from Lake Lar may have occurred at the margins of the basin, through the limestone and lava. However, the fact that the Lake existed at all must indicate that, for at least some time in the past, leakage at the lake margins was insufficient for complete drainage. The prime question is however, whether this leakage could at any time have increased to the extent of draining the Lake and allowing the deposition of the gravel beds in high energy flows.

It is difficult to imagine any process by which the leakage could vary in a periodic manner in order to produce, alternate periods of impounding and drainage in the Lake. Therefore a gradual increase in the mass permeability of the reservoir margins is a more likely process and could account for the eventual drainage of the Lake. Leakage of water through the limestone would have caused solution and a consequent increase in its mass permeability with time. Similarly leakage through the lava could have caused alteration of the rock material. This, associated with the opening up of joints in the massive lava by differential gravity compaction of the underlying sediments, would also have contributed to increased leakage of water through the materials. It is these time dependent effects which were not allowed for by Bailey et al. (1948) in his view that the creation of a dam at the Lar gorge would necessarily mean the recreation of Lake Lar.

Changes in leakage from the Lake provide a possible mechanism to explain the final drainage of the Lake, but they do not adequately explain the earlier periods of drainage.

These can best be explained by the occurrence of early lava dams of low height in the Lar valley. Impounding of water would have occurred behind such dams and the Lake basin would have gradually been infilled with sediments to the top of the dam, or alternatively the lake could have been drained either by leakage or by the dam being breached. Any of these processes would account for the deposition of an upper gravel horizon on account of higher velocity inflows from the rivers. Subsequently, renewed eruptions of Damavand would raise the dam and the process would restart. In order to consider whether these processes adequately explain the sedimentation in the area, information has been sought on the possible height and location of these intermediate dams.

The dam of basic lava at Polour appears to have had a natural spillway level at about 2260 metres, since this is the height to which sediment accumulated in the Haraz valley upstream of the dam. It is considered significant that one of the gravel beds occurs elsewhere in the Lar at an elevation of 2260 metres. It seems likely that the correspondence of levels indicates a common origin for the two sets of sediments in the Lar and Haraz valley behind a single dam of basic lava. However, it has not been possible to established similar correlations for the other gravel beds in the Lar basin.

The complete infilling of the Lar basin up to an elevation of 2700 metres behind the lava dam could also account for the overall succession of sediments and the drainage of the Lake. It has been previously discussed that an increase in leakage from the basin could also have accounted for the final drainage of the Lake. To determine which was the dominant process it is necessary to consider the form of the gorge through which the Lar river flows at present. The limestone gorge is a vertical sided feature which suggests that it originated as a collapsed cavern and hence indicates possible subsurface water flow. The remainder of the valley from the Dalichai conjunction to upstream of Polour is cut into trachyandesites and so it is unlikely that this part of the valley was created by subterranean leakage through the rocks. Overtopping of the lava dam and its consequent erosion is a more likely mechanism. If this is accepted, then it can be reasoned that the Lake Lar became completely infilled with sediments, up to an elevation in excess of 2700 metres (Figure 5.10), with waters spilling over the lava dam eroding the present valley. Leakages from the basin must have been occurring but were of minor importance, at least until the trachyandesitic material had been eroded away.

The formation of the Lar downstream channel from the Dalichai junction seems to have occurred as a series of base level reductions, each new level leading to the development of a terrace in the valley upstream. Temporary base levels appear to have been formed by such features as the top surfaces of limestone beds in the downstream section of the Lar and the upper surface of the landslide debris beneath.

One final factor which will have affected the final drainage of the Lake is movement along faults in the area. Two major faults in the Lar valley appear to have been active after the deposition of the Lar gravels, but before the creation of the Lar terraces. One of these faults has vertically displaced the gravels by about 10 metres. If these fault movements occurred whilst water was still impounded in the Lake, the effects could have been included a major surge of water. This could have had a significant impact on the creation of the present Lar valley.

Much of the discussion on the development of Lake Lar and its final drainage revolves around the age relationships between volcanic eruptions and the deposition of sediments. These ages also provide a guide to the probable climatic conditions in the area. Unfortunately the absolute dating of events is dependant on the single C^{14} dating of organic debris (38500 B.P.) reported by Allenbach (1966) who stated that due to the contamination of this material it was not possible to determine its maximum age. Extensive searches have been made to locate more C^{14} datable materials and to determine the feasibility of carrying out further datings of materials from the Lar basin. It is unfortunate therefore that virtually the only organic debris occurring in the sediments comes from the horizon already sampled and dated by Allenbach, whereas the lavas are understood to be young enough for reliable isotope dating.

It can be concluded that the history of sedimentary and morphological changes in the Lar basin provided new conditions of landsurface with different soil, vegetation and hydrological characteristics. In the former Lake area environmental conditions were such that the surface streams formed in this area were very active for lake sediment delivery. As described in Chapter 6, most of the Lar basin is inaccessible semi-arid mountains, and so any assessment of land cover, morphological changes and sediment delivery requires the use of remote sensing data.

7.2 LANDCOVER ASSESSMENT AND EROSION SOURCES

As described in Chapters 4 and 6, various land cover characteristics in the Lar basin imply different patterns of erosion. The aim of this section is to discuss how the vegetation landcover is likely to give different degrees of protection to the soil and thus to be associated with different levels of erosion. Density of vegetation, the system of root (surface distributed or deep) and seasonal variation were taken into account in assessing the different erosion pattern of various land covers. In studies of alluvial bank materials in Mississipi bluff-line streams, Thorne and Tovey (1981) found the tensile strength of rooted samples to be on average ten times that of unrooted ones. In a general sense, low erosion rates relate to areas of perennial vegetation cover with dense roots and leaves. These are also very good protectors of surfaces in the Lar basin and help prevent erosion. Poor vegetation cover on the other hand, is conducive to severe erosion. Landcover characteristics are discussed below and these imply different patterns of erosion in the Lar basin.

As described in Chapters 4 and 6, the Lar and Khoshkehlar tributaries support only relatively small areas of gentle slopes and terraces covered by high density herb type vegetation. Although such areas can be expected to be protected against surface erosion, bank erosion is very active along the river and terrace erosion is common. On the other hand, there exists about 16% of very poorly vegetated land and some 17% of the area is unvegetated. Both contribute to extensive land surface erosion in the Lar catchment. In the Khoshkehlar catchment, surface erosion is higher than in the Lar because of a high percentage of more easily eroded surfaces: 23% of the area is covered by very poor vegetation. The largest unvegetated area in the Lar basin is in the Alarm sub-basin with 24% of the area entirely unvegetated and 19% poor vegetation. It was expected that the surface erosion in this sub-basin would be higher than in the Lar and Khoshkehlar, but because of the occurance of very hard limestone surfaces, erosion is actually lower than in other sub-basins.

The largest area of very poor vegetation occurs in the Dalichai catchment where 35% is poorly vegetated and 11% of the area is covered by unvegetated volcanic rocks and limestone. In Chapter 4 the physical characteristics of the Dalichai catchment were described having the highest erodible area of all the catchments of the Lar basin mainly

due to severe surface erosion of sediments upstream and tectonic activity in the middle and downstream section.

25% of the Sefid-Ab sub-basin has very poor vegetation and about 18% is unvegetated and so the basin is likely to have the next highest erosion rate after Dalichai. Weathering influences on limestone formations have formed many screes upstream and excess surface water easily delivers this material downstream. In the southern part of the Lake Lar basin, the two sub-basins of Imampahnak and Siahpalas are mostly covered by medium and high density vegetation. In Imampahnak 12% of the catchment area is measured as unvegetated and in Siahpalas only 1.3% of the catchment area is unvegetated: the lowest of all catchments in the Lar basin. Very gentle river gradients and good vegetation cover protect these catchments against surface erosion which falls to a minimum (Table 7.1 and folded veg. map no.2).

Table 7.1: Landcover characteristics in the Lar basin.

Catchment	Very poor vegetation (%)	Unvegetated area (%)	Medium-high density vegetation (%)
Lar	16	17	67
Khoshkehlar	23	4	73
Alarm	19	24	57
Sefid-Ab	25	18	57
Imampahnak	0	13	87
Siahpalas	0	1.3	99
Dalichai	36	11	54
Total	22	13	65

In the Lar basin as a whole 65% of the area is covered with medium to high density vegetation, mostly on the terraces and flat areas along the Lar river channel, Dalichai and Sefid-Ab upstream and in southern parts of the basin at Imampahnak and Siahpalas. These areas are characterised by low rates of surface erosion. However river channels are also cut into the terrace deposits, and so bank erosion is the most important source of material in transport in the Lar basin. 22% of the area is covered with poor vegetation and the remainder is unvegetated. Differences in the rate of the surface erosion can be seen in relation to soil, altitude and hydrological (eg. precipitation and runoff) conditions. Therefore in the southern part of the Khoshkehlar, Lar upstream and northern side of the

basin, surface erosion is higher than other parts of the study area on account of very sparse vegetation, altitude and unstable surface material (see SE on soil erosion map).

As described in Chapter 4 most parts of the erodible area are characterized by ancient scree slopes, landslide deposits and alluvial fans (see Qt, Qf and Qal on geology map) especially in the upstream sections of Sefid-Ab, Dalichai, Alarm and some parts of Lar, Khoshkehlar and the southern part of the basin. Because of the generally low density vegetation cover on these unstable soils and, steep slopes, gully features are also very common in these areas (SE on soil erosion map, Figure 6.26).

It can be concluded that except for the areas of bank erosion in the downstream parts of the basin, high rates of surface erosion characterise 35% of the area because of poor and low vegetation density, unstable soil, altitude and also animal grazing. Low surface erosion rates are related to the areas with medium to high density vegetation cover on terraces and along river channels covering 65% of the basin area (Figure7.1).

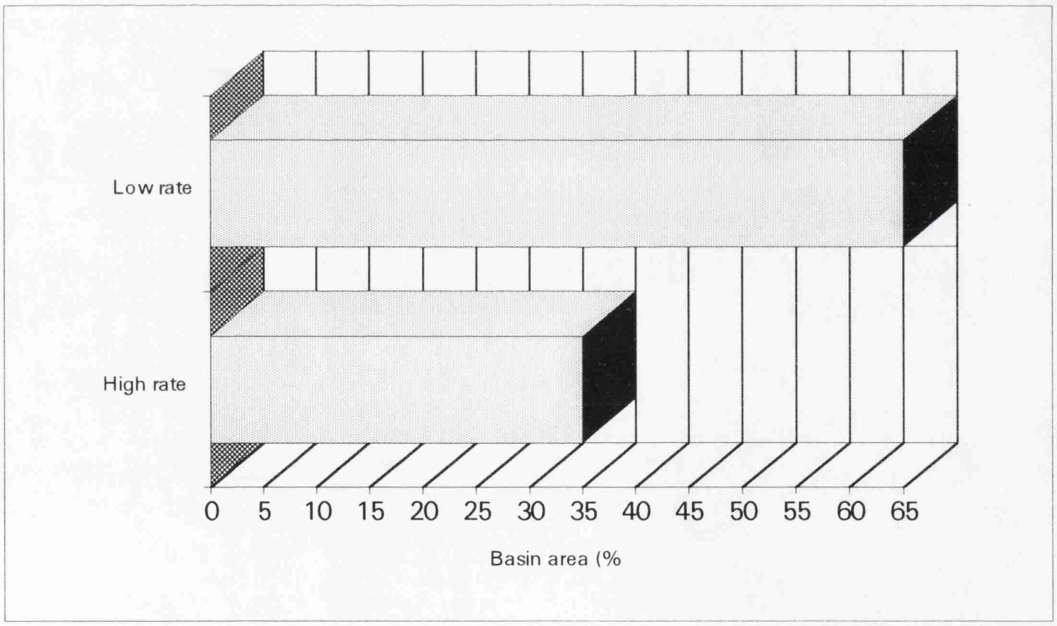

Figure 7.1: Surface erosion rate in the Lar basin (see also Fig.6.26).

7.2.1 Lithologic Characteristics and Erodibility

Lithological information is deduced from maps, field investigation and a number of parameters derived from remote sensing images such as, general geology, landforms, soil, vegetation and spectral characters. Most of these are interdependent and thus

interpretation is generally based on multiple evidence. However, even a single parameter can be helpful in specific situations. As the study area is mountainous, employment of remote sensing techniques is essential for both identification of surface characteristics and morphological changes.

Sedimentary formations are generally identified by compositional layering. The layers of different mineral assemblages possess differing physical attributes and this results in the appearance of regular and often prominent linear features on the images as a result of different spectral characteristics of compositional bands; differences in susceptibility to erosion and resulting differential erosion between hard and soft formations; differing moisture contents depending upon mineral composition and vegetation cover.

Frequently all the above features collectively lead to banding on the KFA-1000, aerial photos and satellite images and resulting linear features are long, and even-spaced. They are few in number in comparison to those produced by foliation in the metamorphic formations and constitute rather distinctive continuous ridges and valleys. This type of banding is the most diagnostic feature of sedimentary terrain.

Vegetation cover and soil depth influence erosion in almost all areas of the catchment. Subaerial erosion, for example, is influenced by soils and vegetation indirectly (e.g. through infiltration influences on mass movement of soil, or vegetation density and canopy influences on the erosivity of rainfall). Also the removal or change of vegetation can alter erosion rates. A general overview of human, vegetation and erosion is presented by Thornes (1987) and several attempts have been made to include vegetation in mathematical models of soil erosion (Thornes, 1985; Kirkby and Neale, 1987).

This type of approach involves tracing specific events of vegetation changes and documenting their effects on hillslopes or in channel systems. Alternatively, observed responses are sometimes traced back to vegetation changes. There is an enormous literature ranging from the prehistoric clearances and war-time destruction to delibrate removal of natural vegetation for agricultural purposes. For example, detailed investigation of alluvial chronologies in northern Europe, heavily supplemented by radiocarbon dates, can indicate the relationships between small land use changes and stream channel response (Starkel, 1977). In the English Lake District, vegetation

changes and erosional features using aerial photographs were mapped successfully (Anderson and Taillis, 1981). Whitlow (1988), working in Zimbabwe, showed that precipitation, soil, slopes and vegetation cover is affected by human factors. Although human population density is emphasised as a major factor in Zimbabwe on soil erosion, it can be considered as the main determinant of vegetation changes and potential erosion.

In the Lar basin three generalised soil, vegetation and erosion maps have been produced by the interpretation of aerial photographs, KFA-1000 and classified images (Figure 7.2-a,b,c). The relationship between soil, vegetation cover and other physical parameters are discussed later in this chapter.

7. 2.1.1 Sandstone Surfaces

Sandstone surfaces usually form topographically prominent features, and drainage density is low to medium in the upper Lar due to the high porosity and permeability of surfaces and steep slopes. The soil cover is variable and on some impure sandstone areas, thicker soil cover has developed. Sandstone mostly supports high density vegetation due to relatively high porosity and good soil cover: in some areas around the Lar stream it supports bushes, whereas the adjoining clay shales support only grass. However, on the higher and steeper land the pure sandstone is barren of vegetation. The spectral characteristics of this formation on KFA-1000 images and grey SPOT images show that the slopes of pure sandstone are generally light-toned, but the overall spectral response over the formation can be highly variable, depending upon the presence of other minerals, weathered soil cover, vegetation and structural orientation.

7.2.1.2 Shale Surfaces

Shales are mostly incompetent, easily erodible and tend to form hollows and valleys in the slightly wetter area to the south of the present lake. In some areas e.g Marghehsar-huh, Pahnak-darreh and upper parts of the Dalichai and Sefid-Ab, there are gently rounded hills, and erosion which in the northern part of basin is more intense. Drainage density is also high and generally well developed with dendritic drainage pattern; gullies tend to be long and gently sloping with V-shaped cross sections. In loose indurated

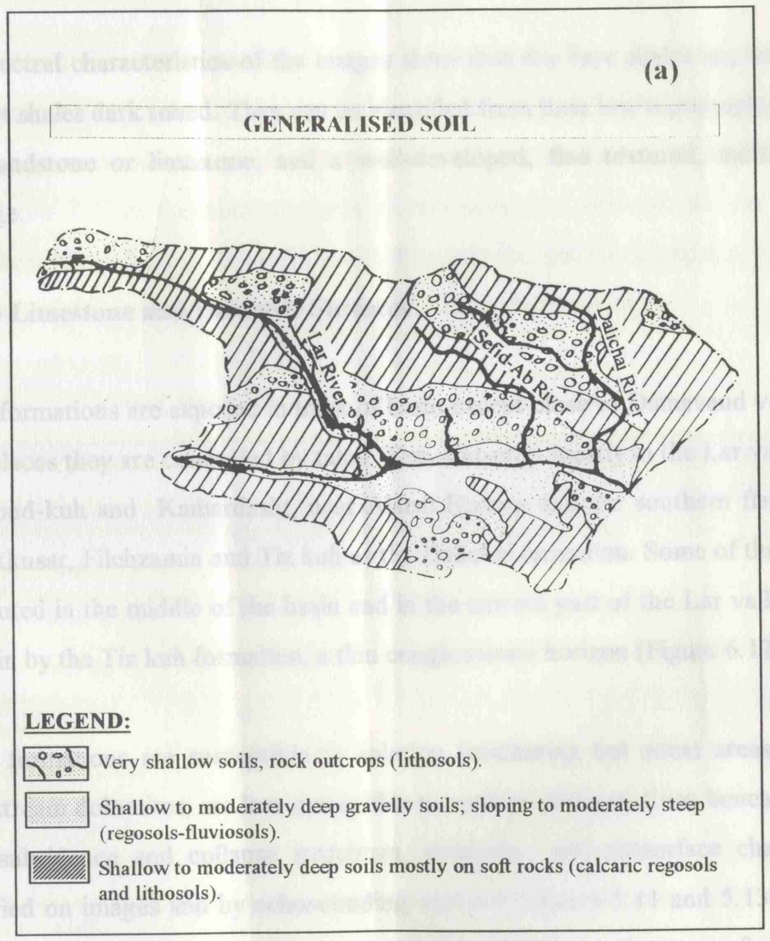

(after Ministry of Agriculture, Iran 1978).

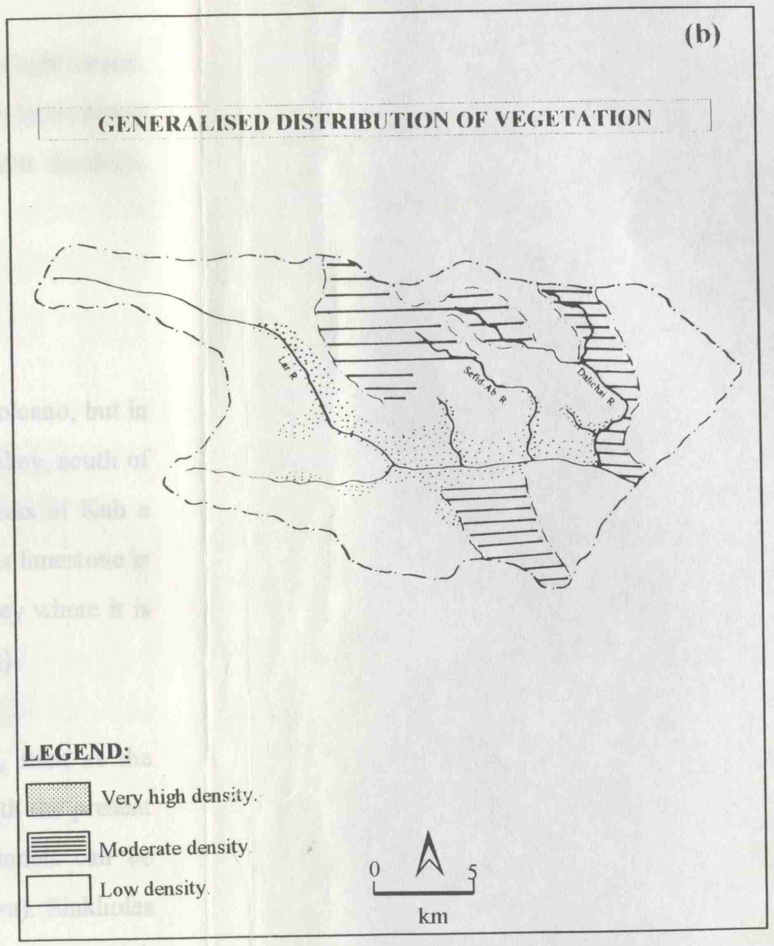

(this map is generalised from Figure 6.27 and folded veg. Map no.2).

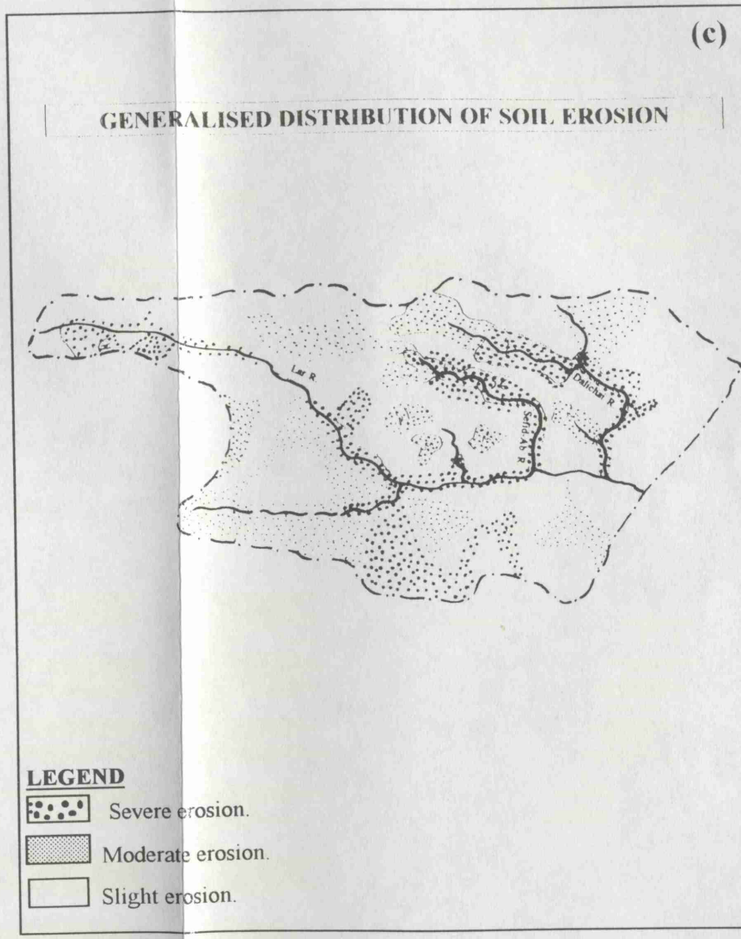

(this map is generalised from Figure 6.26).

Figure 7.2: Generalised Soil (a), Vegetation (b) and Erosion (c) Maps of the Lar Basin.

clayey sediments, the gullies have steeper cross sections and have formed badland topography. The soil cover is mostly thick and dry upstream but moisture rich in the downstream areas with a high density vegetation cover. Clay shales generally have poor cover due to their impervious nature and low water content, and in some areas are nearly barren of vegetation such as the Sefid-Ab upstream section (Figure 6.12).

The spectral characteristics of the images show that dry bare shales appear light toned, and wet shales dark toned. They can be identified from their low topography, intercalated with sandstone or limestone, and a well-developed, fine textured, uniform dendritic drainage.

7.2.1.3 Limestone and Dolomite Surfaces

These formations are exposed in most of basin except close to Damavand volcano, but in most places they are concealed by talus. They out-crop mostly in the Lar valley, south of Karbabud-kuh and Kamardasht, near Alarm Bozorg and the southern flanks of Kuh e Namakkusar, Filehzamin and Tiz kuh as the Dalichai formation. Some of this limestone is distributed in the middle of the basin and in the eastern part of the Lar valley where it is overlain by the Tiz kuh formation, a thin conglomerate horizon (Figure 6.12).

These formations are susceptible to solution weathering but some areas, such as the downstream dolomites, are less susceptible to surface changes. Even beneath the present lake, subsidence and collapse structures, sinkholes, and subsurface channels can be identified on images and by echosounding surveys (Figures 5.11 and 5.13-a). Sinkholes in the lacustrine terraces can be seen, on the top of the limestone formation which continues under the Lake (Figure 5.11). Due to action by surface and subsurface waters these features are often elongated in the direction of prominent jointing. These limestone areas are also marked by low drainage density throughout the Lar basin, and due to low water availability, in some areas the valleys tend to be gorge-like (Figure 6.12). The images show that light coloured calcareous soils often develop on the carbonates. However, as a result of the removal of carbonates in solution, same areas are red in colour as a result of the insoluble residues such as limonite and clays.

Vegetation is sparse on the karst landforms and is variable depending upon weathering and micro climatic conditions. On the images the bare slopes of this formation mostly appear light toned, with low drainage density. The carbonate areas on the images appear similar to sandstones in some dry areas, the lithological distinction between limestone and sandstone requiring field checks.

As discussed above, the results of remote sensing techniques show that lithological and landcover characteristics have contributed to the patterns of erosion in the Lar basin. Thus, gully erosion is mostly found on areas of very shallow soils with rock outcrops (see Figure 7.2) in the northern parts of the basin and also on calcaric regosols and lithosols in Chahelbarreh, Ghooshkhaneh, Khoshkehlar and Lar upstream; all identified as areas of gullying and severe erosion (Table 7.2 and Figure 6.26).

Table 7.2 : Potential surface erosion in the Lar basin.

Catchment	Poor or unvegetated area (%)	Gully area (%)	Erosional soil included gully area (%)	Erosional condition
Lar	33	36	46	M
Khoshkehlar	27	38	51	M
Alarm	43	29	58	M
Sefid-Ab	43	39	49	M
Imampahnak	13	28	23	SL
Siahpalas	1.3	11	19	SL
Dalichai	47	41	68	SE
Total	207.3	222	314	

(**SE**=severe erosion, **M**=Moderate erosion, and **SL**=slight erosion).

The distribution of soil types closely matches the distribution of depositional areas, such as terraces, valley bottoms etc. Therefore, more erodible soil characterise the steeper and more poorly vegetated surfaces (Figure 7.2-a). Most parts of the catchment upstream contain soft rocks with shallow easily erodible soils. These are mostly areas of poor vegetation or are unvegetated (see Figure 7.2-b) exposed limestone and steep slopes. The second major type of soil dominates the middle area (between Lar and Sefid-Ab) and Dalichai western side. Because of weathering and the largely unvegetated nature of this type of soil, gully features are very common, especially in Dalichai upstream and the area

between Lar and Sefid-Ab. Finally, the third type of soil is mostly limited to flat and terraced areas, with moderately steep slopes and high density vegetation. However, because of fluvial activity, bank erosion is active and important.

7.3 THE LAR BASIN EROSION SOURCES AND PATTERNS

The study area is mostly mountainous with a thin soil which covers the basin between 2400 and 5600 metres. Many of the valleys are occupied by ancient alluvial deposits, and for most part the surface waters flow on sedimentary soil formations, except in the eastern side of Dalichai where volcanic formations occur. Sparse vegetation and slope failure also influences the distribution of erosion in the basin.

Land cover changes, are especially important in influencing erosion, transportation and deposition of sediment. In order to evaluate the separability of the different surface cover types found in the Lar dam basin, their surface spectral characteristics were classified using SPOT channels 1-3, Landsat TM and KFA-1000. The technique provided an objective means for assessment of the spectral class discrimination performance of the multispectral bands. The mathematical objective of this technique is to weight and linearly combine a set of discriminating variables (the spectral bands) in a way that a set of a priori established groups are forced to be as statistically distinct as possible (Klecka 1975).

Land cover information in the study area is identified from a number of observations using the images as follows: the general morphological setting; the drainage network; the soil, vegetation and spectral characteristics. Some of these parameters are interdependent and so interpretation is generally based on multiple converging evidence. However, single parameters are often diagnostic in specific situations. The spectral response is highly variable and may be drastically different between weathered and fresh surfaces. Therefore spectral enhancement, followed by visual interpretation is generally preferred for general lithological discrimination purposes as compared to automatic classification approaches (Siegal and Abrams 1976; Abrams and Siegal 1980).

There are two major sources of erosional material in the Lar Basin; erosion from the original surfaces of limestone and volcanic rock formations (limited) and erosion of the former Lake deposits (extensive, because of easy erodibility and delivery downstream).

The principal mechanism of erosion is the action of surface water on the unvegetated surfaces. Common in semi-arid areas, these include: rainsplash, sheet wash, rills, gullies, stream erosion, sub-surface flow and mass movements. In relation to the different physical conditions which were described in lithology and vegetation sections in chapters 4 and 5 (see folded maps no. 1-4), Figure 6.26 shows a three way classification of soil erosion in the Lar basin discussed below catchment by catchment. This map shows that severe erosion mostly occurs in terraces and gullies, moderate erosion is mostly associated with medium vegetation cover and slight erosion is related to exposed hard limestones and volcanic rocks as well as areas of high density vegetation.

7.3.1 Surface Erosion

Rainsplash erosion is the first and most important mechanism of detachment, but as described in Chapter 4 precipitation in the Lar Basin is mostly snow, so its role is limited except in some small parts of the Lar, Khoshkehlar and Dalichai upstream. These parts of the basin also possess poor vegetation cover, steep slopes and erodable Quaternary sediments. Downstream of these sub-catchments, coarser particles are resistant to detachment because of their weight, and clay particles also are resistant because the raindrop energy has to overcome the adhesive or chemical bonding forces which link the minerals comprising the clay particles. This means that soils with high percentages of particles within the most vulnerable range, for example silt loams, loams, fine sands and sandy loams in the southern and eastern parts of the basin are the most detachable. Selective removal of the soil particles by rainsplash can cause variations in soil texture downslope. Since splash erosion acts uniformly over the land surface, its effects in the Lar basin are seen only in the area mentioned above, where stones or vegetation roots selectively protect the underlying soil and splash pedestals or soil pillars are formed which frequently indicate the severity of erosion. However, on the upper parts of hillslopes in the study area especially on convexities, splash transport is the dominant erosion process (Table 7.3 and Figure 6.26; see also folded maps no.1, 2 and Figure 5.16 KFA-1000 image).

Table 7.3: The Lar basin erosion sources and potential.

Catchment Area	Type of Erosion						
	Rainsplash	Sheet	Rill	Gully	Subsurface	Bank	Mass
Lar	M	M	M	SE	-	SE	M
Khoshkehlar	SE	M	M	SE	-	SE	M
Alarm	M	SL	M	M	-	M	M
Sefid-Ab	M	M	M	SE	SL	M	SE
Imampahnak	M	M	M	SL	M	SL	SE
Siahpalas	M	S	M	M	M	SL	M
Dalichai	M	M	M	SE	M	M	SE

(**SE**= severe erosion, **M**= Moderate erosion, and **SL**= slight erosion; this Table produced from Figure 6.26 which was based upon aerial photographs. The potential for erosion is estimated and related to erosion pattern in each subcatchment area).

Sheet or surface erosion removes of a thin layer of soil by the overland flow of water, and can be seen the middle area of the Lar and Khoshkehlar catchments. Production of this erosion in the Lar Basin depends on topography, lithology and vegetation cover. In field checks this was seen in Sefid-Ab, Dalichai upstream and the Lar downstream. Evidence of this kind of erosion in the Lar basin is related to areas of vegetation where the root system is exposed, indicating that the soils in large areas have been washed away. Since the particle size has a profound effect on erosion, sheet erosion occurs in primarily fine grained sediment, since prechannel flow seldom exceeds 0.6 or 0.9 m/sec, and is capable of transporting only the finer grains detached by raindrop impact. Ellison (1945) reported that of the sediment removed by prechannel flow from a silt loam in Ohio, 95% were silt and clay fractions (grain sizes of less than 0.05mm). Only 75% of the grains in the original soil were finer than 0.54mm. Stall et al (1949) present basic data on the grain size distribution of watershed soil and reservoir deposits, which further illustrate the process of selective erosion. The principal watershed soil above Spring Lake, Illinois, contains particles ranging from 70-80% silt size particles and 15-23% clay size particles. The bulk of the sediment deposited in the reservoir averages 50% silt and 45% clay. Similar results obtained from the Lar basin are described in Figures 5.6, 5.7 and show from 60 to 70% fine particle size for the Lake Lar reservoir, and fine particles representing from 50 to 60% at Cheshmehkhooni, Gozaldarreh and Chashmehkhooni (Figure 5.19; see also Figure 3.14 for the area location). The primary source of fine grain

sediment transported to the Lake Lar is likely to be sheet erosion in the Lar basin. This kind of erosion is less important than splash erosion in the study area, but it seems to be more significant in the transportation of particles. Similar results were produced by Disfani (1989) for the Sefid-Rud basin, Iran, a basin with very similar physical conditions to the Lar basin (Table 7.3).

It is widely accepted that rills are initiated at a critical distance downslope where overland flow becomes channelled resulting in scouring of small channels where water concentrates as it flows downslope. The Lar, Sefid-Ab and Dalichai upstream are all characterised by flows of water which erode small discontinous, ephemeral, linear and shallow (Morgan, 1986), channels or rills (see Figure 5.16). The transportation potential of the soil by rills in the Lar Basin is however much greater than that by sheet erosion, because a rill removes and transports both its own product and the particles derived from rainsplash, and inter-rill erosion. A major factor controlling the importance of rill erosion in the study area is the spacing of the rills over the extent of the area affected. In the above mentioned areas, this type of erosion is more readily recognizable and the rills merge in the north and western parts of the Lar basin to form gullies which are almost impossible to overlook. However, the relative quantities of soil movement resulting from rill erosion in the Lar basin are highly variable. Generally, the amount of erosion is higher in areas with higher rainfall, such as the eastern part and the direct force of import causes splash erosion (see Figure 4.6-b), especially where there are very shallow soils, soft rocks, steep slopes and low to medium density vegetation (Table 7.3 also see Figure 7.2 and folded map no.2 and 3). On sloping ground surface splash and rill erosion both shift the soil downhill.

In the semi-arid Lar basin, the southeast, east and northern areas are the most vulnerable to gully erosion, because of the unequal distribution of the landcover as described in Chapters 4 and 5. Bare soil and low density vegetation cover in the upstream areas provide suitable conditions for gully erosion especially on limestone soils. Along the rivers and flat areas where water supports vegetation (such as Lar downstream Imampahnak, Siahplas and the area between Dalichai and Sefid-Ab) gully erosion is much less. Gully features are mostly seen in the upstream area of the Siahplas, Khoshkehlar, Lar, Sefid-Ab and Dalichai sub-basins where steep-sided slopes experience ephemeral flows during precipitation. It seems that the Khoshkehlar sub-basin is more

vulnerable to gully erosion because of ephemeral flows and great variability in the distribution of soil and vegetation cover. In the Lar, Sefid-Ab and Dalichai tributaries, human interference by overgrazing, dry farming, poor soils and steep slopes provide ideal conditions for gully erosion (Table 7.3 and see also Figure 5.13-a).

7.3.2 Bank Erosion

The physiographic characteristics of the basin influence stream erosion in various ways, especially by channel materials and stream hydraulics. Erosion of river bed sediments is important in the Dalichai and Sefid-Ab, and bank erosion dominates in the Lar and Khoshkehlar catchments because of low bed gradients and extensive alluvial deposits in their channels (Table 7.3 and see also Figure 5.2-b the Lar basin sediment map). Also in the western part of the Lar basin in the Lar tributary, channel erosion is proceeding along the stream into recent alluvial deposits as identified on the remote sensing data. In the Kamardasht area (Lar downstream) bank erosion also causes falls and slides of terrace materials, which are then transported as part of the stream load. The physiographic conditions in the middle Lar Basin, downstream of the junction of Khoshkehlar and Lar, produces braided streams due to high discharge and very erodible bank sediments so that the streams are shallow and wide. In Figures 6.17-a and b the terrace areas are most vulnerable to bank erosion because of incision, and falls and slides of the terrace materials are common. These are quickly loosened, separated, and finally transported as part of the stream load.

This process of erosion is an important source of sediment to the Lar system and the results that emerge from analysis of the mechanism, conditions and rates of bank erosion in meandering areas along the Lar river and Sefid-Ab downstream, are achieved by fluvial entrainment, mostly initiated by toppling failure. This mechanism brings about the greatest amounts of planform change and is the process typical of most laterally unstable meandering channels, such as the upper Severn and middle Dane in the UK (Hooke, 1979). In spite of modelling (Thorne and Osman, 1988), and the well known factors influencing slope stability in general, the actual occurrence of shear failures is still not fully understood. Carson et al. (1973) noted a downstream increase in sediment yield in the Eaton basin and ascribed it to increased erosion of the till bank. Sediment yields in Canada (Slaymaker and McPherson 1977) indicate a similar effect, whereby major

contemporary sediment sources may be along the rivers and not in the land surface adjacent. Slaymaker (1977), commenting upon summary sediment yield data of the Lillooet and Fraser basins, proposed that sediment yield increases downstream and reaches a maximum at an intermediate scale where sediment availability is high and land use change has had a major impact. As discussed above a similar effect is observed in the Lar basin especially the lower Lar and Sefid-Ab.

7.3.3 Mass Movement

Mass movement processes in the study area include creep, slides, falls and flows sized about $3m^2$ in Sefid-Ab downstream to $100m^2$ in the Dalichai (see Figure 6.20-a, b and c). These have all been identified from remote sensing data and mapped on a field geomorphology map. Land slides mostly occur in the lacustrine formations in the Lar and lower Sefid-Ab and also in the Dalichai tributary (Table 7.3 and see also folded map no.4). Rock falls also occur in the Dalichai volcanic formation. This has loosened material and makes it easier to erode and transport by water. Secondly it displaces materials downstream into alluvial fans which are then eroded by the river. Mass movement features are easily detected on large scale air photographs in the Lar Basin. The importance of the high spatial resolution of SPOT and TM (respectively 20 and 30 metres) in comparision with the spatial resolution of MSS image (79 metres) (and the increase in spectral bands from 4 in MSS to 7 in TM data) allowed many morphological features, previously poorly represented on MSS data, to be identifiable on TM and SPOT.

Tables 7.3 and 7.2 and Figure 7.2 all show that low density vegetation on shallow soils is coincident with surface erosion especially in the Dalichai, Sefid-Ab, Imampahnak and in the upstream parts of the Lar and Khoshkehlar. Severe gully erosion occurs on erodible lithosols, calcaric regosols and in areas of low to moderate vegetation cover in the Dalichai, Sefid-Ab, Lar and Khoshkehlar upstream.

7.3.4 Subsurface Erosion

As described in Chapter 5 subsurface flow (via pipes or limestone caverns) has an important role in the transportation of sediments in the study area especially after the

dam was constructed. The material in identified sinkholes moves by rolling or in suspension, and in solution in limestones and former Lake deposits. This makes the soil more vulnerable to transportation. Samples from sinkholes show that the soils are mostly fine loess and clay. The volume of lost soil from these holes is estimated later in this chapter. Figure 7.3-*a* shows an evidence of sinkhole in Lake Lar area and in Figure 7.3-*b* shows two springs which appear some about 200m from the dam site as subsurface activity related to features such as Figure 7.3-*a*. In 1994 the Dam Authority reported that after the dam was constructed, 9 springs had appeared along the Haraz river some about 25km between Lar dam and Ab-Ask village. The limestones of the lower formation are very prone to both solution and collapse and so these subsurface pipes and caves are capable of carrying water and sediment out of the Lake (Table 7.3 and Figure 5.13-b).

7.3.5 Sinkhole Development and Lake Drainage

The development of sinkholes is an important morphological change in the study area and 12 separate cases were identified in 1994 (Figures 5.13 and 6.27). This demonstrates activity in the karst formation of the Lake Lar area. The way in which sinkholes are related to the delivery of soil and water from the Lake is also of importance. Certainly morphological changes on the land surface and also in the karst formations will create serious problems for the present dam and any hydraulic planning in future.

There are several possible mechanisms by which these sinkholes could have been produced. The underlying limestone is known to be prone to solution which would lead to surface collapse. Alternatively, they could have been caused by piping or internal erosion of the underlying sediments leading to surface collapse. Finally they could have been produced by the internal collapse of loose structures within the soil deposits; the collapse having been initiated by vibrations associated with morphotectonic changes in the basin. The collapse of material into solution cavities in the underlying bedrock to form sinkholes is thought to constitute the most unlikely mode of origin of the depression in view of the extreme depth to bedrock. In one case, more than 450 metres of sediments occur above bedrock. Similarly, piping is not considered to be a likely mode of formation due to the apparent absence of deposits formed where the piped material emerged. Minor sinkholes which would most likely have developed along the pipe channels are also absent.

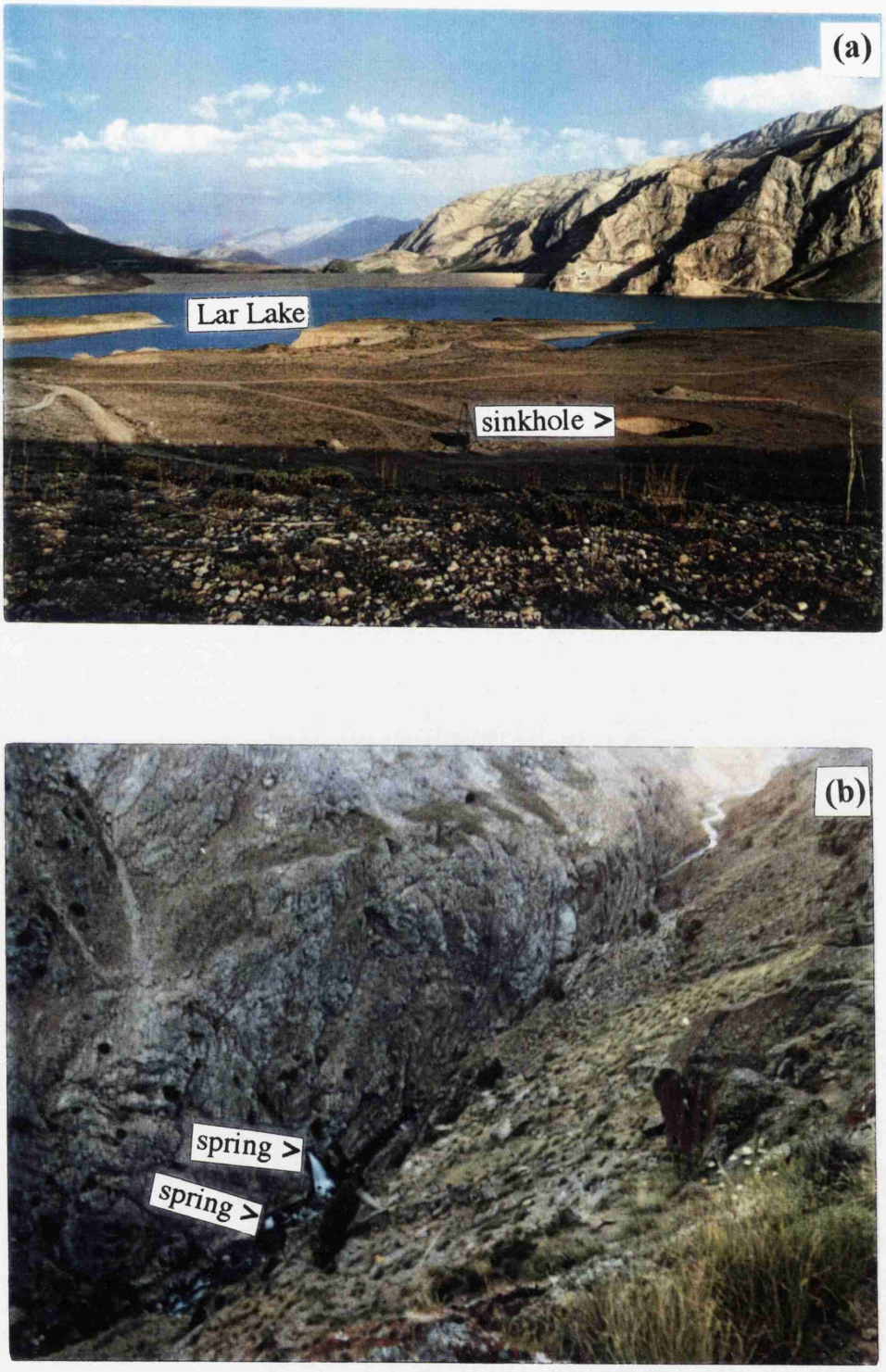

Figure 7.3: Lake Lar and Sinkhole (**a**), Springs in the Lar gorge (**b**) which appeared after the Dam construction *(looking East, Aug. 1994).*

The presence of extensive granular soils in the upper parts of the upper deposits (see section 5.1) is significant in that such soils are capable of being compacted by vibration. This factor combined with the close association between the depressions and known major faults is considered to suggest that depressions are the result of internal collapse of the granular sediments triggered off by movements along the faults and associated tectonic changes.

The sediment loss from two old sinkholes (located in the Southern Lake side) is estimated as 4.24×10^5 t and for two new sinkholes in northern side of the Lake about 0.28×10^5 t. These sediments have been lost via transport through open cavities in the underlying bedrock. In general as described in Chapters 4 and 5, the physical stratigraphy and sediment characteristics of the sediments, shows that they are originally lacustrine deposits, laid on the limestone formation in the Lake area. The chemical characteristics of limestones have made this area more sensitive than would be expected.

7.3.6 Summary

It can be concluded that rainsplash erosion is mostly moderate in the Lar basin except in the Khoshkehlar subcatchment which possess poor vegetation cover, steep slopes and higher rainsplash erosion. Sheet and rill erosion have mostly moderate erosion potential in the study area, but gully erosion has an important role, especially in the Lar, Khoshkehlar, Sefid-Ab and Dalichai sub-catchments because of variability in the soil, poor vegetation and steep slopes. Subsurface erosion is mostly can fined to areas around or inside of the Lake Lar area in the Sefid-Ab, Imampahnak, Siahplas and Dalichai sub-catchments. Bank erosion is significant on terraces especially along the Lar tributary, but is of moderate to slight importance in other areas. The Sefid-Ab, Imampahnak and Dalichai catchment possessing Quaternary sediments on steep slopes are proned to serious mass movement, although other sub-catchments are considered to have a moderate potential against for mass movement.

7.4 PARTICLE SIZE PATTERNS

Iindividual sedimentary particles are best described by their lithology, size, and shape. This allows the separation of facies in depositional materials. At each of these stages the characteristics of the sediment provides insights into the process which transported and deposited them. In many cases in semi-arid river basins the processes are so difficult and infrequent to observe that the sedimentary evidence is the primary indicator of the morphological changes.

As described in Chapter 5 some important factors can be discussed to relation to the sediments found in the Lar basin at different sites. Frequency diagrams from sieved samples from the Lar and Khoshkelar indicate that much sediment is between 0.06-0.002mm and less than 0.002mm (medium coarse silt and clay). Because of the sparse vegetation and grazing upstream, sheet erosion can easily transport these fine particles downstream to be deposited in the fan areas and Lake Lar. The particles of 0.06mm to 2mm, 2-60mm and 60mm to 200mm size (sand, gravel and cobbles) are mostly transported by rill, gully and then stream erosion. In the eastern parts of the study at the Khoshkehlar and Lar catchments, a huge mass of these particles shows that significant activity of rill, gully and stream erosion may be related to seasonal flooding, especially in Khoshkehlar basin. The finer particles occur mainly in the Lake bed at depth and are mostly clay and silt. The grain size distributed with more than 50% larger than 0.062mm are referred to as coarse grained, (in terrace gravels only) and particles with more than 50% in grains of less than 0.062mm as fine grained sediments, mainly in the Lake Lar bed deposits. Fluvial sands are usually moderately sorted and positively skewed since they almost invariably contain silts derived from suspension. Overbank deposits consist totally of silts and fine sands deposited from suspension. Coarse clastic inputs to Lake Lar are mostly deposited at or near the lake margin in Lar, Sefid-Ab and Dalichai deltas, although this material probably also contains material contributed by landslides, debris flows and turbidity currents transported into the central part of lake. The particle size distributions of the marginal deposits are difficult to distinguish from those of fluvial deposits. Far out in the lake some clastic sedimentation occurs by progressive settling out of material from suspension and from turbid underflows of relatively cool and dense inflows. Characteristically, the particle size of deposits falls with distance from the inlets (Smith, 1978). Lake bottom sediments are typically fine grained, with mean size of 0.5-

30μm. Studies of glaciolacustrine rhythmites by Banerjee (1973) and Ashley (1975) showed the deposits to be generally poorly sorted and to range from very fine to very coarse skewed. As described in Chapter 5 and discussed above are characteristics can be recognized Lar Lake (see Table 5.4).

Particle shape results for seven selected sites in the Lar basin showed that Dalichai (see App. Chapter 5, sample-A) with 63% spheres has the maximum amount in the Lar basin. This is because the eastern side of Dalichai subcatchment possesses Lava flows, which produce block material which is then transported very effectively by the river. Along the Dalichai river, rock also commonly breaks off through frost wedging (Figure 6.16-a), and is then transported as bedload. These range from boulders of metres in diameter, transported during very high magnitude floods, to gravel sizes moved in normal conditions. At Dalichai sample site, the size of stream-bed materials significantly decreases with distance downstream because of reduced bed slopes and thus shear stress. This is the result of shape as well as size sorting, by which the more spheroidal materials are transported further downstream, and particles with lesser abrasion are deposited upstream.

In the Lar upstream, the Khoshkehlar subcatchment is a seasonal stream, and has 9% of spheres. This value is less than other catchments in the Lar basin, because these materials are transported from more erodible sediments and over greater distances. The reason for different shapes of the river sediments in the Lar basin, is that at Gozaldarreh and Khoshkehlar the river bed gradients are very gentle and meandering, but these areas possess different lithologies which break down and are abraded at significantly different rates (Sneed and Folk, 1958). The Dalichai tributary has mostly spherical volcanic clasts in the downstream areas, because they have traveled farthest. In the eastern part of the study area, however, the simple picture of a systematic downstream reduction in the size of stream bed sediments is complicated by inputs from seasonal tributaries and bank erosion, flow resistance and channel morphology. Thus, particle size distributions vary across the channel and over time as flow competence falls on the declining limb of a flood pulse.

7.5 SEDIMENT YIELD

7.5.1 Lar Basin Deposition

The erosion sources and patterns discussed above need now to be linked to the location of deposition. The depositional environment of the Lar basin is dominated by the lacustrine deposits of Lake Lar. The characteristics of the upper and lower deposits have however, been found to be rather unusual, and are more sensitive to erosion than would be expected.

Generally the pattern of Lar Basin sediments consists of a sequence that has coarse grain sizes at the top and silts and clays lower down. This is found in boreholes at Chehelcheshmeh and by the sequence of bedded silts and sands found on the right bank of the Lar downstream of Imampahnak (excavation data from the dam authority). Overlying these fine grained deposits at elevations of between 1480 - 2700 metres, are the rather coarser grained silts and sands which make up the middle portion of the upper deposits and which have also been described on the southern side of the present Lake (see Chapter 5 for more detail). Coarse sandy gravel makes up the upper part of the sequence. These are found throughout the basin and at the Lar Gorge. The Lake deposits are mostly distributed in Lar downstream below the Lar and Khoshkehlar conjunction and also in some parts of the Dalichai and Sefid-Ab upstream, and fluvial deposits are widely distributed in other parts of the basin.

7.5.2 Infill of the Lar Lake and Rate of Deposition

Sedimentary infill of the depositional areas was identified using different methods as described in Chapters 3, 5 and 6. Remote sensing and field investigation both confirmed that except for the former Lar Lake deposits, which extended up to about 2700 metres, some small Lakes formed at the same time as the Damavand eruption, between 2800-3500 metres in the Dalichai and Sefid-Ab catchments. The sediment volumes of these lakes are estimated from: (1) sediment concentration techniques; (2) comparison of old topographic maps; and (3) aerial photographs. These were calculated separately to estimate the amount of sediment delivered to the Lar basin.

Sieving analysis from Cheshmehkhooni at Khoshkehlar, at about 2700 metres altitude, identified that the former Lake of the Lar basin extended well into this area (Chapter 5). Also other sample results from Chahelchashmeh and Gozaldarreh show that these formations are related to more widespread lacustrine deposits (Figure 5.19-g) that were idendified from KFA-1000 and aerial photographs before field mapping and sampling (Figure 5.10-a). Some geologists (e.g. Assereto, 1966) have reported that Lake deposits can be found at about 2500 meters, but the present sieving and aerial photo interpretation from the upper Lar provide a revised extent of the Lar Lake (Figures; 5.19-a, b, c and d and 5.10-a,1,2).

7.5.3 Sediment Delivery Estimation from Gauging Data

There are two further routes by which the sediment yield of the Lar catchment can be assessed. The first involves comparison of the rate of infill of Lake Lar with other lakes and the second uses the sediment yield derived from sediment concentration data at river guaging stations.

There has been no specific study of sedimentation of the Lake Lar area but comparative information has been obtained (Energy Ministry Iran, 1971) from the Latian Reservoir located some 20 kilometres to the south west (Figure 5.16). Here, an echo-sounding survey carried out in 1971, 5 years after the lake was flooded, shows that 0.8×10^6 m^3 of sediment per year had been delivered from upstream. Of this, approximately 10% consisted of gravel and boulders deposited as two prominent deltas where the main streams enter the Lake. The remaining finer grained sediment had been carried into the reservoir, over 80% of it entering the Lake during snow-melt. The Lar Basin deposits are very similar to those of the Latian reservoir in overall configuration and particle size distribution, and are likely to have been deposited in a very similar manner. The volume of the Lar Basin deposits is estimated at 198 t/km^2 for an area of 726 km^2 at the dam site. In comparison, the Latian Lake has a similar area (710 km^2), but drier climatic conditions and high erodibility, and has deposits estimated at 690 t/km^2 (Latian data calculated from Energy Ministry Iran, 1971). The only anomalous feature of the Lar basin deposits is the occurrence within the fine grained sediments of gravel beds, indicating phases of high energy flow. The gravels in the Lar sediments were probably laid down during periods when the lake was drained, and this is consistent with the

presence and altitude of a weathered erosion surface in boreholes at on the western bank of the Dalichai. Table 5.11 and Figure 7.4 presents the sediment production from 13 dam basins for comparison with the Lar basin.

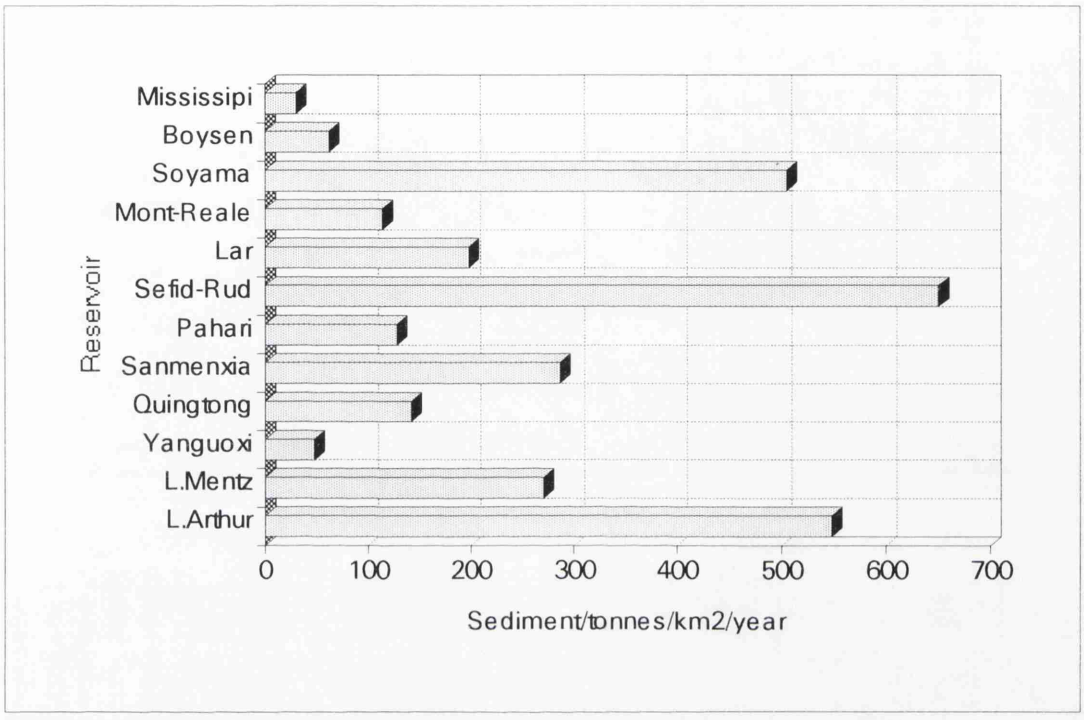

Figure 7.4: Annual average sediment production in reservoirs of the world.

Sediment production for the Lar basin of 198 t a^{-1}/km^{-2} seems a reasonable value since the Latian and Sefid-Rud have high values of 690 t a^{-1}/km^{-2} and 650 t a^{-1}/km^{-2} But both are characterised by over grazing and large areas of either poorly vegetated or unvegetated surfaces. The Latian basin also has a higher erodibility than the Lar because of it is mostly underlain by tuff, tuffaceous shale, and calcareous mudstones, all of which are susceptible to rapid surface erosion (Hezardarreh Formation). Elsewhere, the L. Arthur basin (548 t a^{-1}/km^{-2}) and L.Mentz (271 t a^{-1}/km^{-2}) in Africa, the Soyama in Japan (505 t a^{-1}/km^{-2}) and the Sanmenxia in China (287 t a^{-1}/km^{-2}) are all semi-arid and mountainous environments that are similar to the Lar basin. Clearly the Lar lies in the middle range of values of sediment production (Figure 7.4, see also Table 5.11).

The sediment history of the Lar Basin is summarised in Table 5.12 for the period of before and after dam construction and also for former Lake deposits and selected depositional fan sites (Figure 7.5).

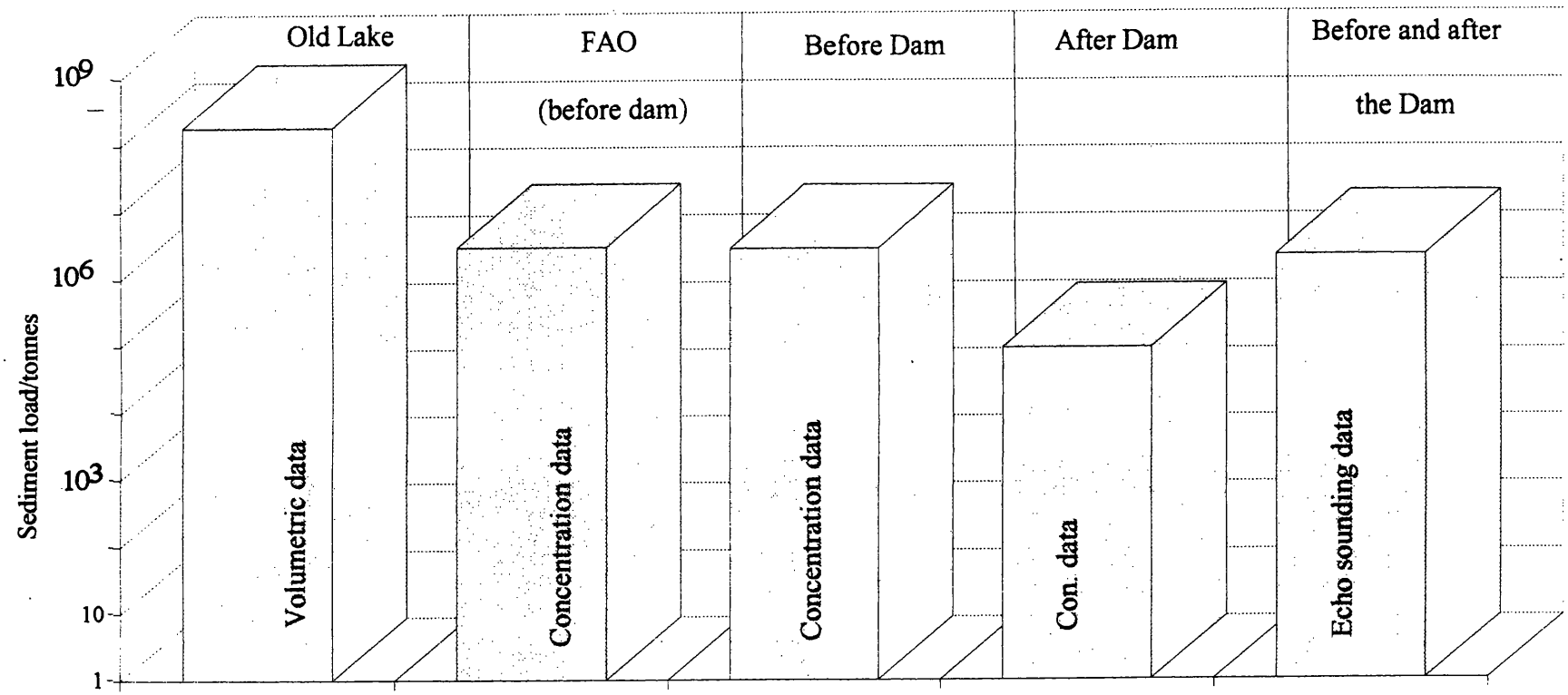

Figure 7.5: Different methods to estimate the infill of the Lar Basin
(FAO is United Nation Food and Agriculture Organisation).

Taking the mean density of the Lar sediments at 2.16 tonnes/m^3, (for method of calculation and range of values see Selby 1993, p.107) the total weight of sediment which has accumulated in the Lar basin is 4×10^{11} t, and it would have taken 26 000 years for the lake to have become completely infilled with sediment. However, sedimentation in the Lar Lake is thought to have commenced about 38500 years ago, as dated from the material from an elevation of 2450 metres (Allenbach 1966). Figure 5.22 shows that approximately $1.58\times10^{11}m^3$ of sediment has accumulated above this elevation (for method see Chapter 3, section 3.3.7 and also Table 5.6-a and b). Thus the minimum sedimentation rate using Allenbach's time scale is approximately $2.5\times10^{8}m^3a^{-1}$: Lake Lar was clearly in existence during the second period of glaciation (Weicheselian) (see Table 7.4).

The relationship between sediment concentration and runoff was summarized in Chapter 5. It was possible to derive the relationships between sediment concentration and river discharge for the Lar river for various periods of the year. The effect of the artificial dam on sediment discharge after 1972-1974 shows a decline which is greater than the decline of water discharge. The relationships for the period 22 years before the Dam was constructed show that the amount of suspended solids at Polour is 115×10^{3} ta^{-1}. Following grain size analysis in different river deposits, it is assumed that 70% of total sediment is suspended and 30% bed load sediment (FAO, 1969), suggesting a total yield of about 164×10^{3} ta^{-1}. This translates to an average sediment yield (concentration and bedload) from the 726 km^2 of the Lar catchment of 226 t a^{-1}/km^{-2} (Table 7.4 and Figure 7.5).

At Polour station, the sediment yield can also be compared for the periods before and after the dam construction. The mean annual sediment load of 1.7×10^{5} t, before the dam shows a reduction to 0.92×10^{5} t after dam construction; a 69% fall in sediment yield to downstream. Daily sediment concentration-discharge relationships for the period of 1965-1986 show falls after dam construction. The sediment yield for a period of 13 year after the Dam construction at Polour station is 7×10^{3} t. In Figure 7.6 a sharp decrease of sediment can be seen between 1973-76 gradually decreasing to the mid-1980's, followed by a small increase up to 1986. One of the reasons for the post-dam fluctuations may be related to the development of sinkhole activity. These sinkholes lose both water and

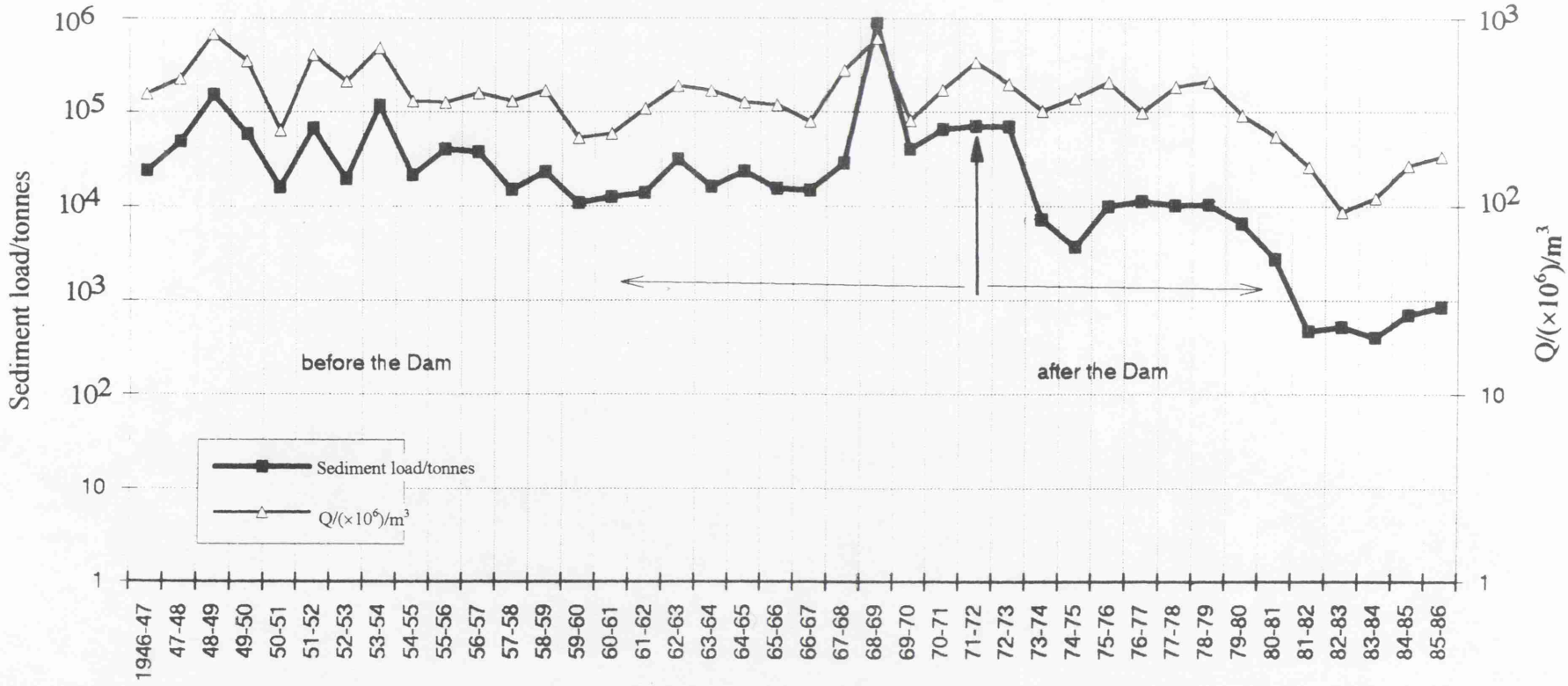

Figure 7.6: Annual sediment load and water discharge at Polour (1946-1986).

sediment and so the dam authority has attempted to control this loss (Figure 7.7). So far this has been unsuccessful and 9 new springs have appeared along a 20 km reach of the Haraz river below the dam (Figure 7.3).

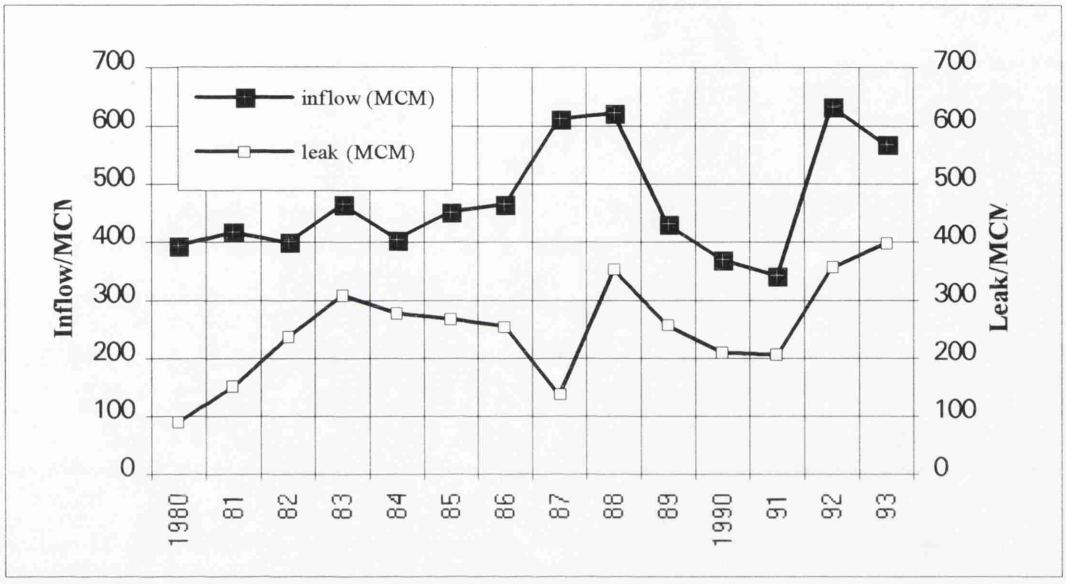

Figure 7.7: Annual inflow and leakage of water of the Lar reservoir [MCM=($\times 10^6 m^3$)].

Table 7.4: Summary of the Lar basin sediment estimation.

Source of Estimate	Total Estimate	Annual Estimate
Topography Map	4 ($\times 10^{11}$t)	5.4 ($\times 10^8 ta^{-1}$)
FAO (before dam1969)	1.6 ($\times 10^5$t)	1.4 ($\times 10^2 ta^{-1}$)
before dam **Polour**	1.7 ($\times 10^5$t)	2.2 ($\times 10^2 ta^{-1}$)
after dam	1.2 ($\times 10^5$t)	1.5 ($\times 10^2 ta^{-1}$)

Karehsang station was selected as a control station at the northern end of the Haraz basin. The catchment it measures covers 18% of the Haraz basin, mainly comprising the Lar basin. The average daily sediment yield at this station is estimated as 1885 t, 1905 t before the dam and 1603 t after the dam. The sediment concentration and discharge relationship before and after the Dam, using Karehsang station as a control station, shows the influence of the 18% area blocked by the Lar dam in the upstream part of the Haraz basin, and there is a very clear relation between these two factors (water and sediment discharge) before the Dam (see Figure 5.32). Similar relationships between daily sediment concentration with discharge and annual sediment can be seen at Polour

station; high fluctuations before the Dam, declining and irregular fluctuations after the Dam (see Figures 5.31 and 7.6).

7.5.4 Patterns of Sediment Delivery From Different parts of the Basin

An alternative method of estimation of sediment volume is to calculate these directly from topographic maps at 1:25 000 scale (British Army, 1945). The amount of deposited sediment in the Lar basin including the former Lake to 2700 metres, is estimated as about $1.58\times10^{11}m^3$, along the Lar river, Dalichai, Alarm and Sefid-Ab upstream between 2800-3500 metres (deposited area). This result is a yield of $208\times10^3m^3/km^2/yr$. The values for sediment volumes reduce with increasing altitude to a minimum value of about 0.25% of total sediment volume occuring between 3000-3100 in Dalichai and Sefid-Ab and a maximum value of 31% of the volume occuring between 2500-2600 metres. This area includes most of the Lake depression. About 89% or $140\times10^9m^3$ was deposited between 2200-2700 metres by the former Lake Lar. This includes 92% of the area of deposits because this Lake extended up to 25 km, and was also receiving all the tributary sediment discharges. In other parts of the Lar, Khoshkehlar, Sefid-Ab, Alarm and Dalichai catchments 11% by volume of the accumulated sediments were deposited in 8% of the area of deposition (Figure 5.22 and see also Table 5.6).

As described in Chapter 5, three delta sites of Gozaldarreh, Sefid-Ab and Dalichai were selected on aerial photographs for calculation of sediment volumes. The amount of accumulated sediment is estimated at about $8.5\times10^5m^3$ or $3.9\times10^3m^3/km^2/a$ (see Chapter 3 section 3.3.7 for calculation method). A comparative study from these three delta fans using photogrammetric techniques results shows the Dalichai with $1.6\times10^3m^3/km^2$ and Gozaldarreh with $1.08\times10^3m^3/km^2$ rates of deposition. At Sefid-Ab, this value is estimated of about $1.2\times10^3m^3/km^2$. Also, subtracting of the results of the 1955 aerial photos from echosounding (1994) shows that the annual change rates are $0.02\times10^5m^3/km^2$ at Sefid-Ab, $0.03\times10^5m^3/km^2$ at Dalichai and $0.008\times10^5m^3/km^2$ at Gozaldarreh fans. Volumetric results from echosounding work estimate that about $14\times10^3m^3$ of sediment has accumulated in fans. The higher annual amount of sediment again shows that Dalichai is highly significant in terms of erosional supply of sediment ($1.6\times10^3m^3/km^2$).

The reasons for the higher erosion rate in Dalichai than in other catchments is related to its physical conditions (described in Chapter 4). Table 7.2 shows that 35% of vegetation cover in this catchment is very poor, much higher than in other sub-basins in the Lar area. Figure 4.14 shows that 68% of the area in this catchment is between 3250-5671 metres with high gradients (see folded map no.1). These characteristics, the steep gradient and the high velocity of the river to combine produce higher erosion rates in Dalichai catchment than in other catchments. The Gozaldarreh site which covers both Lar and Khoshkehlar, has a lower erosion rate than the other two catchments ($1.08\times10^3 m^3/km^2$), probably related to low-medium slope gradients and high density vegetation in the channel area. It is also more stable than Dalichai in terms of tectonic activity.

In some studies of palaeohydrological reconstruction it may prove attractive to relate downstream sediment yields to erosion rates operating within the basin. In this manner estimates of erosion rates could be converted to values of sediment yield or conversely, evidence for past sediment yields could be extrapolated to provide estimates of erosion rates within the basin. However, relationships between sediment yield and drainage basin area proposed by Branson et al. (1981) and employed for the Lar basin three sub-catchments shows (see Figure 7.8) increased sediment yields with decreased basin area. The Dalichai basin with about $196km^2$ shows higher sediment yield in the left end of the curve and the Lar and Khoshkehlar at Gozaldareh shows lower sediment yield in the right end of the curve. The relationship between sediment yield and drainage basin area in Figure 7.8 supports the results from the volumetric method discussed above. The smaller catchments have higher sediment yields and the larger have lower yields in the Lar basin.

7.5.5 General Relationships

A relationship that predicts sediment yield only on the basis of drainage area is necessarily region specific because the simple function cannot account for the effects of local physical conditions (Graf, 1988). Analysis of yield-area relationships for a variety of environments reveals that the sediment yield per unit area nearly always declines with increasing drainage basin size, but the rate of decline varies from one region to another. The relation plotted in Figure 7.8 is derived from two general climatic regions. The curves by Hadley and Schumm (1961), Renard (1972), and Strand (1975) depict

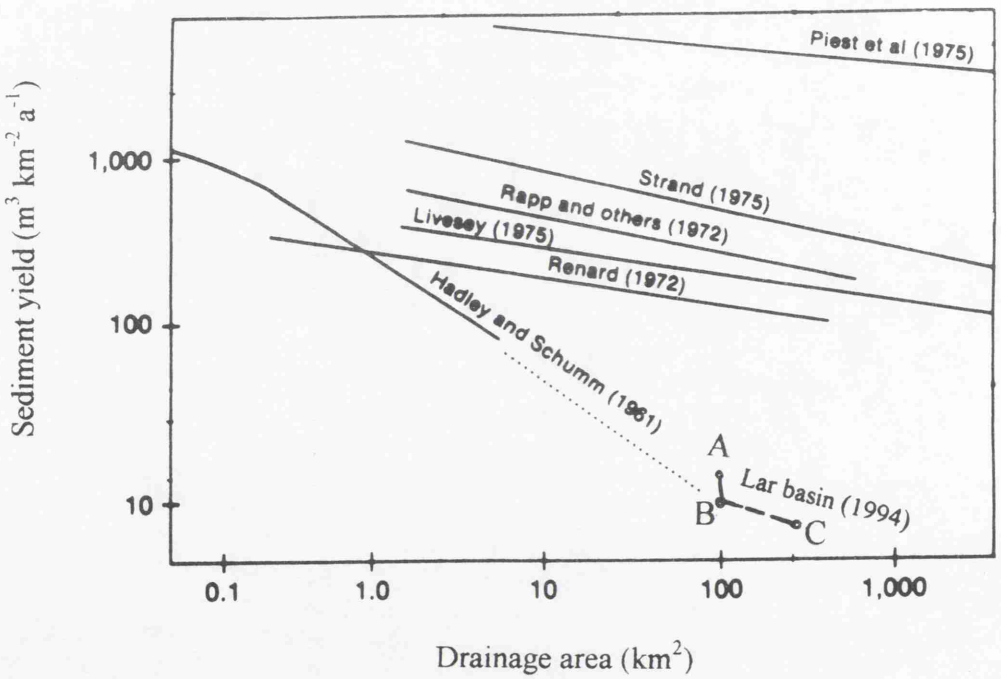

Figure 7.8: Relationship between sediment yield and drainage basin area, A=Dalichai basin, B=Sefid-Ab basin, and C=Lar at Gozaldarreh *(after Branson et al., 1981)*. Dotted line shows an extension to the Hadley and Schumm (1961) curve, derived from the semi-arid SW USA. Note the correspondence between this curve and the Lar and Sefid-Ab catchments.

conditions in the semi-arid area of the southwest of the United States. Data from Livesey (1975) for the upper Mississipi basin (partly semi-arid) is also shown while the top curve data are from a humid-semiarid transition zone in southern Iowa (Piest et al. 1975). The relatively high sediment yield for the Iowa data reflects the input of soils and geology because the basins are developed in highly erodible loess materials. The Lar curve in Figure 7.8 is most similar to the semi-arid Southwest US. Estimated sediment data from the Dalichai, Sefid-Ab and Lar catchments suggest wide applicability of this general rate of decline in sediment yield with increasing area. The reason for the scale related decline in sediment yield of the Lar basin is that sediment eroded from slopes does not immediately make its way to the basin outlet. Temporary storage of sediment eroded from upper slopes on lower slopes is common to both the semi-arid Lar basin and in west America (Leopold et al., 1966). The Dalichai basin with about 196km^2 shows higher sediment yields in the left end of the curve and the Lar and Khoshkehlar at Gozaldareh shows lower sediment yields in the right end of the curve.

Relationships between precipitation and sediment yield have been developed by many workers, both as an end in themselves and as a means of postulating the influence of a changing climate on sediment yields through space-time substitution. The approach was pioneered by Schumm (1975) and applies the relationship between annual sediment yield and effective precipitation, proposed by Langbein and Schumm (1958). This relationship is depicted in Figure 7.9 and has been explained in terms of the interaction of erosive energy and vegetation density. Maximum sediment yields occur at an annual effective precipitation of about 300mm (semi-arid areas). In areas with effective precipitation in excess of 300mm, vegetation growth is promoted and this increases surface protection. In areas with less than 300mm.a^{-1}, the available energy for erosion and transport in limited. This explanation has been termed the Langbein-Schumm rule, by a number of workers and the influence of climatic change on sediment yields can be readily estimated by evaluating the increase or decrease in annual effective precipitation. Effective precipitation is defined as the annual precipitation required to generate a given annual runoff at a standardized annual mean temprature of 50°F and is not, as some workers (e.g. Golubev, 1982) have assumed, equivalent to precipitation minus evapotranspirational losses. But Wilson (1973) suggests that climate cannot be adequately represented by annual quantities, seasonality of rainfall is an important control of erosion. Also Fournier's (1954) index p^2/P accounts for both total annual precipitation

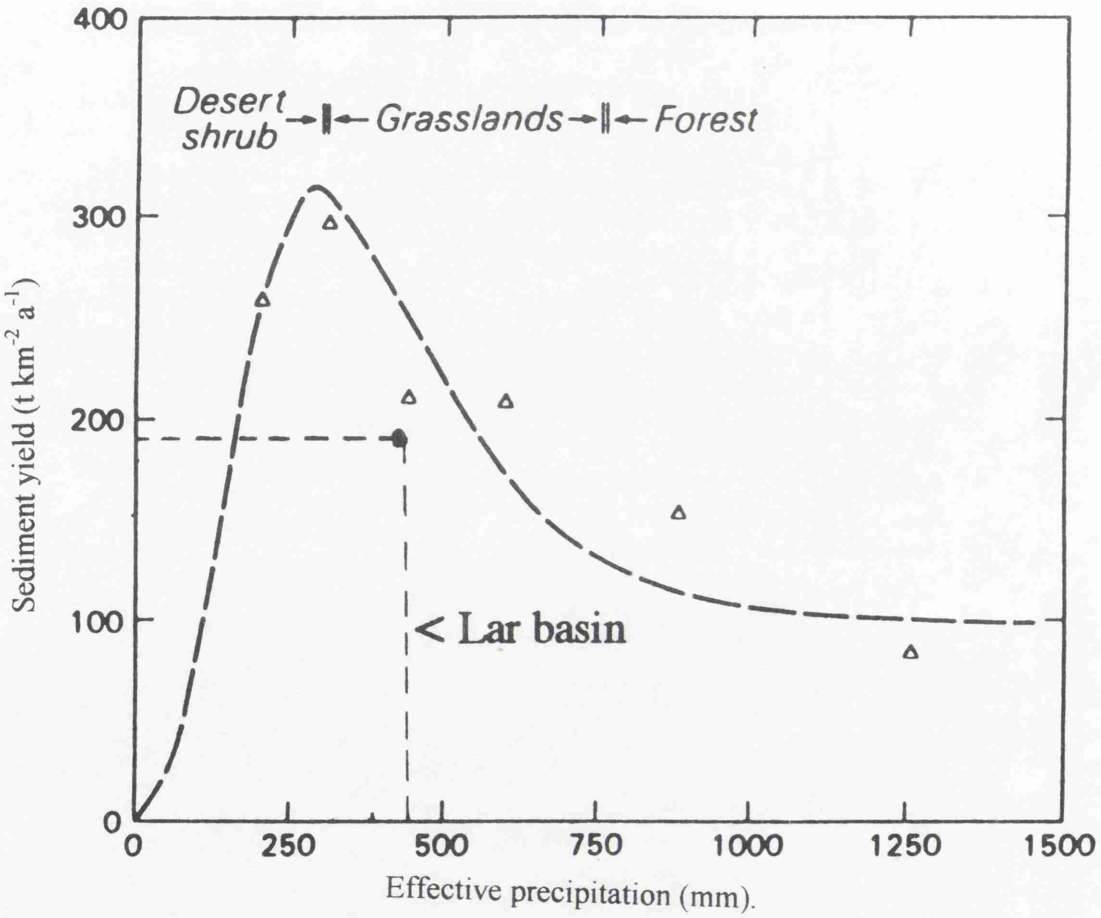

Figure 7.9: The relationship between sediment yield and annual precipitation *(after Langbein and Schumm, 1958).*

(P, mm) and seasonality, where p is the average precipitation of the wettest month. Regional sediment yields are distinguished by this parameter, which is highest in semi-arid seasonal tropical environments, but a relief factor is necessary to rationalize the scatter in a multivariate relationship (Fournier, 1960).

Figure 7.9 was derived using data from 94 river basins by applying a group average technique and the average sediment yields for a series of effective precipitation classes were calculated and the final curve was drawn through these points. To this extent the curve is a statistical abstraction of the raw data and it has been suggested that removal or addition of a small number of key stations could substantially alter the form of the curve. In terms of its general applicability, it can be accepted that the curve was derived from data for rivers in the United States and that the range of climatic conditions represented is therefore limited. However, when the curve is applied to the Lar basin (annual precipitation of 440 mm) it is found to be a reasonable prediction of yield from a grassland catchment. However, in Iran some regions such as the Caspian Sea and Persian Gulf coastal areas (e.g. northern Haraz, Sefid-Rud, Karun and Minab basins) exhibit high sediment yields at values of annual precipitation in excess of 1000 mm (Northern Iran) and less than 300mm (Southern Iran) which do not conform to the pattern suggested by the curve (Energy Ministry, Iran 1979 and Mahab Qouds Ltd., Iran 1985).

7.6 METHOD ASSESSMENT AND CRITIQUE

The previous section has shown that substantial spatial and temporal variations exist in the erosion and sediment yield data within the Lar catchment. This section aims to discuss the methods used in this research, in the light of the review of similar work described in Chapter 2 and the methods in Chapter 3. This Discussion considers the use of remote sensing techniques including; aerial photographs, KFA-1000 images, digital SPOT and Landsat TM images, topographic mapping, echosounding surveys and sediment concentration and water discharge data analysis at selected hydrographic stations in the Lar basin.

7.6.1 Remote Sensing Technique Assessment

This section aims to assess and discuss the remote sensing techniques used for assessing vegetation, erosion patterns, morphotectonic features and sediment deposition areas in the Lar basin as described in Chapter 6. The Lar Basin is a high mountainous area, and achive of the inaccessible parts of which are best addressed using remote sensing data. Therefore Landsat (TM) and SPOT multispectral bands have been employed to identify the land surface characteristics against which to compare aerial photograph and map data. Much of the geomorphology, vegetation and lithology maps were produced by a combination of remote sensing and aerial photography before field checking.

In Chapter 6 both SPOT and Landsat TM data were successfully used to map vegetation and different land surface types in the selected sites. In general both the classification (supervised) and Global Vegetation Index (GVI) were useful for establishing land cover, but for extraction of dry grassland and rangeland areas, the results of the GVI are preferable. For the identification of land surfaces using a system of image processing and up to date ancillary data, supervised classification is preferable to unsupervised classification. More accurate results were obtained from the Global Vegetation Index than the classification system (e.g. MDM, Maximum likelihood and Box classification) because it is simple to apply in areas of varying vegetation density and type. Of the single band images of TM-1,3 and 7 (Figure 6.22) the blue band-1, was most useful for identifying the soil, but dead grass could be confused as bare soil. The utility of red band-3 for differentiating bare soil and senescent vegetation cover was limited. In terms of spatial clarity, the blue band-1 was more useful than the red band-3. The bare soil appeared brighter and easily separable from former farmland, but this was more complicated on Kamardasht area in the western side of the Lake Lar. The reason for different identification between bands 1 and 3 is related to their spectral sensitivity (0.45-0.52μm in band-1 and 0.63-0.96μm in band-3, see also Chapter 2 Figure 2.7). The middle infrared band-7 provided significant information for discriminating the range of different surface types considered in the Lar basin. The band contains enough unique spectral information concerning grey tones to discriminate vegetation from other land covers. The bare soil was clearly separable from the dried vegetation and farmland. However the middle infrared band was more useful for differentiating all surface types.

Three Band Composites of the Study Area: Like the individual TM and SPOT wave bands, visual interpretation of the false colour composites also revealed a wide range of information on the Lar Basin. The composition of three available bands 1, 3 and 7 (Figures 6.17-a) from TM and bands 1, 2 and 3 from SPOT (Figure 6.17-b) show good discrimination of bare soil, vegetated areas and some other surface features. In general the three band composition of the TM and SPOT data are most useful for discrimination of surface types e.g. recent alluvial deposits could be distinguished from ancient alluvial deposits.

Maximum Likelihood Classification Assessment: The maximum likelihood classification of the Lar basin was not fully successful (Figure 6.23 TM bands 1, 3 and 7) as there was a considerable misclassification of vegetation and wet and shaded areas. The classification was successful in clearly delimiting the bare soil boundary, and areas more than 30 metres in size were clearly separable, however dried grass and former agricultural fields were occasionally (e.g. at Gozaldareh) misclassified. The misclassification also occurred with the spectral and field dimension attributes of the smaller vegetation units. Despite the limitations of the maximum likelihood classification for separation of vegetation, it appears that with adequate training data sets, the classification result could be improved. Maximum likelihood proved to be a useful supervised classification when applied to Landsat Thematic Mapper 3 bands composite of the Lar upstream.

Discrimination of surface cover was attempted using the Landsat TM, SPOT (MSS), sequential aerial photographs, KFA-1000 and field investigation. The Landsat TM, SPOT and aerial photographs were also analyzed in order to classify and map the surface covers of the study area. The mapping information thus obtained were used as an input into geomorphology, vegetation, lithology maps of the Lar basin.

The different kinds of data, especially sequential aerial photographs from 1955, suggested that the surface cover of the study area has undergone a great change between 1945 and 1994 (see Chapter, Figure 6.27). The creation of the artificial lake Lar (1974) led to the development of the karstic features (e.g. sinkholes and springs) and the whole Lake bed was vulnerable to the development of sinkholes and erosion. Because of the impoundment of surface water, the overall numbers of sinkholes in the area increased

from two before 1974 to twelve in 1994. A significant difference was observed in the number of holes on the southern side of the Lar channel compared with the northern side, due to the distribution of limestone formations (Tizkuh; see Chapter 5, Figure 5.5) forming Lake substrate at Imampahnak and Siahpalas areas (Cahpter 5, Figure 5.13-a).

Extensive cave development and localized collapse were the most important erosion features of the area. The results of the image analysis implied that, although the increased spatial resolution of the SPOT was sufficient enough to expose the details of the Lar basin, because of the very minute detail of the spectral variation, it was difficult to map the eroded areas precisely. The enhanced images, whilst making the identification of the broad surface types more straightforward, failed to increase the accuracy of the classification. Interpretation of the false colour composite (Figure 6.17-b) indicated that exposed limestone would be recognized with ease, although some difficulty remains in separating dried grass from bare soil and limestone. The middle infrared band was useful in delimiting the senescent grassland from the bare soils and fresh vegetation cover. An interpretation of the maximum likelihood results suggests that broad categories, (vegetation, bare soil, river bed) are separable although in a few cases misclassification between vegetation and bare soil might occur. The FCC's, the ratio images, and maximum likelihood classification maps all provided a general guide to the spatial distribution of the main cover types. As far as erosion in the study area is concerned it appears that the SPOT images are less satisfactory for the clear identification and accurate delimitation of eroded areas, more specifically the separation of bare soil from vegetation. Apparently it seems that for a successful identification and discrimination of bare soil from vegetation in the Lar subcatchments, the SPOT system needs:

- more integration of spectral information within the spectral class so that internal variations remain at minimum. This would enhance the between class variation and hence improve the classification accuracy;
- more spectral bands at the longer wavelength, such as the Landsat TM band 7, are essential. The increased number of spectral hands would increase the possible number of band combinations for better identification and delimitation of bare soil and hence would reduce misclassifications. Analysis of the Landsat Thematic Mapper data suggests that that this is the most useful imagery in the identification of vegetation types in the Lar Basin. The TM bands were better correlated than either KFA-1000

or SPOT imagery with the ground data. Amongst others, soil moisture, vegetation and surface silt were significantly correlated with most of the TM bands.

The TM spectral and spatial resolution were sufficient to expose the spectral class variation of the Lar basin, but were not so detailed as to cause confusion. Because of the spectral and spatial diversity of the surface types in the study area different TM band combinations are essential for effective delimitation of the major surface categories. The overall classification accuracy achieved for the different surface types of the Lar basin with the TM and SPOT show different values (see Appendix Chapter 6). Because of the coarser spatial resolution of the TM data (30 metres) compared with the SPOT data (20 metres) an increase in number of boundary pixels, thereby a decrease in classification accuracy was expected.

The maximum likelihood classification was most useful in classifying the bare soil and least effective for the vegetation. TM bands 1 and 7 were most effective for the discrimination of the Lar surface types. SPOT overlays of filtered bands 1 and 3, and the stretch of the grey tone composite of bands 1, 2 and 3 were useful for bare soil and vegetation determination.

Estimation of the accuracy of classification maps constructed by an image processing system or from aerial photographs requires some independent means for checking the classification. The role of field work was particularly important in checking the interpreted features from the aerial photographs and the classification of the images. For this reason two extensive field work seasons were undertaken during the summers of 1993 and 1994. In certain cases changes to classification boundaries were made but the original interpretation remains largely unchanged. In only very few cases was it necessary to alter the attributed classes. This suggests that conventional aerial photo interpretation is a reliable approach to mapping surface covers in this area. It also suggests that the results arising from a comparison of the maps derived from the interpretation of aerial photographs for different dates can be viewed with some confidence. The availability of aerial photographs and the high level of confidence attributed to their interpretation permits their use as a surrogate to field checking when interpreting the results from the satellite multispectral data sets. In their absence however the role of field survey assumes a greater significance. In this study the interpretation of false colour composites ratio and

classified data for the SPOT and Landsat TM data sets were backed up by comparisons with the aerial photo interpretation and field work. A similar approach has been adopted in other studies to determine the accuracy of the remote sensing data for classifying land surface types (e.g. Justice and Wharton 1981). Nevertheless, the results presented here should be treated with caution yet are, in the best estimates currently a variable for the area.

As described in the previous section results from the discriminant analysis indicated that the TM data set provided an overall higher level of discrimination among the major surface categories, such as the vegetation and bare soil. The image processing system used in SPOT analysis here was the PC-based Dragon image processing system. The imagery was analyzed to examine whether each of the major cover types could be delimited consistently from the others. The subscene was first examined in each of the SPOT bands and then in false colour composites. Band ratios and a maximum likelihood classification were also generated from these data.

Single band imagery shows a large scale variation within and among the land surface types appearing as wide variation in grey tones. Similar levels of variation between surface types were apparent as the blue to red gradations in false colour composites of the three SPOT bands (Figure 6.17-b; False colour composites of the SPOT the Lar basin). Analysis of the false colour composites shows that exposed limestone (colour grey) could be recognised relatively easily. Wetland appeared as dark grey, while the dry area was difficult to separate from the bare soil especially where the bare soil has still a thin veneer of clay mixed with sandstone. The large gullies on the slopes were identified as they appeared black due to moisture and shadow. In the false colour composite, considerable difficulty was encountered in separating bare soil from dried grassland as well as from former grazing land. Finally, analysis of the errors of the classification methods described in Chapter 6, indicates that in spite of some advantages e.g. the saving of time and the accessing of data for an inaccessible area, some misclassification is unavoidable. factor. However, the Dragon method used here, together with field surveying, improves the classification accuracy: the SPOT and TM maximum likelihood classifications were 0.65 and 0.54 in comparison to a Kappa value of 1.0 for perfect accuracy.

Summary of Remote Sensing Techniques: As described previously some of the interpretation of these data was subjective. A more objective way to delineate the main land surface cover types would be through automated classification of the imagery using supervised maximum likelihood classification. Figures 6.23 and 6.24 present the results of the maximum likelihood classification. Ignoring the classification external to the Lar Dam Basin, a subjective assessment of the results from this classification indicated that broad categories such as bare soils, vegetation and gullys are separable with considerable success. Although to a greater extent the exposed limestone has been accurately classified, however, some smaller areas of patchy vegetation and dry, desiccated wetland are misclassified as limestone. Similarly some smaller bare soil units are also misclassified as limestone, especially where subsurface soils were exposed recently by erosion. Such missclassification was rectified here by use of aerial photographs and ground survy.

7.6.2 Sediment Estimation from Topography Maps

As described in Chapter 5 the former Lake Lar deposits extended 25 km up valley and to an altitude of 2700m at Kamardasht and for small Lake of Dalichai to between 2700-3500m altitude. The only existing topography map at 1:25 000 for the whole Lar basin (1945) allowed a successful calculation of the volume of deposited materials. This type of map has a contour interval of 50 metres, and carries an error of ±2.42m (see Table 5.10). The estimated volume of the sediments (this value is a maximum) in the Lar basin ($1.58\times10^{11}m^3$) represents a sediment yield rate of $208\times10^3m^3km^{-2}$. However, reference to Chapter 5 (Table 5.10) indicates that approximately $112\times10^3m^3km^{-2}$ sediment yield is recently delivered from the basin. The reasons for this significant difference is; a) the topograpic map gives only a maximum estimation of sediment yield, and b) the environmental conditions suggest that it was probably wetter than at present time and certainly tectonic activity was an important factor in the high rate of Pleistocene erosion. In spite of this difference, this method can be recommended for use in areas which have no sediment records. It is also a very economical technique (e.g. aerial photographs, echosounding and remote sensing data).

7.6.3 Aerial Photos and Sediment Estimation

Sediment volume estimation for limited areas, like the selected alluvial fans in the Lar basin, needs large scale and high accuracy remote sensing data. Welch et al. (1984) suggest that digital data from stereopairs of two different dates can measure soil loss but this needs field survey and high resolution remote sensing data for reliable estimation. Several studies (e.g. Poole, 1969; Morris et al 1979; Alam and Harris, 1987; Pelletier, 1985 and Palylyk et al 1992) have utilized remote sensing data in studies of soil erosion or very generally in soil loss, and found it useful for the identification of erosion patterns. Thus for more accurate sediment value estimation in the Lar basin, aerial photographs were used to plot contours and to calculate accumulated sediment volumes in alluvial fans. This could be checked in the field for both control points and areas. It seems useful to compare each fan deposit with other methods. This confirmed the results of topography maps, aerial photos and the relationship between sediment yield and drainage basin area (Figure 7.8) that the Dalichai catchment has a higher erosion rate than other catchments (see Chapter 5, Table 5.7).

7.6.4 Echosounding Survey

Construction of an artificial dam caused increased sediment deposition into the Lake deltas. Surveying the delta volumes by echosounding methods resulted in a very close agreement with the sediment volume estimated via aerial photograph and surveying at Gozaldarreh, Sefid-Ab and Dalichai. Similar methods were used in the Latian reservoir, Iran (Ministry of Energy Iran, 1972). Annual echosounding surveying would have given a more accurate estimate of annual volume but this has not been done for the Lar on for any other lake reservoir in Iran. As described in Chapter 5 and discussed earlier in this chapter, there is a significant advantage in this method where the sub-catchments have high erosion rates. This would allow future management plans for soil and water conservation to be highly targeted, especially in semi-arid and mountainous areas and in sparcely vegetated sub-catchments.

7.6.5 Sediment Concentration Analysis

This method is most useful when the river basin has a regular and long period record of water discharge and sediment concentration. Regular daily, monthly and annual data from hydrometric stations are vital for a successful estimate of the long-term basin yields. This was impossible for all hydrographic stations recording both of sediment concentration and water discharge in the Lar basin because of short records, which often had gaps in them. Thus, as described in Chapter 3, procedures for infilling the gaps and extending the data (sediment concentration and water) from adjacent stations were used, but these must be viewed with caution and cannot provide completely reliable results. Finally the use of sediment estimation models, as used in Chapter 5, in relation to the Lar basin as a semi-arid mountainous watershed, can be assessed as follows:

- sediment concentration and water discharge data cannot be adequetly modelled for sediment estimation because of the irregular and inadequate data in the study area. For this reason, therefore the estimation of the sediment concentration should only be used for general comparisons with other estimation methods. The effect of the Lar dam on sediment supply at Polour station and also at Karahsang shows that the relationship between sediment concentration and water discharge can be useful for this purpose and was significant in reducing the sediment concentration after 1974.

- satellite remote sensing data, including SPOT and Landsat images, were very useful for identifying deposition areas and mapping land surface units, but have a lower ground resolution than aerial photos so that they are of limited use for sediment yeild estimation.

- erosion and deposition dynamics in the Quaternary formations of the Lar basin were identified and measured using remote sensing data and field observations. Present erosion is related to vegetation cover and soil characteristics in the study area. An environmental inventory is an essential component in the assessment of the contribution of such phenomena to land surface erosion. This would provide quantitative data of natural and anthropogenic processes and their interrelationships.

7.6.6 Future Work

The data used in this study can be transformed into usable information for management purposes through manipulation of the datasets generated during mapping and field work using GIS procedures. It is important to note the uncertainties present with each type of data in this approach.

- **Vegetation:** For vegetation classification in inaccessible mountainous areas where field work is difficult or impossible (such as some parts of the Lar area), the most useful technique is remote sensing data especially where it is available at high resolution (e.g. SPOT, KFA-1000 or TM). Further, the spectral resolution contained in the colour composite aids in vegetation cover and land use mapping. When required, additional detailed data can be gained if aerial photographs at larger scales are available. Existing maps can also be incorporated in the GIS database.

- **Erosion:** The eroded areas, which are clearly depicted on classified SPOT, TM and stereo KFA-1000 and photographic images, can be mapped using standard interpretation techniques (Bacco, et al. 1989). Simple GIS procedures make it possible to georeference and quantify these features. The stereoscopic images also allow the mapping of geomorphologically defined landscape units, such as terrain mapping units (Verstappen, 1989). A topographic map, for example, permits the construction of digital elevation models (DEM) and the derivation of slope gradient maps. The corresponding terrain mapping unit, land use or slope gradient of the eroded area can be quickly determined by combining the appropriate maps.

- **Sediment estimation:** estimation of the sediment delivery from the basins such as Lar can be achieved by employing regularly recorded (especially daily) data (sediment and water discharge) at gauging stations distribution over the catchment. This does not occur at the present and for successful work in the future, establishment of automatic recorders throughout the basin seems neccessary.

7.7 SUMMARY

The eruption of Damavand blocked both the old Lar valley and the Dalichai valley and the natural dams at southern and western sides of present volcanic cone respectively led to the infill of sequences of sediment up to 2700m and 3500m. The development of the Lakes provided an envoronment which was prone to subsequent morphological changes.

It can be concluded that the results of the imagery analysis imply that the increased spatial resolution was adequate to reveal the details required to meet the study aims, even a small site with intricate variations, such as the Lar basin. However it was also the case that due to minute detail in spectral variation it was difficult to map clearly the eroded land surfaces. However, enhanced imagery allowed better differentiation of the broad surface types.

Field observations in the summers of 1993 and 1994 were used to complete maps and to confirm identified morphological patterns and landcover changes in the Lar basin. Soil sampling and field checking of sediment types which confirmed the limits of the former Lake and enabled better estimates of the sediment deposited in the study area were especially useful. Landcover and landforms were mapped from remote sensing and stereo aerial photographs and KFA-1000 and plotted on the topographic map of the Lar basin using simple photogrammetric equipment. The other maps were derived using the same procedure and input data as in the Lar basin. The most eroded areas are the upstream catchments with alluvial deposits. The relationships between erosional and depositional areas show the significance of severe bank erosion related to the downstram terraces and upstream alluvial fans. Most of the erosion features (rill, gully, rainsplash) are located on slopes gentler than 45% gradient, poor vegetation cover and soft geological formations in the east and northern parts. The critical slope gradient and sparse vegetation for the occurrence of gully erosion, as described for the eastern, southern and northern parts of the basin produces more erosion in these areas. The vegetation characteristics (type and density) that were detected from the remote sensing data were checked in the field for some selected small areas. This was very useful for reduction of the error in classification from the images and on the final vegetation map. Similar work has been done for the lithology and geomorphology maps in the field. Where possible, sediment concentration and water discharge data records were extended and then compared with sediment

estimation by other methods. The hydrometric data was useful for a comparison of sediment supply after and before the dam at Polour station and also some 100 km downstream of the Lar basin, the relationship between sediment concentration and water discharge shows significant impact of the Lar dam after 1974. Apart from estimation from hydrometric data, volumetric methods seem useful for estimation of the sediment delivery because of the problems in the Lar basin recorded data.

In spite of some limitations related to resolution, remote sensing data proved most useful method for establishing landcover for the Lar mountainous area. Maximum likelihood method for this purpose was successul in both SPOT and TM with accuracies of 56% and 64%. Ancillary support for the remote sensing data is best provided by aerial photographs and KFA-1000, together with field checks. Although more accurate estimation of sediment yield depends on gauging records from river basins the lack of data in montainous area like the Lar means that the best method for estimation of yield is via a volumetric model. This need primary knowledge of the deposition area and accurant heights to achieve good results. Data for different dates e.g. aerial photos, maps and surveying, can also be most useful for comparisons of quantitative morphological changes but must be used with qaution.

Sediment estimation methods (photogrammetric plotting and echosounding surveying) used for three catchment deltas, show that the Dalichai catchment despite its smaller size has a high sediment delivery rate ($1.6\times10^{3}m^{3}km^{-2}$). At Gozaldarreh, the Lar (as the largest catchment in the study area), has a low sediment delivery rate ($1.08\times10^{3}m^{3}km^{-2}$). At Polour station, gauging records shows the influence of the artificial dam (after 1974), which reduced sediment load by 69% from 223t $km^{-2}a^{-2}$ before its construction to $153tkm^{-2}a^{-2}$ now.

CHAPTER 8: CONCLUSIONS

8.1 GENERAL REVIEW OF THE RESEARCH

It is useful to recall the research objectives given in Chapter one. The overall aim of the research was to test the usefulness of remotely sensed data (particularly SPOT multispectral, Landsat TM aerial photographs and KFA-1000) and field techniques for geomorphological mapping and sediment delivery studies in the basin of the Lar reservoir northern Iran. Field work and sampling followed to assess the physical properties of the Lar basin sediments. Sampled sediments have been investigated to detail the variation of soil characteristics throughout the sediment sequence, and assess the influence of this on the behaviour of the soils. Finally, estimates of sedimentation in a former Lake (38500 BP) and present sediment delivery from different sub-catchments in the study area were made.

8.1.1 History of Deposits in the Lar Basin

The former Lake Lar was formed about 38500 years ago, (Allenbach 1966) by the blocking of the Lar valley with lava flows from Damavand volcano. The initial Dam had a spillway level at an elevation of about 2150 metres. Before renewed eruptions of Damavand, this early basin was infilled with a coarsening upward sequence of sediments. After the first creation of the lake, were eruptions of basic lavas raised the Dam in the Lar valley to about 2260 metres. These lavas also impounded water in the Haraz river.

The last major eruptions of Damavand raised the natural spillway of Lake Lar to an elevation of about 2560 metres. Sedimentation continued in the Lake until the basin finally became completely infilled after which water spilling over the lava Dam caused it to be breached. Faulting which occurred at about this time is likely to have contributed to the breakup of the Dam.

As the valley of the new Lar River was established the sediments in the basin began to be progressively removed, a prominent set of river terraces being formed in the process. This stage of development is still operating at the present time in the Lar basin.

The stratigraphy and geometry of the Lar Basin sediments have confirmed their origin as lacustrine deposits laid down in the former Lake Lar. Subsequent rivers have carved out prominent sets of river terraces as the sediments have begun to be progressively removed. Different groups of sediments, whilst having a similar origin, in that they were deposited upstream of a lava dam, were probably not interrelated. Thus the maximum elevations reached by the sediments vary from basin to basin. The maximum elevation reached was in the eastern side at Dalichai where sediment was deposited up to an elevation of about 3500 metres. In the Lar valley the Lake reached an elevation of about 2700 metres whilst at Polour a maximum height of sediment of only 2260 metres was attained. These are correlated with spillway levels in the lava flows responsible for damming the individual valleys in the Lar basin.

8.2 SUMMARY OF FINDINGS

8.2.1 Land Surface Mapping from Aerial Photographs and Field Checking

Three major features were identified from aerial photographs: (I) vegetation cover type and density in different areas; (II) morphological features in the basin related to eruptions of Damavand, and the morphological changes in the Lar Basin associated with the present Lake; and (III) sediment volume measurement related to upstream erosional patterns.

In stage (I) aerial photograph interpretation was used to identify different types of vegetation. The aerial photographs of the Lar Basin show different tonal characteristics (see folded maps no.2 and 3). These tonal types are mainly associated with the density of surface vegetation. The highest density of vegetation is related to the flat river terraces, while bare soil (mostly limestone formation with no vegetation) appeared in Kuh e namahkusar, Alarm kuh, Tiz kuh and other limestone ridges in the Lar basin. The overall vegetation cover of the basin was 6% of high density, 41% moderate, 22% poor, 18% very poor and the remaining 13% bare rock and cliffs.

The aerial photographs from about 50 years ago show that the effect of animal grazing is clearly reflected in the surface cover changes of the study area. The area is extensively used by nomads for grazing sheep and goats (Figure 6.27). The dark tones appeared

very smooth and associated with the completely vegetated area, which was observed to a larger extent only in the 1955 aerial photographs. Moderately dark tones were relatively less smooth than the dark tone, reflecting significant degradation of the vegetation due to grazing of large flocks of sheep.

In stage (II) the major erosional forms identified on the aerial photographs include, landslides, sinkholes and gullying. The infill sediments of the Lar basin have been confirmed as of lacustrine origin. The morphological changes can be divided in to old and recent changes in sediments which are identified from aerial photographs in geomorphology map.

In stage (III) aerial photographs were employed to estimate sediment volumes at three selected sites, which were surveyed by echosounding in summer 1994. The sediment volume at Gozaldarreh is greater than at the two other tributaries in the middle and downstream. It is suggested that in the Khoshkeh Lar and Lar tributaries two important factors influence the sediment delivery. The first is the large area of terraces in these catchments which are readily eroded. The second one is the seasonal flow regime on poor or unvegetated areas in the Khoshkeh Lar tributary which deliver a high volume of sediment during the runoff season.

Only moderate morphological changes were identified at Sefid-Ab river mouth, which has the lowest drainage density, low elongation and lower slopes than the other selected sites. The downstream parts of this tributary possess a steeper slope than other tributaries so that the former Lake deposits cannot be seen in the downstream areas before the mouth. The Dalichai is unique in the area due to its physiography and geology. Lacustrine terraces are identified on both sides of the river downstream but in the river bed there is no evidence of terraces. This is related to very large sediment delivery in this tributary which has covered former Lake terraces with bed load derived from the volcanic areas.

8.2.2 SPOT (XS), Landsat (TM) and Land Surface Detection

Landsat and SPOT information offer significant advantages over traditional methods in detecting geomorphological features especially in inaccessible areas such as high

mountains. However, very few remote sensing studies have previously attempted to quantify the land surface changes or soil erosion occurring in upland areas. Much of the Lar Basin has significant geomorphological activity in the upstream parts of catchments, and also has a high potential for karst erosion since the Basin has been blocked by an artificial dam. This has apparently lead to change and caused leakage problems for the reservoir.

The ability to identify quickly the problem areas and to quantify morphological changes are vital for effective water and catchment management. The present study suggests that Landsat TM and SPOT XS can be used to make a rapid first approximation of the erosion in an area, and to identify different parts of a watershed according to the potential for erosion. The need for extensive field investigations is minimised and the use of limited resources is maximised.

Furthermore, this research shows the variation in capability of SPOT, Landsat TM, aerial photographs and KFA-1000 images to identify the land cover and morphological changes in mountainous areas. Photogrammetric plotting methods on aerial photographs proved to be an essential part of the estimation of the rate of soil erosion for the three river mouths in the Lar Basin. Further the sediment concentration, discharge, and sediment sampling results were valuable in estimating the sediment supply processes in the Lar Basin. The results indicate that eroded terrain can be classified employing the original bands of SPOT or Landsat TM. Preliminary data manipulation, such as ratioing was not required but was used for estimating vegetation characteristics.

The classification using the SPOT data gave good results in discriminating between land surface change classes. There were problems in the classification, for example between former farmland and vegetative cover, and it also misclassified bodies of water with large quantities of sediment. On the other hand the TM classification produced good classes of former farmland, bare soil and vegetated areas, but it greatly overestimated the eroded areas. The finer resolution of SPOT produced better identification and classification of changed areas, while the better spectral characteristics of Landsat TM resulted in a better classification of land cover.

The combination of visual interpretation of the stereo KFA-1000, aerial photos data, and multispectral classification of SPOT and Landsat TM data in the identification and classification of morphological changes using field work management proved to be an acceptable method and could be applied for other purposes as well.

8.3 GENERAL CONCLUSIONS

Remote sensing data were successful for identifying the main land cover types and changes in mountainous semi-arid Lar basin. Relatively poor erosion rate estimation based on SPOT and Landsat are directly attributable to their low effectiveness in clearly separating the depositional areas from other land surface in comparison with KFA-1000 and aerial photographs. As was expected, the work described in Chapter 6 confirmed that individual features e.g. rill or first order gullies cannot be identified by means of classification and none of the supervised or unsupervised classifications were successful in identifying small morphological features and their different severities in different sites in the Lar basin. The highest average accuracy of classification was 78% and 59% respectively for SPOT and TM maximum likelihood method, but this decreased to 33% and 52% for SPOT and TM using the Minimum Distance of Mean (MDM). Using maximum likelihood method, it seems that remote sensing data is the best tool for inaccessible parts of the Lar basin, subject to field checking of classification groups. The mapping information obtained from the classification was then used as an input into landsurface maps at the study area.

Except for estimation by FAO (1971) there were no sediment records available for the Lar basin. The soils and landform diversity mainly dictates the erosion features of the Lar basin. Extensive rilling and to some extent localized gullying were the most important erosion features in parts of the Lar basin. The analysis using remote sensing suggest that the three distinct surface types of vegetation cover, soils and slope angles, as identified in the field do exhibit distinctive features of erosion.

After identification of the deposition area in the Lar basin the amounts of infilled sediment estimated from topography maps at 1:25 000 (British Army, 1945) to a maximum of $1.58\times10^{11}m^3$ which represents a value of $2.08\times10^{3}m^3km^{-2}a^{-1}$. Three deltas with major accumulations sediment in the Lar basin were measured by photogrammetric

plotting from aerial photographs and echosounding surveying. The photogrammetric results give sediment yield as follows:

- Dalichai catchment in 1955 was $1.6\times10^3 m^3km^{-2}$ which increased to $1.96\times10^3 m^3km^{-2}$ in 1970 at a rate of $0.02\times10^3 m^3km^{-2}a^{-1}$.
- Gozaldarreh yielded 1.08×10^3 m^3km^{-2} in 1945 which increased to 1.5×10^3 m^3 km^{-2} in 1994 at a rate of $0.008\times10^3 m^3km^{-2}a^{-1}$ increase in delta volume;
- Sefid-Ab yielded $1.2\times10^3 m^3km^{-2}$ in 1955 and increased to $1.9\times10^3 m^3km^{-2}$ in 1970 at a rate of $0.04\times10^3 m^3km^{-2}a^{-1}$.

The echosounding surveys give yield values of;

- $3\times10^3 m^3km^{-2}$ at Dalichai ($0.1 m^3km^{-2}a^{-1}$),
- $1.5\times10^3 m^3km^{-2}$ ($0.075 m^3km^{-2}a^{-1}$) at Gozaldarreh, and
- lower in Sefid-Ab ($1.4\times10^3 m^3km^{-2}$ or $0.035 m^3km^{-2}a^{-1}$).

Both methods show that the Dalichai has a high sediment delivery rate, and this is confirmed by Figure 7.8 showing a relationship between sediment yield and drainage basin area (Branson et al. 1987). The errors in the estimates of sediment from these different methods are:

- ±22% ($\pm0.99\times10^5 m^3$) for the topographic map (Gozaldarreh only),
- ±15% ($\pm0.58\times10^5 m^3$) at Dalichai and ±9% ($\pm0.09\times10^5 m^3$) at Sefid-Ab for aerial photographs, and
- ±2% ($\pm0.11\times10^5 m^3$) at Dalichai; ±3.5% ($\pm0.06\times10^5 m^3$) at Sefid-Ab and ±2% ($\pm0.11\times10^5 m^3$) at Gozaldarreh for echosounding survey.

The calculated errors from the different methods show that the echosounding method, with a range between ±2% and ±3.5%, and also the photogrammetric method, range between ±9% and ±15%, provide reliable estimates of sediment volumes. The 1945 British Army topographic map (±22%) error is greater, but still provides a useful indication of sediment delivery. Sequential gauging data for sediment concentration and water discharge is also required to control for accuracy in sediment yield estimation.

In Chapter 7 a comparison of world reservoirs with the Lar basin has shown that the Lar has a medium sediment production rate (Figure 7.4). The only station (at Polour) with a long gauging record shows a significant influence of the artificial dam, with sediment

load estimated at about 223t $km^{-2}a^{-1}$ before the dam reducing to 155t $km^{-2}a^{-1}$ after it's construction. Finally, from work in Chapters 5 and 6 it can be concluded that the sub-catchments upstream, especially in the Quaternary deposition areas and unvegetated surfaces, are highly dissected by gully erosion and have suffered from surface erosion. In contrast, the flat terrace areas which were expected to be stable areas have been eroded by bank erosion along the river channels. However, based on the deposition of the basin in the past, the continuation of erosion at present, and the constructed dam after 1974 it is likely that areas downstream of the Lar basin (which accounts for 18% area of the Haraz basin) will be subject to reduced deposition rates in the future. This will inevitably impact on future soil fertility in an important agricultural production area on the Caspian plain of Iran.

8.4 SCOPE FOR FUTURE RESEARCH

The estimation of sediment yield from watersheds, with their complex arrangements of slopes and channels, can be accomplished by modelling each slope segment and channel reach, but an approach of this detail would be too costly for most semi-arid catchment studies. Statistical relationships between control factors and sediment yield are cheaper and easier to apply but sacrifice mathematical explanation (Weber et al. 1976). However, such relationships in semi-arid areas are influenced considerably by local factors (e.g. lithology, sediment history) and so are difficult to transfer from place to place. Detailed local information is thus required in all cases.

For large basin areas, like the Lar ($726km^2$), high accuracy of sediment yield estimates depends on the distribution of the gauging stations (sediment concentration and water discharge) in different parts of the area and also their length and regularity of record. But in some parts of the world, especially in inaccessible mountainous areas, establishment of the required equipment is impossible, so volumetric analysis from existing maps and high resolution remote sensing data can be neccessary. This was employed in the Lar basin by use of aerial photos, topographic maps and readily available remote sensing images. To improve this method for mapping of depositional areas, further work needs to be done, and in all cases many control points are required.

Measurement of the vegetation cover characteristics requires field work and ancillary data. In addition, the distribution of erosion rates for land cover should be extended to other factors which influence erosion. The best means for handling this multivariate problem will be gained by adopting a GIS method in the future (Disfani, 1989).

Sequential remote sensing images are required to identify the vegetation changes which are indirect indicators of accelerated soil erosion. The resolution of SPOT (PA 10m), KFA-1000 (5-10m) and aerial photos are good enough for looking at changes which occur in the land as a result of soil erosion. With regard to physical and vegetation characteristics, it is recommended that best results are achieved if the TM images are selected at least earlier than July (the TM used in this work which were dated September 1988, SPOT and KFA-1000 were dated June 1987 and 1991).

Looking to the future it is suggested that although the resolution of the TM (30m) and SPOT XS (20m) is currently an obstacle to the detection of fine erosion features in inaccessible areas, the resolution of SPOT (PA, 10m) and KFA-1000 are much better, also they are much cheaper. These sources of information are recommended for further use. The ease, cost and effectiveness of such studies will be further improved with the use of GIS and GPS technologies.

It is worth noting that approximately three months of effort went into mapping the land cover characteristics for the study area by aerial photograph interpretation, while much less time was spent to reach the same result by using the SPOT and TM digital data using the Dragon method. However, there is a loss of accuracy using remote sensing. The resolution of SPOT and Landsat TM was not enough to identify small feature changes unless supported by aerial photos, KFA-1000 and field checking. The methods are therefore complementary.

From work in Chapter 5 and 6 it was concluded that the land surface changes in vegetation and soil here increasingly related to human impacts via grazing and construction of the artificial dam. Also within the Quaternary deposition area in former Lake Lar and Dalichai wetter climatic conditions in the past period seems to have resulted in eroded land surface and reservoirs infilling. These deposits from former Lakes are also prone to bank erosion along the Lar channel, landslides in the Dalichai

and Sefid-Ab sub-catchment areas and sinkhole development around the present Lake. All of these factors serve to raise questions concerning the long term viability of the Lar dam; the dam is infilling with sediment; sinkholes are appearing in the terraces; leaks have occured downstream; and downstream sediment yield has been adversely affected.

GLOSSARY

Ab (persian): water.

Active system: A remote sensing system that transmits its own electromagnetic emanations at an object and then records the energy reflected or reflected back to the sensor.

Albedo: [1] The ratio of the electromagnetic radiation reflected by a body to the amount incident upon it, often expressed as a percentage; e.g., the albedo of the Earth is 34%. [2] The relativity of a body as compared to that of a perfectly diffusing surface at the same distance from the sun, and normal to the incident radiation.

Analogue image: An image where continuous variation in the object or surface being sensed is represented by continuous variation in image tone.

Ancillary: In remote sensing, secondary data pertaining to the area or classes of interest, such as topographic data. Ancillary data may be digitized and used in the analysis process in conjunction with the primary remote sensing data.

Aperture: The opening in a lens diaphragm through which light passes.

Azimuth: The geographical orientation of a line given as an angle measured clockwise from north.

Bit: [1] An abbreviation of binary digit. [2] A single character of a language employing only two distinct kinds of characters.

BP: Before Present.

Brightness: The attribute of visual perception by which an areas to radiate more or less light.

Brightness value: A image pixel value that represents the amount of radiance striking a detector in a multi-spectral scanner.

CCT: Computer compatible Tape; also known as magnetic tape.

Channel: Synonymous with band. In microBRIAN, band is used exclusively to refer to the traditional naming of the four Landsat MSS channels as bands 4-7.

Chehel (Persian): Forty (40).

Cheshmeh (Persian): Spring 'where water comes up naturally from the ground'.

Classification: The process of assigning individual pixels of a multi-spectral image to categories, generally on the basis of spectral reflectance characteristics.

CNES: Centre National d'Etudes Spatiales, France.

Colour composite: A colour picture produced by assigning the three primary colours to three selected channels of an image. For example, with Landsat MSS data, blue is ordinary assigned to band 4 (0.5-0.6μm), green to band 5 (0.6-0.7μm), and red to band 7 (0.8-1.1μm) to form a picture closely approximating a colour infrared photograph.

Composite photograph: A photograph made by assembling the separate photographs, made by the several lenses of a multiple-lens camera in simultaneous exposure, into the equivalent of a photograph taken with a single, wide-angle lens.

Compositing: Production of a single image by using data from multiple image. This process is applied to AVHRR imagery for cloud removal.

Contrast stretching: Improving the contrast of images by digital processing. The original range of digital values is expanded to utilize the full contrast range of the recording file or display device.

Darreh (persian): Valley

DEM: Digital Elevation Model.

DIAD: Digital Image Analysis and Display.

Digital image: An image having numeric values representing grey tones in which each numeric value represents a different grey tone.

Digital number (DN): The value of a variable recorded for each pixel in an image, usually in the range of 0-255.

DTM: Digital Terrain Model.

Edge enhancement: The use of image filtering techniques to emphasize changes in data values in imagery.

False colour image: A colour image where one or more channels which indicate nonvisible reflectance are expressed as one or more of the red, green and blue additive colour components, so the resulting colours do not correspond to normal visual experience; also called a false colour composite. The most commonly seen false colour image display the near infrared as red, red as green and green as blue.

FAO: United Nation Food and Agriculture Organisation.

Filtering: In analysis, the removal of certain spectral or spatial frequencies to highlight features in the remaining image.

Fourier transform: An optical or digital means of transforming an image from the spatial the frequency domain.

FOV: Field of view.

GCP: Ground Control Point.

GIS: Geographical Information System.

GPS: Global Positioning System.

HRV: High Resolution Visible Scanner.

I^2S: International Imaging System.

IR: infrared.

IRSC: Iranian Remote Sensing Centre.

Irradiation: The impinging of radiation on an object or surface.

ISPRS: International Society of Photogrammetry and Remote Sensing.

ITC: International Institute for Aerospace Survey and Earth Sciences.

Kuh (persian): montain.

Laplacian: A filter in which the central value is subtracted from the average of its neighborhood. The operation enhances edges and its name refers to its identity as a discrete from of the Laplacian derivative. [2] statistic produced by program mCURVA from the average of the first and second eigenvalues of the second partial derivative matrix which indicates the magnitude of the major surface curvature within the filter region.

Lineament: A linear topographical or tonal feature on the terrain and on images and maps, which may represent a zone of structural weakness.

Maximum Likelihood Classifier: Characterises each class by a probability distribution function and allocates pixel to the class with maximum likelihood among the candidate distributions. The most common model for the probability distribution function is the Gaussian distribution in which each class is characterised by its mean and covariance matrix.

Minimum distance classifier: A classification technique that assigns raw data to the class whose mean falls the shortest Euclidean distance from it.

NCC: Iranian National Cartographic Centre.

MSS: Multi-spectral Scanner.

NASA: National Aeronautics and Space Administration (USA).

NOVA: National Oceanic and Atmospheric Administration (USA).

Rud (persian): River.

RSS: Remote Sensing Society (UK).

SAR: Synthetic Aperture Radar.

Sefid (persian): white.

SLAR: Side-Looking Airborne Radar.

SPOT: Satellite Pour l'Observation de la Terre.

Synoptic view: The ability to see or otherwise measure widely dispersed areas at the same time and under the same conditions, such as the overall view of a large portion of the Earth's surface which can be obtained from satellite altitudes.

TIRS: Thermal Infrared Scanner.

TM: Thematic Mapper.

USLE: Universal Soil Loss Equation.

VHF: Very High Frequency.

VHRR: Very High Resolution Radiometer.

Visible wavelengths: The radiation range in which the human eye is sensitive, approximately 0.4-0.7μm.

WMO: World Meteorological Organization.

VTIR: Visible and Thermal Infrared Radiometer.

Zenith: The point in the celestial sphere that is exactly overhead. Constrsts with nadir.

Standard Symbols;

A° = angstrom (10^{-10}m).

α = absorptance.

ε = emittance.

nm = nanometre (10^{-9}m).

θ = angle of incidence.

λ = wavelength.

μ = micro (prefix), 10^{-6}m.

ρ =reflectance.

σ = Stefan-Boltzmann constant.

τ = transmittance.

REFERENCES

Abd Eel-Hady, A.M., Rognon, P., Escadafal, R., Pouget, M. (1989). Contribution of Landsat data (Mss) to Soil survey: Application of the soil of Southwestern Sina (Egypt). *International Journal of Remote Sensing.* **12**(5): 1053-1061.

Abrams, M.J., Siegel, B.S. (1980). Lithologic mapping. In: *Siegal, B.S., Gillespie, A.R. (eds.), Remote Sensing in Geology.* Wiley, New York. pp. 381-418.

Ackers, P. (1972). Sediment transport in channels: an alternative approach. *Hydraulic Research Station, Wallingford, Report no. INT **104**.*

Acton, D.F. and Stonehouse, H.B. (1972). *Experimental program on the application of remote sensing for soil surveys in Saskatchewan.* 1st Canadian Symposium on Remote Rensing of Environment: 295-303.

Addington, J.D. (1975). A hybrid maximum likelihood classifier using the parallelepiped and Bayesian techniques. Technical papers, *50th Annu. Meet. Am. Soc. Photogrammetry:* 772-784.

Al-Abbas, A.K., Swain, P.H. and Baumgardner, M.F. (1972). Relating organic matter and clay content to the multispectral radiance of soils. *Soil Science* **(114):** 477-485.

Alam, M.S. and Harris R. (1986). Study of moorland soil erosion by spectral reflectance. *International Journal of Remote Sensing* **8**(4): 593 608.

Ali, S.I., Chakaraborti, A.K., Iqbaludin and Ansari, I.A. (1988). *Remote sensing applications for water resources investigations in Tons river watershed, Doon valley, Upper Pradesh, India.* 22th Symposium on Remote Sensing of Environment: 851-870.

Almer, A. and Buchroithner, M.F. (1990). *Digital Mapping with High Resolution Sojuz KFA-1000 Images.* 10th EARSEL Symposium: New European Sys., Sensors and Applications, EARSEL: 403-417.

Allenbach, P. (1966). *Geologie und Petrographie des Damavend und seiner Umgebung (Zentral-Elburz), Iran.* Univ. Zurich, Geol. Inst. E. T. H.

Anderson, P. And Tallis, J. (1981). The nature and extent of soil and peat erosion in the Peak District-field survey. In: *Phillips, J., Yalden, D. And Tallis, J. (eds) Moorland Eroison Study, phase 1 (Peak park, Joint Planning Board, Bakewell):* 52-64.

Aniya, M. (1985). Landslide susceptibility mapping in the Amahata river basin, Japan. *Annals AAG.* 75**(1):** 102-114.

Anuta, P.E. (1977). Computer-assisted techniques for remote sensing data interpretation. *Geophysics* **42**: 468-481.

Ashley, G.M. (1975). Rhythmic sedimentation in glacial Lake Hitchcock, Massachusetts Connecticut. In:*Glaciofluvial and Glaciolacustrine Sedimentation,* (eds) Jopling, A.V. and McDonald, B.C. Soc. Econ. Paleontol. And Mineral Pub. **23:** 304-320.

Asserto, R. (1966). *Geological Map of Upper Djadjerud and Lar Valleys (Central Elborz, Iran).* Univ. Milano, Inst. Geol.

Astara, T. (1990). Drainage system analysis by Landsat-3 RBV, Landsat-5 TM and Spot PA. *International Journal of Remote Sensing* **11**(9): 1549-1559.

Atukum, I.B. (1976). Use of aerial photographs in erosion reconnaissance survey and local detailed studies in the Merida Province, Spain. *ITC, Msc Thesis.*

Ayres, Q.C. (1936). *Soil erosion and its control.* McGraw-hill, New York, N.Y. 365 pp.

Bailey, E.B. and Jones, R.C. and Asefia, S. (1948). Notes on the geology of the Elborz mountains, north-east of Tehran, Iran. *London, Quart. Jnl. Geol. Soc: 1-42.*

Baker, V.R. (1986). Fluvial landforms. In: *Short et al. (Eds) Geomorphology from space. NASA SP-486.* US Govt Printing Office, Washington DC. pp. 253-316.

Banerjiee, I. and McDonald B.C. (1973). Nature of esker sedimentation in Glaciofluvial and Glaciolacustrine Sedimentation. In: *Paleontol. And Mineral Pub.* **23:** 132-154.

Barber, D.G., Dean, G.F., Hochheim K.P., Kechy, R.E., McCullaugh G.K. and LeDrew, E.F. (1990). *Measuring historical sediment concentrations with archived Landsat Mss imagery.* 13th Canadian Symposium on Remote Sensing: 36-59.

Bartlett, D.S. and Klemas, V. (1982). In situ spectral reflectance studies of tidal wetland grasses. *Photogrammetric Engineering and Remote Sensing.* 47 **(12):** 1695-1703.

Beaubien, J. (1979). Forest type mapping from Landsat digital data. *Photogrammetric Engineering and Remote Sensing.* 45 **(8):** 1135-1144.

Beaven, P.J. (1984). *A microcomputer based image processing.* Presented in RSS workshop. Reading University, U.K. 12 April 1984.

Beer, C.E., Farnham, C.W. and Heineman, H.G. (1986). Evaluation of sedimentation prediction techniques in western Iowa. *Trans Am Soc Agric Engineering,* **9**:828-831, 833.

Begni, G. (1982). Selection of the optimum spectral bands for the SPOT satellite. *Photogrammetric Engineering and Remote Sensing* **48:** 1613-1620.

Berger, Z. And Jensen, J.R. (1980). Modelling soil loss and flood potential due to organization in humid subtropical southeastern environments. *Proc. 14th Int. Symp. On Remote Sensing of Environment:* 1057-1068.

Bergsma, E. (1974). Soil erosion sequence on aerial photo. *ITC Journal* **3:** 342-376.

Bishop, Y.M.M., Feinberg, S.E., and Holland, P.W. (1975). *Discrete Multivariate Analysis-Theory and Practice.* Cambridge, The MIT Press.

Biswas, R.R. (1978). Landsat data and soil study in a part of the Auranga catchment, India. *International Journal of Remote Sensing* 8(4):541-543.

Bobek, H. (1963). Nature and implications of Quaternary climatic changes in Iran. *Changes of Climate.* UNESCO. 403-413.

Bocco, G., Palacio, J.L. and Valenauela, C.R. (1989). Geomorphological mapping using SPOT for gully erosion assessment. *Procceding of 11th geomorphological cong.* Frankfurt, Germany:111-116.

Bogen, J. (1995). Sediment transport and deposition in mountain rivers. In: Foster et al. (eds), *Sediment and water quality in river catchments.* Wiley: 437-451.

Bohne, E. (1932). Die Steinkohlenvorcommen Persien. *Z. Prakt. Geol.,* **(40):** 113-119, 132-141.

Bout, P. and Derruau, M. (1961). *Le Damavend.* CNRS Centr. Doc. Cart. Geogr., Mem.

Braidwood, R.J. (1963). Summary of prehistoric investigations in Kurdistan in relation to climatic changes, in: *Changes of climate.* UNESCO: 251-254.

Branson, F.A., Gifford, G.F., Renard, K.G., Hadley, R.F. (1981). *Rangeland hydrology.* Kendal/Hunt, Dubuque.

British Army. (1945). *Lar Valley topography map at 1:25000.*

Brooks, C.E.P. and Carruthers, N. (1953). *Handbook of Statistical Methods in Meteorology.* London, UK Met. Office, H. M. S. O.

Browing, G.M., Parish, C.L. and Glass, J. (1974). A method for determining the use and limitations of rotation and conservation practices in the contrast of soil erosion in Iowa. *Journal of American Soc. Agron.,* **39**: 65-73.

Brunsden, D., and Prior, D.B. (1984). *Slope instability.* (eds) Chichester, Wiley.

Bryant, E., Dodge, A.G. and Warren, S.D. (1980). Landsat for practical forest type mapping: a test case. *Photogrammetric Engineering and Remote Sensing.* 46 **(2):** 1575-1584.

Buchanan, M.D. (1979). Effective utilization of colour in multidimensional data presentation. *Processing Soc. Photo. Opt. Instrument Eng.* **199**: 9-19.

Buller, A.T. and McManus, J. (1972). Simple metric sedimentary statistics used to recognize different environments. *Sedimentology.* **18:** 1-21.

Buringh, P. and Vink, A.P.A. (1961). The use of aerial photography in relation to soil erosion and soil conservation. *ITC, Delft,* The Netherland.

Burns, K.L. and Brown, G.H. (1978). "The human perception of geological lineaments and other discrete features in remote sensing imagery." *Remote Sensing of Environment* 7: 163-167.

Campbell, J.B. (1987). *Introduction to Remote Sensing.* New York, London, The Guilford Press, USA.

Campbell, W.J. (1981). An Application of Landsat and computer technology to potential water pollution from soil erosion. *Satellite Hydrology, 5th Annu. William, T. Pecora Symposium on Remote Sensing.* American Water Resources Association, Minneapolis, MN: 616-621.

Carson, M.A. and Kirkby, M.J. (1973). *Hillslope form and process.* Cambridge, Cambridge University Press.

Carter, P. and Jackson, M.J. (1976). The authomated recogniation of urban develipment from Landsat images. *Proc. Symp. Machine Processing of Remotely Sensed data.* Pardue University, Lafayette, I.N.

Carter, V. (1978). Coastal wetlands: role of remote sensing. In: *Coastal Mapping Papers Reprints from Coastal Zone Symposium on Technical, Environmental, Socioeconomic and Regulatory Aspects of Remote Sensing.* SanFrancisco, CA. March 14-16, 1978: 1261-1279.

Carter, V. And Richardson, K. (1981). Landsat digital analysis: implication for wetland management. *7th Int. Symp. on Machine Proc. Of Remotely Sensed Data.* Purdue University: 220-229.

Castleman, K.R. (1977). *Digital image processing.* Prentice-Hall, Englewood Cliffs, N.J.

CENES (Centre National d' Etudes spatiales) (1984). *SPOT satellite-based remote sensing system.* Toulouse, France.

Chalmers, A.I. and Harris, R. (1981). *Band ratios in multispectral analysis of Landsat digital data.* In: Geological and Terrain Analysis, Allan, J.A. and Bradshaw, M. (Eds): The Remote Sensing Society, p. 134.

Chaplo, R. (1974).The significance of bubble structures in borehole samples of fine sand. *Geotechnique* (3): 33-344.

Chavez, H. and Bauer J.(1982). An automatimum kernel-size selection technique for edge enhancement. *Remote Sensing of Environment* **12**(23): 38.

Chen, Z., Hansom, J.D. and Curran, P.J. (1991). The role of the relationship between suspended sediment concentration and spectral reflectance: its implications for the use of Daedaus 1268 data. *International Journal of Remote Sensing* **12**(1): 215-222.

Chow, V.T. (1964). *Handbook of Applied Hydrology.* New York, McGraw Hill.

Chidley, T.R.E. and Drayton, R.S. (1986). Spot simulated imagery in hydrological mapping. *International Journal of Remote Sensing* 7(6): 791-79.

Cihlar, J., Protz, R. And Prevost, C. (1987). *Soil erosion assessment using remote sensing data.* 11th Canadian Symposium on Remore Sensing: 395-407.

Cipra, J.E. (1973). Mapping soil associations using ERTS MSS data. In: *Proceedings of Confer. on Machine Processing of Remotely Sensed data.* LARS. Purdue University. Oct. 16-18. 1973: 3A-10.

Clotet, N. And Gallart, F. (1986). Sediment yield in mountainous basin under by Mediteranean climate. *Annals of Geomorphology,* **60:** 205-216.

Colwel, J.E. (1974). Vegetation canopy reflectance. *Remote Sensing of Environment* **3:** 175-183.

Condit, C.D. and Chavez, P.S. (1979). Basic concepts of computerised digital image processing for geologists. *US Geol. Surv. Bull.* **1462:** Washington DC, 16 pp.

Congalton, R.G., Mead, R.A. (1983). A quantative method to test for consistency and correctness in photointerpretation. *Photogrametric Engineering & Remote Sensing.* **49**(1): 69-74.

Congalton, R.G., Oderwald, R. And Mead, R. (1983). Assessing Landsat classification accuracy using discrete multivariate analysis statistical techniques. *Photogrammetric Engineering and Remote Sensing,* **49** (12): 1671-1678.

Congalton, R.G. (1988). A comparison of sampling schemes used in generating error matrices for assessing the accuracy of maps generated from remotely sensed data. *Photogrammetric Engineering and Remote Sensing,* **54**(5): 593-600.

Cochrane, G.R., Hajic, E.J. (1978). *Landsat mapping of suspended sediment.* 5th Canadian Symposium on Remote Sensing: 104-126.

Cohen, J. (1960). A coefficient of agreement for nominal scales. *Educational and Psychological Measurement.* **20**(1): 37-46.

Colwel, J.E. (1974). Vegetation canopy reflectance. *Remote Sensing of Environment* **3:** 175-183.

Corbel, J. (1964). L' erosion terrestre, etude quantitative (methodes, techniques, resultats). *Annales de Geographie.* **73:** 385-412.

Crapper, P.F. and Hynson, K.C. (1983). Change detection using Landsat photographic imagery. *Remote sensing of Environment.* **13:** 291-300.

Crown, P.H., Pawluk, S. (1972). *Remote Sensing for Soil Rsource.* 1st Canadian Symposium on Remote Sensing: 317-322.

Curran, P.J. (1980). Multispectral remote sensing of vegetation amount. *Prog. Phys. Geogr.* **4:** 315.

Curran, P.J. (1985). *Principles of Remote Sensing.* London, Longman.

Danel, N.M. and Shennan, I. (1987). Landsat TM imagery and mapping vegetation and sediment distribution in the wash estuary. *International Journal of Remote Sensing* **8**(7): 1101-1108.

Davis, L.S. (1975). A survey of edge detection techniques. *Computer Graphic and Image Processing.* **4:** 248-270.

Dedkov, A.P. and Mozzherin, V. (1992). Erosion and sediment yield in mountain regions of the wold. In: *Erosion, Debris Flows and Environment in Mountain Regions,* IAHS Publication 209: 29-36.

Degane, A., Lewis, L. And Dowing, B. (1979). Interactive computer simulation of the spatial process of soil erosion. *Prof. Geogr.* **31:** 184-190.

Delavigne, R. and Thibault, C. (1984). *Recent contribution of satellite remote sensing to the implementation of regional environmental policy in ILe-de France (Paris-Regional) through the qualitative mapping of urban vegetation.* International Symposium on Remote Sensing of Environment (II), Paris, France: 675-691.

Dellenbach, J. (1964). *Contribution a l'est de Teheran (Iran).* Strasbourg.

Dendy, F.E. and Bolton, G.C. (1976). Sediment yield-runoff-deainage area relationships in the United States. *Journal of Soil and Water Conservation. 32:* 264-266.

Disfani, N.M. (1989). *Utility of Spatial Filtering Techniques in Remote Sensing of Erosion in the Sefid-Rud basin Iran.* Ph.D Thesis **University of Glasgow.**

Donald, H.P. (1969). *Slope failure forms: their identification, characteristics and distribution as depicted by selected remote sensor returns.* 6th Symposium on Remote Sensing of Environment: 927-965.

Douville, H. (1904). Mollusque fossiles. In: *Mission Scientifique en Perse,* v.3, n.4, pp.450 pls., Paris.

Dowdeswell, M.R., Gorman, M.R., Macheret, YU.YA., Moskalevsky, M.YU., Hagen, J.O. (1993). Digital comparison of high resolution Sojuzkarta KFA-1000 imagery of ice masses with Landsat and SPOT data. *Annals of glaciology* **17:** 105-112.

Drury, S.A. (1987). *Image Interpretation in Geology.* Chapman and Hall, pp. 283.

Duda, R.D. and Hord, P.E. (1973). *Pattern classification and scene analysis.* New York, Wiley.

Dutra, L.V. and Mascarenhas, N.D.A. (1984). Some experiments with spatial feature extraction methods in multispectral classification. *International Journal of Remote Sensing* **5**(2): 303-313.

Ellison, W.D. (1944). Two devices for measuring soil erosion. *Agricultural Engineering,* **25:** 53-55.

Ellison, W.D. (1944). Some effects of raindrops and surface flow on soil erosion and infiltration, *Transaction American Geophysic Union,* vol. **26** (3): 415-429.

Elwell, H.A. (1978) Combined report of the multisciplinary team on soil loss estimation. *Rohdesia Dep. of cons. exten., unnumbered rep.*

Emery, K.A. (1975). Identification of soil erosion from aerial photographs. *Journal of Soil Conservation Sevice of New South Wales.* **31**(3): 219-240.

Engelund, F. and Hansen, E. (1967). A monograph of sediment transport in alluvial streams. *Teknisk Vorlag, Copenhagen.*

Erni, A. (1931). Decouverte du Bathonien fossilifere dans I'Elburz (Perse du Nord). *Geol. Helv.,* v. 24, n. 2, pp. 164-165, Basel.

Ernst, C.L. and Hopper, R.M. (1979). Using Landsat MSS data with soils information to identify wet land habitats. In: *Satellite Hydrology.* 5th Pecora Memorial Symp. Sioux Falls, SD.: 474-478.

Evans, R. (1980). Mechanics of water erosion and their spatial temporal controls: an emperical viewpoint. In: Kirkby, M.J., Morgan, R.P.C. (eds), *Soil erosion.* Wiley, Chechester. pp. 109-128.

Fantini-Sestani, N. (1965). The geology of the upper Djadjerud and Lar valleys. (II). *Riv. Ital. Paleont. Strat.* v.71, n. 1. Pp.13-108. Milano, Italy.

Fischer, E. (1914). Zur stratigraphie des Mesozoicum in Persien. Zeit. *Deut. Geol. Ges.,* v. 66, pp. 39-46, Berlin.

Fischer, E. (1915). Jura und Kreideversteinerungen aus Persien. Beitr. *Palaeont. Geol. Ost.-Ung.,* v. 27, pp. 207-273. Wien.

Flaxman, E.M. (1972). Predicting sediment yield in Western USA. *Journal of Hydraulic Engineering, American Soc. of Civil Engineers* **198**(12): 2073-2085.

Fleiss, J.L., Cogen, J. and Everitt, B.S. (1969). Large sample standard errors of kappa and weighted kappa. *Psychological bulletin* **72**(5): 323-327.

Fournier, F. (1954). Influence des factors climatiques sur l'erosion du sol estimation des transports solides effectues en suspension par les cours d'eau', *publication. International Association of Scientific Hydrology,* **38:** 283-8.

Fournier, F. (1960). Debit solide des cours d'eau. Essai d,estimation de la perte en terre subie par l'ensemble du globe terrestre, *publication. International Association of Scientific Hydrology,* **53:** 19-22.

Frances, M.J. and Hedges, P.D. (1986). *A hydrological comparison of Landsat TM, MSS and black and white aerial photography.* Symposium on Remote Sensing for Resources Development and Environment Management, Enschede, the Netherlands: 717-720.

Frankline, S. E. (1987). Geomorphometric processing of digital elevation models. *Computers and Geosciences* **13**(6): 603-609.

Franklin, S.E., Rogerson, R.J. and Moulton, J.E. (1987). *Interpretation of a high relief glaciated environment using digital spectral in sothwestern Yukon.* 11th Canadian Symposium on Remote Sensing: 419-427.

Franklin, S. E. and Peddle, D.R. (1990). Classification of SPOT HRV imagery and texture. *International Journal of Remote Sensing* **11**(3): 551-556.

Fung, T. and LeDrew, E.F. (1988). The determination of optimal threshold levels for changes detection using various accuracy indices. *Photogrammetric Engineering & Remote Sensing* **54**(10): 1449-1454.

Gale, S.J. and Hoare, P.G. (1991). *Quaternary Sediments,* Belhaven Press pp:325.

Ganser, A. and Huber, H. (1962). Geological observations in the Central Elborz, Iran. *Mineral. und Petrogr. Mitt* **42**(2): 583-630.

Gardner, T.W. (1988). Fluvial networks analysis by SPOT panchromatic data." *International Journal of Remote Sensing* **10**(11): 1789-1807.

Gerrard, A. J. (1981). *Soil and land forms an integration of geomorphology and pedology,* George Allen and Unwin, London.

Gardner, T.W., and Connors, K.F. (1989). Extraction of fluvial networks from SPOT (Pan) data from low relief arid basin. *International Journal of Remote Sensing.* **10**(11): 1789-1801.

Ghosh, T.K. (1990). Landsat TM data and neotectonic analysis of Mendba river basin, India. *International Journal of Remote Sensing* **12**(12): 2585-2595.

Goldin-Rudahl (1993). *Dragon/ips Image Processing System.* Goldin-Rudahl system Inc. USA.

Golubev, G.N. (1982). Soil erosion and agriculture in the world: an assessment and hydrological implications. In: *Walling, D.E. (ed.), Recent Developments in the Explanation and Prediction of Erosion and Sediment Yield.* International Assoc. of Hydrological Sciences **137:** 261-268.

Gong, P. and Howarth, P.J. (1989). *A modified probabilistic relaxation approach to land cover classification.* Proceeding of IGARSS 89/12th Canadian Symposium on Remote Sensing, Vancover, B.C: 1621-1624.

Gong, P. (1990). A graphical approach for evalution of land-cover classification procedures. *International Journal of Remote Sensing* **11**(5): 899-905.

Gong, P. (1990). An assessment of some factors influencing multispectral landcover classification. *Photogrammetric Engineering and Remote Sensing* **56** (5): 597-603.

Gong, P. and Howarth, P. (1992). "Frequency-Based Contextual Classification and Gray-Level Vector Reduction for Landsat-Use Identification." *Photogrammetric Engineering and Remote Sensing* **58**(4): 423-437.

Gonzalez, R.C. and Wintz, P. (1987). *Digital image processing.* Adddison-Wesley Publishing Company, pp.500.

Gottschalk, L.G and Brune, G.M (1950). Sediment design criteria for the Missouri Basin, Loess hills, U.S. Dept. Agr. Soil Conserv. SCS-TP-97.

Graf, W.L. (1983). Variability of sediment removal in a semi-arid watershed. *Water Resour. Res.* **19:** 643-652.

Graf, W.L. (1988). *Fluvial Processes in Dryland Rivers.* Springer-Verlag. 346 pp.

Gregory, K.J. and Walling, D.E. (1976). *Drainage basin form and process.* Edward Arnold, London.

?Gregory, K.J., Davis, R.J. and Downs, P.W. (1992). Identification of river channel change due to urbanization. *Applied Geography,* **(12):** 299-318.

Gugan, D.J. and Dowman, I.J. (1988). Topographic mapping from SPOT imagery. *Journal of Photogemmetric Engineering and Remote Sensing* **54:** 1409-1414.

Gurnell, A.M. (1995). Sediment Yield from Alpine Glacier Basins. In: Foster et al. (eds), *Sediment and water quality in river catchments.* Wiley: 407-435.

Haack, B., Bryant, N. and Adams, S. (1987). An assessment of Landsat MSS and Tm data for urban and near-urban landcover digital classification. *Remote Sensing of Environment.* **21:**201-213.

Hadley, R.F. (1961). Influence of riparian vegetation on channel shape, northeastern Arizona. *U.S. Geol. Surv. Prof. Pap.* **424-C:** 30-31.

Haralick, R.M. (1979). Statisticsl and structural approaches to texture. *Proceedings of the IEEE.* **67**(5): 786-804.

Haralick, R.M. and Fu, K. (1983). Pattern recogniation and classification. In: *Colwell, R.N. (ed). Manual of remote sensing. Am. Soc. Photogrammetry Remote Sensing,* Falls Charch: 793-805.

Haralick, R.M., Wang, S., Shapiro, L.G. and Campbell, J.B. (1985). Extraction of drainage networks by using and consistent labeling technique. *Remote Sensing of Environment* **18:** 163-175.

Harper, D. (1983). *Eye in the sky, Introduction to remote sensing.* Ministry of Supply and Services, Canada.

Harris, J.W.E., Dawson, A.F. and Goodenough, D. (1978). Evaluation of Landsat data for forest pest detection and damage appraisal surveys in British Colombia. *Environment Canada, Canadian Forestry Service, Pacific Forest Research Centre, Victoria, B.C.* 12 p.

Harris, R. (1987). *Satellite Remote Sensing.* Routledge and Kegan Paul.

Heede, B.H. (1975). Watershed indicators of landform development. In: *Hydrology and water resources in Arizona and the Southwest, Volume 5.* Proceedings, 1975 Meeting, Arizona, American Water Resource Association and Hydrology Section, Arizona Academy of Science: 43-6.

Henderson, F.M. (1990). *Open Channel Flow.* New York, Macmilan.

Hey, R.D. (1982). Gravel bed rivers: form and processes. In: Hey, R.D., Bathurst, J.C. and Thorne, C.R. *(eds), Gravel bed rivers,* Wiley, Chichester, 5-13.

Kirschner, F.R., Kaminsk, S.A., Weismiller, R.A., Sinclair, H.R. and Hinzel, E.J. (1978). Map unit composition assessment using drainage classes defined by Landsat data. *Soil Sci. Soc. of Am. J.* **42:** 768-771.

Hjeelmfelt, A.T. and Cassidy, J.R.J.J. (1975). *Hydrology for Engineers and Planners.* Ames, Iowa, Iowa State University Press.

Hobbs, W.H. (1904). Lineaments of the Atlantic border region. *Geological Society Am. Bull.* **15:** 483-506.

Holz, R.K. and Baker, V.R. (1979) *An examination of fluvial morphological characteristics of western Amazon streams from Apolo-Syuz photographs.* In: Satellite hydrology.American Water Resources Association: 252-259.

Hooke, J.M. (1979). An analysis of the processes of river bank erosion. *Journal of Hydrology.* **42:** 39-62.

Hord, R.M. (1982). *Digital Image Processing of Remotely Sensed Data.* New York, Academic Press. 256 pp.

Horton, R.E. (1932). Drainage basin characteristics. *Am. Geophys Union Trans* **13:** 350-361.

Horton, R.E. (1941). Sheet erosion, present and past. *American Geophys Union* Trans **22:** 299-305.

Horton, R.E. (1954). Erosional development of streams and their drainage basins, hydrophysical approach to quantitative morphology. *Geological Society* Am. Bull. **56:** 275-370.

Hossain, H. and Chaudhury, M.U. (1975). *Study of land formation in Bangladesh whith Landsat-1 images.* 10th Symposium on Remote Sensing of Environment: 1023-1027.

Howard, J.A. (1991). *Remote Sensing of Forest Resources: Theory and application.* Chapman and Hall. 420 pp.

Hsu, S. (1978). Texture tone analysis for automated landuse mapping. *Photogrammetric Engineering & Remote Sensing* **44**(11): 1393-1404.

Hudson, N.W. (1961). An introduction to the mechanics of soil erosion under conditions of subtropical rainfall. *Rhod. Sci. Assoc. Proc.* **49:** 14-25.

Hudson, N.W. (1978). Soil conservation strategies for the future. In: *Rimwanich, S. (Eds), Land conservation for future generations.* Bankok, Dep. of Land Development: 117-130.

Hutton, S.M. and Dincer T. (1979). *Satellite Hydrology,* A.W.R. pp.512.

Ioka, M. and Koda, M. (1986). Performance of Landsat-5 (TM) data in landcover classification. *International Journal of Remote Sensing.* **7**(12): 1715-1728.

Iranian Geographical Organization, (I.G.O.), Tehran (1975). *Topography Maps of the Lar Basin at 1:50 000.*

Iranian Geological Survey Organization (G.S.O.) (1972). *Geological Map of The Central Alborz at 1:100 000.*

Iranian Geological Survey Organization (G.S.O.) (1973). *The Seismicity of Iran (Prelinimary Map of Epicentres and Focal Depths).*

Iranian Geological Survey Organization (G.S.O.) (1987). *Geological map of Tehran at 1:250 000.*

Iranian Geological Survey Organization (G.S.O.) (1991). *Geology map of Amol at 1:250 000.*

Iranian National Cartographic Centre, (N.C.C), Tehran. (1962). *Lar Valley.* topography maps at 1:10 000.

Irons, J.R., Markham, B.L., Nelson, R.F., Toll, D.L., Williams, D.L., Latty, R.S. and Stauffer, M.L. (1985). The effects of spatial resolution on the classification on TM data. *International Journal of Remote Sensing.* 6**(8):** 1385-1403.

Ishaq, A.M. and Huff, D.D. (1974). Application of remote sensing to the location of hydrologically active areas. *Proc. 9th Int. Symp. Remote Sensing of Environment.* Michigan. **(I):** 653-666.

Jackson, R.D. and Slater, P.N. (1983). Discrimination of growth and water stress in wheat by various vegetation indice through clear and turbid atmosphere. *Remote Sensing of Environment* 6(8): 1385-1403.

Jackson, M.J. and Mason, D.C. (1986). The develioment of integrated Geo-information Systems. *International Journal of Remote Sensing.* 7**(6):** 723-740.

Jacobsen, K. (1992). *Advantages and Disadvantages of Different Space Images for Mapping.* International Society for Photogrammetry and Remote Sensing (ISPRS) **29**(2): 162-168.

Jacobsen, K. (1993). *Comparative Analysis of The Potential of Satellite Images for Mapping.* International Society for Photogrammetry and Remote Sensing (ISPRS) IPI, Hannover: 107-113.

Jackson, R.D., Slater, P.N. and Pinter, P.J. (1983). Discrimination of growth and water atress in wheat by various vegetation indices through char and turbid atmospheres. *Remote Sensing of Environment.* **13:** 187-208.

Japan Association on Remote sensing (1993). *Remote Sensing Note.* Nihon Printing Co.Ltd, Tokyo, Japan. pp: 284.

Jensen, J.R. and Toll, D.L. (1982). Detecting residential land-use development at the urban fringe. *Photogrammetric Engineering & Remote Sensing* **48**(4): 629-643.

Jensen, J.R. (1986). *Introductory Digital Image Processing.* Englewood Cliffs, New Jersey, Prentice-HALL.

Jones, R.G.B. and Keech, M.A. (1966). Identifying and assessing problem areas in soil erosion survey using aerial photographs. *Photogrammetric Review.* **27:** 189-197.

Jones, J.G. (1970). Intreglacial volcanoes of the Laugravatn region, Southwest Iceland (II). *Jnl. of Geol.* 78 (2): 127-140.

Jordan, T.R. and Welch, R. (1984). Photogrammetric mapping of soil erosion from low altitude aerial photographs. *Tech. Papers. 50th Annual Meeting, ASP.* (II), ASS-ACSM Convention. March 11-16: 848.

Judson, S. And Ritter, D.F. (1964). Rates of regional denudation in the United States. *Journal of Geophysical Research* **69:** 3395-401.

Justice, C., Wharton, S.W. and Holben, B.N. (1981). Application of digital terrain data to quantify and reduce th topographic effect on Landsat data. *Intternational J. Remote Sensing.* **2:** 213-230.

Karvas, M.L. ed. (1989). Surface Water Modelling: *New Directions for Surface Water Modelling.* IAHS, (181).

Keech, M.A. (1972). Aerial photography applied to the assessment and control of soil erosion caused by water. *Atti delle gironate di studio della la sezione CIGR, Firenze:* 168-177.

Kirkby, M.J. and Neale, R.H. (1987). A soil erosion model incorporating seasonal factors.In:*Gardiner, V. (Ed), International Geomorphology (II).* Wiley: 189-210.

Kirpich, Z.P. (1940). Time of concentration of small agricultural watershed. *Civil Engineering* 10(6): 362.

Kowalik, W.S. and Lyon, R.J.P. (1983). The effects of additive radiance terms on ratios of Landsat data. *Photogrammetric Engineering and Remote Sensing* **49:** 659-669.

Kramer, J. (1991). Production and revision of maps using satellite photography from MKF-6, KATE-140, KATE-200 and KFA-1000 cameras. *Journal of Photogrammetry and Remote Sensing* **(46)**: 31-36.

Kristof, S.J. and Zachary, (1974). Mapping soil features from MSS data. *Photogrammetric Engineering and Remote Sensing* **40:** 1427.

Kristof, S.J., Baumgardner, M.F., Weismiller, R.A. and Davis, S. (1980). Application of multispectral reflectance studies of soils: *pre-Landsat. Machine Peocessing of Remotely Sensed Data Symposium:* 52-61.

Krumbeck, L. (1922). Stratigraische Ergebnisse von Niedermeyers Reise durch persien. *Zentralbl. f. Min.usw.*, Abt.B.

Lamb, H.H. (1961). Fundamentals of climate. In: *Descriptive paleoclimatology,* (ed) Nairn, A.E.M. Interscience publishers. London.

Langbein, W.B. (1947). Topographic Characteristics of Drainage Basins. USA, *American Geological Survey Water Supply: no.968-C.*

Langbein, W.B. and Schumm, S.A. (1958). Yield of sediment in relation to mean annual precipitation. *Transactions American Geophysical Union* **39:** 1076-84.

Larocque, A. (1983). *Seasat-A to detect geomorphological phenomena in St. Lawrence valley, Qubec, Canada.* 8th Canadian Symposium on Remote Sensing: 785-791.

Latty, R.L. and Hoffer, R.M. (1981). Computer-based classification accuracy due to the spatial resolution using per point and pre-field classification techniques. *Machine Processing of Remotely Sensed Data Symp.* West Lafayette, Indiana: 384-392.

Lawler, D.M. (1992). Process dominance in bank erosion systems. In Carling, P.A. and Petts, G.E. (eds), *Lowland Floodplain Rivers, Geomorphological Perspectives,* Wiley, Chichester: 117-144.

Leeder, M.R. (1982). *Sedimentology: process and product.* Allen and Unwin, Boston.

Leopold, L.B., Emmett, W.W., Myrick, R.M. (1966). Channel and hillslope processes in a semi-arid area, New Mexico. *US Geol. Survey. Prof. Paper* **352-G:** 193-253.

Liedtke, J., Robert, A. and Evans, D. (1987). *Discrimination of suspended sediment and littoral features using multespectral video imagery.* 10th Symposium on Remote Sensing: 739-747.

Lillesand, T. and Kiefer, R. (1987, 1993). *Remote Sensing and Image Interpretation.* John Wiley & Sons, pp.750.

Lioyed, C.H. and Eley, G.W. (1952). Graphical solution of probably soil loss formula for the northeastern region. *J. Soil and Water Conserv.* **7:** 189-191.

Livesey, R.H. (1975). Corps of Engineering methods for predicting sediment yields. *Present and prospective technology for predicting sediment yields and sources.* U.S. Dept. Agric. Res. Serv. Publ. ARS-S- **40:** 16-32.

Lo, C.P. (1976). *Geographical applications of aerial photography.* Crane Russak: New York: David and Charles: Newton Abbot, London.

Longoria, A., Zivichin, V., Greshishev, A. and Wallace, B. (1993). *Integration of Geologic and High Resolution Russian Satellite Photography for GIS Applications Covering the Timan Pechora Basin, Russia.* 10th Thematic conference on Geologic Remote Sensing, San Antonio, Texas, USA: (vol.I), 474-479.

Lorenz, C. (1964). Die Geologi des Oberen Karaj-Tales (Zentral Alborz, Iran). *Mitt. Geol. Inst. E.T.H. Univ. Zurich, N.F.,* **(22):** 114-136, Zurich Germany.

Low, F.K. (1967). Estimating potential erosion in developing countries. *Journal of Soil and Water Conservation* **22:** 147-148.

Marceau, D.J.P.J., Dubois, J-M.M. and Gratton, D.J. (1990). Evalution of the grey level co-occurance matrix method for land cover classification using SPOT imagery. *IEEE Transaction on Geoscience and Remote Sensing* **28**(4): 513-19.

Marek, K.H. and Weigelt, A. (1993). *The 3rd Generation of Space Photography.* (ISPRS) International Society for Photogrammetry and Remote Sensing, IPI Hanover: 101-106.

Markham, B.L. and Townshend, J.R.G. (1981). Land cover classification accuracy as a function of sensor spatial resolution. *Proc. 15th Int. Symp. Remote Sensing of Environment.* Michigan. **(III):** 1075-1090.

Marwick, R. (1972). *Site investigation for Lar Dam, Iran.* Civ. Eng. and Pub. Wks. Rev. 67, No 788, March.

Mather, P.M. (1987). *Computer Processing of Remotely Sensed Images An introduction.* Chichester, John Wiley & Sons. pp.352.

Mattews, H.L., Cunningham, R.L. and Peterson, G.W. (1973). Spectral reflectance of selected Pennsylvania soils. *Soil Sci. Soc. Am. Proc.* **37:** 421-424.

Megahan, W.F. (1975). Sedimentation in relation to logging activities in the mountains of central Idaho. *Present and prospective technology for predicting sediment yields and sources.* U.S. Dept. Agric. Res. Serv. Rep. ARS-S-**40:** 74-82.

Mehta, K.M., Sharma, V.C. and Deo, P.G. (1963). Erodibility investigations of soil of Eastern Rajasthan. *Journal of Indian Soc. Soil Sci.,* **11:** 23-31.

Miller, V.C. (1953). *A quantitative geomorphic study of drainage basin characteristics in the clinch mountain area.* Dept. of Geology. **Colombia University.**

Moik, J.G. (1980). Digital processing og remotely sensed images. *NASA SP-431, U.S. Govt. Printing Office.* Washington, D.C.

Moor, G.K. and Waltz, F.A. (1983). Objective procedures for lineament enhancement and extraction. *Photogrammetric Engineering and Remote Sensing* **49:** 641-647.

Morgan, J.D. (1905). Notes sur La geologie de La Perse et sure les travaux paleontologiques de M.H. Douville sur cette region. *C.R.S.G.F.* **5**(4e): 170-189.

Morgan, K.M., Lee, G.B., Kiefer, R.W., Daniels, T.C., Bubenzer, K.D., and Murdock, J.T. (1978). Prediction of soil loss on cropland with remote sensing. *Journal of Soil and Water Conservation.* **33:** 291-293.

Morgan, K.M., Morris, D.R., Lee, G.B. and Kiefer, R.W. (1979). Cropping management using colour infrared aerial photographs. *Photogrammetric Engineering and Remote Sensing* **45(6):** 769-774.

Morgan, K.M., Morris, D.R., Gershaw, G.B. and Kiefer, R.W. (1980). Airphoto analysis of erosion control practices. *Photogrammetric Engineering and Remote Sensing* **45:** 637-642.

Morgan, K.M. and Nalepa, R. (1982). Application of aerial photographic and computer analysis to the USLE for wider erosion studies. *Journal of Soil and Water Conservation.* **37:** 347-350.

Morgan, R.P.C. (1986). *Soil erosion and conservation.* Longman U.K. 93pp.

Morris, J.D., Morgan, K.M., Kiefer, R.W. and Scarpace, F.L. (1979). *Remote sensing as a source of landcover information utilized in the USLE.* 13th Symposium on Remote Sensing of Environment: 1107-1115.

Moss, A.J., Green, P., Hutka, J. (1982). Small channels: their formation, nature and significance. *Earth Surface Processes and Landforms* **7:** 401-15.

Muesksch, M.C. (1984). A splash and sheet erosion model from Landsat data. Proc. *IGARSS'84 Symp., Strasbourg,* ESA SP-215: 295-299.

Musgrave, G.W. (1947). The quantitative evaluation of factors in water erosion: a first approximation. *Journal of Soil and Water Conservation,* **2:** 133-138.

Negev, M. (1967). *A sediment model on a digital computer.* Department of Civil Engineering, Rep. no. 76. **Stanfod University, California.**

Nelson, R. (1985). Reducing Landsat MSS scene variability. *Photogrammetric Engineering and Remote Sensing* **51:**583-593.

Novo, E.M.M., Hansom, J.D. and Curran, P.J. (1989). The effect of sediment type on the relationship between reflectance and suspended sediment concentration. *International Journal of Remote Sensing* **10**(7): 1283-1289.

Novo, E.M.M., Hansom, J.D. and Curran, P.J. (1989). The effect of viewing geometry and wavelength on the relationship between reflectance and suspended sediment concentration. *International Journal of Remote Sensing* **10**(8): 1357-1372.

OKI (Ohaio-Kentucky-Indiana Regional Council of Governments), (1975). A method for assessing rural non-point sources and its application in water quality management. *Water Resources Planning Divesion, EPA.* Washington, DC.

OLeary D.W. and Friedman, J.D. (1976). Lineament, linear and lineation. *Geological Society Am. Bull.* **87**: 1463-1469.

Ovcinnikow, A. (1930). Outline of the geology of the Demavend region. *Bull. Naturalistes Moscou, sect. Geol., 8/4.*

Palylyk, C.L., Crown, P.H., Sauchyn, D.J. (1992).*Temporal monitoring of agricultural soil erosion risk through integrated Landsat and GIS.* 14th Canadian Symposium on Remote Sensing: 108-111.

Pearson, R.L. and Miller, L.D. (1972). Remote sensing of crop biomass for estimation of crop productivity of the short prairie. *Proceeding of the 8th International Symp. on Remote Sensing of Environment.* Ann Arbor, Michigan: p. 1357.

Peli, T. and Malah, D. (1982). A study of edge detection algorithms. *Computer graphics image processing* **20**: 1-21.

Pelletier, R.G. (1985). Evaluating non-point polution using remote sensed data in soil erosion model. *Soil and Water Conservation* **40:** 332-335.

Perrot, T. (1984). *The analysis of Landsat Mss data for characterizing sediment dispersal in the Beaufort sea.* 8th Canadian Symposium on Remote Sensing: 283-291.

Pickup, G. and Chewings, V.H. (1987). Landsat Mss data and forecasting pattern of soil erosion. *International Journal of Remote Sensing* **9**(1): 69-84.

Piest, R.F., Kramer, L.A. and Heineman, H.G. (1975). Sediment movement from loessial watersheds. Present and prospective technology for predicting sediment yields and sources. *US Dept. Agric, Agric Res Serv Publ ARS-S-40,* pp. 130-141.

Pihan, J. (1980). Soil erosion detection using infrared colour oblique aerial photography. In: *Boodt, M.D.E. and Gabriels, D. (eds), Assessment of erosion.* Wiley and Sons. Chichester, U.K.

Pitts, D.E. and Badhwas, G. (1980). Field size, length and width distributions based on LACIE ground truth data. *Remote Sensing Environment.* **10:** 201.

Poole, D.H. (1969). Slope failure forms: their identification, characteristics and distribution as dipicted by selected remote sensor returns. *Proc. 6th Int. Symp. on Remote Sensing Environment.* **(II),** Oct. 13-16, Michigan, Ann. Aebor. U.S.A.: 927-965.

Pratt, W.K. (1978). *Digital image processing.* Wiley, New York.

Ragan, R.M. and Rogers, R.H. (1978). Use of Landsat satellite remote sensing for regional environment planning and management. *XV Convention Pan American Federal of Engineering Societies.* Santiago, Chile.

Rahn, P.H. and Moore, D.G. (1979). Landsat data for locating shallow glacial aquifers in Eastern South Dakota. In: *Satellite Hydrology.* pp.398-404.

Raikes, R. (1967). *Water, weather and prehistory.* John Baker London. Pp.208.

Rassekh, M., Tiedig, F., Vollmer, T. And Weggen, J. (1984). Zur Geologie des Gebietes zwischen Chalus-und Haraz-Tal (Zentral-Elburz, Iran). *Verh. naturwiss. Ver. Hamburg* (NF) **27:** 107-196.

Rees, W.G. (1990). *Physical principles of remote sensing.* Cambridge University Press. 247pp.

Renard. K.G. (1972). Sediment problems in the arid and semi-arid Southwest. *Proc. 27th Annu. Meet. Soil Cons. Soc. Am:* 255-232.

Renfro, G.W. (1975). Use of erosion equations and sediment-delivery ratios for predicting sediment yield. Present and prospective technology for predicting sediment yields and sources. *US Dept. Agric, Agric Res Ser Pub ARS-S-40,* pp. 33-45.

Resenfield, G.H. and Fitzpatrick-Lins, K. (1986). A coefficient of agreement as a measure of thematic classification accuracy. *Journal of Photogrmmetric Engineering and Remote Sensing* **52**(2): 223-227.

Rib, H.T. and Liang, T.A. (1978). Recognition and identification. In: Schuster, R. L, Krizek, R.V. (eds) *Landslides analysis and control. Trans Res Board Nat Res Conucil* USA Space Rep **178:** 34-80.

Richard, J.A. (1993). *Remote Sensing Digital Image Processing: An Introduction.* Spriger-Verlag. pp.340

Richards, K. (1993). Sediment Delivery and the Drainage Network, In: *Channel Network Hydrology: 221-254,* Ed. Beven, K. And Kirkby, M.J., John Wiley & Sons Ltd.

Richards, K. (1982) Rivers *Form and Process in Alluvial Channels.* Methuen, pp.361.

Ripley, P.O., Kalbfleisch, W., Bourget, S.J., and Coper, D.J. (1961). *Soil erosion by water: damage, prevention, control.* Can. Dep. Agriculture, Res Br Publ 1083.

Riviere (1934). Contribution a letude geologique de I'Elbourz. *Rev. Geogr. Phys. Geol. Dynam., v.7. 1-2,* pp: 1-190, 12 pls., 20 tex-figs., Paris.

Robert, K.H. and Baker, V.R. (1979). An examination of Fluvial Morphological Characteristics of Western Amazon streams from Apollo-Soyuz photographs. In: (eds) *Satellite hydrology:* 252-259.

Robinove, C.J. (1982). Computation of physical values from Landsat digital data. *Photogrammetric Engineering and Remote Sensing.* **48:** 781-784.

Roehl, J.W. (1961). Sediment source area, delivery ratios, and influencing morphological factors. *Int Assoc Sci Hydrology Publ* **59:** 202-213.

Rogers, N.W., Selby, M.J. (1980). Mechanism of shallow translational landsliding during summer rainstorms: North Island New Zealand. *Geografiska Annaler* **62-A:** 11-21.

Rohde, W.G. and Pohl, R.A. (1978). Eros data center Landsat digital enhancement techniques and imagery availability, 1977. *Canadian Journal of Remote Sensing* **4**(63): 76.

Rohn, P. (1979). *Remote sensing and bank erosion along the Missori river, South Dakota, USA.* In: Satellite Hydrology.American Water Resources Association: 697-700.

Rooseboom, A. (1975). Sediment transport in rivers and reservoir basins. *D. Sc. (Eng.) Thesis presented to the University of Pretoria, Pretoria, South Africa.*

Rosenfeld, A. and Kak, A.C. (1982). Digital picture processing, 2nd edn, *Academic Press, Orlano, FLA.*

Rothery, D.A. and Drury, S.A. (1984). The neotectonics of the Tibetan Plateau. *Tectonics,* **3:** 19-26.

Royer, A., Vincent, P., Dube, C. and Bonn, F. (1984). *Landsat image and geomorphological interpretation of an area in southern Qubec in Canada (French text).* 8th Canadian Symposium on Remote Sensing: 717-732.

Sabins, F.F. Jr. (1978). *Remote Sensing Principles and Interpretation.* Freeman, San Francisco, 426 pp.

Schecter, R.N. (1976). Resource inventory using Landsat data for area wide water quality planning. *Proc. Symp. on Machine Processing of Remotely Sensed Data.* Purdue University, West Lafayette.

Schumm, S.A. (1956). Evolution of drainage system and slopes in badlands at Perth Amboy, New Jersey. *Bull. American Geological Society* **67**: 597-646.

Schumm, S.A. and Hadley, R.F. (1957). Arroyos and the semi-arid cycle of erosion. *American Journal of Science* **255:** 161-174.

Schumm, S.A. (1975). Quaternary palaeohydrology. In: Wright, H.E. and Frey, D.G. (eds.), *The Quaternary of the United States,* Princeton University Press, Princeton.: 783-794.

Scoging, H., Parsons, A.J., and Abrahams, A.D. (1992). Application of a dynamic overland-flow hydraulic model to a semi-arid hillslope, Walnut Gulch, Arizona. In: Parsons and Abrahams (eds) *Overland flow: Hydraulic and erosion mechanics.* London, UCL Press: 105-145.

Selby, M.J. (1993). *Hillslope Materials and Processes.* Oxford, Oxford University Press, pp.451.

Seubert, C.E., Baumgardner, M.F., Wiesmiller, R.A. and Kirschner, F.R. (1979). Mapping and estimating areal extent of severely eroded soils of selected sites in Northern Indiana: 234-238.

Sgavetti, M. and Ferrari, J. (1988). TM data and study of a modern deltaic depositional system. *International Journal of Remote Sensing* **10**(11): 1613-1627.

Sharifi, M.A. (1978). *Application of remote sensing to the study of the agricultural resources.* 12th International Symposium on Remote Sensing of Environment: 95-111.

Sharpe, C.F.S. (1960). *Landslides and related phenomena.* New York, Colombia University Press.

Shillai, S. (1985). Remote sensing techniques and evalution of hydrological conditions in the southern part of Tami, India. *International Journal of Remote Sensing* **6**(3,4): 447-456.

Shiva, P.C.R. (1988). Landsat data and mapping soil and land resources in parts of Northern Karnataka, India. *International Journal of Remote Sensing* **11**(10): 1889-1900.

Shaw, G.B. (1979). Local and regional edge detectors: some comparisons. In: *Compuetr Graphics and Image Processing.* **9:** 135-149.

Shreve, R.L. (1966). Statistical law of stream numbers. *Journal of Geology.* **4:** 17-37.

Shreve, R.L. (1967). Infinite topographically random channel networks. *Journal of Geology.* **75:** 178-186.

Siegal, B.S. and Abrams M.J. (1976). Geological mapping using Landsat data. *Photogrammetric Engineering and Remote Sensing* **42:** 325-337.

Siegal, B S. and Goeta, A.F.H. (1977). Effect of vegetation on rock and soil type discrimination. *Photogrammetric Engineering and Remote Sensing* **43:** 191-196.

Siegal, B.S., and Gillespie, A.R. (1980). *Remote Sensing in Geology.* Wiley, New York.

Singh, A. (1986). Change detection in the tropical forest environment of North east India using Landsat. In: *Eden, M.J. and Parry, J.T. (eds). Remote Sensing and Tropical Land Management.* Wiley. Pp. 237-254.

Slater, P.N. (1979). A re-examination of the Landsat Mss. *Photogrammetric Engineering and Remote Sensing* **49**(6): 811-833.

Slaymaker, O. (1977). Estimation of sediment yield in temperate alpine environments. In Erosion and solid matter transport in inland water. Proceedings of the Paris Symposium. International Association of Hydrological Sciences. Publ. **122:** 109-117.

Slaymaker, O. and McPherson, H.J. (1977). An overview of geomorphic processes in the Canadian Cordillera. Zeitschrift Fur Geomorphologie. **21:** 169-186.

Smedes, H.W. (1975). The mixture problem in computer mapping of terrain: Improved techniques for establishing spectral signatures, atmospheric path radiance, and transmittance. *Proc. of the NASA Erth Resources Survey Symposium.* Houston, Texaa (Washington D.C.): 1099.

Smith, D.D. (1941). Interpretation of soil conservation data from field use. *Agriculture Enineering.* **22:** 173-175.

Smith, D.D., and Wischmeier, W.H. (1957). Factors affecting sheet and rill erosion. *Transactions, American Geophysical Union,* **38:** 889-896.

Smith, D.D. (1958). Factors affecting rainfallerosion and their evaluation. *International Association of Scientific Hydrology Publication* **43:** 97-107.

Smith, W.O., Vetter, C.P. and Cummings, G.B. (1960). Comprehensive Survey of Sedimentation in Lake Mead, 1948-49. *US Geol. Survey Prof. Paper* (295): 83-102.

Smith, D.I. and Stopps, P. (1978). *The river basin.* Cambridge University Press. 245 pp.

Sneed, E.D. and Folk, R.L. (1958). Pebbles in the lower Colorado River, Texas a study in particle morphogenesis. *The Journal of Geology* **66:** 114-150.

Solaimani, K. (1990). *Haraz river hydrology. M.Sc. Thesis, Persian text,* **Tabriz University,** Tabriz, Iran.

Solaimani, K. (1995-a). *Utilization of Russian Satellite Photography in the Detection of Lava Flows, Damavand Volcano,Iran.* Proceedings of Remote Sensing one day conference, Lecester University: 109-114.

Solaimani, K. (1995-b). *Application of Satellite Photographs in a Morphologic study of the Lar Dam Basin, Iran.* 17th BGRG Postgraduate Symposium, University of Leeds, Proceedings: 84-88.

Solaimani, K. (1996). *Use of Landsat (TM) and SPOT (XS) for the Identification and Mapping of Ancient and Recent Depositions in the Lar Basin-Iran.* Proceedings of the 22nd Annual Conference of the Remote Sensing:393-400.University of Durham.

Sollner, R. (1993). *First Experiences with the Application of Superhigh-Resolution Photographs.* International Mapping from Space, ISPRS.

Somma, J. and Cavayas, F. (1987). *Reconnaisance Geomorphologique D'une Region montagenuse Semi-arid par Teledecation.* 14th Canadian Symposium on Remote Sensing: 449-439.

Stahl, A.F. (1897). Zur geologie von Persian. *Geognostische Berschreibung vo nord-und zentral Persien.* Peterm. Mitt., (26):122-172.

Stahl, A.F. (1911). Persian. *Handb. Reg. Geologie,* v.5, n.8: 1-45. Heidelberg.

Stall, J.B., Gottschalk, L.C., Klingebiel, A.A, Sauer, E.L., De Turk, E.E. (1949). The silt problem at Spring Lake, Macomb, I11., *Illinois State Water Surv. Div. Rept. Invest.* 4.

Stallings, J.H. (1957). *Soil Conservation.* Prentice-Hall, Englewood Cliffs, N.J.

Stephen, P.R., Daigle, J.L. and Cihlar, J. (1982). Use of sequential aerial photographs to detect and monitor soil management changes affecting cropland erosion. *Journal of Soil and Water Conservation.* 37**(2):** 101-105.

Stohr, C.J. and West, T.R. (1985). Terrain and look angle effects upon multispectral scanner response. *Photogrammetric Engineering and Remote Sensing* **51:**229-235.

Stoklin, J., Ruttner, A. And Nabavi, M. (1964). New Data on the Lower Paleozoic and Pre-Cambrian of North Iran. *Geological Survey of Iran,* report no. 1: 29 pp.

Story, M., and Congalton, R.G. (1986). Accuracy Assessment: A user's perspective. *Photogrammetric Engineering and Remote Sensing* **53**(3): 397-399.

Strahler, A.N. (1952). Hypsometric (area altitude) analysis of erosional topography. Bul. *American Geological Society* **63**: 1117-1142.

Strahler, A.H. (1964). Quantitative geomorphology of drainage basin and networks. In: *(ed) Chow, V.Te., Handbook of Applied Hydrology.* New York.

Strahler, A.H. (1980). The use of prior probabilities in maximum likelihood classification of remote sensing data. *Remote Sensing of Environment* **10**: 135-163.

Strakel, L. (1977). Late-glacial and Holocene fluvial chronology in the Carpathian valleys. *Studia Geomorphologica Carpatho-Balancia.* **6:** 121-133.

Strand, R.I. (1975). Bureau of recamation procedures for predicting sediment yield. *Present and prospective technology for predicting sediment yields and sources.* U.S. Dep. Agric. Res. Serv. Pub. ARS-S-40: 10-15.

Sussli, P.E. (1976). The geplogy of the Lower Haraz valley area, Central Alborz, Iran. *Geological Survey of Iran,* Report **(38):**116 pp.

Swain, P.H. and Davis, S.M. (1978). *Remote Sensing: The Quantitative Approach, (eds.).* McMraw-Hill, New York.

Terzaghi, K. (1974). *Shear characteristics of quicksands and soft clays.* Seventh Texas Conference Soil Mechanic, Bureau of Engineering Research University of Texas: 557-618.

Thillai, S., Kumar, S.S., Padhak, P. and Jayaraman, M. (1985). The Evolution of Hydrogeological Condition in the Southern part of Tamil Nadu using Remote Sensing Techniques. *International Journal of Remote Sensing* **6**(3-4): 447-456.

Thomas, A.W., Welch, R. and Jordan, T.R. (1986). Quantifying concentrated-flow erosion on crop-land with aerial photogrammetry. *Journal of Soil and Water Conservation.* **41**(4): 249-252.

Thomson, F.J., Erickson, J.D., Koerber, K. and Harnage, M.L. (1975). A thematic performance optimization study. *Proc. 10th Int. Symp. on Remote Sensing of Environment.* (Ann Arbor, Michigan: EIRM): 85.

Thornes, J.B. (1985). The echology of erosion. *Journal of Geographical Association,* **70:** 222-235.

Thornes, J.B. (1987). The palaeoecology of erosion. In: *Wagstaff, J.M. (ed.), Landscapes and culture.* Basil Blackwell: 37-55.

Thorne, C.R. and Tovey, N.K. (1981). Stability of composite river banks. *Earth Surface Processes and Landforms* **(6):** 469-484.

Thorne, C.R. and Osman, A.M. (1988).River bank stability analysis.II.Applications. *Journal of Hydraulic Engineering* **114**(2): 151-172.

Tietze, E. (1887). Der Vulkan Demavend in Persian. *Jb.K.K. Geol. Reichsanat.,* **(28):** pp.169-206; 1 pl., Wien.

Toll, D.L. (1984). An evaluation of simulated TM data and Landsat MSS data for discriminating urban and regional land use and landcover. *Photogrammetric Engineering and Remote Sensing.* **50:** 1713.

Toll, D.L. (1985). Effect of Landsat (TM) sensor parametres on landcover classification. *Remote Sensing of Environment.* **17:** 129-140.

Tolouie, E., West, J.R., and Billam, J. (1993). Sedimentation and desiltation in the Sefid-Rud reservoir, Iran. In: *(ed) McManus and Duck, R.W., Geomorphology and sedimentology of lakes and reservoirs.* Wiley, pp.278.

Totterdell, C.J. and Nebauer, N.R. (1973). Colour aerial photography in the reapraisal of alpine soil erosion. *Journal of Soil Conservation Service of New South Wales.* **29**(3): 130-158.

Townshend, J. and Justice, C. (1981). Information extraction from remotely sensed data. *Int. J. of Remote Sensing* **2:** 313.

Treitz, P.M., Howarth, P.J., Gong, P., and Crahon, D.J. (1990). Itegrating remote sensing data within a GIS environment for mapping the changing landscape. *Proceeding of 13th Canadian Symposium on Remote Sensing,* Frederition, N.B., Canada. 448-459.

Tueller, P.T. and Booth, D.T. (1975). Large scale colour photography for soil evaluations on rangeland watersheds in the great basin. *Proc. of Am. Soc. of Photogramm.* Phoenix, Arizona: 708-753.

Udden, J.A. (1898). The mechanical composition of wind deposits. *Augustana Library Publications.* **1:** 69 pp.

Ungar, S.G., Merry, C.J., Irish, R., McKim, H.L. and Miller, M.S. (1988). Extraction of Topography from side-looking Satellite System-A case Study with SPOT Simulation. *Remote Sensing of Environment* **26**: 51-73.

Van Doren, C.A. and Bartelli, L.J. (1956). A method of forecasting soil loss. *Agriculture Engineering.* **37:** 335-341.

Van Gendern, J.L. and Lock, B.F. (1977). Testing landuse map accuracy. *Photogrammetric Engineering and Remote Sensing* **(43):** 1135-1137.

Venkat, L. (1984). *Mapping of land soil degradation by Multispectral data, in India.* 8th Canadian Symposium on Remote Sensing: 421-429.

Verstappen, H.Th. (1989). Satellite remote sensing geomorphological survey and natural hazard zoning. *Some new developments at ITC, the Netherlands. Suppl. Geogr. Fis Dinam Quat* **2:** 103-109.

Vita-Finzi, C. (1969). Late Quaternary alluvial chronology of Iran. *Geol. Rundsachau 58,* no. 3: 951-973.

Wagle, B.E. and Hashimi, N.H. (1988). Aerial photograph an analysis of coastal geomorphology of Mabe Island. *International Journal of Remote Sensing* **11**(2): 281-287.

Walling, D.E., Webb, B.W. (1983). Pattern of sediment yield. in Gregory, K.J. (ed.), *Background to paleohydrology.* Chichester, Wiley: 69-100.

Walling, D.E. (1984). Muddy waters move mountains. *The Geographical Magazine, 57:262-267.*

Walling, D.E. (1995). Suspended sediment yields in a changing environment. In: *Changing River Channels;* Gurnell, A. and Petts, G.et (Eds), Wiley and Sons, Chichester: 149-176.

Welch, R., Jordan, T.R. and Thomas, A.W. (1984). A photographic technique for measuring soil erosion. *Journal of Soil and Water Conservation,* **39**: 191-194.

Weber, J.E., Fogel, M.M., Duckstein, L. (1976). The use of multiple regression models in predicting sediment yield. *Water Resources Bulletin,* **12:** 1-17.

Wentworth, C. (1922). A scale of grade and class terms for clastic sediments. *Journal of Geology.* **30:** 377-392.

Whitlow, R. (1988). Potential versus actual erosion in Zimbabwe. *Applied Geography,* **12:**87-100

White, L.P. (1977). *Aerial Photography and Remote Sensing for Soil Survey.* Oxford, Clarendon Press.

White, W.R. (1972). Sediment transport in channels: a general function. *Hydraulics Research Station, Wallingford, Report no. INT 104.*

White, S. (1995). Soil Erosion and Sediment Yield in the Philippines. In: Foster et al. (eds), *Sediment and water quality in river catchments.* Wiley: 391-406.

Williams, J.R. and Berndt, H.D. (1972). Sediment yield computed with universal equation. *Journal of the Hydraulics, Division American Society Civil Engineers* **98**(12): 2087-2099.

Williams, A.R. and Morgan, R.P.C. (1976). Geomorphological mapping applied to soil erosion evaluation. *Journal of Soil and Water Conservation.* **31:** 164-168.

Williams, D.L., Irons, J.R., Markham, B.L., Nelson, R.F., Toll, D.L., Latty, R.S. and Stauffer, M.L. (1984). A statistical evaluation of the advantages of Landsat (TM) in comparison to multispectral scanner data. *I.E.E.E. Trans. Geosci. Remote Sensing.* **22:** 294.

Wilson, L. (1973). Variations in mean annual sediment yield as a function of mean annual precipitation. *American Jurnal of Science,* **273:** 335-49.

Wischmeier, W.H. and Smith, D.D. (1958). Rainfall energy and its relation to soil loss. *Trans. Am. Geophys. Union.* **39:** 285-291.

Wischmeier, W.H., Smith, D.D., and Uhland, R.E. (1958). Evaluation of factors in the soil loss equation. *Agricalture Eng.* **39:** 458-462.

Wischmeier, W.H. and Smith, D.D. (1965). *Predicting rainfall erosion losses from cropland east of the Rocky Montains.* Agriculture Handbook 282. U.S. Dep. of Agriculture, Washington, D.C.

Wischmeier, W.H. and Smith, D.D. (1978). Predicting rainfall erosion losses. *Agricultural Handbook No.* 537, USDA Science and Education Administration.

Wischmeier, W.H. (1978). Use and misuse of the Universal Soil Loss Equation. *Journal of Soil and Water Conservation.* **31:** 5-9.

Wise, D.U. (1982). Linesmanship and practice of linear geo-art. *Bull. American Geological Soc.* **93**: 886-888.

Wood, J.C. (1995). Patterns of erosion and suspended sediment yield in Mediterranean river basins. In: Foster et al. (eds), *Sediment and water quality in river catchments.* Wiley: 365-389.

Woodward, J.C. (1995). Archaeology and human-river environment interactions. In: Lewin, J., Macklin, M.G. and Woodward, J.C. (eds), *Mediterranian Quaternary River Environments.* Balkema, Rotterdam: 99-102.

Yang, C.T. (1972). Unit a stream power and sediment transport. *Journal of the Hydraulics, Diversion American Society Civil Engineers* **98**: *HY10.*

Yang, C.T. (1973). Incipient motion and sediment transport. *Journal of the Hydraulics, Diversion American Society Civil Engineers.* **99:** *HY10.*

Zachary, A.L., Cipra, J.E., Diderickson, R.I, Kristof, S.L. and Baumgardner, M.F. (1972). Application of multispectral remote sensing to soil survey research in Indiana. LARS. *Information Note 110972.* Purdue University, Indiana, U.S.

Zaruba, Q., and Mencl, V. (1969). *Landslides and their control.* Amsterdam, Elsevier.

Zhang, Y., and Yang, Q. (1990). *Remote Sensing Image for Research of Landslide.* 23th Canadian Symposium on Remote Sensing of Environment.

Zingg, Th. (1935). Betrage Zur Schotter analyse; Schweiz. *Mineralog. Pettrog. Mitt.* **(15):** 39-140.

Zingg, A.W. (1940). Degree and length of land slope as it affects soil loss in runoff. *Agricultural Engineering* **21:** 59-64.P.

Zuidam, R.A. (1985). Aerial photo-interpretation. In:*Terrain Analysis and Geomorphologic Mapping.* ITC, The Netherlands. 442 p.

Folded map no.(1)

THE LAR DAM BASIN

SLOPE ANGLES

LEGEND

- 0 - 5%
- 5 - 20%
- 20 - 45%
- 45 - 65%
- > 65%
- Reservoir
- Basin boundary
- River

* Location of study area in relation to Iran

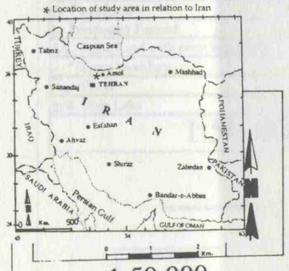

1:50 000

Damavand volcano (5671 m.)

Sefid-Ab river

Dalichai river

Lar river

Khoshkeh-Lar

Kamardasht

THE LAR DAM BASIN
VEGETATION

Folded map no.(2

LEGEND:

- 1-1: Agropyron-Poa bulbosa-Ferule
- 1-2: Oryzopsis-Melica-Ferula
- 1-3: Poa bulbosa-Cousinia
- 1-4: Festuca ovina traxacum
- 1-5: Ferula-Agropyron
- 1-6: Ranunculus-Alopecurus
- 2-1: Asragalus-Onobrychis cornuta-Cousimia-Carex-Poa pulbosa
- 2-2: Astragalus-Euphorbia-Bromus
- 2-3: Astragalus-Poa bulbosa Eremurus-Ferula
- 2-4: Thymus-Astragalus-Salvia-Agropyrom
- 2-5: Salvia-Astragalus-Psathyrostachys pragilis
- 2-6: Onobrychis-Cornata-Bromus-Euphorbia
- 2-7: Onobrychis-Cornata salvia-Bromus
- 2-8: Agropyron-Ferula-Onobrychis
- 2-9: Astragalus-Ferula sp-Bromus tomentellus
- 2-10: Onobrychis cornuta-Astragalus-Cousinia-Bramus
- 2-11: Ferula-Onobrychis-Bromus-Agropyron
- 2-12: Onobrychis-Cornata-Astragalus-Rumex-Bromus
- 2-13: Astragalus-Cousinia-Festuca
- 3-1: Thymus-Bromus
- 3-2: Thymus-Astragalus-Poa
- 3-3: Thymus-Onobrychis cornuta-Agropyron
- 3-4: Agropyron-Acanthotimon
- 3-5: Agropyron-Astragalus
- 3-6: Onobrychis cornuta-Astragalus-Festuca
- 3-7: Festuca-Astragalus
- 4-1: Onobrychis-Eremutrus
- 4-2: Astragalus-Cousinia
- R: Rocky land without Vegetation
- A: Farm Land
- L: Previously Farmed
- S/L: Scree Land with poor Vegetation
- Basin boundary
- River
- Dam Lake

1:50 000

1=Herb Type
2=Shrub-Forbs-Grass Type
3=Shrub and Perennial Grass Type
4=Shrub and Forbs Type

Location of study area in relation to Iran

Lar R.
Sefid-Ab R.
Dalichai R.
Khoshkeh-Lar R.
Kamardasht
Damavand volcano (5671 m.)

(K. Solaimani, Glasgow Univ. 1995)

THE LAR DAM BASIN

SOILS

Folded Map no.(3)

SOIL TYPE

A. MOUNTAINS UNIT:

Aa= High mountains of the Alborz, bare soil, limestone and sandstone.

Ab= High mountains with shallow to moderately gravely soil,*(Regosols-Lithosols).*

Ac= High mountains with shallow gravely and rock outcrops on the soft limestone-sandstone rocks, *(Rigosols-Lithosols).*

Ad= High mountains, Generally very shallow soil on limestone scree,*(Lithosols).*

Ae= High mountains, limestone and marl, shallow to moderate depth soil,*(Calcaric Regosols)*

Af= Damavand Volcanic cone, extensive basic rock and pyroclastic formation, slopes with tuffs

Ag=Damavand Volcano heights, generally have soil, pyroclastic, trachyandesite, *(Lithosols).*

Ah= Damavand Volcano slopes, generally bare soil and rock outcrops, *(Regosols-Lithosols).*

Ai= High mountains, shallow to moderate depth soils, soft rocks and sandy marl.

Aj= Mountainous Shallow soils, with rock outcrops or soft sandy marl and limestone.

Ak= High mountains, Shallow to moderate depth soils, scree, sandstone clay and marl.

B. HILLS: Dissected old flats.

Ba= Shallow to moderately deep soils and continuous with some gravel on sandstone, limestone and conglomerate rocks, *(Regosols - Lithosols).*

Bb= High with shallow soil cover, good vegetation cover, with tuffs and volcanic rocks.

Bc= Shallow deep soil, rock outcrops, and some scree, *(Regosols-Lithosols).*

C. FLAT SURFACES:

Ca= High flats and terraces, with shallow to moderately deep soils on the Pleistocene rocks.

Cb= Upper terraces with deep soil cover, and some scree on the conglomerate rocks, *(Regosols - Calcic camiso's)*

Cc= Moderate topography, Plateaux, with deep soil, cover *(Eutric Regosols Cortic luvisols).*

Cd= Middle flats and terraces, shallow to moderate deep soil and old gravelly alluvial fans.

Ce= Plateaux shallow soil with gravel, *(Regosols - Calcic camisols)*

Cf= Terraces with some gravel, *(Eutric Regosols).*

Cg= Plateaux and terraces with shallow soil cover,*(Regosols-Cambisols 'shallow phase').*

D. GRAVELLY ALLUVIAL FAN SOILS:

Da= River alluvium with gravel beds with very shallow soil,*(Fluvisols).*

Db= River alluvium with moderate soil erosion.

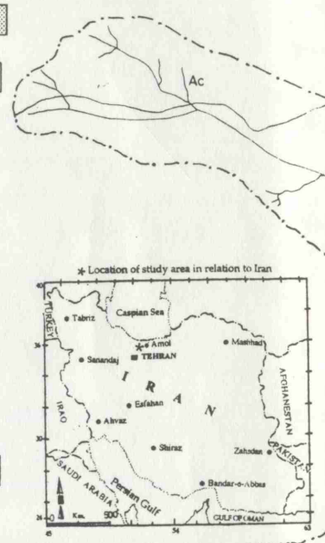

51° 38′ E

THE LAR DAM BASIN
GEOMORPHOLOGY

	LEGEND:
	Terrace border.
	Leakage point.
	Ruins of ancient village.
	Old sinkhole.
	Active sinkhole.
	Recent sinkhole.
	Scree cone detritus of large blocks.
	Alluvial fans.
	Ancient scree slopes and landslide deposits.
	Landslide with topographic scar in rear.
	Cliff.
	Lava flow.
	Overthrust.
	Fault outlier.
	Fault inlier.
	Upthrust.
	Normal fault.
	Vertical fault.
4089	All spot heights are in metres.
	Basin boundary.
3500	Contour.metre.
	Dam Lake.
	Lake shore.
	River.
	River channel.
	Spring.
	Sub-basin boundary.
	Village.

1:50 000

0 1 2 Km.

Damavand volcano (5671 m.)

Lar R.

Sefid-Ab R.

Dalichai R.

Khoshkeh-Lar R.

Kamardasht

POLOUR

K. SOLAIMANI, Univ. of Glasgow, 1994

Particle Shape Analysis

Basin: Lar **Date:** Aug. 1994

Sample Number: B-1 **Location** Dalichai Downstream

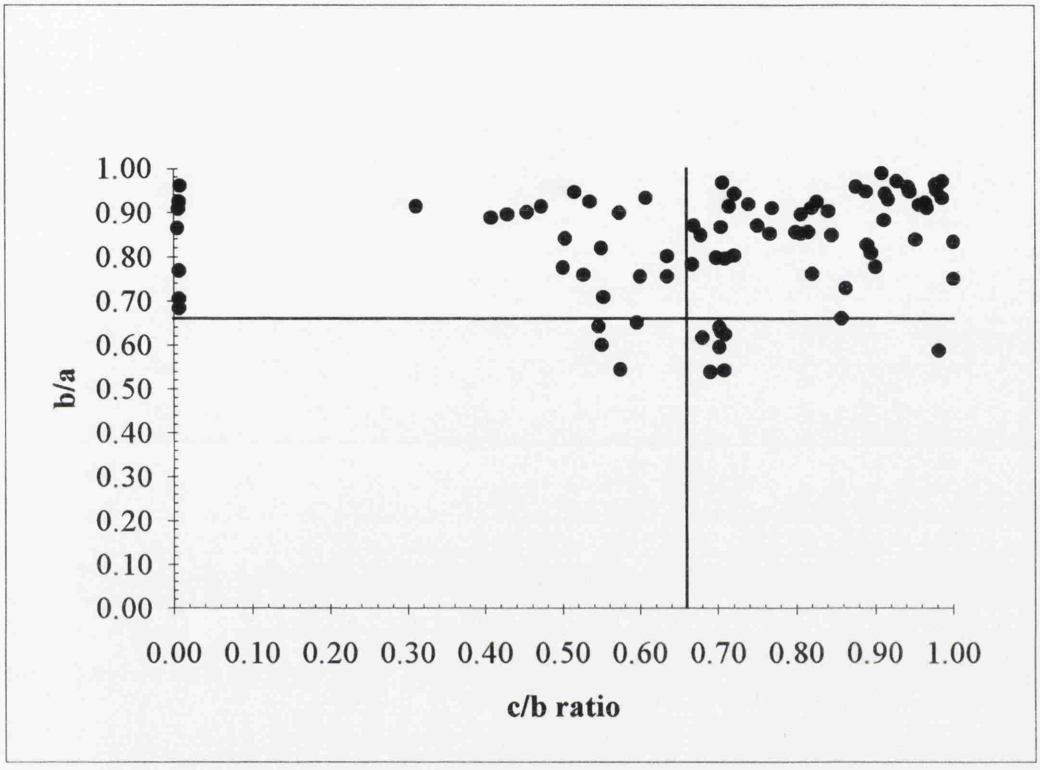

Spheres :	59%	**Blades:**	4%
Discs:	28%	**Rollers:**	9%

Particle Shape Analysis

Basin: Lar **Date:** Aug. 1994

Sample Number: B-1 **Location** Dalichai Upstream

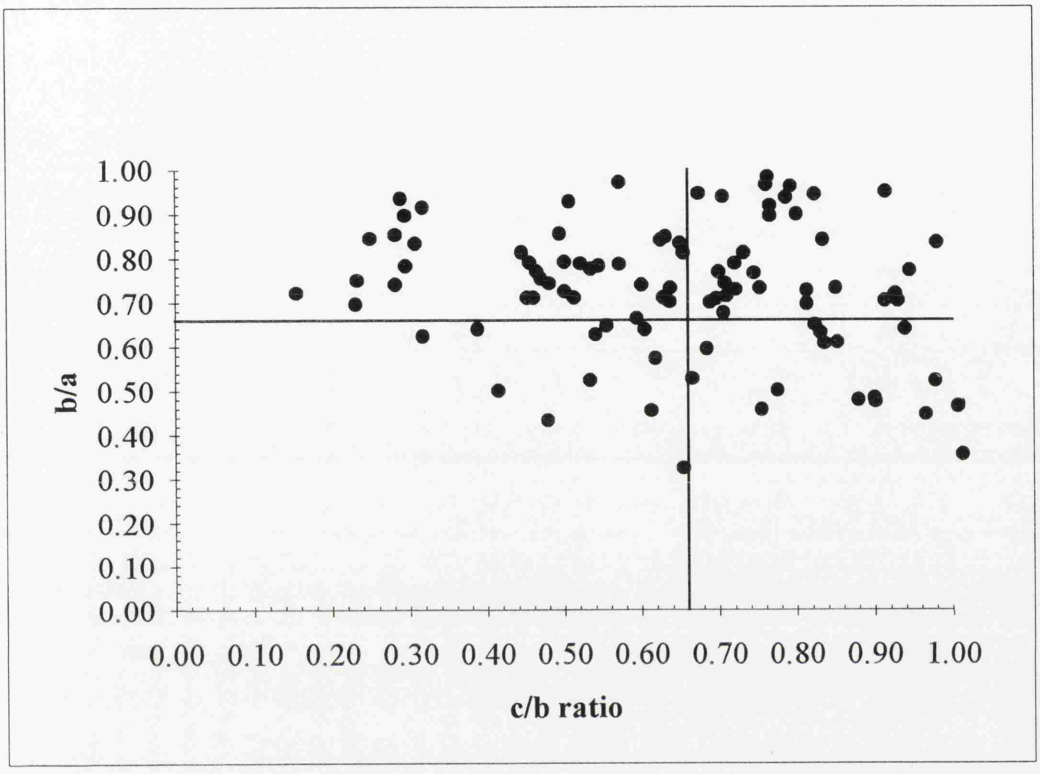

Spheres : 33% **Blades:** 11%

Discs: 40% **Rollers:** 16%

Particle Shape Analysis

Basin: Lar **Date:** Aug. 1994

Sample Number: B-1 **Location:** Sefid-Ab

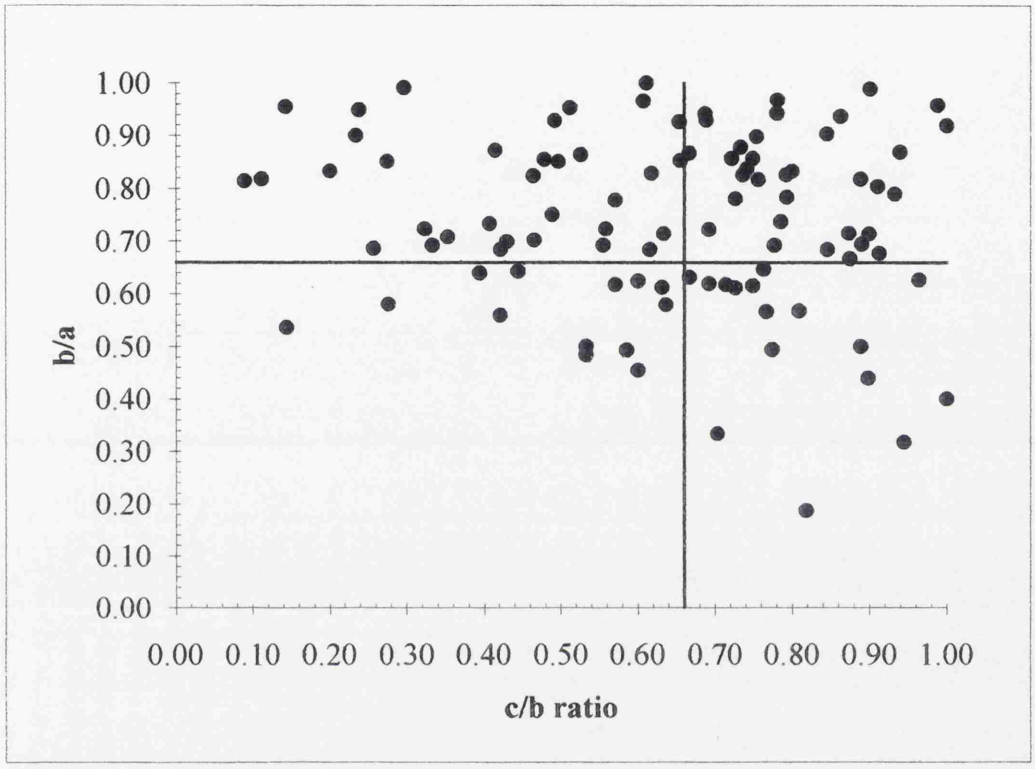

Spheres : 35% **Blades:** 13%

Discs: 35% **Rollers:** 17%

Particle Shape Analysis

Basin: Lar **Date:** Aug. 1994

Sample Number: C-1 **Location:** Ab-Sefid (Asb-Kalak)

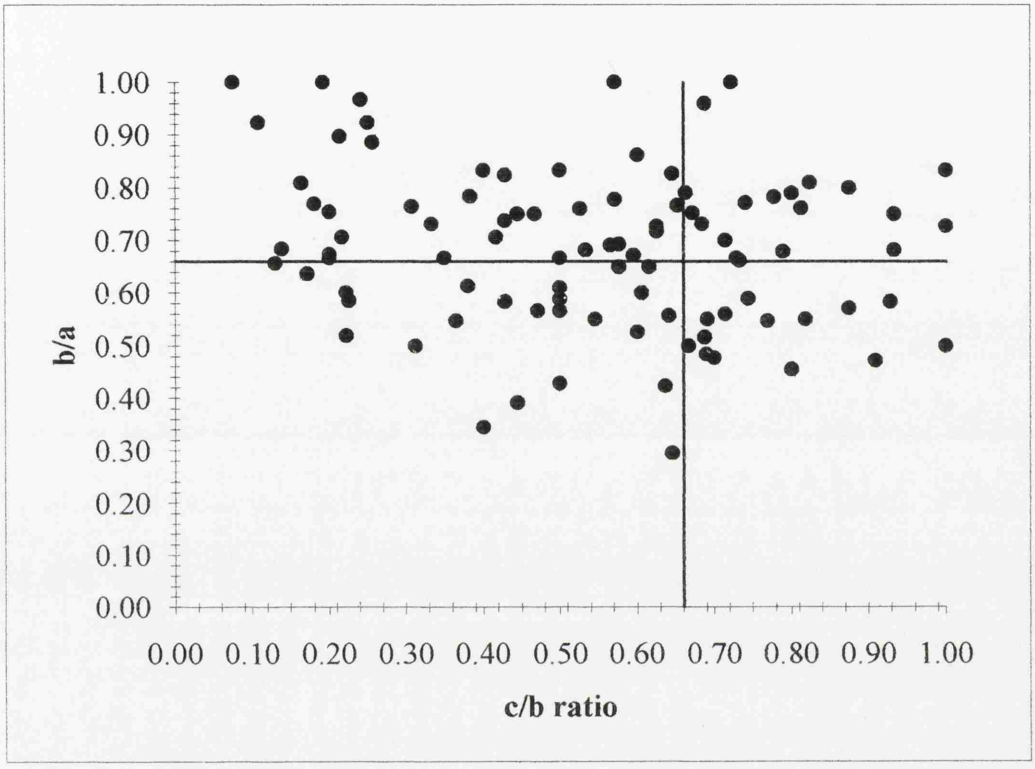

Spheres : 20% **Blades:** 24%

Discs: 40% **Rollers:** 16%

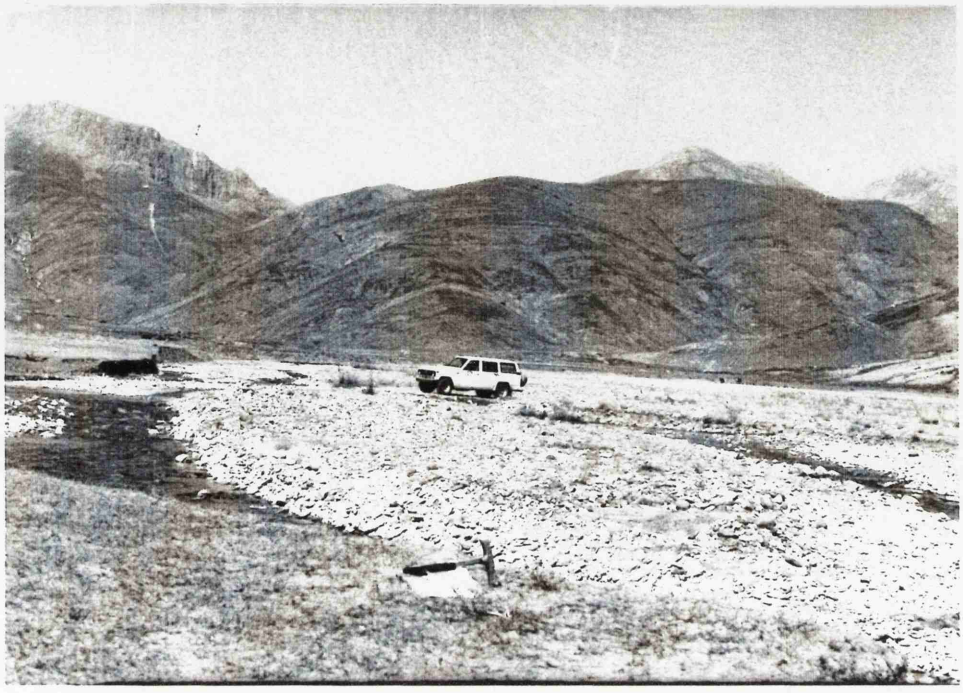

Particle Shape Analysis

Basin: Lar **Date:** Aug. 1994

Sample Number: D-1 **Location:** Khoshkehlar+Galesardab

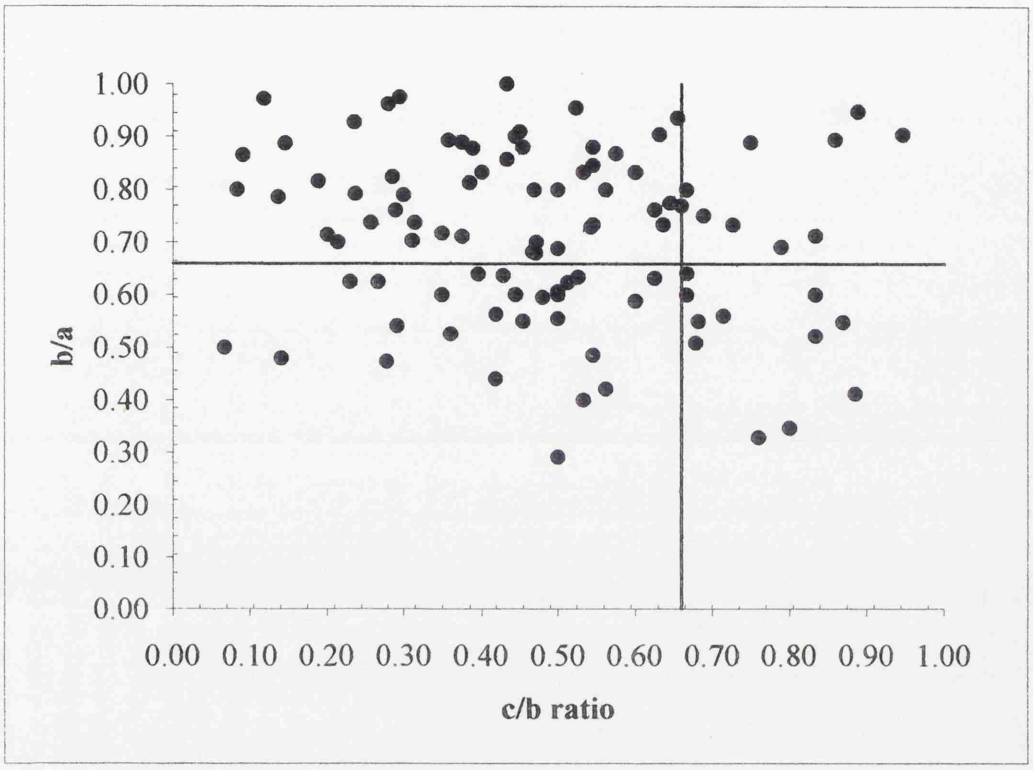

Spheres : 9% **Blades:** 26%

Discs: 53% **Rollers:** 12%

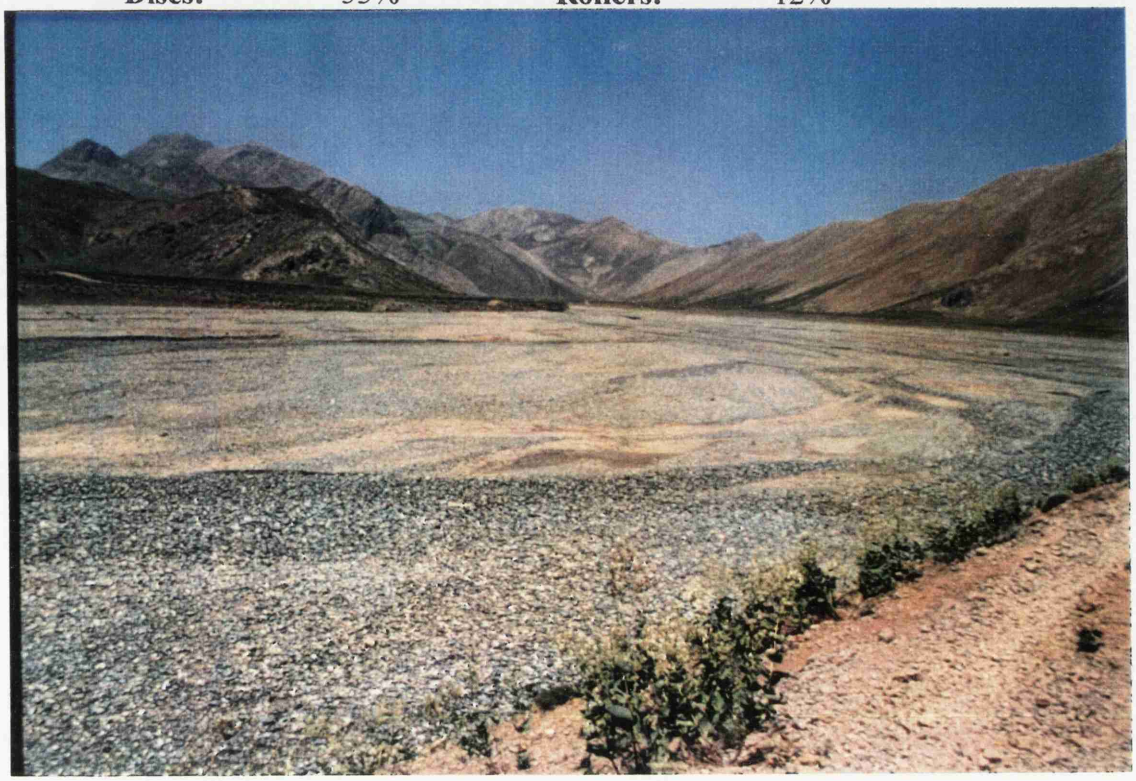

Particle Shape Analysis

Basin: Lar **Date:** Aug. 1994

Sample Number: E-1 **Location:** Gozaldarreh

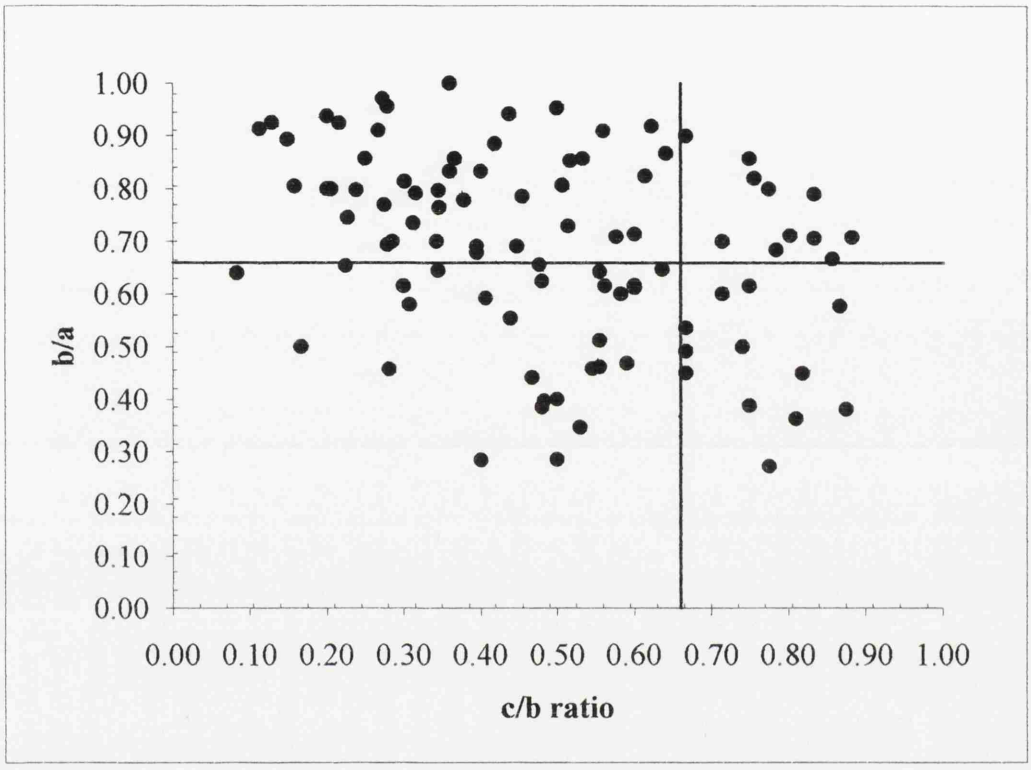

Spheres : 11% **Blades:** 28%

Discs: 49% **Rollers:** 12%

Particle Shape Analysis

Basin: Lar **Date:** Aug. 1994

Sample Number: F-1 **Location:** Imamzadeh Yorghidar

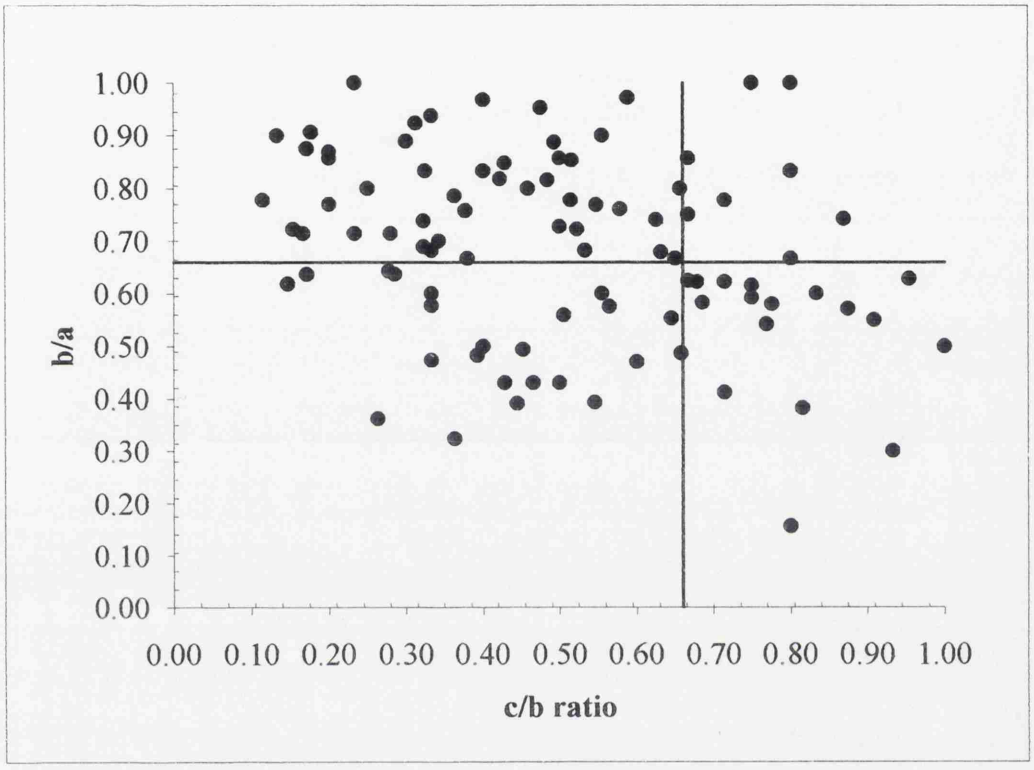

Spheres : 10% **Blades:** 23%

Discs: 49% **Rollers:** 18%

Appendix Chapter 6

6.1 SPOT-HRV (High Resolution Visible)

SPOT-1 was launched on February 1986, SPOT-2 on January 1990 (Figure Ap.6.1). The payload for SPOT consists of two identical High Resolution Visible (HRV) elevation imaging systems and auxiliary tape recorders. Each HRV is designed to operate in either two modes of sensing include; - 10 m resolution Panchromatic (black & white) P-mode or a 20 m resolution Multispectral Xs-mode (colour infrared). The HRV is a pushbroom scanning system and does not employ a scanning mirror. The incoming radiation is reflected by a fixed optical mirror, before it is registered. Each HRV contains CCD subarrays. A 6000 element subarray is used in the panchromatic view. Three 3000 element subarrays are employed in the Xs-mode. Data are effectively encoded over a 256 digital number range and are transmited to ground at a rate of 25 Mbps at 8253 Mhz.

6.1.1 Orbital and Recording Options

The sensors on board the TIROS and NIMBUS satellites in the 1960s provided remotely sensed imagery with ground spatial rasolutions of approximately 1000×1000 m and were the first to reveal the potential of space as a vantage point for earth resource observation. The multispectral Landsat MSS and TM sensor systems developed in the 1970s and early 1980s provided imagery with spatial resolutions of 79×79 to 30×30 m. The SPOT sensor system has a special resolution of 10×10 to 20×20 meters and provides several other innovations in remote sensor system design (Begni, 1982, CNES, 1984).

- When the instruments are pointed so as to cover adjacent image fields at nadir, the total swath with is 117 km and the fields overlap by 3 kilometers. This positioning is denoted "Twin-Vertical" (Figures App.6.2 and App.6.3). At off-nadir view both system can be tilted up to 475 km from the subsatellite track. The swath width will increase from 60 km to 80 km and the minimal reviewing time frame will be 5 days instead of 26 days nominally. This opens 11 viewing options for a given ground object at a latitude of 45 degree.

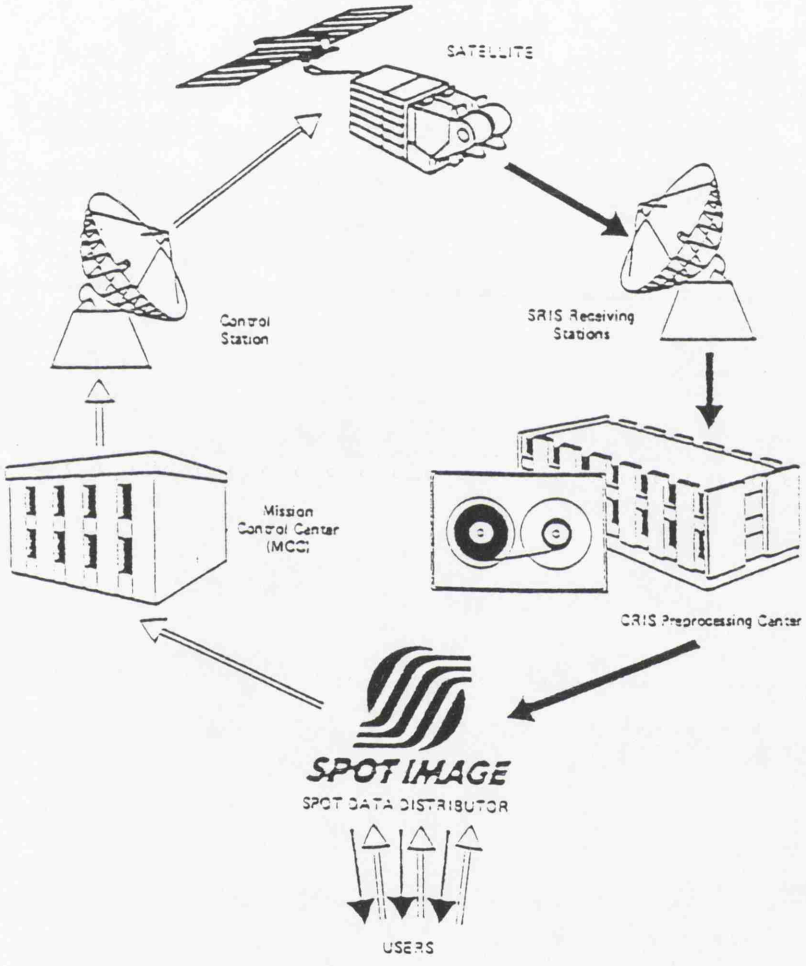

Figure App.6.1: General organization of the SPOT system (source; CNES 1988).

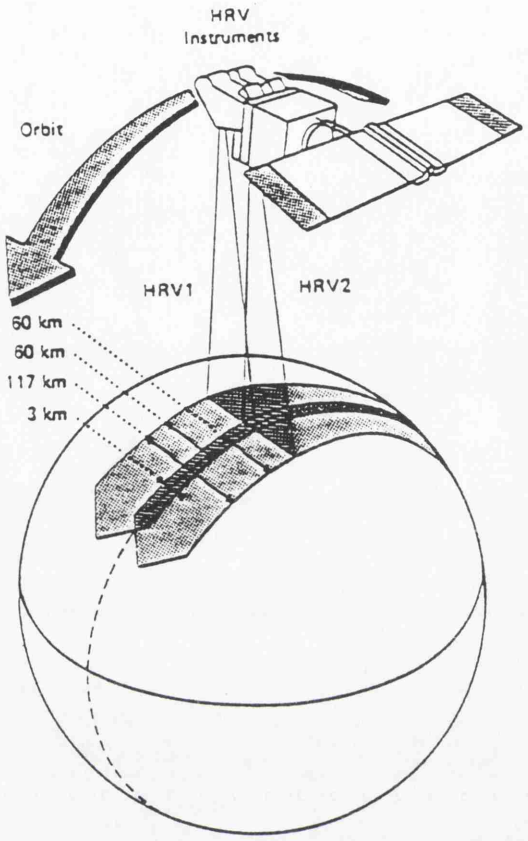

Figure App.6.2: Ground strips imaged by HRVs 1 and 2 in the twin-vertical viewing configuration.

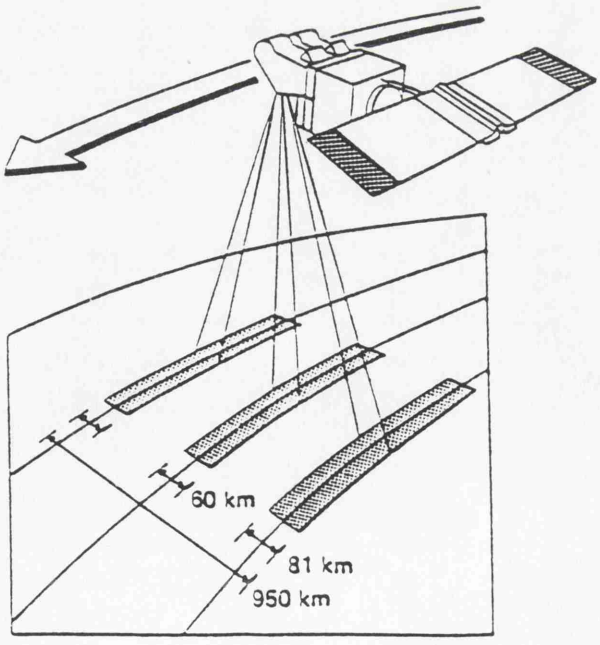

Figure App.6.3: Observable corridor and ground strips using vertical and oblique viewing.

- Stereoscopic imaging is also possible due to off nadir viewing capability of the HRV. For two consecutive days the stereo-base-length is half the flight altitude.

6.1.2 Multispectral Scanner Imagery

Multispectral scanner systems are desined to sense energy in a number of narrow spectral bands simultaneously. This mod analysis utilizes three spectral band as follows:

Green (0.5-0.59μm), Red (0.61-0.68μm), and Near-infrared (0.79-0.89μm). These three bands together ensure improved spectral response to chlorophyll and specifically to a response peak in the green band, strong absorption in the red band, and prononced response in the near-infrared band, which cannot be perceived by the human eye, (Figure App.6.4). Figure Appendix 6.5 shows comparison mode between multispectral (Xs) as foregoing and panchromatic mode (P) in a single spectral band extending from 0.51 to 0.73μm.

6.2 LANDSAT

The experiments from manned satellite and the results and success of the semipermanent meteorological satellite systems encouraged NASA to initiate a series of high resolution orbital systems aimed at the biological and physical resources at the earth. The first Earth Resources Technology Satellite (ERTS-1) was launched by NASA on the 23 1972, using a nimbus platform.(Figure Ap.6.6 a&b).It was subsequently renamed Landsat-1, to complement the oceanographic Satellite Seasat, and eventually the administration of the Land series passed first to NOAA and then to a commercial company, EOSAT. The 918-km Llandsat orbits passed within 9 degree at the poles, and circled the Earth once every 103 minutes. Descending orbits crossed the Equator at an angle of 9 degree at around 09.30h local time.The Landsat series is sun-synchronous, and Images are illuminated by the mid- morning sun at relatively low elevation. (Table Appendix 6.2).

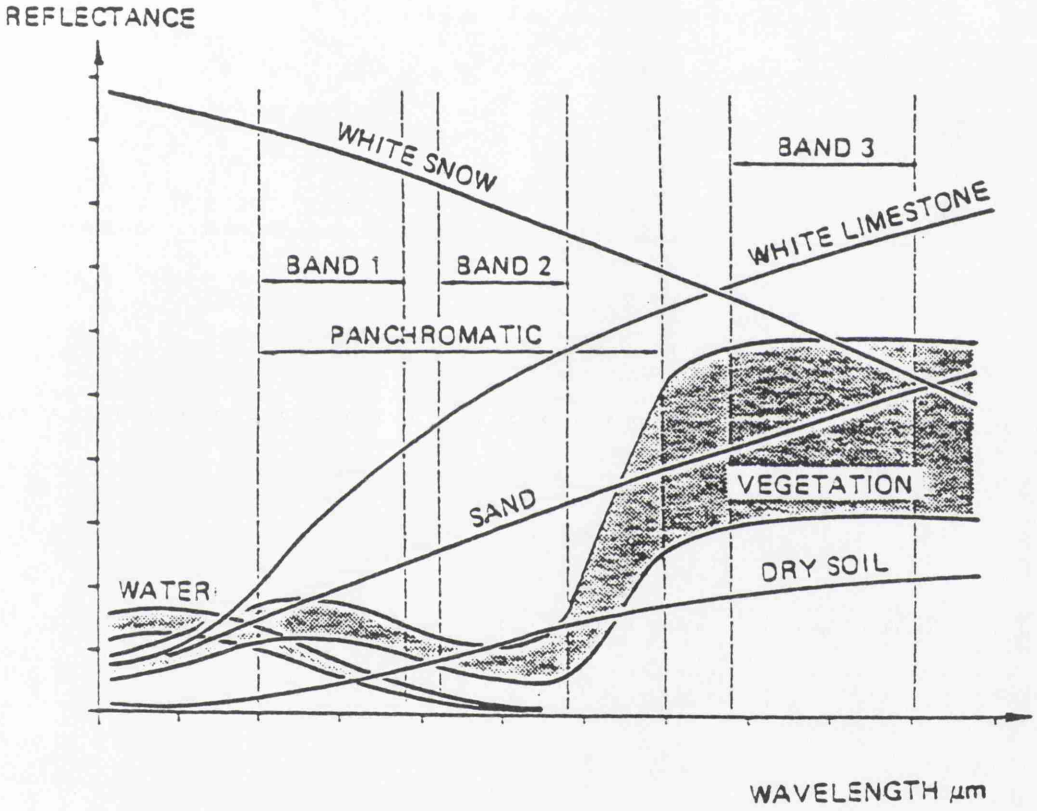

Figure App.6.4: Typical spectral signatures and SPOT special bands (source; CNES, 1988).

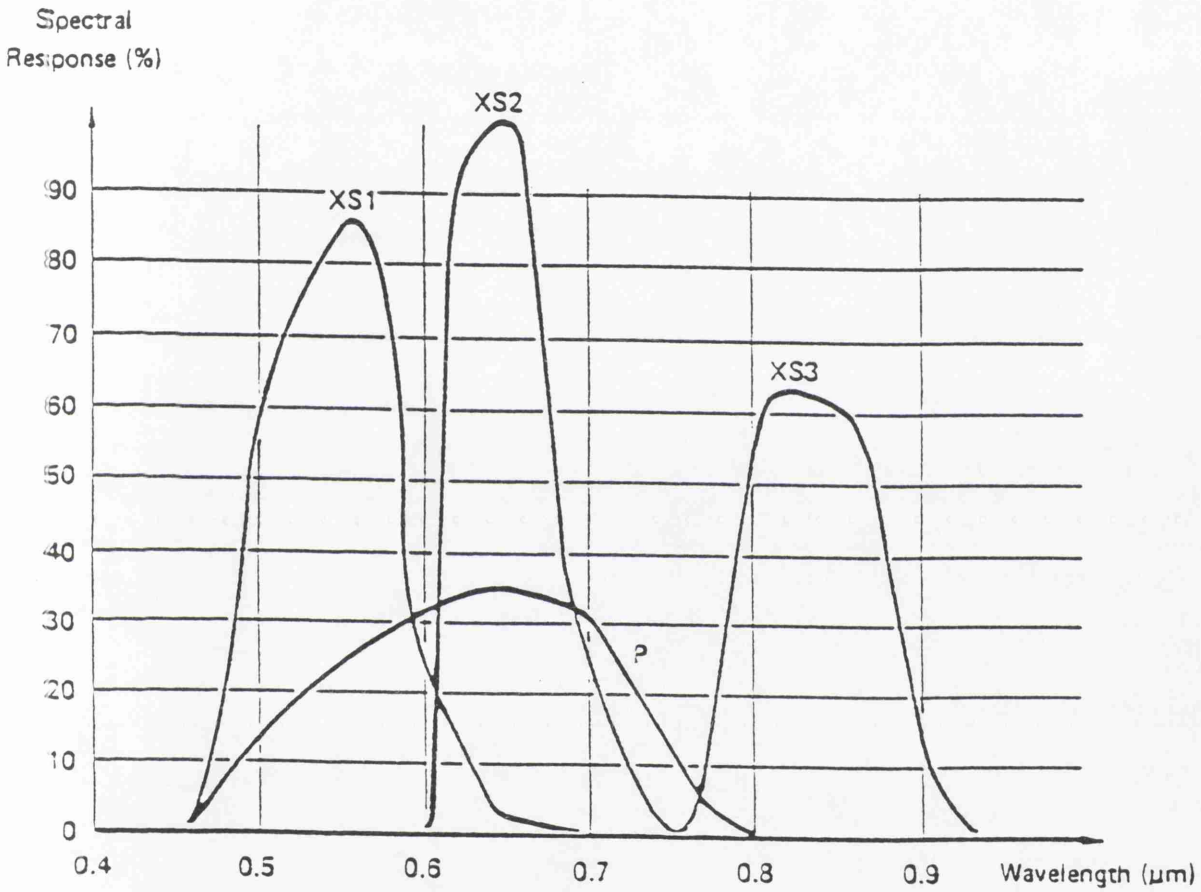

Figure App.6.5: Typical spectral response of HRV imaging instruments (source; CNES, 1988).

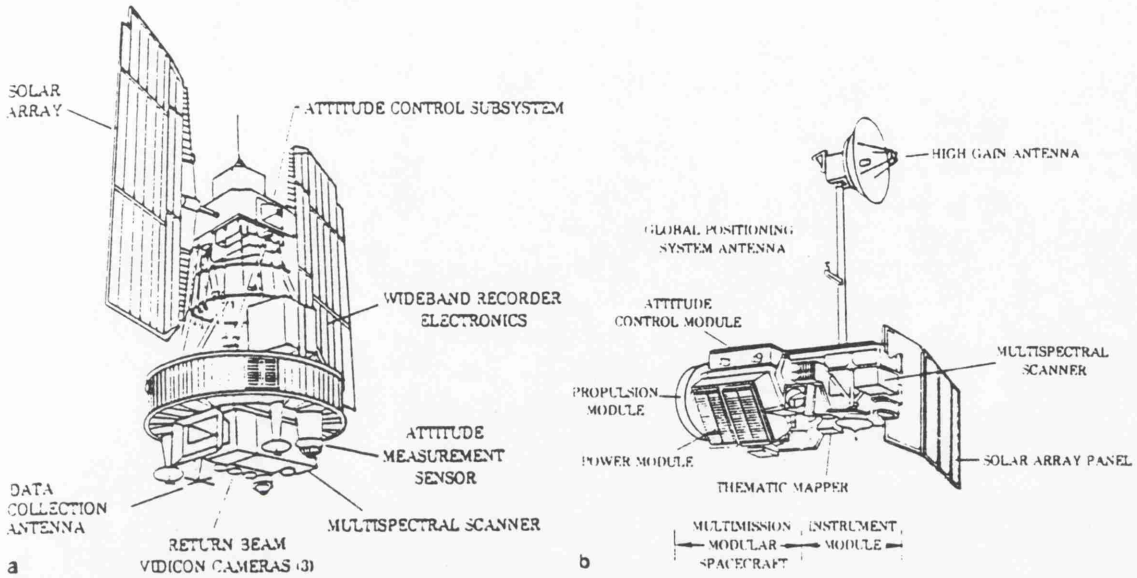

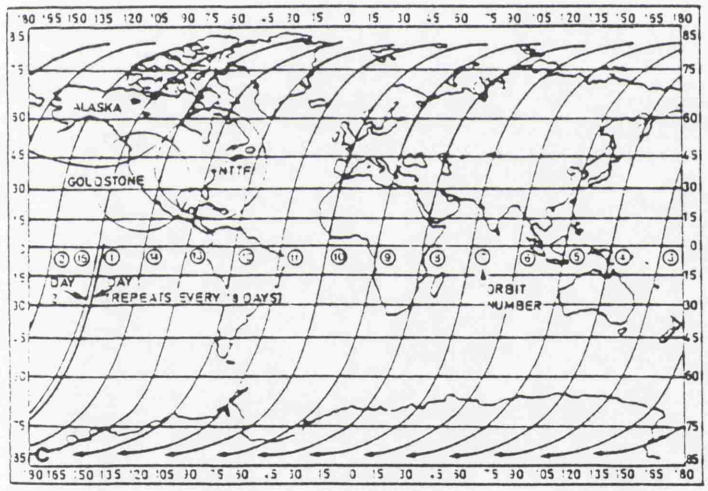

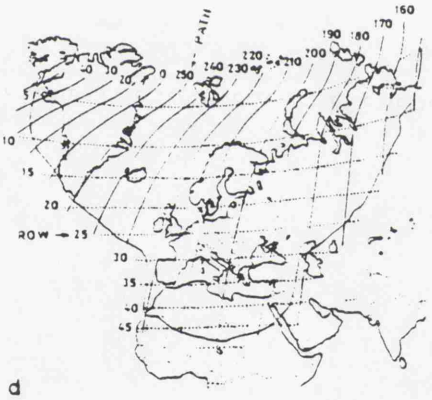

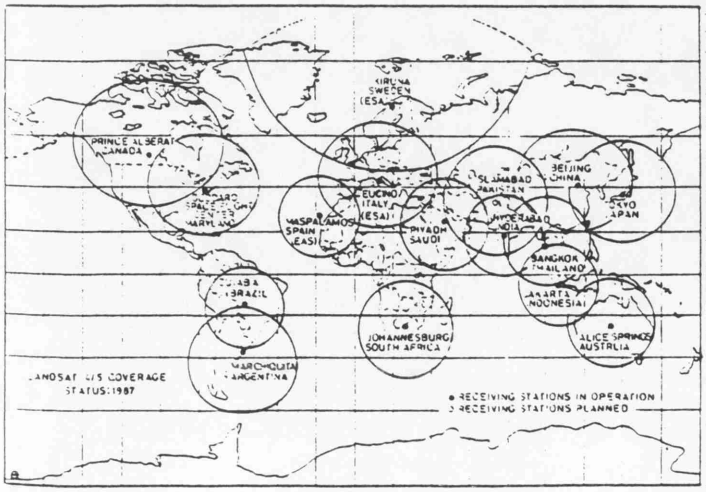

Figure App.6.6: Design of Landsat-1, 2 and 3 (a); Landsat-4 and 5 (b). Typical ground face of Landsat (1, 2 and 3) for one day (only southbound passes shown) (c). System of path and row numbers used for global indexing and referencing of satellite image data (d). Location and area coverage of various receiving stations of Landsat data, (e). (All Figures after NASA 1976-78).

6.2.1 MSS Sensor

It is the multispectral scanning system (MSS) which has the Landsat programme a tremendous success. The MSS records data in 4 spectral channels (Table App.1) and therefore total of 24 detectors are used concurrently. It,s ground resolution cell is 79×79 m; however, sampling of the signal is carried out in an overlapping fashion, such that sampling interval corresponds to only 56 m on the ground, in scan direction. A Landsat MSS scene is nominally 185×185 km in dimension (Figure App.6-7). A detailed performance characteristic of the MSS sensor have been given by Stater (1979). Markham and Barker (1983) and Rice and Malila (1983).

6.2.2 RBV Sensor

The Return Beam Vidiocon (RBV) sensor was used in the Landsat-1,2 and 3 mission. Landsat-1 and 2 carried a set of three RBV cameras in multispectral mode (spectral ranges: 0.47-0.57μm=green, 0.58-0.68μm=red and 0.69μm=infrared) and the wavelength spectral was provided by filters mounted over the camera lenses. Each RBV image covered an area of about 185×185 km^2 on ground, corresponding to the Landsat MSS scene. Landsat-3 carried a set of two broad band and panchromatic RBV cameras (spectral range 0.5-0.75μm), each of which imaged a adjacent areas of about nominally 98×98 km on ground, concurrently.

6.2.3 TM Sensor

This sensor collects, filters and detects radiation in a similar km swath. It records in seven spectral bands which include medium and thermal infrared. It provides a spatial resolution of 30 meters, except on the thermal infrared band, where it is 120 meters. The high spectral resolution is achieved by sensitive detectors and an 8-bit quantization in the analo-to digital conversion process gives 256 gry levels(Table App.6.2). TM images are useful for image interpretation for a much wider range of application than Landsat MSS images because it has both an increase in the number of apectral bands and an improvement in spatial resolution.

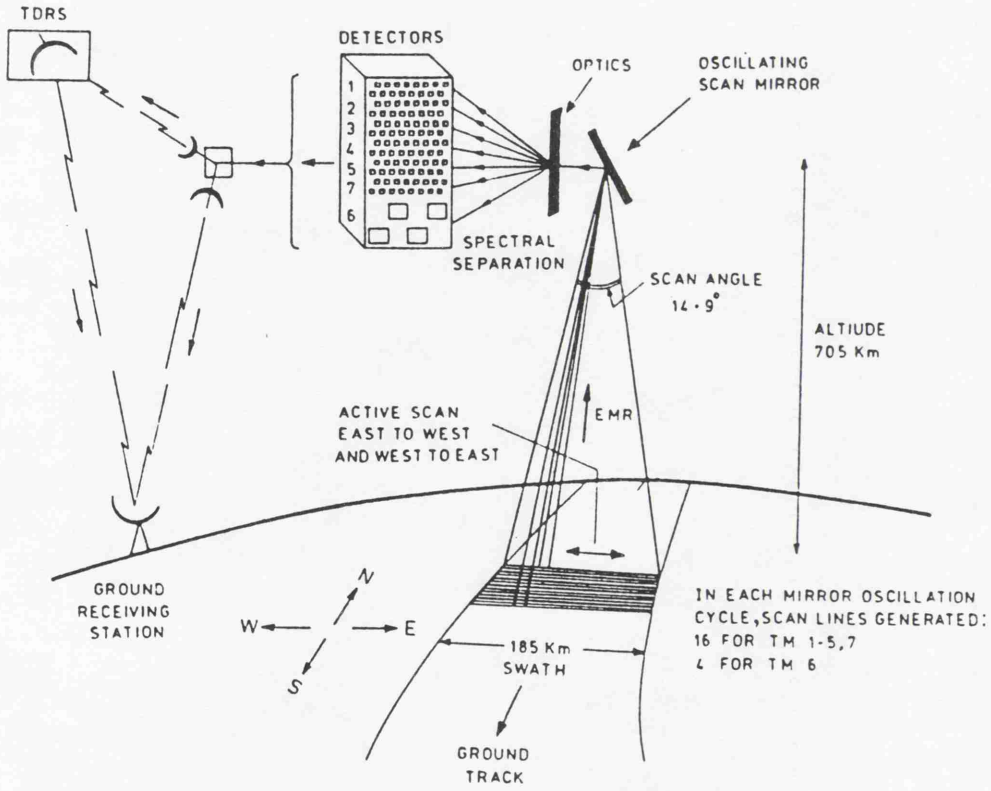

Figure App.6.7: Landsat TM scanning arrangement. The sensor recorders data in 7 bands (1-7). The detectors in the VNIR region are placed at the primary focal plane and those in the SWIR-TIR region at the cooled focal plane. A total of 16 scan lines are concurrently generated for bands 1 to 5 and 7 and four lines for band 6.

6.3 USED REMOTE SENSING DATA

Table Appendix 6.1: Used Remote Sensing Data in This Study.

Type of Data	Obtained From
Lansat (TM	Sept. 1988, Iranian Remore Sensing Centre.
SPOT (XS)	June 1987, Ministry of Agriculture-Iran.
KFA-1000	at 1:270000 scale, (1990), Iranian Geographical Organization.
Aerial photos	at 10000, (1991) Iranian Geographical Organization.
Aerial photos	at 1:20000, (1970) Iranian National Cartographic Centre.
Aerial photos	at 1:55000 Iranian Geographical Organization.

Table Appendix 6.2: Landsat (MSS and TM) and SPOT (MSS and Panchromatic) sensor specifications.

Sensor type	Band number	Spectral sensitivity (μm)	Resolution (m)
	Landsat	**1 and 2**	
RBV	1	0.47-0.75 (green)	80
RBV	2	0.58-0.58(red)	80
RBV	3	0.69-0.83(near infrared	80
MSS	4	0.5-0.6(green)	79
MSS	5	0.6-0.7 (red)	79
MSS	6	0.7-0.8 (near in.)	79
MSS	7	0.8-1.1 (near in.)	79
	Landsat	**3**	
RBV		0.5-0.75 (pn)	30
MSS	4	0.5-0.6 (green)	79
MSS	5	0.6-0.7 (red)	79
MSS	6	0.7-0.8 (near in.)	79
MSS	7	0.8-1.1 (near in.)	79
MSS	8	10.4-12.6 (far in.)	237
	Landsat	**4 and 5**	
TM	1	0.45-0.52 (blue-green)	30
TM	2	0.52-0.60 (green)	30
TM	3	0.63-0.69 (red)	30
TM	4	0.76-0.90 (near in.)	30
TM	5	1.55-1.75 (mid in.)	30
TM	6	10.4-12.5 (far in.)	120
TM	7	2.08-2.35 (mid in.)	30
MSS	1	0.5-0.6 (green)	82
MSS	2	0.6-0.7 (red)	82
MSS	3	0.7-0.8 (near in.)	82
MSS	4	0.8-1.1 (near in.)	82
		SPOT	
MSS	1	0.5-0.59 (green)	20
MSS	2	0.61-0.68 (red)	20
MSS	3	0.79-0.89 (near in.)	20
Panchromatic		0.51-0.73	10